IMAGE PROCESSING AND INFORMATICS LABORATORY

Department of Radiology
University of Southern California

2008 Annual Report

SUMMARY

"Character is like the foundation of a house - it is below the surface."- Unknown

The Image Processing and Informatics Laboratory (IPILab) continues to remain steadfast in its lifelong mission during the year 2007: R&D novel medical imaging informatics concepts, infrastructure, and clinical applications; and training interdisciplinary scientists and academicians in Medical Imaging Informatics. During this period of continued bleakness in the landscape across the national scientific research community with regards to the shrinking NIH funding, the IPILab has continued its stride in receiving research supports, and maintained a steady turnover of matured scientists moving out into other academic institutions and industry; recruited young scientists to launch new research directions and emphases; and cultivated further industrial collaborations. Some of the accomplishments are detailed:

1. Education and Training

We have reached the midpoint of our five-year T32 Training Grant from the National Institute of Biomedical Imaging and Bioengineering (NIBIB), National Institutes of Health (NIH), DHHS entitled: "Biomedical Imaging Informatics Training Program" effective September, 1, 2005 – August 31, 2010, totaling about US$1.6 million. The PI and Co-PI are Dr. H.K. Huang of Radiology and Biomedical Engineering Departments (BME) and Dr. Michael Khoo of BME, respectively. Some accomplishments: One of our previous M.D. T32 trainees has received the four-year prestigious distinguished USC Provost's award to complete his Ph.D. in BME. Existing trainees continue receiving national recognition as first authors in national presentations, proceedings papers and peer-reviewed chapters and papers. We have four new recruits: Two new Ph.D. students with certain unique characteristics, one is from the University of Texas (BME) (we forgave the bitterness, but insisted he was not allowed to discuss the 2006 Rose Bowl BCS Championship game during office hours); the other is a current USC BME Ph.D. candidate from Under-Represented Minorities (URM), a high priority in the T32 mandate. Two Post Doctoral Fellows, one from the USC Radiology Residency Program; and one medical school graduate from the University of Hawaii who is applying for Radiology Residency at USC this summer.

In addition to the T32 training grant, we have been a longtime participant of the USC Summer Undergraduate Research Programs with funding awarded to recruit bright young undergraduate students around the nation searching for future academic research directions. This program continues to be important bedrock for the future of not just our lab, but for the national Medical Imaging Informatics research arena with the emergence of a new generation of young potential interdisciplinary scientists. Some previous Summer Undergraduate Research Candidates have also gone on to participate with the T32 training program.

Milestones for our staff members: Aifeng Zhang received her Ph.D. degree from the BME Department and has accepted a Post Doctoral fellowship with IPILab. Zheng Zhou completed his Post Doctoral training and accepted a position within the research division of a new and innovative Medical Imaging corporation. Arkadiusz Gertych also completed his Post Doctoral training and has accepted a position within a prestigious Minimally Invasive Surgical lab at nearby Cedars Sinai Hospital. Sinchai Tsao, a Ph.D. candidate has just received a Society of Imaging Informatics in Medicine (SIIM) fellowship to pursue his Ph.D. study. Additionally, Bing Guo, M.D. completed her Master's Degree in Medical Imaging and Imaging Informatics BME program at USC and has joined the USC Radiology clinical IT services team which manages the RIS/PACS/VR systems across the USC Health Sciences campuses.

Two international fellows, Dr. Xiang Wu Zheng, Professor of Radiology, Wenzhou Medical College, China as a Distinguished Research Fellow and Elisa Talini, M.S., Research Associate, University of Pisa, Italy completed their training in Medical Imaging Informatics. Ms. Talini is part of the growing consortium participating in our International Data Grid project which includes: Hong Kong, Sao Paulo, Brazil, and Pisa, Italy.

2. Research Projects

We have continued in our new areas of Medical Imaging Informatics research: 1) a DICOM-RT based ePR system with Decision Support for Managing patients treated with Proton Beam Therapy; 2) CAD for Neurological Pathologies including Multiple Sclerosis detection and management on MRI, small Acute Intracranial Hemorrhage detection on CT, and image-based in characterization of ischemia and hemorrhage in stroke patients; 3) CAD-PACS Integration Toolkit; 4) A surgical ePR system for Image-Guided Minimally Invasive Spinal Surgery (MISS); and 5) Clinical validations of bone age assessment. The DICOM-RT ePR system was invited as a paper to Radiographics, and two bone age assessment results were invited for submission to Radiology during another successful RSNA conference in November 2007. Our existing long term research projects: Data Grid, wireless PDA Server have continued to progress. We have over four participating clinical sites for the Bone Age Assessment research including Women's and Children Hospital, USC; Hong Kong; Pisa, Italy; Tehran, Iran; and Taiwan with two other potential sites at NIH/NLM and Korea. Several of these researches are continuously being supported by extramural finds including NIH, U.S. Army Medical Research and Materiel Command, and the private industry.

3. Industrial Collaborations

IPILab has continued to venture into establishing R&D collaborations with the private industry in anticipation of the dwindling NIH research support. To name a few: Working with Guardian Technologies to develop the well-received CAD product showcased at the 2007 RSNA Technical exhibit; Cedara in their PACS workstation display software; Calgary Scientific, Inc. in 3-D display package, and MI^2 in the ePR System for MISS. We are also in communication with multiple manufacturers for collaborations in daily clinical operations of the bone age assessment, AIH CAD, and CAD/PACS Integration toolkit.

We are in the process of planning to move IPILab from the current picturesque location in the Marina del Rey to a new site in the heart of the Health Science Campus at USC. Although, we will miss the view of the marina, we look forward to an even more successful and exciting year of research collaboration with clinicians and scientists throughout the campus without the physical limitations of distance in the metropolitan Los Angeles area. You are welcome to visit us at that time and please check our website periodically for the time of relocation.

As described in the Table of Contents, this 2008 Annual Report includes materials related to IPI R&D plans and current results, selected published and in-press papers during the year, as well as preprints to appear in the *Proceedings of the International Society for Optical Engineering (SPIE) in Medical Imaging*, San Diego, California, February 16-21, 2008.

Our research has been supported by:

- NIH/NIBIB R01 EB 00298
- NIH/NLM Training Grant T15 LM07356
- NIH/NIBIB Biomedical Imaging Informatics Training Grant T32 EB 00438
- USAMRMC/Henry M. Jackson Foundation Subaward 53-5149-5600
- USAMRMC/TATRC AAMTI Subaward 2007011185
- USC Undergraduate Research Award No. 22-2149-6044
- USCRA Research Fund 3051-00
- Array Corporation, Japan
- Guardian Technologies, USA
- MI^2, USA

TABLE OF CONTENTS

STAFF AND COLLABORATORS

Faculty and Administrative

Edward V. Grant, M.D., FACR.
Professor and Chairman,
Department of Radiology

H.K. Huang, D.Sc., FRCR (Hon.), FAIMBE
Professor of Radiology and BME
Director, IPI

Vicente Gilsanz, M.D.
Professor of Radiology and Pediatrics

James William Hill, M.D., J.D.
Clinical Assistant Professor,
Department of Radiology

James Sayre, Ph.D.
Professor of Biostatistics and Radiological Science,
University of California, Los Angeles (UCLA)
Consultant

Cammy Huang, Ph.D.
Lecturer, Computer Science Dept,
Director of Scientific Outreach, WGLN
Stanford University
Consultant

Marco A. Gutierrez, Ph.D.
Invited Professor, Heart Institute of University of Sao Paulo,
Visiting Distinguished Research Fellow

Xiangwu Zheng, M.D.
Professor, Wenzhou Medical College, Zhejiang
Visiting Distinguished Research Fellow

Angelica Virgen
Administrative Assistant

Michael C.K. Khoo, Ph.D.
Professor and Chairman,
Department of Biomedical Engineering (BME)

Brent J. Liu, Ph.D.
Associate Professor of Radiology and BME
Deputy Director, IPI

Greg T. Mogel, M.D.
Associate Professor of Radiology, Asst Prof. of BME

Ewa Pietka, Ph.D. D.Sc.
Professor, Technical University of Silesia, Poland
Visiting Professor of Radiology

Jianguo Zhang, Ph.D.
Professor, Shanghai Institute of Technical Physics, The Chinese Academy of Science
Visiting Professor of Radiology

Maria YY Law, MPhil, BRS, Ph.D.
Associate Professor
The Hong Kong Polytechnic University
Visiting Associate Professor of Radiology

Heinz U. Lemke, Ph.D.
Visiting Research Professor of Radiology

Elisa Talini, M.S.
University of Pisa
Visiting Fellow

Mary Hall
Administrative Assistant

Post Doctoral Fellows

Aifeng Zhang, Ph.D.

Arkadiusz Gertych, Ph.D.

Zheng Zhou, Ph.D.

NIH T32 Post Doctoral Fellows

Paymann Moin, M.D.

James Fernandez, M.D.

Alexis Wong, M.D.

NIH T32 Pre Doctoral Fellows

Jasper Lee, B.S., Ph.D. Student

Kevin Ma, B.S., Ph.D. Student

Anika Joseph, M.S., Ph.D. Candidate

Research Assistants

Mark W. Haney, M.D.
USC Provost Fellow, Ph.D. Student

Heston K. Kwong, M.D., MBA, M.S.,
Ph.D. Candidate, Hong Kong Polytechnic University.

Jorge Documet, M.S.
Ph.D. Candidate
Lab Manager

Anh Le, M.S.
Ph.D. Candidate

Sinchai Tsao, M.S.
Ph.D. Candidate

Bing Guo, M.D.

2007 Summer Students

Tony Mo, B.S.
University of Southern California

Alan Sangnil,
University of Southern California

Joshua Uyeda,
University of Southern California

Carlo Fernandes,
University of Michgan

EQUIPMENT LAYOUT AND NETWORK CONFIGURATION

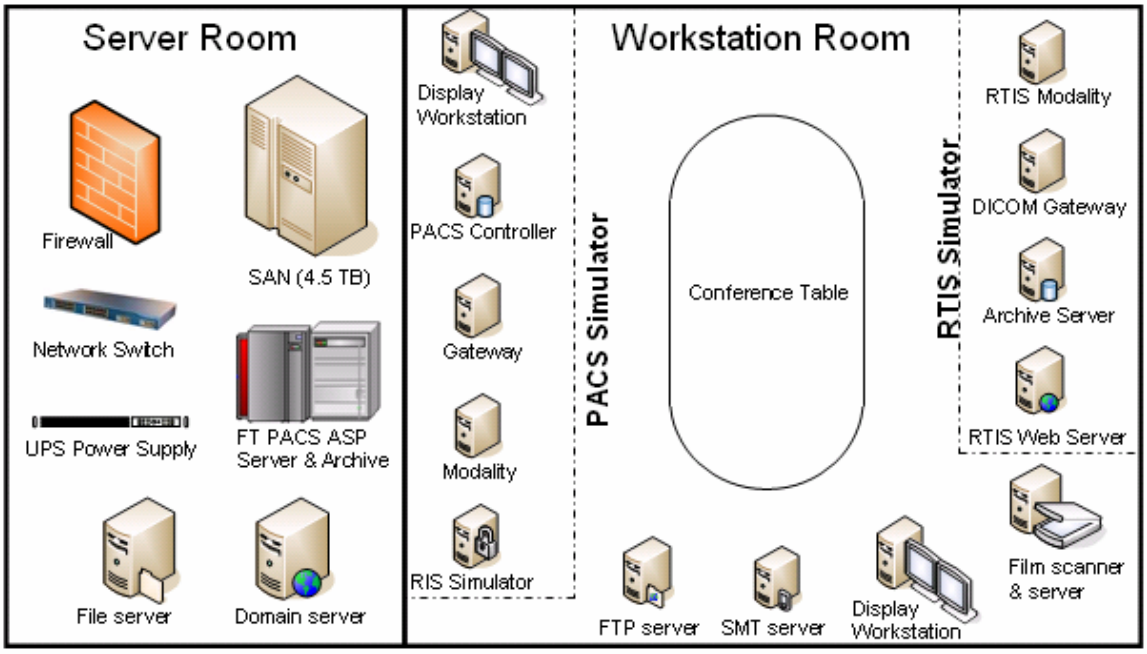

Figure 1. Equipment Layout

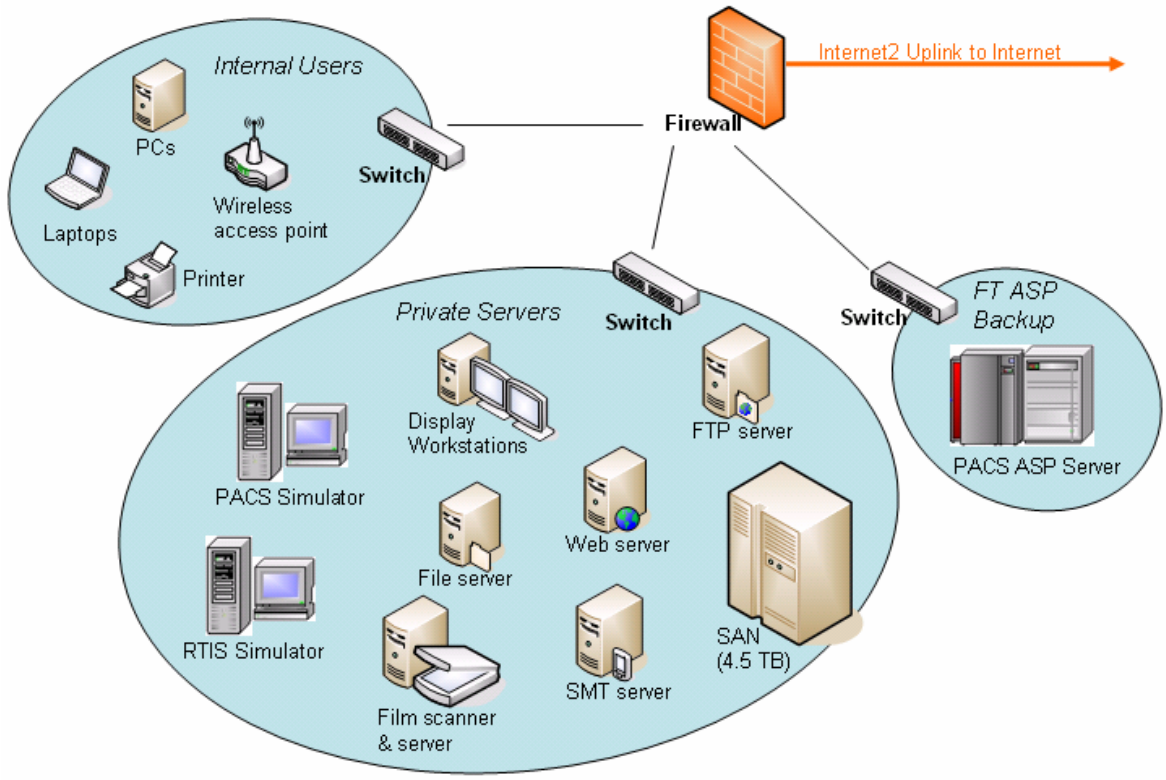

Figure 2. Network Configuration

NATIONAL AND INTERNATIONAL COLLABORATING SITES AND WEBSITE

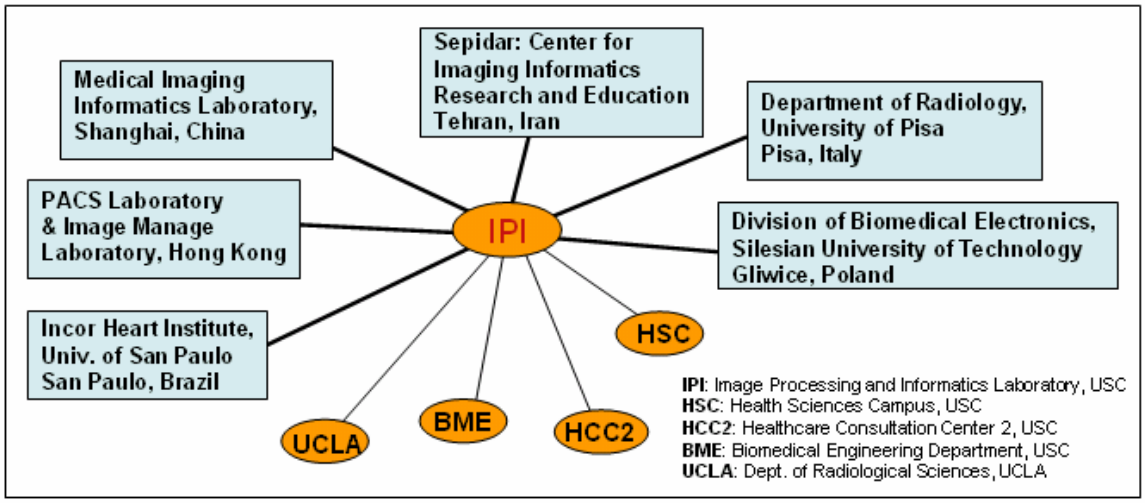

Figure 3. National and International Collaboration Sites

Figure 4. Website

RSNA 2007 POSTERS AND PAMPHLET

USC UNIVERSITY OF SOUTHERN CALIFORNIA

Image Processing and Informatics Lab

A DICOM Structured Report Viewer and Automatic Workflow for CAD-PACS Integration in a Clinical Environment Based on IHE Workflow Profiles.

A Le[1], MS, Z Zhou[2], PhD, J Documet[1], MS, S Tsao[1], MS, A Zhang[1], PhD, B Liu[1], PhD, HK Huang[1], DSc, FRCR (Hon.)

[1] Image Processing and Informatics Laboratory
Department of Radiology and Biomedical Engineering, University of Southern California
[2] U-System, Inc., San Jose, CA

In this presentation, we demonstrate:

- A protocol for the integration of CAD Structured Report into PACS clinical workflow.
- An automatic workflow of CAD-PACS integration.
- Examples of CAD Structured Report displays on web-based viewer.

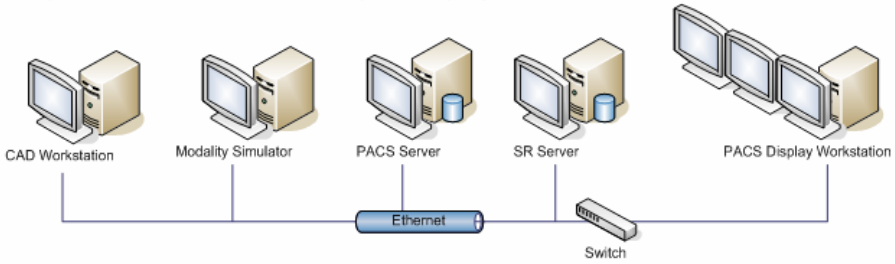

Courtesy of R2 Technology, Dr. Matthew Brown, Dr. Tao Chan and Dr. Arkadiusz Gertych.

USC UNIVERSITY OF SOUTHERN CALIFORNIA

Image Processing and Informatics Lab

A Fault-Tolerant Metadata Database Design for Sharing Quantitative Results in Imaging-based Clinical Trials

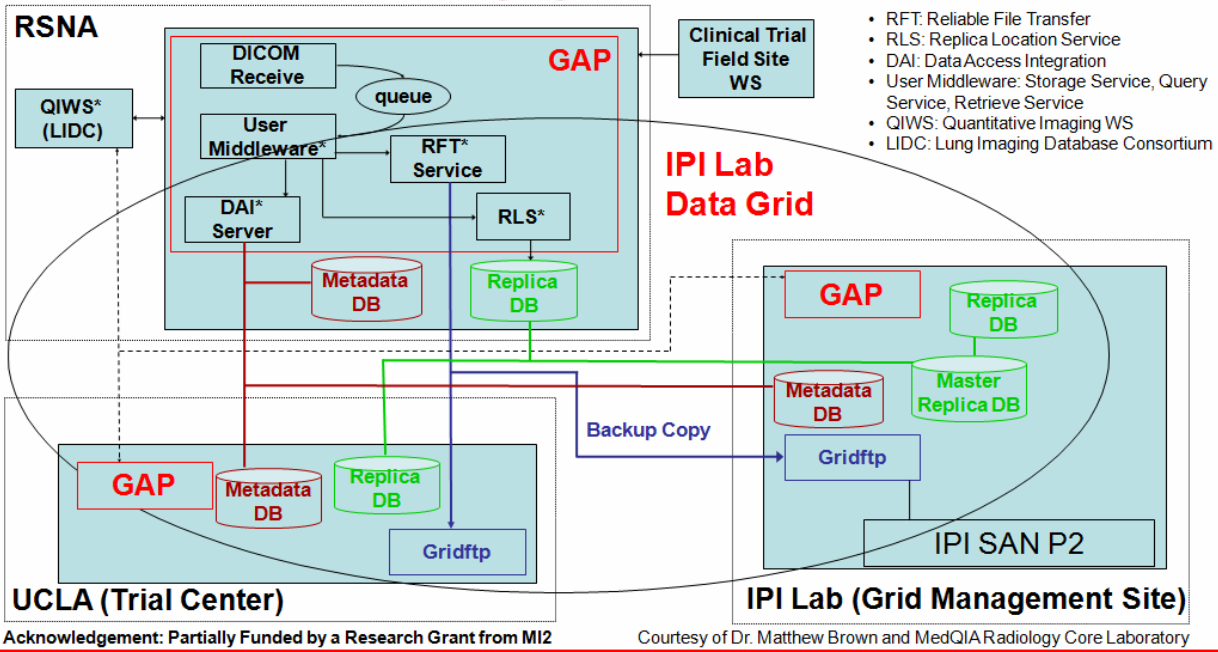

- RFT: Reliable File Transfer
- RLS: Replica Location Service
- DAI: Data Access Integration
- User Middleware: Storage Service, Query Service, Retrieve Service
- QIWS: Quantitative Imaging WS
- LIDC: Lung Imaging Database Consortium

Acknowledgement: Partially Funded by a Research Grant from MI2

Courtesy of Dr. Matthew Brown and MedQIA Radiology Core Laboratory

USC UNIVERSITY OF SOUTHERN CALIFORNIA

Image Processing and Informatics Lab

Data Grid for Enterprise PACS
Tier 2 Storage and Disaster Recovery

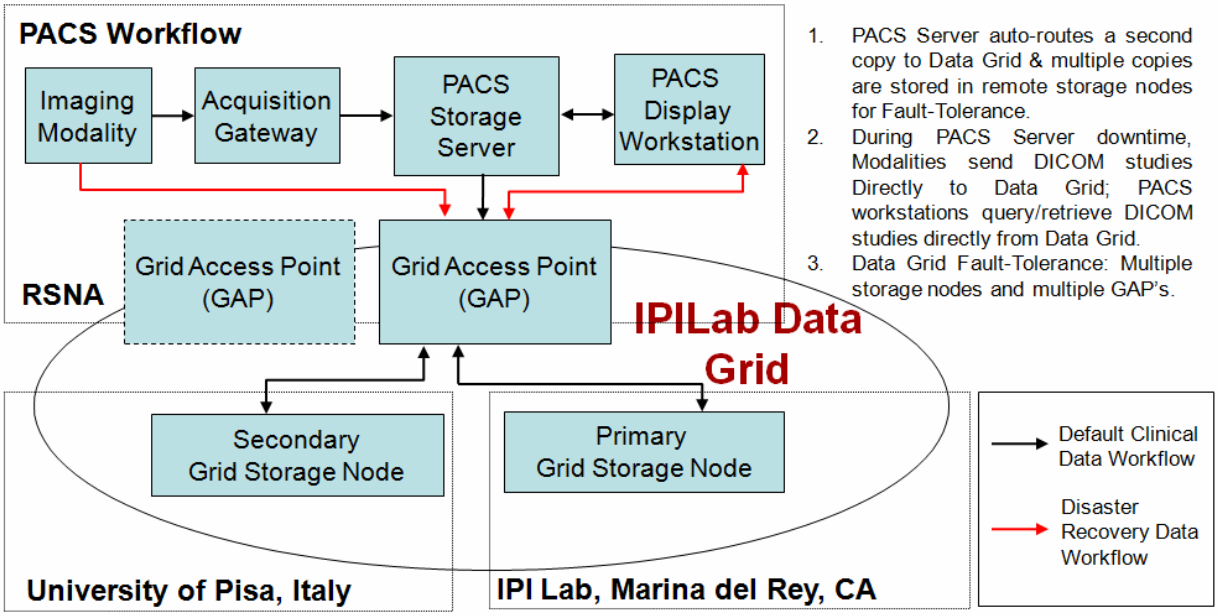

1. PACS Server auto-routes a second copy to Data Grid & multiple copies are stored in remote storage nodes for Fault-Tolerance.
2. During PACS Server downtime, Modalities send DICOM studies Directly to Data Grid; PACS workstations query/retrieve DICOM studies directly from Data Grid.
3. Data Grid Fault-Tolerance: Multiple storage nodes and multiple GAP's.

Acknowledgement: Partially Funded by a Research Grant from MI2

USC UNIVERSITY OF SOUTHERN CALIFORNIA

A DICOM-RT Radiation Oncology ePR with Decision Support Utilizing a Quantified Knowledge-base from Historical Data

J Documet, BS [1]; B Liu, PhD [1]; A Le, MS [1]; A Gertych, PhD [1], J DeMarco, PhD [2]

1 – Department of Radiology, Keck School of Medicine University of Southern California, Los Angeles, USA

2 – UCLA Department of Radiation Oncology, Los Angeles, California, USA

Learning Objectives

- Analyze historical patient data and create a quantified knowledge base for decision support to improve the planning of treatments.
- Integrate DICOM-RT objects from different vendors currently disseminated in multiple systems.
- Provide a standardized platform for developing decision-support tools.
- Present initially developed tools to see the future potential research.

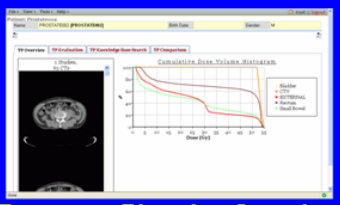

Treatment Planning Overview

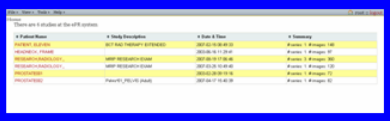

Worklist

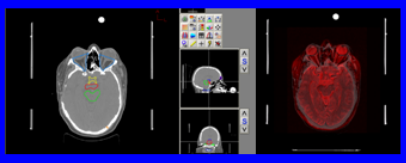

MR/CT Fusion Display Tool

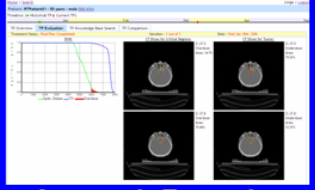

Automatic Extraction of Hot Spots

3-D Conformal RT | Head & Neck PT

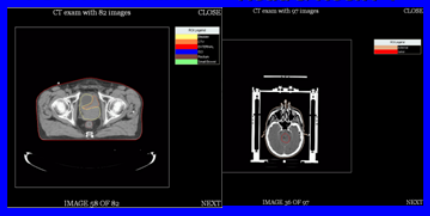

Study Visualization

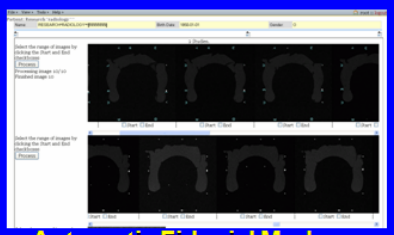

Automatic Fiducial Markers Extraction Tool

This research has been partially funded by USAMRMC/Henry M. Jackson Foundation Subaward 53-5149-5600

Computer-aided Diagnosis (CAD) of Small Aneurysms of Circle of Willis

B Guo, MD [1]; X Zheng, MD [2]; A Gertych, PhD [1]; B J Liu, PhD [1]; H K Huang, DSc[1]; S Tsao, MS;[1]

1 - Department of Radiology, Keck School Medicine University of Southern California, Los Angeles, USA

2 – First Affiliated Hospital of Wenzhou , WenZhou, China

IN THIS PRESENTATION…

We Demonstrate: **A CAD system to detect aneurysms of Circle of Willis :**

1) CAD algorithms and method used in the system ;

2) Quantitative measurements of vascular diameters of the Circle of Willis to aid in the diagnosis process;

3) Present differences in quantitative measurements for both a normal case and a case with small aneurysm;

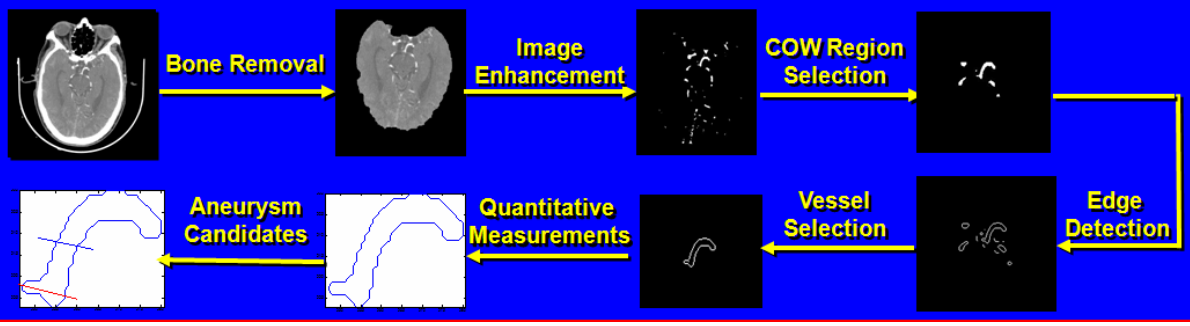

Implementation of Collaborative Healthcare in Grid-Based Cross-Enterprise Images Sharing with IHE XDS-I Integration Profile

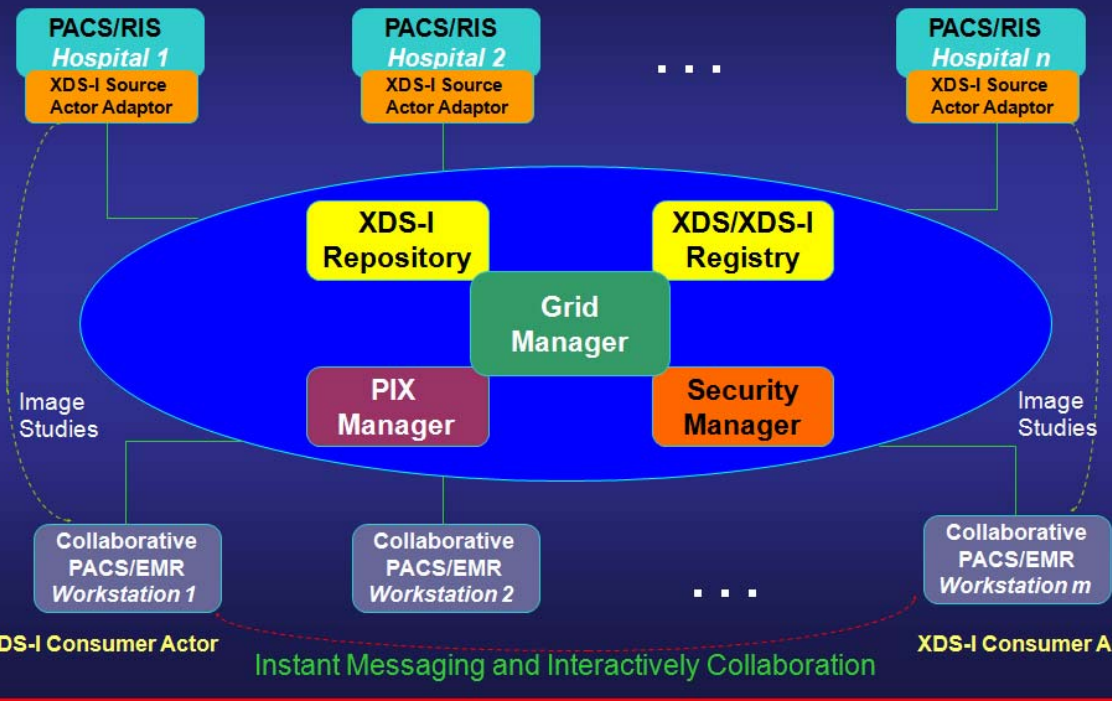

A Vendor Agnostic Real-time Patient Dashboard to Monitor the Patient Workflow in a Radiology Department

J Documet, BS [1]; B Liu, PhD [1]; K Wang [1]; R Shrestha, MD MBA [2]

1 - Department of Radiology, Keck School of Medicine University of Southern California, Los Angeles, USA

2 - Radiology Informatics, University of Pittsburgh Medical Center, Pittsburgh, Pennsylvania, USA

Learning Objectives:

- A vendor agnostic dashboard. With useful clinical information from different systems in a single display.
- Display of real-time clinical and workflow metrics. With email notifications when procedure times are exceeded.
- Display of related reports from RIS. Each different RIS vendor has an interface for flexibility.
- Display and distribution of patients' DICOM images obtained from the PACS. System integration always needed.
- Data mining tools to add business intelligence to identify trends and workflow efficiency. Management can take better decisions.

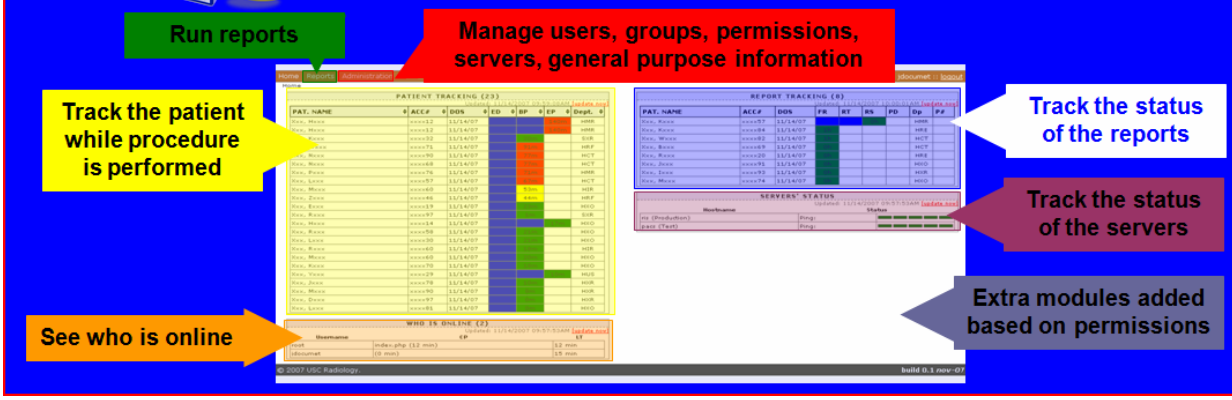

Image Sharing and Distribution in a Regional Health Information Organization (RHIO) through the utilization of a DICOM, IHE, and HL7 Compliant Data Grid Using XDS

UNIVERSITY OF SOUTHERN CALIFORNIA

Sander Chao, Anh Le, Kevin Ma, Jasper Lee, Brent Liu, HK Huang

Image Processing and Informatics Lab

RHIO

RHIO With Centralized Data Grid Database and Storage

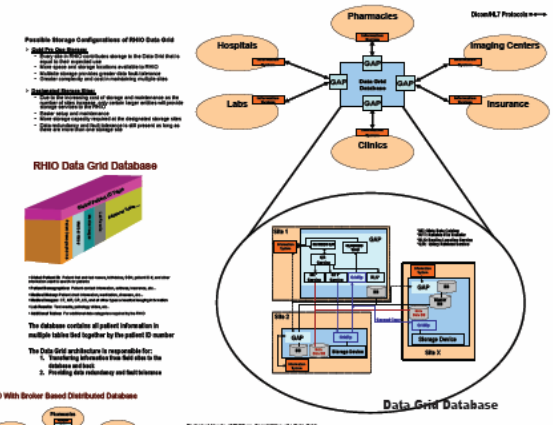

Data Grid

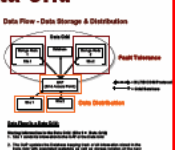

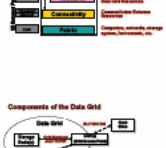

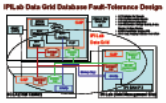

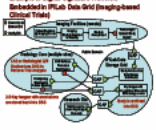

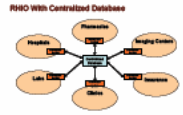

University of Southern California

USC Viterbi School of Engineering

Keck School of Medicine of USC

Image Processing and Informatics Laboratory

RSNA 2007 Connecting Radiology November 25–30, 2007 Chicago

IPILab
Presentations and Exhibits

4676 Admiralty Way,
Suite 601
Marina Del Rey, CA 90292
(310) 448 9440
http://www.ipilab.org/

Dear Colleagues and Friends of IPILab,

Welcome to another exciting year of IPILab's presentations and exhibits at RSNA 2007.

This year we are presenting:

InfoRAD Exhibits	8
Education Exhibits (Electronic Posters)	5
Scientific Posters	1
Scientific Papers	1

Our InfoRAD or Computer Exhibits as well as our education exhibits will be available for viewing:

Sunday	8:00 am - 6:00pm
Monday - Thursday	7:00 am - 10:00 pm
Friday	7:00 am - 12:45 pm

This year we have 2 scientific poster / paper presentations:

Tuesday November 27, 2007 - Scientific Paper
5:20 pm - 5:30 pm @ N229
Cross-Racial Discrepancies of Growth Patterns in Bone Age Assessment
Aifeng Zhang, PhD, Han K. Huang, ScD, James Sayre, PhD, Linda Vachon, MD

Tuesday November 27, 2007 - Scientific Poster
12:15 pm - 01:15 pm @ Lakeside Learning Center
Fuzzy System Design for Bone Age Assessment of Children in Multiple Regions of the Hand
Aifeng Zhang, PhD, Arkadiusz Gertych, PhD, Sinchai Tsao, MS, Brent Liu, PhD, Han K. Huang, ScD

If you have any queries or questions please don't hesitate to contact us.

Brent J. Liu, PhD
Deputy Director
IPILab &
Informatics Division, Dept of Radiology
Assistant Professor of Radiology and Biomedical Engineering
University of Southern California

2007 IMAGE PROCESSING AND INFORMATICS LABORATORY (IPILab)
STAFF AND COLLABORATORS

Faculty and Administration

Edward V. Grant, M.D., FACR.
Professor and Chairman, Department of Radiology

H.K. Huang, D.Sc., FRCR(Hon.), FAIMBE
Professor of Radiology and BME
Director, IPI

Vicente Gilsanz, M.D.
Professor of Radiology and Pediatrics

James William Hill, M.D., J.D.
Clinical Assistant Professor, Department of Radiology

James Sayre, Ph.D.
Professor of Biostatistics and Radiological Science, UCLA
Consultant

Cammy Huang, Ph.D
Virtual Labs Project Director, SUMMIT
Director of Scientific Outreach, WGLN (Wallenberg Global Learning Network)
Lecturer, Dept of Computer Science, Stanford U.
Consultant

Heinz U. Lemke, Professor
Technical University Berlin
Visiting Research Professor of Radiology

Michael C.K. Khoo, Ph.D.,
Professor and Chairman, Department of Biomedical Engineering (BME)

Brent J. Liu, Ph.D.
Associate Professor of Radiology and BME
Deputy Director, IPI

Greg T. Mogel, M.D.
Associate Professor of Radiology

Ewa Pietka, Ph.D. D.Sc.
Professor, Technical University of Silesia, Poland
Visiting Professor of Radiology

Jianguo Zhang, Ph.D.
Professor, Shanghai Institute of Technical Physics, The Chinese Academy of Science
Visiting Professor of Radiology

Maria YY Law, MPhil, BRS, Ph.D.
Associate Professor
The Hong Kong Polytechnic University
Visiting Associate Professor of Radiology

Tao Chan, M.D., Ph.D.
Consultant

Postdoctoral and Visiting Fellows

Xiangwu Zheng, M.D.
Professor, First Affiliated Hospital of Wenzhou Medical College

James Reza F. Fernandez, M.S., MD
NIH T-32 Fellow

Marco A. Gutierrez, Ph.D.
Invited Professor, Heart Institute of University of San Paulo

Lucy (Aifeng) Zhang, Ph.D.

Paymann Moin, M.D.
NIH T-32 Fellow

Research Fellows and Assistants

Jorge Documet, M.S.
Ph.D. Candidate

Anika Joseph, M.S.
NIH T32 Fellow, Ph.D. Candidate

Heston K. Kwong, M.D., MBA, MS.
Ph.D. Candidate, Hong Kong Polytechnic University

Jasper Lee, B.S.
NIH T32 Fellow, Ph.D. Student

Bing Guo, M.D. M.S.

Anh Le, M.S.
Ph.D. Candidate

Sinchai Tsao, M.S.
Ph.D. Candidate

Mark Haney, M.D.
USC Provost Fellow, Ph.D. Student

Kevin Ma, B.S.
NIH T32 Fellow, Ph.D. Student

Undergraduate Trainees

Joshua Uyeda
Dept of Biomedical Engineering
University of Southern California

<--InfoRAD Exhibits-->

<--Education Exhibits-->

<--InfoRAD Exhibits-->

InfoRAD CODE: LL-IN5215-H

A DICOM Structured Report Viewer and Automatic Workflow for CAD-PACS Integration in a Clinical Environment Based on IHE Workflow Profiles

***Anh Le, MS**, Zheng Zhou, PhD, Brent Liu, PhD, Han K. Huang, ScD*

PURPOSE/AIM

1. To review DICOM Structured Report Standard and IHE Post Processing Workflow Profiles. 2. To present a protocol for the integration of CAD Structured Report into diagnosis workflow. 3. To provide examples of how CAD Structured Report displays on web-based viewer. 4. To demonstrate automatic workflow of CAD-PACS integration.

CONTENT ORGANIZATION

1. Significance and complexity of DICOM-SR for CAD. 2. Integration of the technologies for CAD-SR and diagnosis workflow. 3. Web-based DICOM-SR Viewer for CAD application using key note image with annotation toggle mode. 4. Automatic workflow for CAD application in clinical environment using IHE Post-Processing Profiles. 5. Examples of integrated CAD results with the diagnosis workflow.

SUMMARY

1. Integration of CAD results into diagnosis workflow is achievable using DICOM standard and IHE profiles. 2. The DICOM SR Viewer with user friendly design can greatly enhance the visualization of CAD results. 3. The automatic workflow tracks and logs the CAD process in radiology workflow. 4. CAD-PACS integration does not alter CAD results. Thus, the proper integration will improve usage of CAD for more accurate analysis and faster assessment in the clinical decision-making process.

InfoRAD CODE: LL-RO3260

A DICOM-RT Radiation Oncology ePR with Decision Support Utilizing a Quantified Knowledge-base from Historical Data

***Jorge Documet, MS**, John DeMarco, PhD, Anh Le, MS, Arkadiusz Gertych, PhD, Brent Liu, PhD*

PURPOSE/AIM

To improve turnaround time for radiation therapy of cancer patients by providing retrospective analysis tools to assist physicists and physicians during the therapy planning process. To permit offline treatment dose calculations and plan evaluation, allowing participants to compare and quantify treatment planning algorithms using DICOM-RT objects

CONTENT ORGANIZATION

Develop a scalable and expandable ePR system with DICOM-RT to: - analyze historical patient data and create a quantified knowledge base for decision support to improve the planning of treatments. - integrate DICOM-RT objects from different vendors currently disseminated in multiple systems. - provide a proactive mechanism with alerts and notifications to reduce the approval time in the treatment planning process. The ePR will be used by dosimetrists, physicists, and radiation oncologists.

SUMMARY

Integrating local stored data from different treatment planning systems into a centralized and modular ePR can serve as a data mining repository for retrospective analysis. The ePR displays DICOM-RT objects including CT images, contours, DRRs, DVHs in a web-based fashion. In addition, alerts can be sent every time a major event occurs, such as approval requests or physician completion tasks. The ePR supports quantification and comparison of offline treatment dose calculation and plan evaluation.

InfoRad CODE: LL-IN5251-D

A Vendor Agnostic Real-time Patient Dashboard to Monitor the Patient Workflow in a Radiology Department

***Jorge Documet, MS**, Rasu Shretha, MD, Kevin Wang, Brent Liu, PhD*

PURPOSE/AIM
To develop a patient dashboard that will help to improve and optimize the workflow processes in a radiology department, monitoring every stage of the clinical care process within radiology. In addition, the new approach will allow one to track, measure and throttle these processes, as well as identify and minimize bottlenecks in the process flows.

CONTENT ORGANIZATION
To develop an extensible, scalable and secure web-based Patient Dashboard, which is a web portal to access reports about patients and tools for managing the workflow from a single interface. This vendor agnostic dashboard provides: - display of real-time clinical and workflow metrics. - display of related reports from RIS. - display and distribution of patients' DICOM images obtained from the PACS. - data mining tools to add business intelligence to identify trends and workflow efficiency.

SUMMARY
This exhibit implements a Patient Dashboard for the Radiology Department that can monitor ongoing clinical and workflow metrics. The real-time monitoring of the flow of the patient in the radiology department will use data points entered in the Radiology Information System (RIS) and it will be displayed in a 'patient dashboard' on either PCs or mobile devices. The primary users of this application will be administrative staff, technologists and PACS administrators.

InfoRad CODE: LL-IN5236-D

Computer-aided Diagnosis (CAD) of Small Aneurysms of Circle of Willis

***Bing Guo, MD**, XiangWu Zheng, MD, Arkadiusz Gertych, PhD, Brent Liu, PhD, Han K. Huang ScD, Mark Haney, MD, Paymann Moin, MD*

PURPOSE/AIM
To use CAD to detect small aneurysms (<=5mm) of Circle of Willis. To use CAD to derive 3-D anatomical information with anatomical names, size, and diameter on CTA images for medical education.

CONTENT ORGANIZATION
Cerebral aneurysm most likely occurs around the Circle of Willis. Some of these are manifested as small aneurysms that are difficult to detect during diagnosis which may lead to severe bleeding into the brain tissue and life-threatening. We have developed a CAD system to detect small aneurysms (<=5mm) of Circle of Willis based on a 3-D model of Circle of Willis. The 3-D model contains quantitative measurements of various vascular diameters of the Circle of Willis based on 30 non-aneurysm cases.

SUMMARY
The CAD provides automatic segmentation and measurement in prediction of intracranial aneurysms which can be used to provide a second opinion for physicians. Thirty clinically confirmed small cerebral aneurysm cases were used to test the sensitivity, specificity and accuracy of the CAD. The false positives were removed by use of a rule-based classification method. Experimental results suggest that the CAD system is reliable, fast and easy to use.

InfoRAD CODE: LL-IN5226-B

A Data Grid for Enterprise PACS Tier 2 Storage and Disaster Recovery

***Jasper Lee, BS**, Zheng Zhou, PhD, Elisa Talini, MS, Kevin Ma, BS, Brent Liu, PhD, Han K. Huang, ScD*

PURPOSE/AIM
The current solution for Enterprise PACS Tier 2 or backup storage is costly and difficult to maintain and operate. In this presentation, we demonstrate a Data Grid system that federates all available storage devices at the enterprise level to provide a virtual, distributive and cost-effective solution for clinical enterprise PACS tier 2 storage.

CONTENT ORGANIZATION
1. Review of current enterprise PACS tier 2 storage solutions 2. The Data Grid concept and system architecture 3. The data flow of using Data Grid for enterprise PACS Tier 2 storage and disaster recovery 4. Demonstration of storing images from a clinical enterprise PACS to the Data Grid 5. Demonstration of accessing images in the Data Grid from the enterprise PACS workstation 6. Demonstration of automatic Data Grid backup and disaster recovery

SUMMARY
We have developed a Data Grid system for enterprise PACS tier 2 storage and disaster recovery. The Data Grid has been applied to a clinical enterprise PACS that consists of three commercial PAC systems. Results demonstrate that the Data Grid can be utilized for Enterprise PACS tier 2 storage and disaster recovery.

InfoRAD CODE: LL-IN5250-B

A Fault-tolerant Metadata Database Design for Sharing Quantitative Results in Image-Based Clinical Trials Based on the IHE XDS Profile

***Jasper Lee**, BS, Zheng Zhou, PhD, Elisa Talini, MS, Kevin Ma, BS, Brent Liu, PhD, Matthew Brown, PhD*

PURPOSE/AIM
In the 2006 RSNA, a Data Grid was demonstrated for storage and distribution of medical images. However there still lacks a fault-tolerant means to share quantitative trial results within the Data Grid. We demonstrate a fault-tolerant metadata database design for image-based clinical trials based on the DICOM Structure Report and IHE XDS profile.

CONTENT ORGANIZATION
This exhibit demonstrates a fault-tolerant storage and sharing of quantitative trial results within the Data Grid. It will cover: A. System design of the fault-tolerant metadata database architecture. B. Storage of quantitative trial results in DICOM SR format in the Data Grid. C. Automatic replication of clinical trial results in the Data Grid for fault-tolerance. D. Sharing of clinical trial results in the Data Grid. E. Storage and user designated distribution of DICOM images in the Data Grid.

SUMMARY
We demonstrate a fault-tolerant metadata database system within the Data Grid for image-based clinical trials. Based on the IHE XDS profile, storage and sharing of DICOM SR and clinical trial quantitative results can be performed within the Data Grid. This fault-tolerant design is critical for applying the Data Grid in image-based clinical trials.

InfoRAD CODE: LL-IN5215-H

A DICOM Structured Report Viewer and Automatic Workflow for CAD-PACS Integration in a Clinical Environment Based on IHE Workflow Profiles

***Anh Le, MS**, Zheng Zhou, PhD, Brent Liu, PhD, Han K. Huang ScD*

PURPOSE/AIM

1. To review DICOM Structured Report Standard and IHE Post Processing Workflow Profiles. 2. To present a protocol for the integration of CAD Structured Report into diagnosis workflow. 3. To provide examples of how CAD Structured Report displays on web-based viewer. 4. To demonstrate automatic workflow of CAD-PACS integration.

CONTENT ORGANIZATION

1. Significance and complexity of DICOM-SR for CAD. 2. Integration of the technologies for CAD-SR and diagnosis workflow. 3. Web-based DICOM-SR Viewer for CAD application using key note image with annotation toggle mode. 4. Automatic workflow for CAD application in clinical environment using IHE Post-Processing Profiles. 5. Examples of integrated CAD results with the diagnosis workflow.

SUMMARY

1. Integration of CAD results into diagnosis workflow is achievable using DICOM standard and IHE profiles. 2. The DICOM SR Viewer with user friendly design can greatly enhance the visualization of CAD results. 3. The automatic workflow tracks and logs the CAD process in radiology workflow. 4. CAD-PACS integration does not alter CAD results. Thus, the proper integration will improve usage of CAD for more accurate analysis and faster assessment in the clinical decision-making process.

InfoRAD CODE: LL-IN5237-H

Visual and Quantitative Assessment of Multiple Sclerosis Lesions in Comparative 3-D MR Studies

***Arkadiusz Gertych, PhD**, Alexis Wong, MD, Han K. Huang, ScD, Alan Sangnil, Carlo Fernandes*

PURPOSE/AIM

2D MRI has become the study of choice for diagnosis, monitoring of progression in multiple sclerosis (MS). In clinical practice evaluation of current and previous studies is manual. This onerous task of counting 2D and 3D lesions by the expert can be automated using computer aided detection (CAD) by providing quantitative results in 2D and 3D space

CONTENT ORGANIZATION

Anatomical and pathological knowledge guided 3D CAD approach has been developed to quantify MS lesions in MR comparative studies. The CAD first localizes the brain mask (BM) in T1 sequences and segments MS lesions in the BM in FLAIR sequences. Lesions are detected and counted. Their areas and volumes in 2D and 3D spaces are calculated. The CAD graphical interface with 3D rendering capability provides quantitative results and visualization of lesions within BMs in comparative MR studies.

SUMMARY

We have developed a 3D CAD method to quantify MS lesions. This novel approach includes side-by-side comparison and visualization with quantitative findings for progression comparison in 3D. It can facilitate neuroradiologist s diagnosis efficiency and improve accuracy in the evaluation of global progression of MS disease. Our validation data set contains 55 MS exams, 30% of them are comparison studies. The pilot study with this data set demonstrates very good correlation with expert's readings.

InfoRAD CODE: LL-IN5238-B

Quantification of Hippocampal Volume and Detection of MR Signal Abnormalities in the Diagnosis of Mesial Temporal Sclerosis

***Arkadiusz Gertych, PhD**, Alexis Wong, MD, Mark Haney, MD, Brent Liu, PhD*

PURPOSE/AIM

Diagnosing mesial temporal (hippocampal) sclerosis (MTS)can be challenging for the radiologist. Particularly difficult is the comparative evaluation of the bilateral hippocampi on multiple MR sequences. The purpose is to demonstrate the utility of mesiotemporal structures quantification and lesion detection in improving both the speed and accuracy.

CONTENT ORGANIZATION

Our clinical dataset currently contains 12 confirmed MTS and 15 control MR exams respectively. Based on this dataset we have developed an automated computer-aided diagnosis (CAD) algorithm which first detects and then analyzes the hippocampi using volumetric and intensity measurements. The CAD utilizes joint features of FLAIR and T1 sequences to emphasize anatomical and pathological findings within the hippocampi. Findings are superimposed onto MRI and displayed via graphical interface.

SUMMARY

The CAD has enhanced capabilities vs. those previously presented. The new features are lesion outline and volumetric measurements of the hippocampus. The ability to show a size discrepancy between the hippocampi in a particular MR slice provides additional information to the radiologist and may support current approach in the diagnosis of MTS. Evaluation of this method using the clinical dataset shows improved reading time, subjectivity, accuracy and also high correlation with expert s verdict.

<--Education Exhibits-->

Education Exhibit CODE: LL-IN6851

The Utilization of Imaging and Informatics Decision Support Tools Based on DICOM-RT and DICOM-RT-ION Objects for Therapy Treatment Planning

***Brent Liu, PhD**, Anh Le, MS, Jorge Documet, MS, Arkadiusz Gertych, PhD, Reinhard Schulte, MD, Maria Law, ScD.*

PURPOSE/AIM
To present Decision-Support Tools developed based on DICOM-RT and RT-ION objects with quantitative measurements and knowledge base for therapy treatment planning. These tools are add-on features for a DICOM standard ePR system of cancer patients and can expand the clinical efficiency and efficacy of therapy treatment planning.

CONTENT ORGANIZATION
1) Learn about the DICOM standard with DICOM-RT and DICOM-RT-ION Objects and workflow models for radiation and proton therapy for cancer patients and the differences in treatments. 2) Development and differentiation of decision-support and visualization tools with quantitative measurements and knowledge base for therapy treatment planning. 3) Discover the impact of Imaging Informatics and decision-support tools in the field of Image-Intensive Radiation and Proton Therapy for cancer patients.

SUMMARY
1) The DICOM-RT and DICOM-RT-ION objects have significant potential as a platform for developing additional decision support tools. 2) An Imaging and Informatics approach towards developing the quantitative measurements and knowledge base is demonstrated for radiation and proton therapy planning. 3) The development of DICOM-based decision-support tools allows open system integration, global data distribution and analysis, and sharing of best-practice treatment plans from multiple facilities.

Education Exhibit CODE: LL-IN6879

The Workflow and Procedures for Integrating Standalone Compute-aided Detection (CAD) Workstations with a Clinical PACS with Real-World Examples

***Anh Le, MS**, Zheng Zhou PhD, Brent Liu, PhD, Han K. Huang, ScD*

PURPOSE/AIM
A CAD-PACS integration toolkit for integrating standalone CAD workstations with a clinical PACS has been demonstrated in 2006 RSNA. In this presentation, we illustrate the workflow and procedures of the CAD-PACS integration by showing examples from some commercially available CAD applications using this toolkit.

CONTENT ORGANIZATION
1. Current CAD workflow in clinics 2. The CAD-PACS Integration toolkit based on DICOM Standard and IHE workflow profiles to facilitate the integration of standalone CAD with a PACS 3. The workflow and procedures of CAD-PACS integration using the CAD-PACS toolkit 4. Examples of integrating various CAD applications with a PACS using the CAD-PACS toolkit 5. Discussion 6. Summary

SUMMARY
We have developed a CAD-PACS integration toolkit for integrating a standalone CAD workstation/server with a PACS using DICOM secondary capture (SC), DICOM Structured Report (SR) and the Integrating Healthcare Enterprise (IHE) Post-Processing Workflow Profile. The workflow and procedures of the CAD-PACS integration using this toolkit is illustrated with examples. These examples demonstrate that the toolkit is an effective solution for integrating standalone CAD applications with a clinical PACS.

Education Exhibit CODE: LL-IN5282

Image Sharing and Distribution of a Regional Health Information Organization (RHIO) through the Utilization of a DICOM, IHE, HL7 Compliant Data Grid Using XDS

***Sander Chao, MS**, Anh Le, MS, Kevin Ma, BS*

PURPOSE/AIM
To design and develop a Data Grid Architecture with XDS to support fault-tolerant storage and sharing of patient images and information between hospitals, pharmacies and other organizations forming a Regional Health Information Organization.

CONTENT ORGANIZATION
(1) Introduction to RHIO
(2) Workflow & Dataflow Analysis of a RHIO
(3) RHIO System Requirements
(4) Extending the Data Grid Architecture to Support RHIO s
(5) Future Work

SUMMARY
The flexible storage, access architecture, and security compliance of the Data Grid provides solutions well suited towards handling the diverse storage and distribution needs of a RHIO by integrating the storage of information with XDS into a single system for access by all. We present the workflow analysis of one example RHIO and designed a Data Grid Architecture that can provide a secure and fault-tolerant solution for storing and distributing patient images and information.

Education Exhibit CODE: LL-IN6848

CAD of the Radius for Bone Age Assessment of Older Children

***Sinchai Tsao, MS**, Arkadiusz Gertych, PhD, Aifeng Zhang, PhD, Brent Liu, PhD, Han K. Huang, ScD*

PURPOSE/AIM
Current bone age assessment techniques are inadequate in assessing bone age of older children (15-18 yrs). We will demonstrate how a CAD technique using radius growth plate degree of fusion features is able to assess the bone age of older children in order to provide decision support for Pediatric Radiologists.

CONTENT ORGANIZATION
1. *Brief overview of the Bone Age Assessment MethodologyCompare and Contrast Clinical Methodology and Computational / CAD Methodology*
2. *Current Challenges in Assessing Bone Age*
3. *CAD Methodology of the Radius bone to address Current Challenges.*
4. *System Performance Results and Comparison with Phalangeal-based Bone Age Assessment Method.*
5. *Discussion and Conclusion*

SUMMARY
1. *The major teaching points are:*
2. *Illustrate Current Challenges in Bone Age Assessment of older children and how radius feature addresses these issues.*
3. *Show the clinical and medical knowledge analyzed to develop additional decision support.*
4. *Outline the integration of CAD of the Radius and what it means to Pediatric Radiology.*
5. *Illustrate how the integration of new Radius features affects the overall performance of our Bone Age Assessment CAD system for older children.*

Education Exhibit CODE: LL-IN6883

Assuring Image Security within a Data Grid for Image-based Clinical Trials Using Lossless Digital Signature Embedding and a HIPAA-compliant Auditing System

***Jasper Lee BS**, Zheng Zhou, PhD, Brent Liu, PhD, Matthew Brown, PhD, Bing Guo, MD, Jorge Documet, MS*

PURPOSE/AIM
To develop a secure solution for medical image access and transfer within the Data Grid for imaging-based clinical trials without interruptions to the workflow using a lossless DICOM image encryption methodology and HIPAA-compliant auditing system.

CONTENT ORGANIZATION
A. *Introduction to imaging-based clinical trials and current Data Grid architecture design.*
B. *Discuss image integrity and auditing needs that are critical for further implementation of the Data Grid in imaging-based clinical trials.*
C. *Present LDSE and H-CAS as novel image-integrity methodology and activity logging solution for storage and distribution of medical images within the Data Grid.*
D. *System Design & Implementation*
E. *Preliminary Results*
F. *Discussion*

SUMMARY
Lossless Digital Signature Embedding (LDSE) and HIPAA-Compliant Auditing System (H-CAS) are significant Data Grid management features that provide image security and auditing for imaging-based clinical trials. This exhibit reviews: A.Security concerns in a Data Grid for imaging-based clinical trials. B.DICOM image-integrity authentication and auditing system for all image access and transfer activity in the Data Grid. C.Seamless integration into existing Data Grid workflow for clinical trials.

<--Scientific Posters-->

Scientific Poster CODE: LL-PD2098-R09
SESSION: Pediatric (Musculoskeletal)

Fuzzy System Design for Bone Age Assessment of Children in Mulitple Regions of the Hand

***Aifeng Zhang, PhD**, Arkadiusz Gertych, PhD, Sinchai Tsao, MS, Brent Liu, PhD, Han K. Huang, ScD*

DATE:	***Thursday, November 29 2007***
START TIME:	***12:15 PM***
END TIME:	***01:15 PM***
LOCATION:	***Lakeside Learning Center***

PURPOSE
A computer-aided-diagnosis (CAD) method for bone age assessment (BAA) has been developed based on phalangeal regions of interest (ROI). In order to improve the accuracy for young children, carpal ROI was incorporated. In consideration of the missing feature problem and imprecise nature of relationship between bone growths and chronological age, a rule-based fuzzy inference system was developed to assess the bone age. Two goals of this paper are to develop a fuzzy system for carpal ROI, and a modular and extensible model integrating carpal ROI with the existing phalangeal ROIs analysis. Fuzzy system design, training and testing have been accomplished and BAA results obtained from the fuzzy system have been evaluated with our data collection of 1,400 normals.

METHOD AND MATERIALS
A digital hand atlas has been developed with 1,400 normal children hand images of Caucasian, African American, Hispanic, and Asian. Carpal bone analysis of each hand image yields six morphological features, which were taken as the input into the carpal fuzzy sub-system. During the training process, the output was set as the subject s chronological age since the normality of children was ensured. An automatic training algorithm was used to generate Gaussian membership functions for inputs and output and then rules for each sub-system, one for each category by race and gender. To assess the bone age of a given hand image, two steps are involved: A fuzzy bone age BA1 was obtained from the existing phalangeal sub-system and BA2 from carpal sub-system; BA1 and BA2 were then integrated into the final fuzzy BA which yields a precise bone age through the defuzzification procedure using center of gravity method.

RESULTS
The integrated fuzzy system takes the features from both regions as input and predicts the bone age. This fuzzy system can process a dynamic number of inputs in case one or several ROIs detection fails.

CONCLUSION
This presentation demonstrates the use of a modular and extensible fuzzy inference system to integrate both phalangeal ROIs and carpal ROI for BAA.

CLINICAL RELEVANCE/APPLICATION
This presentation demonstrates the applicability of the fuzzy system for BAA based on morphological bony features of multiple hand ROIs.

<--Scientific Papers-->

Scientific Paper CODE: VP32-08
SESSION: Pediatric Series: Trauma/Emergency Imaging II

Cross-Racial Discrepancies of Growth Patterns in Bone Age Assessment

***Aifeng Zhang, PhD**, Han K. Huang, ScD, James Sayre, PhD, Linda Vachon, MD*

DATE:	***Tuesday, November 27 2007***
START TIME:	***05:20 PM***
END TIME:	***05:30 PM***
LOCATION:	***N229***

PURPOSE
The most commonly used standard in Bone Age assessment (BAA) of children today, the Greulich and Pyle Atlas (G&P), was developed in the 1950s with subjects recruited from a narrow region of Caucasian populations. Due to progressive changes in ethnic origins and environment during the past 50-60 years, G&P atlas may not be fully applicable to today s children. This presentation addresses two issues: "Is G&P atlas still applicable to today s children?", and "Do different ethnicities have different BONE growth patterns?".

METHOD AND MATERIALS
A digital hand atlas was developed with normal children hand images of four populations, including Caucasian, African American, Hispanic, and Asian with Ages 0–18 years. Two pediatric radiologists performed independent readings on each case based on the G&P atlas. This presentation is based on first cycle data with 1,100 cases. Using chronological Age as the gold standard, paired-sample t-tests were performed on two readings to study the performance of G&P atlas in eight categories by race and gender. To study the differences in great details, the entire Age range was divided into four Age subsets, for male (1-7, 8-10, 11-15, 16-18 years) and female (1-5, 6-9, 10-13, 14-18 years) respectively. Cross-racial comparisons of the difference between the averAge of two readings and chronological Age were then conducted by analysis of variance (ANOVA).

RESULTS
The t-tests observed that using the G&P atlas, radiologists are able to assess BONE Age accurately for African American and Caucasian male population. However, significant discrepancies of about 4 months were observed in Asian and Hispanic ($p<.05$). ANOVA results showed that compared with African American and Caucasian, over-readings of one year in male and 8 months in female for Asian and Hispanic occurred, mostly in 10-13 of female and 11-15 of male.

CONCLUSION
Genetic differences with influences from nutritional and environmental changes may cause variations in growth patterns, thereby influencing BONE Age assessment process.

CLINICAL RELEVANCE/APPLICATION
The discovered cross-racial discrepancies is a possible consideration in pediatric radiology training when applying G&P atlas to today s children.

<--International Collaborators-->

InfoRAD CODE: LL-IN5262-B

Implementation of Collaborative Healthcare in Grid-based Cross-Enterprise Images Sharing with IHE XDS-I Integration Profile

***Jianguo Zhang, PhD**, Jianyong Sun, PhD, Yuanyuan Yang, MS, Jin Jin, Tonghui Ling, MS, Kai Zhang, BS*

PURPOSE/AIM
A number of hospitals in Shanghai, China are piloting an EHR solution. In this presentation, we will demonstrate the implementation of collaborative healthcare between multiple hospitals in a grid-based image sharing system fully aligned with the IHE XDS-I integration profile.

CONTENT ORGANIZATION
The XDS-I compliant EHR solution for image/report sharing are developed based on grid concept with Service-Oriented Architecture, and consists of Master Node, Agent Node and User Node, which are synonymous with the XDS-I Registry, Repository, Source and Consumer actors. The collaborative operations include instant message, interactive remote control of image viewing shared between radiologists and physicians, and intelligent content delivery based on event-driven work flows among the hospitals.

SUMMARY
A solution has been installed in four hospitals in Shanghai and tested for collaborative operation on shared image data. The results are extremely positive and demonstrate that the collaborative features implemented in a grid-based sharing system can scale effectively to serve for regional collaborative healthcare.

Education Exhibit CODE: LL-IN6881

A Real Case PACS Enterprise in Italy: Feasibility of a Data Grid Solution for Backup and Disaster Recovery with a Web-based Centralized Management System

Elisa Talini, MS, Jasper Lee, BS, Zheng Zhou, PhD, Davide Caramella, PhD, Han K. Huang, ScD

PURPOSE/AIM
Due to the large amounts of images and the heterogeneous architecture of PACS systems in an Enterprise PACS environment, a Data Grid is presented as the solution for Backup and Disaster Recovery as well as data integration and sharing between heterogeneous PAC systems. A unique web-based access interface for Data Grid administrators is presented.

CONTENT ORGANIZATION
1. A real case scenario: PACS Enterprise in Tuscany, Italy. 2. Data Grid concepts and its extension to DICOM services developed to apply within a heterogeneous PACS environment 3. Data Grid as a possible solution for Backup and Disaster Recovery in Tuscany sub regions. 4. Data Grid as the proposed solution for integration between heterogeneous PACS systems in a regional Enterprise PACS 5. Web-based Data Grid Users and Management System for Enterprise PACS: functionalities and features 6. Feasibility Study and Results 7. Summary

SUMMARY
The Data Grid allows incorporation of PACS systems in an enterprise environment providing a powerful and scalable solution. Scalability is a key concept for developing an Enterprise PACS because of the enormous amount of acquired data and images involved. The web-based management system allows easy-to-use data management and permits access to the Data Grid components easily without lengthy login processes at each Grid component.

Education Exhibit CODE: LL-IN6877

A CAD Integrated Content-based Retrieval System for Multilocational Image Distribution Environment

Douglas K.S. Ng, Fuk-Hay Tang PhD, Maria Law, DSc

PURPOSE/AIM
1.By studying this exhibit, the learner will understand the working principle of CAD integrated image content retrieval method for PACS. 2. The learner will be aware of the feasibility of using distributed computing method for detection of particular image pattern.

CONTENT ORGANIZATION
A. Why image content retrieval is necessary B. How mutli-locational web-based server enhance data mining for combining different PACS C. The Structure of multi-location web-based image distribution system D. Working examples of such system E. Concluding remarkings

SUMMARY
Textual information is not sufficient for finding images with similar pattern in a PACS. An intelligent computer-aided detection system is developed to retrieve images based on image content. This system consists of a coordination server (CS) which is developed to integrate PACS servers distributed at different locations using web-based technology to facilitate data inter-change while the autonomy of individual PACS servers is preserved.

PREPRINTS FROM SPIE 2008

Web-based Computer-aided-diagnosis (CAD) System for Bone Age Assessment (BAA) of Children

Aifeng Zhang[1], Joshua Uyeda[1], Sinchai Tsao[1], Kevin Ma[1], Linda A. Vachon[2], Brent J. Liu[1], H.K. Huang[1]

[1]Image Processing & Informatics Lab, Department of Radiology, ISI/USC, Marina Del Rey, CA 90292
[2]Los Angeles County Women's and Children's Hospital Los Angeles, CA 90033

ABSTRACT

Bone age assessment (BAA) of children is a clinical procedure frequently performed in pediatric radiology to evaluate the stage of skeletal maturation based on a left hand and wrist radiograph. The most commonly used standard: Greulich and Pyle (G&P) Hand Atlas was developed 50 years ago and exclusively based on Caucasian population. Moreover, inter- & intra-observer discrepancies using this method create a need of an objective and automatic BAA method. A digital hand atlas (DHA) has been collected with 1,400 hand images of normal children from Asian, African American, Caucasian and Hispanic descends. Based on DHA, a fully automatic, objective computer-aided-diagnosis (CAD) method was developed and it was adapted to specific population. To bring DHA and CAD method to the clinical environment as a useful tool in assisting radiologist to achieve higher accuracy in BAA, a web-based system with direct connection to a clinical site is designed as a novel clinical implementation approach for online and real time BAA. The core of the system, a CAD server receives the image from clinical site, processes it by the CAD method and finally, generates report. A web service publishes the results and radiologists at the clinical site can review it online within minutes. This prototype can be easily extended to multiple clinical sites and will provide the foundation for broader use of the CAD system for BAA.

1. INTRODUCTION

Bone age assessment (BAA) of children is a clinical procedure frequently performed in pediatric radiology to evaluate the stage of skeletal maturation based on a left hand and wrist radiograph. The most commonly used standard: Greulich and Pyle (G&P) Hand Atlas was developed 50 years ago and exclusively based on Caucasian population. [1] Moreover, inter- & intra-observer discrepancies using this method create a need of an objective and automatic BAA method.

A digital hand atlas (DHA) has been collected with 1,400 hand images of normal children from Asian, African American, Caucasian and Hispanic descends. Based on DHA, a fully automatic, objective computer-aided-diagnosis (CAD) method was developed based on phalangeal and carpal bone features. Adapted to specific populations, the CAD method achieved high BAA accuracy. [2-7]

To bring DHA and CAD method to the clinical environment as a useful tool in assisting radiologist to achieve higher accuracy in BAA, a client-server system with direct connection to a clinical site is designed as a novel clinical implementation approach for online and real time BAA.

2. METHODS

2.1 Standard Clinical Workflow

The standard clinical workflow of BAA at clinical site is as following: Hand X-ray from the CR modality is sent to gateway and then to PACS server. Radiologist reviews images on PACS WS and assesses the bone age (Figure 1). [8]

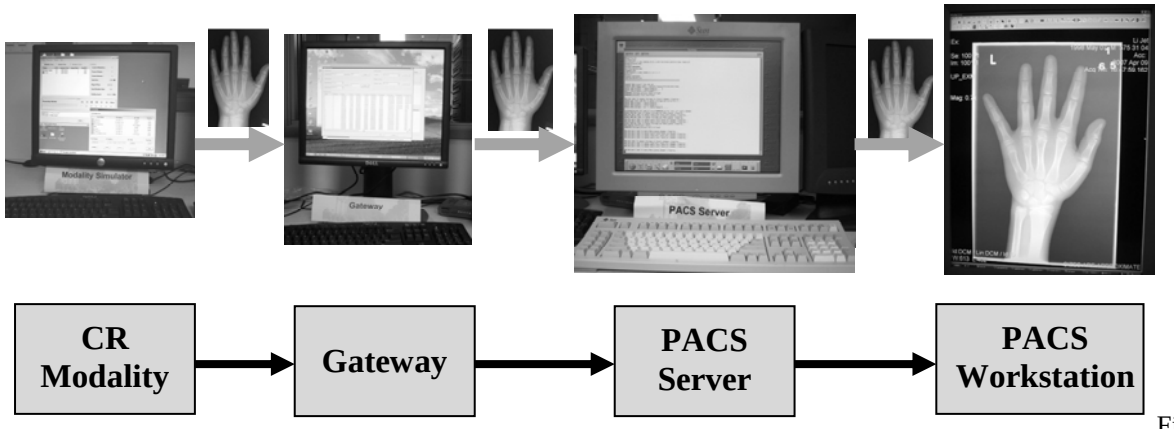

Figure 1. Normal Clinical Workflow

2.2 Web-based BAA CAD Clinical Implementation

To minimize the disruption of the PACS clinical workflow, a client-server system was developed as a novel clinical implementation approach. Utilizing web technology and DICOM (Digital Imaging and Communications in Medicine) standard, CAD method was integrated with PACS for online BAA. [9,10]

In the CAD system clinical implementation workflow (Figure 2), a second copy of the hand image from CR modality is sent to the CAD server with secure internet connection. The CAD server receives the image and processes it. The CAD report is then generated automatically. The radiologist at the clinical site can log into the website and review CAD results from a PACS WS. The web-based CAD report display application allows multiple users with specific patient list. For each radiologist, clinical decisions (without and with the aid of CAD) including readings and growth abnormality are captured and stored in the clinical database.

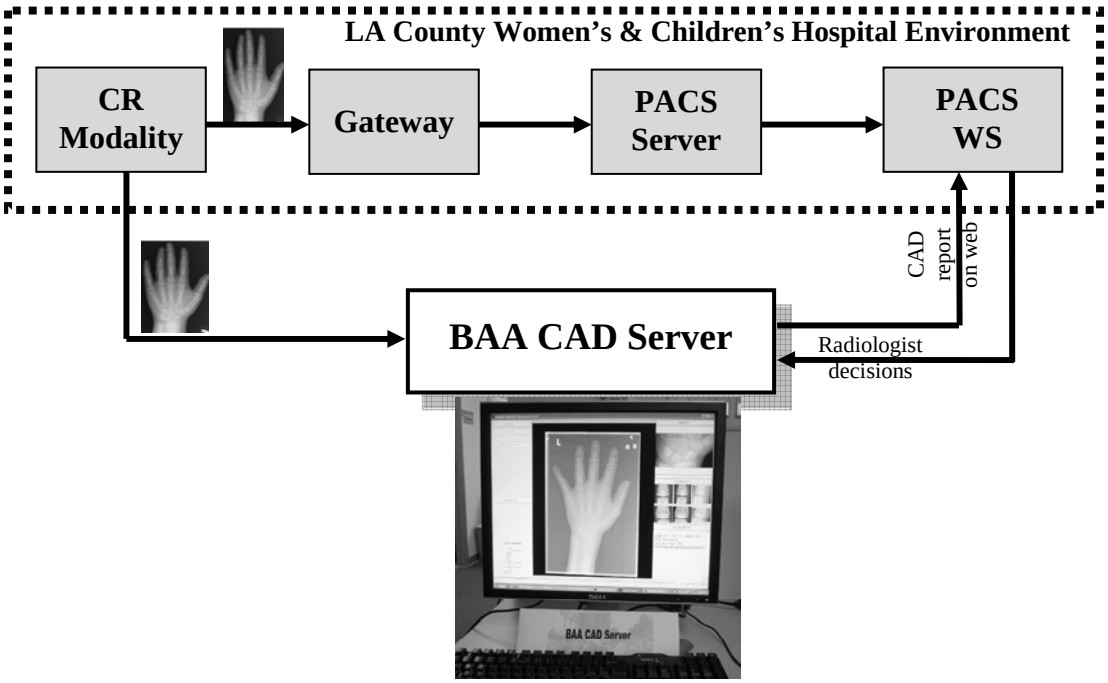

Figure 2. Clinical Implementation Workflow

2.3 BAA CAD Server Design

The core of the system, CAD server includes the following major components (Figure 3): DICOM receiver, CAD engine, web service and clinical database. The DICOM receiver utilizes the DCMTK toolkit to listen and receive the hand image from CR modality over the Internet using DICOM Storage protocol [11]. The CAD engine is then triggered to segment the hand images, extract bony features for automatic bone age assessment by fuzzy logic. The CAD report is then generated automatically at CAD server. The web service automatically updates the clinical database and publishes the CAD report for radiologist at the clinical site to review online.

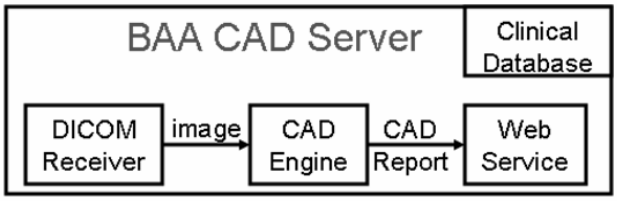

Figure 3. Major components in CAD server

The purpose of the web GUI is for the radiologists to be able to select and view the DICOM hand images from the patient list. The GUI provides the race and gender of the patient and it allows the radiologists to enter their initial reading into the database after reviewing the original patient hand image. After the initial reading has been entered, the CAD BAA result is shown with: 1) CAD assessed bone age; 2) patient displayed in the normal development graph for the corresponding racial group and 3) the best match image found from the DHA. The radiologist is then allowed to input a second reading for the hand image after reviewing the CAD results.

2.3 Laboratory Simulation at IPILAB

An existing PACS simulator developed at the laboratory simulates the PACS clinical workflow. This testbed system has been utilized to test the CAD server and PACS integration. Figure 4 shows the CAD server at left, and the four major components of the PACS simulator on the right: modality simulator, gateway, PACS server and PACS workstation (WS).

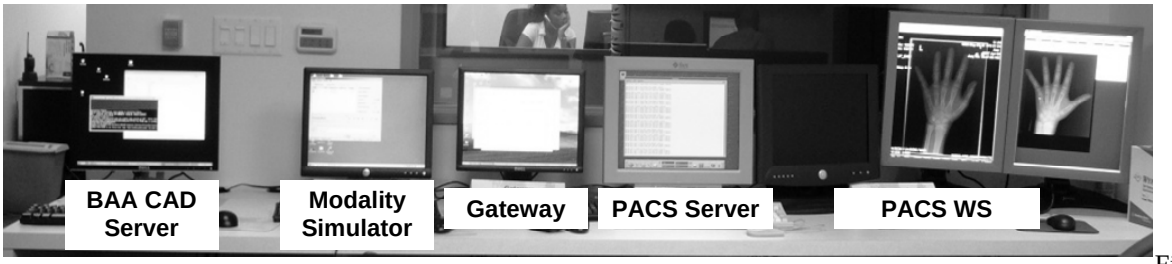

Figure 4. BAA CAD server and PACS simulator at IPILAB

3. RESULTS

The CAD server and PACS integration has been successfully implemented on an existing PACS simulator developed at our lab. A number of clinical images were tested for the entire workflow. A fully automatic workflow was achieved without manual interaction. This system is currently being implemented in multiple clinical sites. The hand image is sent from the modality to the CAD system and the CAD results are displayed on the PACS WS for radiologists to review. Figure 5 shows an example of web GUI.

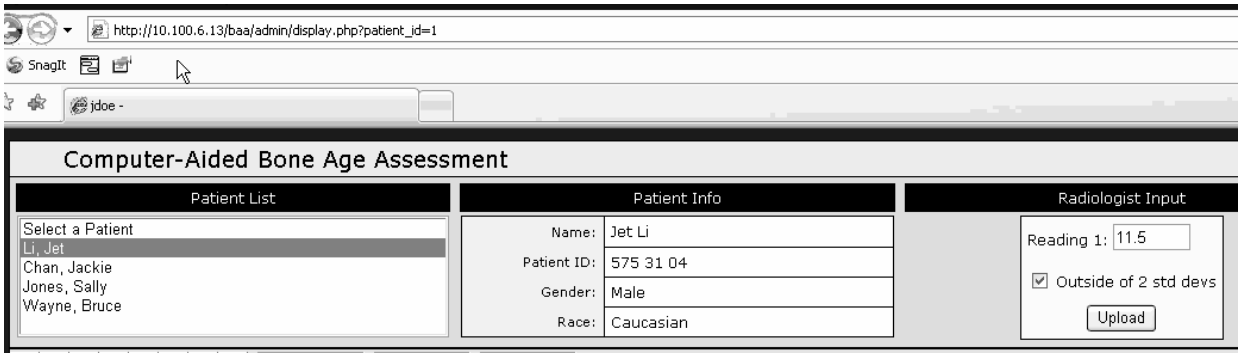

(a)

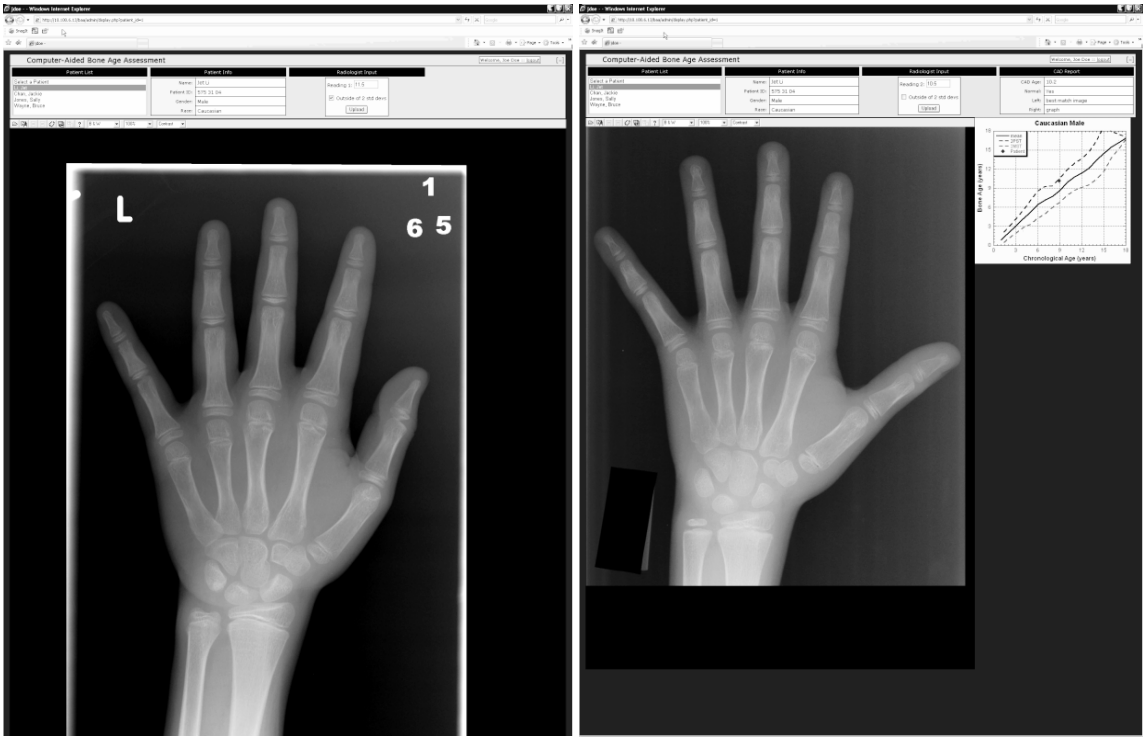

(b) (c)

Figure 5. Web GUI (a) Patient list, patient information table and radiologist's initial reading; (b) First page with patient's original hand image; (c) Second page with CAD results; Radiologist can input the second reading.

4. DISCUSSIONS AND CONCLUSIONS

This paper presents a novel clinical implementation approach for a CAD system using web technology for online and real time BAA. It brings DHA and CAD methods to the clinical environment as a useful tool in assisting radiologist to achieve higher accuracy in BAA. This also allows data collection in the atlas to be continuously enriched with normal cases selected from the clinical environment. This web-based prototype can be easily extended to multiple clinical sites and will provide the foundation for broader use of the CAD system for BAA. By equivalence test on the means of two assessments (without and with aid of CAD), the statistical analysis will allow us to validate that the DHA and CAD can assist radiologists and residents to achieve higher accuracy of BAA.

ACKNOWLEDGMENT

This work has been supported by NIH R01 EB 00298.

REFERENCES

1. Grelich W, Pyle S, *Radiographic Atlas of Skeletal Development of Hand Wrist*, Stanford, CA: Stanford University Press, 1959.
2. Pietka E, Pospiech-Kurkowska S, Gertych A, Cao F, Huang HK, "Computer-Assisted Bone Age Assessment: Image Analysis And Fuzzy Classification", Radiology, 225(P), 751, 2002.
3. Pietka E, Gertych A, Pospiech S, Cao F, Huang HK, Gilsanz V, "Computer Assisted Bone Age Assessment: Image Processing and Epiphyseal/Metaphyseal ROI Extraction," IEEE Trans. Medical Imaging, 20, 715-729, 2001.
4. Pietka E, Pospiech S, Gertych A, Cao F, Huang HK, Gilsanz V, "Computer Automated Approach to the extraction of epiphyseal regions in hand radiographs," Journal of Digital Imaging, 14, 165-172, 2002.
5. Pospiech-Kurkowska S, Pietka E, Cao F, Huang HK, "Fuzzy System for the Estimation of the Bone Age from Wavelet Features", Proc. BIOSIGNAL 2002
6. Gertych A, Zhang A, Sayre, J, Pospiech-Kurkowska, S., Huang, H.K, "Bone Age Assessment of Children using a Digital Hand Atlas," Computerized Medical Imaging and Graphics, May, 2007.
7. Zhang A, Gertych A, Liu BJ, "Automatic Bone Age Assessment for Young Children from Newborn to 7-Year-Old Using Carpal Bones", Computerized Medical Imaging and Graphics, May 2007
8. Huang HK, PACS and Imaging Informatics: Basic Principles and Applications, Wiley & Sons, NJ, p. 44, 504-507, 2004.
9. Zhang A, Zhou Z, Gertych A, Liu BJ, Zheng X, Huang HK, "Integration of Bone Age Assessment CAD Results with the PACS Diagnostic Workflow Utilizing DICOM Structure Report", Scientific Poster, RSNA 2006
10. Zhou Z, Liu BJ, Le AH, " CAD-PACS Integration Tool Kit Based on DICOM Secondary Capture, Structured Report and IHE Workflow Profiles", Computerized Medical Imaging and Graphics, May 2007
11. dicom.offis.de - DICOM Software made by OFFIS - DCMTK – DICOM, http://dicom.offis.de/dcmtk.php.en

Bone age assessment in Hispanic children: Digital hand atlas compared the Greulich and Pyle (G&P) atlas

James Reza Fernandez[a], Aifeng Zhang[a], Linda Vachon[b], Sinchai Tsao[a]

a. Image processing and Informatics Laboratory, Dept. of Radiology, Keck School of Medicine, USC, Marina del rey, 90292

b. Women's and Children's Hospital, Dept. of Radiology, Keck School of Medicine, USC

ABSTRACT

Bone age assessment is most commonly performed with the use of the Greulich and Pyle (G&P) book atlas, which was developed in the 1950s. The population of the United States is not as homogenous as the Caucasian population in the Greulich and Pyle in the 1950s, especially in the Los Angeles, California area. A digital hand atlas (DHA) based on 1,390 hand images of children of different racial backgrounds (Caucasian, African American, Hispanic, and Asian) aged 0-18 years was collected from Children's Hospital Los Angeles. Statistical analysis discovered significant discrepancies exist between Hispanic and the G&P atlas standard. To validate the usage of DHA as a clinical standard, diagnostic radiologists performed reads on Hispanic pediatric hand and wrist computed radiography images using either the G&P pediatric radiographic atlas or the Children's Hospital Los Angeles Digital Hand Atlas (DHA) as reference. The order in which the atlas is used (G&P followed by DHA or vice versa) for each image was prepared before actual reading begins. Statistical analysis of the results was then performed to determine if a discrepancy exists between the two readings.

Keyword: Bone Age Assessment, Digital Hand Atlas

1. INTRODUCTION

Bone age assessment (BAA) has long been a screening method for skeletal growth in children. The left hand and wrist is X-rayed and it is compared to the bones of a standard atlas, most often the Greulich and Pyle (G&P) atlas. This involves visual comparison of the patient's hand image with images in the atlas, and a subjective closest match selected by the radiologist yields the patient's bone age (Figure 1). The G&P atlas was assembled in the 1950s based on Caucasian children born in the United States with mainly North European ancestry, ranging in age from newborn to eighteen years. It has not been updated since its initial publication. The current United States population is ethnically diverse and the environment in which children are living has changed. Therefore, a new digital hand atlas been developed to address these issues of diversity.

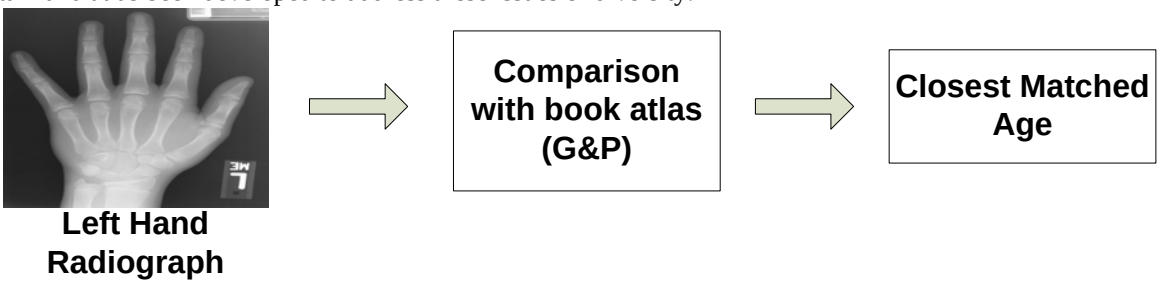

Figure 1. Clinical bone age assessment procedure

In present-day Los Angeles, CA, the majority of the population consists of persons of Hispanic or Latino origin[7] as shown in Figure 2. .

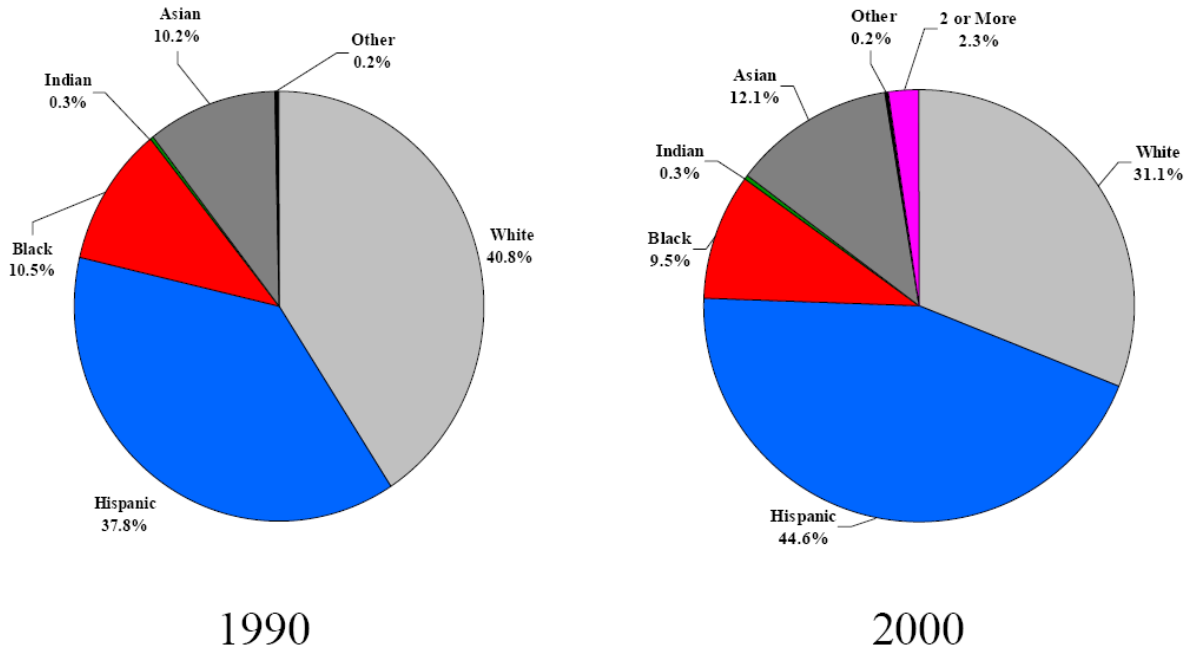

Figure 2. Ethnic composition of LA County according to the Census Bureau[8]

2. METHODS

2.1 Data Collection - Building of the Digital Hand Atlas

A digital hand atlas was developed with 1,390 left hand computed radiography films of normal Caucasian (CA), African American (AA), Hispanic (HI), and Asian (AS); male (M) and female (F), ranging from 0-18 years. The number of cases spread evenly among the races. Each hand image and the subject's demographic data, along with two or four radiologists' readings were populated into a mysql database. Figure 3 is a sample hand image.

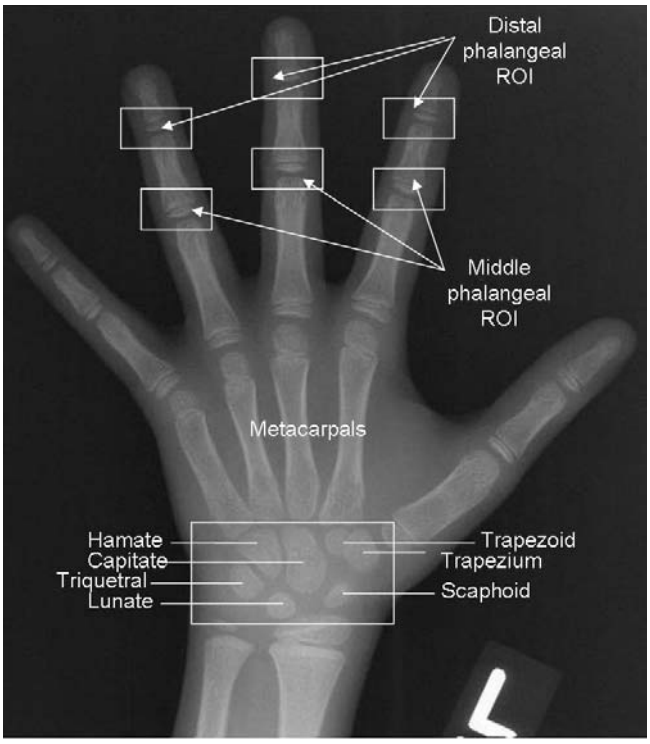

Figure 3 - Sample Hand Image from the CHLA data collection process.

2.2 BAA of Hispanic Children

To validate the usage of DHA as clinical standard in Hispanic Children, radiologists and residents evaluated the clinical hand image twice, each time using the DHA and the G&P atlas. The order of atlases to be used was randomly assigned to each image. The following is the step-wise approach used (Figure 4):
Radiologists and residents evaluated the clinical hand images from the Hispanic Male and Female groups twice, each time using the DHA and the G&P atlas, and the order of atlases to be used was randomly assigned to each image to eliminate bias. The following is the step-wise approach used (Figure 3):

1) A randomized order set of which atlas to use first, the G&P or the DHA, is prepared

2) A Left hand and wrist X-ray is automatically sent to the PACS workstation for viewing by a radiologist

3) The radiologist then reads the X-ray using either the G&P atlas followed by the DHA, or the DHA followed by the G&P, depending on the order in step 1;

4) Statistical analysis will then be performed on the results obtained from those readings to determine if there is any statistical significance when using the digital hand atlas versus the G&P atlas.

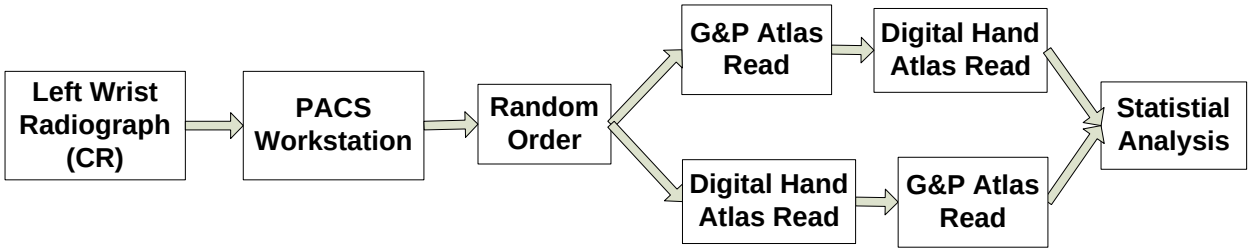

Figure 4. Clinical workflow of bone age assessment for Hispanic children

3. RESULTS

From data in the DHA, it was found that radiologists over-estimate the age of Hispanic children by an average 0.8 years as compared to their African American and Caucasian peers age 10-14 years. Figures 5 and 6 show the plots of readings between Hispanic female and African American female populations from a study by Zhang et al[2]. The readings for Hispanic children as compared to African American and Caucasian children are comparable, except in the 10-14 years age group.

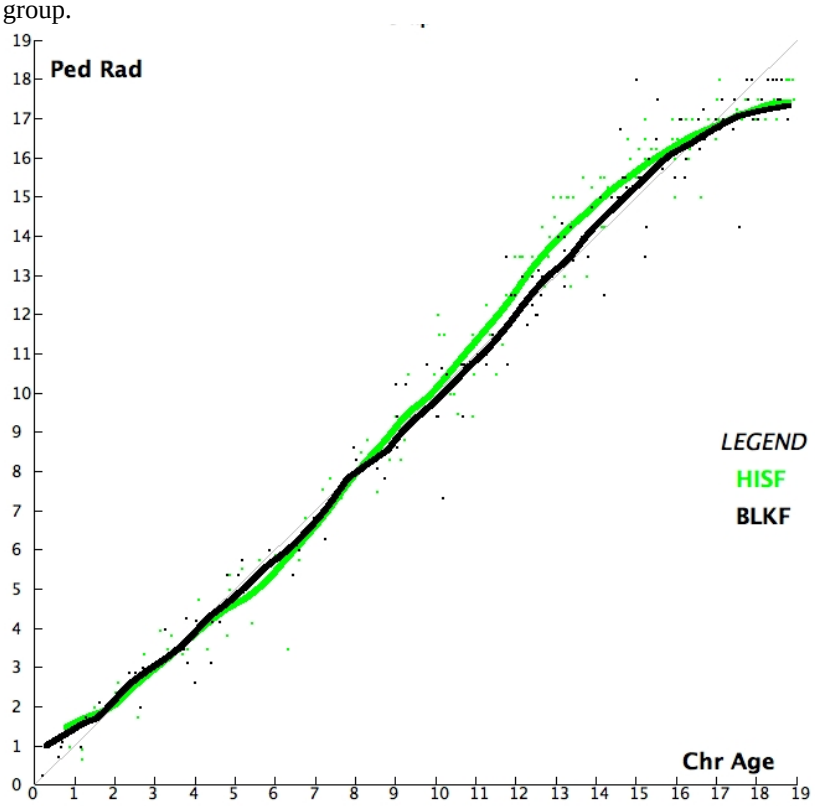

Figure 5. Hispanic female and African American female comparison

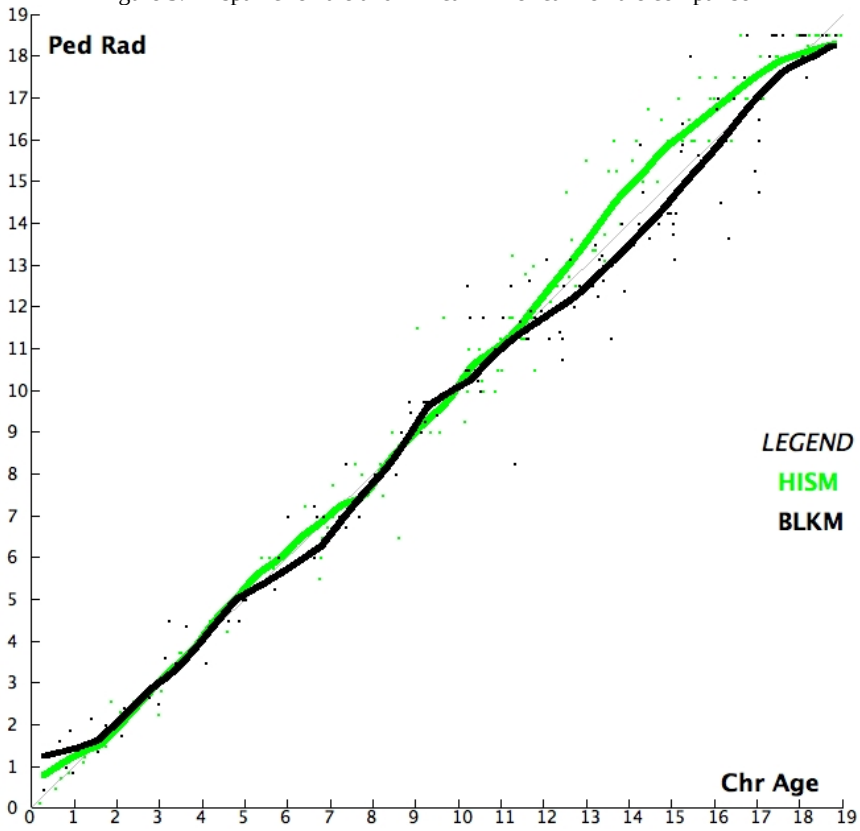

Figure 6. Hispanic male and African American male comparison

Paired-sample t-test is performed on the two readings of Hispanic Children based on the G&P atlas and DHA. Significant discrepancies were discovered, especially for ages 10-14 years.

4. DISCUSSIONS AND CONCLUSIONS

The results of this illustrated that the accuracy of the Greulich and Pyle atlas can be improved by taking ethnic population and gender into account, especially in Hispanic children age 10-14 years. Other studies[9,10] have shown that using the standards of the Greulich and Pyle to determine bone age is not entirely accurate given today's diverse population. Based on these findings, it is likely that further analysis of the bone age analysis of Hispanic children age 10-14 years using the DHA and the G&P atlas will further validate data collected in that study. This study also proposes that a computer aided detection scheme based on DHA can be of use in.BAA of Hispanic children.

ACKNOWLEDGMENT

This work has been supported by NIH R01 EB 00298.

REFERENCES

[1] W. Grelich, S. Pyle, Radiographic Atlas of Skeletal Development of Hand Wrist, Stanford, CA: Stanford University Press, 1959.

[2] A Zhang et al. "Is Greulich and Pyle Atlas still a Good Reference for Bone Age Assessment?", SPIE Medical Imaging, Feb 2007

[3] A. Gertych, A. Zhang, J. Sayre, S. Pospiech-Kurkowska, H.K Huang, "Bone Age Assessment of Children using a Digital Hand Atlas", J Comp Med Imag & Graphic, 31(4-5), May, 2007.

[4] Zhang, A. Gertych, B. J. Liu, "Automatic Bone Age Assessment for Young Children from Newborn to 7-Year-Old Using Carpal Bones", J Comp Med Imag & Graphic, 31(4-5), May, 2007.

[5] E. Pietka, S. Pospiech-Kurkowska, A. Gertych, and F. Cao, "Integration of computer assisted bone age assessment with clinical PACS," Comput Med Imaging Graph, vol. 27, pp. 217-28, 2003.

[6] E. Pietka, A. Gertych, S. Pospiech, F. Cao, H. K. Huang, and V. Gilsanz, "Computer-assisted bone age assessment: image preprocessing and epiphyseal/metaphyseal ROI extraction," IEEE Trans Med Imaging, vol. 20, pp. 715-29, 2001.

[7] United States Census Bureau. http://quickfacts.census.gov/qfd/states/06/06037.html

[8] Southern California Association of Governments Census Data. http://www.scag.ca.gov/census/

[9] RT Loder, DT Estle, K Morrison, D Eggleston, DN Fish, ML Greenfield, KE Guire. "Applicability of the Greulich and Pyle skeletal age standards to black and white children of today." Am J Dis Child, 147(12), pp. 1329-33, Dec 1993.

[10] FK Ontell, M Ivanovic, DS Ablin, TW Barlow. "Bone age in children of diverse ethnicity." AJR Am J Roentgenol. 169(2), pp.1395-8, Dec 1996.

Integrating DICOM Structure Reporting (SR) into the Medical Imaging Informatics Data Grid

Jasper Lee, Anh Le, Brent Liu
Image Processing & Informatics Laboratory, USC 90292, CA

ABSTRACT

The Medical Imaging Informatics (MI^2) Data Grid developed at the USC Image Processing and Informatics Laboratory enables medical images to be shared securely between multiple imaging centers. Current applications include an imaging-based clinical trial setting where multiple field sites perform image acquisition and a centralized radiology core performs image analysis, often using computer-aided diagnosis tools (CAD) that generate a DICOM-SR to report their findings and measurements. As more and more CAD tools are being developed in the radiology field, the generated DICOM Structure Reports (SR) holding key radiological findings and measurements that are not part of the DICOM image need to be integrated into the existing Medical Imaging Informatics Data Grid with the corresponding imaging studies. We will discuss the significance and method involved in adapting DICOM-SR into the Medical Imaging Informatics Data Grid. The result is a MI^2 Data Grid repository from which users can send and receive DICOM-SR objects based on the imaging-based clinical trial application. The services required to extract and categorize information from the structured reports will be discussed, and the workflow to store and retrieve a DICOM-SR file into the existing MI^2 Data Grid will be shown.

Keywords: DICOM-SR, Structured Reporting, Data Grid, CAD, Clinical Trials

1. INTRODUCTION

1.1. Medical Imaging Informatics Data Grid

With the rapid rate at which medical imaging data is being accrued, the need for storage and securing medical data is becoming increasingly apparent for healthcare sites as well as medical research groups. Over the past three years, a medical imaging data grid for DICOM radiological images has been developed at the Image Processing and Informatics Lab at the University of Southern California. An application of the MI^2 Data Grid has been a thoracic imaging research group at UCLA where multiple imaging field sites work with the radiology core to conduct clinical trials of the lung. The MI^2 Data Grid has the ability to store multiple copies of DICOM studies in a virtualized and distributed storage system that has DICOM store, query and retrieve capabilities. It is an integration of DICOM standards, fault-tolerant services, grid services, and Integrated Healthcare Enterprise concepts. Built on the open source Globus Toolkit, the IPILab has been able to utilize robust security and file management services.

1.2. Need for DICOM Structured Reporting in Research

At the IPILab where the Medical Imaging Informatics Data Grid is developed, the projects involving computer aided detection (CAD) typically utilize CAD servers perform image processing methods on inputted DICOM imaging studies. The CAD applications produce results in the form of quantitative reports with references to key note images documenting the CAD findings. These reports follow the DICOM Structured Report (SR) standard, which has been adopted into the DICOM standard in 1999 as Supplement 23 [7]. Below in Figure 1 is the revised DICOM model with DICOM-SR added. Since the IPILab utilizes the Medical Imaging Informatics Data Grid to store DICOM imaging studies, research involving data mining and clinical evaluations of CAD applications can benefit from a distributive and DICOM-compliant medical imaging data grid that supports the SR results that hold CAD findings. The MI^2 Data Grid serves as a novel and robust virtualized storage system for CAD research if it can support both DICOM images as well as DICOM structured reporting.

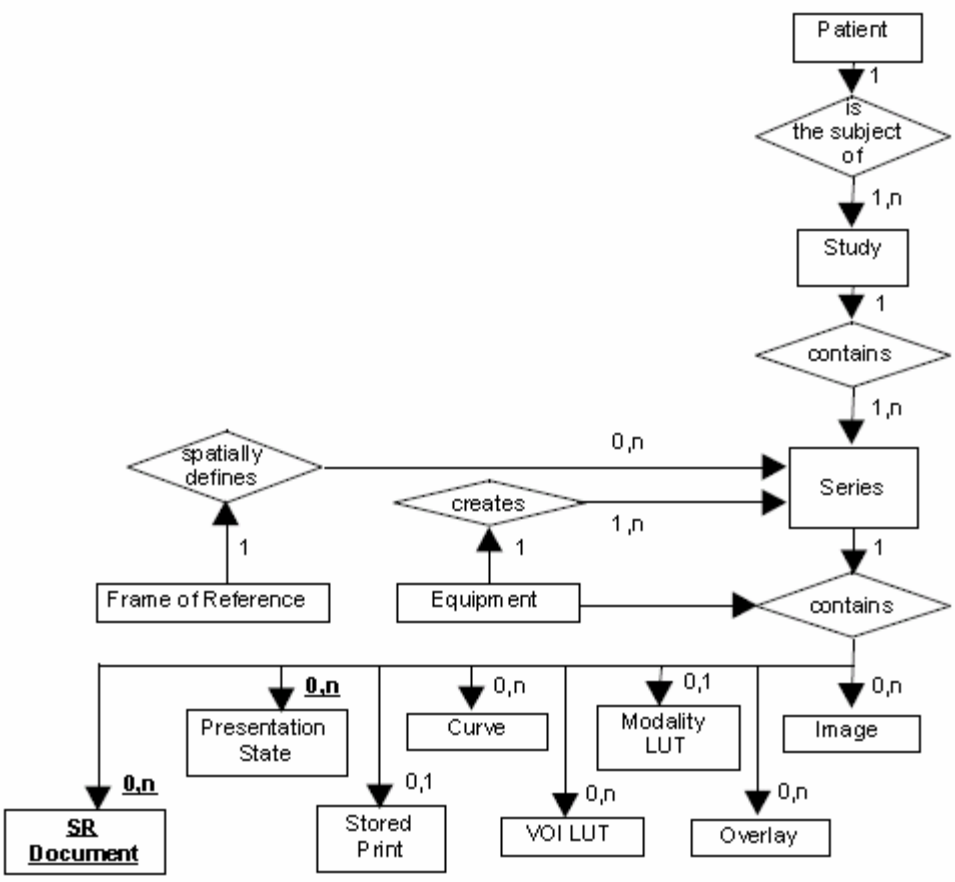

Fig.1. DICOM Model (abbreviated) with DICOM-SR[4]

1.3. Benefits of DICOM SR

The DICOM structured reporting (SR) standard has been underway over the past few years and its benefits are numerous [2]. Its overall purpose is to enhance the expressiveness, precision and clarity of clinical documentation. Clinical documentation has a broad range depending on the medical group, but the unifying characteristic is that its content includes all or some of text, coded values, numeric values, persons name, date and time, reference to DICOM images or waveforms, and spatial and temporal coordinates in reference images. The SR classes first introduced in Supplement 23 of DICOM fully support conventional free text reports and structured information with well-defined semantics. The SR allows users to link text and other data to particular images or waveforms and to store the coordinates of findings, which brings the connection of visual data and textual data. In other words, SR documents can refer to any number of images or waveforms and contain description of images and waveforms' specific features.

2. METHODOLOGY

In this discussion, we will use one of the first accepted DICOM chest CAD SR templates to demonstrate the integrated workflow of the DICOM-SR and the Medical Imaging Informatics Data Grid. A DICOM-SR can include a wide range of medical documentation, but our initial database design is based on a chest CAD SR tree structure. Seen in Figure 2 is a display sample of a chest CAD SR document. The design challenges involved to integrate DICOM-SR into the MI^2 Data Grid are a DICOM-SR receiver service at the grid-access-points, additional DICOM-SR databases, and modified DICOM query/retrieve services. The implementation has been simplified because it already supports the DICOM standard. However, the workflow is complicated by the format in which DICOM imaging studies are stored.

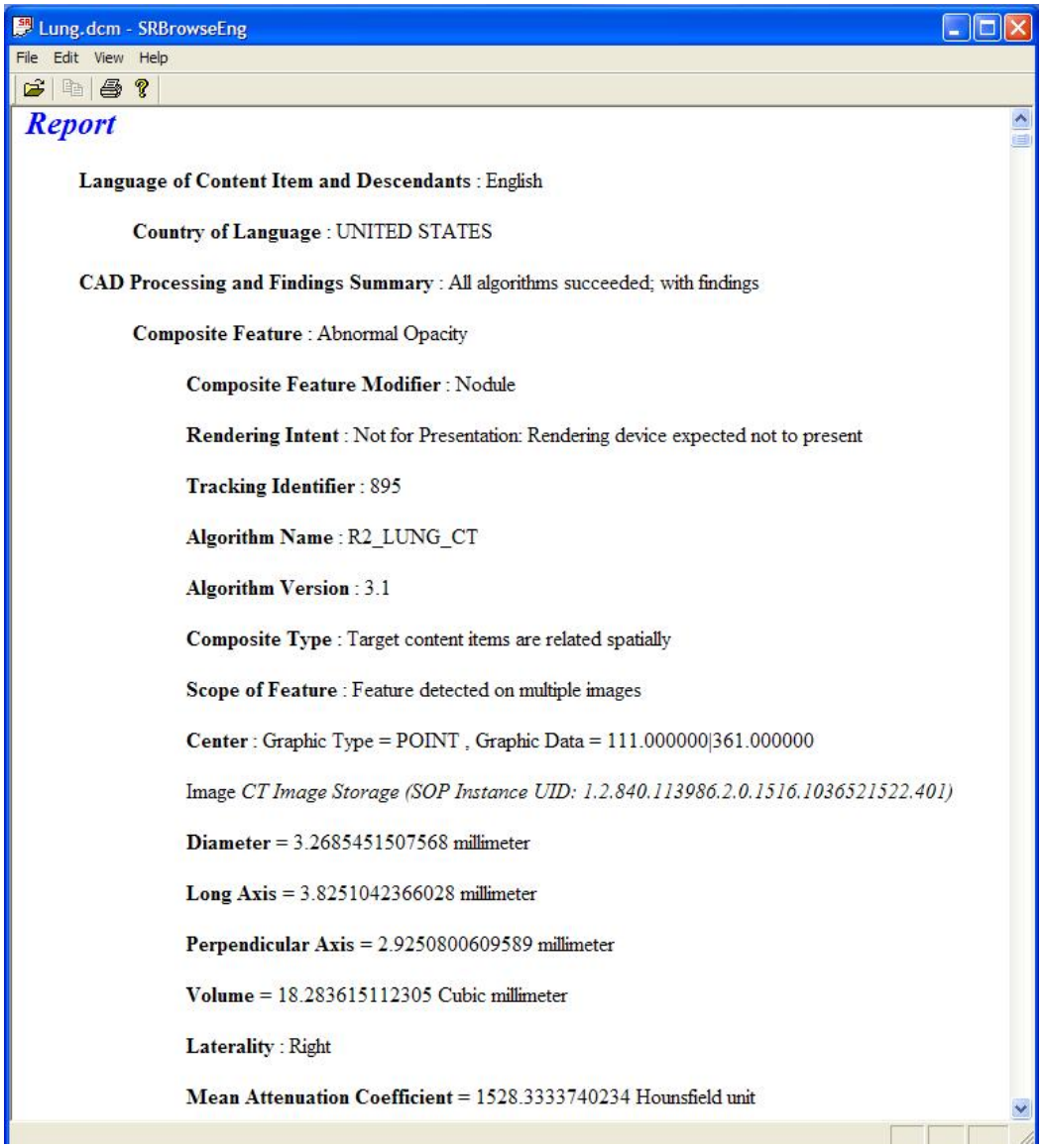

Fig. 2. Sample DICOM-SR document provided by IPILab, USC.

2.1 MI^2 Data Grid Architecture

The design architecture of the Medical Imaging Informatics Data Grid is seen in Figure 3. There is a DICOM service layer built onto the Globus Toolkit, which provides security and file transfer middleware features necessary for the Medical Imaging Informatics Data Grid. At the bottom hardware layer, there are storage nodes, multiple databases, and Internet2 network connectivity. The three main databases are the DICOM metadata database to store basic DICOM header information, the Replica Location Database that belongs to the Globus Replica Location Service, and the DICOM-SR Database to hold report text, values, and image SOP instance reference links.

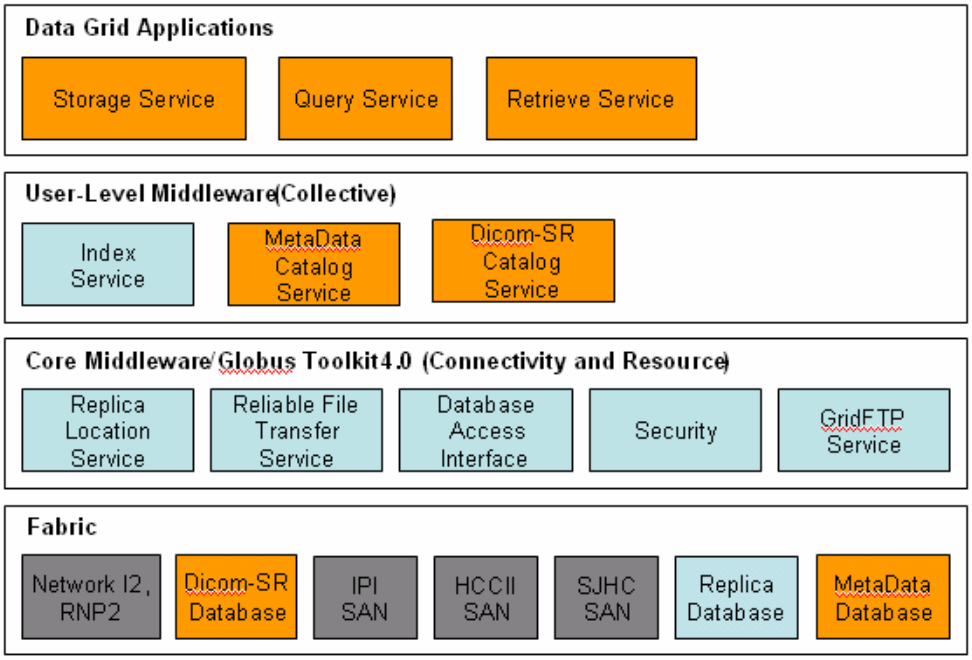

Fig. 3. Overview Architecture of Medical Imaging Informatics Data Grid
Orange: developed at IPILab, Blue: Globus Toolkit, Grey: hardware

The overall data grid system implemented at the IPILab is drawn in Figure 4 below. A grid-access-point (GAP) is the DICOM-compliant gateway into the MI^2 Data Grid for each physical site, managing DICOM store and query/retrieve just like a PACS. The main benefit behind the GAP is that it speaks DICOM language with the outside world, and utilizes security and faster reliable file transfer protocols across public domain within the MI^2 Data Grid. The result is a distributable storage system that seamlessly utilizes remote storage space within a proven secure grid environment.

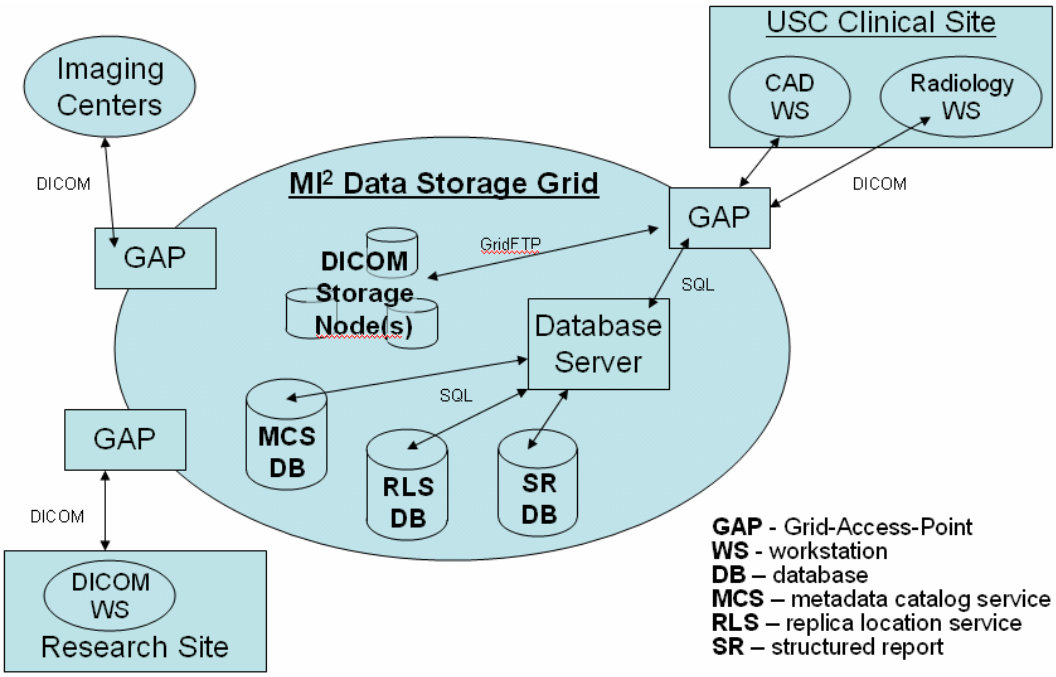

Fig. 4. Workflow Overview of Medical Imaging Informatics Data Grid at the IPILab

2.2 Workflow Overview

After an imaging center such as a CT for thoracic imaging has completed a DICOM imaging study, copies can be pushed to the local PACS and Medical Imaging Informatics Data Grid for primary and secondary storage,

respectively, and then a CAD server for image processing. CAD applications on the server can detect and quantify potential biological target markers in the DICOM study and presents its findings in a report, which have predominantly been proprietary in the past. However, DICOM structured report standard is gradually creating template for more CAD applications as well as other forms of document types such as a radiologist's report [3]. This DICOM structured report, while being a standard, is flexible to cover user's diverse demands.

2.2.1 Storage of DICOM-SR into the MI^2 Data Grid

When a DICOM-SR file is sent to the Medical Imaging Informatics Data Grid via the grid-access-point (GAP), the DICOM header information gets extracted to be linked to its respective DICOM images, identified by Study UID. The SOP Class UID is also extracted to identify whether it is an SR and if it is a basic, enhance, or comprehensive SR [1]. The entering SR is added as a new series into the metadata database, and a field is marked as being an SR. Figure 1 draws up the general DICOM model with the DICOM-SR document at the series level. Figure 5 below is the workflow for storage of DICOM-SR. After the metadata database has been updated with the typical DICOM header information, it is sent to the Replica Location Service Images for distribution into the MI^2 Data Grid storage nodes. Images for the DICOM SR should have already been stored into the MI^2 Data Grid at two or more remote storage repositories depending on each grid-access-point's backup policy. It is important that the SR files are stored into the same storage repositories as its referenced imaging studies so both can be retrieved in one process. Furthermore, we would want them to both be available in case a storage node goes down. Transfers of DICOM-SR across public domain within the MI^2 Data Grid utilize security and GridFTP protocols provided by the Globus Toolkit 4.0 middleware.

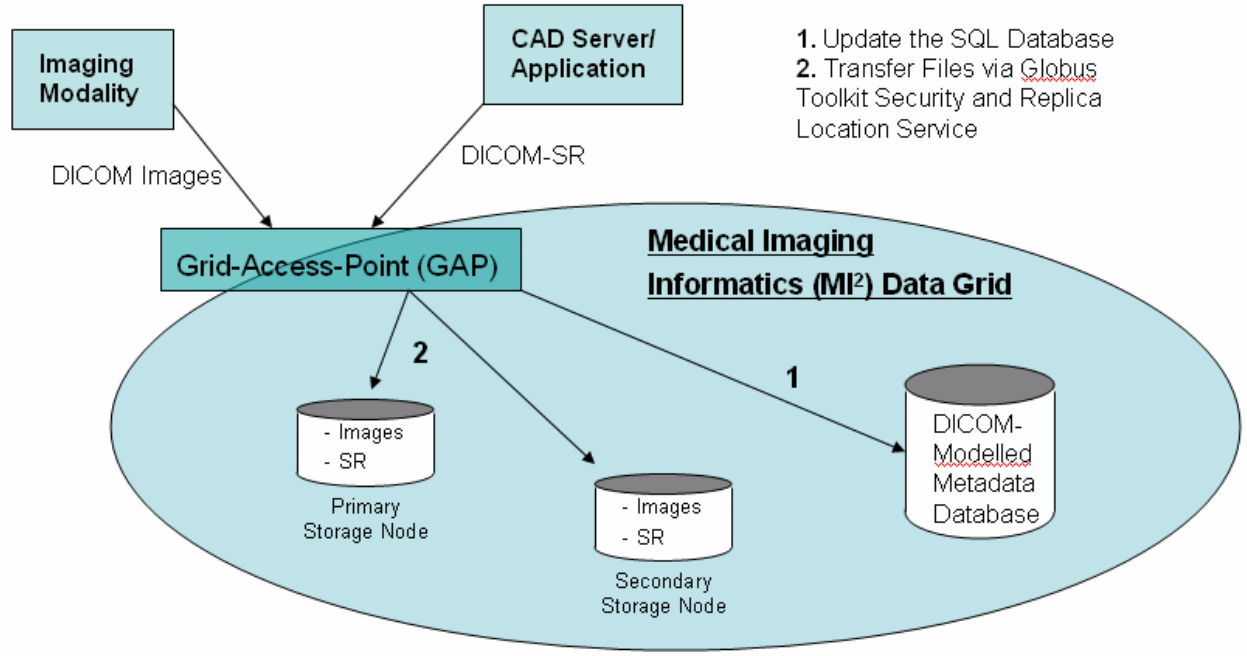

Fig. 5. Storage Workflow of DICOM-SR into the MI^2 Data Grid from CAD Application.

2.2.2 Query/Retrieve the DICOM Structured Report

When a radiologist or researcher queries the MI^2 Data Grid from either a DICOM-SR compliant viewing workstation or web-based interface, he or she will see the DICOM structured report as a series under the patient-study hierarchy. To retrieve the SR, they would have to retrieve the entire patient study from the MI^2 Data Grid because performs its query / retrieve at the study level. When the grid-access-point receives the retrieve request with patient and study UID, it calls on the Replica Location Service to find where the primary copy of the DICOM study is and gets first the images and then the SR, if available, from the remote storage node via GridFTP protocol. This method of retrieval is secured using the Globus certificate authorization services and faster than DICOM transfers thanks to GridFTP.

2.3 MI^2 Data Grid Database Design to Support DICOM

The Medical Imaging Informatics Data Grid has a metadata database that followed the DICOM-model hierarchy for DICOM header information. To support DICOM-SR, the existing database tables that was designed based on the real world DICOM model was slightly expanded at the series level to mark whether the series is an SR. The database for the Replica Location Service did not have to be changed because the SR file is simply another file to be distributed and retrieved by the DICOM query / retrieve service in the MI^2 Data Grid.

In development are extended database tables to support SR content based on the DICOM-SR class IOD [1]. This can enable querying of the MI^2 Data Grid for DICOM studies with SR files that have certain values and findings. Given an interface that could query the MI^2 Data Grid for this DICOM-SR database, researchers would be able to do data-mining and SR content-based querying. However, the challenge is to design a generic database to accommodate the recursive tree-structure and variable content values of a DICOM-SR. An initial database has been set up based on the DICOM chest CAD SR standard. Figure 6 diagrams the top levels of the content tree that the database is built on.

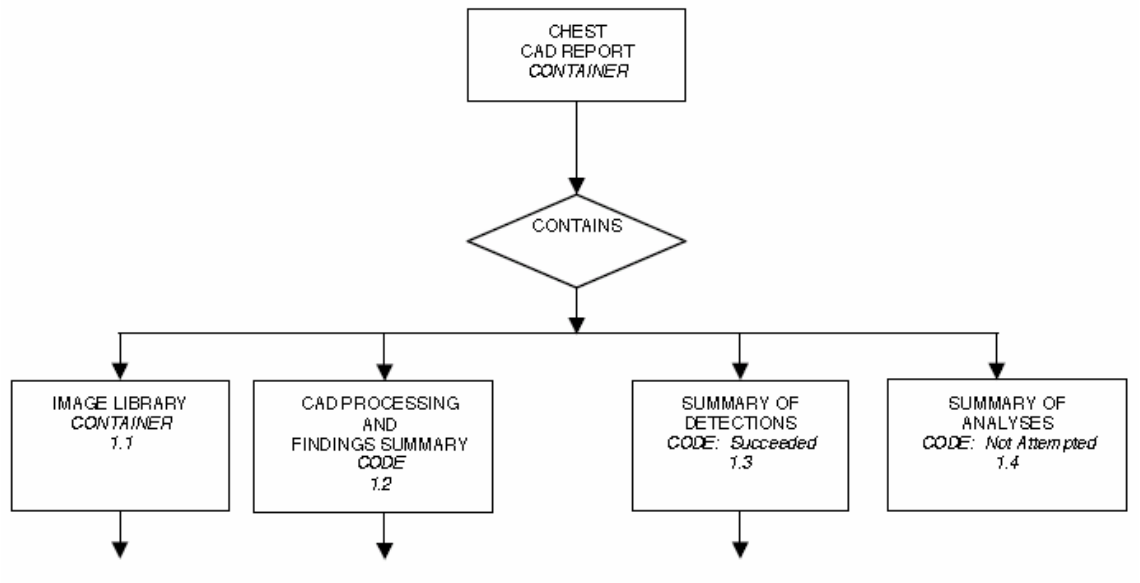

Fig. 6. Content Tree Root for a Sample Chest CAD SR [6]

3. RESULTS and DISCUSSION

This integration of DICOM-SR files with the Medical Imaging Informatics Data Grid provides users with a single access method to manage DICOM images and structured reports in a grid infrastructure. Multiple copies are distributed and available for fault-tolerant retrieval using the DICOM compliant grid-access-points. The grid-access-point can receive both DICOM images and DICOM-SR files, categorize them using the DICOM modeled database, and save them to multiple remote storage nodes with a secured GridFTP protocol using the Globus Toolkit. Users can query/retrieve from the MI^2 Data Grid using a DICOM viewing workstation that supports DICOM Structured Report standard.

The benefits of supporting DICOM-SR in the Medical Imaging Informatics Data Grid is that it opens doors to diagnostic reporting as well as quantitative value analysis. CAD generated structured reports are only one of the many types of structured documents that are involved in the DICOM-SR standard. It can also include waveforms, medical documents such as ultrasound measurements, cardiac procedure logs, and radiologist reports. Furthermore, DICOM-SR documents enable quantified measurements and diagnostic findings to be referenced to the DICOM imaging studies and key note images.

By supporting the DICOM-SR standard, the Medical Imaging Informatics Data Grid can promote sharing of vendor-independent CAD results across the public domain in a secured and robust DICOM grid repository. The benefits can be seen in clinical trials, CAD application testing, and healthcare enterprises. Furthermore, applications that can query the MI^2 Data Grid for the SR-specific content can open doors to data mining of DICOM-SR content.

4. CONCLUSION

As CAD applications are developed in the medical imaging field and the DICOM-SR becomes a widely accepted standard to document radiological and medical reports, the Medical Imaging Informatics (MI^2) Data Grid is able to support DICOM-SR storage and query/retrieve within the same system as its DICOM images. Medical imaging modalities, radiology workstations, PACS, and now even CAD workstations can connect to a local grid-access-point where their images are securely stored and can access both image studies and the corresponding DICOM-SR objects.

5. REFERENCES

[1] DICOM Supplement 23 : Structured Reporting Storage SOP Classes. <www.nema.org> (accessed Dec. 07)

[2] Bidgood, Dean. "DICOM-SR: Requirements, Applications, Benefits" <medical.nema.org/dicom/srworkshop/sr.intro.bidgood.20000329.print.ppt> (accessed Dec. 07)

[3] Hussein, Rada, MSc., et al. "DICOM Structured Reporting," RadioGraphics 2004; 24:891-896

[5] DCM4CHE. <www.dcm4che.org> (accessed Jan. 2008)

[6] DICOM Supplement 65: Chest CAD SR SOP Class. <www.nema.org> (accessed Dec. 07)

[7] Harry Soloman. "Electronic Reports: HL7 CDA (Clinical Document Architecture) and DICOM SR (Structured Reporting)," RSNA 2006 course

Assuring Image Authenticity within a Data Grid Using Lossless Digital Signature Embedding and a HIPAA-Compliant Auditing System

Jasper C. Lee, Kevin C. Ma, Brent J. Liu
Image Processing and Informatics Laboratory, Dept. of Radiology
Keck School of Medicine, USC, Marina del Rey, 90292

ABSTRACT

A Data Grid for medical images has been developed at the Image Processing and Informatics Laboratory, USC to provide distribution and fault-tolerant storage of medical imaging studies across Internet2 and public domain. It is a grid-based DICOM storage repository to promote multi-institution and international healthcare collaboration. Although back-up policies and grid certificates guarantee privacy and authenticity of grid-access-points, there still lacks a method to guarantee that the sensitive DICOM images have not been altered or corrupted during transmission across a public domain. This paper takes steps toward achieving full image transfer security within the Data Grid by utilizing DICOM image authentication and a HIPAA-compliant auditing system. The 3-D lossless digital signature embedding procedure involves a private 64 byte signature that is embedded into each original DICOM image volume, whereby on the receiving end the signature can to be extracted and verified following the DICOM transmission. This digital signature method has also been developed at the IPILab. The HIPAA-Compliant Auditing System (H-CAS) is required to monitor embedding and verification events, and allows monitoring of other grid activity as well. The H-CAS system federates the logs of transmission and authentication events at each grid-access-point and stores it into a HIPAA-compliant database. The auditing toolkit is installed at the local grid-access-point and utilizes Syslog [1], a client-server standard for log messaging over an IP network, to send messages to the H-CAS centralized database. By integrating digital image signatures and centralized logging capabilities, DICOM image integrity within the Medical Imaging and Informatics Data Grid can be monitored and guaranteed without loss to any image quality.

Keywords: Medical Imaging and Informatics, Data Grid, Lossless Digital Signature Embedding, HIPAA-Compliant Auditing System, Image Integrity and Security

1. INTRODUCTION

1.1 Data Storage Grid for Medical Images

The Medical Imaging Informatics Data Grid developed at the IPILab has become a viable and cost-saving solution for storage and sharing of DICOM images for multi-site healthcare and imaging research institutions. It uses software developed at the IPILab and open-source grid technology by Globus® Toolkit to store and query/retrieve medical and radiological images securely and quickly from geographically distributed storage nodes. Its applications have included backup solution for an enterprise PACS[2], primary storage for image-based clinical trials[3], and international collaborative research in medical imaging processing at the IPILab. Each grid node is called a Grid Access Point (GAP) and is set up at local sites to act as the gateway into the Medical Imaging Informatics Data Grid. When DICOM images of a study are sent to a GAP, the DICOM header information is extracted and updated in the Data Grid's database and are then sent to the storage nodes using grid-ftp protocol to two or more pre-configured storage nodes. The GAP also has query/retrieve functions that DICOM compliant. The Data Grid is a fault tolerant and continuous availability model for DICOM storage and distribution in clinical PACS and imaging research.

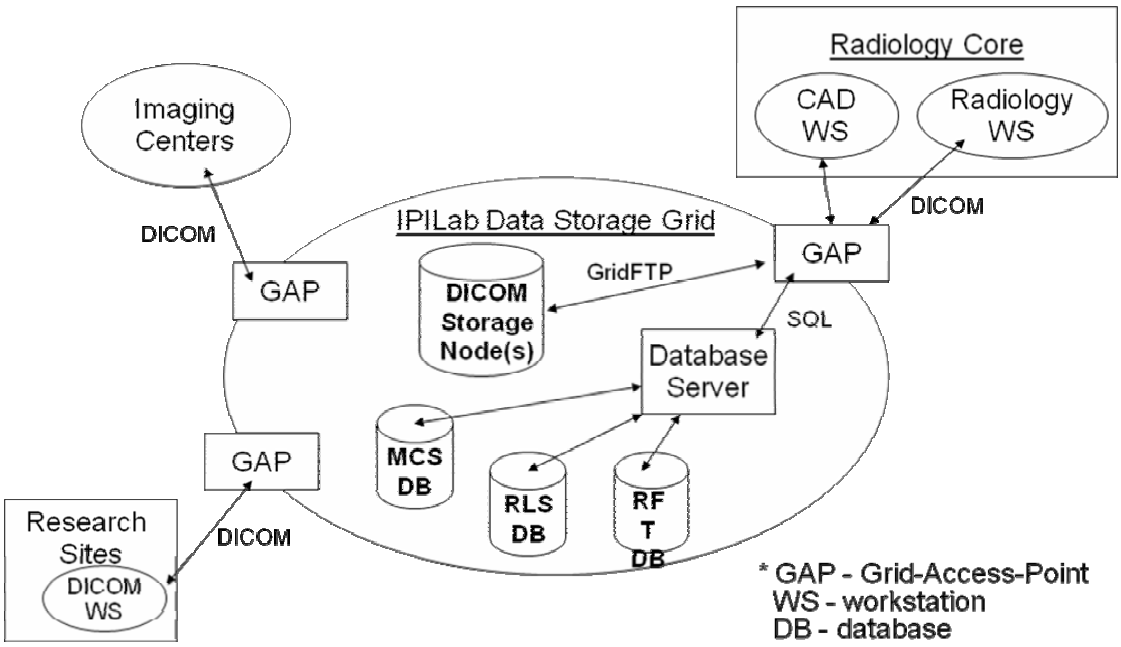

Fig. 5 Sample Diagram of Data Grid in Clinical Trials. RFT stands for Reliable File Transfer, RLS stands for Replica Location Service, and MCS stands for Metadata Catalog Service.

1.2 Network and Image Security within Data Grid

Because the Data Grid utilizes public networks to transmit DICOM images, it presents a concern over security during file transmission. There are three general characteristics of network security – privacy against unauthorized individuals, authenticity of data source, and integrity against altering or destroying of the image itself. The recent Data Grid software addresses privacy and authenticity issues using grid security certificates, Transfer Layer security and key cryptography[4]. However, the integrity of the image data is not addressed, as stated by the Health Insurance Portability and Accountability Act (HIPAA) [5]. This paper describes how the Data Grid adapts security measures to ensure image integrity and security, as well as secure and complete data transfer logging. A Lossless Digital Signature Embedding system (LDSE) has been designed in the IPILab for image encryption during image data transfer. A HIPAA-Compliant Auditing System (H-CAS) has also been designed and tested in the IPILab for activity logging in a Picture Archiving and Communication System (PACS) [6]. The integrated system is robust and does not compromise the Data Grid's own flexibility and efficiency.

2. METHODS

In this section, we will present a novel Lossless Digital Signature Embedding (LDSE) workflow and verification algorithm to maintain image data integrity within the Data Grid. We will also present a HIPAA-Compliant Auditing System (H-CAS) architecture that logs activities at each GAP and storage node to record system activity, authentications, data transfers, and provide alerts for unauthorized actions based on HIPAA guidelines. Both LDSE and H-CAS are needed to achieve adequate image and data security in Data Grid.

2.1 Lossless Digital Signature Embedding Design

LDSE is an image encryption method that embeds a unique digital signature in images of a DICOM study. Because it is lossless, the original images can be restored, thus preventing compromising diagnostic qualities. A three-dimensional signature is used for multi-slice studies such as CT, MR, and US exams. This is to ensure no loss of images data with a single digital

signature. The following description of the system includes digital signature generation, DS embedding, DS extraction, and verification.

2.1.1 Signature Generation

There are several possible algorithms to generate the signature for 3-D digital signature embedding (DSE), notably Random Pixel and RS groups (Regular and Singular).[4] The method chosen here is the RS groups DSE because of the higher compression ratio of the extracted bit stream from the images. Take a medical image of N x M pixels, first the image is divided into disjoint groups of *n* adjacent pixels ($x_1, x_2, \ldots, x_n$). A discrimination function 'f' is defined that computes the correlation coefficients of each group G. Equation 1 shows how to calculate f. An invertible operation F ("flipping" function) is defined on P such that F(F(x)) = x for all x in P.

$$f(x_1, \ldots, x_n) = \sum |x_{i+1} - x_i|, 1 \leq i \leq n-1 \quad (1)$$

From the relationship between f(F(G)) and f(G), three groups can be derived:

Regular Group: f(F(G)) > f(G)
Singular Group: f(F(G)) < f(G)
Unuseable: f(F(G)) = f(G)

At a selected bit plane, the pixels corresponding to the Regular (R) group are 1, and those corresponding to Singular (S) group pixels are 0. This bit plane becomes the digital signature.

For a multi-image study with *n* images, a pseudo random sequence of n numbers is generated, and all of the images in the study are rearranged based on this sequence of *n* numbers. A hash value is computed for all of the pixels in the rearranged image study. The hash value then becomes the digital signature for all *n* images. This is the 3-D digital signature generation.[1]

2.1.2 Embedding Process

Since most pixels in a medical image do correlate with its adjacent groups, it is expected that f(G) values are smaller than f(F(G)) for most cases. Therefore, there are more R groups than S groups, thus the signature is mostly 1's. To make room for the digital signature (DS), the DICOM image is losslessly compressed until there is enough bits for the DS. Then the DS is appended to the compressed bit stream. Figure 2 shows the diagram of the embedding process.

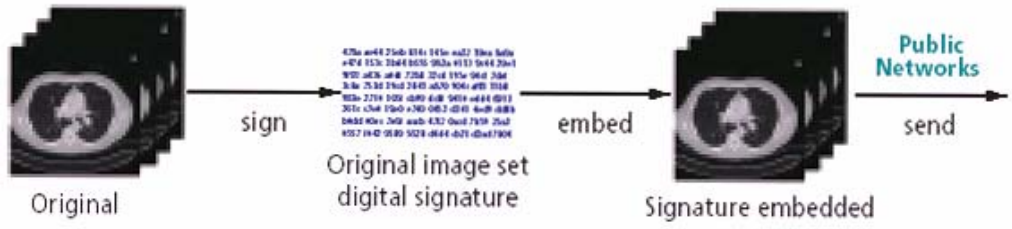

Fig. 6. Diagram of Digital Signature Embedding. The destination of DICOM send is the local GAP, which redirects the embedded images to storage nodes in the Data Grid.

One of the new features in LDSE-Data Grid integration is location-specific digital signature. After a GAP receives an embedded image study, the program extracts the DICOM images and further appends a unique GAP identifier. The several copies of the images in the Data Grid thus have different digital signatures based on where the images were originally sent into a specific GAP.

2.1.3 Extracting and Verification Process

The digital signatures can be extracted by reversing the embedding process. When an image set in the Data Grid is retrieved from one of the multiple storage nodes to the GAP, the digital signatures are extracted and verified at the GAP before DICOM sending to the querying workstation or web server. For 2-D RS Group signatures, the image goes through a series of decompression and RS-Group reconstructions. For 3-D digital signatures, the images are first

arranged in the same random order, signature extracted and verified, and images restored to the original order in the study. The verification process of digital signatures includes generating new signature from decompressed images to match against the extracted signature, as well as matching the extracted signature against a database of signatures. The latter way is used in matching location-specific signatures with origins of image studies.

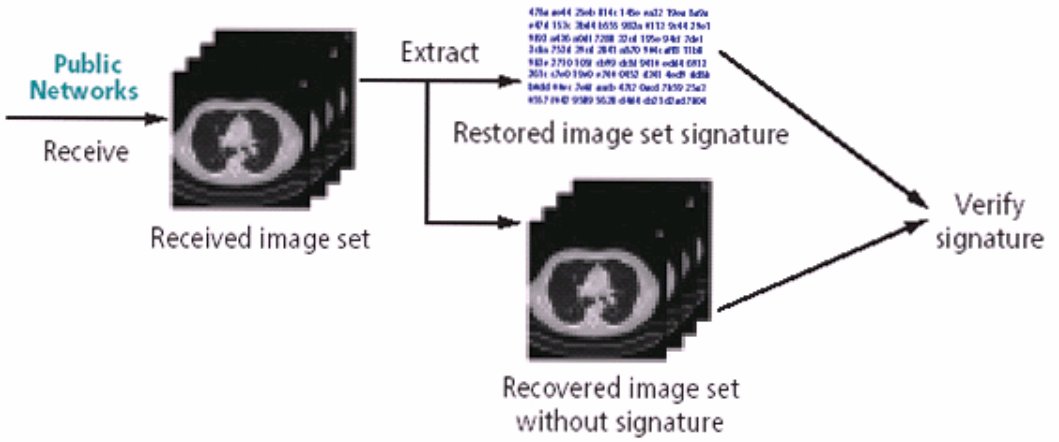

Fig. 7 The Diagram of the Extraction and Verification Process of LDSE. After images are received after a query, the signature is extracted and images restored, and then the signature is matched against the restored image and/or a signature database.

2.2 HIPAA-Compliant Auditing System Design

The architecture of H-CAS for Data Grid should record activities at all GAP's, as well as combine individual logs into a master log. An existing H-CAS has been developed in IPILab for a hospital PACS system[5]. It employs a layered structure to detail each steps and functions needed for a complete auditing and alert system. The architecture is broken down into two main parts: a record layer and an audit layer. Figure 4 shows the diagram of the H-CAS system.

2.2.1 Record Layer

The record layer is the most basic layer in the structure. The logs includes changes in grid services, user information that initiates a transaction, the DICOM Study UID accessed, the type of access, data source (identity of GAP and storage node), timestamp of activity, success/failure of access, and success/failure of LDSE verification. The logs are flexible such that new categories and items can be added to the record layer, which is installed at each GAP locally.

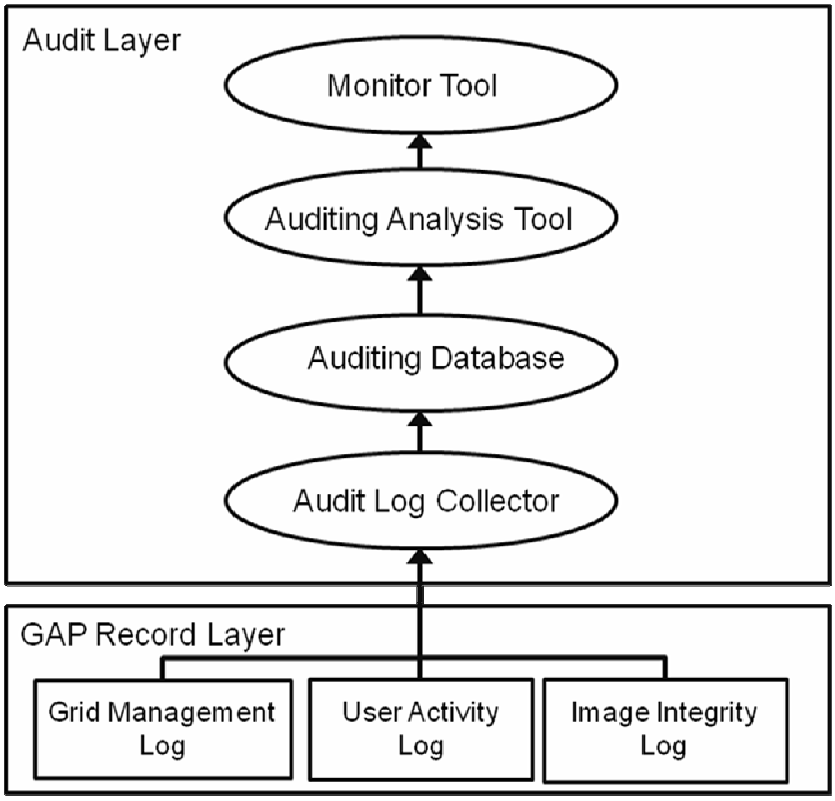

Fig. 8 Diagram of the H-CAS architecture.

2.2.2 Audit Layer

The audit layer has the most important components in the architecture, as it collects all audit logs from nodes and stores them in a database. The Audit layer includes a log collector, auditing database, log analysis tool, and monitoring tool. A log collector periodically extracts all of the logs at each GAP and stores it in the audit database. The database stores information from the logs in a tabulated format. Columns include DICOM header information, timestamps, activity descriptors, grid node identifiers, and success/failure of processes. The audit analysis tool looks into the audit log database to find any abnormal log activities and unauthorized accesses. HIPAA-compliant rules and regulations define scenarios and activities of concern. The monitor tool takes the form of a web-based server that allows the system administrator to monitor system activity and generates alert messages and notifications from the results of data analysis tool.

2.3 System integration with Data Grid

The software toolkit for both LDSE and H-CAS are portable and included as add-ons with a new GAP installed on a unix-based machine. When the toolkit is installed and grid security is updated, the database of existing GAP is updated. At the same time, databases for LDSE and H-CAS are both updated to incorporate the new additions to the grid infrastructure.

Unique LDSE for individual GAPs are realized by using GAP's public and private keys as digital signatures. Public and private keys are stored in a database of GAP locations, along with IP address, AE title, etc. In this way, when a user receives an image study, by extracting the digital signature the user is able to know where the image study originates from. GAP-specific signatures also enable H-CAS to record the origins of data during data retrieval activities. This access log is recorded in the "Image Integrity Log" in the record layer. In the events of DSs failing to be verified, the errors are recorded in H-CAS and a notification is sent by the monitoring service.

To test the workflow of Data Grid with the combined security system, several test runs are designed. Test runs include CT, MR, CR images with 2-D and 3-D LDSE. Images are pushed into the Data Grid and then queried and retrieved to verify digital signatures. H-CAS is then

checked to see if it successfully records such activities. Unauthorized user access scenario is tested. Digital signatures are then altered to created errors in the verification process, which then should be recorded by H-CAS. A new GAP is installed and added to the Data Grid. The scenarios are tested again to see if LDSE and H-CAS responds to the new GAP.

3. RESULTS AND DISCUSSION

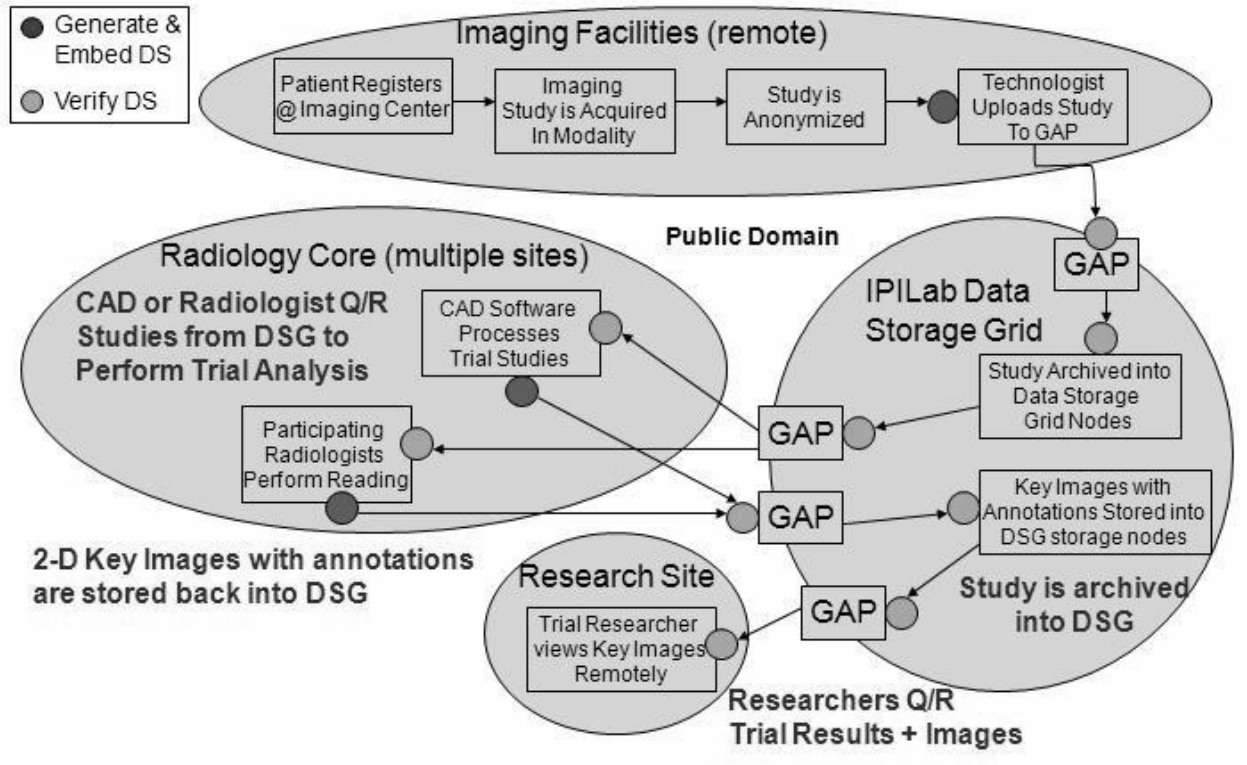

Fig. 9 A simulated LDSE workflow in a clinical trials setting. This simultaneously tests LDSE verification system and HIPAA-compliant user authentication.

The integration of LDSE and the H-CAS system into the Data Grid is still ongoing. Figure 5 below describes the workflow involved for a clinical trial utilizing the IPILab Data Storage Grid with LDSE embedding and verification. The red dots represent the embedding procedure of the digital signature into DICOM images. The green dots represent the physical workflow locations where the digital signature is extracted and verified for image integrity. The H-CAS system receives LDSE logs from all GAP's and storage nodes using Syslog messaging and SSL encryption. A web-based monitoring application is also being developed to communicate with the H-CAS database and will function as the audit layer's monitoring tool and user interface for the system administrator.

4. CONCLUSION

The need for image integrity when DICOM images are transmitted over public networks is important especially in grid-based storage applications. Exposure to public networks is easily seen as an unsafe place to send patient-sensitive data. There are tools that can be utilized to ensure image data integrity and log activity of all transactions within the Data Grid. Lossless Digital Signature Embedding is a method developed at the IPILab and addresses image data integrity issues that have previously been absent in the medical imaging Data Grid. By combining the DICOM image-integrity authentication method and a HIPAA-compliant auditing system into the Data Grid, the Data Grid can meet HIPAA-compliance security requirements and better meet the patient data privacy requirements of imaging-based clinical trials. It provides a

solution to guarantee DICOM images transferred within the Data Grid are kept exactly the same as the original image sent in from the user.

REFERENCES

[1] Syslog, http://www.loriotpro.com/Products/SyslogCollector/SyslogDataSheet_ENv3.php (accessed Dec. 2007)

[2] B Liu, Z Zhou, J Documet. "Utilizing Data Grid Architecture for the Backup and Recovery of Clinical Image Data" Computerized Medical Imaging and Graphics 29 (2005), 95-102

[3] Z Zhou, J Dodumet, L Chan et al. "The Role of a Data Grid in Worldwide Imaging-Based Clinical Trials" 2006, USC UPU: Marina del Rey

[4] Z Zhou, HK Huang, B Liu. "Digital Signature Embedding for Medical Image Integrity in a Data Grid Off-Site Backup Archive" SPIE Med. Imag. Conference Proceeding: PACS and Imaging Informatics, February 2005

[5] J. Fridrich, M. Goljan, R. Du. "Lossless Data Embedding – New Paradigm in Digital Watermarking" EURASIP Journ. Appl. Sig. Proc., vol. 2002, no.2 pp. 185-196, 2002

[6] B Liu, Z Zhou, HK Huang "A HIPAA-Compliant Architecture for Securing Clinical Images" SPIE Med. Imag. Conference Proceeding: PACS and Imaging Informatics, February 2005

[7] A Chervenak, I Foster, C Kesselman, et al. "The Data Grid: Towards an Architecture for the Distributed Management and Analysis of Large Scientific Datasets" Journal of Network and Computer Applications, 23:187-200, 2001

[8] XQ Zhou, HK Huang, SL Lou. "Authenticity and Integrity of Digital Mammography Images" IEEE Trans. Medical Imaging, vol. 20, no. 8, pp. 784-791, 2001

[9] HIPAA Security Standard. http://www.hipaadvisory.com/regs/finalsecurity/

[10] Conducting a HIPAA security audit http://searchdomino.techtarget.com/news/article/0,289142,sid4_gci912158,00.html

[11] Z Zhou, B Liu, HK Huang et al. "A RIS/PACS Simulator Integrated with the HIPAA-Compliant Auditing Toolkit" SPIE Med. Imag. Conference Proceeding, February 2005

Automated Bone Age Assessment of Older Children using the Radius

Sinchai Tsao*[a], Arkadiusz Gertych[b], Aifeng Zhang[a], Brent J. Liu[a], Han K. Huang[a]
[a]Image Processing and Informatics Laboratory, Department of Radiology,
Keck School of Medicine, University of Southern California,
Suite 601, 4676 Admiralty Way, Marina Del Rey, CA 90292;
[b]Department of Surgery, Minimally Invasive Surgical Technologies Institute, Cedars-Sinai Medical Center, 8700 Beverly Blvd, Davis 4021, Los Angeles, CA 90048, USA

ABSTRACT

The Digital Hand Atlas in Assessment of Skeletal Development is a large-scale Computer Aided Diagnosis (CAD) project for automating the process of grading Skeletal Development of children from 0-18 years of age. It includes a complete collection of 1,400 normal hand X-rays of children between the ages of 0-18 years of age. Bone Age Assessment is used as an index of skeletal development for detection of growth pathologies that can be related to endocrine, malnutrition and other disease types. Previous work at the Image Processing and Informatics Lab (IPILab) allowed the bone age CAD algorithm to accurately assess bone age of children from 1 to 16 (male) or 14 (female) years of age using the Phalanges as well as the Carpal Bones. At the older ages (16(male) or 14(female) -19 years of age) the Phalanges as well as the Carpal Bones are fully developed and do not provide well-defined features for accurate bone age assessment. Therefore integration of the Radius Bone as a region of interest (ROI) is greatly needed and will significantly improve the ability to accurately assess the bone age of older children. Preliminary studies show that an integrated Bone Age CAD that utilizes the Phalanges, Carpal Bones and Radius forms a robust method for automatic bone age assessment throughout the entire age range (1-19 years of age).

Keywords: Bone Age Assessment, CAD, Image Processing, Skeletal Imaging

INTRODUCTION

Current Issues in Bone Age Assessment Methods

Bone Age Assessment is used in Pediatrics to determine the stage of a subject's bone maturity during its growth from 0 to 19 years of age. Delayed or accelerated bone growth relative to a child's chronological age may be an indication of a pathological growth pattern. Examples of diseases that may cause pathological growth patterns include growth hormone deficiency, hypothyroidism, Sotos syndrome and other genetic and non-genetic pathologies. The Greulich and Pyle atlas published in 1950 form the basis of clinical bone age assessment. Radiologists use the hand radiographs of children from the G&P atlas along with descriptions of hand bone growth stages to assess a patient's bone age. Other more recent but less commonly used methods include the Tanner and Whitehouse or TW2 Method developed in 1975. However both methods require the Radiologist to compare and manually judge stages of growth relative to an atlas. Our CAD method attempts to quantify features that correlate well with bone maturity and growth and completely automate the process of bone age assessment.

Previous Work

Previous work by Pietka, Gertych, Pospiech-Kurkowska, et al [10] used the Phalanges as the ROI for feature extraction. The dynamic changes in the Phalanges in children between the ages of 7 to 16 (male) or 14 (female) years of age provided information for bone maturity assessment within this age range. Later work by Zhang et al [4] using size and shape-based features of the Carpal Bones allowed for assessment of younger children. To allow for complete assessment of Bone Age in all children, another ROI was necessary. The Radius was chosen as the ROI of

choice for older children because of its late fusion of the proximal Metaphysis and distal Epiphysis. This phenomenon is documented in the Greulich and Pyle Atlas as being later in the Radius as compared to the Phalanges. Thus allowing for assessment in the degree of fusion at the older age range using wavelet transformation based features similar to those used in the Phalanges. Due to the differing morphology between the Phalanges and the Radius, however, a new methodology is still necessary to extract the smaller sub-image of the growth plate region that will be used for feature extraction via wavelet transform. This segmentation technique is based on knowledge about the generalized morphology of the wrist. Using this knowledge along with defined landmarks, the Radius is identified and the bounding box for the sub-image is segmented from the larger wrist ROI.

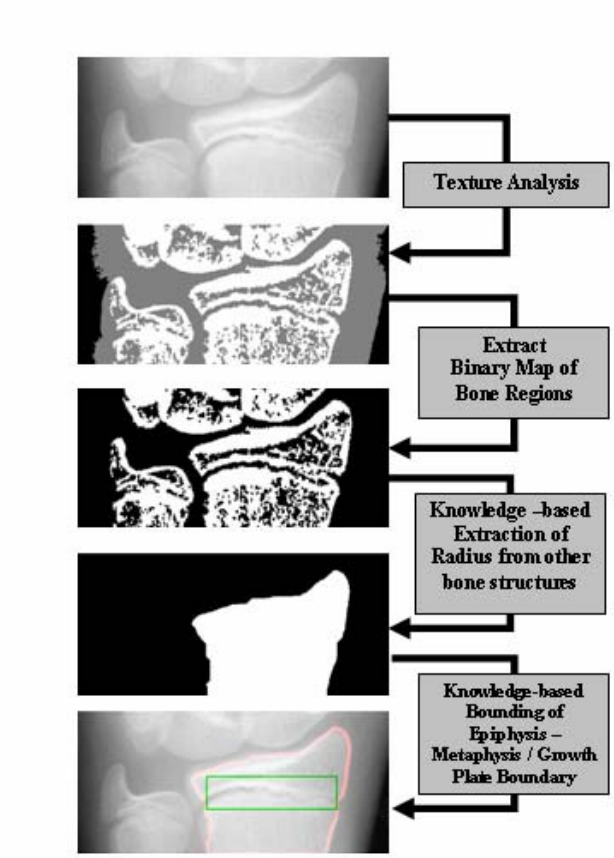

Fig. 10. Outline of Image Processing algorithm to extract Growth Plate ROI from the larger Wrist ROI.

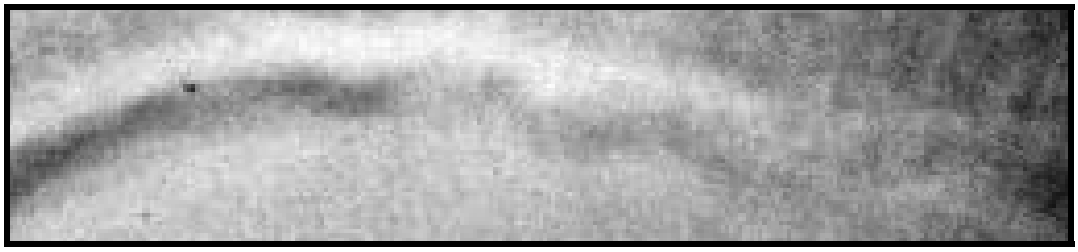

Fig. 11. Enlarge Image showing the extracted Growth Plate ROI. Note the horizontal pattern that denotes the boundary between the epiphysis and metaphysis. This boundary lessens and eventual disappears as the child grows.

Methods

Localizing the Radius

This initial methodology was developed based on previous work in the phalangeal ROI in the hand. The wrist region is segmented from the overall image via a set of landmarks based on the location of the Phalanges and the hand midline. The wrist ROI is then extracted as shown in figure 1. Through textural analysis, the pixels are grouped into three sub-textures (Bone, Soft Tissue and Background) as shown in the second image in figure 1. The bone-based texture is then removed from the other two textures. A binary image shows the location of all pixels that are part of that texture group. Using knowledge of the morphology of the wrist, the Radius is selected from all other bone structure and an overall outline of the bone is formed using image processing techniques such as erosion and dilation. In addition, knowledge of the location of the Epiphysis and Metaphysis of the Radius allows missing smaller structures that may be identified as separate objects to be merged to form the image of the Radius as seen in image number 4 in figure 1. Using the width and centerline of the Radius, a box containing the growth plate is drawn automatically by the CAD algorithm. The sub-image extracted from the segmentation process illustrated by figure 1 is shown in figure 2.

Features Extraction

After the growth plate ROI is segmented (figure 2), the sub-image is then passed onto the features extraction algorithm, which calculates the energy, orientation and number of edges in the sub-image and provides 12 quantitative measurements using the wavelet transform developed for the phalanges [10]. Six of the features that show most correlated variation with bone maturity are selected and passed on to a Mamdani fuzzy inference system. For each feature, a set of membership functions are formed from training using 48 images from males of ages 14 to 18 years of age. Using statistical analysis of feature values between age groups of 14, 15,16,17,18 and 19 years, groups that showed too much variation were merged.

Fuzzy Classification and Computation of Bone Age

The feature set for the images are divided into the two male and female cohorts for bone age computation, since the growth patterns and in male and female children are different[1]. For each feature, a set of 3 to 6 Gaussian membership functions were formed using the standard deviation and means from the data. Each of these membership functions represented a specific age group and depending on the feature value will contribute to each of the computed bone age output differently. A set of simple aggregation rules dictated how the membership functions were aggregated into the output membership function. The output membership functions were also Gaussian-based and depended on the standard deviation and mean of the chronological age of the 149 image training set. For our preliminary system testing we used the same image set for training and testing.

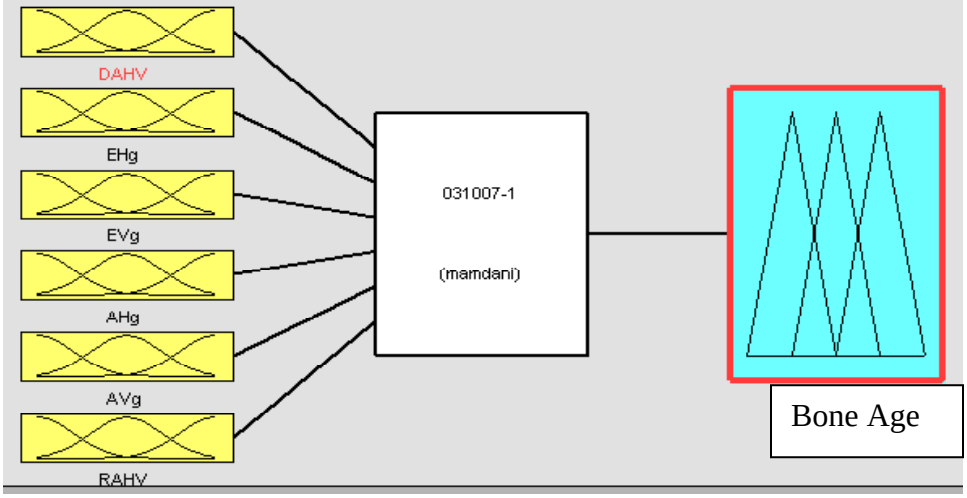

Fig. 12. Mamdani Fuzzy Inference System used to aggregate the feature values and derive a Bone Age based on feature values. The system requires training with a data set of normal children.

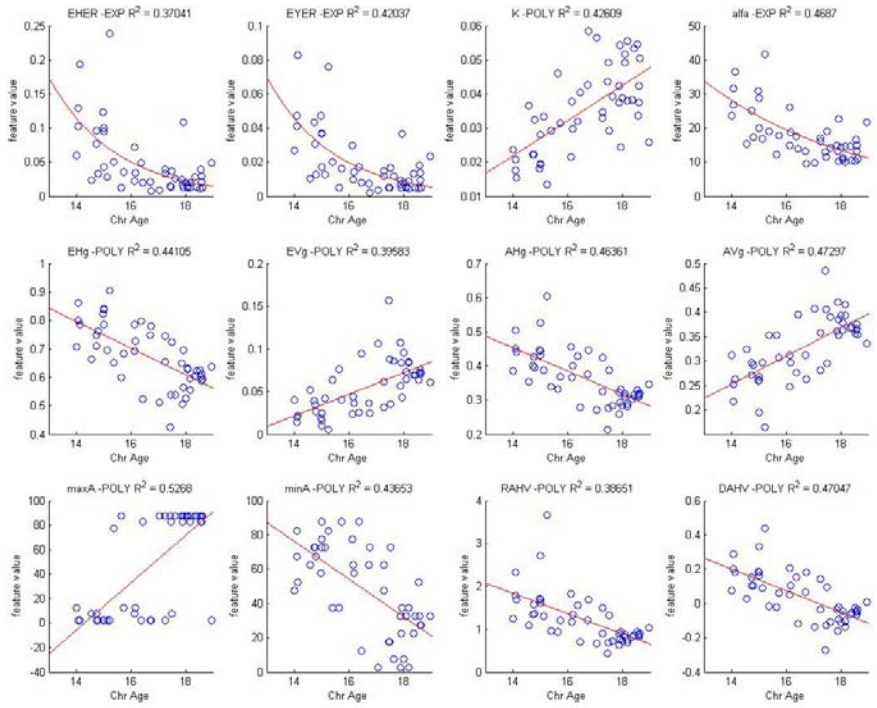

Fig. 13. Feature values for the male cohort.

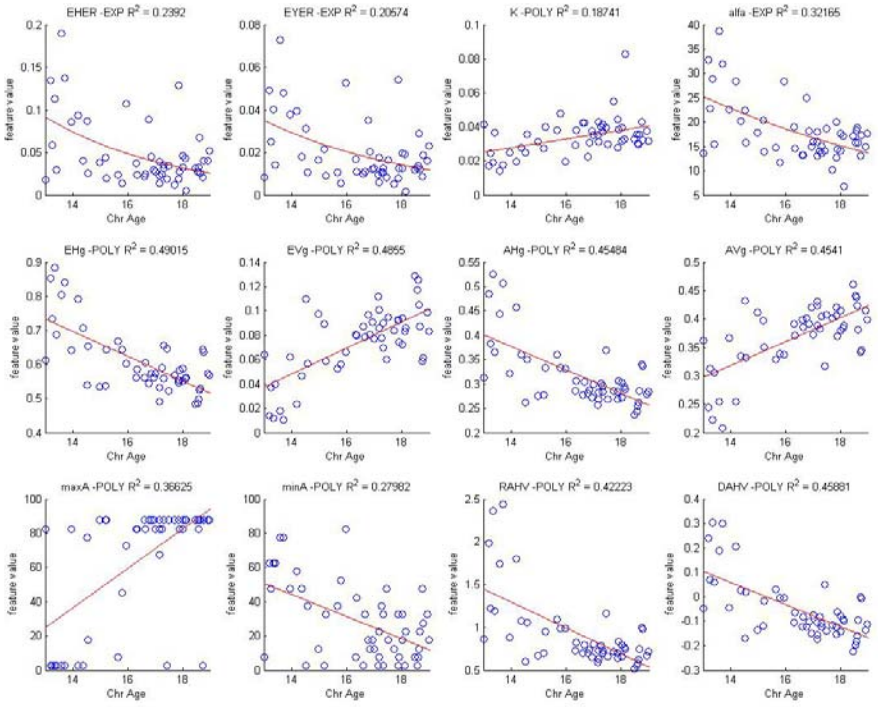

Fig. 14. Feature Values for the Female Cohort

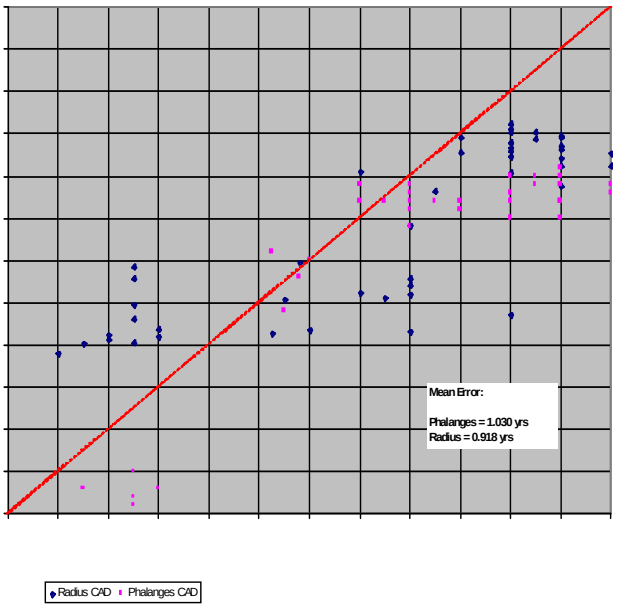

Fig. 15. CAD Age versus Pediatric Radiologist's Reading for the Male Cohort

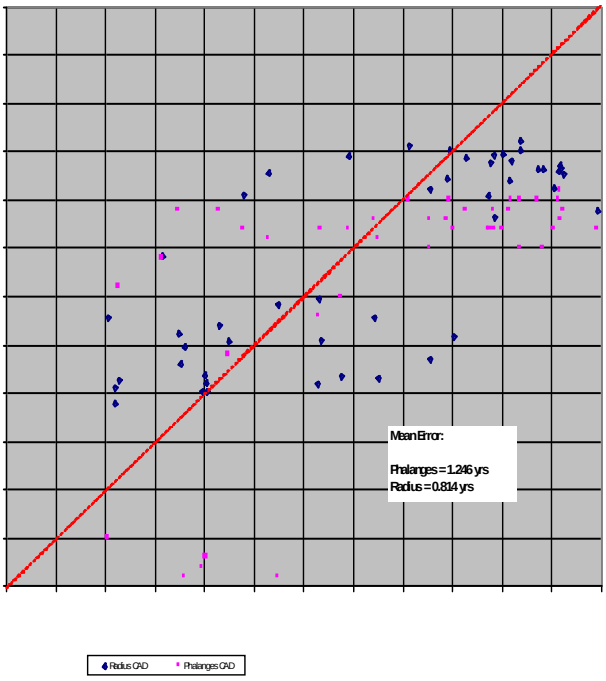

Fig. 16. CAD Age versus Chronological Age for the Male Cohort

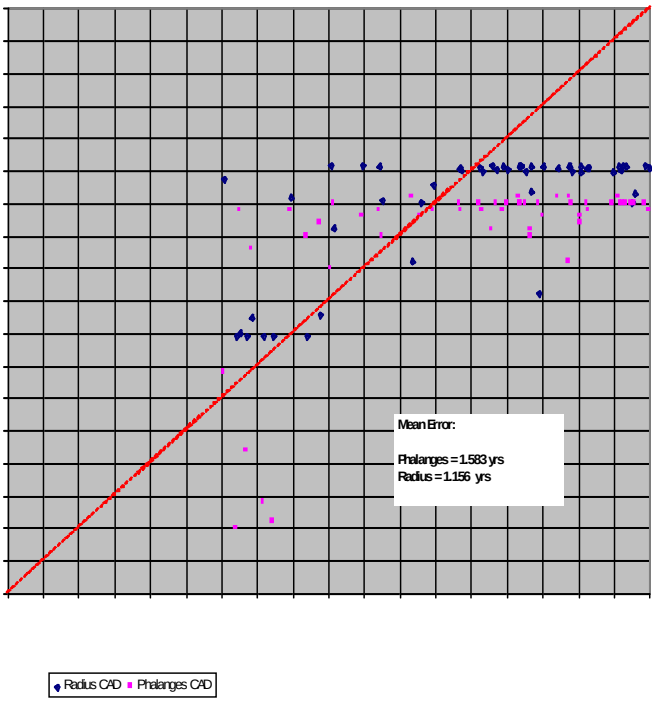

Fig. 17. CAD Age versus Chronological Age for the Female Cohort

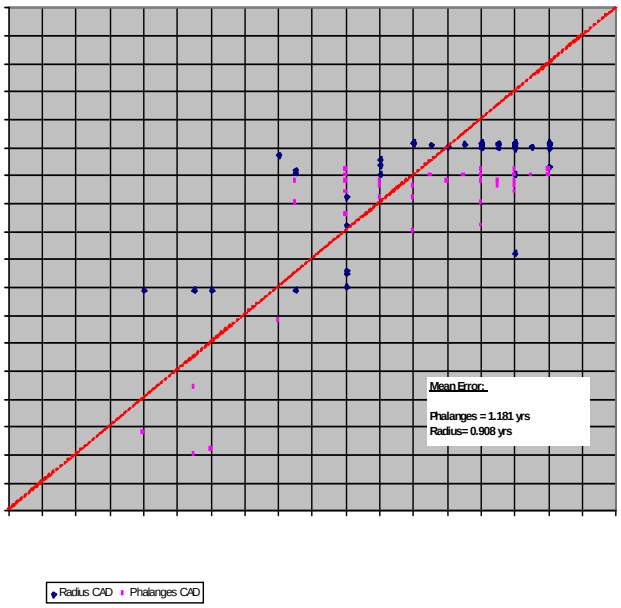

Fig. 18. CAD age Versus Pediatric Radiologist's Reading for the Female Cohort

Table 1. Mean Absolute Error of the system for the Male Cohort using Phalanges and Radius based on the Chronological Age and Reading of the Pediatric Radiologist as the gold standards. The absolute mean difference for the male cohort between the Pediatric Radiologist's reading and the normal child's chronological age is 0.650 years.

	Phalanges	Radius
ChrAge	1.246 yrs	0.814 yrs
Reading	1.030 yrs	0.918 yrs

Table 2. Mean Absolute Error of the system for the Female Cohort using Phalanges and Radius based on the Chronological Age and Reading of the Pediatric Radiologist as the gold standards. The absolute mean difference for the female cohort between the Pediatric Radiologist's reading and the normal child's chronological age is 0.700 years.

	Phalanges	Radius
ChrAge	1.583 yrs	1.156 yrs
Reading	1.181 yrs	0.908 yrs

Results

With our initial test group of Caucasian Children between the ages of 14 and 19, there were 149 images that were used for testing. The chronological age of these children does not differ more than 3 years from the projected bone age that the Pediatric Radiologist determined. The Caucasian Children also provide us with homogeneity in ethnic background in our dataset in case there are differences in growth patterns due to ethnic background. From previous experience we also found that the Caucasian dataset has the most consistent in image quality.

Our initial results show that we were able to correctly segment out the growth plate region approximately 50% of the time. Errors were a result from (1) an inability to differentiate between the carpal bones and the radius (2) mistaking the Ulna for the radius (3) unable to locate the growth plate sub-region of the carpal bone accurately. More work needs to be done to improve the accuracy of segmentation or have fail safe mechanisms when the Radius or the growth plate region cannot be segmented. In the final integrated system, images where the Radius cannot be used will rely on the phalangeal data for bone age assessment.

The results of the feature extraction are shown in figure 3 and 4, correlation coefficients are calculated from either a linear regression or exponential regression depending on the feature and were indicated by either "POLY" for linear polynomial or "EXP" for exponential. We chose to use both measures because the fuzzy inference system was able to mimic both types of trends during training. The trends indicate that the features allow for differentiation between the lower age range of 14 to 15 and the higher age range of 17 to 19 years of age but not any higher in age range resolution.

Figures 6 to 9 shows our preliminary results of the system after the fuzzy inference engine has computed the bone age based on the radius' features. The computed CAD bone age for the new Radius results and the previous Phalangeal results are compared to the chronological age as well as the Radiologist's Readings. Tables 1 and 2 show the generalized error for the overall testing set. Relative to chronological age, the new system showed a decrease of about 0.3 years for males and 0.4 years for females.

Discussion

The G&P atlas acknowledges natural growth variation in males from 14 to 17 years of age to have a standard deviation of 10.72 to 13.05 months. [1] Therefore, any variation of our result to within the order of 1 year can be attributed to natural variation in the population. In addition, our current system based on the Phalanges tapers off at 16 years of age for females and 17 years of age for males. Therefore any ability to differentiate between the pre-16 or pre-17 years of age and the higher age group of 18 and 19 will be contributed significantly to the overall fuzzy bone age result. This is because final system integration will allow the Phalangeal features to be aggregated with the Radii features and weighed using the fuzzy inference system to yield a final CAD bone age result.

The R-squared correlation coefficients for Radius are much lower than that of the Phalanges (approx 0.8 and above) for their optimal operational age range from 5 to 14 years. The computed bone age results show the effects of the lack of correlation in the features. Relative to the gold standard of the chronological age, it shows a stepwise output, with many of the computed bone ages clustered at 15.5 years and 17.5 years. The system however still show improvements over the Phalanges in this age range but most likely reflect the fact that Phalanges have already fully developed at this age range and no longer have enough variability for bone age assessment.

Future Work

The current image segmentation techniques have a high failure rate (50 %), improvements can be made looking at current error cases. Common problems include mistaking the Ulna for the Radius and having an incomplete segmentation of the Radius. Adding improvements to the current image segmentation algorithm will decrease the failure rates and increase the accuracy of the segmentation. The features are highly sensitive to whether the demarcation of the epiphysis and metaphysis is captured therefore better segmentation will yield better feature values.

For CAD system to have accuracy over the entire 0-19 year age range, the radii information has to be integrated with the current system that uses the carpal and phalangeal information for Bone Age Assessment. How this will be done and to ensure maximum reliability and performance has yet to be determined. The difficulty lies in the fact that at lower age ranges the current Radii methodology will not work as a method to determine bone age, similarly the carpal data will not work on older children, therefore, a reliable method must be developed to cover the whole age range by efficiently aggregating information from each of the different regions.

Acknowledgements

The authors would like to thank National Institutes of Health for their support of this research as well as the Society of Imaging Informatics in Medicine for their continuing support for this project through their imaging informatics training grant.

REFERENCES

[1] W. Grelich, S. Pyle, “Radiographic Atlas of Skeletal Development of Hand Wrist,” Stanford, CA: Stanford University Press, 1959

[2] J.M. Tanner, R.H. Whitehouse, “Assessment of Skeletal Maturity and Prediction of Adult Height (TW2 Method),” Academic Press London, 1975.

[3] A. Gertych, E. Pietka, B.J. Liu, “Segmentation of Regions of Interest and Post-segmentation Edge Location Improvement in Computer-Aided Bone Age Assessment,” Pattern Anal Applic. April 2007;10 (2):115-123.

[4] A. Zhang, A. Gertych, B.J. Liu, “Automatic Bone Age Assessment for Young Children from Newborn to 7-Year-Old Using Carpal Bones,” JCMIG 2007

[5] A. Gertych, A. Zhang, J. Sayre, S. Pospiech-Kurkowska, H.K. Huang. Bone Age Assessment of Children using a Digital Hand Atlas, Comput Med Imaging Graph. 2007 Jun-Jul;31(4-5):322-31

[6] A. Zhang, A. Gertych, B.J. Liu, "Automatic Bone Age Assessment for Young Children from Newborn to 7-year-old using Carpal Bones," Comput Med Imaging Graph. 2007 Jun-Jul;31(4-5):299-310.

[7] A. Zhang, A. Gertych, B.J. Liu, H.K. Huang, S. Kurkowska-Pospiech, „Carpal Bone Segmentation and Features Analysis in Bone Age Assessment of Children," Proceedings of RSNA Conference, Chicago, pp.688 2005.

[8] A. Zhang, A. Gertych, B.J. Liu, H.K. Huang, "Data Mining for 'Average' Image Based on Phalangeal and Carpal Bone Features in a Large-scale Digital Hand Atlas," Proceedings of RSNA Conference, Chicago, 2006

[9] A. Zhang, S. Tsao, J. Sayre, A. Gertych, B.J. Liu, H.K. Huang, "Is Greulich and Pyle Atlas still a Good Reference for Bone Age Assessment?" Proceedings of SPIE Medical Imaging, February 2007.

[10] E. Pietka, A. Gertych, S. Pospiech, F. Cao, H.K. Huang, V. Gilsanz. Computer-assisted bone age assessment: image preprocessing and epiphyseal/metaphyseal ROI extraction. IEEE Trans. Med. Imaging. Aug 2001;20(8):715-729.

RadSearch: A RIS/PACS Integrated Query Tool

Sinchai Tsao*[a], Jorge Documet[a], Paymann Moin[a], Kevin Wang[a], Brent J. Liu[a]
[a]Image Processing and Informatics Laboratory, Department of Radiology,
Keck School of Medicine, University of Southern California,
Suite 601, 4676 Admiralty Way, Marina Del Rey, CA 90292;

ABSTRACT

Radiology Information Systems (RIS) contain a wealth of information that can be used for research, education, and practice management. However, the sheer amount of information available makes querying specific data difficult and time consuming. Previous work has shown that a clinical RIS database and its RIS text reports can be extracted, duplicated and indexed for searches while complying with HIPAA and IRB requirements. This project's intent is to provide a software tool, the RadSearch Toolkit, to allow intelligent indexing and parsing of RIS reports for easy yet powerful searches. In addition, the project aims to seamlessly query and retrieve associated images from the Picture Archiving and Communication System (PACS) in situations where an integrated RIS/PACS is in place -- even subselecting individual series, such as in an MRI study. RadSearch's application of simple text parsing techniques to index text-based radiology reports will allow the search engine to quickly return relevant results. -This powerful combination will be useful in both private practice and academic settings; administrators can easily obtain complex practice management information such as referral patterns; researchers can conduct retrospective studies with specific, multiple criteria; teaching institutions can quickly and effectively create thorough teaching files.

Keywords: NLP, PACS, RIS, Data Mining, Radiology, Radiology Reports

1. INTRODUCTION

1.1 Previous Work

Previous work has shown that a RIS database can be searched and radiology report text can be parsed and indexed. Desjardins and Hamilton showed that radiology reports can be extracted and indexed with minimal disturbance of the clinical workflow while complying with HIPAA and IRB requirements. Current trends in improving standards in Radiology Reporting as well as current practices of report voice recognition dictation using standard templates demonstrate predictability in the location of information within the format of the radiology report. Classification tools such as Index Medicus (IM), Medical Subject Headings (MeSH), International Classification of Disease (ICD), Systematized Nomenclature of Medicine (SNOMED), Unified Medical Language System (UMLS) and RadLex are built to classify large volumes of medical literature for easy searching. RadSearch's end goal is to apply the same concept to Radiology Reports within the RIS.

1.2 RadSearch Toolkit

The toolkit builds upon current functionalities in previous work by (1) parsing the radiology report intelligently into multiple clinically relevant subsections (2) linking the search results to PACS studies. This will enable administrative users of the toolkit to track referral patterns, perform receiver operating characteristic (ROC) analysis, and track billing codes for studies. The toolkit also allows researchers to easily perform large, complex retrospective PACS-based studies by querying for one or more study indications, findings, impressions, diagnostic codes or any other indexed criteria. Finally, the RadSearch toolkit allows educators to easily compile interesting cases and quickly assemble teaching files. In short, RadSearch will enhance radiological informatics support for three main groups: Administrators, Researchers, and Educators.

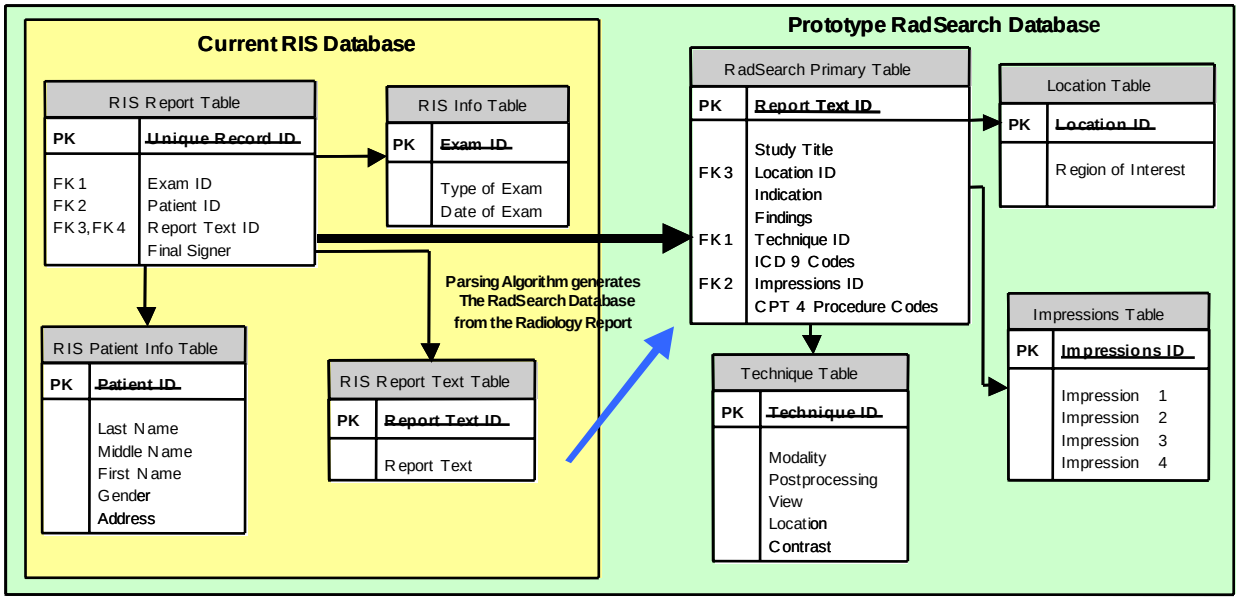

Fig. 1. Prototype Database Schema

2. METHODS

2.1 Natural Language Processing (NLP) -based Approaches

There have been numerous approaches to the data mining Radiology Text information in the RIS database. Taira et al. , Friedman et al. as well as other groups have approached the problem by classification for the specific type of Radiology Reports such as Chest X-rays or Mammograms using Natural Language Processing Techniques. Leximer, a NLP engine at Massachusetts General Hospital, went further to describe referral trends by classifying pathological findings. Nuance Inc. the company behind Leximer, also offers applies similar techniques to improve billing by NLP-based classification of billing codes. However, there have yet to be a tool that allow for generalized searches of the RIS database for teaching file generation or retrospective studies that also have PACS integrated image retrieval.

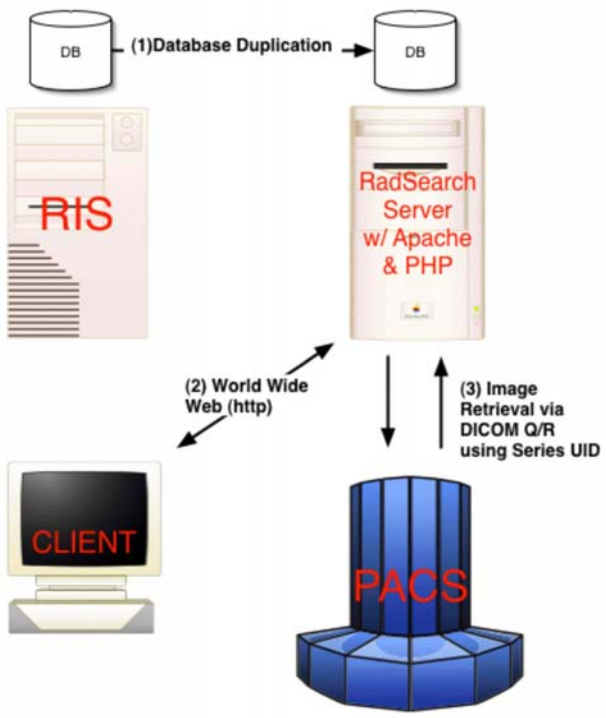

Fig. 2. Overall System Diagram.

2.2 Lexicons and Synonymity

Current work have also concentrated in including synonymity and uniformity to searches of Medical Literature (Journals and other publications) using thesauruses such as Unified Medical Language System or Radiological Society of North America (RSNA)'s RadLex (Radiology Lexicon) for Radiology. These lexicons can just as easily be employed in Radiology Report searches and can be achieved in two ways. (1) Using the lexicons as a pure thesaurus, therefore searching of one specific term will search for all related terms. (2) Pre-Classification of the text with specific unified key terms for specific sub-headings and convert all queries to use those key terms. The later approach has advantages with increased search speed and accuracy since the text data can be indexed using those key terms.

2.3 RIS/PACS Integration

Integrated PACS/RIS solutions have shown that it is possible to link RIS radiology reports back to PACS image series using the Series Instance UID portion of the RIS radiology report table. However, none of the current tools allow RIS data mining techniques with PACS integration.

3. RESULTS

3.1 System Architecture

The system is developed utilizing a SUSE linux box running a postgreSQL database as well as an Apache web server with PHP enabled. It employs current PHP scripting technology to perform database manipulations as well as to display results via a web interface. Advantages to using this

architecture is that server-side scripting languages such as PHP do not require a compilation step and have an easy to use interface with html for displaying results on the web. PACS connections will be run using the open-source DCMTK toolkit executables called by PHP scripts.

3.2 Radiology Text Report Parsing

The current system has links from the RIS database to a text file that contains the Radiology reports. Our goal is to breakdown the RIS text into broad fields such as: Study Title, Location, Indications, Findings, Technique and Impressions. We can then index the database based on these subsections. This allows the users to make more precise searches based on the aforementioned fields. An initial parsing algorithm employs a simple method of detecting each of the subtitles and parsing the text into each of the subsections. Subsections not detected is left null. The detected values are then populated into the database and indexed for expedited searching. The PHP scripts will handle both the retrieval of the text file containing the Radiology Text report, parsing, as well as population back into the database using the proposed schema in figure 1. Future advanced Natural Language Processing algorithms can be applied to enhance and improve the parsing step further and, thus improve the overall performance of the toolkit.

3.3 Forming Queries

Queries to the system is formed by specifying key terms for each of the subfields indicated in figure 1. This can include patient demographic data as well as information contained within the Radiology Report. The results will then be returned in the form of a list of Radiology Reports that matched that query along with links to related images.

3.4 Integration with PACS and as a Study Management Tool (SMT)

PACS integration comes in when the user decides to view images related to the desired Radiology Report. PACS images are query-retrieved and displayed in a presentation state (JPEG) as specified in the DICOM convention for WADO (Web Access for DICOM Objects). The system can also function as a study management tool that allows the images to be moved via DICOM standards to other DICOM nodes for CD burning, display on a PACS workstation, etc. This is done via the Series Instance UID attached to the desired Radiology Report. The Series Instance UID allows the RadSearch server to query-retrieve all series images from the PACS for the user or initiate a DICOM C-MOVE to move images to another DICOM node.

3.5 System Operation Considerations

To minimize disruption of the clinical RIS system, the system database is duplicated to a postgres SQL database on the RadSearch Server. The system will have weekly duplication sessions during non-peak times such as Sunday nights. PACS connections and query-retrieval will be based on an as-needed basis and should not effect the current clinical operations of the PACS system. Early uses of the system are limited to teaching file generation. IRB approval for use as a retrospective clinical research tool will be implemented when the system has been tested for reliability. User authentication as well as usage logging is also implemented to ensure HIPAA and IRB compliance.

4. DISCUSSION

4.1 RadSearch versus other RIS Data Mining Approaches

RadSearch's approach differs from the other approaches in two folds (1) RadSearch includes PACS integration (2) RadSearch allows for higher specificity in the Radiology Report by parsing the report into subsections. PACS integration is essential as it allows the user to preview the desired images on the same interface as the RIS search engine. Previously, the user would have to obtain the patient name or ID from the search interface and search for it within the PACS via a PACS workstation before being able to determine if those images are what the user is looking for. With PACS integration, RadSearch will allow the user to seamlessly preview the images together with the list of potential Radiology Reports.

Ability to search within specific fields is also important, as the appearance of a term in one subsection of the report may have different meaning than if it appeared within another subsection. Therefore, this ability to search within subsections will improve specificity, accuracy and quality of the user query.

4.2 Future Work

We intend RadSearch to be a platform for future work. The next obvious step is to use a Lexicon to build a classification engine so as to allow for synonimity in searching. We plan to integrate the RadLex lexicon system, since it is build specifically for Radiology. Other possibilities include classification of findings, techniques and indications in the examinations to allow for statistical data mining.

REFERENCES

[1] Bashyam, V. and R.K. Taira, Indexing anatomical phrases in neuro-radiology reports to the UMLS 2005AA. AMIA Annu Symp Proc, 2005: p. 26-30.

[2] Bashyam, V. and R.K. Taira, A study of lexical behaviour of sentences in chest radiology reports. AMIA Annu Symp Proc, 2005: p. 891.

[3] Ceusters, W., P. Spyns, and G. De Moor, From natural language to formal language: when MultiTALE meets GALEN. Stud Health Technol Inform, 1997. **43 Pt A**: p. 396-400.

[4] Ceusters, W., P. Spyns, and G. De Moor, From syntactic-semantic tagging to knowledge discovery in medical texts. Int J Med Inform, 1998. **52**(1-3): p. 149-57.

[5] Cho, P.S., R.K. Taira, and H. Kangarloo, Syntactic parsing of medical reports using evolutionary optimization. AMIA Annu Symp Proc, 2005: p. 920.

[6] Desjardins, B. and R.C. Hamilton, A practical approach for inexpensive searches of radiology report databases. Acad Radiol, 2007. **14**(6): p. 749-56.

[7] Friedman, C., et al., A general natural-language text processor for clinical radiology. J Am Med Inform Assoc, 1994. **1**(2): p. 161-74.

[8] Hripcsak, G., et al., Use of natural language processing to translate clinical information from a database of 889,921 chest radiographic reports. Radiology, 2002. **224**(1): p. 157-63.

[9] Hripcsak, G., et al., Unlocking clinical data from narrative reports: a study of natural language processing. Ann Intern Med, 1995. **122**(9): p. 681-8.

[10] Hsiao, C.H., et al., Developing a medical image content repository for e-learning. J Digit Imaging, 2006. **19**(3): p. 207-15.

[11] Huang, Y. and H.J. Lowe, A grammar-based classification of negations in clinical radiology reports. AMIA Annu Symp Proc, 2005: p. 988.

[12] Huang, Y. and H.J. Lowe, A novel hybrid approach to automated negation detection in clinical radiology reports. J Am Med Inform Assoc, 2007. **14**(3): p. 304-11.
[13] Huang, Y., et al., Improved identification of noun phrases in clinical radiology reports using a high-performance statistical natural language parser augmented with the UMLS specialist lexicon. J Am Med Inform Assoc, 2005. **12**(3): p. 275-85.
[14] Jakobovits, R., et al., Enabling clinicians, researchers, and educators to build custom web-based biomedical information systems. Proc AMIA Symp, 2001: p. 279-83.
[15] Kahn, C.E., Jr. and C. Thao, GoldMiner: a radiology image search engine. AJR Am J Roentgenol, 2007. **188**(6): p. 1475-8.
[16] Pyrros, A., et al., A Bayesian approach for the categorization of radiology reports. Acad Radiol, 2007. **14**(4): p. 426-30.
[17] Reiner, B.I., N. Knight, and E.L. Siegel, Radiology reporting, past, present, and future: the radiologist's perspective. J Am Coll Radiol, 2007. **4**(5): p. 313-9.
[18] Spyns, P., Natural language processing in medicine: an overview. Methods Inf Med, 1996. **35**(4-5): p. 285-301.
[19] Spyns, P., et al., Medical language processing applied to extract clinical information from Dutch medical documents. Medinfo, 1998. **9 Pt 1**: p. 685-9.
[20] Szolovits, P., Adding a medical lexicon to an English Parser. AMIA Annu Symp Proc, 2003: p. 639-43.

Development and Deployment of a Comprehensive Electronic Patient Record

Marco A. Gutierrez
Heart Institute, University of Sao Paulo, Medical School
Sao Paulo, Brazil
marco.gutierrez@incor.usp.br

Sergio S. Furuie
Heart Institute, University of Sao Paulo, Medical School
Sao Paulo, Brazil
sergio.furuie@incor.usp.br

Fabio A. Pires
Heart Institute, University of Sao Paulo, Medical School
Sao Paulo, Brazil
fabio.pires@incor.usp.nbr

***Abstract*— The goal of the current study is to describe the experience of the Heart Institute (InCor) in the implementation of a patient-oriented Electronic Patient Record (ePR) integrated with the Picture Archiving and Communication System (PACS) in an open-source three-tier architecture. The system was designed in modules that permits patient admission, discharge and transfer (ADT), registration of medical activities, registration of diagnoses and therapy, order entry and access of all patient data, including vital signals, images and lab tests. The modules are integrated in a single Web-based application allowing the easy and fast navigation through the modules. In order to maintain the quality of patient care in an efficient and cost-effective manner, thin clients workstations in a Linux environment were used. To access the patient information users have to perform an authentication procedure that uses LDAP protocol, which also defines a profile to the users. The system is fully integrated to the InCor´s PACS, allowing instant access to the image database from applications that requires this information, such as diagnostic reports. For displaying the images a Java DICOM viewer was implemented. On the server side, a Java DICOM server was designed to allow communication with all DICOM modalities.**

Keywords- Electronic Patient Record, Interoperability, Medical Images, Modeling

I. INTRODUCTION

The integration of medical images as part of the Electronic Patient Record (ePR) can be defined as a set of relevant patient information stored in digital format that allows adequate medical assistance delivered to the patient even in distinct places and scenarios [1]. The pursuit of an efficient and comprehensive ePR has stimulated several groups [2,3,4,5,6,7]. The potential advantages of an ePR over a traditional paper-based patient record involve distributed and simultaneous access, high availability, fast information retrieval, better quality, higher confidence. The capability to establish access control policy, including audit trail and digital signatures, assures higher level of privacy than conventional paper-based records. Furthermore, the inclusion of medical images and the integration of data from different systems make possible a more comprehensive ePR.

The Heart Institute (InCor) is a medium to large hospital specialized in cardiovascular diseases with nearly 600 beds. It is also an educational institution that attends more than 280,000 outpatients and performs more than 4,300 complex surgeries per year. In the last few years, InCor has been committed to the goal of integrating all relevant information within the institution. As part of this strategy, InCor has successfully created a system for transmission, archiving, retrieval, processing and visualization of Medical Images and created also a Hospital Information System (HIS) that stores the institution administrative and clinical information. These integrated subsystems form InCor's Electronic Patient Record (ePR). InCor is also facing a challenge that is becoming very common in the healthcare field: the need of exchanging information among different institutions. Since InCor is one of the six institutes of the University of São Paulo Medical School Hospital (HC) and each institute has its own information system, exchanging information among the institutes is also a very important issue. This work describes the experience in the effort to develop a functional and comprehensive ePR, which includes lab exams, images (static dynamic and 3D), clinical reports, documents and even real-time vital signals. This paper addresses also the integration of distributed and heterogeneous ePR.

II. MATERIAL AND METHODS

Beyond a simple interchange of data, we need to deal with a more complex level of integration. The desired level of interoperability can be achieved through the use of standards such as: UML - Unified Modeling Language [8]; DICOM - Digital Imaging and Communications in Medicine [9] for archiving and communication of medical images; CORBA - Common Object Request Broker Architecture [8] for heterogeneous and distributed objects; PIDS - Patient Identification Service [10]; COAS - Clinical Observation Access Service [11] and CIAS - Clinical Images Access Service [12].

A key point in the development is the modeling of patient data, including medical images as part of the global patient information. We developed an object-oriented representation of the whole clinical image domain and its integration to our HIS. Representation of images is based on DICOM3 standard for communication and storage of medical images. This standard incorporates associated data such as identification of the patient, performed study, image acquisition context and image interpretation findings. DICOM3 standard describes a patient-oriented model that is well suited to follow all information related to a patient. However, as the main purpose of the project is to allow a higher level of complexity on searches, we expanded the model proposed on the standard in

order to fulfill the requirement of retrieving medical images from any attribute. The new model allows the representation of different image modalities, integration of these modalities in a same study, investigation of similar images from different patients and contextual visualization and processing of clinical images [13].

Another important issue is that ePR is constantly evolving; therefore the architecture should be flexible enough to accommodate new functionalities and technologies.

The implementation was based on client-server architecture via Web servers connected to several databases and subsystems: HIS, image (PACS) database, document database, signal monitors and resource access decision (RAD) subsystem (fig. 1).Clinical and Administrative Data

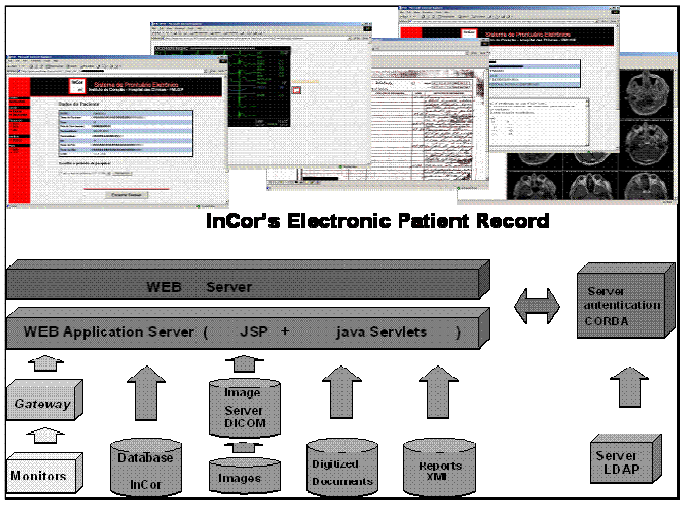

Figure 1. Overview of proposed integrated Electronic Patient Record

A. *Clinical and Administrative Data*

The Hospital Information System (HIS) has been developed in a three-tier architecture using Oracle 9i as the database layer, Oracle Forms as the application layer and WEB browsers at the user layer.

The structured information of the HIS is formed from several clinical information modules that permit patient admission, discharge and transfer (ADT), registration of medical activities, registration of diagnoses and therapy, order entry and access to all patient data, including vital signals, images and lab tests. The ADT module collects patient demographic and insurance data, allocates room and bed and registers medical procedures and diagnosis. After a patient is admitted and a room and a bed are allocated, all main patient data is available to the medical staff through a concise graphical interface [7]. The billing module permits that the patient data and the specification of all procedures are transferred to external information systems including the Brazilian Public Health System (SUS) and the insurance companies. The data is transferred electronically and provides billing information based on standardized tables about patient demographics, insurance and performed procedures. The HIS is integrated to the PACS in three points (Fig. 2): a) modality worklist to schedule exams; b) medical reports tools; and c) visualization of the images. The worklist server allows the integration of all exams with patient clinical and administrative information. The Medical Report module allows the authorized physicians to design the layout of the report, based on a drag and drop mechanism. The medical reports are associated to the medical images inside the HIS and are available for visualization in the iView, together with the complete set of images. The physician with proper authorizations can then select images that best illustrate the report. The viewer is called from inside the HIS, transparently for the user, since the interface is the same (WEB pages) in spite of different technologies of the implemented PACS and HIS. When the clinician wants to see the images related to a patient or exam, a new browser window is opened pointing to a Web page that is part of the PACS system. This page creates a JNLP (Java Network Launching Protocol) file that calls an external Java application (the viewer) that presents the images to the user. The performance of the joint work between PACS and HIS depends on the servers, network and processing capabilities of viewing machine. A typical figure for a network of 100 Mbit/s without server limitation, and a Pentium IV (3GHz, 512 MB of RAM) as viewing machine, is a rate of 15 frames per second for cineangiographic images.

The ePR currently stores more than 11 GB/day of data and receives more than 12,000 hits per day.

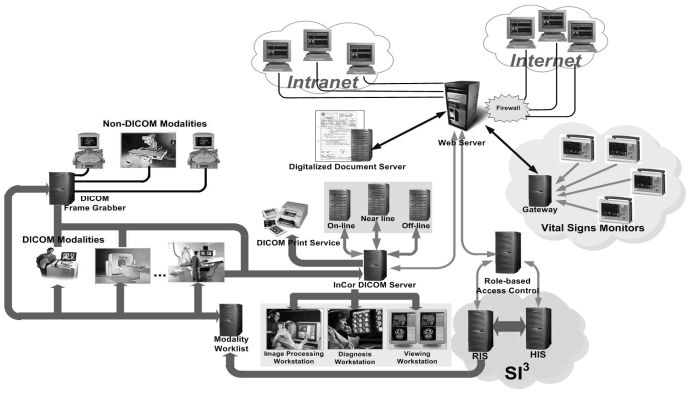

Fig. 2. Overview of proposed integrated Electronic Patient Record

B. *Medical Image Data*

The proposed image data model is a specialization of the Clinical Information Model, for the particular case in which the events involve the generation or manipulation of medical images. It is also described in details in [13].

Our PACS (Picture Archiving and Communication System) is based on DICOM3 standard and all image generators send their images to our institutional DICOM servers. The DICOM servers archive the images in the storage subsystem and update the image database and HIS database. Currently, the institution has the following medical scanners, most of them are DICOM compliant:

- Five (5) CATH labs (hemodynamic): 3 of them are ACRNEMA, whose data are converted to DICOM;
- Two (2) Magnetic Resonance
- Two (2) spiral CT;
- Nine (9) Nuclear Medicine scanners, including 1 PET
- Seventeen (17) ultra-sound/echocardiographs, whose video data are acquired and converted to DICOM.

The proposed architecture for storage combines online, nearline and offline modes in an asynchronous flow of data [14]. The flow is controlled by a manager software based on information archived in a database. The online storage is based on a RAID-5 magnetic disk system with 4 TB (TeraBytes) of capacity. The access time is clinically adequate (less than 3s) using fast networking (fast Ethernet and Gigabit Ethernet.) For the nearline storage we have used a jukebox of DLT (Digital Linear Tapes) with 48 slots and 4 drives with 3.5 TB of storage capacity. The offline storage is simply the tapes on the shelves.

We have also developed DICOM viewer in java that is able to handle dynamic images at 30 frames per second.

C. Real-time Vital Signals

Real-time vital signals, such as EKG and respiration of patients in surgery and intensive care are obtained via patient monitors (Siemens, models SC7000 and SC6002XL) able to communicate with other computerized systems via HL7 protocol (Health Level Seven) [16]. Since the data from bed monitors are integrated to EPR, vital signals can be viewed on-line by authorized users via an in house developed web application and can also be accessed through wireless handheld devices. All communication between the network of monitors and the hospital network is carried out through an implemented HL7 server (Fig. 3) that integrates the data from the monitors with the HIS. For security and performance reasons, there is no direct routing of TCP/IP packages between the two subnetworks (general hospital and monitors). The server is then the only bridge between the two systems and acts as an application gateway that feeds the monitors with basic information such as patient demographic data and also presents specific information such as clinical laboratory results.

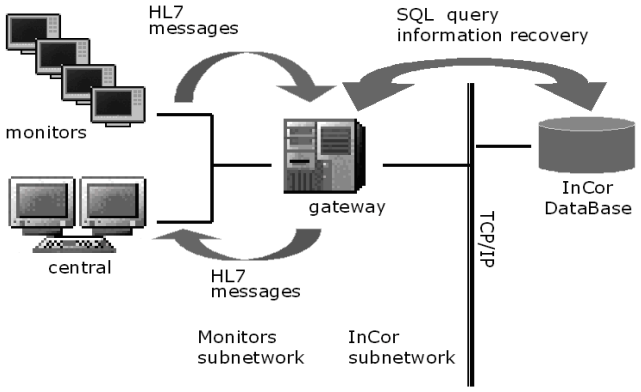

Fig. 3. Scheme for the integration of vital signals to the system

D. Integrating Distributed and Heterogeneous ePR

A single person produces a huge amount of information during his/her life. Having this information available in a way that it could be easily retrieved is important not only for the patient, but also for research purposes. Since each Medical Institution usually has its own information system, which uses a particular combination of database management system, programming language, operational system, data structure and hardware platform, the task of retrieving the complete medical record for a single patient is highly complex. Even inside a single healthcare institution, information is commonly distributed over different departmental systems, which also have a particular combination of software and hardware platforms. This inherently heterogeneous environment makes the task of integrating healthcare information a challenge to be met.

The integration of distributed and heterogeneous systems can be attained with the use of middleware objects that work as interfaces between different systems. We have utilized middleware based on CORBA [8], since it allows integration of a large variety of heterogeneous environments and it is also an open international standard. However, CORBA is not enough to deal with clinical information exchange. OMG has defined some services for Healthcare area. Specifically, we are using three of them: PIDS, COAS and CIAS.

The proposed architecture is composed by four basic services (middleware), as shown in figure 3. The Patient Identification Service (PIDS) retrieves patient demographic information. This service provides a standard method for locating person identifiers and their associated records across facilities and enterprises. The Clinical Observation Access Service (COAS) is a mechanism for retrieving clinical observations data from information repositories and applications. The Clinical Images Access Service (CIAS) retrieves medical images. This service permits search of images of a single patient or based on images characteristics, as body part, equipment, modality, and so on. The Image Processing Service contains several image processing methods, as blurring, zooming, segmentation, etc. Clients of the distributed system, that could be running in any software and hardware platform, can access these services through CORBA interfaces.

E. Access Control

Designing proper models for authorization and access control for the electronic patient record is essential to wide scale use of the ePR in large health organizations. We have proposed a contextual role-based access control (RBAC) authorization model for ePR [17]. The implemented RBAC regulates user's access to computers resources based on organizational roles [18] and extends the proposed National Institute of Standards and Technology (NIST, USA) RBAC reference model. A contextual authorization uses environmental information available at access time, like user/patient relationship, in order to decide whether a user is allowed to access an ePR resource. This model was implemented using Lightweight Directory Access Protocol (LDAP), Java programming language and the CORBA

Security Service and Resource Access Decision Facility. With these open and distributed standards, heterogeneous ePR components can request user authentication and access authorization services in a unified way across multiple platforms.

The proposed model is consistent with the Health Insurance Portability and Accountability Act of 1996 (HIPAA) recommendation to regulate access to patient health information. The run-time components of contextual RBAC authorization model is formed by a set of administrative tools, a contextual RBAC authorization server and the implementations of context interfaces.

The authorization model representation was stored in a hierarchical directory service, with access and data scheme description standardized by LDAP protocol [19]. Administrative tools allow privileged users to manage the ePR authorization policies stored at LDAP server. The contextual RBAC authorization implementation was integrated into a Java/CORBA server. It is in charge of user authentication, session management and access authorization decision. Authentication and session management are done through implementations of **PrincipalAuthenticator** and **Credentials** standard interfaces of the CORBA Security Service [20]. Access authorization decision service is available through an implementation of **PolicyEvaluator** standard interface of the Resource Access Decision Facility [21] from Object Management Group. Contexts are implemented in Java as dynamic libraries loaded at run-time using the Java Extension Mechanism.

III. RESULTS

Currently, user authentication and access decision services has been used daily at InCor. The process for deployment of our solution was based on the following steps: definition of roles; load of user's profiles from personnel software into LDAP server and assignment of respective roles; creation and use of authorizations by the applications that compose the ePR. So far 1900 users have been registered and assigned to some of 51 professional roles. Furthermore, complex access control logic can stay outside the application, though considering the necessary context to grant or deny permission. Thus, changes in authorization logic do not imply changes in application code. Another benefit is the conflict policy resolution that considers the need to know principle. Conflicts can be determined according to the authority and responsibility defined to each role via associated authorizations. Only the actions that configure real conflicts of interests are forbidden to a user with conflicting roles assigned. Finally, automatic role activation leaves the user free from explicit selection of a role, making RBAC transparent to final users.

In terms of volume, since mid of 2000, more than 10 TB of DICOM images have been stored and integrated using the proposed architecture. The ePR stores more than 5 GB/day of data and presents more than 1400 hits per day. The proposed storage subsystem allows six months of visibility for rapid retrieval (online mode) and more than two years for automatic retrieval using the DLT jukebox.

The distributed access of all integrated data is carried out via web browsers through our network with around 1000 terminal clients. The clients can be conventional microcomputers or LINUX thin-client.

IV. DISCUSSION

Implementing a comprehensive ePR is a huge challenge that several centers in the world are pursuing. We described our experience and our vision about ePR. It includes several important and relevant pieces of information, but it is not comprehensive enough yet. Some features have not been integrated such as material control. However, the proposed model allows the representation of any medical document, as well as procedures, guidelines and clinical observations.

Realistically, a common patient has records in several ePRs. It is clear the importance of interoperability among distributed and heterogeneous ePR to collect distributed information about a specific patient. This is a very complex issue that we are also addressing. We are proposing CORBA services such as COAS and CIAS for integration of heterogeneous and distributed systems. We strongly believe that the use of non-proprietary standards is the path that will make a comprehensive Electronic Patient Record a reality. The proposed approach is based on standards such as CORBAmed specifications, DICOM and XML.

ACKNOWLEDGMENT

This work has been partially supported by Grant #2436 of the National Network for Education and Research (RNP), the National Council for Scientific and Technological Development (CNPq), Grant No. 300499/2005-1 and the Zerbini Foundation.

REFERENCES

[1] Liu G.C., Cooper JG., Schoefflerb K.M.; Hammond E. (2001). Standards for the Electronic Health Record Emerging from Health Care's Tower of Babel . Proceedings of AMIA 2001.

[2] Grimson J. (2001) Delivering the electronic healthcare record for the 21st century. International Journal of Medical Informatics, 64: 111-127.

[3] Berg M. (2001) Implementing information systems in health care organizations: myths and challenges. International Journal of Medical Informatics, 64: 143-156.

[4] Katehakis D, Lelis P, Karabela E, Tsiknakis M, Orphanoudakis S: (2000) An Environment for the Creation of an Integrated Electronic Health Record in HYGEIAnet, the Regional Health Telematics Network of Crete. TEPR 2000, Your Connection to Electronic Healthcare, San Francisco, CA, May 9-11, 2000, Vol. 1, pp. 89-98.

[5] Cimino,J.J., Li,,J., Mendonca,E.A. (2000) An Evaluation of Patient Access to Their Electronic Medical Records via the World Wide Web., Proc. of 19th Symposium on Computer Applications in Medical Care.

[6] Adelhard, K Holzel, D., Uberla, K. (1999) Design elements for a computerized patient record, Methods. Inf. Med. 38 187–193.

[7] Tachinardi U, Furuie SS, Bertozzo N, Moura L, Gutierrez MA, Melo CP. (1995). Hypermedia patient data retrieval and presentation through www. Proc. of 19th Symposium on Computer Applications in Medical Care: 551-555.

[8] OMG. (1996) Object Management Group, Manual 1996 http://www.omg.org.

[9] ACR-NEMA (1988) American College of Radiology, National Electrical Manufacturer Association, ACR-NEMA Digital imaging and communication standard: version 2.0, NEMA standards publication N0. 300-1988.

[10] OMG (1998a) Person/Patient Identification Service. February http:// www.omg.org/pub/docs/corbamed/96-11-02.rtf.

[11] OMG (1999a) Clinical Observation Access Service Final. http:// www.omg.org/cgi-bin/doc?corbamed/99-03-25

[12] OMG (2000a) Clinical Image Access Service Revised Submission. http://www.omg.org/cgi-bin/doc?corbamed/00-02-01

[13] Nardon, F.B.; Rebelo, M.S., Furuie, S.S., Moura, L. (2000) Modeling the Electronic Patient Record- The Heart Institute of São Paulo Case. Toward an Electronic Patient Record (TEPR'2000) Proceedings, San Francisco, p 150 164.

[14] Furuie SS, Bertozzo N, Yamaguti M., Gutierrez M.A.(2002) A Flexible Storage Architecture For Large PACS. IEEE Computers in Cardiology ,September 22-25, 2002, Memphis, USA

[15] Furuie SS,Tachinardi U ,Bertozzo N, Gazetta M ,Ramos J A, Teixeira JC. (2001) Digitized Paper-Based Medical Records as Part of a HIS/PACS. Radiology, 221 (P) Fascículo: suppl. RSNA 2001:761.

[16] Health Level Seven. (1996) HL7 Version 2.3 Specification. 1996.

Development of a mobile HIS/PACS workstation to assist critical cardiac patients in an intensive care unit

Marco A. Gutierrez[*a], Idagene A. Cestari[b], Gina Hamamoto[a],
Simão Bacht[a], Marina S. Rebelo[a], João E.M.M. Silva[a], Silvia G. Lage[c]
[a]Informatics and [b]Bioengineering Divisions and [c]Intensive Care Unit, Heart Institute,
University of Sao Paulo Medical School, São Paulo, Brazil

ABSTRACT

The current study describes the experience in the implementation of a mobile HIS/PACS workstation to assist critical cardiac patients in an Intensive Care Unit (ICU). Recently, mobile devices connected to a WiFi network were incorporated to the Hospital information System, providing the same functionalities of common desktop counterpart. However, the use of commercially devices like PDAs and Pocket PCs presented a series of problems that are more emphasized in the ICUs 1) low autonomy of the batteries, which need constant recharges; 2) low robustness of the devices; 3) insufficient display area to show medical images and vital signals; 4) data entry remains a major problem and imposes an extra time consumption to the staff; 5) high cost when fully equipped with WiFi connection, optical reader to access bar codes and memory. To address theses problems we developed a mobile workstation (MedKart) that provides access the HIS and PACS systems, with all resources and an ergonomic and practical design to be used by physicians and nurses inside the ICU. The system fulfills the requirements to assist, in the point-of-care, critical cardiac patients in Intensive Care Units.

Keywords: Mobile computing, point of care, pacs, electronic patient record.

1. INTRODUCTION

The health care information at the point of care (POC) is a universal need by any health care professional. The advance in mobile computing technologies and applications such as medical reference, drug references, guide lines and patient information can improve the assistance at POC and the information needs of the health care professional at this point. The adoption of mobile computing adds value to clinical practice by giving clinicians access to patient clinical information where and when the information is needed. Moreover, such technology can improve the exchange of information between health care professionals, reducing medical errors due to inadequate access to clinical data and providing clinical decision support at the POC.

In the last years, the use of mobile computing has become an important tool in health care and has grown in popularity between health care professionals. Lu et al. [1] review most of the contributions in this area and classify the applications in five domains: decision support, administrative support, documentation, professional activities and education or research.

The decision support applications include access to patient information, medical calculation, drug reference electronic textbooks, real-time information access, diagnostic data management and laboratory result retrieval. The administrative support applications include scheduling, billing, charge capturing and tracking and reimbursement. Drug reference was the most important use of PDA in nursing [2]. Schneider reported use of a handheld computer in an emergency nursing setting [3]. Silva et al. reported the use of PDAs to document pharmacist cognitive services and estimate potential reimbursement [4]. Lynx et al. described the implementation of a PDA-based pharmacist intervention system in a hospital [5].

Despite of the growing adoption of mobile computing in health care, there are major complaints about personal digital assistants and barriers to their use. The most important barriers in this technology are: 1) Personal factors - large fingers

[*] Correspondence: marco.gutierrez@incor.usp.br; phone +551130695385; fax +551130695311; Heart Institute (InCor), University of Sao Paulo Medical School, Av. Dr. Eneas de Carvalho Aguiar, 44, CEP-05403-000, São Paulo, BRAZIL

(too big for the buttons) and poor eyesight (cannot read the small fonts), memory problem (forgot to carry the device), comfort with technology, comfort with the device and dependency or over-reliance on the device; 2) Ineffectiveness - Brody's study showed that documenting pharmacists' clinical interventions on PDAs did not appear to be more effective or efficient than documenting on paper [6]; 3) Non-integrated Electronic Patient Records (ePRs) - Most medical facilities do not have integrated ePRs. Ideally, the handheld system should be integrated with the hospital's electronic patient record system, to allow direct entry and access of patient data [7]; 4) Data entry – The common mechanism with graffiti is unintuitive and not easy to use [8,9]; 5) Physical design - Size, weight, limited battery power and small screen: most users think that PDAs should be smaller and lighter but have the largest screen possible [8,9]; Low robustness devices - Fears of breaking the device make some users limit their uses to avoid damaging it [8,9]; Security and bandwidth - An integrated input/output device with data encryption at both ends of transmission should be developed to meet security needs. Broadband wireless access is needed for faster transmission [10];

The goal of the current study is to describe the experience of the Heart Institute (InCor) in the implementation of a mobile HIS/PACS workstation to assist critical cardiac patients in an Intensive Care Unit (ICU). The system was developed as part of our efforts in to construct a complete HIS/PACS solution to permit patient admission, discharge and transfer (ADT), registration of medical activities, registration of diagnoses and therapy, order entry and access of all patient data, including vital signals, images and lab tests. Recently, mobile devices connected to a WiFi network were incorporated to the Hospital System providing the same functionalities of its common desktop counterpart. However, the use of commercially devices like PDAs and Pocket PCs presented a series of problems. These problems are more emphasized in ICUs, where patients are in critical conditions and decisions must be taken at the bed-side.

Based on the lessons learned using commercial mobile devices we developed a mobile kart (MedKart) with all resources, such as a, terminal connected to the WiFi network, 15" LCD monitor, membrane keyboard to simplify cleaning, optical reader to access bar code information, extra batteries to provide up to 6 hours of continuous use and an ergonomic and practical design to be used by physicians and nurses inside the ICU.

2. METHODOLOGY

2.1. Development and deployment of a HIS and PACS systems

InCor is a medium to large specialized hospital in cardiovascular diseases with nearly 600 beds. It is an educational institution that attends more than 280,000 outpatients and performs more than 4,300 complex surgeries per year.

The Hospital Information System (HIS) has been developed in a three tier architecture using Oracle 10g as the database layer, Oracle Forms as the application layer and WEB browsers at the user layer. The structured information of the HIS is formed from several clinical information modules that permit patient admission, discharge and transfer (ADT), computerized provider order entry (CPOE), registration of medical activities, registration of diagnoses and therapy, order entry and access to all patient data, including vital signals, images and lab tests. The ADT module collects patient demographic and insurance data, allocates room and bed and registers medical procedures and diagnosis. After a patient is admitted and a room and a bed are allocated, all main patient data are available to the medical staff through a concise graphical interface. The billing module permits that the patient data and the specification of all procedures is transferred to external information systems including the Brazilian Public Health System (SUS) and the insurance companies. The data is transferred electronically and provides billing information based on standardized tables about patient demographics, insurance and performed procedures.

In order to provide proper support for clinical decisions and therapies, there are several medical equipments that generate images. Currently, the institution has the following medical scanners, most of them DICOM [12] compliant:

- Five (5) CATH labs (hemodynamic): 2 are DICOM compliant and 3 are ACRNEMA 2.0, whose data are converted to DICOM and properly stored;
- Two (2) Magnetic Resonance;
- Two (2) spiral CT;
- Nine (9) Nuclear Medicine scanners, including 1 PET;
- Seventeen (17) ultra-sound/echocardiographs, whose video data are acquired and converted to DICOM (developed prototype is in assessment).

A Picture Archiving and Communication System (PACS) was built based on the DICOM 3.0 standard [12] and in WEB technology. The PACS is completely integrated with HIS using the DICOM Modality Worklist [12] specification in a manner that patient name and identification are performed only in the ADT module. This workflow avoids any mistake in the patient identification during the process involved in the image acquisition.

The PACS architecture is composed of two parts: DICOM servers, responsible for the integration of the image acquisition equipments across the hospital and a WEB interface for management and retrieval of the images. The management via Intranet gives flexibility to associate new equipments and allows monitoring of the services. The recovery of images allows that any authorized user (in the Intranet) have access to the images even without a DICOM client, only using a WEB browser and the Java Runtime environment [11]. The DICOM Java viewer, called iView (Figure 1), was developed at InCor and is easily integrated to the system [13] using Applet or WebStart technologies. When an image study is opened, the iView groups the images in series according to acquisition parameters, modality, and anatomy. Each series is shown as a thumbnail. In case of images from dynamic acquisition process, the thumbnails are also dynamic, showing the series in animation mode. To open a series, the user applies a double click over the desired series which is downloaded to the client computer, and then made available for online viewing and analysis. For dynamic series the images are shown in animation mode, offering cine loop viewing with speed control, forward/backward play, pause and stop functions. The iView offers support for all image formats.

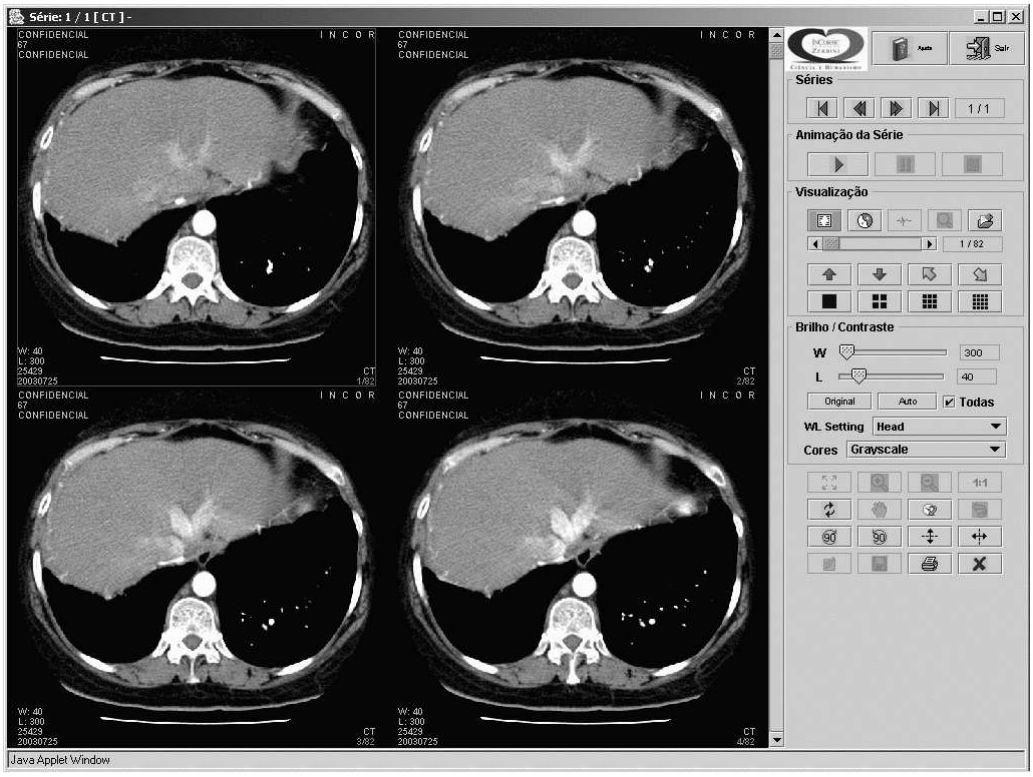

Figure 1 – The Java DICOM Image Viewer

Real-time vital signals, such as EKG and respiration, of patients in surgery and intensive care unit are obtained via special patient monitors (Siemens, models SC7000 and SC6002XL) that are able to communicate with other computerized systems using HL7 protocol (Health Level Seven) [14]. All communication between the network of monitors and the hospital network is carried out through an implemented HL7 server that integrates this type of data with the HIS. Since the data from bed monitors are integrated to EPR, vital signals can be viewed on-line by authorized users via an in house developed web application. All communication between the network of monitors and the hospital network is carried out through an implemented HL7 server (Figure 2) that integrates the data from the monitors with the HIS. For security and performance reasons, there is no direct routing of TCP/IP packages between the two sub-networks (general hospital and monitors). The server is then the only bridge between the two systems and acts as an application gateway that feeds the monitors with basic information such as patient demographic data and also presents specific

information such as clinical laboratory results. Figure 2 depicts the main elements involved on the integration of vital signal monitors, which can also be accessed through mobile devices.

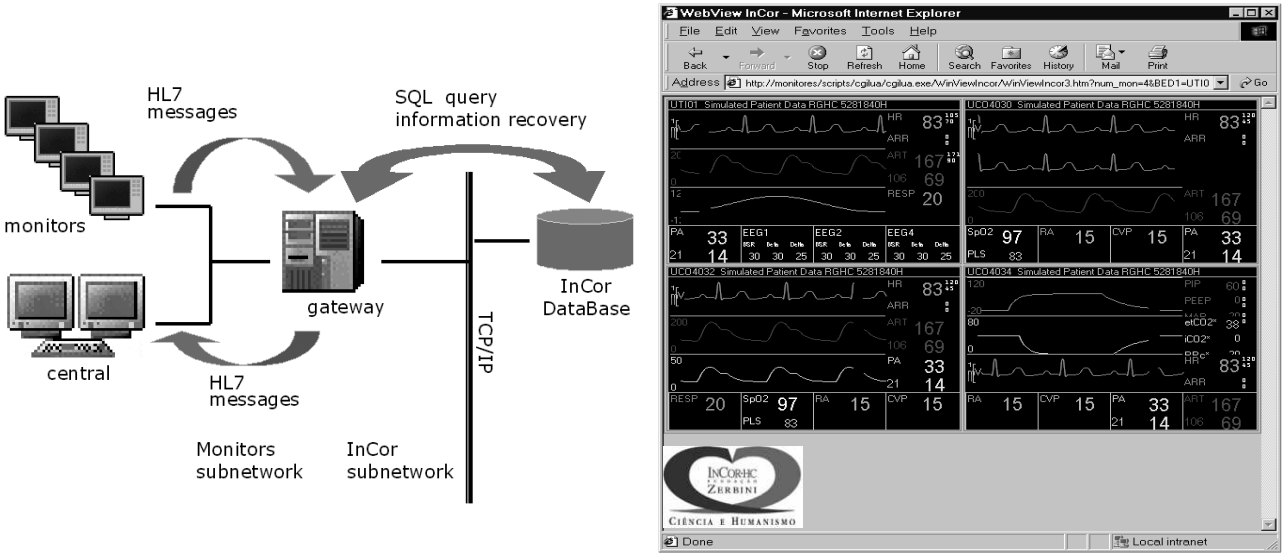

Figure 2 – The main elements for the integration of vital signals to the system (left) and a typical screen showing the signals in real time on the ePR (right)

2.2. User Access and Control

Designing proper models for authorization and access control for the electronic patient record is essential to wide scale use of the ePR in large health organizations. A contextual role-based access control (RBAC) authorization model for EPR was proposed [15]. The implemented RBAC regulates user's access to computers resources based on organizational roles [16]. A contextual authorization uses environmental information available at access time, like user/patient relationship, in order to decide whether a user is allowed to access an ePR resource. This model was implemented using Lightweight Directory Access Protocol (LDAP), Java programming language and the CORBA Security Service and Resource Access Decision Facility. Moreover, all data stream is encrypted with the Security Socket Layer (SSL) version 3.0 protocol. With these open and distributed standards, heterogeneous ePR components can request user authentication and access authorization services in a unified way across multiple platforms.

The proposed model is consistent with the Health Insurance Portability and Accountability Act of 1996 (HIPAA) recommendation to regulate access to patient health information. The run-time components of contextual RBAC authorization model are formed by a set of administrative tools, a contextual RBAC authorization server and the implementations of context interfaces.

The authorization model representation was stored in a hierarchical directory service, with access and data scheme description standardized by LDAP protocol [17]. Administrative tools allow privileged users to manage the ePR authorization policies stored at LDAP server.

2.3. The Need of a Mobile HIS/PACS Workstation

Intensive care units are complex environments, where rapid access to clinical information can be life-determining. Clinical information technologies such as ePRs, Computerized Provider Order Entry (CPOE), Clinical Decision Support Systems (CDSS), and Picture Archiving and Communication Systems (PACS) may profoundly affect ICU performance and clinical outcomes. The availability and use of information technology at the point of care may favorably impact clinical endpoints, costs, and efforts to improve quality of care [18, 19].

When participating in an assessment about the efficiency on searching clinical information, most of the ICU hospital staff (physicians and nurses) stated that they usually spend a great deal of time searching for patient and medical

information using workstations located far from the point of care. They added that the time spent on looking for information could be considerably reduced. Most physicians and nurses thought that a PDA would be ideal for reading information about the patients and medical information central to their work. However those devices were inefficient in essential tasks, such as prescribing in the CPOE, viewing images in PACS and data entry operations.

The conclusions of this initial analysis were: a) there should be a better system for finding correct information; b) all information should be collected and accessed at the point of care, so mobility is mandatory; c) there should also be a faster way to access, to write and to change clinical information at the point of care.

3. RESULTS

3.1 The MedKart Concept

A new concept to assist critical patients at the bed-side was then proposed and deployed. It is based on a mobile kart – called MedKart - that comprises all resources needed for the ICU application, such as:

- a terminal connected to the WiFi network, to attend the mobile requirement;
- a 15" LCD monitor, that provides a better viewing of the graphical PACS and HIS interfaces;
- a membrane keyboard, water resistant and that simplifies the cleaning;
- an optical reader, to access bar code information;
- extra batteries, to provide up to 6 hours of continuous use;
- an ergonomic and practical design, specially featured to be used by physicians and nurses inside the ICU.

Figure 3 shows the final assembly in different views of the MedKart.

The system is fully integrated to the InCor's PACS and to the network of vital signals monitors, allowing instant access to the image database and vital signals in real-time at the bed side.

The DICOM viewer was specially designed to run on MedKart side, decreasing server and network burden and allowing great local flexibility. On the server side, a Java DICOM server was designed to allow communication with all DICOM modalities.

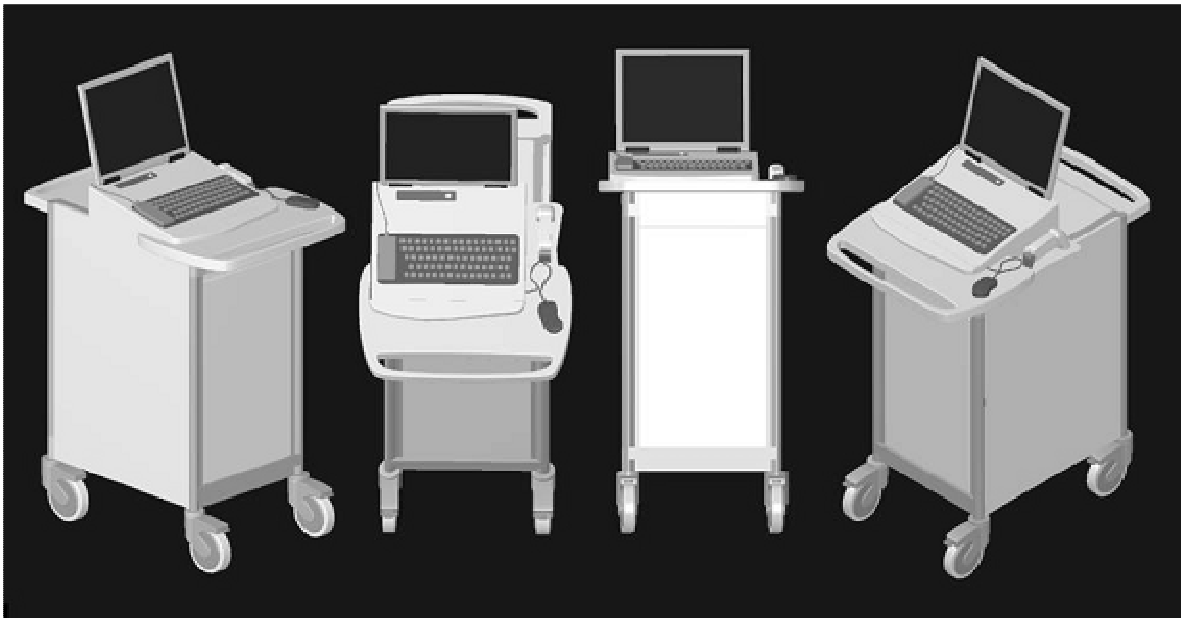

Figure 3 - The MedKart, a mobile terminal to assist critical cardiac patients in an Intensive Care Unit (ICU)

Figure 4 shows the final assembly of the MedKart including all functionalities described in this section.

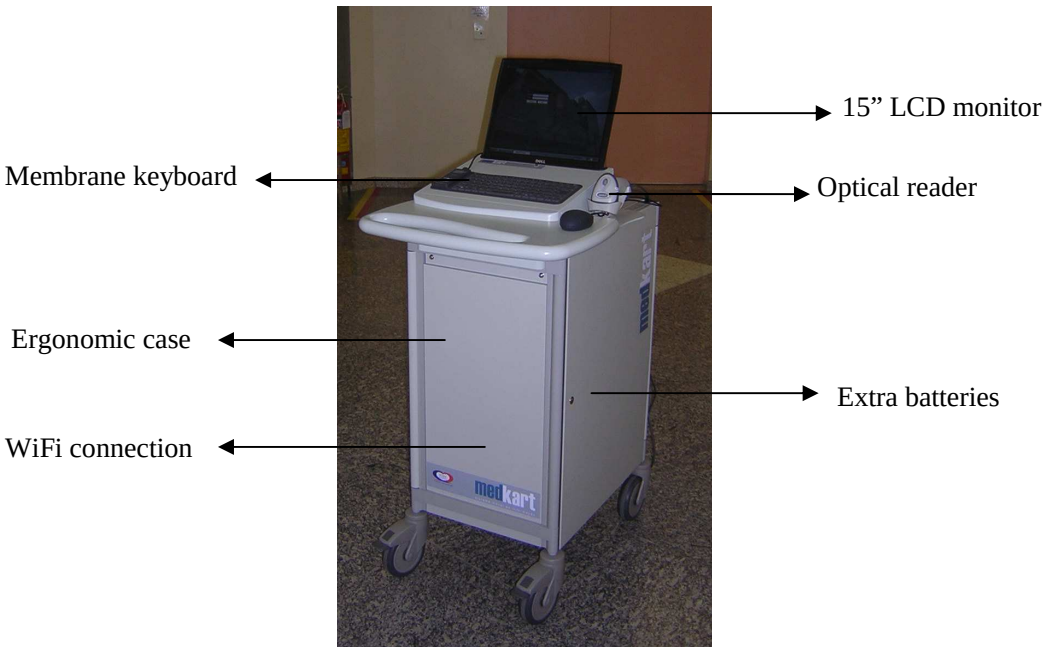

Figure 4 – The final assembly of the MedKart and its functionalities.

The software modules are integrated in a single Web-based application allowing the easy and fast navigation through the modules. To access the patient information, stored in a SQL database (Oracle 10g), users have to perform an authentication procedure that uses LDAP protocol including a profile definition to the users, which is based on their role at the Institution. The set of applications and patient information available to the user is dependent on the user’s profile. Moreover, in the application level all data stream is encrypted with the Security Sock Layer (SSL) version 3.0 protocol

The WiFi infrastructure was deployed and includes four Access Points (APs), to provide full access to InCor’s network. All forty beds at Intensive Care Unit (ICU) devoted to critical cardiac patients are actually covered by this WiFi infrastructure. To improve the security in the network layer, a combination of two mechanisms was used in the communication between the MedKart and the InCor’s network. Each AP allows the connection of just the devices with known Ethernet MAC addresses previously registered in each AP Access Control Lists (ACLs). This avoids any unauthorized device to explorer backdoors in the network.

The second security mechanism used was the WiFi Protected Access protocol (WPA). The WPA protocol encrypts all transactions between MedKart and the InCor’s network. The WPA was chosen due its powerful security technology for Wi-Fi networks when compared with Wired-Equivalent Privacy (WEP). It provides strong data protection by using encryption as well as strong access controls and user authentication. WPA utilizes 128-bit encryption keys and dynamic session keys to ensure your wireless network's privacy and enterprise security. There are two basic forms of WPA: WPA Enterprise (requires a Radius server) and WPA Personal (also known as WPA-PSK). Either can use TKIP or AES for encryption [20].

WPA-PSK is basically an authentication mechanism in which users provide some form of credentials to verify that they should be allowed access to a network. This requires a single passphrase entered into each WLAN node (Access Points, Wireless Routers, client adapters, bridges). As long as the passphrase matches, a client will be granted access to a WLAN.

Encryption mechanisms used for WPA and WPA-PSK are the same. The only difference between the two is in WPA-PSK, authentication is reduced to a simple common passphrase, instead of user-specific credentials.

The passphrase may be from 8 to 63 printable ASCII characters or 64 hexadecimal digits (256 bits). If you choose to use the ASCII characters, a hash function reduces it from 504 bits (63 characters * 8 bits/character) to 256 bits (using also the SSID). The passphrase may be stored on the user's computer at their discretion under most operating systems to avoid re-entry. The passphrase must remain stored in the Wi-Fi access point.

Security is strengthened by employing a PBKDF2 key derivation function. However, the weak passphrases users typically employ are vulnerable to password cracking attacks. To protect against a brute force attack, a truly random passphrase of at least 20 characters should be used, and 33 characters or more is recommended.

The Pre-Shared Key (PSK) mode of WPA is considered vulnerable to the same risks as any other shared password system - dictionary attacks for example. Another issue may be key management difficulties such as removing a user once access has been granted where the key is shared among multiple users, not likely in a home environment.

3.2 Assessment of the use of MedKart

To evaluate the MedKart in terms of usability, acceptance and functionality, a questionnaire to the physicians and nurses at ICU was prepared (n=10). The questions dealt with the need of information, functions and usability in the MedKart. Table 1 shows the results after analysis of the answers.

Table 1. Evaluation parameters in terms of usability, acceptance and functionality collected from a questionnaire submitted to the physicians and nurses at ICU.

Evaluation parameter	Answers	*n*
Acceptance and usability	Very useful	5
	Useful	5
	No useful at all	0
	No opinion	0
Function used	CPOE at the bed side	7
	To view images, lab tests and reports	10
	Drug administration and material used	2
Event or condition of use	During the daily visit	5
	After the daily visit to change procedures	5

The analysis of the answers shows that all users found the system useful in some way when compared to the traditional workstations or to previous tests with commercial mobile devices. All of them could use the graphical PACS application. This is a highlight of the MedKart concept when compared to PDAs, since its 15'' LCD monitor allows a comfort manipulation of graphical interfaces and quality visualization of the medical images. The visualization of the patient images, tests and reports at the POC is a factor that can decrease the time for clinical decisions. The reason why only few responders use the drug administration and material modules is still being analyzed. The use of the system during the daily visit by half of the responders saves them the extra time needed for updating the patient information after the daily visit, thus fulfilling their needs for reduction of time to update the system and to search for patient information.

4. CONCLUSION

Intensive care units are complex environments, where rapid access to clinical information can be life-determining. The availability and use of information technology at the point of care, especially in ICUs, may favorably impact clinical endpoints, costs, and efforts to improve quality of care. In this work a new concept to assist critical patients at the bed-side, which is based on a mobile kart was described. The system fulfills the requirements to assist, in the point-of-care,

critical cardiac patients in an ICU. The whole solution permits, not only the access and distribution of medical information at the bed-side, but the integration in a consistent and secure environment, without the need to switch between different applications. Medical images are retrieved as needed and displayed in the same Web-based work place. The complete system is under clinical evaluation with a database of more than 1.2 million patients, 130,000 medical images and real-time visualization of vital signals.

ACKNOWLEDGES

This work was supported in part by National Council for Scientific and Technological Development (CNPq) Grants 552026̃2002-6 and 300499/2005-1 and Zerbini Foundation. The authors are especially grateful to the physician and the nursing staffs at InCor's ICU for their assistance and collaboration. The whole IT team at InCor has contributed in different ways, and the authors are thankful to them.

REFERENCES

[1] Y. Lua, Y. Xiaoa, A. Searsb, J.A. .Jack. A review and a framework of handheld computer adoption in healthcare. Intl. J. Med. Informatics, **74**, 409-422 (2005).
[2] Y. Stolworthy, RNs are mobilizing, 10-24 (2003).
[3] T. Schneider, Easy access to a world of information: using a handheld computer, J. Gen. Intern. Med. **27** (2001).
[4] M.A. Silva, G.R. Tataronis, B. Maas, Using personal digital assistants to document pharmacist cognitive services and estimate potential reimbursement, Am. J. Health Syst. Pharm. **60**, 911—915 (2003).
[5] D.H. Lynx, H.R. Brockmiller, R.T. Connelly, S.Y. Crawford, Use of a PDA-based pharmacist intervention system, Am. J. Health Syst. Pharm. **60**, 2341—2344 (2003).
[6] J.A. Brody, Implementing a personal digital assistant to document clinical interventions by pharmacy residents, Am. J. Health-Syst. Pharm. **58**, 1520—1522 (2001).
[7] S.E. Lapinsky, J. Weshler, S. Mehta, M. Varkul, D. Hallett, T.E. Stewart, Handheld computers in critical care, Crit. Care **5**, 227—231 (2001).
[8] Y. Lu, J. Lee, L. Xiao, A. Sears, J. Jacko, K. Charters, Why don't physicians use their personal digital assistants (PDAs)? Proc. AMIA Symp. 405—409 (2003).
[9] A.S. McAlearney, S.B. Schweikhart, M.A. Medow, Doctors' experience with handheld computers in clinical practice: qualitative study, Br. Med. J. **328**, 1162(2004) .
[10] E.S. Hall, D.K. Vawdrey, C.D. Knutson, J.K. Archibald, Enabling remote access to personal electronic medical records, IEEE Eng. Med. Biol. Mag. **22**, 133—139 (2003).
[11] M. A. Gutierrez, S. S. Furuie, M. S. Rebelo, F. A. Pires, and R. A. Moreno, "Implementation of an integrated hospital information system using an open-source three-tier architecture," in Proc. SPIE, **5371**, 23-30 (2004).
[12] Digital Imaging and Communications in Medicine (DICOM), National Electrical Manufacturers Association, DICOM Committee, 2000.
[13] M. Santos and S. S. Furuie, "High performance web viewer for cardiac images," in Proc. of SPIE, **5371**, 391-401 (2004).
[14] Health Level Seven. HL7 Version 2.3 Specification. 1996.
[15] G. H. M. B. Motta, S. S. Furuie. A Contextual Role-Based Access Control Model for Electronic Patient Record. IEEE Transactions on Information Technology in Biomedicine, **7(3)**,:202-207 (2003).
[16] D.F. Ferraiolo, R. Sandhu, D. Gravila, D.R. Kuhn, R. Chandramouli Proposed NIST standard for role-based access control, ACM Trans.Info. Syst. Security, **4**, 224-274 (2001)
[17] W. Yeong, T. Howes, S. Kille, Lightweight Directory Access Protocol. Internet Engineering Task Force – IETF, In: http://www.ietf.org/rfc/rfc1777.txt?number=1777(1995)
[18] R. Amarasingham, P. J. Pronovost, M.D. West, C. Goeschel, T, Dornan, D. R. Thiemann, N.R. Powe. Measuring Clinical Information Technology in the ICU Setting: Application in a Quality Improvement Collaborative, J Am Med Inform Assoc. **14**, 288 –294 (2007);.
[19] M. Berglunda, C. Nilssona, P. Revaya, G. Peterssonb, G. Nilssonb. Nurses' and nurse students' demands of functions and usability in a PDA, Int. J. Med. Inf. **76**, 530–537 (2007).
[20] A. S. Tanenbaum, Computer Networks, fourth edition, Prentice Hall PTR, New Jersey, 2003.

A novel multidimensional medical image display framework based on Visualization Toolkit

Jie Shuai[*a], Jianyong Sun[a], Jianguo Zhang[a]
[a] Laboratory for Medical Imaging Informatics, Shanghai Institute of Technical Physics, Chinese Academy of Sciences, Shanghai 2000832

ABSTRACT

PACS display workstations usually display medical image volumes in one single pattern at one time. Though some image workstations may offer three orthogonal views for orientation, users are not allowed to view different patterns of three dimensional objects simultaneously. In this paper, we propose a novel framework that integrates different rendering methods by utilizing the pipeline mechanism of Visualization Toolkit (VTK). VTK is an open source software system for 3D computer graphics, image processing, and visualization. On the basis of VTK, this image display framework can display multidimensional medical images in two different patterns, Multi-Planar Reconstruction (MPR) and Maximum/Minimum Intensity Projection (MIP), at the same time with most freedom by allowing users to configure viewpoint freely, what we call Free-MPR, and to shift between different patterns unlimitedly. Furthermore, the framework can be easily applied to medical image workstation or Web-based network application for it is provide as a plug-in that can be integrated conveniently. The preliminary testing results showed that our developed MedViewCtrl display framework can be integrated into any Windows Program based display software or Internet Explore Web Browser to provide multiwindow and multidimensional medical image visualization functionality for higher volume medical image data sets.

Keywords: Medical Image Display, Multidimensional Visualization, Free-MPR, VTK

1. INTRODUCTION

1.1 Background

As multi-Slice CT imaging modalities are used widely in the world, the three dimensional (3D) even four dimensional (4D) image workstations have already become common diagnosis means for radiologists. The multidimensional medical image workstations usually display volume data in one single pattern simultaneously, such as Multi-Planar Reconstruction (MPR) and Maximum Intensity Projection (MIP), the most used two patterns by radiologists. Although some applications offer three orthogonal views for orientation and positioning, users cannot create and view the volume of different patterns at the same time. Yet it does help a lot when radiologists making diagnosis to be shown 3D and 2D information together.

[*] shuaijie@live.com; phone (86)-021-65420850-45300

In addition, interactive manipulation is primary in visualization. Unfortunately, not all image workstations give enough freedom to users when rendering volume. Free to change the visual angle (Free-MPR) and free to set the rendering pattern is what we are going to satisfy.

Furthermore, in favor of the wide spread application of medical image visualization, a small and flexible 3D display framework relatively is more suitable for Chinese radiologists and physicians as there are no so many powerful yet huge and resources consuming workstations in clinical environment. So, it is very useful to develop a 3D plug-in display component which can run on most single computers or be used in web environment.

1.2 Open source approach for multidimensional visualization

It is clear that there is a trend to develop free plug-in, lightweight and more efficient 3D display software for medical image visualization. Our aim is to develop a plug-in based open source software for multidimensional visualization. Visualization Toolkit (VTK) is an open source software system for 3D computer graphics, image processing, and visualization which supported C++ and Java. We develop VTK classes according to the features of medical image data and optimize the processing algorithms to improve the efficiency.

2. METHODS

2.1 The Visualization Toolkit (VTK)

The Visualization Toolkit is an open source and cross-platform software library. VTK includes a wide variety of visualization algorithms including scalar, vector, tensor, texture, and volumetric methods; and advanced modeling techniques such as implicit modeling, polygon reduction, mesh smoothing, cutting, contouring, and Delaunay triangulation. VTK supports C++ and several interpreted interface layers of other languages, such as Java, Tcl/Tk and Python.

2.2 Pipeline mechanism

After medical image are formed into 3D volume data, they enter the processing pipeline. The volume data consist of discrete spacial points, isotropy or anisotropy, holding the information of position and value. From these 3D points, lines, planes, surfaces and other data objects are constructed. Due to the pipeline mechanism, every data object possesses multiple inputs and outputs. That is, all data objects may share one input. (See Fig. 1)

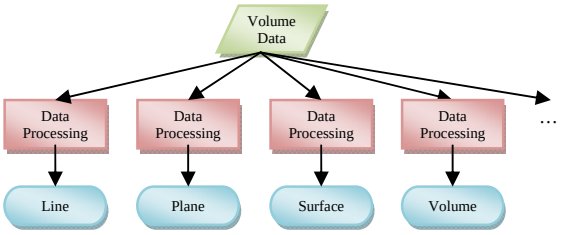

Fig. 1. Diagram of pipeline image processing and visualization mechanism. The same volume data are applied to different processing for various data objects.

One input volume data may produce several data objects. All these objects exist simultaneously and function severally. Besides, because all data objects are sharing the same input, any changes on the input data will affect the output data objects. This inherent trigger mechanism effects directly and rapidly.

2.3 Interaction between rendering patterns

For the three dimensional volume data, the different rendering objects can be constructed with different pipelines. Given the visual angle, we can extract the projecting plane for MPR visualization and construct the MIP visualization. Each rendering pattern may have more than one instances. For example, there probably are 3 MPR objects and 2 MIP objects at the same time. (See Fig. 2)

In addition, all data objects interact with correlative ones. Restricted by the screen, all 3D display objects are projected to 2D plane for rendering. A spacial plane may appear to be a line on the screen. So from different visual angle, display object has various representations while they are actually one thing. In each rendering pattern, a 3D object is represented by one data object. These objects represent the same physical 3D dataset and are able to interact with others because they share the same input data. Taking advantage of such reciprocity, data objects representing one thing in different rendering patterns combine together. (See Fig. 3)

On the other hand, a rendering pattern is a representation of the medical image data volume. Hence all rendering patterns are correlative with each other. By sharing one data source, the memory occupation is reduced greatly.

2.4 MedViewCtrl

MedViewCtrl is a research and plug-in display framework we designed and developed for medical image processing and visualization. A large set of image processing and visualization methods for multidimensional medical images as well as advanced methods for specific organs and clinical tasks are included. MedViewCtrl is implemented in C++ and ultimately provided as dynamic

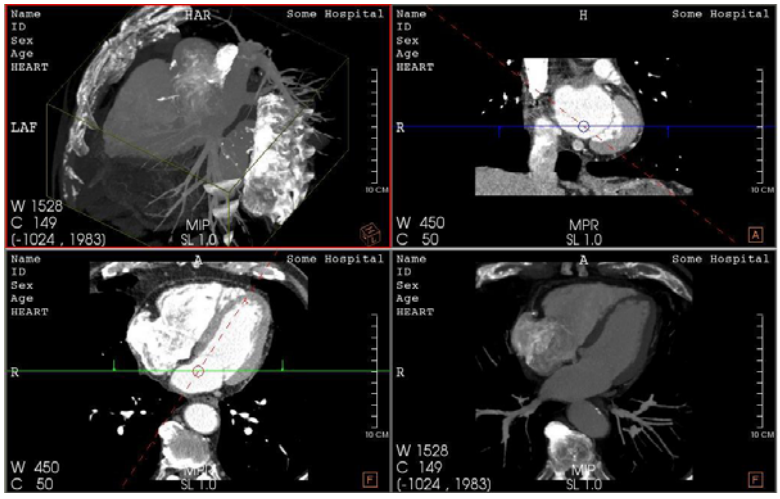

Fig.2. Screenshot of the visualization of a patient's heart with two MIP objects (upper left and bottom right) and two MPR objects (upper right and bottom left). The highlight red frame includes the upper left MIP object and the red color on behalf of the projecting plane of the upper left MIP object. This plane was represented by red dotted lines on the upper right MIP object and the bottom left MPR object severally.

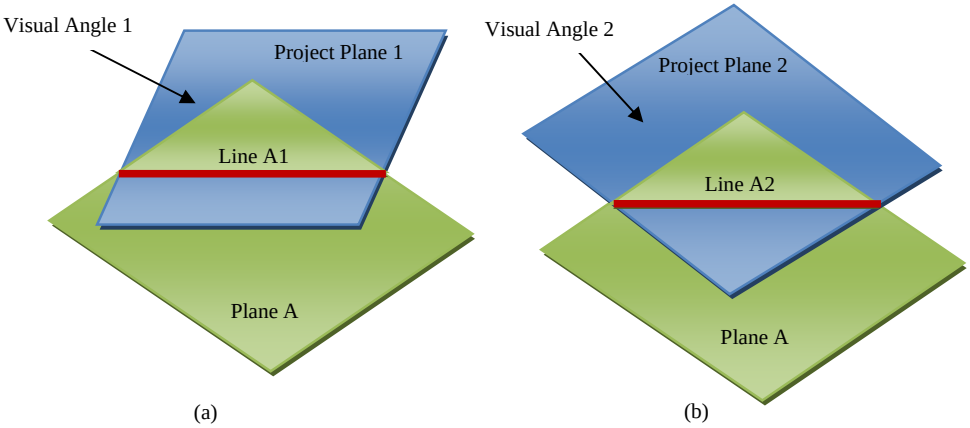

Fig.3. Diagram of the correlation between different data objects. The spacial plane A is projected to the project plane and represented by a line. (a) From visual angle 1, plane A is represented by line A1 on project plane 1. (b) From visual angle 2, plane A is represented by Line A2 on project plane 2. Actually we know line A1 and line A2 are both on behalf of plane A, so line A1 and line A2 correlate with each other and associate with plane A. If plane A moves, line A1 and line A2 will change responsively.

linked library. The original aim to design MedViewCtrl is to achieve a simple and fast multidimensional visualization of multi-modality medical images conforming to DICOM standard and is applicable to ordinary performance computer.

Program Interface

MedViewCtrl is a dynamic linked library and is callable by any window programs as long as given a win handler and transferred the medical image data including spacial information. Medical images of DICOM format consist of pixel data and several sets of attributes. And patient orientation, slice thickness, image size, image spacing, and slope angle are necessary parameters for visualization. Theoretically, with these values the 3D volume is ready to be reconstructed.

For further configuration and to provide more information about the medical images, more image attributes are transferred. Such as window width and window center to set the default display. (See Fig. 2. The left two and upper right rendering objects are set to default window level and window width.)

Data Processing

While the image data is transfer to MedViewCtrl, a dataset of VTK defined type is constructed. This dataset is the data source of all rendering patterns. Then the pipeline of data processing starts.

We define MPR and MIP property classes to render different patterns. Every property defines a set of data objects associated with its rendering pattern. For example, the indicating lines representing other planes on top of one rendering pattern. (See Fig. 2. The red dotted

line and green solid line in left bottom MPR rendering window are associated with the MPR property within the window.) These properties do not manipulate the original data source but decide how to display it by setting the parameters as visual angle, zooming rate, projecting plane, and etc. Theoretically, besides MIP and MPR, all visualization methods are applicable to the processing pipeline. Having been developed for several dozen years, most algorithms for volume rendering and surface rendering are stable, effective and widely accepted. Given the algorithms, it's not difficult to define the project function from volume data to projecting plane for screen rendering. Yet considering the software efficiency and practicability, we have chosen MPR and MIP, the two most practical and most commonly used methods, as the main rendering patterns.

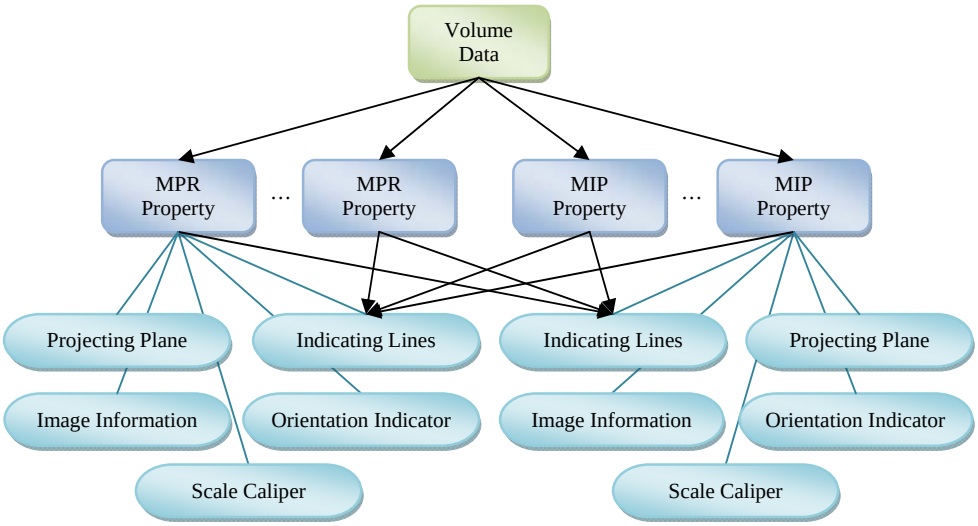

Fig.4. Diagram of the relation between MPR and MIP properties and associated data objects. Through MPR and MIP methods, the volume data is projected to the projecting plane to be rendered on the screen. In this figure, the solid black arrows indicate the data flow through the pipeline, and the blue lines indicate the associations between rendering patterns as MPR and MIP properties and object data as the indicating lines, projecting plane, orientation indicator, scalar caliper and image information. Since there may exist several rendering patterns, one render pattern have more than one indicating lines. The number of lines depends on the number of rendering patterns.

Rendering Frame

Each rendering pattern associates with a rendering window class which is defined as MedWindow in MedViewCtrl. MedWindow is based on vtkOpenGLRenderWindow, a VTK class inherits from vtkWindow which based on C++ class CWnd and hence can be created by windows handler of the calling program of MedViewCtrl conveniently. One rendering window is independent of others. Basically we take four rendering windows to display the volume from orthogonal visual angles and as a whole. (See Fig. 5.)

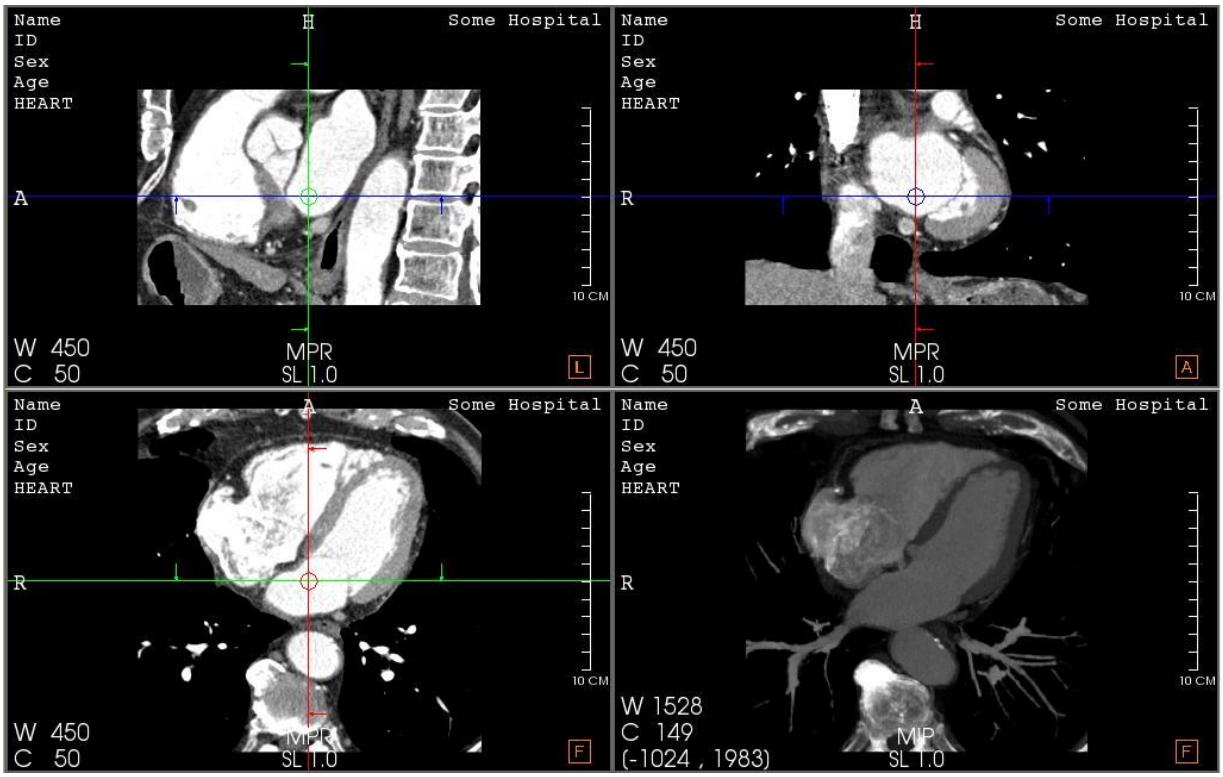

Fig.5. Screenshot of the visualization of a patient's heart. The upper left window displays the sagittal projecting plane of MPR. The upper right window shows coronal projecting plane of MPR. And the bottom left window shows the axial projecting plane of MPR. The bottom right window display MIP from axial visual angle. Each window is a MedWindow instance based on vtkWin32OPenGLWindow and CWnd.

Provided the handler of parent window, MedViewCtrl create the visualization fame composed by several rendering windows. (See Fig. 2, 5, 6) Since in C++ a parent window is capable to have several child windows, MedViewCtrl frame may have many rendering windows. In other words, users are able to create as many rendering patterns as they want and to change the layout of those rendering windows. (See Fig. 6)

Visualization Implementation by Using VTK

The Visualization Toolkit (VTK) provides a powerful system to render three dimensional image data. Generally the input data are formed into structured dataset. If the spaces between pixels are consistent, in other words the points are arranged on a regular, rectangular lattice, the points construct a structured points dataset. (See Fig. 7. (a)) Most medical images of CT and MRI are regular spacing. Otherwise, the points construct a rectilinear grid dataset because they have regular topology but partially regular geometry. Sometimes, the radiologist performs a scan with irregular spaces. In this kind of situation, data in each single image are regular because each image is composed of the same number of rows(X axis) and the same number of columns(Y axis) of pixels and the spaces between pixels are regular. But it's not regular on Z axis because of the inconsistent spaces between images. If we want to reconstruct a volume by all images, they can only be formatted as rectilinear grid. (See Fig. 7. (b)) But for the ultrasonic images produced by sector scan, the images are arranged with

certain angles. The geometry of dataset is completely irregular and thus formatted as structured grid. (See Fig. 7. (c))

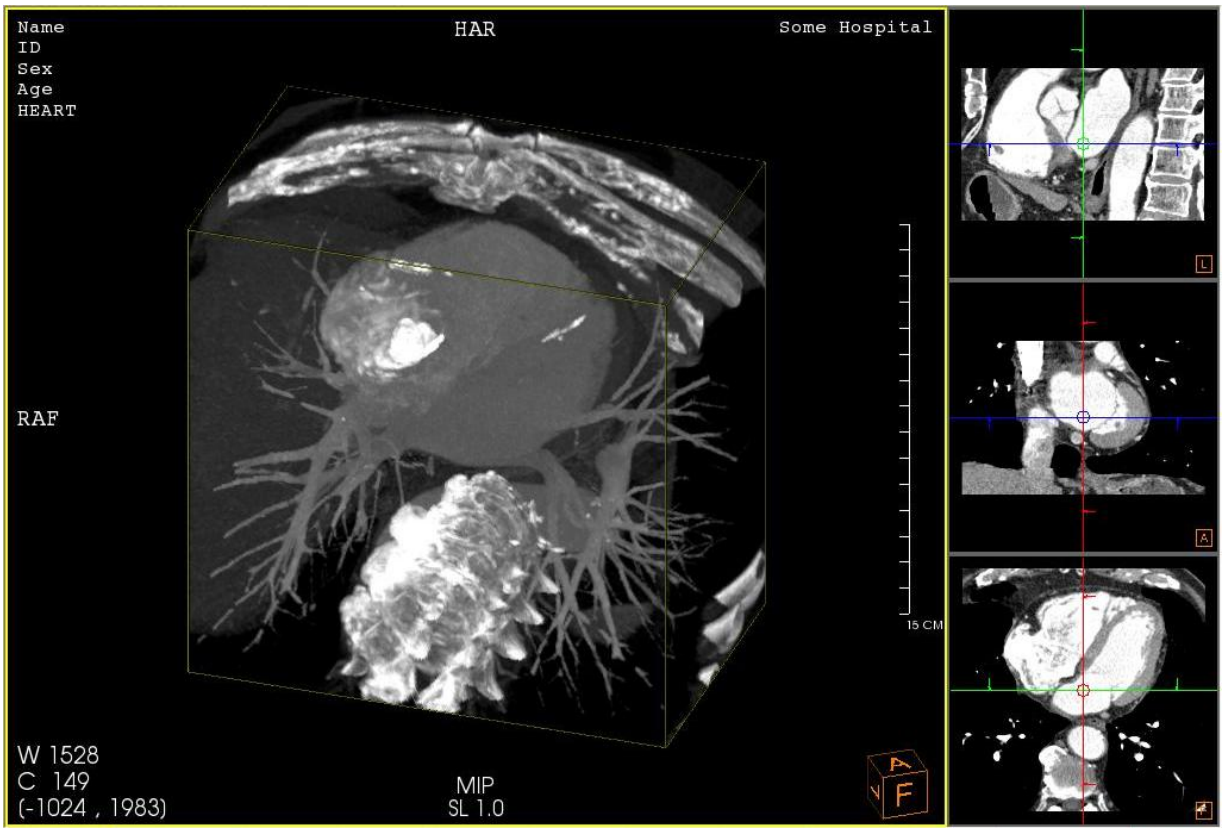

Fig.6. Screenshot of the visualization of a patient's heart with another type of layout. The left rendering window shows the MIP object and its associated data objects as orientation labels. The right three rendering windows display the three orthogonal projecting plane of MPR as sagittal, coronal, and axial view respectively.

The visualization networks of VTK consist of process objects and data objects. Dataset pass through several process objects as filters and are terminated by mappers or sinks. VTK integrates many visualization algorithms, such as ray cast algorithm for MIP rendering. We make some modification on these provided classes to suit our visualization framework. We render MPR as a plane object by mapping texture onto the projecting plane and render MIP as a volume object using Ray Cast algorithm for volume rendering. (See Fig. 8.)

Besides the MPR and MIP objects, the associated projecting plane, indicating lines, orientation indicator, scalar caliper and patient information (See Fig. 4.) are also rendered within the same vtkRenderWindow. Due to the pipeline mechanism of VTK, every data object may have more than one input. vtkRenderWindow consists of a collection of vtkRenderer as input. Similarly, vtkRenderer includes a collection of vtkActor. That's how we display multiple data objects within a window. When actualize the frame in C++, we make a new class of window to expand the function, such as shifting the layout.

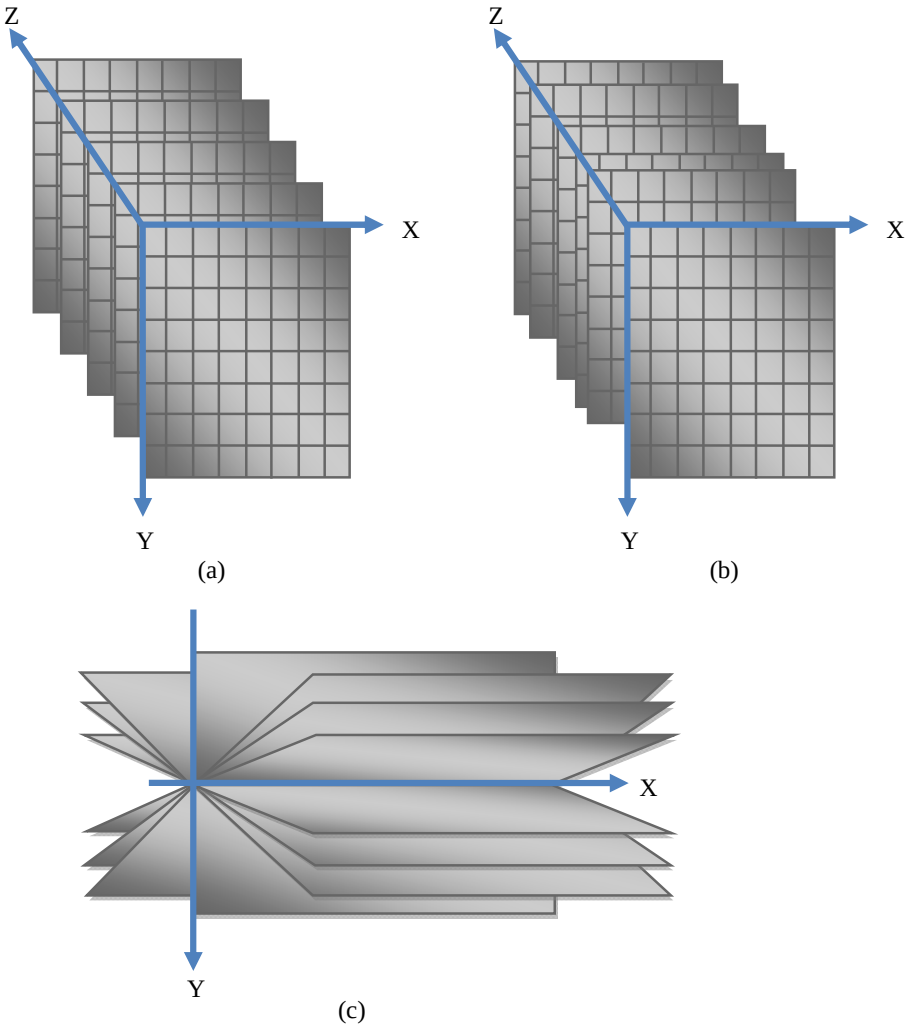

Fig.7. Diagram of VTK definition of dataset types for medical images. (a)Structured Points. All voxels are arranged on regular, rectangular lattice and both the topology and geometry of the dataset are regular. Most CT and MRI images are of this type. (b)Rectilinear Grid. Voxels in X and Y axes are regular arranged while in Z axis all images are parallel but have irregular spacing. The topology is regular and the geometry is partially regular. (c)Structured Grid. Although every single image is kind of regular lattice, the arrangement of images is irregular. It's the typical geometry of ultrasonic images. The topology of this kind of dataset is regular and the geometry is irregular.

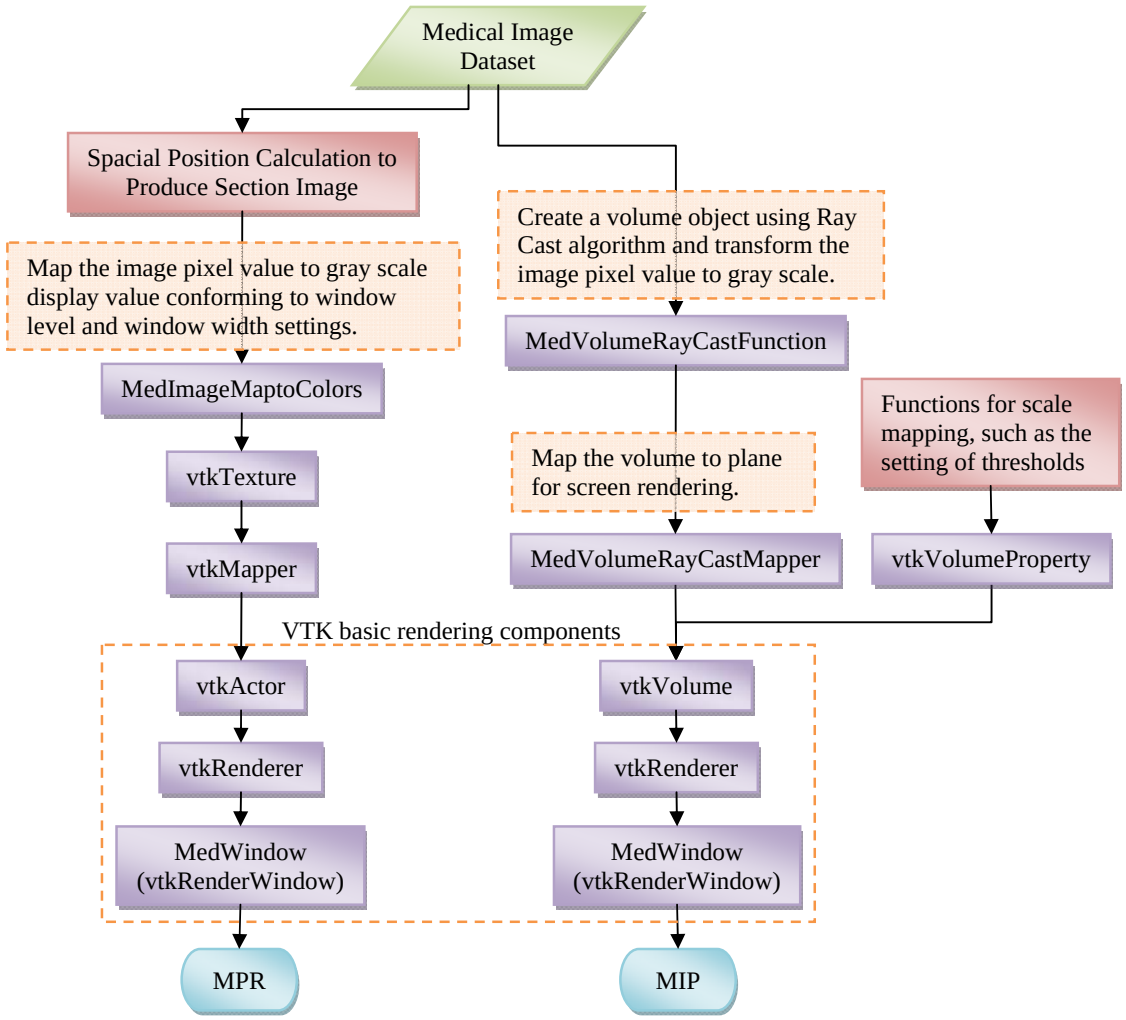

Fig. 8. The pipeline structure of visualization of MedViewCtrl based on VTK. This figure show the data flow and main functions and classes used to render MPR and MIP objects. The classes MedImageMaptoColors, MedVolumeRayCastFunction, and MedVolumeRayCastMapper are modified based on the VTK classes vtkImageMapToColors, vtkVolumeRayCastFunction, and vtkVolumeRayCastMapper to suit the features of medical images and to improve the performance and efficiency of three dimensional calculation. The vtkActor, vtkRenderer and vtkRenderWindow are the three necessities to render an object in VTK. MedWindow inherit from vtkRenderWindow.

3. RESULTS

Our developed MedViewCtrl framework can be integrated into any Windows Programs or Internet Explore Web Browser to provide multiwindow and multidimensional medical image visualization. All rendering windows are correlative and may correspond to the events of other window or user inputs. For example, when the status is set to unify window level and window width, a change of window level or window width in one rendering window will affects on all rendering windows. Each rendering window display an object of MIP or MPR pattern and other associated data object, such as indicating lines, projecting plane, orientation

indicator, scalar caliper and patient/institute information. The rendering pattern is exchangeable between MPR and MIP without modifying the volume data. All operation on the MPR or MIP objects, such as cropping, moving, window level and window center adjusting, and etc., do not affect the original image data.

The interface of software is straightforward and easy to use. Users are not restricted to the rendering pattern any more. Every rendering object is independent but correlative. Almost all CT and MRI images can be rendered by MedViewCtrl framework. The whole framework is small with a size of 525Kb. While together with all necessary VTK libraries, the size is only 18.8M. Compared with popular image workstations, MedViewCtrl is rather lightweight software, but provided with primary visualization functions. Moreover, it holds a novel framework that is more freely and efficient.

4. DISCUSSION AND CONCLUSIONS

As shown in Figure 8, our multiwindow, multidimensional visualization framework bases on VTK. Image data are reconstructed into VTK dataset and processed in a pipeline system. The modified VTK pipeline mechanism performs with high efficiency and low occupation of memory and system resources. Thought VTK provides most popular visualization methods, we do some modification to improve the performance according to characteristics of medical image, such as value range and spacial arrangement. As modularly designed, the framework can be expanded by adding new visualization methods. Having consulted several radiologists and taking the efficiency into account, we adopted the two most used and most useful visualization methods, MPR and MIP.

Further work on MedViewCtrl may focus on higher efficiency and more powerful functions. There is great potential improvement of performance by optimizing the hardware programming together with software scheme. The Graphic Processing Unit (GPU) is programmable, and may boost the efficiency dramatically by coding targeting on our visualization procedure. Besides, Web-based 3D visualization is another important application of the MedViewCtrl. After all, high performance, easy to use, and great freedom have always been what we are chasing for.

REFERENCES

1 The Visualization Toolkit. http://www.vtk.org.

2 VTK 5.1.0 Documentation. http://www.vtk.org/doc/nightly/html.

3 W. Schroeder, L. Avila, and W. Hoffman. Visualizing with VTK: A tutorial. *IEEE Computer Graphics and Applications*, 20(5):20-27, 2000.

4 W. Schroeder, K. Martin, and B. Lorensen. *The Visualization Toolkit, An Object-Oriented Approach To 3D Graphics, 2nd edition*. Kitware Inc., 1997.

5 D.J. Kruglinski, S. Wingo, and G. Shepherd. *Programming Visual C++, 5th edition*. Microsoft Press Redmond, 1998.

A Novel Strategy to Access High Resolution DICOM Medical Images Based on JPEG2000 Interactive Protocol

Yuan Tian, Weihua Cai, Jianyong Sun, Jianguo Zhang
Laboratory for Medical Imaging Informatics
Shanghai Institute of Technical Physics, Chinese Academy of Sciences, China

ABSTRACT

The demand for sharing medical information has kept rising. However, the transmission and displaying of high resolution medical images are limited if the network has a low transmission speed or the terminal devices have limited resources. In this paper, we present an approach based on JPEG2000 Interactive Protocol (JPIP) to browse high resolution medical images in an efficient way. We designed and implemented an interactive image communication system with client/server architecture and integrated it with Picture Archiving and Communication System (PACS). In our interactive image communication system, the client can make simple requests which identify the resolution, quality and region of interest and download selected portions of the JPEG2000 code-stream instead of downloading and decoding the entire code-stream. After receiving a request form a client, the server downloads the requested image from the PACS server and then replies the client by sending the appropriate code-stream. We also applied this approach to a PDA-based wireless medical system in which large medical images can be transmitted through wireless network and be displayed on the lower resolution screen of a PDA in an efficient way.

Keywords: JPEG2000, JPIP, PACS, resolution scalability, spatial random access, Window of Interest(WOI), Personal Digital Assistant (PDA)

1 INTRODUCTION

Image compression has been used to increase the communication efficiency and storage capacity. JPEG2000 offers many features to support interactive access to large images [1][2]. These include highly efficient compression, resolution scalability, quality scalability and spatial random access. JPIP, part 9 of JPEG2000, is an interactive protocol standard for viewing JPEG 2000 images in a client-sever system [3]. It utilizes the scalable features of JPEG 2000 code-stream and allows the client to fetch the window of interest image without directly accessing the compressed target file. Clients can request different kind of images or code-streams (a low resolution image or a specific region of interest in high quality) from the same image stored on JPIP server. With JPIP high resolution medical images can be browsed efficiently under the condition of low-speed connection or low power devices with limited resources.

In this paper we used JPIP to design and implement an interactive image communication system. In this system, the client firstly requests a low resolution image to preview, and then selects a WOI to display in high quality. Many operations such as zoom and pan are provided to browse large images efficiently. A cache is maintained and managed on the client side to

store the parts of JPEG2000 code-stream that have already been transmitted from the server. Some study proposed to use empty packets to reconstruct tile data in order to raise transmission efficiency of JPT-stream [5]. In this paper, we used a set of empty packets to reconstruct the code-stream on the client side to provide image information outside the WOI. On the server side, after receiving a request form a client the server downloads the requested image from the PACS server and then replies the client by sending the appropriate code-stream. Many mechanisms such as cache model management, local image database management, session and memory management are adopted to facilitate the process of responding. We also used JPIP in a PDA-based wireless medical system. With embedded software, PDA can be used to browse large medical images efficiently by accessing the JPIP server. This system was tested successfully with DELL X51V Pocket PC and 802.11g wireless network.

The organization of this paper is as follows. Section 2 gives a brief overview of JEPG2000 and JPIP. Section 3 describes the system design and implementation details. Section 4 contains the results, and Section 5 provides concluding remarks.

2 METHODOLOGY

2.1 Some Relevant Aspects of JPEG2000

2.1.1 Resolution Scalability

JPEG2000 is the latest international still image compression standard. Rather than using Discrete Cosine Transform (DCT), JPEG2000 adopts Discrete Wavelet Transform (DWT) and Embedded Block Coding with Optimized Truncation (EBCOT) [1][2]. DWT decomposes the image into a lower resolution and three detail subbands: HL, LH and HH. *D* stages of DWT analysis result in 3*D*+1 subbands: LH_d, HL_d, HH_d and LL_D, d = 1,2,…,D. Figure 1 shows a computed tomography image decomposed into 10 subbands by a 3-level DWT. DWT provides resolution scalability, so the image can be decoded at reduced resolutions from a subset of the compressed DWT subbands. This property allows JPEG2000 code-stream to be delivered in a manner which matches the user's desired display resolution.

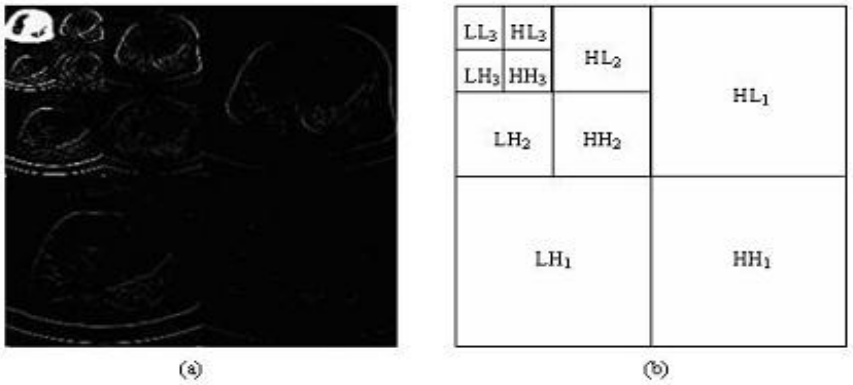

Figure 1. (a) 3-level DWT of a CT image. (b)Subband LH*d*, HL*d*, HH*d* and LL*3*, d = 1,2,3.

2.1.2 Spatial Random Access

JPEG2000 provides two image partitioning schemes for spatial random access: tiles and precincts [1]. The image can be spatially divided into rectangular tiles prior to compression and each tile is coded independently. The tiles that cover the region of interest can be extracted from the code-stream to offer spatial accessibility. Tile-based method relies exclusively on tiles to provide spatial random access.

D-level DWT decomposes the image into D+1 resolutions: LL_d, d=0,1,2,…,D. Resolution LL_D contains only one subband, while all other resolutions LL_d contain the three detail subbands LH_{d+1}, HL_{d+1} and HH_{d+1}, d = 0,1,2,…,D-1. Each subband is partitioned into rectangular code-blocks, each of which is independently coded into a finely embedded bit-stream. Precincts may be interpreted as partitions of LL_d, d = 1,2,…,D. A precinct on LL_d consists of code-blocks from the same spatial region within the subbands which belong to image resolution LL_d. Figure 2 illustrates the relationship between precincts and code-blocks. Because code-blocks which affect limited spatial regions are coded independently, the precinct-based method offers spatial random access even if the entire image is compressed as a single tile. Compared with the tile-based method, the precinct-based method provides a finer spatial accessibility. This property perfectly suits interactive image browsing, especially in the case of viewing very large images with a low-speed connection.

2.1.3 Code-Stream Structure

Associated with each precinct is a corresponding data-stream, which is organized into packets. A packet which is the smallest accessible portion in the JPEG2000 code-stream is uniquely identified by four parameters: image component (C), resolution level (R), precinct (P), and quality layer (L). Figure 3 illustrates the JPEG2000 code-stream structure, which consists of a main header followed by one or more tile-streams and an End-of-Code-stream (EOC) marker. Each

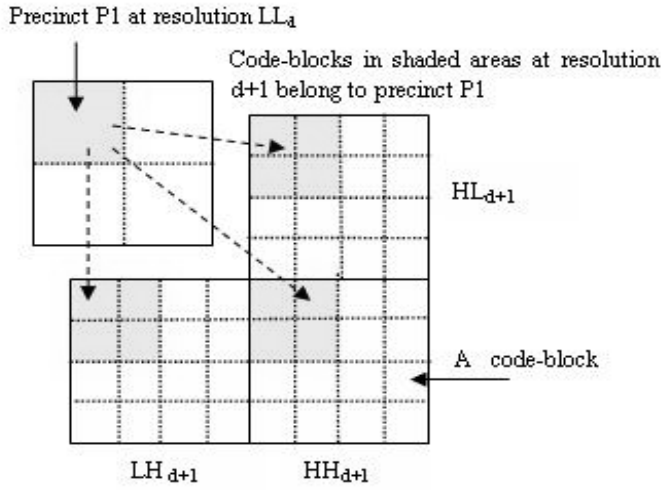

Figure 2. Precincts and code-blocks.

tile-stream is comprised of a tile header followed by the tile's packets which are sequenced in the code-stream according to one of five progression orders denoted LRCP, RLCP, RPCL, PCRL and CPRL. Packets that correspond to a specific resolution, component, layer or spatial region can be extracted from the code-stream to display the interested part of a image which makes it possible that we only need to transmit the interested packets to a client instead of transmitting the entire code-stream [1].

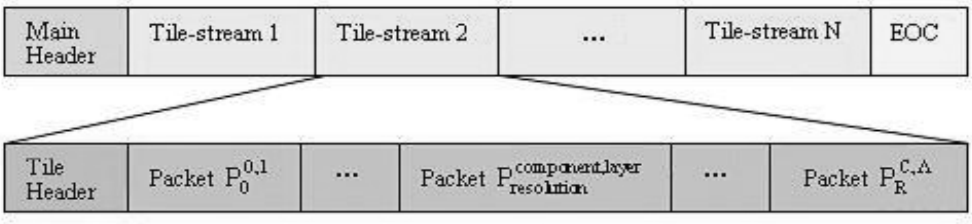

Figure 3. JPEG2000 code-stream structure

2.2 Overview of JPEG2000 Interactive Protocol

2.2.1 Client-Server Architecture

JPIP (JPEG2000 Interactive Protocol) is Part 9 of the JPEG2000 image compression standard. JPIP specifies a protocol consisting of a structured series of interactions between a client and a server by means of which image file metadata, structure and partial or whole image code-streams may be exchanged in a communications efficient manner [3]. JPIP utilizes JPEG2000 scalable features to allow the client to request the window of interest (WOI) of an image that are applicable to the client's needs without directly accessing the compressed target file. Figure 4 provides an overview of JPIP client-server architecture structure [4]. The client uses the WOI request to define the resolution, spatial region, component and layer of interest. After receiving a request from a client, the JPIP server generates appropriate response stream (precinct-based streams, tile-based streams or whole images) from the target compressed image. The client contains a cache of the data previously transmitted by the server and the server may maintain a model of the client's cache to avoid transmitting the data the client already has. The client can decompress the JPEG2000 stream in the cache and render the WOI before waiting for new data to arrive. As the client receives more data, the cache contents grow and decompressing and rendering are repeated to refine the image quality (LRCP progression mode) or increase the image resolution (RLCP or RPCL progression mode). The JPIP protocol can be used over several different transport environments such as HTTP, TCP and UDP.

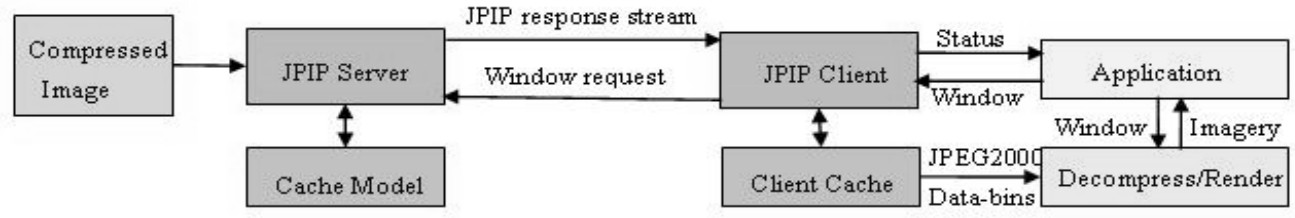

Figure 4. JPIP client-server architecture

2.2.2 JPP-stream and JPT-stream media types

JPIP partitions JPEG2000 code-stream into a collection of "data-bins" which contain portions of a compressed image representation. JPIP defines two partitioning schemes, based on either precincts or tiles. In the case of precinct-based scheme, each tile header is assigned its own data-bin and each precinct is assigned to a data-bin which contains the precinct data-stream. In the case of tile-based scheme, each tile is assigned a single data-bin. In both cases, the code-stream's main header is assigned its own data-bin [3][4].

JPIP uses JPP-stream and JPT-stream as media types to present JPEG2000 code-streams and file format data. The JPIP server delivers response data with either JPP-stream type or JPT-stream type. Each media type consists of a concatenated sequence of messages, where each message contains a portion of a single data-bin preceded by a message header. Each message is completely self-describing, so that the sequence of messages may be terminated at any point and messages may be re-ordered without losing their meaning. Precinct data-bins and tile header data-bins appear only within the JPP-stream media-type and tile data-bins shall be used only within the JPT-stream media type. Both JPP- and JPT-stream media types use the main header data-bin and metadata-bins [3].

2.2.3 Caching and Sessions

As already noted, the client can contain a cache to store all information received previously from the server, so the server need not retransmit this information in response to future requests. The JPIP protocol defines two different types of requests: stateless requests and requests which belong to a session [3][4]. The purpose of sessions is to reduce the amount of explicit communication required between the client and server. Within a session, the server may maintain a model of the client's cache so that it can send only those portions of the compressed image data or metadata which the client does not already have in its cache. A stateful request contains cache model manipulation statements which are to be processed to update the server's cache model before determining the data that should be returned to the client in response to the request. As for stateless requests, the server need not maintain state information between requests, so the client should identify the information about its cache contents with each request to avoid the transmission of redundant data.

2.2.4 Client Request and Server Response

The JPIP request consists of a sequence of fields, such as target identification fields, session and cache management fields, view-windows request fields and so on [3]. Each request field is a "name=value" pair. In HTTP, multiple fields are joined with an "&" character and the request may be part of the query field of a GET request (after the "?" character), or the body of a POST request. View-window field contains 3 two-dimension parameters. The size parameters (sx and sy) and the offset parameters (ox and oy) specify the width and height of the desired image region and the top-left corner of that region, with respect to a whole image that has the given frame size (fx and fy). For example, a client wishing to fill a 640 × 480 display with the whole image could make a request as follows "fsiz=640,480&rsiz=640,480&roff=0,0". If none of the available image resolution in the

JPEG2000 code-stream corresponds exactly to the requested frame size, the JPIP server can modify the request parameters in aspect ratio. The JPIP response consists of the following elements: status-code, reason-phrase, jpip-response-header and return data [3]. In HTTP, the status code and the reason phrase appear in the status line, the JPIP response headers appear in the HTTP response headers and the return data (if any) appears in the HTTP entity-body. If the server has modified the request fields, these modified fields should be included in the JPIP response headers using header names which are constructed by prepending the name of the modified request field with the string "JPIP-". The return data is either JPP-stream or JPT-stream terminated by a single EOR (End Of Response) message.

3 SYSTEM IMPLEMENTATION

3.1 Image Compression

Firstly, we used JPEG2000 image compression standard to compress DICOM images. There are two different partition methods in JPEG2000 to provide spatial random access based on either precincts or tiles. In order to compare the two partition methods, we used them to compress a computered tomography image respectively (compress the image without tiles and with 128×128 tiles, the code-stream size is 190,506 bytes and 173,093 bytes respectively) and extracted five different view-windows from the two code-streams. Table 1 shows the performance between the two methods. When the tiles align perfectly with the requested view-window, the tile-based method transmits fewer data than the precinct-based method because there is no redundant data need to be transmitted. But usually the view-window is not perfectly covered by tiles, in such cases the precinct-based method has a better performance.

Table 1. The performance of spatial random access.

Requested View-window	Transmitted Bytes	
	JPP-stream	JPT-stream
fsiz=512,512&roff=0,0&rsiz=256,256	47,000	42,735
fsiz=512,512&roff=128,128&rsiz=256,256	65,761	48,301
fsiz=512,512&roff=64,192&rsiz=256,256	68,753	101,108
fsiz=512,512&roff=96,160&rsiz=290,192	74,741	91,938
fsiz=512,512&roff=156,82&rsiz=256,256	82,608	100,522

The precincts from resolution LL_D contain low frequency information of the image, so the reconstructed image by the precinct-based method provides much more navigation context for the client as illustrated in Figure 5.

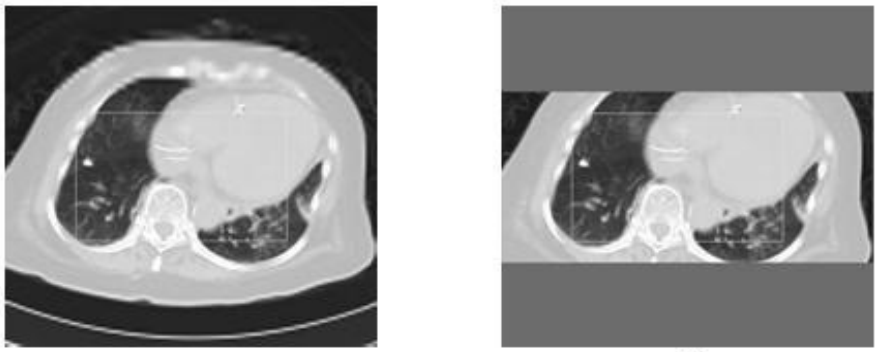

Figure 5. The view-window request is "fsiz=512,512&roff=96,160&rsiz=290,192". (a) The image is compressed without using tiles. (b)The image is divided into 128×128 tiles.

From the results stated above we can see that the precinct-based method is more efficient than the tile-base method and is well suited to the efficient communication of images. So we compressed DICOM images using precinct-based method without using tiles.

Both precinct size and resolution number affect image compression ratio. As the precinct size or the resolution number increases, the image compression ratio increases. But if the precinct size or the resolution number is too large, the efficiency of spatial accessibility will decrease. Considering both storage capacity and communication efficiency we used 3-level reversible wavelet decomposition (four resolutions) and 32×32 precinct size at all resolutions as the compression parameters.

3.2 System Architecture

Our interactive image communication system is based on client-server architecture (Figure 6). The JPIP clients communicate with the JPIP server through intranet or internet and the PDA clients can access the JPIP server via 802.11b wireless network. We implemented JPIP on HTTP protocol. The JPIP client sends HTTP GET requests containing JPIP requests in query field to the JPIP server. Before responding the client, the JPIP server retrieves requested images from the PACS server, stores them into local image database and loads the image data (DICOM header and encoded pixel data) into memory. When the same image is requested the second time, the JPIP server will read the image data directly from its memory. This will speed the response process greatly. The database and memory management will be discussed later. The server response is JPP-stream which contains a sequence of messages and each message contains the data from a single packet. The client parses the response stream, stores the received packets into its cache and renders the interested view-window.

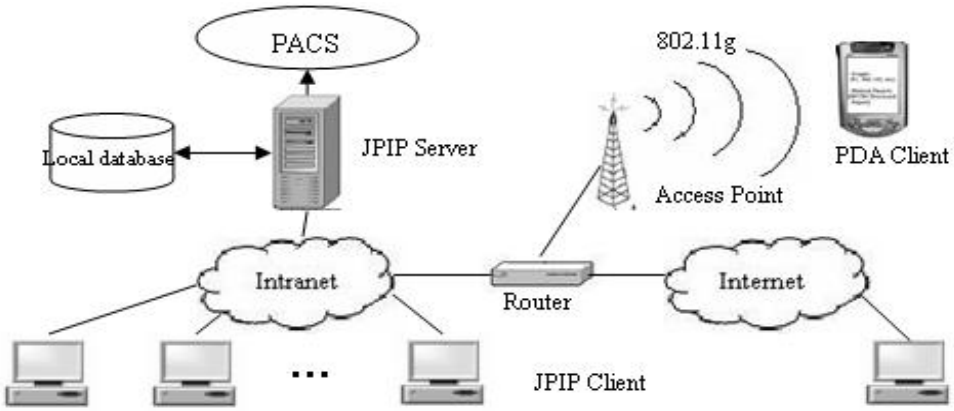

Figure 6. Architecture of the interactive image communication system

3.3 Database and Memory Management

A local image database is maintained on the server side. The purpose of maintaining an image database is to facilitate the responding process. When an image is requested the second time, the JPIP server doesn't need to download the image again. As we know, a DICOM image is identified by patient UID, study UID, series UID and image UID, so in the memory the image objects are organized in hierarchical structure. When a new request is arrived, the server firstly finds the requested image in its memory. If the image is already in the memory, the server can read image data directly; otherwise the server will find the image in local database. Similarly, if the image exists in local database, the server loads image data into memory form its hard disk; if not, the server will download the image form PACS server and then store it on local hard disk, insert the image information into database and load the image data into memory. Each image object in memory has a life period which is defined by the period from last access time to current time. If the life period of an image object is too long and exceeds a given limit, the image object will be removed from memory.

3.4 Cache and Session Management

On the client side, the client cache stores the packets received from the JPIP server and each packet is identified by four parameters: resolution, layer, component and precinct. Before rendering the view-window, the needed packets will be extracted from the cache and be reorganized into a JPEG2000 code-stream. On the server side, a cache model is maintained for each session. The cache model stores information of each packet about whether this packet is received by the client, so the JPIP server can avoid sending redundant data to the client. The client request contains a "model" field which describes the data-bins the client has received from last request. Using this "model" field (if one exists) the JPIP server firstly updates the cache model and then formulates its response. Both additive explicit and implicit forms are used for bin-descriptor values to facilitate the efficient exchange of cache model information. Currently, we only associated a cache model and one channel with each session. When a request for new session is arrived, the JPIP server will generate a random number as the channel ID and send it back to the client. In future requests, the client will use this channel ID to communicate with the server.

4 RESULTS

4.1 Resolution Scalability

We used a computed radiography image with original size of 2048×2500 pixels to demonstrate the interactive features of this image communication system. The size of the original image and the lossless compressed image are 9.76 Mbytes and 5.18 Mbytes respectively. There are four available resolutions embedded in this compressed image and the client can request and display the image at any interested resolution. The following stateful request was used to retrieve a quarter resolution of this image:

<<GET jpip?target=cr.dcm&fsiz=256,313&roff=0,0&rsiz=256,313&type=jpp-stream&cnew=http HTTP/1.1
>>JPIP-cnew:cid=18136
… (Rest of the response to request)

The type request field indicates the type of requested return data and the cnew request field asks the server for a new channel and identifies the transport protocol to be used during communication with this channel. The JPIP server extracted the relevant packets from the compressed file, assigned a channel ID and generated a sequence of messages to respond the client. The data transmitted in the network is 113 Kbytes which is only 2.13% of the full compressed image. With a low resolution image to preview, the client can easily choose the interested region to view in higher resolution. This is particularly useful when viewing images on limited bandwidth networks and when using low power devices with limited display capabilities such as mobile devices. Figure 7(a) shows the resulting image at PACS image workstation.

At the image workstation, image is displayed progressively by resolution where the progression in each resolution is by quality. When more data is arrived, the client repeats decompressing and rendering to increase the image resolution or refine the image quality.

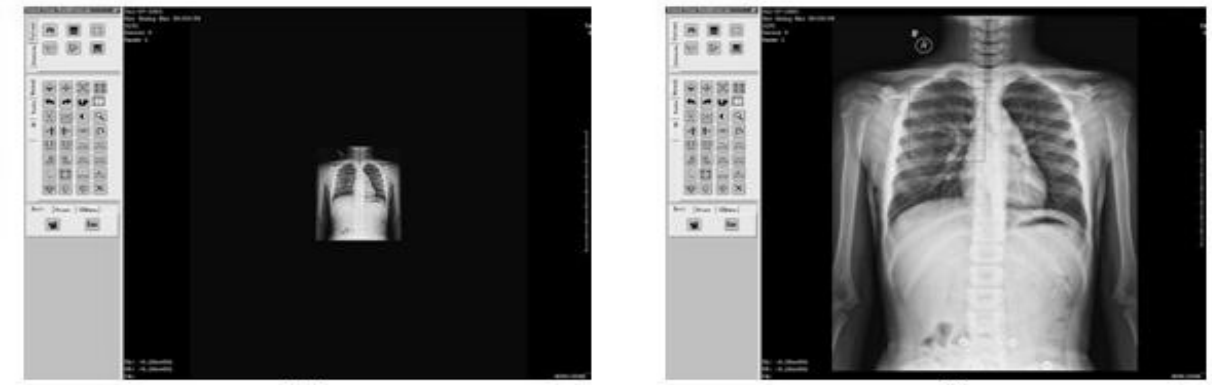

Figure 7. (a) The image is viewed at quarter resolution. (b) Spatial random access: Image reconstructed by the JPIP client at view-window: fsiz=2048, 2500&roff=504,504&rsiz=512,512.

4.2 Spatial Random Access

After downloading a low resolution image to preview, the client can zoom in on any interested part of this image. The following stateful request was used to retrieve a lossless 512×512 WOI which is offset by (504,504) pixels from the top left corner of the image:

```
<< GET jpip?target=cr.dcm&fsiz=2048,2500&roff=504,504&rsiz=512,512&type=jpp-
stream&model=Hm,H,r0
        &cid=18136 HTTP/1.1
>>  … (Response to request)
```

In this request, the model request field tells the server the client already had the main header ,tile header and all data-bins at resolution level 0 in its cache and the cid request field identifies the channel ID. The server updated the cache model and then responded to the request by sending 362 Kbytes of information relevent to the requested WOI. At the client side we used a set of empty packets to reconstruct the code-stream, so the image information outside the WOI can also be decoded and displayed. This approach provides some navigation context about regions outside the WOI. Figure 7(b) shows the resulting reconstructed image at the PACS image workstation where the WOI marked by red square box is reconstructed at full quality and regions outside the WOI are reconstructed with a lower quality. The client can navigate in the image by changing the WOI. This time the client only reconstructs the WOI image instead of the full image to reduce the decoding time. After decoding the reconstructed WOI image, the new WOI will be rendered at full quality.

4.3 PDA use case

For the case of browsing high resolution medical images on a PDA, we used DELL X51V Pocket PC and 802.11b wireless network. The PDA device features a 624MHz Inter XScale PXA270 processor, 64 MB flash ROM and a 480×640 TFT screen. The operating system is windows mobile 5.0. An embedded JPIP client software was built in the PDA to communicate with the JPIP server. To demonstrate the result, we requested the same computed radiography image. Firstly we retrieved a low resolution image to preview, and then selected a WOI to zoom in. Figure 8 shows the resulting image on the PDA.

Figure 8. Browsing high resolution image on a PDA: (a) Low resolution image preview. (b) Reconstructed WOI image at view-window: fsiz=1024,1250&roff=256,384&rsiz=256,256.

In figure 8 (a) the image is viewed at quarter resolution with size of 256×313 pixels. The red square box can be moved to select a region of interest to zoom in. For viewing the details of a interested region, we only reconstructed the WOI image without reconstructing regions outside the WOI since PDA has limited hardware resources. Figure 8 (b) demonstrates a 256×256 WOI which is offset by (256,384) pixels from the top left corner of half resolution image. The red square box in the icon image on the left of figure 8 (b) shows the position of the current WOI in full image. This box can be moved to change the WOI and navigate in the image. Some simple image processing tasks such as zoom, pan and window settings changing are provided on the PDA client to browse high resolution image efficiently.

4.4 Performance of JPIP server

In order to test the performance of the JPIP server under heavy load, we used Mercury LoadRunner to generate 100 Virtual Users to access JPIP server simultaneously. We started 20 Virtual Users every 30 seconds and after 2.5 minutes the 100 Vusers ran simultaneously for 1minute, and then these Vusers were stopped gradually. This scenario lasted 6 minutes and 17 seconds in total. To run the test we used 50 images including computed radiography image, computed tomography image and magnetic resonance image among which each Vuser requested two images randomly and did a series of interactions with JPIP server about these images. The JPIP server was tested on DELL OptiPlex 745 desktop PC with Inter core2 CPU 1.86GHz and 1.00GB memory. Figure 9 shows the resulting graphs.

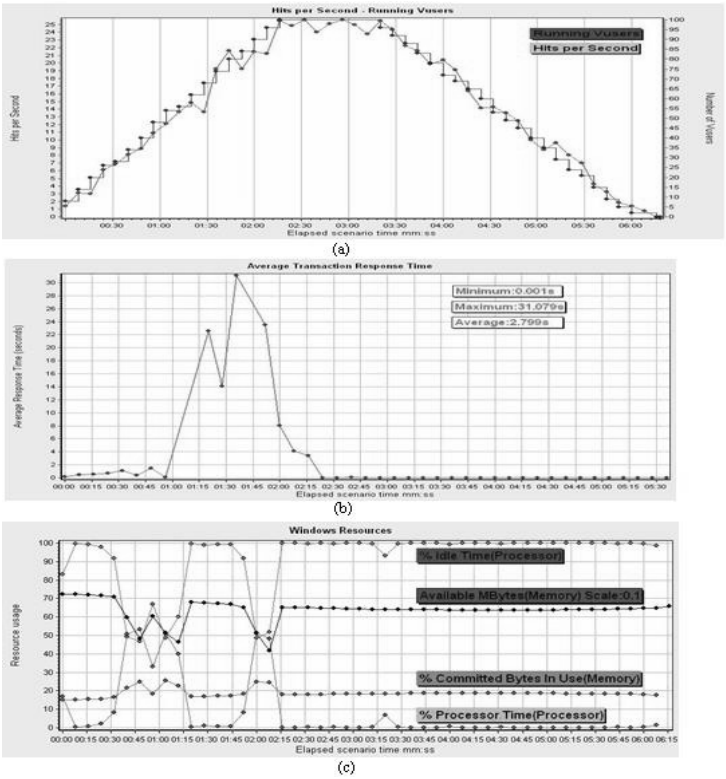

Figure 9. Performance of JPIP server under load tested by Mercury LoadRunner: (a) Hits per Second and Running Vusers. (b) Average Response Time. (c) Windows Resources.

Figure 9 (a) displays the number of running virtual users and requests during each second of the test. The number of Hits per Second increases as the number of Vusers increases. In whole scenario there were 5,470 hits (requests) in total and 14.471 hits per second in average. All the requests were responded correctly by JPIP server. The average response time to each request is showed in Figure 9 (b). The most time consuming part of the server application is to downloading image from PACS server and transforming the format of image (especially the computed radiography image), so when more and more Vusers started, the requests for new images increased and the response time became longer. The maximum and minimum response time is 31.079s and 0.001s and the average response time is 2.799s. Figure 9 (c) shows the status of resources (CPU, memory) used on JPIP server measured during the test. We can see from this graph that the JPIP server ran stably during the whole scenario.

5 CONCLUSIONS

JPIP is a flexible and efficient image browsing protocol. Based on JPIP, our interactive image communication system which is integrated successfully with PACS enables high resolution medical images to be transmitted and browsed efficiently across wide area network or can be used in enterprise applications. We also used JPIP in a PDA-based wireless medical system in which large medical images can be transmitted through wireless network and be displayed on the lower resolution screen of a PDA in an efficient way.

REFERENCES

[1] D. Taubman and M. Marcellin. JPEG2000: Image Compression Fundamentals, Standards and Practice. Kluwer Academic Publishers, 2002.

[2] ISO/IEC 15444-1 JPEG2000 image coding system Part 1:Core coding system.

[3] R. Prandolini, G. Colyer, and S. Houchin, "15444-9:2004 JPEG 2000image coding system - Part 9: Interactivity tools, APIs and protocols– JPIP," Final Publication Draft Revision 3, ISO/IEC JTC 1/SC29/WG 1 N3463, November 2004.

[4] D. Taubmana and R. Prandolini, "Architecture, Philosophy and Performance of JPIP: Internet Protocol Standard for JPEG2000," International Symposium on Visual Communications and Image Processing(VCIP2003), 2003.

[5] Junichi Hara, "An Implementation of JPEG 2000 Interactive Image Communication System", Circuits and Systems, 2005. ISCAS 2005. IEEE International Symposium on 23-26 May 2005 Page(s):5922 - 5925 Vol. 6..

A DICOM-RT radiation oncology ePR with decision support utilizing a quantified knowledge-base from historical data

Jorge R. Documet*[a], Brent Liu[a], Anh Le[a], Maria Law[b]
[a]Image Processing & Informatics (IPI) Laboratory, Radiology Department, University of Southern California, Marina del Rey, CA 90292, USA
[b]Department of Health Technology and Informatics, The Hong Kong Polytechnic University, Hong Kong, China

ABSTRACT

During the last 2 years we have been working on developing a DICOM-RT (Radiation Therapy) ePR (Electronic Patient Record) with decision support that will allow physicists and radiation oncologists during their decision-making process. This ePR allows offline treatment dose calculations and plan evaluation, while at the same time it compares and quantifies treatment planning algorithms using DICOM-RT objects. The ePR framework permits the addition of visualization, processing, and analysis tools, which combined with the core functionality of reporting, importing and exporting of medical studies, creates a very powerful application that can improve the efficiency while planning cancer treatments.

Usually a Radiation Oncology department will have disparate and complex data generated by the RT modalities as well as data scattered in RT Information/Management systems, Record & Verify systems, and Treatment Planning Systems (TPS) which can compromise the efficiency of the clinical workflow since the data crucial for a clinical decision may be time-consuming to retrieve, temporarily missing, or even lost. To address these shortcomings, the ACR-NEMA Standards Committee extended its DICOM (Digital Imaging & Communications in Medicine) standard from Radiology to RT by ratifying seven DICOM RT objects starting in 1997 [1,2]. However, they are not broadly used yet by the RT community in daily clinical operations. In the past, the research focus of an RT department has primarily been developing new protocols and devices to improve treatment process and outcomes of cancer patients with minimal effort dedicated to integration of imaging and information systems. Our attempt is to show a proof-of-concept that a DICOM-RT ePR system can be developed as a foundation to perform medical imaging informatics research in developing decision-support tools and knowledge base for future data mining applications.

Keywords: Radiation Oncology ePR, Quantified knowledge base, DICOM, DICOM-RT, Decision support, web

1. INTRODUCTION

The current various proprietary systems that are involved in the process of planning cancer treatment are disseminated throughout the Radiation Oncology department which makes integration and sharing of the information challenging. Even with DICOM-RT compliant systems from vendors, there still is a lack of Medical Imaging Informatics tools to quantify knowledge from these standardized DICOM-RT objects. Thus, standard data that can be imported to the ePR combined with analysis and visualization tools will provide better decision support tools for the physicians.

In order to perform treatment planning and to track the progress of the treatment of prostate cancer patients, clinically relevant data needs to be retrieved from various sources. For example, treatment records for a single RT session would either be stored on paper or within an RT information management system. Most of these systems can receive DICOM PACS studies which are used to perform treatment planning. However, the treatment planning systems (TPS) generate image-related data such as isodose curves and structure contours overlaid on diagnostic images. RT image data such as reference images either come from a simulator or from the TPS (eg, DRR's). Finally, each RT modality may have verification images (eg, portal images) acquired for a treatment session. In order to review a patient's case with prostate cancer, the physician and physicist must interface with these various data sources which increase time in the RT department. Although some RT image data (eg, portal, simulator, DRR, etc) are already DICOM-RT compliant, there are still pertinent data from both the TPS and the record and verify systems (eg, critical structure curves, isodose lines,

dose volume histogram (DVH) curves, etc) that have yet to be addressed. Virtually each RT modality contains a separate proprietary treatment planning system with no standard for sharing the pertinent clinical data.

With the emergence of PACS as an imaging informatics tool, it has improved the workflow efficiency within the Radiology Department [3]. RT and the utilization of image-guided RT Systems to treat tumors have benefited from PACS and the DICOM standard by utilizing clinical images from Radiology. However, the real benefit to an RT department is to extend the experience and knowledge gained from system integration of PACS and modalities to the various sources of clinical data dispersed within the RT department. To date within the RT department, one of the biggest challenges towards an effective and efficient clinical workflow is integrating pertinent image and image informatics data into one source point for all clinical users. These include a lack of formal methodology to define the clinical workflow of tumor cases, lack of system integration, and insufficient IT experts in RT-related applications. The need for an integrated solution utilizing a DICOM-based ePR server becomes apparent. In addition, the redesign of workflow to incorporate the information will help to enrich not only the electronic patient records but also provide a platform for researching and developing decision-support tools. Given this backdrop, the implementation of a DICOM ePR server would be an effective and efficient one-stop-shop source for tracking the treatment progress of patient's with prostate cancer by merging the data from the various sources and present them in a user interface that will be designed for ease-of-use. In addition and more importantly, it provides a foundation of standardized data objects with which to build a knowledge base and data mining tools for clinical decision-support that would have been much more challenging to accomplish without standardization of this RT imaging and informatics data within the ePR system. [4]

This research aims to present a scalable and expandable ePR system with DICOM-RT compliance that can analyze historical patient data and create a quantified knowledge base for decision support to improve the planning of cancer treatments. Measurements of overdose of critical structures and underdose of tumor regions form part of this knowledge base. This ePR integrates DICOM-RT objects from different vendors currently disseminated in multiple systems, and it also provides a mechanism with alerts and notifications in order to reduce the approval time in the treatment planning process. The ePR has been built using PHP5 (Pre Hypertext Preprocessor) language for the server side and a combination of javascript, and web technologies for the client side. The ePR will be used by dosimetrists, physicists, and radiation oncologists. In developing the ePR and its infrastructure including quantified knowledge, we have applied this methodology to Prostate Cancer patients receiving 3D Conformal Radiation Therapy.

2. METHODS AND MATERIALS

2.1 Workflow for prostate cancer

One of the most important first steps for system integration and development and ePR withof clinical image and information systems is to research the workflow model of the clinical operations. Since the focus of this research will be on patients with prostate cancer, the workflow related to these particular treatment cases will be studied. A general clinical workflow model for radiation treatment of prostate cancer cases was developed for the Departments of Radiology and Oncology at UCLA (University of California Los Angeles) as shown in Figure 1. Although this workflow is tailored to one clinical site, the general workflow steps are common across all RT departments. The treatment starts when the patient is diagnosed with prostate cancer. The patient then meets with the physician(s) to determine what the best treatment for the patient is. If radiotherapy is the one chosen, at this time it will be also determine which type will be performed. At this stage a diagnostic CT is acquired and those images will serve for the planning done at the next steps. After CT images are taken, the virtual simulator images and preliminary objects are created. As shown in figure 1, there is a variety of TPS at the RT department at UCLA, which are utilized depending on the history of the patient; for our workflow analysis we found that an important decision for treatment is whether the patient has had any prior surgery. Either way, the radiologist and the radiation oncologist review the patient's case and the radiation oncologist defines the initial plan parameters such as dose limits and constraints, critical structures, and tumor volume to be treated. After the initial parameters are set then the physicists' team computes the plan based on the dose constraints on the corresponding TPS. An iterative process is then started between the radiation oncologist and the physicists' team until the final plan is approved. This is what we have called the feedback loop, which represents the inverse treatment process and can become tedious and time consuming if many iterations are needed. This becomes the area of focus where decision-support tools may benefit during the decision-making. If more a priori knowledge and robust quantification and visualization tools can be included during the decision-making process of the initial plan parameters, then it is possible to reduce the overall time needed for treatment planning.

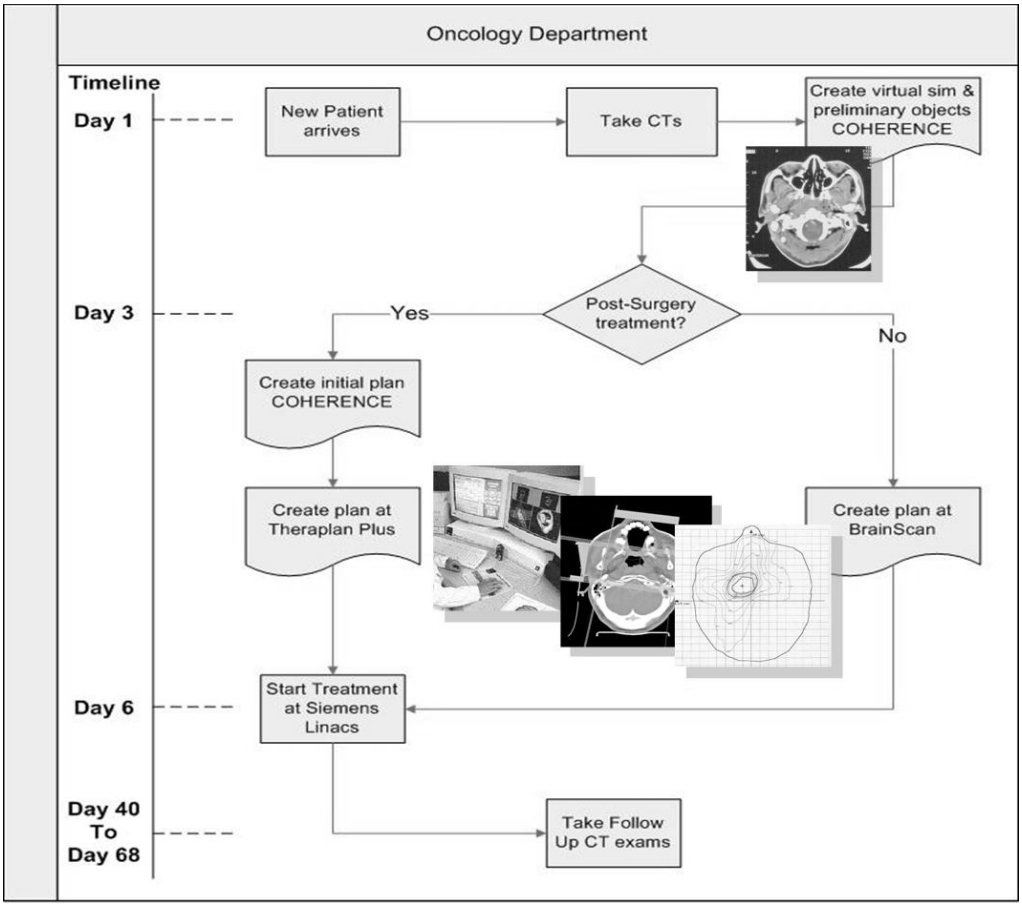

Fig. 1. The workflow at UCLA for prostate cancer patients. Usually a treatment can last from 40 to 68 days. The ePR will try to help reducing the 3-day interval that takes to get a plan for treatment at the RT department. The users via the web interface can see the status of the plans and contribute to improve the efficiency of the planning stage.

2.2 The ePR architecture

The ePR is a web based application that complements the current TP systems in a RT department. It is a primary goal to be easily included in the workflow in the current planning of cancer cases, thus it should not be considered as a replacement to any existing application. The design has considered having the capability to add necessary modules as required. At the current time, the modules that we have designed include the DICOM, data mining and knowledge base as depicted in Figure 2 below. The DICOM module allows the ePR to receive DICOM and DICOM-RT objects from either the PACS or any TPS that can export DICOM-RT objects. The knowledge base module will be a set of rules for data extraction and data compilation related to a specific type of cancer, thus, different types of cancer will have a different set of rules but both will share the same mechanisms for extraction and compilation. The data mining module will interpret the data collected by the knowledge base and it will further classify it for later retrieval; one of the features of this module is to identify possible trends and correlation on the data collected from the different systems that take part on the planning of cancer treatments. The database module is needed to interact with the MySql database where the data is stored. The programming language utilized to develop the ePR is PHP5 running on an Apache 2.0 web server. The platform where the ePR is installed is a Windows XP Professional Pentium 4 and 2.5 GB of memory, but we have also tested the application on a linux server.

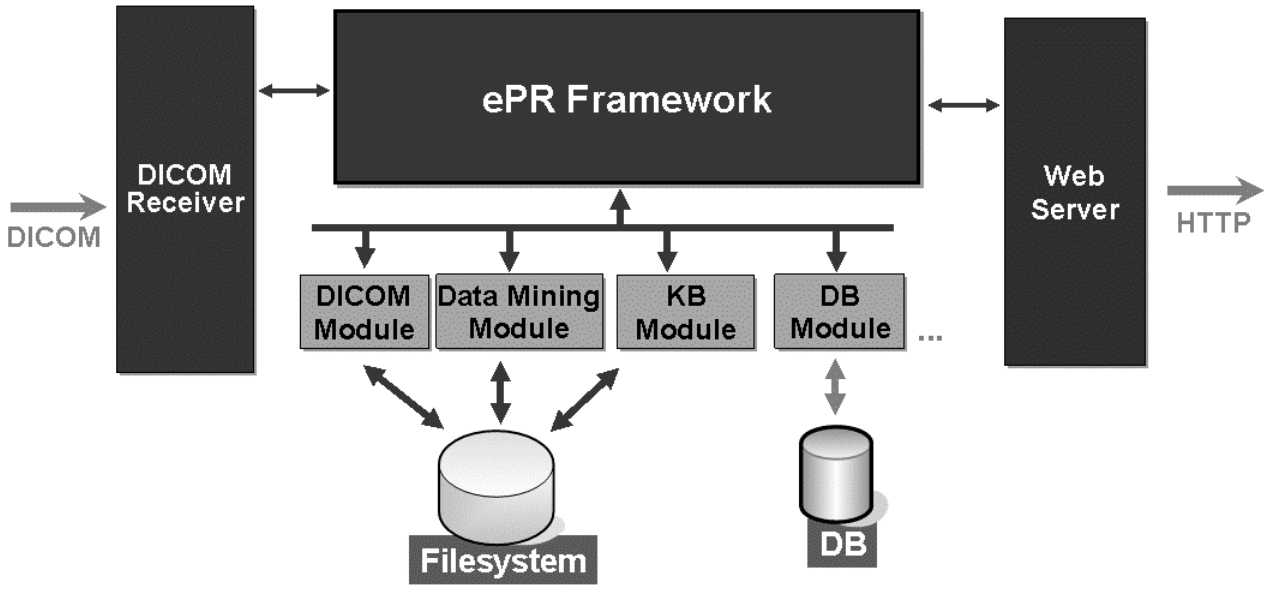

Fig. 2. The architecture of the ePR. The DICOM receiver from one end listens for incoming DICOM data, then the data is extracted from the DICOM objects (including RT objects) and populated to the database. From the data collected the Data Mining and Knowledge based modules perform the proper analysis of the data and it is saved back to the database. The users via the web interface can browse the knowledge and also contribute to it by uploading new cases.

2.3 Defining the knowledge base

Utilizing the clinical workflow model as a basis, a clinical scenario is identified where decision-making is crucial from the physician and the tools to help this decision-making process are lacking. The first objective is to define the knowledge. The starting point for defining knowledge is based on the expert's ability, in this case, the oncologist and the physicist, to utilize data and other criteria in evaluating, grouping, and defining certain clinical characteristics that are extracted from the standardized DICOM-RT objects stored within the ePR system. Query and search engine tools will be researched and developed to mine the knowledge base which can potentially assist in the clinician's decision-making process, such as when the oncologist needs to review a treatment plan and determine whether it should be approved or further modified and would like to reference previous treatment plans to gain an understanding of what criteria was used to approve previous plans. Additionally, quantification and visualization tools will be developed to extract and present pertinent knowledge for the clinician to review and utilize as a decision support tool. The knowledge base will be designed in an object-oriented and modular fashion so that additional knowledge and new object classes defined in the future can be easily integrated without affecting the overall design. This medical imaging informatics approach is a unique and novel approach towards development of clinical decision-making tools for the RT field. Although current manufacturers have the ability to develop such tools within the TPS, their primary focus has been on high-computational complex calculations and re-calculations of treatment plans. In addition, they have been slowed in part by the lack of availability of standardized DICOM-RT data objects. [5]

Currently we have identified the radiation therapy dose, the dose volume histogram (DVH) from the dose as key information for data mining. The information stored on the RT Structure set as well as in the Regions of Interest (ROI) form also part of the knowledge base that we consider important for the decision support tools.

3. RESULTS

The ePR system has been successfully tested at the IPI (Image Processing and Informatics) Laboratory from data collected at the Radiation Oncology department at UCLA. The collected data includes DRR images, CT images, Structure Sets and Radiation Therapy Plans for prostate cancer cases treated on 3D conformal TPS. We have been able of replicating RT specific data such as DVH curves, isodose curves and ROI contours. These data objects were exported in the DICOM-RT format and imported into our ePR system. Extracted knowledge includes overdose for critical

structure regions and underdose for tumor regions, which are key whenever an iterative process during treatment planning happens. As mentioned in sections above, the long-term goal of the ePR is to provide with an initial plan that was data mined through a historical database of treatment plans that would be a good starting point for a new plan. In that process, the users of the ePR will be able of dynamically interact with the data via a web interface. Figure 3 shows a screenshot of this interface; in this case, we can dynamically display the different ROIs from a particular study and show them on the corresponding CT slice. We are currently working on having a dynamic interface to provide the users with a mechanism to extract which slices on a given CT case will receive an overdose amount according to a manual constraint of dose; this way the users will be able of fine tuning the treatment parameters at the ePR. The interaction of the users will allow the ePR to increase the amount of knowledge for later data mining scenarios.

We are currently working developing the data mining tools to extract the quantified knowledge for decision-support.

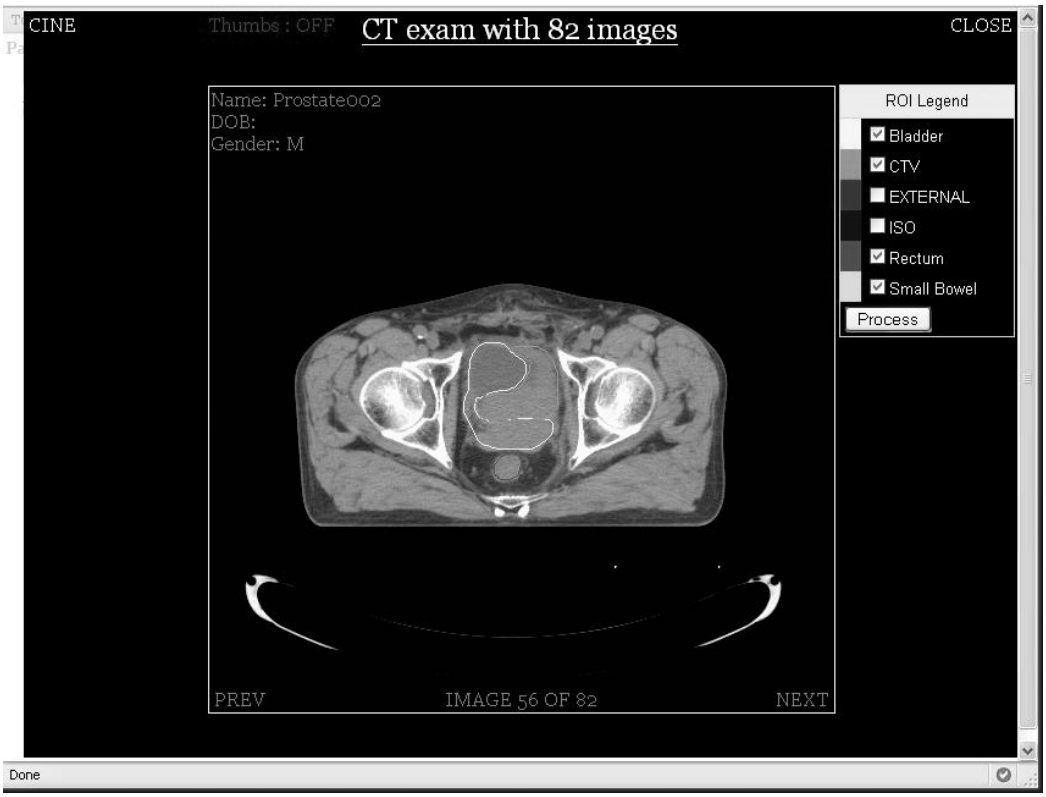

Fig. 3. An screenshot of the ePR. The Graphical User Interface (GUI) allows the users to interact with the data stored on the ePR. In the screenshot shown above the users can dynamically select the ROI curves that they will like to display on top of the CT images. Both, the curves data points and the names of the ROIs are extracted from the RT objects that were sent to the ePR.

4. DISCUSSION

Integrating data from different treatment planning systems into a centralized and modular ePR can serve as a data mining repository for retrospective analysis. The repository will include values from automatic processing of the information from the DICOM-RT objects and as well from input data entered by the users. The ePR displays DICOM-RT objects including CT images, contours, DRRs, DVHs in a web-based fashion. In addition, the ePR can also send alerts every time a major event occurs, such as approval requests or physician completion tasks.

In our current stage we are still developing the DICOM-RT based ePR system for managing patients with prostate cancer particularly treated with 3D Conformal RT. This effort has been performed in collaboration with the Radiation Oncology Department at UCLA. It is important to mention that our ePR has been designed to extend its capabilities to include other type of cancer cases, i.e. brain lesions, or even different radiation treatment methods such as proton therapy cases. Data obtained from sample prostate cancer cases where the treatment was planned on 3D conformal TPS was

collected and integrated within the ePR system as an initial first step. A methodology was introduced for the development of decision-support tools based on the standardized DICOM-RT data within the ePR system. As a first step proof of concept of how crucial standardized RT data can be, a clinical scenario was developed where knowledge base was defined and quantification and visualization tools were designed to extract the knowledge and display it for a decision-making process. By implementing this DICOM-RT based ePR system, both clinical image and related informatics data are integrated into a one-stop source of pertinent clinical information necessary for making treatment decisions within the RT department and throughout the healthcare enterprise. The initial results show the confirmation that the integration of DICOM-RT objects was correct and that it can be stored and displayed similar to what is displayed within the proprietary systems. More importantly, with the availability of standardized DICOM-RT data, further knowledge base and decision-support tools development can be realized to aid the clinicians in critical decision-making processes. Future work includes the complete development and collection of the knowledge base and decision support tools as well as a clinical evaluation of the decision-support tool development.

REFERENCES

1. Digital Imaging and Communications in Medicine (DICOM), Supplement 11: Radiotherapy Objects, 1997.
2. Digital Imaging and Communications in Medicine (DICOM), Supplement 29: Radiotherapy Treatment Records and Radiotherapy Media Extensions, 1999.
3. Huang HK. 1999. PACS: Basic Principles and Applications. Wiley & Sons, NY, p. 521.
4. Law M.Y.Y., Huang H.K., Zhang X., Zhang J. The Data Model of a PACS-Based DICOM Radiation Therapy Server. Proceedings of the SPIE Medical Imaging, 5033, pp 128-129, 2003.
5. Liu BJ, Law M, Huang HK, Zee CS, Chan L, A DICOM-RT ePR Radiation Therapy Information System for Managing Brain Tumor Patents, Proceedings of SPIE Medical Imaging, 5748, pp 105-115, 2005.

The Workflow and Procedures for Automatic Integration of a Computer-Aided Diagnosis Workstation with a Clinical PACS with Real World Examples

Anh Le[a,b], Lam Mai[b], Brent Liu [a,b], HK Huang[a,b]
[a]Dept. of Radiology, USC, 4676 Admiralty Way Ste 601, Marina del Rey, CA, USA 90292;
[b]Dept. of Biomedical Engineering, USC, University Park, Los Angeles, CA USA 90089.

ABSTRACT

Digital Imaging and Communications in Medicine (DICOM) has standardized structure reports (SR) to fully support conventional free-text reports, images, and structured information, thus enhancing the precision, clarity, and value of clinical documents. The SR standard provides the capacity to link key images, region of interest within images, and measurement as result of Computer-Aided Diagnosis (CAD) process. Accordingly, SR bridges the traditional gap between CAD and PACS. Last year we presented an open and universal CAD-PACS integration toolkit that could seamlessly integrate standalone Computer-Aided Diagnosis (CAD) workstations with a clinical PACS based on Structure Report (SR) and IHE Post-Processing. In this presentation, we illustrate the workflow and procedures of CAD-PACS integration by showing examples from some available CAD applications using the toolkit. This proper integration will improve usage of the CAD applications for more accurate analysis and faster assessment in the clinical decision-making process.

Keywords: PACS, DICOM, Structured Report, Integrating the Healthcare Enterprise, CAD

1. INTRODUCTION

With the advanced technology in both image acquisition and the image interpretation, PACS studies have yielded better and more accurate diagnosis. Also, methods of interpretation have also benefited from advances in computer technology, which further elevates the development of computer aided diagnosis/detection (CAD) [1-4]

CAD is a computerized analysis method to obtain quantitative measurements from medical images along with clinical information to give clinicians and radiologists a "second opinion" to assess the clinical state of a patient under consideration more objectively [13]. CAD software can be in a stand-alone CAD workstation, or be integrated in the PACS as PACS-based CAD. In order to utilize the CAD results more efficiently and timely, CAD should be integrated with daily clinical HIS/RIS/PACS operation. In this paper workflow and procedures of the integration of CAD with PACS using a CAD-PACS integration toolkit with real world examples are presented.

2. METHODS

2.1. CAD-PACS Integration Toolkit

CAD-PACS© is a software toolkit using DICOM and IHE designed for the integration of CAD results with PACS workflow. This CAD software toolkit can be used in a standalone CAD workstation, a CAD server, or installed in a PACS workstation. Figure 2 depicts the architecture of the CAD-PACS© which has three versions DICOM-SC™, DICOM-PACS-IHE™, and DICOM-CAD-IHE™.

1. DICOM-SC™ uses the DICOM Screen Capture (SC) service which is simple but with limitation for clinical research because data mining of key quantified data is not possible. It uses screen capture to store CAD results for viewing purpose. [14-15]

2. DICOM-PACS-IHE™ uses the DICOM Structured Report (SR) [5] service and several IHE Workflow Profiles [6], the methodology is elegant but requires part of the toolkit to be installed in PACS server which would need the collaboration with the PACS manufacturer during the integration. [14,15]
3. DICOM-CAD-IHE™ also uses DICOM SR and Key Image Note IHE Profiles, this method reduces the necessity to altering the current PACS Server, but CAD results are stored in the CAD server only.

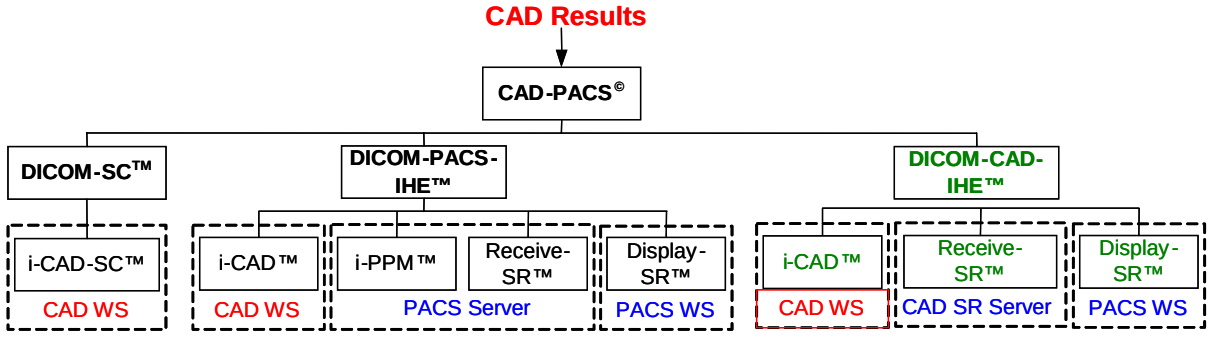

Figure 1. Left: The original design of CAD-PACS© integration toolkit with two versions: The DICOM--SC™, and the DICOM-PACS-IHE™. Right: DICOM-CAD-IHE™ is an extension from the second version by adding the capability of the toolkit for the CAD Server. The three modules i-CAD™, Receive-SR™, and Display-SR™ are the same in both DICOM-PACS-IHE™ and DICOM-CAD-IHE™ version.

The main component of the DICOM-CAD-IHE is the CAD SR Server, which is the storage of all of the CAD results in DICOM SR objects. It also includes three modules from second version [14], which are i-CAD, Receive-SR, and Display-SR. However, with the new component, CAD SR Server, the Receive-SR is not installed on the PACS Server to eliminate difficulties in implementation of PACS from vendors, and avoid an interruption of current workflow. Besides, the function and design of each module in this version is slightly different from last version to accommodate the change in architecture of the whole CAD-PACS integration system.

2.2. Architecture of CAD-PACS Toolkit: DICOM-CAD-IHE™ version

2.2.1. The i-CAD™ Module

The i-CAD module resides in CAD WS [7], providing methods to create DICOM-SR as a mean for integration. The function of each module is described as following:

1. DICOM-SR Module creates the DICOM-SR objects from information given by CAD results. Once the CAD process is done, the output is produced, which will trigger this module to create DICOM SR object content automatically. The DICOM SR object content will include the CAD summary of finding, image references and any numerical values of CAD measurement.
2. CAD-SR Module receives the DICOM SR object content from DICOM-SR Module, append the patient information to create DICOM SR file.
3. DICOM-SR C-Store SCU sends the DICOM SR file to CAD SR Server to archive.
4. DICOM-SR C-Store SCP receives DICOM study/images from PACS Server and triggers the CAD process.

2.2.2. CAD SR-Server with Receive-SR™

The CAD SR-Server is implemented as a separate server to be responsible for just DICOM-SR, storing both the DICOM SR files and contents of DICOM SR in the database. With the Receive-SR function [2], this server has DICOM capability readily query and retrieve images from PACS and receive DICOM SR from CAD WS. CAD SR Server will be used to store DICOM SR objects and content, all medical images still resides in PACS. The function is described as following:

1. The Web Server utilizes open-source Apache HTTP Server as the main component, with PHP (Hypertext Preprocessor) language as server side scripting. This Web Server is responsible of accepting HTTP request from client WS, and serving HTTP response for DICOM SR reports chosen from display patient worklist.
2. The DICOM-SR DB stores the results SR in database.
3. The DICOM SR C-Find SCU supports DICOM images query from PACS WS.

4. The DICOM SR C-Move SCU retrieves DICOM study/images from PACS Server for viewing purpose.
5. The DICOM SR C-Store SCP receives DICOM SR sent from CAD WS.
6. The DICOM SR Translator captures the metadata and content of DICOM SR to store in the database.

2.2.3. The Display-SR™

The Display-SR™ is a combination of client side modules, which is built using javascript, flash and activeX libraries. They provide user an interface for viewing DICOM SR and interacting with the CAD DICOM SR results. The function is described as following:

1. The DICOM-SR Viewer gives user the customized format for viewing DICOM SR files.
2. The DICOM Image Viewer adds the basic functionality for viewing referenced images, such as zoom, pan and windows level.
3. The Annotation Exchanger provides methods to display CAD results overlay on original image retrieved from PACS. The CAD results can be location, measurement, boundaries of lesions detected by CAD application.

2.3. Workflow of CAD-PACS Integration System

Last year, we have presented workflow of DICOM-SC and DICOM-PACS-IHE versions of the CADPACS toolkit. In this paper, we present the workflow of the DICOM-CAD-IHE. The step of the integration in Figure 2 are referred by the numerals and explained in below paragraphs accordingly.

1. *PACS PUSH*: PACS server pushes DICOM studies to CAD WS for CAD process. If the PACS Server cannot push the DICOM studies, the SR-Server can query the PACS for DICOM studies and push them to CAD WS. The CAD results are converted to DICOM SR by i-CAD upon completion of CAD process.
2. *CAD PUSH*: The i-CAD pushes the DICOM SR CAD results to CAD SR Server, which consists of a Receive-SR component and a SR-Database to store CAD results.
3. *Web-based SR Display*: The web-based Display-SR component at the PACS WS queries and retrieves DICOM SR CAD results from the CAD SR Server.
4. *Referenced Images within SR*: The Display-SR automatically query and retrieve images referenced in the DICOM SR in the PACS Server for reviewing both original images and SR.

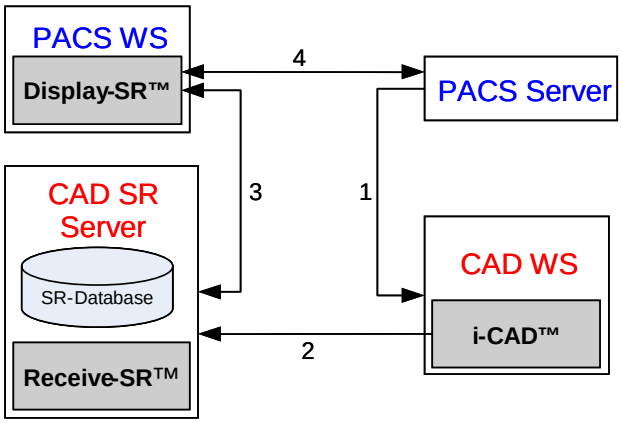

Figure 2. Workflow of the CAD-PACS integration system

2.4. Configuration

Figure 3 shows the configuration of CAD-PACS Integration System [16]. This configuration, utilizing PACS simulator [9, 10], has been presented at the 93rd Scientific Assembly and Annual Meeting of RSNA 2007 (Education Exhibit).

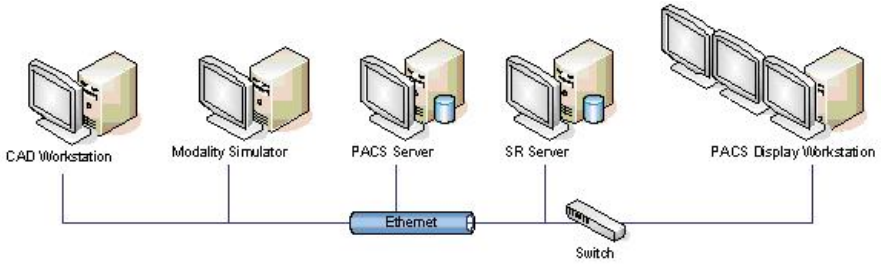

Figure 3. The CAD-PACS Integration System Configuration

3. REAL WORLD EXAMPLES

3.1. Integration using in-house CAD Software

Figure 4 shows the initial step to push images from PACS to CAD WS for process. This integration step demonstrates the ability of CAD SR Server to query the PACS server for study/images when the CAD WS has not yet been integrated with PACS for images, and RIS has not yet been implemented to order images from PACS for CAD processes. The arrow next to each study represents the study which doesn't have the DICOM SR stored in SR Server. The user will use the arrow to push the study to CAD WS.

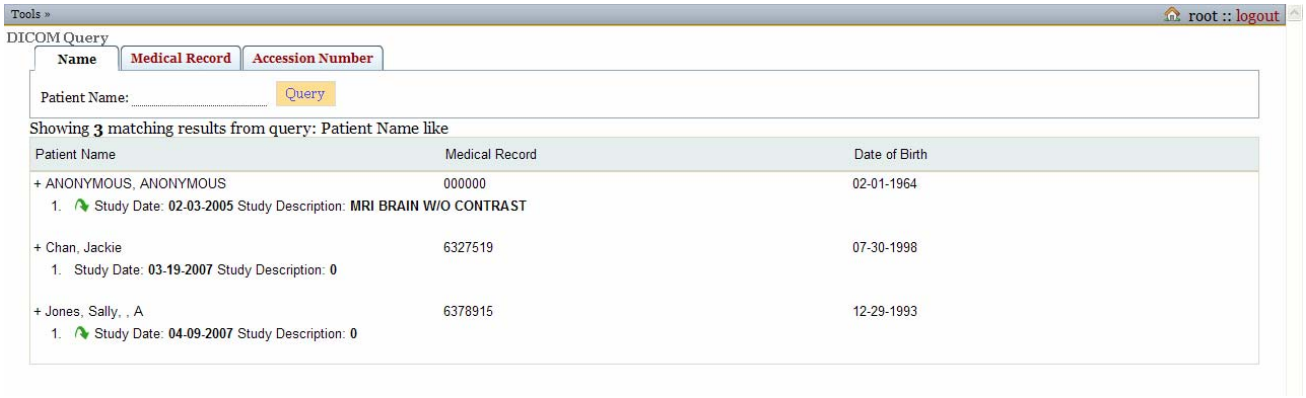

Figure 4. PACS PUSH step from PACS WS using CAD SR Server interface.

After the study is pushed to CAD WS, the i-CAD Module installed in CAD WS will receive images and the CAD process is started (Figure 5a). In this example, we use the bone age assessment CAD [12]. Figure 5b shows the step of CAD process and send the final DICOM SR to SR-Server. The CAD SR Server receives the new DICOM SR objects and updates the patient worklist as shown in Figure 5.

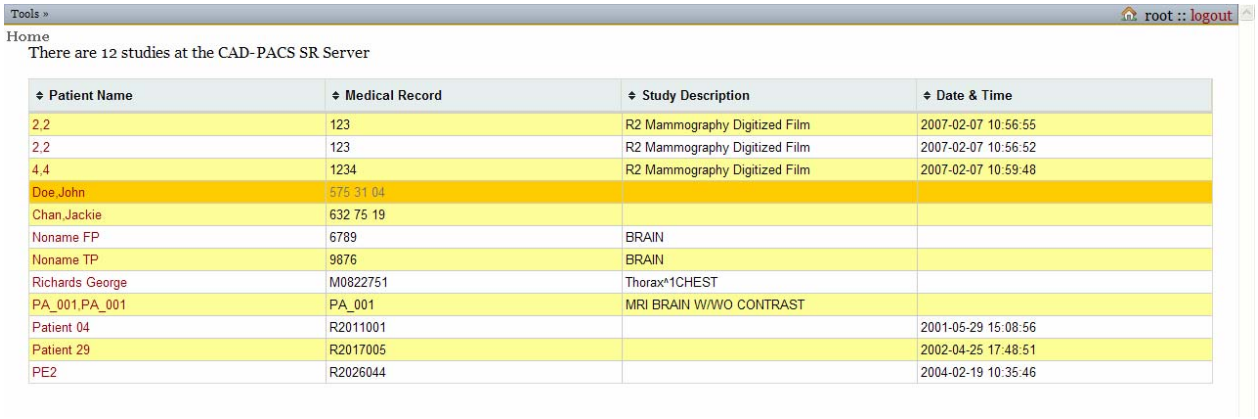

Figure 5. Patient worklist interface of CAD SR Server.

3.2. Integration using DICOM-SR from Commercial CAD Vendor

Figure 6 shows a DICOM SR Viewer and DICOM Image Viewer for referenced images. The DICOM SR objects and DICOM Images in this example is obtained from R2 Tech/Hologic [8]. The top is the patient information, left is the display for DICOM SR report and the right shows the mammography with lesion identified. The location of lesions or nodules is extracted from DICOM SR and this information is then transferred to the Image Viewer to display as annotations on top of original DICOM mammography.

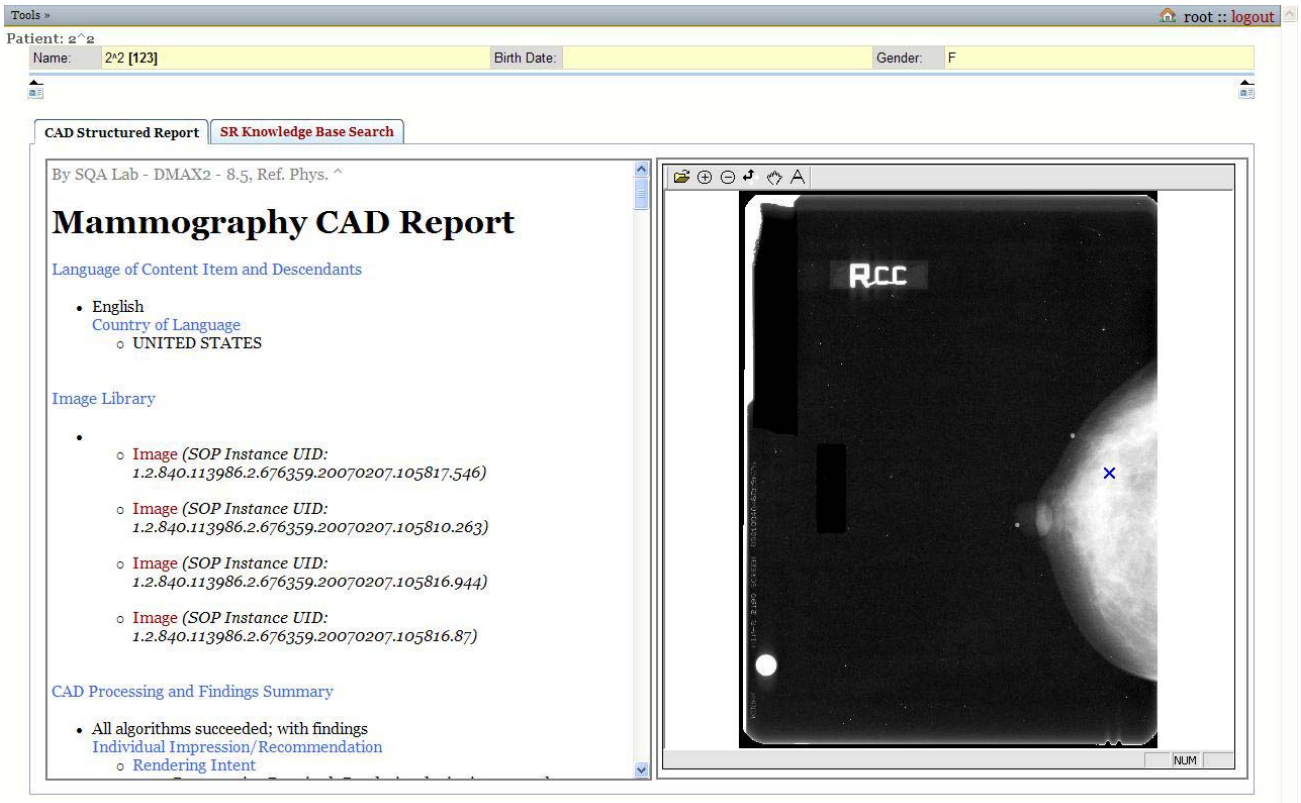

Figure 6. DICOM SR viewer and DICOM Image Viewer (DICOM Files: Courtesy R2 Tech/Hologic)

4. DICUSSION

Both DICOM-PACS-IHE™ and DICOM-CAD-IHE™ use DICOM SR service and several IHE profiles. In the second version implementation, the methodology requires several modules of the toolkit to be installed in the PACS server [14], which would need the collaboration of the PACS manufacturer. The integration would require time and patience from the integrator because of the protective culture of PACS business. The third version also uses DICOM SR and Key Image Note IHE Profile, but this version reduces the necessity of altering the current PACS server, but the CAD results are stored in CAD Server and not in PACS. This version is favored by the CAD manufacturers because they have the ability to install the toolkit on their CAD server and integrate CAD results with clinical workflow using DICOM SR objects. The DICOM SR provides the data format allowing CAD results, text, images, graphics and annotation to be directly store in the DICOM SR compliance PACS or CAD Server. With the implementation of CAD SR Server, the data in DICOM SR can be extracted for data mining purposes in future.

5. FUTURE WORK

The workflow and procedures of the automatic integration of CAD with clinical PACS using CAD-PACS toolkit has been presented. Our experiments show various CAD applications integrated with the toolkit and the CAD results with PACS using DICOM SR. In the current workflow, the study order or integration with current clinical RIS is currently in development. Figure 7 shows our next step of development to make the CAD integration complete.

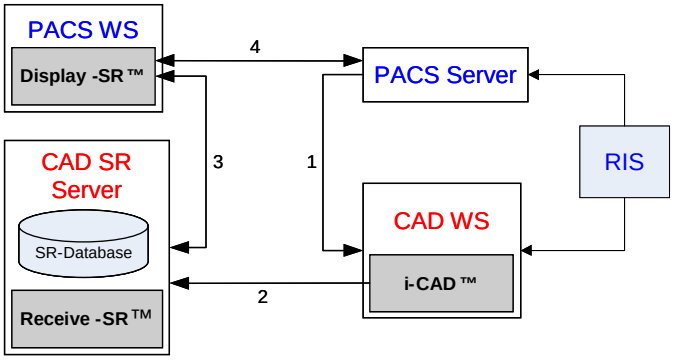

Figure 7. The next step for integration RIS of CAD-PACS toolkit.

REFERENCES

1. M.L. Giger, K. Doi, H. MacMahon, Image feature analysis and computer-aided diagnosis in digital radiography: 3. Automated detection of nodules in peripheral lung fields, Med. Phys. 15 (1988) 158-166.
2. M. McNitt-Gray, Lung nodules and beyond: approaches, challenges and opportunities in thoracic CAD, CARS 2004, 896-091.
3. K. Doi, et al., Computer-Aided Diagnosis in Medical Imaging, Elsevier, New York, 1999.
4. Huang HK, PACS and imaging informatics. Hoboken, NJ: John Wiley & Sons, 2004.
5. DICOM, http://medical.nema.org/, accessed on January 10 2008.
6. IHE, http://www.ihe.net/, accessed on January 10 2008.
7. P. Heffernan, H. Zhang, Software architecture for a CAD server, CARS 2004, 861-866.
8. R2 Technology Inc., http://www.r2tech.com/main/home/index.php, accessed on January 10 2008.
9. Z. Zhou, H. K. Huang, F. Cao, B. J. Liu, J. Zhang, and G. T. Mogal, Educational RIS/PACS Simulator, SPIE Medical Imaging, vol. 4, pp. 139-147, 2003.
10. M. Y. Y. Law, Z. Zhou, New direction in PACS education and training, J. Computerized Medical Imaging and Graphics, vol. 27, pp. 147-156. 2003.
11. E. Pietka, A. Gertych, S. Pospiech, F. Cao, H.K. Huang, V. Gilsanz, Computer Assisted Bone Age Assessment: Image Processing and Epiphyseal/Metaphyseal ROI Extraction, IEEE Trans. Medical Imaging, 20, 715-729, 2001.
12. E. Pietaka, S. Pospiech, A. Gertych, F. Cao, H.K. Huang, V. Gilsanz, Computer Automated Approach to the Extraction of Epiphyseal Regions in Hand Radiographs, Journal of Digital Imaging, 14, 165-172, 2002.
13. Doi K. Compter-aided diagnosis in medical imaging: Historical review, current status and future potential. J. Computerized Medical Imaging and Graphics 31 (2007):198-211
14. Zhou Z, Le A, Liu B, and Huang HK. PACS-CAD toolkit for integrating an independent CAD workstation to diagnostic workflow, Proc. SPIE Int. Soc. Opt. Eng. 6516, 651609 (2007)
15. Zhou Z, Liu BJ (2007) CAD-PACS Integration Tool Kit - Based on DICOM Screen Capture (SC) and Structured Report (SR) and IHE Workflow Profiles, Comput Med Imaging Graph 31(4-5): 346-352
16. Le A, Zhou Z, Zhang A, Tsao S, Documet J, Liu B, Huang HK. A DICOM Structured Report Viewer and Automatic Workflow for CAD-PACS Integration in a Clinical Environment Based on IHE Workflow Profiles. Presented at the 93rd Scientific Assembly and Annual Meeting of RSNA 2007 (Education Exhibit)

The Design and Implementation of Decision Support Tools of Proton Beam Therapy Treatment Planning of Brain Cancer Patients

Anh Le [a], Jorge Documet [a], Anika Joseph[a], Reinhard Schulte [b], Brent Liu [a]
[a]Dept. of Radiology, University Southern California, , Marina del Rey, CA 90292
[b]Dept. of Radiation Medicine, Loma Linda University Medical Center, Loma Linda, CA 92354

ABSTRACT

Last year, we presented methodology to perform knowledge-based medical imaging informatics research on specific clinical scenarios where brain tumor patients are treated with Proton Beam Therapy (PT). In this presentation, we demonstrate the design and implementation of quantification and visualization tools to develop the knowledge base for therapy treatment planning based on DICOM-RT-ION objects. Proton Beam Therapy (PT) is a particular treatment that utilizes energized charged particles, protons, to deliver dose to the target region. Similar to traditional Radiation Therapy (RT), complex clinical imaging and informatics data are generated during the treatment process that guide the planning and the success of the treatment. Therefore, an Electronic Patient Record (ePR) System has been developed to standardize and centralize clinical imaging and informatics data and properly distribute data throughout the treatment duration. To further improve treatment planning process, we developed a set of decision support tools to improve the QA process in treatment planning process. One such example is a tool to assist in the planning of stereotactic PT cases where CT and MR images need to be analyzed simultaneously during treatment plan assessment. These tools are add-on features for DICOM standard ePR system of brain cancer patients and improve the clinical efficiency of PT treatment planning. Additional outcome data collected for PT cases are included in the overall DICOM-RT-ION database design as knowledge to enhance outcomes analysis for future PT adopters.

Keywords: DICOM, DICOM-RT, DICOM-RT-ION, ePR, Decision Support, Proton Therapy

1. INTRODUCTION

Proton Therapy is a type of particle therapy which utilizes protons beam to irradiate target site. The power of protons is that higher doses of radiation can be used to control and manage cancer while significantly reducing damage to healthy tissue and vital organs. Similar to traditional radiation therapy (RT), PT relies heavily on clinical imaging and informatics for decision and treatment. In radiology, the advancement of Picture Archiving and Communication Systems has tremendous impact on the management of radiological images in radiology departments and improve workflow and turn around time in radiology department [1]. In contrast, radiation oncology still lacks such an information system for radiation oncology imaging informatics data. A lot of effort has been done in creating superior treatment planning systems (TPS) and building better machines for radiation, but little effort has been made in building such a standardized ePR system that could help oncologist and physicists to centralize all necessary information for a better treatment, especially in proton therapy. The data are scattered in various standalone and proprietary systems. This led to concept of an electronics patient record (ePR)[2-4].

For the last few years, we have developed an ePR which can be used as a conceptual storage and distribution solution for oncology imaging and informatics data in a standardized fashion. Because the data is standardized, the ePR can be used as a platform to develop a set of analysis, visualization and comparison tools playing a supporting role in oncologists' and physicists' decision making processes during daily practice [4]. In the diagram of general clinical workflow for PT patient (Figure 1), the dotted line box emphasizes an example where the process can be improved by eliminating the work in feed back loop.

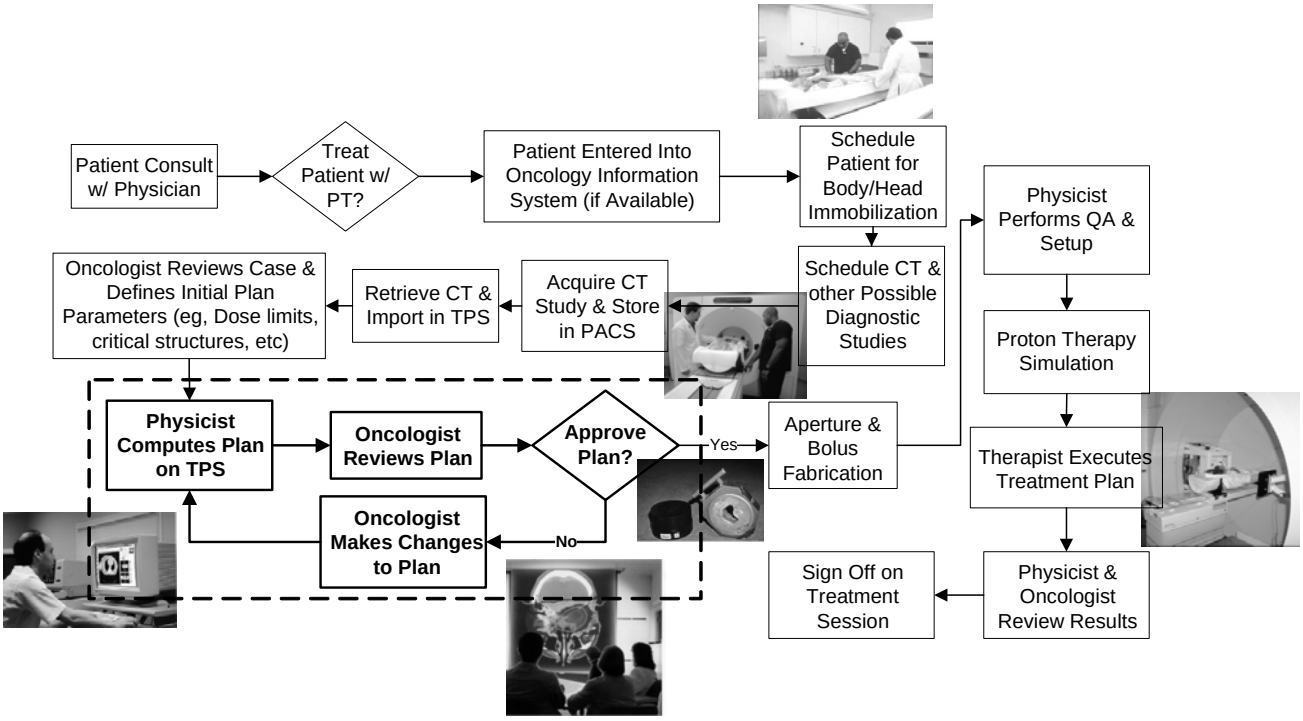

Figure 1: General Clinical Workflow for PT of Cancer Patients.

In this paper, we present the initial step for building decision support tools for proton therapy treatment for brain cancer patients. Its availability and functions do not overlap with current TPS but rather complement them by improving overall patient treatment planning through using the quantified knowledge developed within the ePR. Institution and PT facilities could utilize this DICOM-RT ePR system as central system with outcomes research and decision support for research, education and clinical services in future.

2. METHODS

The medical imaging informatics infrastructure (MIII) has been developed and used widely in some of the applications to utilize PACS images and related data for large scale horizontal and longitudinal clinical service, research and education [1]. The MIII components and their logical relationship are shown in Figure 1. We have extended this methodology in building an electronic patient record (ePR) to standardize and centralize clinical data and properly distribute data throughout the treatment duration. In this paper our focus is on components in three layers from the bottom.

USER'S APPLICATION SOFTWARE				
Research	Clinical Service	Education		
DATABASE & KNOWLEDGE BASE MANAGEMENT DATA MINING & DATA RETRIEVAL				
Image Processing/ Analysis	**Visualization**	**Graphic User Interface**	Security	Communication Networks
PACS & MEDICAL IMAGE & RELATED DATABASE				

Figure 2: MIII components and their logical relationship. [1]

The ePR decision support tools are developed based on DICOM images, DICOM-RT and DICOM-RT-ION objects with clinical collaboration from Loma Linda University Medical Center (LLUMC) Proton Beam Therapy facility and its

oncologists and physicists. The design and implementation consisted of three main steps: data collection (first layer), development of tools prototype (second layer), and knowledge database structure (third layer).

2.1. Data Collection

The DICOM standard has been well established for data and information exchanged and it has been successful for clinical imaging system in radiology, particular in PACS. DICOM standard assures that image and related data acquired from equipment from different vendors can communicate and integrate into a system by using its DICOM objects and formal metadata. Currently, six DICOM radiology objects has been established for transmission and storage radiotherapy images and related information using in PT [6]. These DICOM objects are: RT image, RT structure set, RT dose, RT ION plan and RT ION treatment record. Figure 3 shows a portion of DICOM model in 'real world' that is currently used for PT.

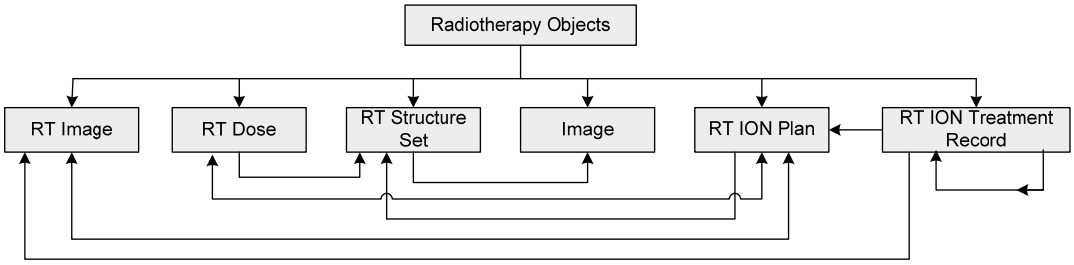

Figure 3: Portion of DICOM model of real world, showing only DICOM objects using PT

Generally, the sources of these DICOM data come from a treatment planning system, oncology information system and PT systems. DICOM data is imported into our ePR system. Images and related information are extracted as knowledge for the knowledge base and can be utilized to develop tools. Even DICOM standard is assumed, some of the legacy systems do not have the DICOM capacity. The superior architecture and design of an ePR system allows users to have the ability to receive non-DICOM data from various PT related imaging and information systems and convert them into the DICOM format [5]. The data collection is still ongoing on at LLUMC.

2.2. Development of Tools Prototype

The ePR system is developed based on a web-based model with the framework using PHP (Hyper Preprocessor) language for the server side and a combination of javascript, flash, activeX libraries. This architecture allows the ability of integrating many applications, such as analysis, visualization and comparison tools, to the ePR. Each tool is a plug-in to the whole system and can be manage using administration interface. Figure 4 shows the architecture of the ePR The DICOM receiver from one end listens for incoming DICOM data, then the data is extracted from the DICOM objects (including RT objects) and populated to the database. From the data collected the Data Mining and Knowledge based modules perform the proper analysis of the data and it is saved back to the database. These Data Mining and Knowledge base modules can be used to store treatment plan as well as following-up data for further outcome analysis. The users via the web interface can browse the knowledge and also contribute to it by uploading new cases [5].

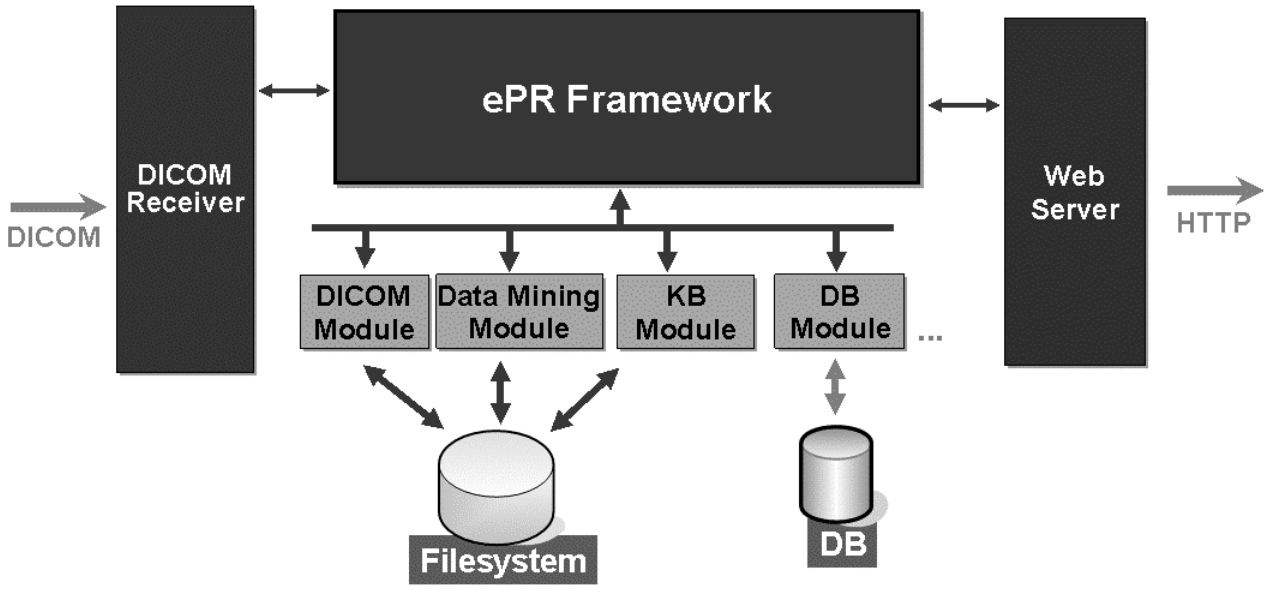

Figure 4: The architecture of the ePR.

For the decision support tools, the development has three phases: Phase 1) Discussion with oncologists/physicist to identify useful tools; Phase 2) Development of standalone applications; and Phase 3) Integration of applications as a tool in the ePR system.

a. Identifying & Designing the appropriate tool: An Example

One of the common radiation treatments for brain cancer is the use of stereotatic radiosurgery (SRS). The goal of SRS is to use high-intensity precisely focused radiation to treat tumors, arterial-venous malformations (AVM) and other diseases using a three-dimensional coordinates system. In SRS, a very high dose is applied to the area of tumor in only one dose fraction, therefore SRS requires a very high accuracy in treatment planning and patient setup during treatment. Currently, MR and CT images are both use in treatment planning: CT provides imaging (structure) for planning and MR provides imaging of the diseased area (tissue) to help in diagnosis and planning. To have as accurate of a plan, the physicist or dosimetrist has to manually register these two images set to outline the target object for treatment.

Since each system utilized during the course of treatment have different coordinates system, the physicist or dosimetrist again needs to find an appropriate transformation to map the treatment plan on TPS to the location of patient in the proton treatment room. The method widely used for this purpose is fiduciary markers which are implanted within the patient. Fiduciary markers are needed to define anatomical coordinates with high accuracy. Measured coordinates are used to create a global reference providing an easy-to-track feature in MRI images which follows movements of the marked subject. Images of the same patient produced with two different systems may be correlated by knowing fiduciary marker locations in the area imaged by both systems.

For those purpose, we identify two tools: MR/CT fusion and fiducially marker translation tool for treatment planning for stereotactic proton therapy.

b. Development of standalone applications

Based on the clinical needs and requirements, the next phase is to develop the tools within standalone applications. The reasons for this allow for multiple developers to work on the different applications before integrating within the ePR system. However, it is important to stress that this is possible because the data within the ePR system will be

standardized by the DICOM-RT and DICOM-RT-ION framework for Proton Therapy. The MR/CT fusion tool is developed using traditional image transformation and rigid registration. The fiducial marker translation tool is first developed under Matlab language and complied into a standalone application.

c. Integration tools to ePR system

Once each of the applications are developed and tested independently, then they can be integrated within the ePR system as a tool within the graphical user interface (GUI) and called within the web-based infrastructure using ajax technology. All tools are integrated into the ePR system and are based on standardized DICOM-RT and DICOM-RT-ION objects.

2.3. Knowledge Database

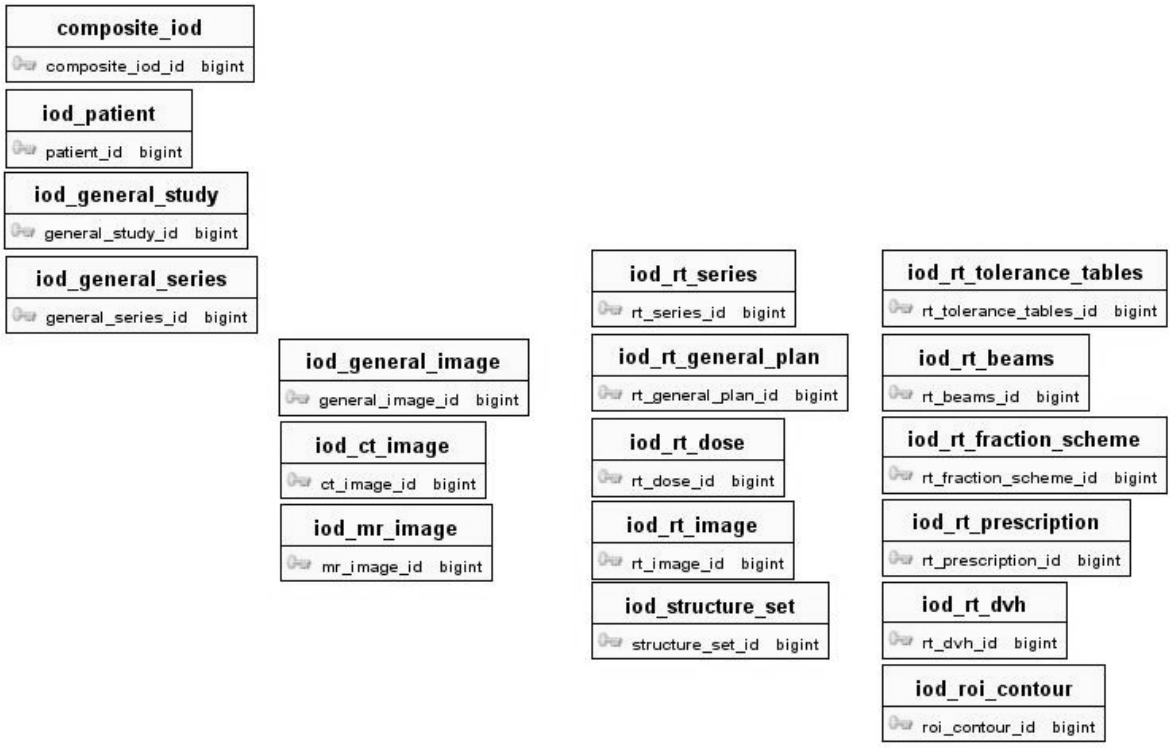

Figure 5: Knowledge Database Structure

Knowledge is defined and quantified based on the expert's ability to utilize data and other criteria in evaluating, grouping and defining certain clinical characteristics. In this case, the knowledge base is designed in object-oriented and modular fashion so that additional knowledge and new object classes defined in the future can be easily integrating without affecting the overall design. The database have different sub-groups to take care of differing groups of data. The data extracted from the DICOM standard are organized very close to DICOM standard and made flexible for changes in the future. A few database tables with primary keys are shown in Figure 5. The first column from the left represents the metadata in DICOM objects, the second column are the image data, and the two right columns are the knowledge extracted from DICOM-RT objects.

3. RESULTS

We have successfully integrated DICOM-RT data from two prostates cancer cases treated with 3D conformal and PT data from one brain cancer patient cancer treated with stereotatic proton therapy case, as shown in Figure 6. The patient

demographics are extracted from DICOM images, RT and RT ION objects. This is important because the DICOM-RT standards allow such an ePR system to store various types of Radiation and Proton Therapy treatment types integrated within a single system based on the patient, which is the strengths of the ePR.

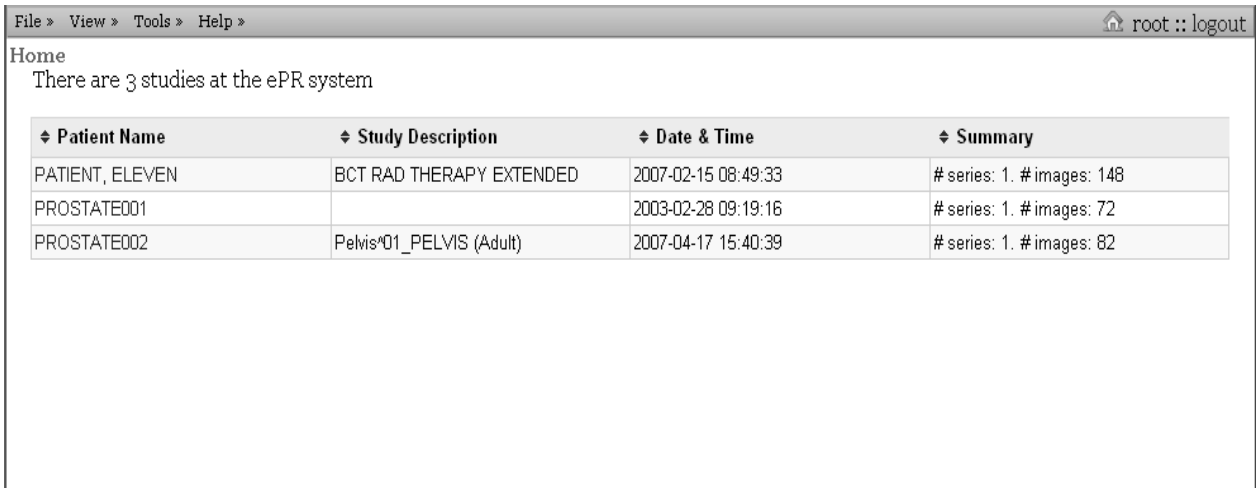

Figure 6: Patient Worklist

Figure 7 shows the MR/CT image fusion tool for tumor delineation in treatment planning for stereotactic proton therapy. The tool loads two set of images (Figure 7a) for users to identify the registration point to be used for fusion. After the user is satisfied, the fused MR and CT images are displayed. A slider bar allows the user to interactively view more or less of each image overlaid on each other. (Figure 7b). The final image show both CT structural image as well as MR tissue structure with color washing to enhance vision.

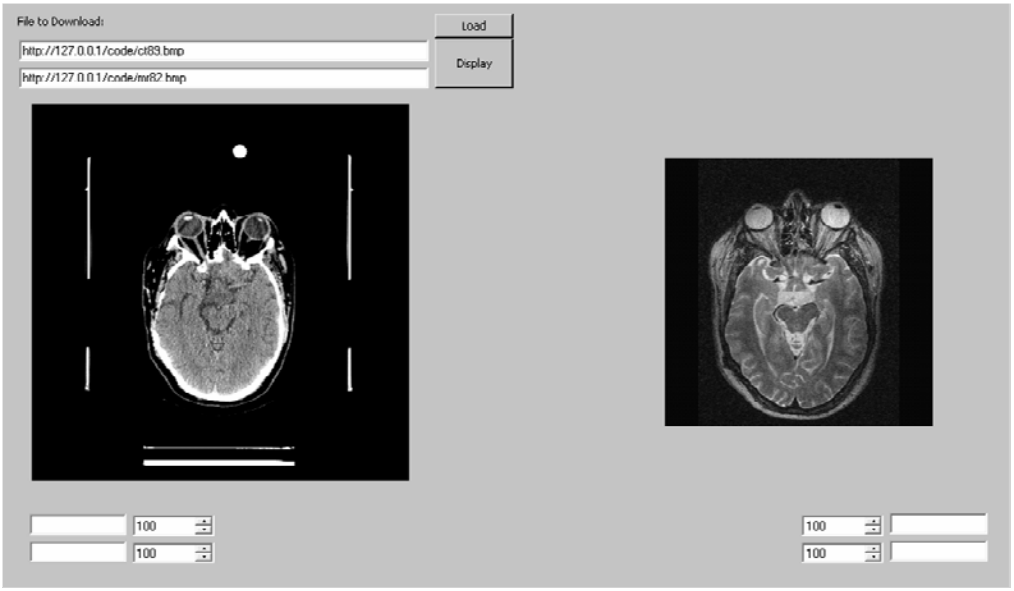

(a)

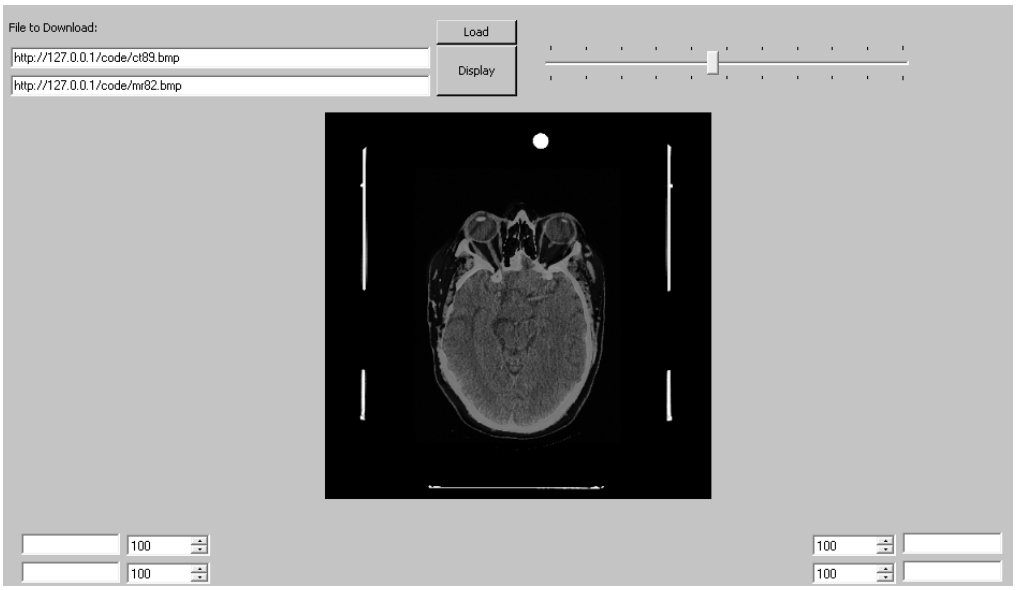

(b)

Figure 7: MR/CT Image Fusion Tool

Figure 8 shows the screen shot of the fiducial marker translation tool for treatment planning for stereotactic proton therapy. The image shown in this screen shot are MR image of a general phantom. The coordinates, in DICOM format, are automatically extracted and correspond to numbered markers on the image. This tool also produces a text file (on the right) containing all the coordinates. In a stereotactic case these extracted coordinates are then entered to another conversion software to obtain corresponding coordinates for patient set up within the Proton treatment room.

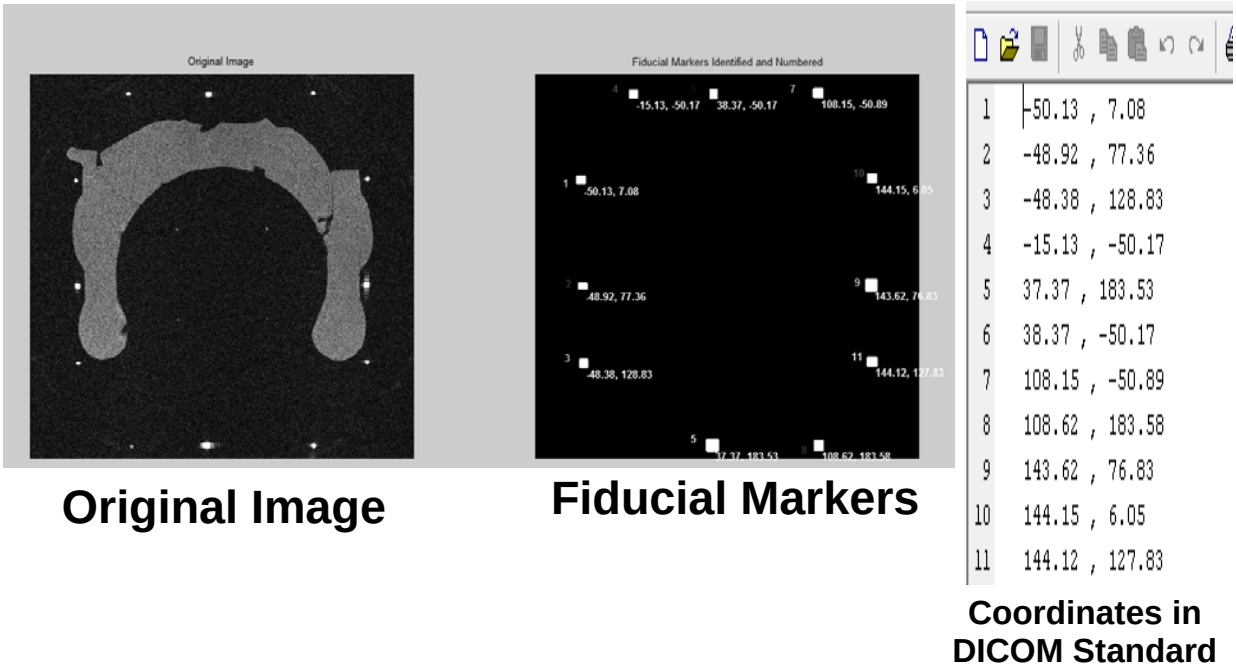

Figure 8: Fiduciary Makers Translation Tool

4. SUMMARY

Standardization of DICOM-RT and DICOM-RT-ION objects eliminates the challenges in assessing crucial data from proprietary treatment systems. Moreover, utilizing DICOM objects in our ePR System can capture PT data and treatment outcomes at multiple institutions. With the Web-based structure of the system, global utilization of multiple PT sites and data becomes more feasible. DICOM-RT and DICOM-RT-ION objects together with knowledge form a standardized and normalized platform for comparison against other treatment modalities which utilize the same standardized data objects. With the scalable and flexible framework of ePR system, various tools can be integrated to support treatment process, such as MR/CT image fusion and fiduciary marker translation tools in this paper.

REFERENCES

[1] Huang HK. PACS and Imaging Informatics: Principles and Applications. John Wiley & Sons, Hoboken, New Jersey (2004).

[2] Law M.Y.Y., Huang H.K., Zhang X., Zhang J. The Data Model of a PACS-Based DICOM Radiation Therapy Server. Proc. of the SPIE on CD-ROM, Medical Imaging 2003, 128-129, San Diego, CA, U.S.A (2003)

[3] Liu B., Huang H.K., Law M., Le A., Documet J., Gertych A. A knowledge-based Imaging Informatics Approach to Managing Patients Treated with Proton Beam Therapy. Proc. of SPIE Medical Imaging, 6516:651616(2007).

[4] Document J., Liu B., Le A., Law M. A DICOM-RT Radiation Oncology ePR with Decision Support Utilizing a Quantified Knowledge-base from Historical Data, Proc. of SPIE Medical Image, (2008).

[5] DICOM Standard 2008. ftp://medical.nema.org/medical/dicom/2008/ (2008).

SELECTED PEER REVIEWED REPRINTS AND PREPRINTS

Effect of a Computer-aided Diagnosis System on Clinicians' Performance in Detection of Small Acute Intracranial Hemorrhage on Computed Tomography[1]

Tao Chan, H. K. Huang

Rationale and Objectives. To analyze the effect of a computer-aided diagnosis (CAD) system on clinicians' performance in detection of small acute intracranial hemorrhage (AIH) on computed tomography (CT).

Materials and Methods. The authors have developed a CAD scheme that used both image processing techniques and anatomic knowledge based classification system to improve diagnosis of small AIH on CT. A multiple-reader, multiple-case receiver operating characteristic (ROC) study was performed. Twenty clinicians, including seven emergency physicians, seven radiology residents, and six radiology specialists were recruited as readers of 60 sets of brain CT, including 30 cases that show AIH smaller than 1 cm, and 30 controls. Each reader read the same 60 cases twice, first without, then with the prompts produced by the CAD system. The clinicians ranked their confidence in diagnosing a case of showing AIH, which produced the ROC curves.

Results. Significantly improved performance is observed in emergency physicians, average area under the ROC curve (Az) increased from 0.8422 to 0.9294 ($P = .0107$) when they make the diagnosis without and with the support of CAD. Az for radiology residents increased from 0.9371 to 0.9762 ($P = .0088$). Az for radiology specialists increased from 0.9742 to 0.9868, but was statistically insignificant ($P = .1755$).

Conclusions. CAD can improve the clinicians' performance in detecting AIH on CT. In particular, emergency physicians can benefit most from the CAD and improve their performance to a level approaching that of the average radiology residents.

Key Words. Observer performance study; receiver operating characteristic; computer-aided diagnosis; computed tomography; acute intracranial hemorrhage.

Acute intracranial hemorrhage (AIH) is recent (<72 hours) bleeding inside skull. It can be the result of stroke or complication of head injury. The presence or absence of AIH requires different treatment strategies and its identification is of prime importance for triage of patients suffering from acute neurologic disturbance or head injury. However, it is well recognized that clinical findings cannot accurately differentiate between patients with AIH and those who suffer from other neurologic emergencies. Therefore neuroimaging findings are essential for immediate management decision making (1–4). Computed tomography (CT) has been the modality of choice for evaluating suspected AIH because it is widely available, quick to perform, and compatible with most life support devices. On CT images, acute blood clot shows higher attenuation than normal brain parenchyma (5). The contrast between AIH and the adjacent structures depends on intrinsic physical properties of blood clot including the density, volume, location; relationship to surrounding

Acad Radiol 2007; xx:xxx

[1] Department of Health Technology and Informatics, The Hong Kong Polytechnic University, Hung Hom, Hong Kong (T.C.); Image Processing and Informatics Laboratory, Department of Radiology, Keck School of Medicine, University of Southern California, Marina del Rey, CA (H.K.H.). Received March 25, 2007; accepted September 21, 2007. Address correspondence to T.C. e-mail: taochan@hkcr.org

doi:10.1016/j.acra.2007.09.022

structures; and technical factors including scanning angle, slice thickness, and windowing (6). Although diagnosis of AIH on CT is usually straightforward, identification of the demonstrable AIH on CT can become difficult when the lesion is inconspicuous (eg, small or being masked by normal structures, or when the reader is inexperienced).

In most parts of the world outside the United States, acute care physicians, including emergency physicians, internists, or neural surgeons, are the only ones to read the CT images at odd hours, when radiologists' expertise may not be immediately available. This may not be a desirable arrangement because the skill of acute care physicians regarding interpretation of brain CT has been shown to be imperfect (7). Even radiology residents can, albeit infrequently, overlook hemorrhage on brain CT (8). Therefore the authors have developed a CAD system that identifies small AIH to help in the management of patients suffering from acute neurologic disturbance or head injury in an emergent setting (9).

This study aims to evaluate the effect of CAD on clinicians' performance in detection of small acute intracranial hemorrhage by the use of multiple-reader, multiple-case receiver operating characteristic (MRMC ROC) approach.

MATERIALS AND METHODS

Computed-assisted Diagnosis Algorithm

Research in computer-assisted diagnosis (CAD) has been around for more than 20 years (10,11). Its concept is to provide computer output to aid human observers in detection or interpretation of images. CAD schemes generally involve some similar components or image processing/analysis steps. To begin, images need to be digitized if not already in a digital format. After preconditioning of images, which usually involve denoising or filtering, segmentation is usually performed. This extracts the relevant portions or features of the image. Then the segmented regions would be characterized by quantification of different image features. At last, the quantified features can be correlated with known pathologic entities to formulate the diagnosis.

The CAD system under evaluation was fully automatic and was designed to process DICOM images in their indigenous format and file structure.

The basic workflow of our CAD algorithm is summarized in Fig 1. Skull, by virtue of its exceptionally high olding. Morphologic opening is performed to remove remaining connections that may exist between intracranial contents and scalp. Afterwards, scalp and other extrinsic structures become separated from the centrally located intracranial contents by regions of void that represent removed bones. The intracranial contents can subsequently be segmented by selectively removing elements that are not contiguous with the central component.

The segmented intracranial contents undergo preprocessing steps which include median filtering for noise reduction and adjustment for CT cupping artifacts. This produces a more homogeneous background on which abnormalities become more conspicuous.

The brain is realigned into the conventional orientation after automatic localization of mid-sagittal plane and boundaries of the whole series of images. This is necessary as images obtained in an emergent setting are often not optimally positioned.

Then high-attenuation components are segmented as candidate AIH from each of the axial sections. The segmentation is based on combined processes of top-hat transformation, which essentially selects pixels of higher attenuation than those in their vicinity, and subtraction between the two sides of the brain about the midline, which highlights regions of higher attenuation than its contralateral anatomic region. The parameters are adjusted such that a moderate number of AIH candidates are generated, so not to miss some small lesions.

Many image features of the candidates, including mean and variation of attenuation, area, long and short axis diameters, relative orientation, are quantified. In addition, the candidate AIHs are given anatomic context by registration against a purposely developed coordinate system. This coordinate system is conceptually similar to the commonly used Talairach coordinate system (12), but is different in that it can be readily applicable for relatively thick section axial images obtained using ordinary clinical protocols.

Coordinates on the coordinate system have their own anatomic label as a result of a normalization procedure using axial brain CT normal subjects obtained using a clinical protocol. Through the registration process between the study in question and the normalized coordinate system, individual pixel location of the brain in question is correlated with a coordinate location of the normalized brain and its embedded anatomic label.

The image features and coordinates of the candidates provide the inputs for the rule-based classification system

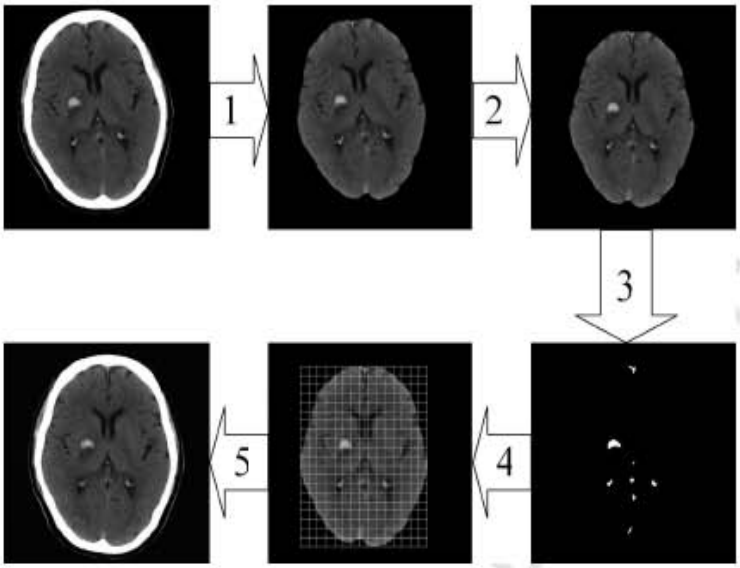

Figure 1. Flow chart and the intermediary outputs after successive steps of the algorithm. Basic components of a usual computer-assisted diagnosis, including image preprocessing, image segmentation, image analysis, and classification are all used. 1. Intracranial contents segmented using thresholding and morphologic operations followed by preprocessing steps that reduce noise and computed tomography cupping artifacts. 2. Intracranial contents aligned by locating mid-sagittal plane and boundaries of the brain. 3. Acute intracranial hemorrhage (AIH) candidates extracted using combined method of top-hat transform and left-right comparison. 4. AIH candidates rendered anatomic meaning by registration against a purposely developed coordinate system. 5. Genuine AIH distinguished from mimicking variants or artifacts by the rule based classification system, using both image features and anatomical information. The intracerebral hemorrhage in right basal ganglia is correctly identified as genuine AIH and outlined in red, whereas the mimics are outlined in blue.

variants and artifacts. The classification is possible because genuine AIH or normal variants tend to follow certain patterns at some typical anatomic locations.

Finally, the outputs of the algorithm are displayed as images with overlay of red perimeters surrounding the genuine AIH as determined by the system. The original images and the corresponding CAD output images are displayed side by side, one axial section at one time in stack mode. The user can scroll through the whole series of synchronized original images and corresponding CAD output images. This arrangement is to facilitate comparison between the original and the CAD output images.

The CAD was trained using 40 positive cases that contained different types of AIH smaller than 1cm across, and 80 controls that were normal or showed pathology other than AIH. The described coordinate system was normalized using 65 studies from the 80 controls that showed normal findings.

The system was subsequently validated using 22 positive cases and 44 controls. In the validation test, the system achieved sensitivity of 83% on a per lesion basis, and false positive rate of 0.29 per case or 0.020 per image (9).

Although the aforementioned performance indicators of the CAD itself are promising, evidence that the system can complement the skills of clinicians and hence enhance the diagnostic accuracy of clinicians using the system is still lacking in the referenced article. Such evidence from observer performance study will be provided in the subsequent sections.

CAD Evaluation

A CAD system can only prove to be useful should its output be beneficial to the human observer in terms of making correct diagnoses. In other words, the CAD system should provide outputs that identify lesions that may otherwise be missed by the human observer. As opposed to early unsuccessful attempts to replace radiologists by computers in the 1960s and 1970s, current CAD schemes now aim to assist readers in making diagnoses by providing quantitative analysis of radiologic images. Therefore

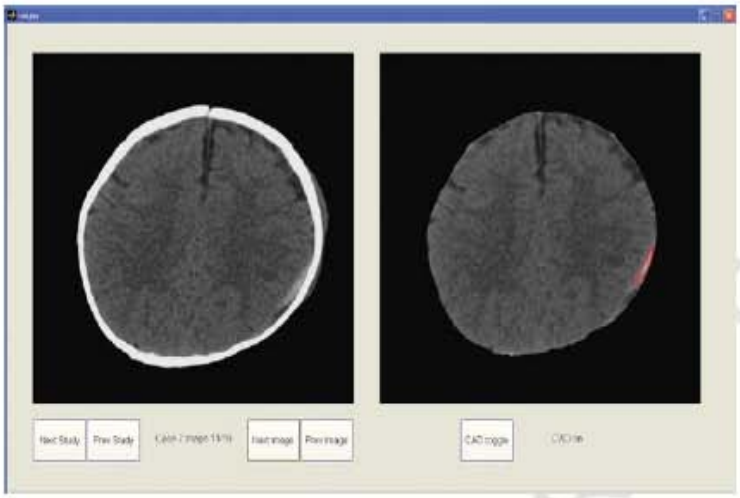

Figure 2. Screen capture of the graphical user interface used in the current observer study. The original images were displayed in the left window in stack mode. In the second reading, the output images of computer-assisted diagnosis were displayed in the right window. An output image contained the segmented and realigned intracranial contents, and acute intracranial hemorrhage was outlined. The original and computer-assisted diagnosis output images were scrolled in synchrony.

investigations of possible human-computer interaction such as the ROC studies are necessary (13). The MRMC ROC paradigm has been commonly used in the evaluation of CAD systems, which is not only efficient in terms of resource requirement (ie, fewer readers and cases are required for a specified precision), but also produces results that can generalize to the populations of readers and cases from which the samples were drawn (14,15).

Observer Performance Study

All the readers and cases are recruited from a 1,200-bed acute hospital in Hong Kong. Institutional review board approval has been obtained for this study.

Seven emergency physicians (EP), with 5–9 years (average 6.4 years) of experience in emergent brain CT interpretation, seven radiology residents (RR) with 1–4 years of experience (average 2.3 years), and six board-certified radiology specialists (RS) with 7–30 years of experience (average 17.8 years) were invited to participate in the evaluation of the CAD system. One of the specialists (subject 5) is a fellowship trained neuroradiologist with 12 years of experience.

Sixty sets of axial brain CT images, of thickness between 5 mm to 10 mm, made up the test cases used in the observer performance study. All were emergency brain CT performed on a single detector CT scanner (HiSpeed CT, GE Medical Systems, Milwaukee, WI). All images were axial images obtained parallel to the orbitomeatal line, at 120kV and 80–200mA. Thirty cases showed AIH, the radiologic diagnosis being established by consensus of two experienced neuroradiologists who did not participate in the observer study. In 26 of the cases, presence of AIH was considered unambiguous by the radiologists. In the other four, the diagnoses were concluded with follow-up CT/magnetic resonance imaging. AIH of different types, including intracerebral hemorrhage, intraventricular hemorrhage, subarachnoid hemorrhage, subdural hemorrhage, and extradural hemorrhage, have been included.

All intracerebral hematomas included in this study were smaller than 1 cm in long axis diameter, whereas all extraaxial hematomas were thinner than 1cm. Only small hematomas were included because detection of large hematomas is straightforward and unlikely to be problematic for clinicians. The other 30 cases revealed either normal findings or pathology other than hemorrhage, which included acute and chronic infarct, ischemia, and tumor.

The readers were asked to read the original images using a graphical user interface specifically implemented for this study, as shown in Fig 2. One axial section was displayed at one time. The readers could scroll through the images of a particular case back and forth. The experiment was conducted in a radiologist's reporting room, where ambient light was low. They were allowed to ad-

just the brightness of the screen to suit their individual needs, but image windowing has not been provided because this on its own could be considered one form of diagnostic aide (16). In particular, we suspect windowing can bias against people less familiar with its use, especially emergency physicians. The readers were instructed to record their confidence in detecting AIH on a scale from 1 (absolute absence of AIH) to 10 (absolute presence of AIH). Readers were also instructed to interpret the score of 5 and 6 as indeterminate, with 5 erring on the side of absent AIH and 6 otherwise. Immediately after they have finished all 60 cases, they would reread the images, now with the CAD output images displayed side by side with the corresponding original images. Both the original and the CAD output images would scroll together in synchrony. They again recorded their confidence level in the same way.

The readers were informed that during the CAD training and validation tests, the CAD had produced sensitivity of 80%–85% on a per lesion basis and a false positive rate of less than one in three cases in earlier tests, but performance for individual case may depend on size and contrast difference of lesions it contains. They were also reminded that the actual accuracy of the CAD output in the sample cases during the ROC study that they were going to read might be better or poorer than the quoted figures reflecting difference in case selection.

The recorded data were subject to MRMC ROC analyses using the freely available software DBM MRMC developed by the University of Chicago (17). The program was based on the Dorfman-Berhaum-Metz method (14) that allows generalization to the population of readers and cases. The ROC curve was obtained by maximum likelihood estimation of the binormal distributions that best fit the rating data of the readers.

Because it was believed by many, including most of the participants in the test, that the diagnosis of AIH is an all or none question, it is also desirable to present the results in some conventional indicators that are more familiar to clinicians and are based on a yes/no type of response. The scores were placed into two categories of 1–5 and 6–10, which dichotomize the results in to absence/presence of AIH. The sensitivity/specificity pair and positive/negative predictive values are calculated accordingly.

In addition, the frequency when the use of CAD resulted in actual change of diagnosis during the experiment, as opposed to mere change in confidence of one particular diagnosis or another, was examined. The diagnosis of absence/presence of AIH for individual case was determined based on the aforementioned method of dichotomization the score ratings. Frequency of the change in diagnosis and the correctness of such changes were recorded. This information can reflect the impact that use of CAD may have in actual clinical practice with altered diagnostic decisions that affect management options.

RESULTS

All the results quoted in subsequent sections refer to those calculated on per case or per patient basis.

The average area under the ROC curve (Az) values scored by individuals before and after CAD are presented in Fig 3. Only 1 of the 20 subjects (subject 18) scores marginally lower Az after CAD. The other 19 people all attained a variable degree of increment after use of CAD. F3

Significantly improved performance is observed in EP, Az increased from 0.8422 to 0.9294 ($P = .0107$) when they make the diagnosis without and with the support of CAD. Az for RR increased from 0.9371 to 0.9762 ($P = .0088$). Az for RS increased from 0.9742 to 0.9868 ($P = .1755$), but was statistically insignificant. The results are shown in Fig 4. F4

It was observed that performance of EP with support of CAD approached that of the RR without CAD. The performance of the RR with CAD became similar to that of RS in this specific experimental condition, when the readers were limited to viewing the images without the benefit of windowing or tiling images. This signifies that the CAD can improve reader performance as well as reduce variability among different clinician groups.

The sensitivity, specificity, and positive and negative predictive values were calculated for each reader both before and after use of CAD (Table 1). It was demonstrated that both sensitivity and specificity improved for each group. The gain is most remarkable for EP, in whom the average sensitivity/specificity improved from 73.3%/81.4% to 80.5/90.5%; less for the RR: from 86.2%/88.1% to 93.8%/92.9%; and least for the RS: from 92.2%/93.3% to 95%/94.4%. T1

Again, it was observed that results of EP with support of CAD approached that of the RR without CAD, and the results of the residents with CAD approached those of the specialists without CAD.

After use of CAD, the positive predictive values improved from 80.1% to 89.5% for EP, from 88.4% to

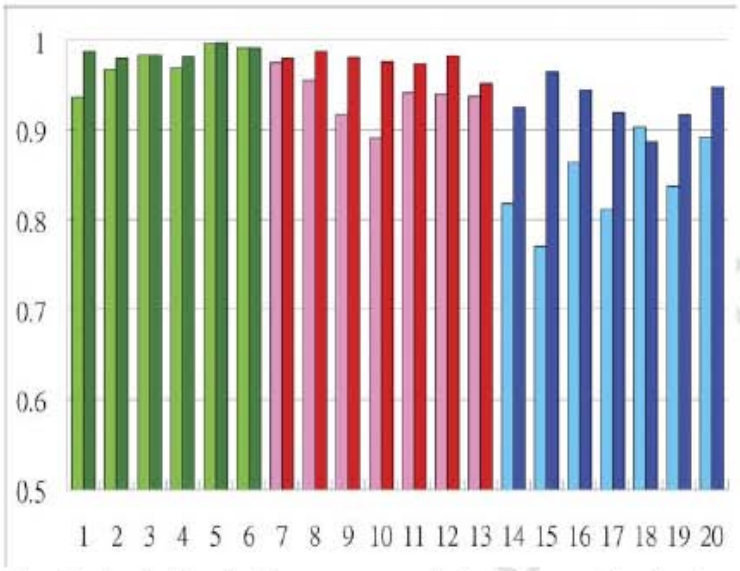

Figure 3. Bar chart showing the average area under the receiver operating characteristic curve before (light) and after (dark) use of computer-assisted diagnosis. The marginal increase shows greatest increase in emergency physicians, less for the radiology residents, and least for the radiology specialists. Subjects 1–6 are radiology specialists (green), 7–13 are radiology residents (red), and 14–20 are emergency physicians (blue).

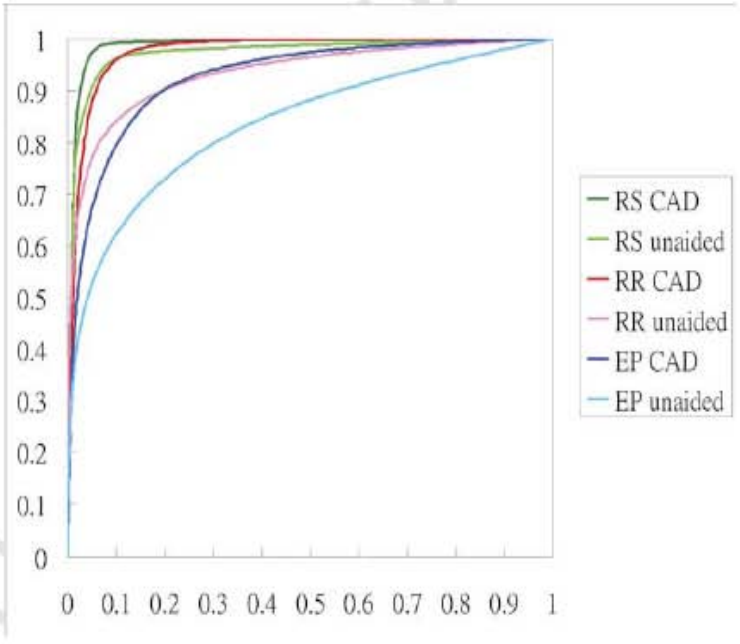

Figure 4. Receiver operating characteristic of detection of acute intracranial hemorrhage among different clinician groups. EP: emergency physicians; RR: radiology residents; RS: board certified radiology specialists; UA: unaided reading mode; CAD: computer-assisted diagnosis reading mode.

Table 1
Average Performance Indicators Including Sensitivity, Specificity, Positive Predictive Value, and Negative Predictive Value for Different Clinician Groups With and Without Computer-Assisted Diagnosis Support

	Emergency Physicians		Radiology Residents		Board-Certified Radiology Specialists	
%	Unaided	Computer-Assisted Diagnosis	Unaided	Computer-Assisted Diagnosis	Unaided	Computer-Assisted Diagnosis
Sensitivity	73.3	80.4	86.2	93.8	92.2	95.0
Specificity	81.4	90.5	88.1	92.9	93.3	94.4
Positive predictive value	80.0	89.5	88.4	93.0	93.3	94.5
Negative predictive value	75.7	82.5	86.7	93.8	92.6	95.1

All indicators in all clinician groups are improved after use of computer-assisted diagnosis.

Table 2
Number of Cases in Which Clinicians Change Their Diagnostic Decision After CAD

	EP	RR	RS
Correct change (% of actual no. of change)	46 (79.3%)	29 (90.6%)	7 (100%)
Incorrect change (% of actual no. of change)	12 (20.7%)	3 (9.4%)	0 (0%)
Frequency of change in decision	58	32	7
% Change in decision/total possible change	13.8% (58/420)	7.6% (32/420)	1.9% (7/360)

CAD: computed-assisted diagnosis; EP: emergency physician; RR: radiology residents; RS: radiology specialists.
The proportion of correct change relative to incorrect change increased from EP to RR to RS. The total and relative number of change decreased from EP to RR to RS.

93.0% for RR, and from 93.3% to 94.5% for RS, respectively.

The negative predictive values also improved from 75.7% to 82.5% for ER, from 86.7% to 93.8% for RR, and from 92.6% to 95.1% for RS.

Again, it was observed that these conventional indicators of diagnostic accuracy of EP with support of CAD approached that of the RR without CAD, and the results of the RR with CAD approached those of the RS without CAD.

When diagnostic decision for each individual case was considered, it was found that use of CAD corrected the diagnosis far more frequently than misled the readers to a wrong diagnosis. For the EP, use of CAD led to 46 correct changes (beneficial effect) in diagnosis and 12 wrong changes (detrimental effect) of the maximum number of possible change of 420 (seven readers × 60 cases). For the RR, the figures were 29 versus 3 of 420. For the RS, the figures were 7 and 0 of 360. Thus use of CAD is associated with change in diagnosis in decreasing order of relative frequency from EP (13.8%) to RR (7.0%) to RS (1.9%). On the other hand, the relative frequency of correct change versus incorrect change show increasing trend from 79.3%:20.7% for EP, to 90.6%:19.4% for RR, to 100%:0% for RS (Table 2).

DISCUSSION

CAD for Clinicians Other Than Radiologists

Many CAD schemes have focused on high volume screening examinations, where detection of abnormality is rare and tedious but crucial. We envisage that CAD can also help in emergency situations, when expert human observers—in our scenario, neuroradiologists—may not be readily available. This is when observers of less expertise need to promptly make the crucial decisions, and hence second opinions in the form of a CAD output may make a significant improvement in outcome.

When the contexts and users are different, the performance requirements of the CAD can be different and the CAD needs to be adjusted so as to produce the most accurate human-computer diagnostic system.

It has been pointed out that CAD may actually degrade human interpretation under certain conditions (18), which design and assessment should therefore take this into ac-

count. The target users of the current CAD system are EP and other acute care physicians, and probably RR as well. It is different from other existing CAD targeted for expert radiologists. This can potentially raise the stake of a wrong suggestion provided by CAD, because the less skilled reader may be less capable of judging whether the output is correct or not.

Results from the current study also supported that observers less skillful in image interpretation are more prone to be affected by the wrong outputs of a CAD. This was reflected by difference in the number of change into a wrong diagnosis after use of CAD for the three groups of clinicians studied. As such, the potential of detrimental effect attributable to CAD may require more careful consideration. Fortunately, the number of mistakes was outweighed by the correct changes attributable to use of CAD. However, in the hands of EP, false positives were still substantial.

Effective use of CAD requires training and experience with the system. For the cases used in this ROC study, the CAD system, on its own, achieved sensitivity of 90% (27/30) and specificity of 90% (27/30) on a per-case basis. It was noteworthy that EP can improve their performance in terms of both sensitivity and specificity with CAD, just like the RR, but the sensitivity of EP with CAD is still lower than that of CAD alone. Detailed discussion with the participating EP revealed that they mistook some of the correct prompts of the CAD to be false-positive outputs and erroneously disregard such cues. It has also been pointed out that they were more prone to accept some of the wrong outputs. It is therefore inferred that more education about AIH and the CAD system is more important for users of less expertise in image interpretation and is necessary before the CAD system can be effectively used.

Choice of Small Lesion in Development and Validation of the CAD

The CAD system itself and the current study have focused on detection of small AIH, because it is conceivable that the small ones are those that cause diagnostic difficulty. At the developmental stage of the CAD, pilot study comprising 23 AIH cases of a wide range of sizes confirmed the intuition that sensitivity for cases including large (>1 cm) AIH reached 100% for CAD (Chan T, unpublished data). It is recognized that detection of large AIH by the CAD may be a technically trivial task. In addition, it may not be clinically useful for a CAD to detect large AIH, because these lesions pose little diagnostic challenge to clinicians, despite the fact that such small AIH represents only a minority of lesions encountered in clinical setting. It is these lesions where human observers are imperfect and may benefit from external assistance.

In an internal audit conducted at the first author's institute, a total of 3,341 emergent brain CT were performed for initial evaluation of head injury or neurological disturbance over a 6-month period. Of these, 279 cases were reported to show AIH, making the prevalence of AIH among emergent brain CT 8.35% (279/3,341). Furthermore, 62 of the 279 cases showed only blood clots defined as small by the criteria mentioned earlier; hence, prevalence of small AIH was 1.86% (62/3,341) (Chan T, unpublished data). These figures illustrate that negative cases usually predominate in real clinical settings. But the proportion of normal cases is only 50% in the sample of the current MRMC ROC protocol; therefore, it can be expected that the relatively infrequent detrimental effect of wrongly label AIH as a result of false-positive output may magnify in clinical practice, when proportion of normal cases is much higher. Hence false positives produced by the CAD may cause more mistaken diagnosis. We have improved this possible detrimental effect by keeping the false-positive rate to a 0.29 per set of brain CT, which is much lower than that reported for many CAD systems (9). However, this would still produce 29% false positives, with respect to patients. False-positive rates need further improvements or radiology oversight remains essential. Also, because specificity and sensitivity were improved, it is expected that the system can improve the performance even when the proportion of cases showing only small AIH in clinical setting is much lower than that in the current experiment.

Limitations of the Study

The choice of small AIH also facilitates comparison between unaided and CAD reading. By employing more difficult cases, statistical power of the experiment would be increased (19). The downside is that such a "stress test" contains nonrepresentative samples with disproportionate number of difficult cases, which affects the generalizability of the results to the general population.

Different types of AIH have been included in the experimental dataset. There were 6 cases showing subarachnoid hemorrhage, 4 cases showing extradural hemorrhage, 3 cases showing subarachnoid hemorrhage, 2 cases showing intracerebral hemorrhage, 1 case showing intraventricular hemorrhage, and 13 other cases showing a combina-

tion of two or more types of AIH. It is possible that the CAD may produce variable effect on different type of AIH, which may require further study that includes ample sample for each particular type of AIH.

There were images obtained using different slice thicknesses in the dataset, although the algorithm was designed to be handle images obtained using different protocol. It is still open to question whether the use of nonuniform imaging protocol affects the result of the CAD output and its evaluation. Again, the exact effect could only be addressed when ample sample obtained using different imaging protocol is available for further study.

The RS are a mixed group of radiologists with different skill levels. The group included one neuroradiologist, whose performance was, as expected, the best among all the readers. The results therefore may not be directly generalizable to groups with specific credentials (eg, general radiologist or neuroradiologist), which would require further experiments with adequate number of reader in each different group.

The experimental procedure required that readers read all the cases without CAD support first, before they reread the same cases with CAD support after minimal delay. This design is more closely related to the sequential than the independent reading mode as described by Kobayashi (20). The independent mode is the conventional method for conducting observer studies, when reading of images without and with CAD support are separated by a period so long that readers should have no recollection of the cases. For evaluation of CAD or other forms of adjuncts, the sequential mode, in which readers read each case first without, then with CAD support, is the favored mode. It is because it mimics the way the CAD is supposed to be used, hence the potential benefit of the first reading to the second reading is a realistic experimental design rather than a bias (21). In addition, the sequential mode is more efficient in terms of reader time. We have modified the method by having the readers complete the readings in unaided mode first because we suspect that readers may change their level of suspicion or vigilance during the experiment should they become affected by feedback available from the CAD in a similar previous case. In other words, we hoped to avoid the training effect during the course of the study. Despite the notion that any second reading per se may improve the detection of abnormalities, it has been demonstrated that ROC studies on CAD employing either sequential reading mode or independent reading mode, where the expected benefit of second reading should be absent, would produce very similar reader variance and measured results are virtually the same for both reading modes (22).

It is recognized that the current study did not measure the performance in terms of lesion localization. The major flaw is that a true-positive response may be result of detection of noise or other mimicking artifacts rather than the genuine lesion. To provide this information, a location specific ROC or free response ROC study is required (15). This type of study would be more demanding because of the requirement of establishing the lesion database and the additional investment in readers' reading time. In many instances, the AIH may span several sections; therefore, the exact definition of correct localization can be elusive. After all, the presence or absence of AIH is more important than the quantity and precise localization of lesion. Therefore we selected a patient level ROC evaluation that is sufficient to decide if the CAD can be beneficial for clinical management.

It is widely accepted that MRMC ROC is very efficient in the evaluation of diagnostic systems including CAD. However, even when the results are generalizable to the reader and case population under the study condition, whether or not the gain in performance can realize its beneficial impact in the clinical environment is a matter of debate (23). For the current study, some tools that can enhance visualization of AIH (eg, windowing and tiling images) were not made available to the readers, which could affect reduce the effect of CAD in actual clinical practice, when such tools are used.

Future Improvement

Parameters and hence performance of the CAD system may require adjustment according to the way the system is used. For example, supposing the CAD is intended to be used in the emergency department for triaging patients suffering from head injury who may be admitted if AIH is demonstrated, or undergo a short observation period; otherwise, high sensitivity is more important than low false-positive rate. The system can also be adjusted to suit the users' characteristics (eg, when the CAD is to be used by radiologist as a second reader), it can also afford to be more sensitive than specific, as suggested by our results that radiologists tend to be less affected by wrong outputs.

It has been recognized that incorporation of information in addition to the image data itself can potentially improve the performance of the CAD (24). Some other patient information available in the DICOM header (eg, sex and age) or other sources (eg, history of head injury)

can be used to modify the behavior of the program to further improve the diagnostic yield.

The CAD system was designed to work on conventional axial sections obtained from an old machine. It is recognized that thick section images and use of spiral CT are becoming substandard and the value of the CAD for thin section images from new multidetector row CT machines need to be evaluated in future studies. The authors have been adapting the system to images obtained from a 64-slice multidetector row CT. The initial impression was that even more accurate results could be achieved because the images from multidetector row CT are less prone to artifacts and contrast between AIH and normal parenchyma is higher, mainly because thinner sections make volume averaging less of a problem even for small lesions.

Another issue that needs to be considered before the CAD system can be put into clinical practice is integration into the workflow of acute care physician or the emergency department. It is different from most of the current CAD systems designed for screening or routine reporting purpose, for which speed is of less concern. For applications to be useful for immediate management, immediate availability without significant additional cost of time is of utmost importance. Possible ways of integration include setting up an application server that connects with the PACS system, or better still, direct incorporation of the system into clinical PACS.

CONCLUSION

Diagnosis of small AIH can be difficult, especially for acute care physicians who may need to interpret brain CT without the support of radiologists during odd hours. The design of a CAD system for AIH on CT has been described and evaluated by ROC analysis. Results from this observer performance study confirmed that clinicians, including both emergency physicians and radiology residents, improved their performance in detection of small AIH when they read brain CT with CAD.

REFERENCES

1. Broderick JP, Connolly S, Feldman E, et al. Guidelines for the management of spontaneous intracerebral hemorrhage: a statement for healthcare professionals from a special writing group of the Stroke Council, American Heart Association. Stroke 1999; 30:905–915.
2. Panagos PD, Jauch EC, Broderick JP. Intracerebral hemorrhage. Emerg Med Clin North Am 2002; 20:631–655.
3. Mullins ME. Modern emergent stroke imaging: pearls, protocols, and pitfalls. Radiol Clin North Am 2006; 44:41–62.
4. Jagoda AS, Cantrill SV, Wears RL, et al. Clinical policy: neuroimaging and decisionmaking in adult mild traumatic brain injury in the acute setting. Ann Emerg Med 2002; 40:231–249.
5. Norman D, Price D, Boyd D, et al. Quantitative aspects of computed tomography of the blood and cerebrospinal fluid. Radiology 1977; 123: 335–338.
6. Cohen W, Wayman L. Computed tomography of intracranial hemorrhage. Neuroimaging Clin N Am 1992; 2:75–87.
7. Schriger DL, Kalafut M, Starkman S, et al. Cranial computed tomography interpretation in acute stroke: physician accuracy in determining eligibility for thrombolytic therapy. JAMA 1998; 279:1293–1297.
8. Wysoki MG, Nassar CJ, Koenigsberg RA, et al. Head trauma: CT scan interpretation by radiology residents versus staff radiologists. Radiology 1998; 208:125–128.
9. Chan T, Huang HK. Computer aided diagnosis of small intracranial hemorrhage. Comput Med Imaging Graph 2007; 31: •. AQ: 2
10. Ducan J, Ayache N. Medical image analysis: progress over two decades and the challenges ahead. IEEE Trans Pattern Anal Machine Intel 2000; 22:85–106.
11. Erickson BJ, Bartholmai B. Computer-aided detection and diagnosis at the start of the third millennium. J Digit Imaging 2002; 15:59–68.
12. Talairach J, Tournoux P. Co-planar stereotaxic atlas of the human brain: 3-dimensional proportional system: an approach to cerebral imaging. New York: G. Thieme; 1988.
13. Doi K. Current status and future potential of computer-aided diagnosis in medical imaging. Br J Radiol 2005; 78:S3–S19.
14. Dorfman DD, Berbaum KS, Metz CE. Receiver operating characteristic rating analysis. Generalization to the population of readers and patients with the jackknife method. Invest Radiol 1992; 27:723–731.
15. Wagner RF, Beiden SV, Campbell G, et al. Assessment of medical imaging and computer-assist systems: lessons from recent experience. Acad Radiol 2002; 9:1264–1277.
16. Lev MH, Farkas J, Gemmete JJ, et al. Acute stroke: improved nonenhanced CT detection—benefits of soft-copy interpretation by using variable window width and center level settings. Radiology 1999; 213: 150–155.
17. LABMRMC. Available at http://xray.bsd.uchicago.edu/krl/KRL_ROC/software_index.htm. Accessed November 5, 2007.
18. Alberdi E, Povykalo A, Strigini L, et al. Effects of incorrect computer-aided detection (CAD) output on human decision-making in mammography. Acad Radiol 2004; 11:909–918.
19. Metz CE. Some practical issues of experimental design and data analysis in radiological ROC studies. Invest Radiol 1989; 24:234–245.
20. Kobayashi T, Xu XW, MacMahon M, et al. Effect of a computer-aided diagnosis scheme on radiologists' performance in detection of lung nodules on radiographs. Radiology 1996; 199:843–848.
21. Metz CE. Fundamental ROC analysis. In: B. J., K. H.L., and V.M. R.L., eds. Handbook of medical imaging. Vol 1. Physics and psychophysics. Bellingham, Wash: SPIE Press, 2000; 751–769. AQ: 3
22. Beiden SV, Wagner RF, Doi K, et al. Independent versus sequential reading in ROC studies of computer-assist modalities: analysis of components of variance. Acad Radiol 2002; 9:1036–1043.
23. Gur D. ROC-type assessments of medical imaging and CAD technologies: a perspective. Acad Radiol 2003; 10:402–403.
24. Partain CL, Chan HP, Gelovani JG, et al. Biomedical Imaging Research Opportunities Workshop II: report and recommendations. Radiology 2005; 236:389–403.

A Computer-Aided Diagnostic System using a Global Data Grid Repository for the Evaluation of Ultrasound Carotid Images

Marco Antonio Gutierrez[(1)], Silvia Helena Gelas Lage[(1)], Jasper Lee[(2)], Zheng Zhou[(2)]
1: Informatics Division and Critical Care Unit, Heart Institute (InCor), University of São Paulo Medical School, São Paulo, Brazil
2: Image Processing & Informatics (IPI) Laboratory, Department of Radiology, University of Southern California, California, USA
marco.gutierrez@incor.usp.br

Abstract

A computer-aided diagnostic (CAD) method of calculating lumen and wall thickness of carotid vessels is presented. The CAD is able to measure the geometry of the lumen and plaque surfaces in ultrasound carotid images using a least-square fitting of the active contours obtained automatically from the vessels border. To evaluate the approach, ultrasound image sequences from 30 patients were submitted to the procedure. The images were stored on an international data grid repository that consists of three international sites: IPI Laboratory at University of Southern California, USA; Heart Institute at University Sao Paulo, Brazil, and Hong Kong Polytechnic University, Hong Kong. The three chosen sites are connected with high speed international networks including the Internet2, and the Brazilian National Research and Education Network (RNP2). The Data Grid was used to store, backup, and share the ultrasound images and analysis results, which provided a large-scale and a virtual data system.

1. Introduction

The use of digital imaging technology has become a key component in both basic research and clinical practice. Although advances in data acquisition technology have improved the resolution and speed at which we can collect image data, most researchers have access to a limited image repository mainly due to lack of efficient software for managing, manipulating, and sharing large volumes of data [1]. In general, the image collection in research and clinical studies intrinsically creates a distributed database, as it involves many hospitals and/or centers in different locations. In addition, the amount of data generated by some imaging procedures can be so large that it is not efficient to concentrate them in a single computing center. As an example, a single study to evaluate ultrasound images of the carotid for the assessment of the degree of atherosclerotic disease has an average size of 64 Mbytes (250 images, 16 sec of acquisition time). This quantity linearly increases with time and a full transfer over the network from the acquisition site to a central repository would be large enough to saturate the available commodity connections.

Despite of the problems involving the manipulation and sharing of large medical image volumes, current image acquisition equipments do not have the software or computational power for the state-of-the-art data post-processing, typically available at computer-aided diagnostic (CAD) systems. Typically, on-line computation is oriented towards image acquisition and reconstruction. As a result, computationally demanding tasks are performed off-line, on desktop workstations after the completion of an exam. This has the adverse consequence of delaying the interpretation and communication of radiological results and makes adoption of advanced imaging techniques inefficient for radiologists.

On the other hand, making the whole image database available to authorized users, regardless of the data distribution, would provide several advantages. For example, a CAD system could be tested and trained on a much larger data set, with an improvement of its performance in terms of both sensitivity and specificity. The CAD system could be used as a real time selector of images, with a remarkable reduction of the delay between image acquisition and diagnosis. Moreover, data associated to the images, or metadata, would be available to select the proper input for epidemiology studies or for the training of new radiologists.

In this work, we present a CAD system method to segment carotid vessels in a large scale data grid repository. The operator selects a region-of-interest (ROI) in a series of carotid images obtained from B-mode ultrasound. This set of images is convolved with the corresponding partial derivatives of the Gaussian filter. The filter response is used to compute a 2D gradient magnitude image in order to refine the

Seventh IEEE International Symposium on Cluster Computing and the Grid(CCGrid'07)
0-7695-2833-3/07 $20.00 © 2007 IEEE

vessel's boundaries. Using an active contour technique the geometry of the lumen and the plaque surface are determined automatically. The near wall media-adventitia (NWMA), far wall media-adventitia (FWMA) and far wall lumen-intima (FWLI) borders are obtained by a least-square fitting of the active contours result. The distance between NWMA and FWLI (vessel diameter) and between FWLI and FWMA (far wall intima-media thickness) are obtained for all images and the mean value is computed during systole and diastole. To evaluate the approach, ultrasound image sequences from 30 patients were submitted to the procedure. The images were stored on an international data grid repository that consists of three international sites: Image Processing and Informatics (IPI) Laboratory at University of Southern California, USA; InCor (Heart Institute) at Sao Paulo, Brazil, and Hong Kong Polytechnic University, Hong Kong. The three chosen sites are connected with high speed international networks including the Internet2, and the Brazilian National Research and Education Network (RNP2). The Data Grid enables the three sites to share the image data and to analyze the results to improve the clinical research outcome.

2. Methods

2.1. Grid technologies

Grid technologies provide mechanisms for sharing and coordinating the use of diverse resources and thus enable the creation, from geographically and organizationally distributed components, of virtual computing systems that are sufficiently integrated to deliver desired quality of service. These technologies include a high-performance hardware and software infrastructure to provide: a) security solutions that support management of credentials and policies when computations span multiple institutions; b) resource management protocols and services that support secure remote access to computing and data resources and the co-allocation of multiple resources; c) information query protocols and services that provide configuration and status information about resources, organizations, and services; d) data management services that locate and transport datasets between storage systems and applications.

Several large-scale Data Grids, such as TeraGrid (http://www.teragrid.org/) and Data Replication for LIGO (http://www.globus.org) have been established for fast movement of large amount of data among multiple research institutes. A Data Grid [2] specifically for clinical image backup and disaster recovery has been developed previously at IPI (Image Processing & Informatics Laboratory) using the Globus Toolkit 4 (GT4) [3]. This Data Grid was designed to utilize the strengths of grid technology along with PACS (Picture Archiving and Communication Systems)/DICOM (Digital Imaging and Communications in Medicine) technology for storing and distributing clinical images [4,5]. In particular, some PACS/DICOM resources are embedded within the five layer grid architecture. These include Storage services, Query services, Retrieve services, which are integrated with the DICOM standard protocols in addition to the use of other Data Grid Services. The five layer architecture of the Data Grid embedded with DICOM technology is shown in Figure 1, which illustrates some of the basic components already developed at IPI, such as the Metadata Catalog Service. The three services in Data Grid Applications layer are not the standard Grid Services defined in the GT4. These services include Storage services, Query services, Retrieve services, which are integrated with the DICOM standard protocols in addition to the use of other Data Grid Services.

The experience and knowledge learned from the Data Grid for clinical image recovery has been utilized to design the Data Grid architecture for CAD assessment of carotid wall thickness.

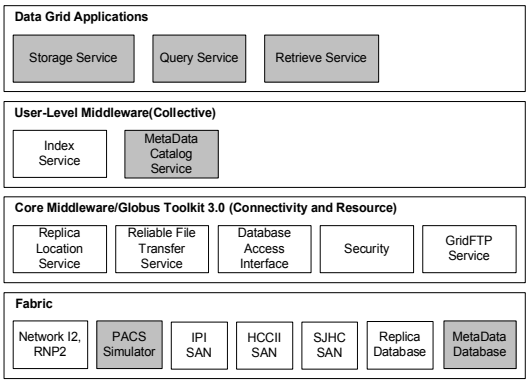

Figure 1. Five-layer architecture and the contents of the Data Grid for clinical image backup: The combination of 2nd and 3rd layers of connectivity and resource, respectively, are sometimes referred to as the Core Middleware. Gray-shaded boxes represent components developed or modified at the IPI Lab.

2.2. Carotid wall thickness in ultrasound images

Non-invasive ultrasonic B-mode imaging is an increasingly important method for studying progress

and regress of atherosclerotic lesions in the carotid artery. Figure 2 shows a representative B-mode ultrasound image of the carotid artery and a schematic illustration of the relevant leading edges of echo responses. Previous studies [6,7] have shown that the leading edges can be mapped to the following interfaces: near-wall intima-lumen, far-wall lumen-intima and far-wall media-adventitia. The lumen diameter (LD) is defined as the distance between the media-adventitia interface of the near-wall and the lumen-intima interface of the far-wall. The far-wall intima-media thickness (IMT) is defined as the distance between the far-wall lumen-intima and the far-wall media-adventitia interfaces.

The complete geometry of the carotid vessels can be manually determined using B-mode ultrasound. However, this approach is a time consuming procedure and based on subjective operator assessment that inevitably results in inter and intra-observer variability. Efforts have been made to make the measurement less operator dependent by introducing automated image analysis procedures.

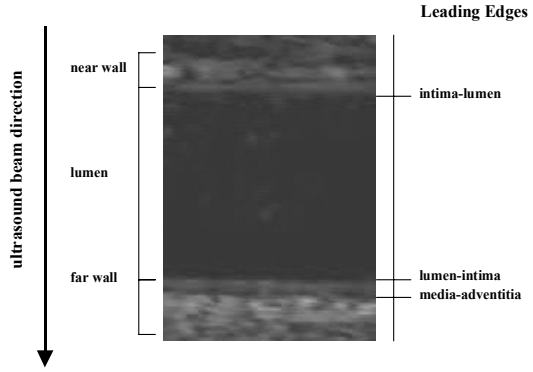

Figure 2. Interfaces between carotid tissue layers obtained from B-mode ultrasound.

2.3. Artery boundary enhancement

To enhance border detection accuracy, a multiscale border identification was implemented using filters in the form of scaled convolution operators [8]. The scale space of an image is constructed through convolution of the image with a two-dimensional (2D) Gaussian density kernel with zero mean and standard deviation:

$$G(\vec{x},\sigma)=\frac{1}{\sqrt{2\pi\sigma^2}^{D}}e^{-\frac{\|\vec{x}\|^2}{2\sigma^2}} \quad (1)$$

where D denotes the dimension of the input domain. A blurred replica of the original image is obtained by convolution with $G(\vec{x};\sigma)$ for a specific σ. The stack of images as a function of increasing scale parameter σ is coined a linear scale space. Hence, as σ increases the detailed object structures vanish, while gross structures persist.

Based on these features a scaled artery image is used to identify the approximated position of the near and far walls. Two complementary images, based on the gradient value in y-direction are obtained: one that enhances pixel values transitions from high to low echoes, such as edges encountered in near wall tissue interfaces, and other that enhances pixel values transitions from low to high echoes (such as edges encountered in far wall tissue interfaces). Figure 3 shows the boundary enhancement of the near and far wall.

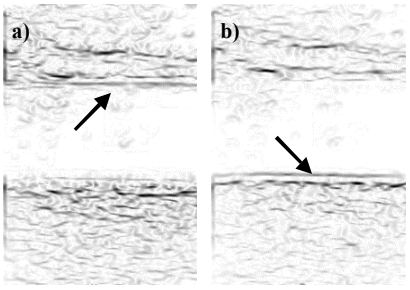

Figure 3. Boundary enhancement of the near wall a) and far wall b)

The contour of each wall is modeled following the Geometrically Deformed Model proposed by Lobregt and Viergever [9].In this model, a set of vertices which are connected by straight line segments or edges forms the basic contour structure (Figure 6). The position of a vertex V_i is represented by a vector p_i, and the edge between V_i and V_{i+1} by a vector d_i. The contour deformation is caused by a combination of forces which act on the vertices. The resulting acceleration in vertex V_i is denoted by a vector a_i.

The contour local curvature at a vertex V_i is defined as the difference between the directions of the two edge segments that join at that location:

$$\hat{c}_i = \hat{d}_i - \hat{d}_{i-1} \quad (2)$$

The local tangential unit vector $\hat{t}_i$ is defined as the normalized sum of the unit vectors of two joining edge segments:

$$\hat{t}_i = \frac{\hat{d}_i + \hat{d}_{i-1}}{\left\| \hat{d}_i + \hat{d}_{i-1} \right\|} \quad (3)$$

The local radial direction at a vertex V_i is obtained from $\hat{t}_i$ by a rotation over $\pi/2$ radians:

$$\hat{r}_i = \begin{bmatrix} 0 & 1 \\ -1 & 0 \end{bmatrix} \hat{t}_i \quad (4)$$

2.5. Dynamic force formulation

In the model definition, the dynamic in each vertex V_i must satisfy the Newton´s second law,

$$\begin{aligned} F_i &= F_{\text{int},i} + F_{ext,i} + F_{damp,i} \\ F_i &= \mu_i a_i \end{aligned} \quad (5)$$

where μ_i is a coefficient that has a mass unit, $F_{damp,i}$, $F_{\text{int},i}$ and $F_{ext,i}$ are the damping (or viscous), the internal and the external forces, respectively.

The internal force can be estimated from the local contour curvature along the local r-axis,

$$F_{\text{int},i} = \left(c_i \cdot \hat{r}_i \right) \quad (6)$$

The external force acting in each vertex can be approximated by some image feature. In this paper we used the information obtained from the local image gradient as the external force.

The damping force is proportional to the velocity of the vertex and points in opposite direction:

$$F_{damp,i} \approx -k.v_i \quad (7)$$

The total force F_i acting on a vertex is a weighted combination of damping, internal and external

$$F_i = w_{\text{int}} F_{\text{int},i} + w_{ext} F_{ext,i} + w_{damp} F_{damp,i} \quad (8)$$

where w_{int}, w_{ext} and w_{damp} are the weighting factors.

The deformation process over the contour is implemented as a numerical time integration process in which the complete state of the contour is calculated at a sequence of discrete positions in time [16,17]. A set of state equations controls the deformation process in terms of position, velocity and acceleration of each vertex on the contour:

$$\begin{cases} p_i(t+\Delta t) = p_i(t) + v_i(t) \\ v_i(t+\Delta t) = v_i(t) + a_i(t).\Delta t \\ a_i(t+\Delta t) = \dfrac{1}{m_i} F_i(t+\Delta t) \end{cases} \quad (9)$$

where $p_i(t+\Delta t)$, $v_i(t+\Delta t)$ and $a_i(t+\Delta t)$ define the position, velocity and acceleration, respectively, of the vertex in a incremental time Δt. The vertex mass, m_i, is setting constant for all vertices and the resulting force, F_i, is calculated using equation (8).

3. Results

3.1. Data collection

A sequence of B-mode ultrasound images of the carotid artery was acquired with spatial resolution of 456 x 576 pixels, 8 bits/pixel, 15 frames /sec and acquisition time of 16 sec. This setup gives an average data size of 64 Mbytes/exam (250 images). The Data Grid was used to store, backup, and to share the ultrasound images and to analyze the results, which provided a large-scale and a virtual data system. The exams were stored on an international data grid repository that consists of three international sites: Image Processing and Informatics (IPI) Laboratory at University of Southern California, USA; InCor (Heart Institute) at Sao Paulo, Brazil, and Hong Kong Polytechnic University, Hong Kong. The three chosen sites are connected with high speed international networks including the Internet2, and the Brazilian National Research and Education Network (RNP2).

The Data Grid enables the three sites to share the image data and to analyze the results to improve the clinical research outcome (Figure 4).

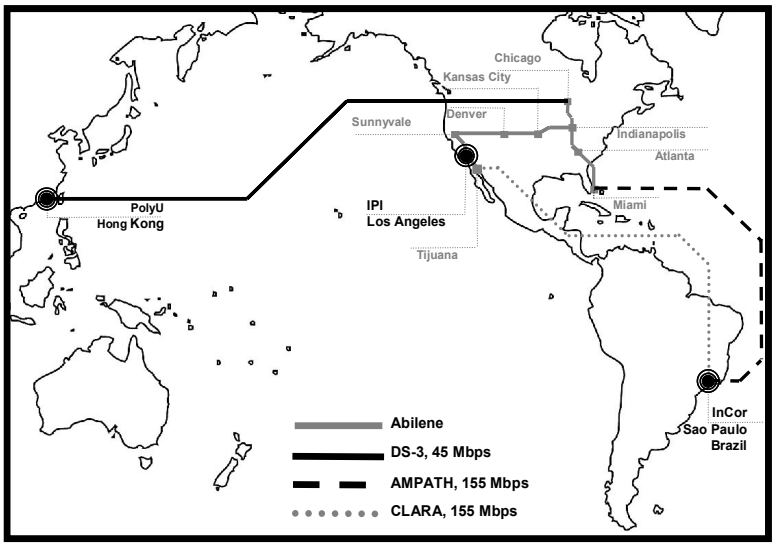

Figure 4. Topology of the International Internet-2 Connectivity Between the Three Sites Linking IPI/USC in North America, InCor in South America, and PolyU in Asia. Note that the Routing Path from InCor to PolyU utilizes AMPATH instead of CLARA which is the routing path between IPI and InCor.

3.2. Evaluation procedure

After the retrieval of an exam previously stored in the Data Grid, the operator selects a region-of-interest (ROI) in a series of carotid images. This set of images is convolved with the corresponding partial derivatives of the Gaussian filter. The filter response is used to compute a 2D gradient magnitude image in order to refine the vessel's boundaries. Using an active contour technique the geometry of the lumen and the plaque surface are determined automatically. The near wall media-adventitia (NWMA), far wall media-adventitia (FWMA) and far wall lumen-intima (FWLI) borders are obtained by a least-square fitting of the active contours result. The distance between NWMA and FWLI (vessel diameter) and between FWLI and FWMA (far wall intima-media thickness) are obtained for all images and the mean value is computed during systole and diastole.

In this evaluation a total of 180 images from 30 patients (3 images in diastole and 3 images in systole for each patient) were analyzed, all of which included manually defined interfaces for reference. The minimum and maximum artery diameters were measured for each patient using the manual and the automatic procedure. However, for clinical purposes, some interactive tools for manual tracing were incorporated to the model to correct remaining detection errors in regions with poor image quality. In order to study the variability between the automatic and manual definition of artery boundaries, the pooled mean, $\overline{\mu}$, and the standard deviation, σ, for the difference between automated and manual measurements of lumen diameter were computed. The coefficient of variation, CV, was calculated according to:

$$CV = \left(\frac{\sigma}{\overline{\mu}\sqrt{2}} \times 100 \right)\% \qquad (10)$$

The strength of the relationship between automated and manual methods is indicated by the correlation, $R_{a,m}$, between the two measurements:

$$R_{a,m} = \frac{Cov_{a,m}}{\sigma_a . \sigma_m} \qquad (11)$$

where $Cov_{a,m}$ is the covariance between the automated and manual and σ_a and σ_m are the standard deviation of automated and manual measurements, respectively.

The results obtained for the means ($\mu_{a,m}$) and standard deviations ($\sigma_{a,m}$) for the differences between the automatic and manual methods and for the parameters $CV_{a,m}$ and $Corr_{a,m}$ are summarized in Table 1.

Table 1. Lumen diameter (LD) and Intima-Media Thickness (IMT) measured using automatic and manual methods (n=30). The difference, Δ, the coefficient of variability, CV and the correlation, $Corr_{a,m}$, between both measurements are also presented

	Automatic $\mu_a \pm \sigma_a$ (mm)	**Manual** $\mu_m \pm \sigma_m$ (mm)	**Difference** Δ $\mu_{a,m} \pm \sigma_{a,m}$ (mm)	**Variability** CV (%)	**Correlation** $Corr_{a,m}$
Lumen Diameter (diastole)	7.85 ± 1.01	7.78 ± 1.01	0.13 ± 0.09	0.83	0.99
Lumen Diameter (systole)	6.81 ± 1.06	6.77 ± 1.05	0.12 ± 0.10	1.00	0.99
Intima-Media Thicknes	0.72 ± 0.14	0.63 ± 0.12	0.09 ± 0.06	6.16	0.90

4. Conclusions

Measurements of lumen diameter (LD) and intima-media thickness (IMT) of carotid and femoral arteries from B-mode ultrasound are defined as the average distance of interfaces between vessel tissue layers. In order to determine the interface location a manual tracing is commonly used. However, this approach is a time consuming procedure and based on subjective operator assessment. We have proposed a method that uses the active contour technique where the external forces are proportional to the local image gradient obtained from a multiscale analysis. The automated measurements, when compared to those obtained by manual tracing, are equally accurate and the coefficients of variability between both methods are below 1.0% for Lumen Diameter and 6.5% for Intima-Media thickness measurements.

In this paper, we present a Data Grid testbed for evaluation of ultrasound carotid images. Three international sites were used for store, query and retrieve of medical images. The laboratory prototype of this DICOM compliance Data Grid has been completed. Currently, the three International sites have been connected, and we are implementing the Data Grid at the Hong Kong Polytechnic University, and the Heart Institute at Sao Paulo, Brazil.

Once the Data Grid testbed for research and clinical study is established, we can incorporate the multiple trials databases into the Data Grid in the future. The multiple trials databases are equally important as the image data. Such a Data Grid can provide three benefits to the trials databases: 1) fault-tolerance, 2) data and result sharing using for instance the DICOM Structured Reporting, and 3) dynamic creation and modification of data model to support any new trial or change of trials.

5. Acknowledgements

This work has been supported by Grant No. 2436 of the National Network for Education and Research (RNP), Scientific and Technology Ministry, Grant No. 300499/2005-1 of the National Council for Scientific and Technological Development (CNPq and the Zerbini Foundation.

6. References

[1] R. Bellotti, P. Cerello, S. Tangaro, V. Bevilacqua, M. Castellano. Distributed medical image analysis on a Grid infrastructure. *Future Generation Computer Systems*, 23:475-484, 2007.

[2] B.J. Liu, M.Z. Zhou and J. Documet, Utilizing data grid architecture for the backup and recovery of clinical image data, *Computerized Medical Imaging and Graphics* 29 (2005), 95-102.

[3] I. Foster, Globus Toolkit Version 4: Software for Service-Oriented Systems, *IFIP International Conference on Network and Parallel Computing*, Springer-Verlag LNCS 3779, 2005, 2-13.

[4] H.K. Huang, PACS and Imaging Informatics: *Basic Principles and Applications*, Wiley & Sons, NJ, 2004.

[5] B.J. Liu, F. Cao, M.Z. Zhou, G. Mogel and L. Documet, Trends in PACS Image Storage and Archive, *Computerized Medical Imaging and Graphics* 27 (2003), 165-174.

[6] C. Liguori, A. Paolillo, A. Pietrosanto. An automatic measurement system for the evaluation of carotid intima-media thickness. *IEEE Transaction on Instrumentation and Measurement*, 50(6):1684-1685, 2001.

[7] A. Zahalka, A. Fenster. An automated segmentation method for three-dimensional carotid ultrasound images. *Physics in Medicine and Biology*, 46:1321-1342, 2001.

[8] J.J. Koenderink. The structure of images. *Biological Cybernetics* 1984;50:363-370.

[9] S. Lobregt, M. Viergever. A discrete dynamic contour model. *IEEE Trans. Medical Imaging*, Vol.14, No. 1, pp.12-24, 1995.

A Continuous Glucose Monitoring System in Critical Cardiac Patients in the Intensive Care Unit

A Murakami[1,2], MA Gutierrez[1,2], SHG Lage[1], MFS Rebelo[1], RHG Guiraldelli[2], JAF Ramires[1]

[1] Heart Institute, University of Sao Paulo, Medical School, Sao Paulo, Brazil
[2] Polytechnic School, University of Sao Paulo, Sao Paulo, Brazil

Abstract

Some studies show that a tight glucose control appears to have clinical benefits for cardiac patients at Intensive Care Unit (ICU). However, it requires glucose readings every few hours in a tiresome operation.

In the present study, a real time glucose monitoring system was implemented to control critical cardiac patients at ICU. For this, a commercially available Holter-like glucose monitor was used. A PocketPC was connected to the glucose monitor, downloading the collected data every 5 min, so real time readings could be obtained. The readings were transmitted using the HL7 communication standard to an Electronic Patient Record and to a bedside monitor at the ICU in real-time.

These results have shown that the proposed methodology is a promising application to the ICU, providing a better treatment for critical cardiac patients.

1. Introduction

The association between diabetes mellitus and cardiopathies is very common, leading patients to a poor prognosis. Since the Diabetes Control and Complications Trial (DCCT), it is well known that a tight glucose control, i.e, keeping glycemia in a restricted normal range, is beneficial for diabetic outpatients [1]. Van den Berghe showed that the same procedure could reduce mortality between Intensive Care Unit (ICU) patients [2]. Though these works did not confirm the relationship between tight glucose control and cardiopathies, others give some evidences. Tight glucose control, according to the DIGAMI study group, reduces mortality between diabetic patients after a myocardial infarction [3]. Furnary et al. showed the reduction of the incidence of deep sternal wound infection after open heart surgery [4]. Despite of its benefits, implementing a tight glycemic control on an ICU patient requires glucose readings every few hours, along with insulin infusion rate adjustments, in a tiresome operation.

Due to the difficulties of the conventional methods, several new ways of continuously measuring glycemia has been studied in the last decades [5]. The research efforts generated a few commercially available glucose sensors, like the MiniMed CGMS (Medtronic Diabetes), GlucoWatch (Cygnus) and GlucoDay (A. Menarini). Still, there are several open issues, like accuracy, generation of real time readings, applicability at ICU and integration to hospital information systems.

In the present study, a real time glucose monitoring system for ICU patients, named as "vMonGluco", was implemented. For this purpose, a commercially available Holter-like glucose monitor was used. The readings were transmitted through a WiFi network using the Health Level Seven (HL7) communication protocol, a standard for integration of medical systems [6]. The collected information was stored in an Electronic Patient Record. They were also shown on a bedside monitor at the ICU, so the medical staff could easily access the glucose readings.

2. Methods

2.1. Real-time glucose readings

To produce the glucose readings the MiniMed Continuous Glucose Monitoring System (CGMS, Medtronic Diabetes) was used [7]. The MiniMed CGMS consists of a disposable subcutaneous glucose sensor, connected by a cable to a pager-sized glucose monitor.

The CGMS uses a glucose oxidase based platinum electrode, which produces an electrical current when in contact with glucose. This sensor is inserted under the skin, in contact with the interstitial fluid. The electrical current is linearly dependent upon the concentration of the glucose. Hence, by scaling the current with appropriate constants, an estimation of the glucose concentration can be determined. A linear regression calibration method is used to estimate these constants.

CGMS readings must be calibrated at least 4 times daily against standard capillary glucose measurements, which are used to retrospectively calibrate the sensor readings at the time of data analysis. Each sensor is meant to be worn for up to three days.

The sensor readings collected by CGMS must be downloaded into a PC at the end of using period. A MiniMed Com-Station, physically linked to the PC through a serial connection, acts as a docking station for CGMS to transfer the data to the PC. When initialized, MiniMed Solution Software V3.0C downloads the data stored onboard and applies a regression calibration algorithm, finally obtaining the glucose readings.

CGMS is approved for use in outpatients by the Food and Drug Administration (FDA), but it is not designed for producing real-time glucose information. The glucose data calibration, as performed by MiniMed's software, is a once off process, based on all the calibration points entered on the measuring period. To use CGMS in real-time, it is necessary to download the sensor readings every 5 min. Also, the calibration must be performed each time the monitor produces a new current value.

We implemented a software module into a PocketPC (HP/COMPAQ iPAQ) to address the two issues. The PocketPC is connected to the Com-Station through a serial cable (Figure 1). A software module, named as "vMonGluco Client", periodically downloads the data stored into the CGMS memory every 5 min. The data interpretation, i.e., the translation of the current generated at the electrode into blood glucose concentration is performed by vMonGluco. After data calibration, the glucose values are plotted in real-time at the PocketPC screen. The values are also parsed into a HL7 message and transmitted to a HL7 server.

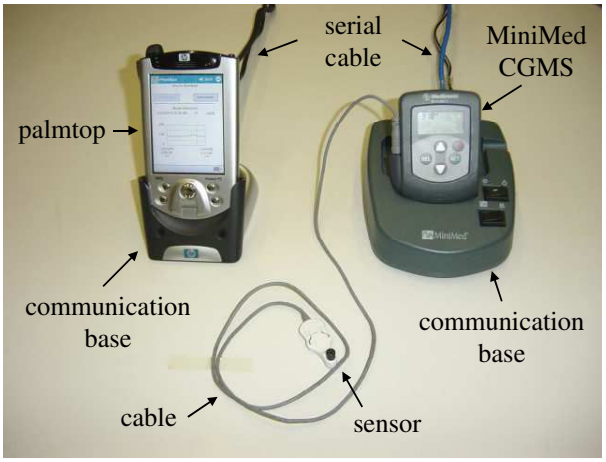

Figure 1. MiniMed CGMS connected to the palmtop.

2.2. Integration to the electronic patient record

The HL7 messages, containing the glucose readings, are received by a HL7 server, named as "vMonGluco Server". The vMonGluco Server transmits the glucose readings to the bedside monitoring system using the HL7 protocol.

The bedside monitoring system is based on Siemens monitors (Siemens Medical Solutions), models SC7000 and SC6002XL, linked to a dedicated network. All communication between the dedicated monitoring network and the hospital network are performed through a gateway using HL7 messages.

The vMonGluco Server also stores the collected information into the Electronic Patient Record. The information can be easily accessed through a Web interface (Figure 2).

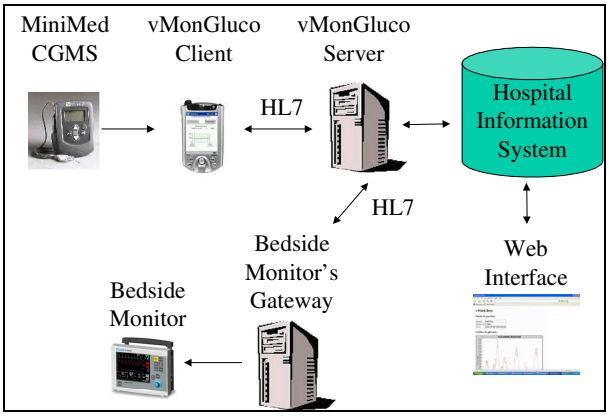

Figure 2. The vMonGluco architecture.

2.3. Accuracy tests on patients

To verify the accuracy of the glucose readings, 12 (twelve) hyperglycemic patients, with some kind of cardiopathy, were selected at the Heart Institute's clinical ICU to use the equipment for a few days. The patients had an average age of 70.6 ± 15.4 years. After consent was obtained, a glucose sensor was placed subcutaneously on the patient's abdomen or upper arm using a proper insertion device. The sensor was connected to the MiniMed CGMS monitor. One hour after the insertion a standard capillary glucose reading (fingerstick) was performed and the result was registered into the CGMS for calibration. Fingersticks were performed using the Accu-Check Advantage glucometer (Roche Diagnostics) every two hours. Every six hours, the CGMS was calibrated using a fingerstick reading.

To allow the periodic download of the sensor's data, the CGMS was mounted on the MiniMed Com-Station. A PocketPC computer, running the vMonGluco Client software, was connected to the MiniMed Com-Station. This way, real-time glucose readings were obtained

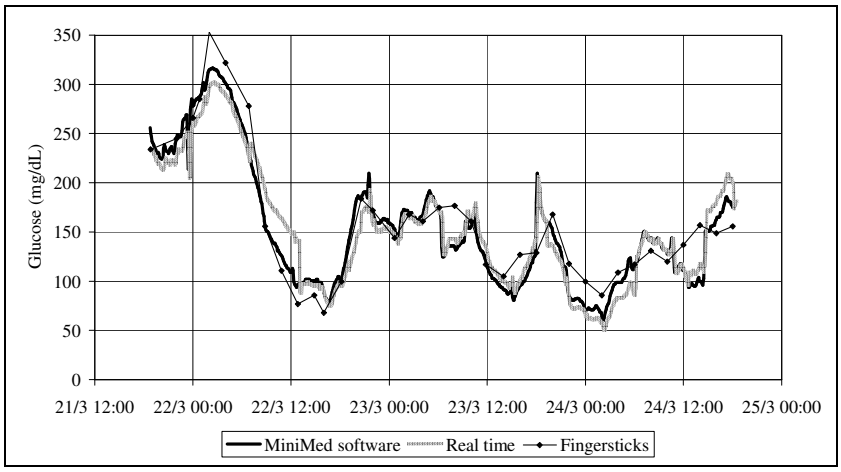

Figure 3. Glucose readings from one of the patients.

Following the data acquisition period, the values stored into the MiniMed CGMS were downloaded into a standard PC. In a retrospective way, the MiniMed Solutions Software (version 3.0C) generated glucose readings, which were compared to the fingersticks and to the real-time readings registered by vMonGluco software (Figure 3).

3. Results

Using the MiniMed as a "gold-standard", the difference between post-processing and vMonGluco readings (real-time) was -1.4 ± 23.5 (n=9,008). The correlation coefficient between the two types of measurements was r=0.92. Table 1 shows the complete statistics.

When comparing the vMonGluco readings (real-time) to the fingersticks, we obtained a difference of -13.8 ± 49.2 (n=318) and the correlation coefficient between the two types of measurements was r = 0.77 (Table 2).

The Clarke grid [8] was also used for the analysis. When comparing the MiniMed software readings to the fingersticks, the following results were obtained: zone A = 81.4%, B = 17.5%, C = 0%, D = 1.1%, E = 0%. For the real time readings, the results were: zone A = 66.5%, B = 31.8%, C = 0%, D = 1.1%, E = 0.6%.

Table 1. Comparison between MiniMed software readings and vMonGluco (correlation coefficient r = 0.92).

Range	N	MiniMed average	vMonGluco average	Difference	Difference (%)	Absolute Difference
< 100 mg/dL	1,125	81.9	88.1	6.1 ± 17.6	9.2 ± 26.2	13.9
100 - 149 mg/dL	3,495	126.3	128.1	1.8 ± 17.9	1.3 ± 13.9	12.1
150 - 199 mg/dL	2,599	170.4	168.2	-2.2 ± 21.2	-1.3 ± 12.3	14.0
200 - 249 mg/dL	1,041	222.3	213.0	-9.3 ± 34.5	-4.1 ± 15.6	22.6
>= 250 mg/dL	748	298.0	284.2	-13.9 ± 33.3	-4.8 ± 11.2	22.6
Total	**9,008**	**158.8**	**157.4**	**-1.4 ± 23.5**	**0.4 ± 16.1**	**15.0**

Table 2. Comparison between real time readings and fingersticks (correlation coefficient r = 0. 77).

Range	N	Fingersticks average	vMonGluco average	Difference	Difference (%)	Absolute Difference
< 100 mg/dL	45	82.0	103.0	21.0 ± 27.4	35.6 ± 61.1	27.1
100 - 149 mg/dL	95	123.1	124.0	0.9 ± 28.5	1.2 ± 23.2	21.6
150 - 199 mg/dL	87	170.9	158.5	-12.4 ± 33.0	-7.0 ± 19.5	25.1
200 - 249 mg/dL	52	219.6	197.5	-22.1 ± 42.4	-10.0 ± 19.5	36.1
>= 250 mg/dL	39	328.8	247.4	-81.5 ± 74.2	-23.8 ± 19.8	85.0
Total	**318**	**171.4**	**157.6**	**-13.8 ± 49.2**	**-1.1 ± 34.4**	**33.5**

4. Discussion and conclusions

The results obtained by the MiniMed software are comparable to the ones found in the literature [7,9]. As shown on Table 1 and 2, greater deviations can be found at low (< 100 mg/dL) and high (> 250 mg/dL) glucose values. As suggested by Goldberg et al. [9], this could be explained by fingersticks inaccuracy during hypoglicemia in hypotensive patients [10]. However, a larger study must be addressed for a more conclusive analysis.

The results of the vMonGluco, the proposed real-time method are similar (r=0.92) to the ones obtained by post-processing using MiniMed software. The Clarke grid analysis result (98.3% of the readings in zones A an B) suggests that the real-time glucose readings are clinically meaningful and, thus, a promising tool at the ICU work, especially when used together with other glucose measuring methods.

The implemented vMonGluco architecture offers a reasonable solution for fast communication and storage of the generated information. The use of a standard communication protocol, such as HL7, allowed an easy integration to prior existing systems.

In conclusion, the results suggest that the proposed methodology is a promising application at the ICU, providing a better treatment for critical cardiac patients.

Acknowledgements

This work was partially supported by the National Council for Scientific and Technological Development (CNPq), grants 471143/2001-4 and 303664/2002-9, and Zerbini Foundation. This project would not be possible without Medtronic Diabetes support, offering CGMS monitors, sensors, software, and standard hospital glucose meters. The authors are especially grateful to Medtronic group based in Brazil. The authors wish to thank the medical and nursing staff at the Heart Institute's ICU for their assistance. The whole IT team at the Heart Institute has contributed in different ways, and the authors are thankful to them.

References

[1] The Diabetes Control and Complications Trial Research Group. The Effect of Intensive Treatment of Diabetes on the Development and Progression of Long-Term Complications in Insulin-Dependent Diabetes Mellitus. The New England Journal of Medicine 1993;329(14):977-86.

[2] Van den Berghe G. How does blood glucose control with insulin save lives in intensive care? The Journal of Clinical Investigation 2004;114(9):1187-95.

[3] Malmberg K. Prospective randomised study of intensive insulin treatment on long term survival after myocardial infarction in patients with diabetes mellitus. British Medical Journal 1997;314:1512.

[4] Furnary AP, Zerr KJ, Grunkemeier GL, Starr A. Continuous Intravenous Insulin Infusion Reduces the Incidence of Deep Sternal Wound Infection in Diabetic Patients after Cardiac Surgical Procedures. Annals of Thoracic Surgery 1999;67(2):352-62.

[5] Pickup J, McCartney L, Rollinsky O, Birch D. In vivo glucose sensing for diabetes management: progress towards non-invasive monitoring. British Medical Journal 1999;319(7220):1–4.

[6] Health Level Seven. Health Level Seven Implementation Support Guide for HL7 Standard Version 2.3. USA: Health Level Seven, 1998.

[7] Gross TM, Bode BW, Einhorn D, Kayne DM, Reed JH, White NH, Mastrototaro JJ. Performance Evaluation of the MiniMed Continuous Glucose Monitoring System during Patient Home Use. Diabetes Technology and Therapeutics 2000;2(1):49-56.

[8] Clarke WL, Cox D, Gonder-Frederick LA, Carter W, Pohl SL. Evaluating Clinical Accuracy of Systems for Self-Monitoring of Blood Glucose. Diabetes Care 1987;10(5):622-28.

[9] Goldberg PA, Siegel MD, Russel RR, Sherwin RS, Halickman JI, Cooper DA, Dziura JD, Inzucchi SE. Experience with the Continuous Glucose Monitoring System in a Medical Intensive Care Unit. Diabetes Technology and Therapeutics 2004; 6(3):339-347.

[10] Atkin SH, Dasmahapatra A, Jaker MA, Chorost MI, Reddy S. Fingerstick Glucose Determination in Shock. Annals of Internal Medicine 1991;114:1020-24.

Address for correspondence:

Marco Antonio Gutierrez
Av. Dr. Eneas de Carvalho Aguiar, 44
05403-900 – Sao Paulo – SP – Brazil
marco.gutierrez@incor.usp.br

Automatic Bone Age Assessment for Young Children from Newborn to 7-Year-Old Using Carpal Bones*

Aifeng Zhang, Arkadiusz Gertych, Brent J. Liu

Image Processing & Informatics Lab, Department of Radiology, University of Southern California, Marina Del Rey, CA 90292, USA

* *Paper accepted to be published in Journal of Computerized Medical Imaging and Graphics*

ABSTRACT

A computer-aided-diagnosis (CAD) method has been previously developed based on features extracted from phalangeal regions of interest (ROI) in a digital hand atlas, which can assess bone age of children from ages 7 to 18 accurately. Therefore, in order to assess the bone age of children in younger ages, the inclusion of carpal bones is necessary. However, due to various factors including the uncertain number of bones appearing, non-uniformity of soft tissue, low contrast between the bony structure and soft tissue, automatic segmentation and identification of carpal bone boundaries is an extremely challenging task. Past research works on carpal bone segmentation were performed utilizing dynamic thresholding. However, due to the limitation of the segmentation algorithm, carpal bones have not been taken into consideration in the bone age assessment procedure. In this paper, we developed and implemented a knowledge-based method for fully automatic carpal bone segmentation and morphological feature analysis. Fuzzy classification was then used to assess the bone age based on the selected features. This method has been successfully applied on all cases in which carpal bones have not overlapped. CAD results of total about 205 cases from the digital hand atlas were evaluated against subject chronological age as well as readings of two radiologists. It was found that the carpal ROI provides reliable information in determining the bone age for young children from newborn to 7-year-old.

Keywords: *Bone Age Assessment, Computer-aided-diagnosis, Carpal Region of Interest, Carpal Bone Segmentation, Anisotropic Diffusion, Canny Edge Detection, Feature Extraction, Fuzzy Classification*

I. INTRODUCTION

The determination of skeletal maturity (‘bone age’) plays an important role in diagnostic and therapeutic investigations of endocrinological problems and growth disorders of children [1, 2]. In clinical practice, the most commonly used bone age assessment method is atlas matching by a left hand and wrist radiograph against the Greulich & Pyle (G&P) atlas [3] which contains a reference set of normal standard images. However, besides the fact that the data in G&P atlas was collected in 1950’s, this method strongly depends on experience of the observer, leading to considerable inter and intra-observer discrepancy. Therefore, an updated data collection and an objective method are desirable.

A computer-aided-diagnosis (CAD) method [4-8] has been previously developed in our laboratory based on features extracted from regions of interest (ROI) in phalanges from a digital

hand atlas. 1,103 left hand and wrist radiographs of normal children, from newborn to 18 years old, were acquired at the Childrens Hospital Los Angeles (CHLA) and digitized at IPI (Image Processing and Informatics Lab, USC). The data was evenly distributed into four races (Asian, Caucasian, African-American and Hispanic) for both gender (Male and Female). Each case was read by two radiologists independently. Figure 1 shows an example image with phalangeal and carpal ROIs superimposed.

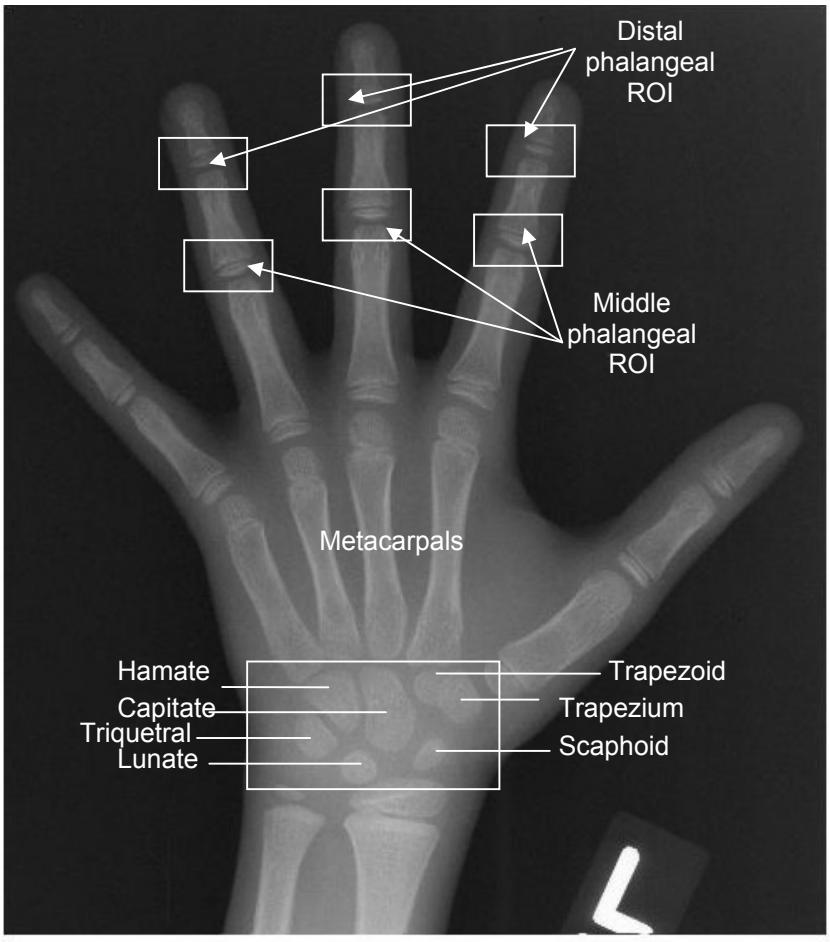

Figure 1. A left hand and wrist radiograph marked with 6 phalangeal ROIs and carpal ROI (box at the bottom)

For children above 6 of female or 8 years old of male, Phalangeal feature analysis was very reliable. Therefore, CAD method yields very accurate bone age assessment. However, for ages below 5 ~ 7, the phalangeal analysis fails to extract the features correctly in some cases, especially in very young children. This is due to the following problems: first, soft tissue deteriorates the border and makes the segmentation between epiphysis and metaphysis an extremely difficult task. Second, the developments of epiphysis of the six phalangeal ROIs are not parallel. Third, it is not reliable to locate the phalangeal ROIs correctly if the hand is rotated when the upright hand position is not achieved during acquisition. Lastly, the phalangeal ROIs analysis is sensitive to bending of fingers during acquisition.

Therefore, in order to achieve similar degree of accuracy in bone age assessment for children of all ages, we hypothesized that the CAD method may benefit from the augmentation of features extracted from the carpal ROI of young children. Medical studies [1, 2, 9] verified the value of

carpal bone in determining the bone age of young children. Past research work on carpal bone segmentation has been done by Pietka [10] utilizing dynamic thresholding. However, due to the limitation of the algorithm, carpal ROI have not been taken into consideration in the bone age assessment procedure.

This paper described a knowledge-based carpal ROI analysis for fully automatic carpal bone segmentation and feature analysis for bone age assessment by fuzzy classification. Table 1 shows the reliability of phalangeal and carpal ROIs analysis for different age groups in CAD system. The carpal bone segmentation and feature extraction were proven to be very reliable for young children before the carpal bones start to overlap. Combining with the existing phalangeal ROI, it improved the accuracy of computerized bone age assessment for young children significantly. Hence, accurate bone age assessment was ensured for the entire age range.

ROI / Age group (years)	Phalangeal ROI Analysis	Carpal ROI Analysis
0 – 5 (female) 0 – 7 (male)	Size & shape analysis of epi-metaphysis - Feature extraction is not reliable	Size & shape analysis of carpal bones - Feature extraction is reliable
6 – 12 (female) 8 – 12 (male)	Size & shape analysis of epi-metaphysis - Feature extraction is reliable	Degree of overlapping of carpal bones - Feature extraction is not reliable
13 – 18 (female & male)	Degree of fusion of epi-metaphysis - Feature extraction is highly reliable	

Table 1. Reliability of ROI analysis for different age groups in CAD method.

II. MATERIALS AND METHODS

A. Growth pattern of carpal bones

At the early stage of development, carpals appear as dense pin points on a radiograph. During development, they increase in size until reaching their optimal sizes and characteristic shapes. Figure 2 shows an ROI image with seven carpal bones appearing.

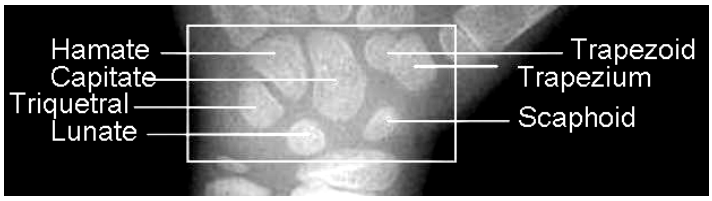

Figure 2. Description of carpal bones in a hand radiograph

Figure 3 demonstrates the growth pattern of carpal bones of Asian males from newborn to 7 years old. Carpal bones ossified in chronological order, Capitate, Hamate, Triquetral, Lunate,

followed usually by Scaphoid, then either the Trapezium or the Trapezoid. [3, 11] Female developments noticeably more advanced than male by as many as 3 years.

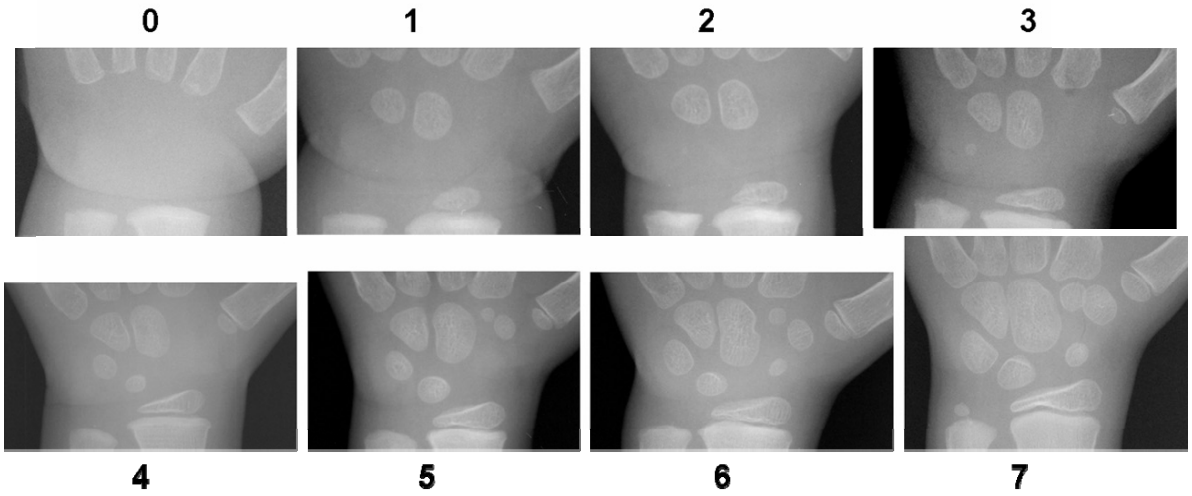

Figure 3. Growth pattern of carpal bones of Asian male from newborn to 7-year-old. The number represents the corresponding age group for each image

Medical study [9] indicated that, due to the nature of carpal bone maturity, their analysis does not provide accurate and significant information for patients older than 7-12 years of age. This is due to the fact that carpal bones start overlap at age around 7 years old in male and 5 in female. In this stage of development the phalangeal analysis yields more reliable information. Therefore, in this research, carpal bone analysis focuses on age group from 0 to 7 for male and 0 to 5 for female.

B. CAD methodology overview of carpal ROI analysis

The workflow of carpal ROI analysis procedure which includes seven steps is shown in Figure 4. The carpal bone region of interest was first extracted from the entire hand image (Figure 1, 1). Due to the non-uniform background and noise, the carpal bone ROI was subjected to an anisotropic diffusion filter (2) which smoothed out the noise and preserves the edges at the same time. Then, the object contours were extracted by the Canny edge detector (3). A series of knowledge-based operations based on morphological properties of segmented objects were implemented in order to single out the carpal bones by eliminating the non-carpal bones (4). The carpal bones contours went through feature extraction phase which yields the inputs into the fuzzy classifiers to assess the bone age (5, 6, 7). This section discusses the procedure in the following order: carpal bone segmentation, carpal bone identification, feature analysis and bone age assessment using fuzzy logic.

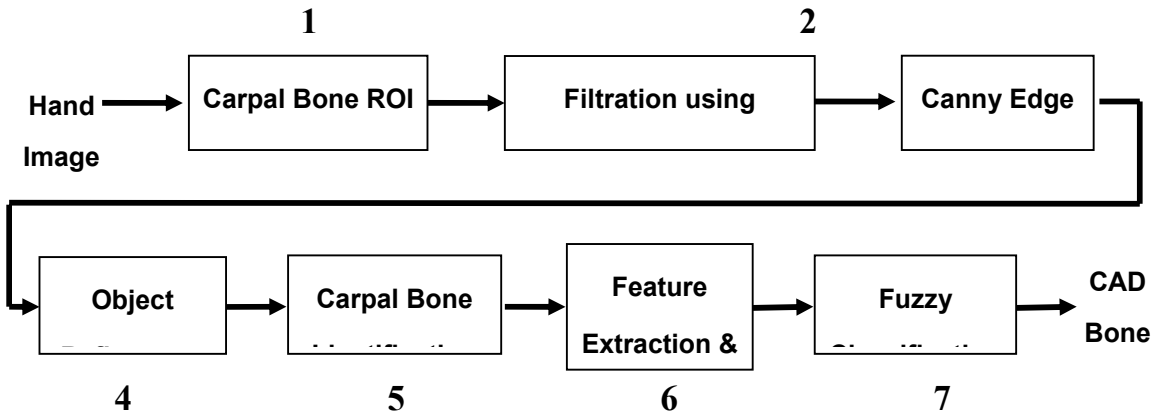

Figure 4. Carpal ROI analysis workflow with 7 steps

C. Carpal bone segmentation

1. Carpal ROI extraction from entire hand image

The first step (in Figure 4) was to locate and extract carpal ROI for further analysis. Figure 5 shows the procedure. A binary hand silhouette was obtained by adaptive thresholding of the hand image with background removed. The carpal ROI was then located in the hand silhouette after artifacts deletion. The upper edge of the carpal ROI was found by scanning a horizontal line and searching for the junction between the second and third metacarpal bone. Perpendicular to the upper edge of the image, starting from its middle, two lines were scanned one pixel at a time toward the left and right borders of the image. The first line on both sides that did not intersect the wrist, fixed the left and right border, respectively. The lower edge of the CROI was the line that intersected the forearm with the minimal width. It was determined by scanning the forearm, one line at a time, from the proximal end of the hand and moving toward the distal end. The carpal ROI was defined within these four edges.

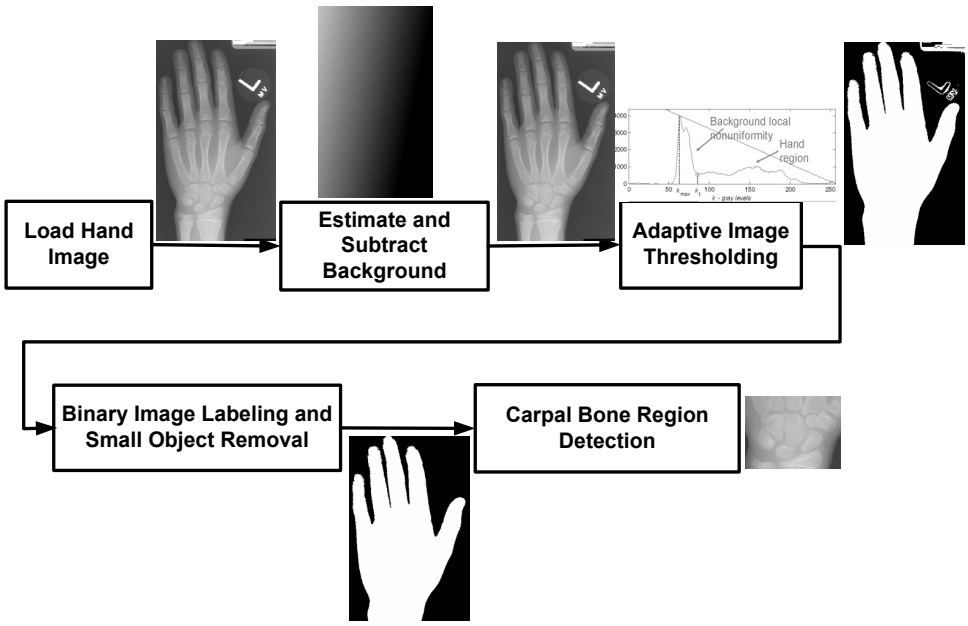

Figure 5. The procedure of carpal ROI extraction from the entire hand image

2. Image smoothing by anisotropic diffusion

Carpal bones in the image are generally poor in contrast. Furthermore, the bone edges are often degraded by noise and artifacts. In order to better differentiate carpal bones from the background, an anisotropic diffusion filter proposed by Perona and Malik [12] was applied to the carpal ROI image. (Second step in Figure 4)

This filter was able to greatly reduce noise in homogeneous areas of carpal ROI images while preserving the edges and contrast associated with bony structures. The principle is to smooth out noise locally by diffusion while at the same time preventing diffusion across object boundaries. The diffusion coefficient is chosen to vary spatially based on a measure of edge strength to encourage intra-region smoothing in preference to inter-region smoothing. The diffusion process achieves piecewise smoothing while preserving the relevant image edges.

Figure 6(a) and Figure 6(b) show the original carpal ROI image and the result after anisotropic diffusion filtration respectively. The comparison of profiles along one horizontal line (same position in both images) which runs across the capitate and hamate is given in Figure 6c) and 6(d). It demonstrates that noise is greatly suppressed by the diffusion process while the sharp edges are well preserved.

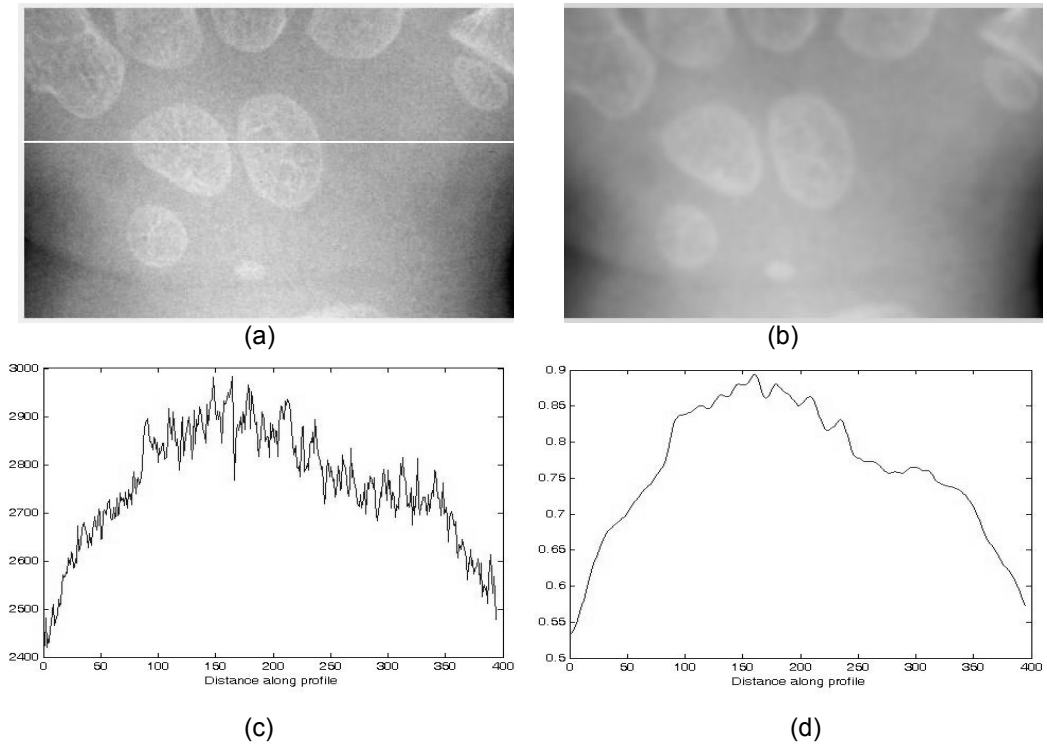

Figure 6. Illustration of anisotropic diffusion filtration (a) Original carpal bone ROI image (b) The result image after anisotropic diffusion filtration (c) profile of the original image along the horizontal line (d) profile of the filtered image along the horizontal line

Size and shape of carpal bone are the characteristics related with skeletal development. Bony texture inside the carpal bone is not the factor that radiologist investigate in assessing the bone age. The next step is to segment the carpal bones from the carpal ROI image.

3. Edge detection by Canny

Edge detection by Canny method (third step in Figure 4) was performed on the smoothed ROI image. The Canny edge detector finds linear, continuous edges and is known as the optimal edge detector. [11, 13, 14] The Canny method differs from other edge-detection methods in that it uses two different thresholds, and includes the weak edges in the output only if they are connected to strong edges. Figure 7 shows an example of a filtered image by using the anisotropic diffusion (shown in Figure 7(b)) and the edges detected by Canny method. This method is less likely than the others to be confused by noise and the carpal bones were detected as closed-contours.

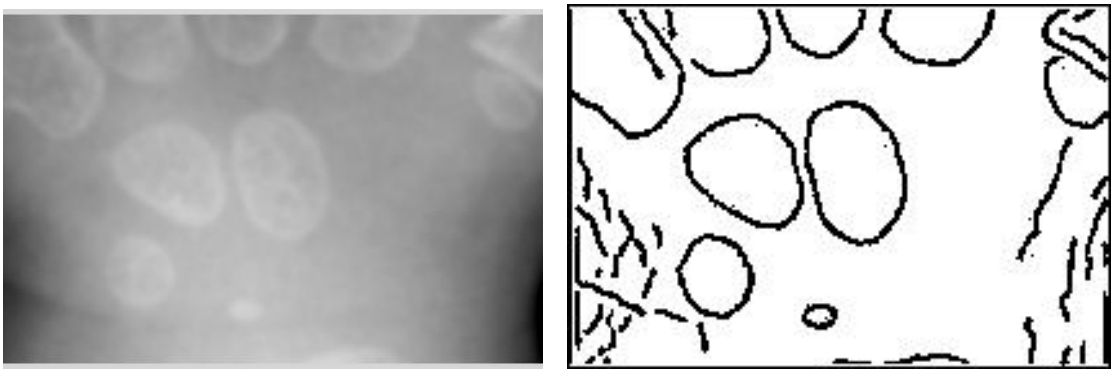

Figure 7 Canny edge detection example (a) Original image (Figure 6 b) (b) Result image after Canny edge detection

4. Objects refinement

The carpal ROI includes carpal bones and parts of the radius, ulna, and metacarpals. Before the features that describe the carpal bones were extracted, the carpal bones themselves needed to be identified from the result of Canny edge detection. An original image and the final result after object refinement (fourth step in Figure 4) are shown in Figure 8 (a) and (b) respectively.

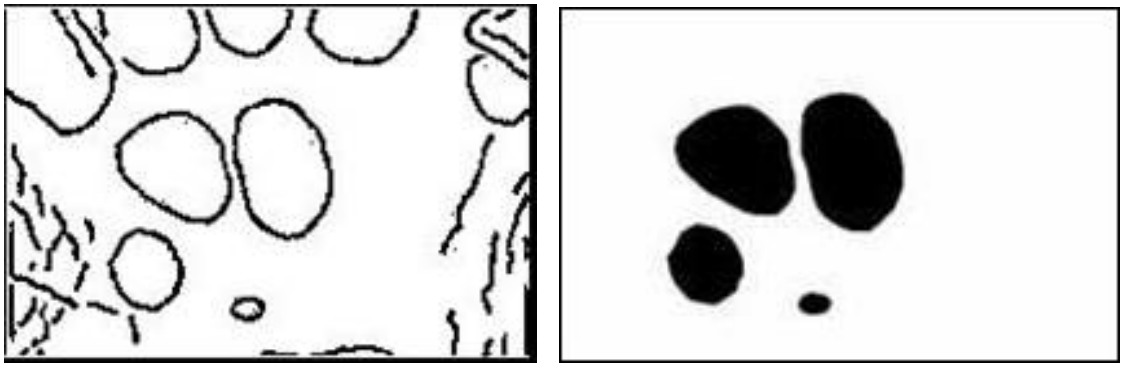

Figure 8. The goal of objects refinement procedure (a) original image (Figure 7 b) (b) image after objects refinement

Knowledge-based morphological operations were used to clean-up the objects. The removal of non-carpal bones was performed in several steps. In the first step all objects that touch the CROI borders were extracted and eliminated. These include the metacarpal bones, wrist bones including ulna and radius touching the CROI borders. In the second step straight and short lines and spots were removed. Eccentricity, a morphological property, of each object was used to

identify the carpal bones. It measures how far the object deviates from a circle. Figure 9 shows an ellipse that has the same area as the segmented carpal bone. Eccentricity is defined as the ratio of the distance between the foci (F_1 and F_2) to the major axis; i.e. $\left(\frac{\overline{F_1F_2}}{\overline{AB}}\right)$.

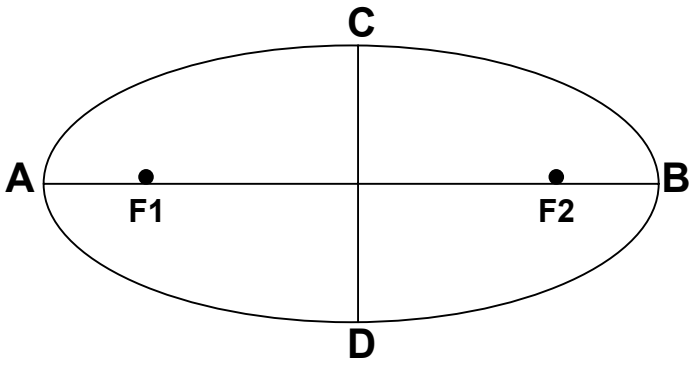

Figure 9. Illustration of an ellipse with foci (F1 and F2) and major axis (between A and B). Eccentricity is defined as the ratio of distance of F1 and F2 and major axis

Based on our experiments, the eccentricity of carpal bone falls between 0.1 and 0.9 and can be used as a prior knowledge. Therefore, objects which have eccentricities under 0.1 or above 0.9 were eliminated. In the third step objects were filled and closed-contour objects were selected based on solidity, a morpholoical property of each object. A convex hull for each filled object is first found as the smallest convex polygon that can contain the object. The proportion of pixels in its convex hull that are also in the studied object is then defined as solidity. The objects, which solidities are above 0.5, were taken as the closed-contour objects. The others were discarded. Figure 10 shows the final carpal bone contours overlapped on a carpal bone region image.

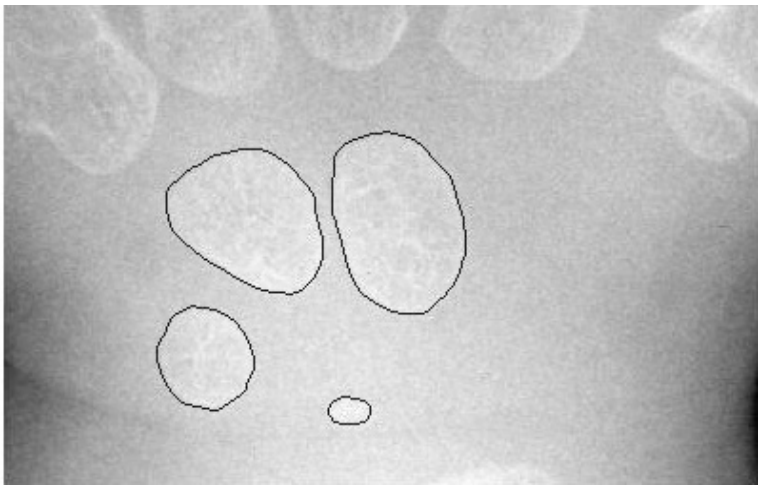

Figure 10. Final segmentation results super-imposed on the original carpal ROI shown in Figure 6 (a)

D. Model-based carpal bone identification

From the carpal bone contours, the post-processing procedure utilizing a prior knowledge was developed to identify the bones (fifth step in Figure 4). The Capitate is the first bone to appear in chronological order and the biggest one among all the carpal bones. It is also the most reliable bone to segment out. A polar coordinate system with the origin at the center of gravity of the Capitate, which was identified as the largest object, was built. The major axis was set as the original normal axis of the polar system. The carpal ROI was then divided into five empirical regions shown in Figure 11. The positions of regions define the prior knowledge about where a carpal bone should be located in the carpal ROI.

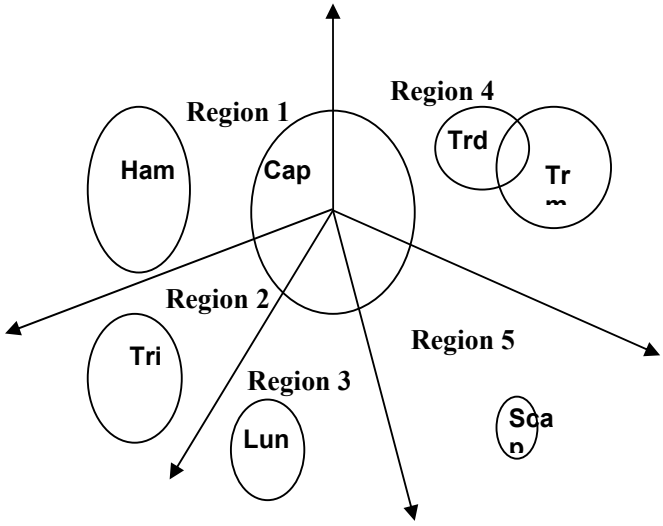

Figure 11. Carpal bone identification model. The polar coordinate system with the centroid of the capitate as the origin is divided into five regions. Based on a priori anatomical knowledge, each of which houses a carpal bone(s): Capitate, Hamate, Triquetral, Lunate, Scaphoid, Trapezium and Trapezoid

The center of gravity of each object was then computed based on polar coordinates. Each object was assigned to the region it belongs to, based on the polar angle and radius of each object. The identification model is hand rotation invariant because the major axis of Capitate follows the rotation of the hand. Figure 12 shows the one example case with identified carpal bones.

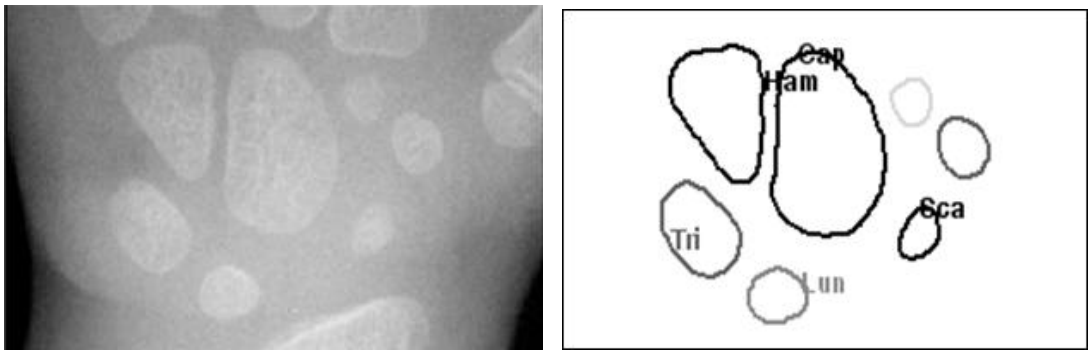

Figure 12. A Carpal bone identification example a) Original carpal ROI image, b) Identified carpal bones - Cap: Capitate, Ham: Hamate, Tri: Triquetral, Lun: Lunate and Sca: Scaphoid.

The first two bones which appear in chronological order, Capitate and Hamate, were selected for further analysis. The other identified bones which appear later will be analyzed for future refinement in case that Capitate and Hamate are failed to extract because of fusion with each other.

E. Feature analysis

From the identified carpal bones, features related to the bony growth were extracted for bone age assessment. (Sixth step in Figure 4)

1. Morphological feature extraction

To describe the size and shape of the carpal bones identified, four morphological features were extracted from Capitate and Hamate. Feature 1 measures equivalent diameter, which specifies the size of the object. An ellipse that has the same normalized second central moments as the region was found for each bone. Feature 2 is eccentricity which we defined in Section C.4. The value of eccentricity is between 0 and 1. Feature 3 is solidity (also refer to C.4). Feature 4, triangularity measures the ratio of equivalent diameter and the product of major axis length and minor axis length.

2. Feature selection

To evaluate the performance of each feature in assessing the bone age, correlation with the chronological age was analyzed. Among all the features, sizes of Capitate and Hamate have the most significant correlations with age, which are over 0.90. To simplify the feature space, all features which have the correlation above 0.60 were selected and form the feature space for bone age assessment. Table 2 shows the correlation coefficients for selected features from an example category of one race and one gender.

Table 2. Correlation coefficients for selected features. High correlation is marked with double asterisks.

	Capitate			**Hamate**		
	size	eccentricity	triangularity	size	eccentricity	triangularity
Correlation Coeff.	.94 (**)	.74(**)	-.65(**)	.92 (**)	.70(**)	-.62(**)

F. Bone age assessment using fuzzy logic

The last step in carpal ROI analysis (Seventh step in Figure 4) is to assess the bone age using fuzzy classification based on the features extracted and selected from the Capitate and Hamate. Two characteristics of carpal bone features make bone age assessment difficult. First, the growth of carpal bones does not have a linear relationship with chronological age. The imprecise nature leads to the inter- and intra-observer discrepancy. Second, some features may be missed by the segmentation and feature extraction procedure. Most of past attempts of using linear approach failed because it is insufficient to model the growth pattern. Fuzzy logic [15-18] incorporates a simple and rule-based approach and is suitable for this application because it is robust and does not require precise and noise-free inputs. As long as some features from any bone are provided, it is sufficient to activate the fuzzy system to generate the output.

The three features, size, eccentricity and triangularity extracted from Capitate and Hamate each were taken as an input into the fuzzy classifier. The system was broken into smaller sub-classifiers based on Capitate and Hamate respectively. Figure 13 shows the workflow of the fuzzy classification for bone age assessment.

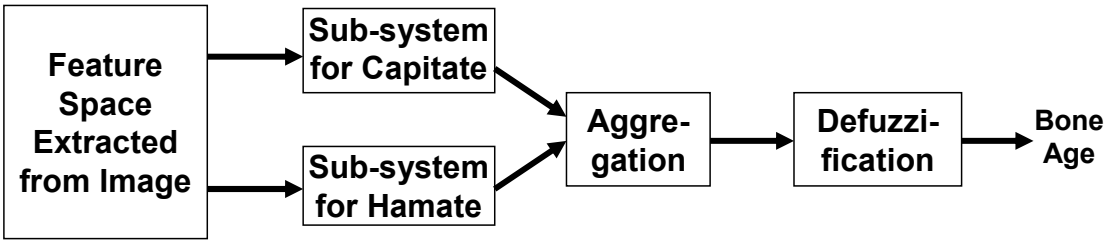

Figure 13. Fuzzy classification workflow for bone age assessment.

An automatic training algorithm with the features from our normal data collection was developed for fuzzy classifiers. The output was set as the subject chronological age since the normality of children was ensured for each case during data collection. The data of young children from newborn to age group of 7 (male) or 5 (female) was divided into age groups with an interval of one year. Therefore, total of 8 (0,1,2,…7 for male) or 6 (0,1,2,…,5 for female) initial Gaussian membership functions were generated for each input feature (size, eccentricity, and triangularity) and output (chronological age). The mean and standard deviation of each feature from each age group were calculated and taken as the Gaussian parameters for the corresponding membership functions. Merging of adjacent membership functions was then performed based on the *t*-test of the mean difference for specific feature between adjacent age groups. The same merging procedure was performed for output depending on the inputs. Fewer number of membership functions simplifies the processing logic and even improving the fuzzy logic system performance. Figure 14 use Caucasian male as an example to show the groups of membership functions for the three features (Figure 14 a, b and c) of Capitate and output (Figure 14 d) as chronological age.

A firing strength for each output membership function is computed. Then a max-min rule operation was applied to combine the inputs logically to produce output response values for all expected inputs. It took two steps. A *min* fuzzy operation was first applied to integrate the multiple inputs of features for each output class. Then the active conclusion was combined by finding the *max* from all the classes.

Take the Capitate of Caucasian male as an example, after feature extraction it yields input features (Size:89.5, Eccentricity: 0.636, Triangularity: 0.0294) shown in Fig. 15 (a), (b), and (c), an output membership function (CAD bone age based on the Capitate) was derived shown at the bottom graph of Figure 15 (d).

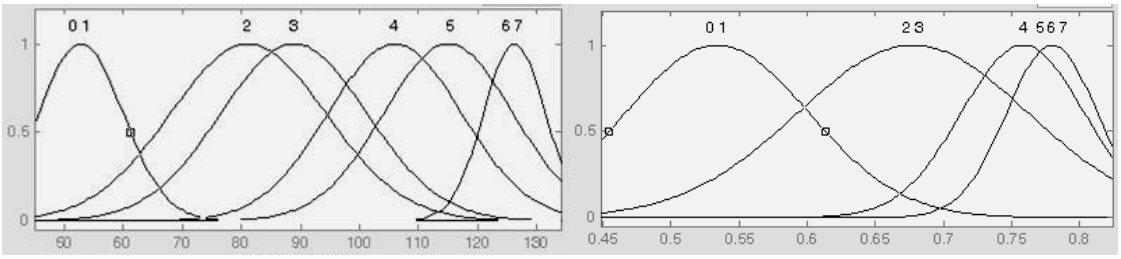

(a) Size **(b) Eccentricity**

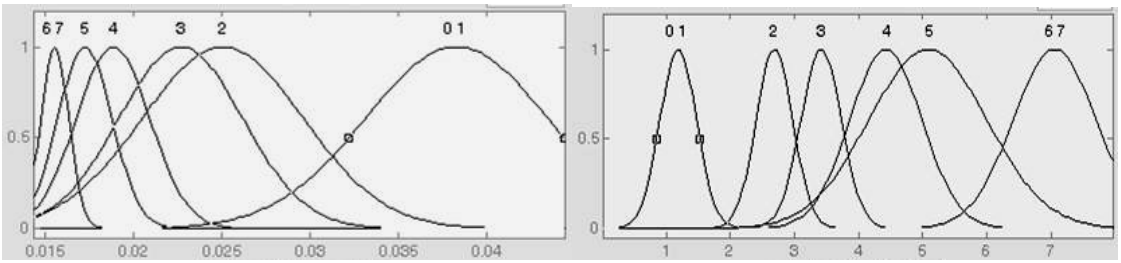

(c) Triangularity **(d) Chronological Age**

Figure 14. Four membership functions of Capitate sub-classifier for Caucasian male category. In this fuzzy logic training, a normal distribution curve is used to represent a membership function using the mean and standard deviation obtained from each feature. (a), (b), and (c) are the three input features: size, eccentricity, and triangularity, the x-axis is the value of the corresponding feature. The output membership function (d) is the chronological age represented by the x-axis. Each of the four y-axes represents degree of the membership function which has a range from 0 to 1. Number on top of each membership function represents the chronological age group. Multiple numbers appear together if membership functions for adjacent groups were merged, for instance, age group 0 and 1 in a). These membership functions were derived from the data collected from each age group

A final output (CAD bone age) needs to be aggregated from the sub-systems based on the Capitate and the Hamate, respectively. It was determined by finding the logic *mean* of the two outputs. The defuzzification process used center of gravity method to obtain a final CAD bone age.

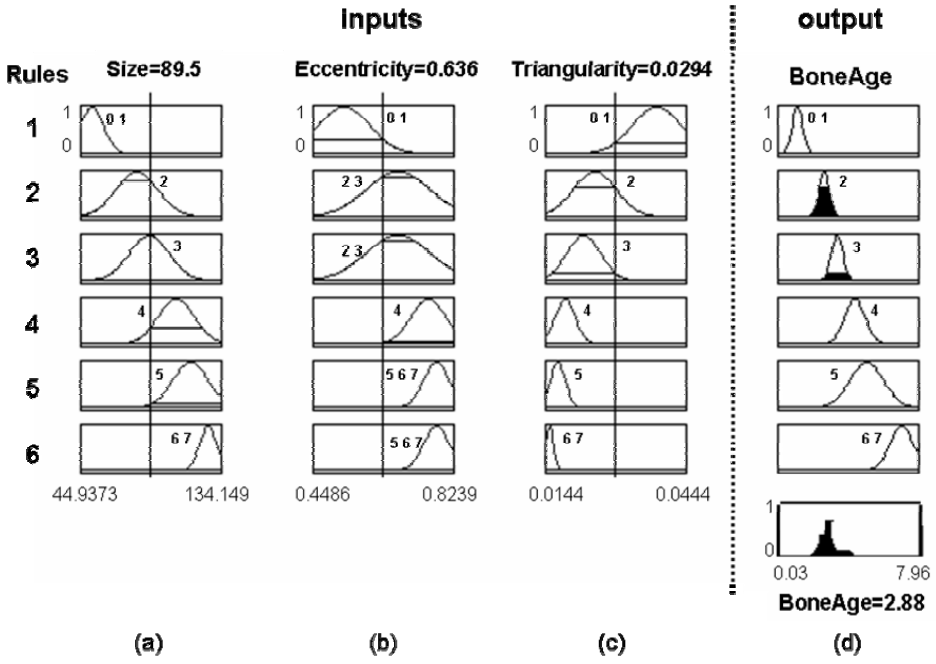

Figure 15. An example of using fuzzy classification for CAD bone age assessment of a given Caucasian male based on membership functions depicted in Fig. 14. Membership functions for each of the three input features (size, eccentricity, and triangularity; columns a, b, and c), and one output which is the chronological age, (column d) are reoriented vertically forming six rules (1, 2, …, 6) based on Fig. 14. Three extracted features from the hand image are: size: 89.5, eccentricity: 0.636, and triangularity: 0.0294, represented by three vertical lines at each of the three columns, respectively. The output is the aggregation of the solid areas under each rule, which yields a crisp CAD bone age as 2.88 year old shown in the bottom graph in column (d).

G. System evaluation

Three types of tests were conducted to evaluate the performance of using the fuzzy logic for bone age assessment. Test 1 separated the data into eight categories of four races and two genders. Classifiers were trained and tested on each case from each category. Test 2 had two categories for female and male with four races combined together. Test 3 combined the entire data collection into one universal category.
For the above three tests, CAD bone age assessed by fuzzy classification was evaluated against chronological age which was taken as the gold standard as the normality of each case was ensured. The same evaluation was performed on readings. The CAD bone age results were plotted with the average reading of two radiologists against chronological age. The mean difference of each of the two readings versus chronological age or CAD bone age versus chronological age was computed by paired t-test.

III. RESULTS

Hand images for females of age groups from 0 to 5 and males from 0 to 7 from the entire data collection of 205 images went through the carpal ROI analysis, including carpal bone segmentation, feature extraction and fuzzy classification for bone age assessment. The segmentation and CAD bone age results are presented in this section.

A. Segmentation success rate

Due to the reasons described in section 1, phalangeal ROI segmentation is not reliable for young children. The comparison of the bone age assessment results for both female and male using phalangeal versus phalangeal and carpal features together are shown in Figure 16. The striped bars show the percentage of successfully processed cases with phalangeal ROI only. However, after carpal ROI analysis was included, the percentage of successfully processed cases (gray bars in Figure 16) was improved significantly especially for age groups from newborn to 3 years. Figure 15 (a) shows the results for female and (b) for male.

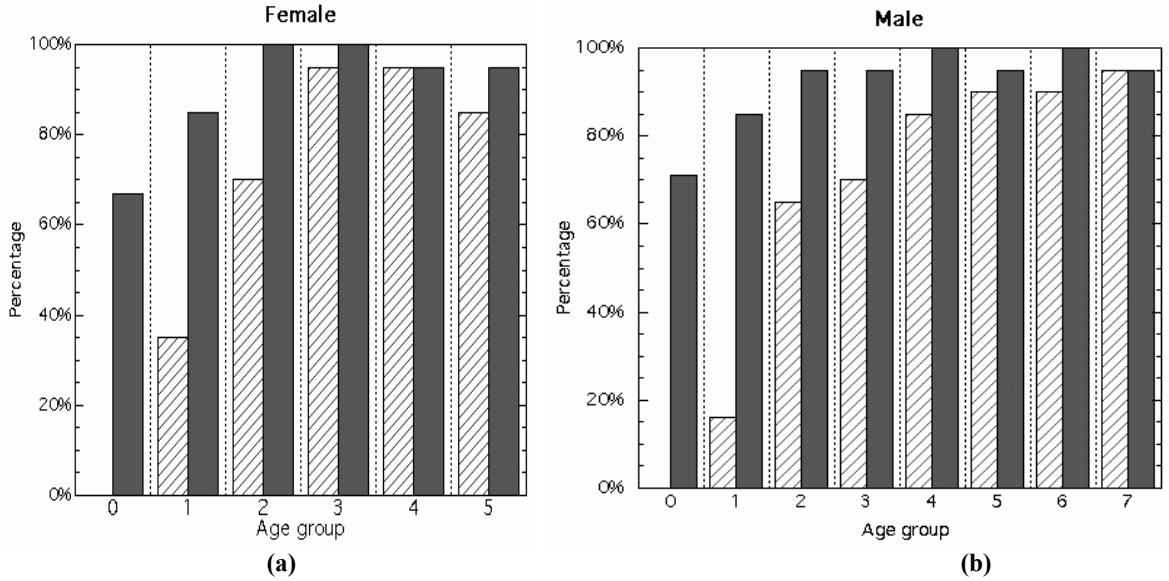

(a) **(b)**

Figure 16. Percentage of successfully processed cases of all four races. Striped bars represent the percentage for phalangeal ROI analysis only and gray bars stand for the percentage after the inclusion of carpal ROI. (a) is for female of 6 age groups from 0 to 5, (b) is for male of 8 age groups from 0 to 7.

The results show that the percentage of success rate is close to 100 percent at age above 2 years old. For case below 2 years, the success rate is about 80 percent. This is due to the general poor contrast of hand images for young children because of the low bone density and thick soft tissue. It leads to the difficulty in segmenting the carpal bones from background. This could be improved by using adaptive diffusion parameters based on the contrast of individual carpal ROI image and will be considered for future work.

B. Plots

The CAD results based on carpal ROI were compared with the average reading of two radiologists. Figure 17 shows the results set for eight categories from test 1. Figure 18 is the results set for two categories from test 2. Figure 19 is for the universal category from test 3. The CAD results generally follow the average reading of two radiologists comparing with the chronological age.

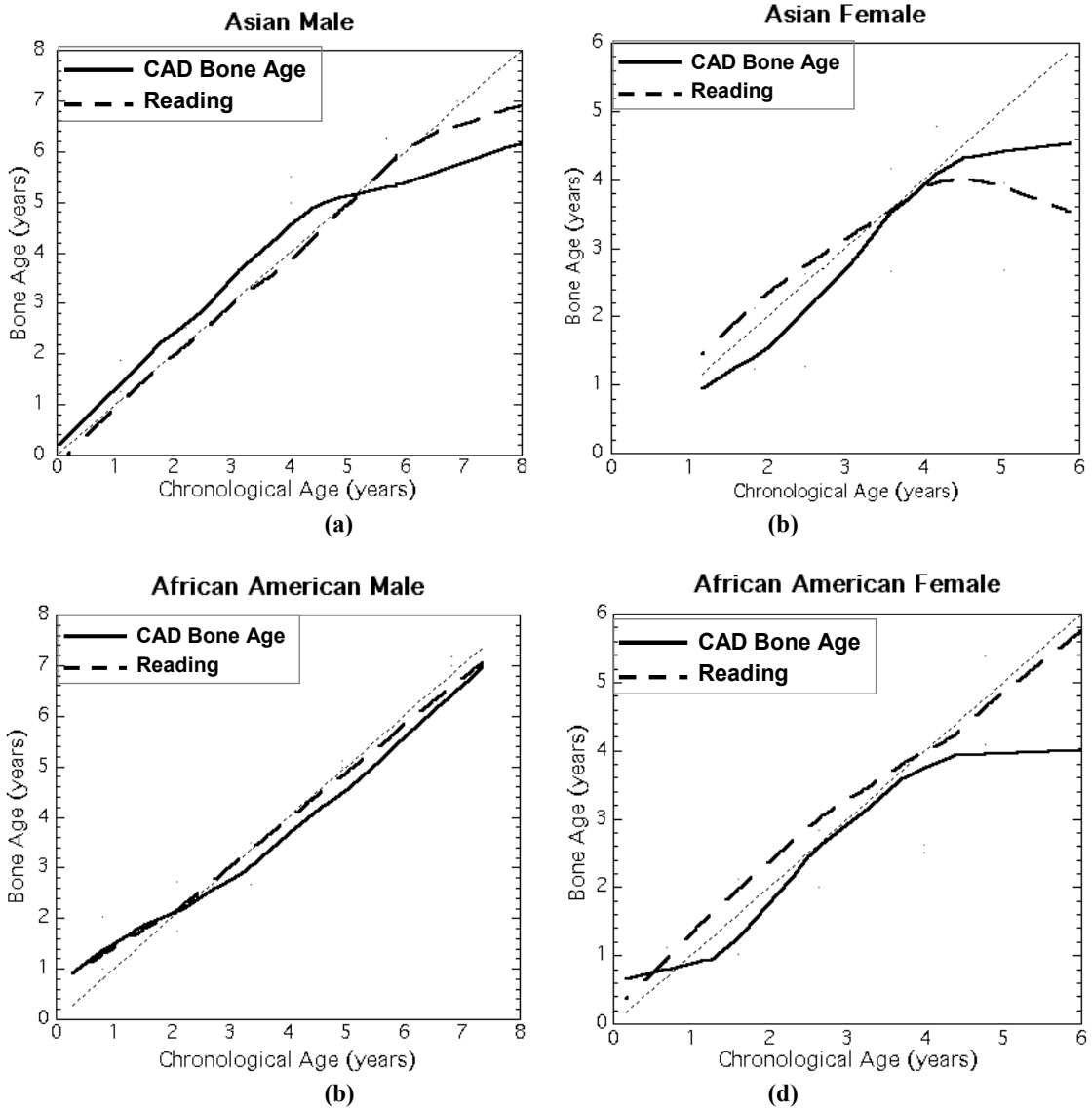

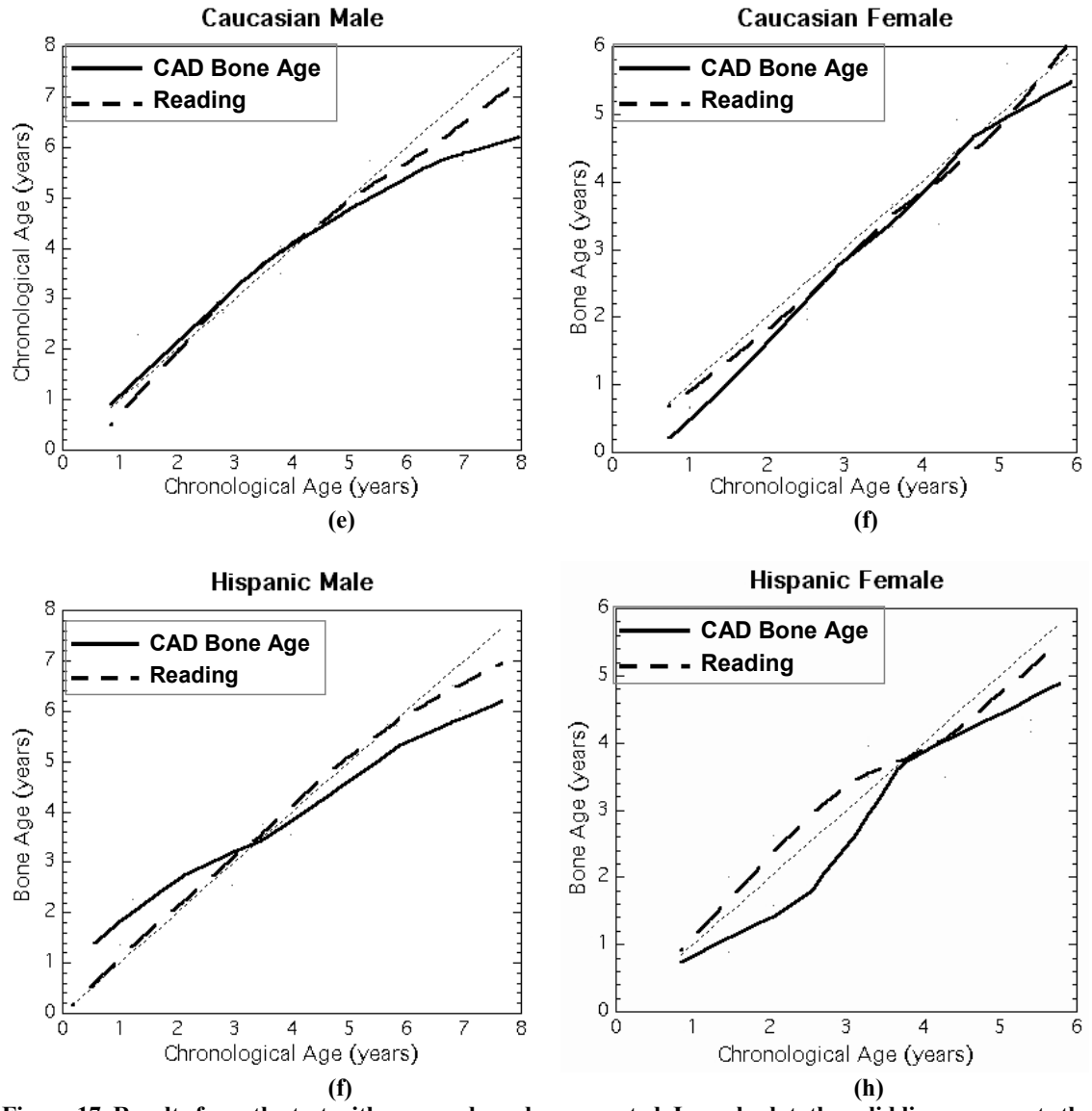

Figure 17. Results from the test with race and gender separated. In each plot, the solid line represents the CAD results and dashed line represents the average reading of two radiologists. See Section IV Discussion for discrepancies

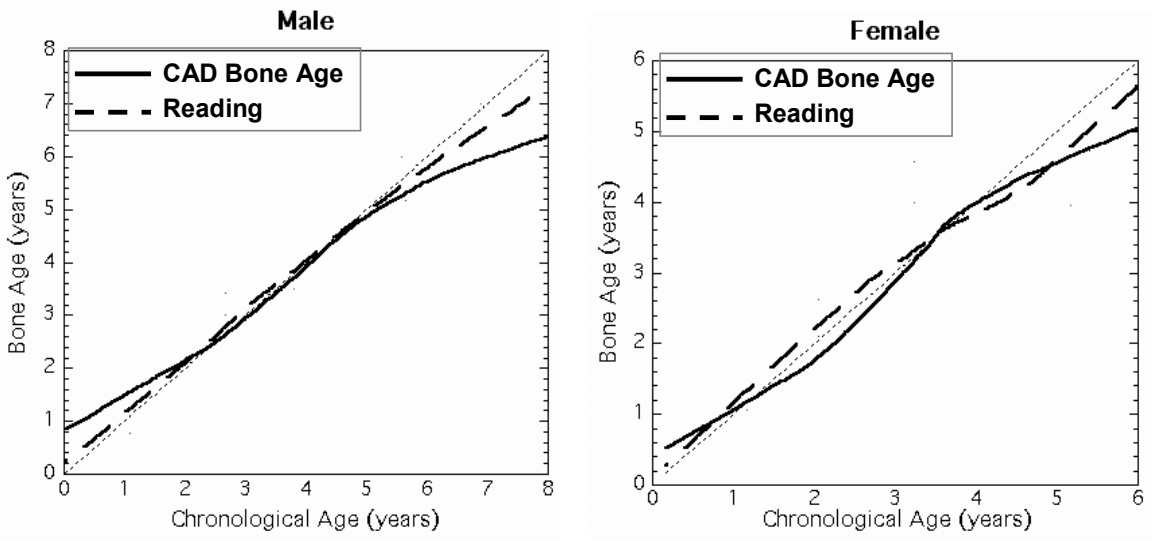

(a) (b

Figure 18. Results from the test for two genders with four races combined. In each plot, the solid line represents the CAD results and dashed line represents the average reading of two radiologists. See Section IV Discussion for discrepancies

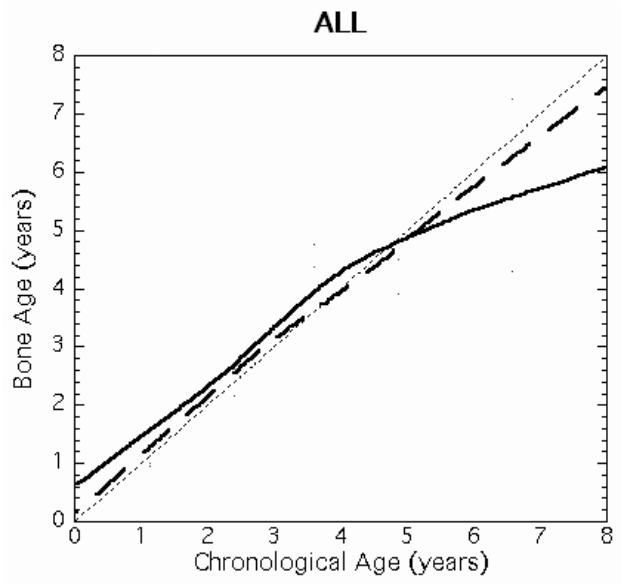

Figure 19. Results from the test for one universal category with both races and genders combined. In this plot, the solid line represents the CAD results and dashed line represents the average reading of two radiologists. See Section IV Discussion for discrepancies

C. CAD evaluation

Paired-samples *t*-test for the above three tests was performed against chronological age for two readings and CAD result. The following tables show the mean difference between reading 1, reading 2 and CAD result versus chronological age. The number with asterisk represents the difference is significant at p-value < .05.

Table 3. CAD evaluation for test 1 with races and genders separated. Significant mean difference (in year) is indicated by an asterisk.

	Asian		African American		Caucasian		Hispanic	
	Female	Male	Female	Male	Female	Male	Female	Male
Reading 1	.19	-.05	-.08	-.13	.12	.02	.07	-.04
Reading 2	.19	.23	.01	-.03	.14	.25*	-.11	.08
CAD BA	.46*	.16	.27	.12	.28*	.20	.36*	.20
No. of Cases	**21**	**28**	**21**	**30**	**22**	**34**	**22**	**27**

Table 4 CAD evaluation for test 2 with two genders, each gender is combined with four races, and test 3 has only one universal category. Significant mean difference (in year) is indicated by an asterisk

	Test 2		Test 3
	Female	Male	
Reading 1	.08	-.05	.00
Reading 1	.06	.13*	.10*
CAD BA	.25*	.20*	.01
No. of Cases	**86**	**118**	**204**

From the evaluation Tables 3 and 4, we can see that the CAD result based on carpal ROI analysis is comparable to the readings within the mean difference of half year.

IV. DISCUSSION AND CONCLUSION

A method of carpal ROI determination, carpal bones segmentation, feature extraction and fuzzy classification for bone age assessment was developed and tested on the 205 young children from the data collection in the digital hand atlas (see Introduction). The percentage of successfully processed cases was improved significantly over the one with phalangeal ROI analysis only. This demonstrates that the feature extraction of carpal ROI is reliable for young children. (Third column, first row of Table 1)

The CAD results by fuzzy classification were evaluated by comparison with readings and chronological age. The CAD results shown in Section III.B based on carpal ROI features follow the readings comparing with chronological age, with the verification from statistical analysis in III.C. The results verified the value of carpal ROI in assessment of skeletal development for young children.

Furthermore, carpal ROI has advantages over phalangeal ROI in bone age assessment for young children in that the appearance of carpal ROI in the radiograph is not influenced by finger bend

and hand rotation during acquisition. This happens frequently since straight fingers and upright position of the hand is hard to achieve in young children.
However, a general observation could be drawn from the curves of Figure 16, 17 and 18, that the CAD results have large discrepancy to the chronological age after age of 5.50 for male and 4 for female. This phenomenon appears in radiologists readings also. The possible reason is that after this point, the growth of Capitate and Hamate slow down and carpal ROI does not reflect very accurate information. The other bones which appear later than Capitate and Hamate, identified by the knowledge-based model (Figure 10) could be taken into consideration to improve the accuracy for these age groups by augmentation of feature space for bone age assessment.
The diverse growth patterns in different race and gender were observed from curves of average reading of radiologists shown in Figure 16. This justifies that it is necessary to distinguish the race in bone age assessment. Two evaluations of two readings in Table 3 and 4 show the inter-observer discrepancy between two radiologists on the same data collection.
The CAD bone age based on carpal ROI could be integrated with phalangeal ROI to provide more accurate bone age assessment. With up-to-date data collection and objective and fully automatic bone age assessment, the CAD system integrated with PACS [19] could provide the radiologists second opinion and help improve the accuracy in clinical practice.

Acknowledgements

This work has been supported by NIH R01 EB 00298.

References

1. Tanner JM, Healy MJR, Goldstein H, Cameron N, *Assessment of Skeletal Maturity and Prediction of Adult Height (TW3 Method)*, WB Saunders, London, 2001.
2. Kirks D, *Practical Pediatric Imaging, Diagnostic Radiology of Infants and Children*, (Little, Brown & Company, Boston/Toronto), 1st ed., 1984, chap. 6, pp. 198-201.
3. Greulich WW, Pyle SI, Radiographic Atlas of Skeletal Development of Hand Wrist. Stanford CA. Stanford University Press, 1959.
4. Pietka E, Gertych A, Pospiech S, Cao F, Huang HK, Gilsanz V, Computer *Assisted Bone Age Assessment: Image Processing and Epiphyseal/Metaphyseal ROI Extraction*, IEEE Trans. Medical Imaging, 20, 715-729, 2001.
5. Pietka E, Pospiech S, Gertych A, Cao F, *Integration of Computer Assisted Bone Age Assessment with Clinical PACS*, Computerized Medical Imaging and Graphics, 1-12, 2002.
6. Cao F, Huang HK, Pietka E, Gilsanz V, *Digital Hand Atlas and Web-based Bone Age Assessment: System* Design and Implementation, Computerized Medical Imaging and Graphics, 297-307, 2000.
7. Zhang A, et al. *Data Mining for Average Images in a Digital Hand Atlas*. Proceedings of SPIE Medical Imaging, Vol. 5371, pp. 251-258, February 2004.
8. Huang HK, Zhang A, Liu B, Zhou Z, Documet J, King N, Chan WC, *Data Grid for Large-Scale Medical Image Archive and Analysis*. Proceedings of the 13th ACM International Conference on Multimedia, pp. 1005-1013, 2005.
9. Johnston FE, Jahina SB: *The contribution of the carpal bones to the assessment of skeletal age*. Am. J. Phys. Anthrop., 1965, 23, 349-354.
10. Pietka E, Kaabi L, Kuo ML, Huang HK, *Feature extraction in carpal-bone analysis*, IEEE transaction on medical imaging, Vol. 12, No.1, Mar 1993.

11. Zhang A, Gertych A, Liu B, Huang HK, Pospiech S, *Carpal Bone Segmentation and Features Analysis in Bone Age Assessment of Children*. Proceedings of RSNA Conference, Chicago, pp. 688, 2005.
12. Perona P, Malik J, *Scale-space and edge detection using anisotropic diffusion*, PAMI 12(7), pp. 629-639, 1990.
13. Canny JF, *Finding edges and lines in images*, Master thesis, Massachusetts Institute of Technology, 1983.
14. Canny JF, *A computational approach to edge detection*, IEEE transaction PAMI, Vol. 8(6), p. 679, 1986.
15. Ross TJ, *Fuzzy Logic with Engineering Applications,* 2nd edition, John Wiley & Sons Ltd, England, 2004
16. Zadeh LA, *Fuzzy sets*, Information and Control, Vol. 8, pp. 338-353, 1965
17. Zadeh LA, *Fuzzy Logic*, Computer, Vol. 1, No. 4, pp. 83-93, 1988.
18. Zadeh LA, *Knowledge representation in fuzzy logic*, IEEE Transactions on Knowledge and Data Engineering, Vol. 1, pp. 89-100, 1989.
19. Huang HK, *PACS and Imaging Informatics*: Basic Principles and Applications, Wiley & Sons, NJ, 2004, p. 504-507.

Bone Age Assessment of Children using a Digital Hand Atlas*

Arkadiusz Gertych[1], Aifeng Zhang[1], James Sayre[2,1] , Sylwia Pospiech-Kurkowska[3], H.K Huang[1]

[1] - Image Processing and Informatics Laboratory, Department of Radiology, University of Southern California, 4676 Admiralty Way, Suite 601, Marina del Rey, CA 90292

[2] - Department of Radiological Sciences, University of California, Los Angeles

[3] - Institute of Electronics, Department of Biomedical Engineering, Silesian University of Technology, Akademicka 16, 44-100, Gliwice Poland

* *Paper accepted to be published in Journal of Computerized Medical Imaging and Graphics*

ABSTRACT

We have developed an automated method to assess bone age of children using a digital hand atlas. The hand Atlas consists of two components. The first component is a database which is comprised of a collection of 1,400 digitized left hand radiographs from evenly distributed normally developed children of Caucasian (CA), Asian (AS), African-American (AA) and Hispanic (HI) origin, male (M) and female (F), ranged from 1 to 18 year old; and relevant patient demographic data along with pediatric radiologists' readings of each radiograph. This data is separate into eight categories: CAM, CAF, AAM, AAF, HIM, HIF, ASM, and ASF. In addition, CAM, AAM, HIM, and ASM are combined as one male category; and CAF, AAF, HIF, and ASF are combined as one female category. The male and female are further combined as the F & M category. The second component is a computer-assisted diagnosis (CAD) module to assess a child bone age based on the collected data. The CAD method is derived from features extracted from seven regions of interest (ROIs): the carpal bone ROI, and six phanlangeal PROIs. The PROIs are six areas including the distal and middle regions of three middle fingers. These features were used to train the eleven category fuzzy classifiers: one for each race and gender, one for the female, one male, and one F & M, to assess the bone age of a child. The digital hand atlas is being integrated with a PACS for validation of clinical use.

Keywords: *bone age assessment of children, digital hand atlas, computer aided diagnosis, feature extraction, fuzzy logic*

1. INTRODUCTION

Bone age assessment (BAA) is a common radiological examination used in pediatrics to determine any discrepancy between a child's skeletal age (the developmental age of their bones) and their chronological age (in years, taken from birth date). The examination is straightforward to perform, involving a single view of the left hand which includes all relevant regions of interest within the hand and wrist (Fig. 1). A difference between chronological age and skeletal age may suggest abnormalities in skeletal development. Delayed or accelerated appearance of ossification centers caused by an illness may serve as an example. Assessment of skeletal age is helpful in the monitoring of growth hormone therapy and diagnosis of endocrine disorders. BAA is also

performed when surgery for correcting deformities of the long bones or the vertebral column is planned. Bone age determinations are also commonly used to predict individual's final height [1].

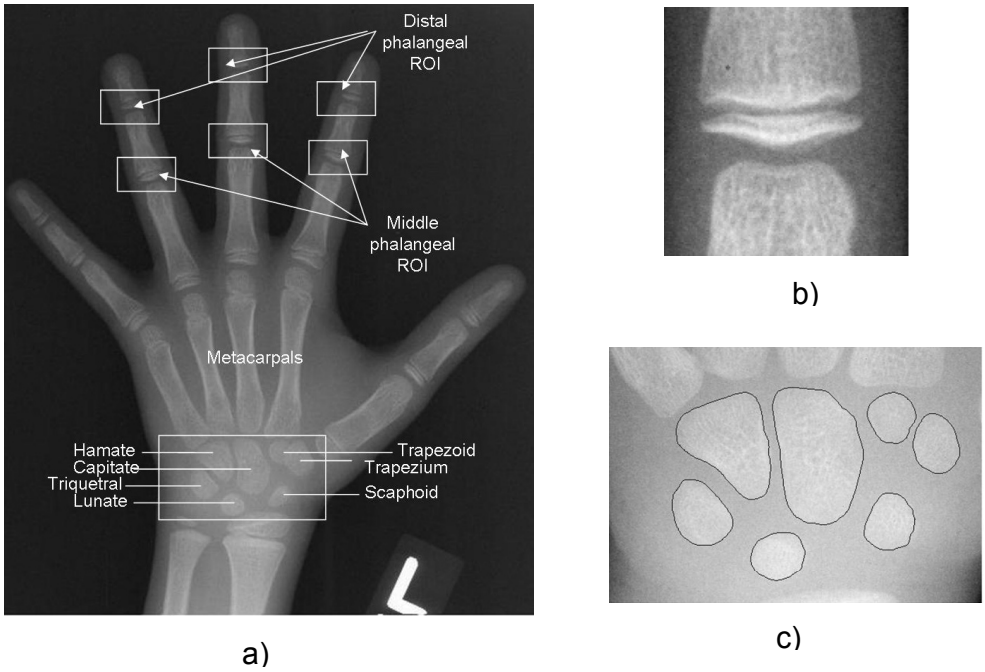

Figure 1. An example of hand image radiograph with superimposed regions of interest: a) a hand image with seven ROIs, b) the phalangeal region of interest (PROI), c) the carpal bones region.

The classical method of skeletal bone age assessment (BAA) utilizes the recognition of changes in the radiographic appearance of the maturity indicators in a hand-wrist radiograph by comparison with a reference data set which consists of series of radiographs grouped according to sex and age. The most commonly used reference standard is the atlas published by Greulich and Pyle (G&P) [1]**.** They were derived from the population of the middle socioeconomic class of Caucasian children from Midwest, USA from 1931-1942. The atlas remains unchanged from its initial publication and is commonly used in clinical practice to assess bone age of children of Caucasian, African American, Hispanic, Asian, and other descent. The examination is subjective because the radiologist analyzes each individual bone of the hand and wrist, determines an overall bone age, and finally fits the amalgamated results into a closest match to the reference radiographs in the atlas. Using the G&P atlas, inter-observer reading differences ranging from 0.37 to 0.6 years and intra-observer reading differences from 0.25 to 0.47, even up to 0.96 years have been reported [2, 6]. The average time of a single case reading depends on radiologist's clinical experience and falls within 2 - 5 minutes.

More objective methods are also available [3-5], (TW1, TW2, TW3). The radiological patterns of ossification centers were derived from the population of 3000 normal British boys and girls. An overall bone age is derived from the sum of the developmental scores from all of the individual ossification centers. Because this approach is both complicated and time consuming, it is seldom used in clinical practice, particularly in the United States.

In this paper, we describe an automated method to assess bone age of children using a digital hand atlas. The hand Atlas consists of two components: a database which is a collection of 1,400 digitized left hand radiographs from evenly distributed normally developed children of Caucasian, African-American, Hispanic and Asian origin, male and female, ranged from 1 to 18

year old. Relevant patient demographic data along with pediatric radiologists' readings of each radiograph were also included. Currently, 1,390 are included in the database. The second component is a computer-assisted diagnosis (CAD) module to assess a child bone age based on the collected data. The CAD method is derived from features extracted from seven regions of interest (ROIs), the six phanlangeal and one carpal bone ROIs.

First, the concept of the Digital Hand Atlas and the data collection is described. Next, a hand image processing work flow of the CAD is introduced. Quantitative features extraction from ROIs is followed by the preprocessing of the hand image. The final bone age assessment based on extracted quantitative features is obtained by means of an array of fuzzy classifiers. The integration of the digital hand Atlas with a PACS for validation of clinical use is presented.

2. DATA COLLECTION OF THE DIGITAL HAND ATLAS

Rationale

During past years, numerous results have demonstrated that variations in skeletal maturation in prepubertal children are greater than those reflected in the Greulich and Pyle atlas. More precisely, prepubertal American children of European (EA) descent have significantly delayed skeletal maturation when compared with those of African descent. Also, postpubertal EA males have significantly advanced skeletal maturation when compared with postpubertal African American males [7]. Therefore, it is apparent that multiethnic pediatric population normal images are needed in order to more accurately assess today's children bone age. We started to collect normal children hand images in the late 90s through the support of grants supported by the National Institutes of Health. The process of data collection was conducted at the Childrens Hospital of Los Angeles (CHLA). Candidates for this study underwent a protocol approved by the institutional review board for clinical investigations. A physical examination by a pediatric endocrinologist was performed to determine health and Tanner stage of sexual development of all subjects. According to the clinical examinations, their skeletal development had been confirmed as normal. Measurements of height, trunk height and weight were also obtained. The bone age of each normal was evaluated by at least two pediatric radiologists from the left hand radiograph according to the method of G & P atlas. Each radiograph was digitized to a 2Kx2K image using a laser film scanner (Array, Tokyo, Japan); and the patient demographic records were manually entered via the scanner GUI (graphical user interface) and saved as a DICOM file. An example of data stored in the DICOM file is presented in Table 1.

Table 1. An example of image header fields in a hand image DICOM file.

DICOM Field Name	Date of Birth	Date of Examination	Chronological Age	Patient Race	Patient Sex	Tanner Index	Trunk Height	Body Height	Body Weight	Reading R1	Reading R2
Unit	dd/mm/yy	dd/mm/yy	years	-	-	-	cm	cm	kg	years	years
Field value	26/02/89	25/06/98	9.33	CAU	M	1.0	71.12	137.8	39.1	9.0	9.5

Data Collection

The data collection was scheduled in two separate cycles. In the first cycle a total number of 1103 left hand radiographs of normally developed children of four races: Caucasian (CA), African American (AA), Hispanic (HI), and Asian (AS) for both male and female [8, 9] have been collected. The data collection protocol is given in Appendix A, with the hand positioned as presented in Fig. 1.

For each race and gender, five images per age group for children aging from one to nine years, and ten images per age group for older have been collected respectively. During an almost 10 year period of collecting the data in this cycle, groundwork of the methodology of developing the CAD for bone age assessment has also been established [10-13].

The data was evaluated as normal comparing to: (1) the body mass index (BMI) for children based on the growth chart from National Health and Nutrition Examination Survey [14], (2) Tanner maturity index, and (3) chronological age vs. skeletal age based on the 1940 Brush Foundation Study. Comparison to (1) and (2) shown that the data is normal. According to comparison with (3), bone age assessment with first cycle data was consistently lower between ages 5-14 for boys and girls in every ethnic origin. A difference of approximately ten months was observed between item (3) and data collected.

Because of the difference in item (3), in order to increase the statistical power of the first cycle data set we started a second cycle data collection with additional 287 images for the rapid maturation stage of children from ages 5 to 14 year old. A summary of first and second cycle data from the Digital Hand Atlas as of today is presented in Table 2 (a-b).

Table 2a. Digital Hand Atlas: the summary of the first cycle data collection.

First cycle of data collection: each case is with two readings								
Age group/Category	ASIF	ASIM	BLKF	BLKM	CAUF	CAUM	HISF	HISM
00	1	2	4	5	3	3	1	4
01	5	5	5	5	5	5	5	5
02	5	5	5	5	5	5	5	5
03	5	5	5	5	5	5	5	5
04	5	5	5	5	5	5	5	5
05	5	5	5	5	5	5	5	5
06	5	5	5	5	5	5	5	5
07	5	5	5	5	5	5	5	5
08	5	5	5	5	5	5	5	5
09	5	5	5	5	5	5	5	5
10	10	10	10	10	10	10	10	10
11	10	10	10	10	10	10	10	10
12	10	10	10	10	10	10	10	10
13	10	10	10	10	10	10	10	10
14	10	10	10	10	10	10	10	10
15	10	10	10	10	10	10	10	10
16	10	10	10	10	10	10	10	10
17	10	10	10	10	10	10	10	10
18	10	10	10	10	10	10	10	10
Images total / category	136	137	139	140	138	138	136	139
Images total	1,103							

Table 2b. Digital Hand Atlas: the summary of the second cycle data collection.

Second cycle of data collection: each case is with four readings								
Age group/Category	ASIF	ASIM	BLKF	BLKM	CAUF	CAUM	HISF	HISM
05	3	4	4	4	2	5	5	4
06	1	1	4	2	2	3	5	4
07	2	2	4	4	3	4	5	5
08	4	0	5	5	4	5	4	5
09	2	2	4	5	3	2	5	5
10	5	4	2	5	2	1	4	2
11	2	5	0	5	3	4	5	4
12	4	5	5	5	4	3	5	5
13	5	5	5	5	4	2	5	5
14	3	2	2	4	1	0	4	4
Images	31	30	35	44	28	29	47	43
Images total	287							

Hand Image Database

A Hand Image Database containing the image data collected along with patient demographic data and radiologist readings can be browsed using the following link: http://www.ipilab.org/BAAweb/. Fig. 2 shows a screen shot of a page retrieved from the eleven year old Asian female data.

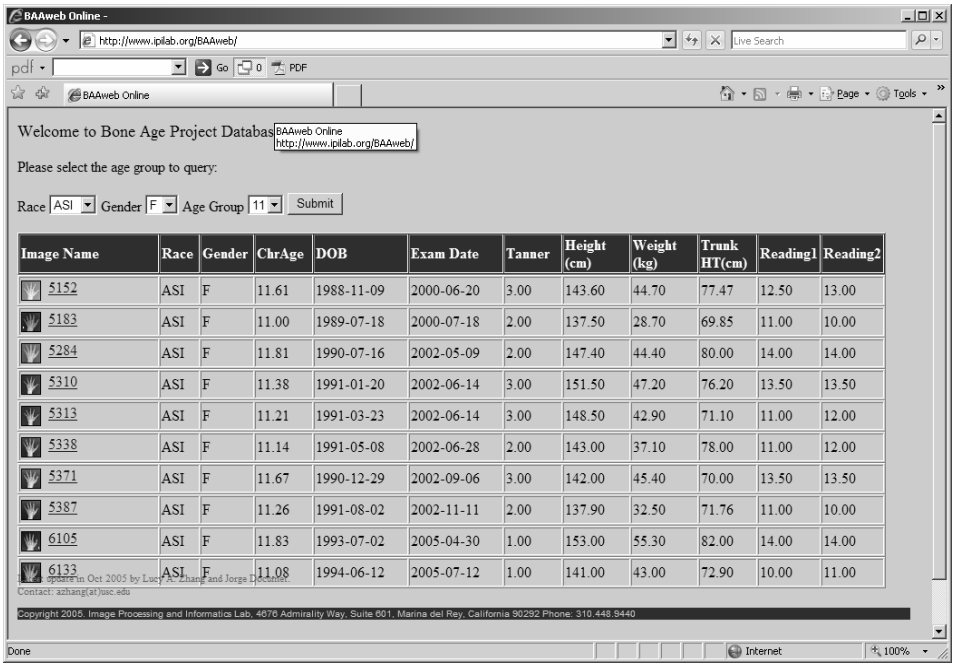

Figure 2. A GUI window of the bone age assessment web site with hand image database. The website provides hand images, information about subjects' demographic data and radiologists' readings.

3. THE CAD MODULE

CAD using the data collected described in Section 2 for the BAA has been designed and implemented to provide an objective assessment of a child's skeletal age as an aid to the pediatric radiologist's reading. The collected data together with features extracted related to skeletal development from phalangeal ROIs [15] and the Carpal bone ROI [17] were transformed into knowledge rules of fuzzy classifiers [16] for bone age assessment. The Digital Hand Atlas is a combination of the collected data and the CAD module. A work flow of the CAD is presented in Fig. 3 which consists of five steps: 1) image preprocessing, 2) ROIs determination, 3) phalangeal and carpal bones features extraction, 4) fuzzy classifiers, and 5) aggregation of fuzzy classifier results to obtain the bone age assessment.

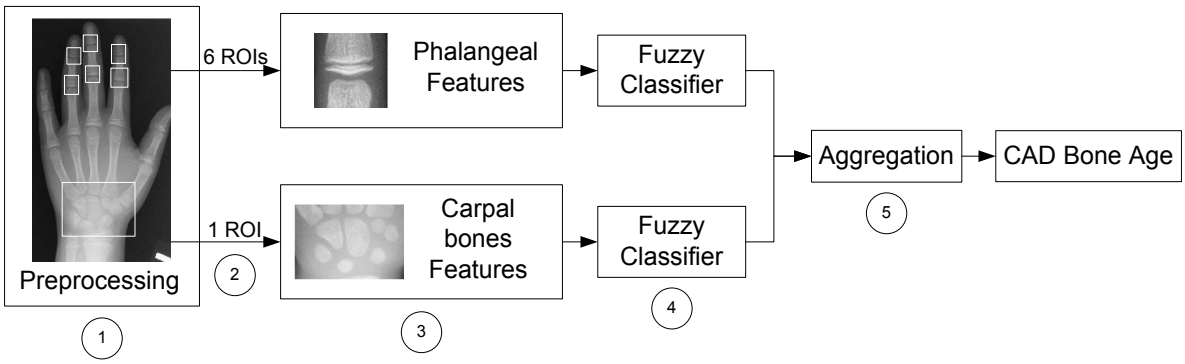

Figure 3. Five steps of the CAD workflow. Located seven regions of interest is subjected to features extraction and category classifiers provide fuzzy information about boner age derived from the regions of interest. Final bone age is calculated after the aggregation procedure

Image Pre-Processing, ROI Determination, Feature Extraction

Image preprocessing includes background suppression and radiological markers removal (see Fig. 1 stripes and background nonuniformitiy may not be well visible in this example, except for the "L" marker). [12, 13] Next, six distal and middle phalangeal ROIs (PROIs) of three middle fingers [13] and the carpal bone ROI are located [11]. Fig. 1 left shows six PROIs and the carpal bone ROI, and the right is the magnification of a PROI and the carpal bone ROI, [17]. Considering first the six PROIs, eleven features were extracted from each ROI. [16,18,19] Two feature sets, those features related to size and shape of the epiphysis, and the wavelet features derived from stage of fusion advancement of the epiphysis, describe the degree of bone development in this single PROI. Similar procedures were performed for each PROI. As a result, a total of twelve feature sets were obtained, two from each PROI. Methods of feature extraction have been discussed in details in previous publications [10-19]. These twelve feature sets were used to train twelve PROI fuzzy classifiers for bone age assessment contributed by PROIs features.

The Category Fuzzy Classifier and Aggregator

The data from 1 – 18 years shown in Table 2 was separated into eight categories (CAM, CAF, AAM, AAF, HIM, HIF, ASM, and ASF) for race and gender comparison study. In addition, CAM, AAM, HIM and ASM were combined as one male category; and CAF, AAF, HIF, and

ASF were combined as one female category. The male and female were further combined as one universal F & M category. Therefore we developed one category fuzzy classifier for each of the eleven categories.

For each category, the category fuzzy classifier using the PROIs feature sets was trained as follows. For each PROI, there were two classifiers, one was based on the shape and size features, and the other was based on wavelet features. The design and training of these two classifiers were based on Mamdani's original concept [21], and applied to phalangeal ROIs discussed in details in Ref [16]. The design and training of each category fuzzy classifier using the carpal bone ROI is given in [17]. Fifty percents of the collected images were used for training, and the other 50% for evaluation.

The design of the category fuzzy classifier is an open architecture model meaning that if fuzzy results from other ossification centers are provided they can be appended to the existing structure before the defuzzification (or aggregation) step, for example in each category classifier, the carpal bone ROI classifier could be appended to the phanlangeal ROI classifiers for bone age assessment [17].

The final BAA was derived from the aggregation of BAA results from the phalangeal ROIs and carpal ROI. In general, carpal bone ROIs determines the bone age of boys from 1 to 7, and girls from 1 to 5; phalangeal ROIs determine the bone age for both sexes above age 13. For girls from 6 – 12, and boys from 8 -12, both carpal ROI and phalangeal ROIs contribute. The final bone age value was obtained by defuzzication with the center of gravity method. Fig. 6 middle left illustrates the concept of the aggregation of 12 PROI classifiers and the carpal ROI classifier to form the combined bone age value in a category fuzzy classifier.

Graphical User Interface

A graphical user interface (GUI) was designed to visualize CAD operation steps (Window 1) and results (Window 2). After the hand image is sent to the CAD and the processes are completed, the CAD workstation Window 1 displays the patient data (Fig. 4, Left), image with superimposed ROIs (Middle) and segmentation results (Right). In addition, detailed messages about currently CAD performed step can also be visualized in the Lower Right of Fig. 4 using a scroll bar at the bottom). The CAD results are shown in Window 2 as depicted in Fig. 5.

Integration of CAD BAA with PACS

The digital atlas has been integrated with a research PACS using a CAD-PACS integration toolkit for validation study [20]. The toolkit is based on the DICOM (Digital Imaging and Communications in Medicine) Standard and IHE (Integrating the Healthcare Enterprise) workflow profiles. The toolkit has two modules, the DICOM-based SC (secondary capture) module, and the DICOM – IHE module, both modules can output the CAD BAA results as shown in Fig. 5. The former module, a fast integration method, allows the CAD GUI results shown in Figs. 5 to be directly displayed on the PACS workstations using the DICOM SC. However, PACS workstations can only display these results but can not assess the image or the textual contents directly. The DICOM – IHE module is based on the DICOM Structured Report (SR) standard and the IHE Post-Processing Workflow Profile protocol. The integration is more elaborated but the PACS workstations, in addition to displaying CAD results as shown in Figs. 5, can also access the CAD result images and data for other research, teaching, and clinical services applications. Zhou [20] in this Special Issues provides detail description of the integration methods. Fig. 6 shows the workflow of the integration of CAD BAA with PACS. Within the

dotted lines is the domain of the Digital Atlas, and PACS hardware components are the image acquisition and workstations. The CAD toolkit is integrated with the PACS software.

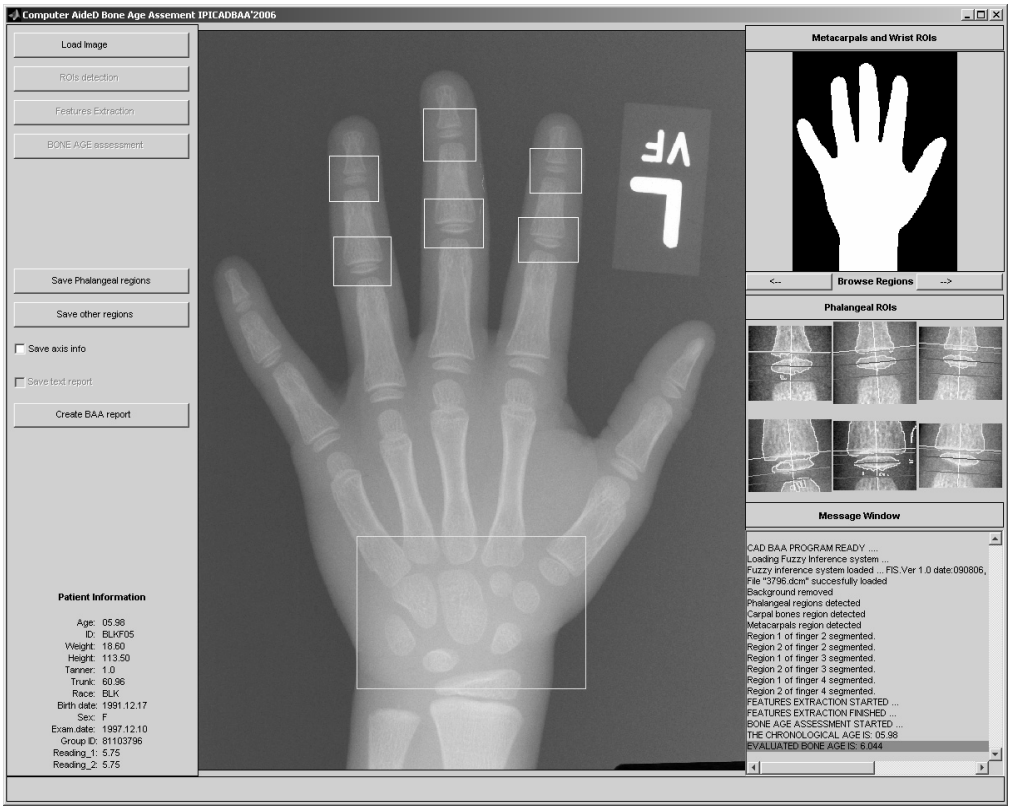

Figure 4. Graphical user interface of the CAD for BAA. The analyzed hand image with superimposed ROIs is in the GUI center. Patient data is on left side, right part of the GUI contains segmentation results and message window.

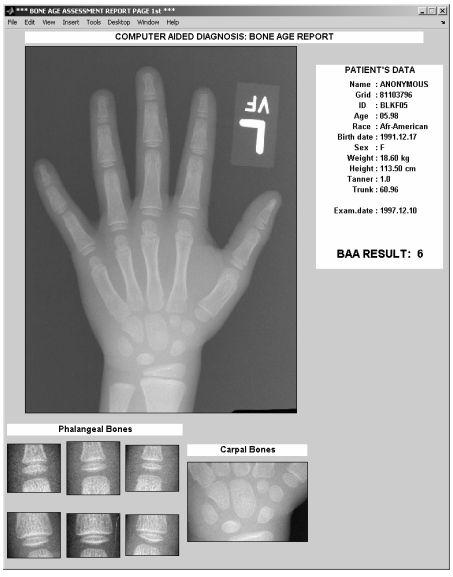

Figure 5. An example of a CAD report window with automatically extracted ROIs together with analyzed hand image. Patient data and CAD result are displayed in the upper right.

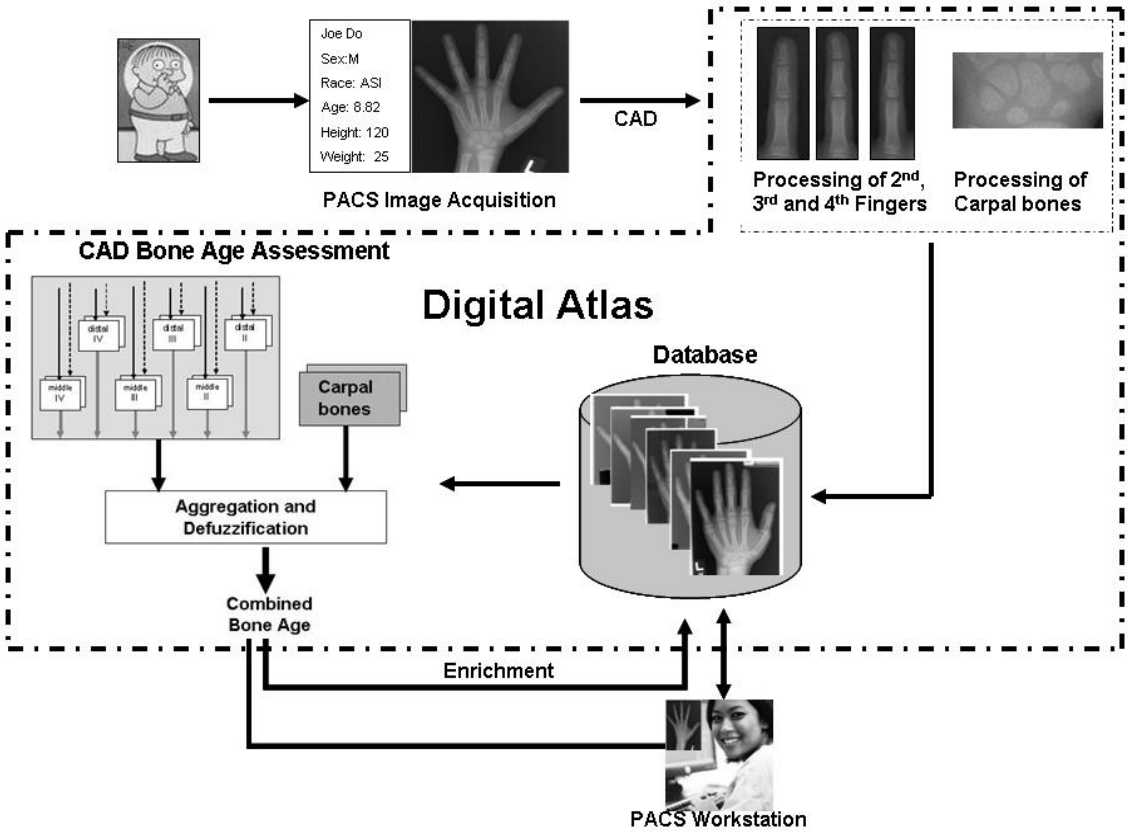

Figure 6. The workflow of CAD and PACS integration. Acquired hand image is processed by the CAD and compared with hand images in the database. The Digital Hand Atlas can be enriched by CAD bone age results.

4. RESULTS

With the large-scale data collection and elaborated design of the CAD module, many different types of meaningful clinical results could emerge. In this section, we provide results related to the evaluation of data collection methodology and its effect on the CAD bone age assessment. In particular, the effect of quality assurance protocol (QAP) to the performance of image analysis algorithm, the accuracy of image analysis algorithm in the phanlangeal ROIs (PROI), and the improvement of the CAD method in bone age assessment with the addition of second cycle data collection (See Table 2a,b) are given.

Effect of Quality Assurance Protocol (QAP) to the Performance of Segmentation Algorithm

Since data collection spanned about ten years, QAP is important to assure the consistence and quality of the data collected (See Appendix A). During the data collection process, by incorporating the QAP, about 5% of cases misspelled dates and other numeric data in the DICOM study description field were detected and corrected. Forty six images failed to pass the Step 1 of the QAP work flow (Appendix A) and were replaced by others. Main reasons were the hand placement was not aligned properly during the X-rays exam, and/or numerous artifacts on the image. Application of the Step 3 of the QAP also greatly improved the passage of all 1,400

images through the CAD in terms of smooth running of the CAD. All cases that caused errors were investigated and more robust error detection was implemented.

Evaluation of the image analysis algorithm

The evaluation of segmentation results involved 300 selected hand images from the second cycle data collection. The set covered distal and middle regions of interest with all possible stages of epiphyseal development, from those with epiphyses distinct in appearance, to epiphyses partially and completely fused with the metaphyses, otherwise. Other than these conditions, the selection process was random. The PROIs were automatically located in the hand image by the CAD software. All segmented regions with outlined cartilage and bony structure were presented to two radiologists of different clinical experience and training. Results of segmentation of each region were evaluated by these radiologists to one of three categories: *good*, *acceptable*, *unacceptable*. They were blind to the child's age, sex and race. Their subjective results are presented in Table 3. The average number of regions classified as *good* was 79.7%, and regions classified as *good* or *acceptable* was 93.7% which demonstrate that the automatic segmentation of the cartilage and bony structures is acceptable by the radiologists. For results in carpal bone ROI, see [17].

Table 3. Experts' evaluation of PROIs outlined by the CAD. The average number of regions classified as *good* is 79.7%, and regions classified as *good* or *acceptable* is 93.7%

Expert	*good*	*acceptable*	*unacceptable*
Expert 1	72.81%	19,94%	7.25%
Expert 2	86.5%	8.08%	5.24%

Improvement of the CAD method with the addition of second cycle data collection

In Section 3 we described that the CAD consists of eleven fuzzy classifiers each of which is used to assess the bone age of the eleven categories: CAM, CAF, AAM, AAF, HIM, HIF, ASM, and ASF, female only, male only, and female and male (F & M) together, respectively. These eleven classifiers were trained in two times, with data from the first cycle collection, and with data from both cycles (first and second) collection. We discuss here the improvement of the CAD method for bone age assessment of the first eight categories with the addition of second cycle data collection. Comparison between races indicated that the addition of second cycle data collection does improve the performance of the CAD based on the comparison of the CAD bone age assessment (BAA) with the chronological age. Improvement is in the sense that less discrepancy between races was observed. Table 4 depicts an example of the girl BAA, where Table 4a) is the result using the first cycle data only, and Table 4b is the results using both first and second cycle data. The girl bone age development according to the female gender was divided into four stages as a gauge of comparison shown in the bottom of both Tables 4a) and 4b).

Table 4a. Performance of the CAD Bone Age Assessment based on comparison with chronological age using first cycle data. The girl bone age development was divided into four stages as a gauge of comparison shown in the bottom. * indicates that the comparison has p-value < 0.05 which is significant.

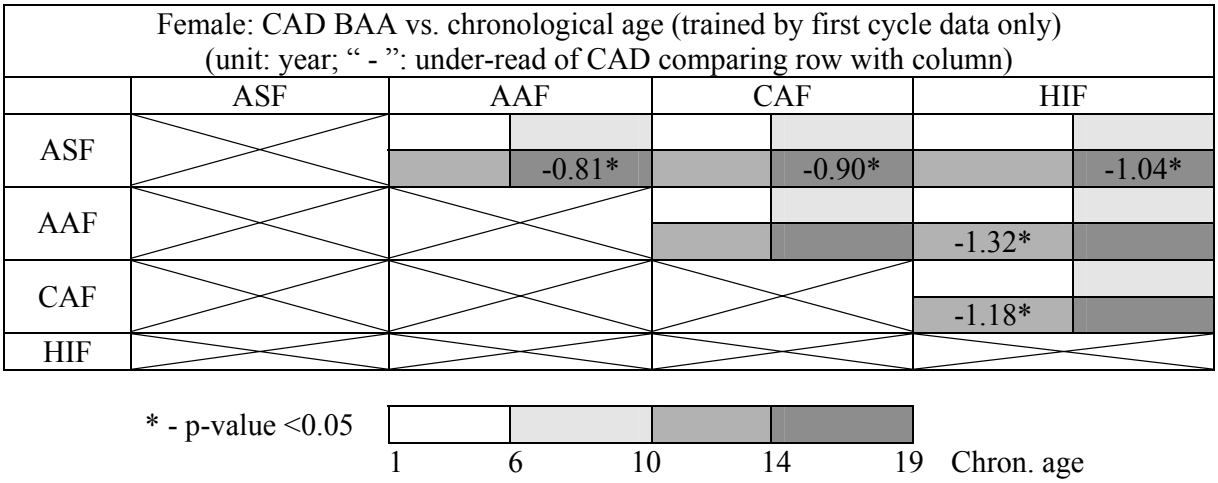

Table 4b. Performance of the CAD Bone Age Assessment based on comparison with chronological age using both first and second cycle data. Improvement is in the sense that less discrepancy between races was observed. The girl bone age development was divided into four stages as a gauge of comparison shown in the bottom. * indicates that the comparison has p-value < 0.05 which is significant

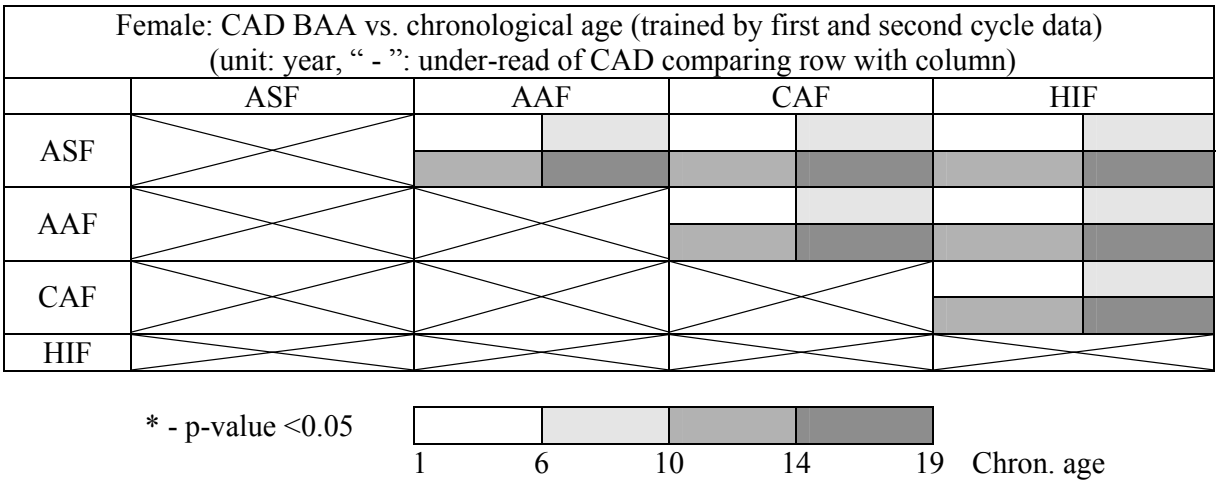

5. DISCUSSION AND SUMMARY

An overview of the computerized approach to bone age assessment utilizing Digital Hand atlas is presented. The Digital Hand Atlas serves as a reference data set reflecting current skeletal development of normal subjects of four descents, living in the US, in particular in the Los Angeles area. The Atlas is comprised of two components, a digital hand database with a

collection of 1,400 digitized left hand radiographs and relevant data from evenly distributed normally children of Caucasian (CA), Asian (AS), African-American (AA) and Hispanic (HI) origin, male (M) and female (F), ranged from 1 to 18 year old; and a CAD module for bone age assessment. The automatic CAD approach utilizing quantitative knowledge of the Digital Hand Atlas can provide bone age value based on radiological findings sensitive to developmental changes.

We are in the beginning of validating and evaluating the performance of the digital hand atlas. Three types of results have been obtained: the effect of quality assurance protocol (QAP) to the performance of image analysis algorithm, the accuracy of image analysis algorithm in the phanlangeal ROIs (PROI), and the improvement of the CAD method in bone age assessment with the addition of second cycle data collection. Bone age assessment for children has been assessed based on the 1950 Greulich and Pyle Atlas (G & P) from a homogeneous population. With today's diverse ethnicities in the US, the G & P atlas may no longer be a good reference. We are in the process of analyzing the Digital Atlas results to address the following questions:1. Does ethnicity and gender have different bone growth patterns? 2. Does the bone age of ethnic origins differ? 3. Is the bone growth for boys and girls different? And 4. Is the G & P atlas still a good reference for bone age assessment of today's children?

The atlas has been integrated with PACS which can directly access the hand image of a patient from the PACS and return the bone age assessment results to PACS workstations for on-line assisting clinicians to assess the bone age. The digital atlas can be expanded in bone age assessment of subjects of other ethnic origins by collecting digital hand images following the data collection protocol and the training of the fuzzy classifiers with methods discussed in this paper.

Acknowledgements

The authors would like to thank Alexis Wong, MD, and Bing Guo, MD, for their kind help in validating the segmentation results. This research work has been sponsored by NIH R01 EB 00298.

APPENDIX A

Quality Assurance Protocol of the Images collected for the Digital Hand Atlas

Testing and developing of a CAD requires the image data to be properly collected according to a standard protocol. Also, high quality of the data should be maintained if the images are intended to be used in a decision making process. A quality assurance protocol (QAP) has been developed and implemented in order to meet such needs. The QAP encompasses a manual and visual inspection of the image and the evaluation of its suitability for the automatic CAD process. The workflow of the QAP is presented in Fig. A1 which consists of four steps. Step1 can be completed by the operator whereas Steps 2-4 are non-interactively performed by the CAD.

In Step1 (Fig. A1) the quality is first visually justified by the operator utilizing the graphical user interface of the CAD. If the hand image is not aligned properly with respect to the image plane, then it is immediately rejected. In Step 2, a comparison between the radiologist readings and the chronological age is performed. The image is rejected if the difference between the chronological age and the radiologist bone age reading is larger than a certain threshold *trh*. In this protocol, *trh* value has been set to three years. In Step 3, the content of the DICOM image header containing

the subject's demographic data is compared with the data in the documentation used during the digitization procedure. Any inconsistencies between the documentation and patient record require corrections. In Step 4, image preprocessing procedures could reveal artifacts caused by nonuniform background, underexposed film borders, scratches and radiological markers that may cause difficulties in automatic image processing [12, 13]. Finally CAD results like: regions of interests and bone age value are evaluated. In Step 4 the CADBA result is also compared with subject's chronological age. If the discrepancy is smaller than the predefined threshold *trh*; the same as used in Step 2, then this image is subjected to the acceptance procedure and appended to the existing data collection. Otherwise it requires a CAD verification step to be taken. In such cases, the image will be subjected to bone age recalculation after a modification of the CAD.

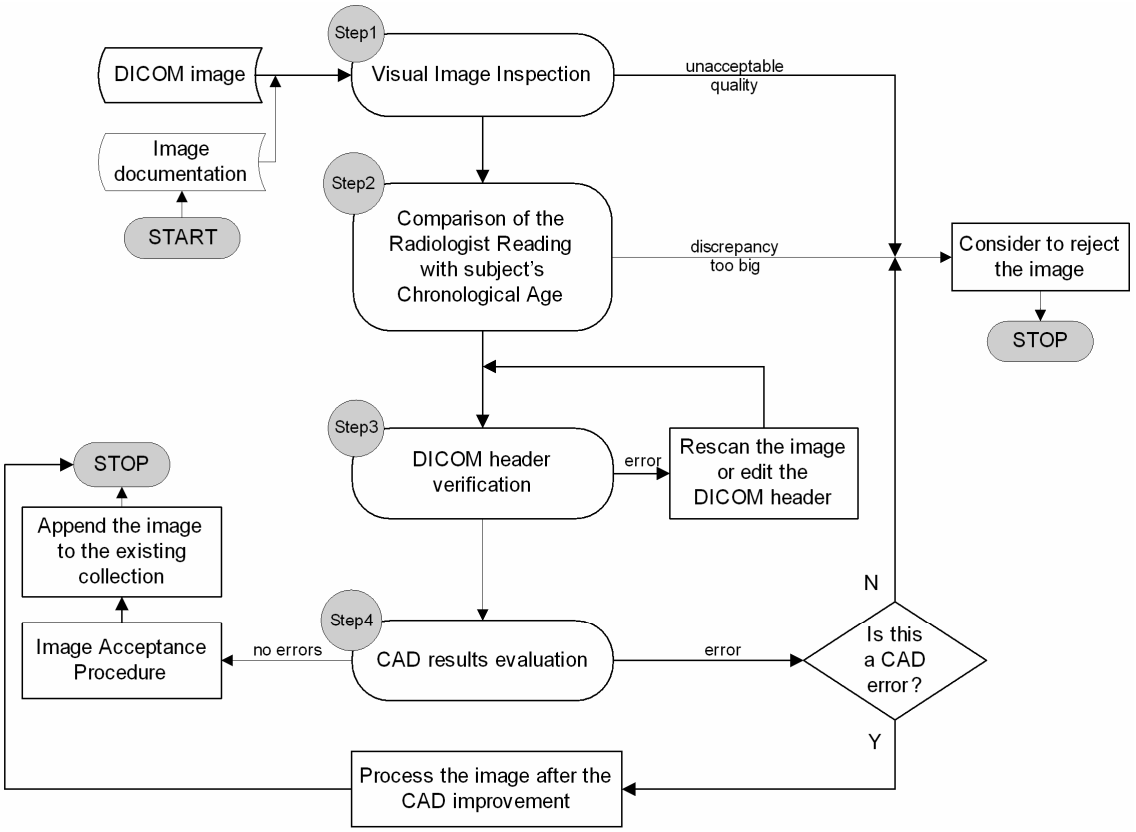

Figure A1. The quality assurance protocol work flow with the CAD in the loop. Image inspection Step 1 and DICOM header verification: Step 2, 3 are performed first. In Step 4 errors and comparison of CAD result are evaluated. Acceptance of the CAD results allows appending the image to the existing collection.

In summary, the QAP applied to the Digital Hand Atlas encompasses checking the image features and patient data at various levels. Image quality is assessed in terms of correct hand placement, presence of image artifacts and capability of radiological findings extraction performed by the CAD. Verification of subject's demographic data can be performed in the QAP by the CAD operator or the CAD; however the latter option can be modified in a more automated fashion. Images that failed to comply with the QAP protocol have been replaced by other images. Using the QAP, the reliability of the data collected for the Digital Hand Atlas has been improved.

References

[1] Greulich WW, Pyle SI, Radiographic Atlas of Skeletal Development of Hand Wrist. Stanford University Press 2nd ed, Stanford CA, 1971.
[2] Roch AF, Rochman CG, Davila GH, Effect of training of replicaability of assessment of skeletal maturity (Greulich-Pyle), Amer. Journal of Roentgenology, 1970, vol. 108, pp. 511-515
[3] Tanner JM. Growth at adolescence, 2nd ed. Oxford: Blackwell Scientific Publications, 1962.
[4] Tanner JM, Whitehouse RH, Assessment of Skeletal Maturity and Prediction of Adult Height (TW2 Method). Academic Press, London, 1975.
[5] Tanner JM, Healy MJR, H. Goldstein, N. Cameron, Assessment of Skeletal Maturity and Prediction of Adult Height (TW3 Method), Third edition, W. B. Saunders, London 2001.
[6] King DG, Steventon DM, O'Sullivan MP, Cook AM, Hornsby VP, Jefferson IG, King PR, Reproducibility of bone ages when performed by radiology registrars: an audit of Tanner and Whitehouse II versus Greulich and Pyle methods. Br J Radiol 1994;67:848–851.
[7] Mora S, Boechat MI, Pietka E, Huang HK, Gilsanz V, Skeletal Age Determinations in Children of European and African Descent: Applicability of the Greulich an Pyle Standards. Pediatric Research, 2001;50(5):624-628, 2001.
[8] Cao F, Huang HK, Pietka E, Gilsanz V, Digital hand atlas for Web-based bone age assessment: System design and implementation. Computerized Medical Imaging and Graphics, 2000;24:297-307.
[9] Cao F, Huang HK, Pietka E, Gilsanz V, Dey PS, Gertych A, Pospiech-Kurkowska S, Image database for digital hand atlas, SPIE Med. Img., Proceedings of the SPIE, 4(24):461-470, 2003.
[10] Pietka E, McNitt-Gray MF, Huang HK, Computer-assisted phalangeal analysis in skeletal age assessment. IEEE Trans. on Medical Imaging, 1991;10:616-620.
[11] Pietka E, Kaabi L, Kuo ML, Huang HK, Feature extraction in carpal-bone analysis, IEEE Trans. on Medical Imaging. 1993;12:44-49.
[12] Pietka E, Gertych A, Pospiech S, Huang HK, Cao F, Computer assisted bone age assessment: Image pre-processing and ROI extraction, IEEE Trans on Medical Imaging 2001;20:715-729.
[13] Pietka E, Pospiech S, Gertych A, Cao F, Huang HK, Gilsanz V, Computer Automated Approach to the extraction of epiphyseal regions in hand radiographs, Journal of Digital Imaging 2001;14:165-172
[14] http://www.cdc.gov/growthcharts/
[15] Pietka E, Gertych A, Pospiech-Kurkowska S, Cao F, Huang HK, Gilsanz V, Computer Assisted Bone Age Assessment: Graphical User Interface for Image Processing and Comparison, Journal of Digital Imaging, 2004;17(3):175-188.
[16] Pietka E, Pospiech-Kurkowska S, Gertych A, Cao F, Integration of Computer assisted bone age assessment with clinical PACS. Comp. Med. Img. Graph, 2003;27:217-228.
[17] Zhang A, Gertych A, Liu BJ, Bone Age Assessment for Young Children from Newborn to 7-Year-Old Using Carpal Bones, Journal of Comp. Med. Img. Graph (*in press*)
[18] Pietka E, Gertych A, Witko K, Informatic infrastructure of CAD system, Computerized Medical Imaging and Graphics, 2005;29:157-169.
[19] Gertych A, Pietka E, Liu BJ, Segmentation of Regions of Interest and Post-Segmentation Edge Location Improvement in Computer-Aided Bone Age Assessment. Pattern Analysis and Application Journal (*in press*)
[20] Zhou Z, CAD-PACS Integration Tool Kit based on DICOM Secondary Capture, Structured Report and IHE Workflow Profiles. Journal of Comp. Med. Img. Graph (*in press*)
[21] Mamdani EH. Application of fuzzy algorithms for control of simple dynamic plant. Proc IEEE 1974; 121:1585-8

BOOK CHAPTER REPRINTS AND PREPRINTS

CHAPTER 3

Principles of X-ray Anatomical Imaging Modalities

Brent J Liu, HK Huang

ABSTRACT

This chapter provides basic concepts of various X-ray imaging modalities. The first part of the chapter addresses digital X-ray projection radiography which includes digital fluorography, computed radiography, X-ray mammography, and digital radiography. The key components belonging to each of these imaging modalities will be discussed along with basic principles to reconstruct the 2D image. The second part of the chapter focuses on 3D volume X-ray acquisition which includes X-ray CT, Multislice, Cine, and 4D CT. The image reconstruction methods will be discussed along with key components which have advanced the CT technology to the present day.

INTRODUCTION

This chapter will present X-ray anatomical imaging modalities which cover a large amount of the total number of diagnostic imaging procedures. X-ray projection radiography alone accounts for 70% of the total number of diagnostic imaging procedures. In this chapter, we will only focus on digital X-ray anatomical imaging modalities, which include digital fluorography, computed radiography, X-ray mammography, digital radiography, X-ray CT, and multislice, CINE, and 4D X-ray CT.

There are two approaches to convert an analogy-based image to digital form. The first is to utilize existing equipment in the radiographic procedure room and only change the image receptor component. Two technologies, computed radiography (CR) using the photostimulable phosphor imaging plate technology, and digital fluorography, are in this category. This approach does not require any modification in the procedure room and is therefore more easily adopted for daily clinical practice. The second approach is to redesign the conventional radiographic procedure equipment, including the geometry of the X-ray beams and the image receptor. This method is therefore more expensive to adopt, but the advantage is that it offers special features like low X-ray scatter which would not otherwise be achievable in the conventional procedure.

DIGITAL FLUOROGRAPHY

Since 70% of the radiographic procedures still use film as an output medium, it is necessary to develop methods to convert images on films to digital format. This section discusses digital fluorography which converts images to digital format utilizing a video camera and A/D converter.

The video scanning system is a low cost X-ray digitizer which produces either a 512 K or 1 K digitized image with 8 bits/pixel. The system consists of three major components: a scanning device with a video or a CCD (charge-coupled device) camera that scans the X-ray film, an analog/digital converter that converts the video signals from the camera to gray level values, and an image memory to store the digital signals from the A/D converter. The image stored in the image memory is the digital representation of the X-ray film or image in the image intensifier tube obtained by using the video scanning system. If the image memory is connected to a digital-to-analog (D/A) conversion circuitry and to a TV monitor, this image can be displayed back on the monitor (which is a video image). The memory can be connected to a peripheral storage device for long-term image archive. Figure 1 shows a block diagram of a video scanning

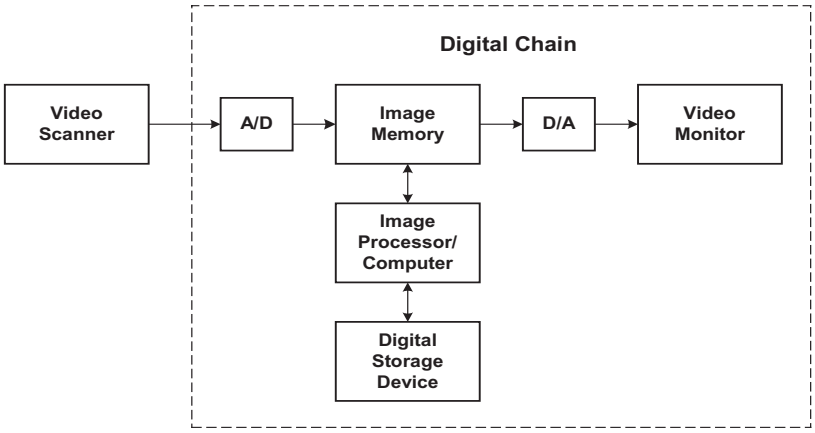

Fig. 1 Block diagram of a video scanning system, the digital chain is a standard component in all types of scanner.

system. The digital chain shown is a standard component in all types of scanner.

Video scanner system can be connected to an image intensifier tube to form a digital fluoroscopic system. Digital fluorography is a method that can produce dynamic digital X-ray images without changing the radiographic procedure room drastically from conventional fluorography. This technique requires an add-on unit in the conventional fluorographic system. Figure 2 shows a schematic of the digital fluorographic system with the following major components:

(1) *X-ray source*: The X-ray tube and a grid to minimize X-rays scatter.
(2) *Image receptor*: The image receptor is an image intensifier tube.
(3) *Video camera plus optical system*: The output light from the image intensifier goes through an optical system, which allows the video camera to be adjusted for focusing. The amount of light going into the camera is controlled by means of a light diaphragm. The camera used is usually a plumbicon or a CCD (charge couple device) with 512 or 1024 scan lines.

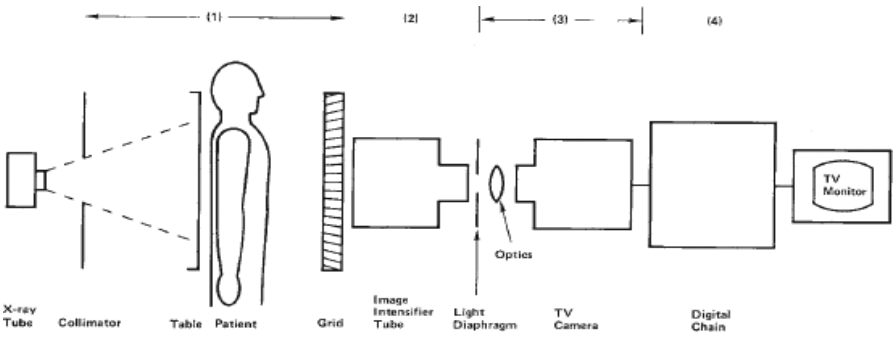

Fig. 2 Schematic of a digital fluorographic system coupling the image intensifier and the digital chain. See text for key to numbers.

(4) *Digital chain*: The digital chain consists of an A/D converter, image memories, image processor, digital storage, and video display. The A/D converter, the image memory, and the digital storage can handle $512 \times 512 \times 8$ bit image at 30 frames per second, or $1024 \times 1024 \times 8$ bit image at 7.5 frames per second. Sometime the RAID (redundant array of inexpensive disks) is used to handle the high speed data transfer.

Fluorography is used to visualize the motion of body compartments (e.g. blood flow, heart beat), the movement of a catheter, as well as to pinpoint an organ in a body region for subsequent detailed diagnosis. Each exposure required in a fluorography procedure is very minimal compared with a conventional X-ray procedure.

Digital fluorography is considered to be an add-on system because a digital chain is added to an existing fluorographic unit. This method utilizes the established X-ray tube assembly, image intensifier, video scanning, and digital technologies. The output from a digital fluorographic system is a sequence of digital images displayed on a video monitor. Digital fluorography has an advantage over conventional fluorography in that it gives a larger dynamic range image and can remove uninteresting structures in the images by performing digital subtraction.

When image processing is introduced to the digital fluorographic system, dependent on the application, other names are used, for example, digital subtraction angiography (DSA), digital subtraction arteriography (DSA), digital video angiography (DVA), intravenous video arteriography (IVA), computerized fluoroscopy (CF), and digital video subtraction angiography (DVSA).

IMAGING PLATE TECHNOLOGY

Imaging plate system, commonly called computed radiography (CR), consists of two components: the imaging plate and the scanning mechanism. The imaging plate (*laser-stimulated luminescence phosphor plate*) used for X-rays detection, is similar in principle to the phosphor intensifier screen used in the standard screen/film receptor. The scanning of a laser-stimulated luminescence phosphor imaging plate also uses a scanning mechanism (Reader) similar to that of a laser film scanner. The only difference is that instead of scanning an X-ray film, the laser scans the imaging plate. This section describes the principle of the imaging plate, specifications of the system, and system operation.

Principle of the Laser-Stimulated Luminescence Phosphor Plate

The physical size of the imaging plate is similar to that of a conventional radiographic screen; it consists of a support coated with a photo-stimulable phosphorous layer made of $BaFX:Eu^{2+}(X=Cl,Br,I)$, Europium-activated barium-fluorohalide compounds. After the X-ray exposure, the photo-stimulable phosphor crystal is able to store a part of the absorbed X-ray energy in a quasistable state. Stimulation of the plate by a 633 nanometer wavelength helium-neon (red) laser beam leads to emission of luminescence radiation of a different wavelength (400 nanometer), the amount of which is a function of the absorbed X-ray energy [Fig. 3(B)].

The luminescence radiation stimulated by the laser scanning is collected through a focusing lens and a light guide into a photomultiplier tube, which converts it into electronic signals. Figure 3(A)

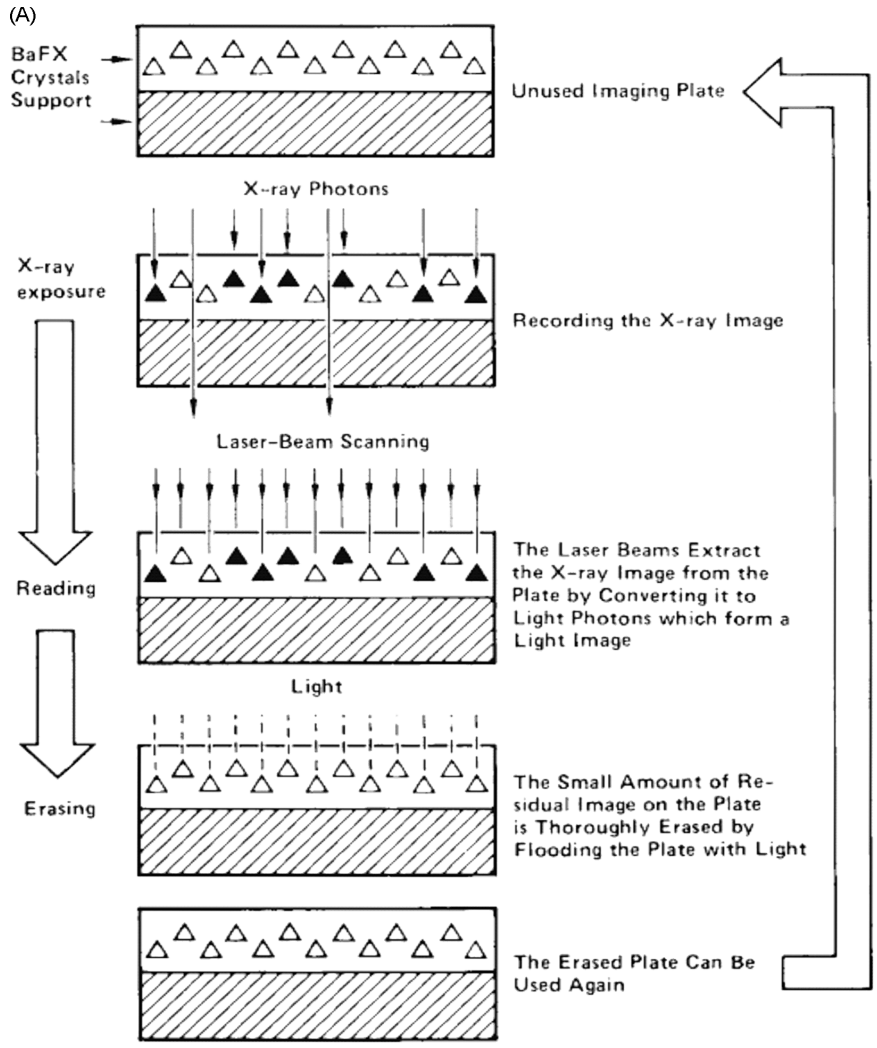

Fig. 3 Physical principle of laser-stimulated luminescence phosphor imaging plate. (A) From the X-ray photons exposing the imaging plate to the formation of the light image. (B) The wavelength of the scanning laser beam (b) is different from that of the emitted light (a) from the imaging plate after stimulation (courtesy of J Miyahara, Fuji Photo Film Co Ltd).

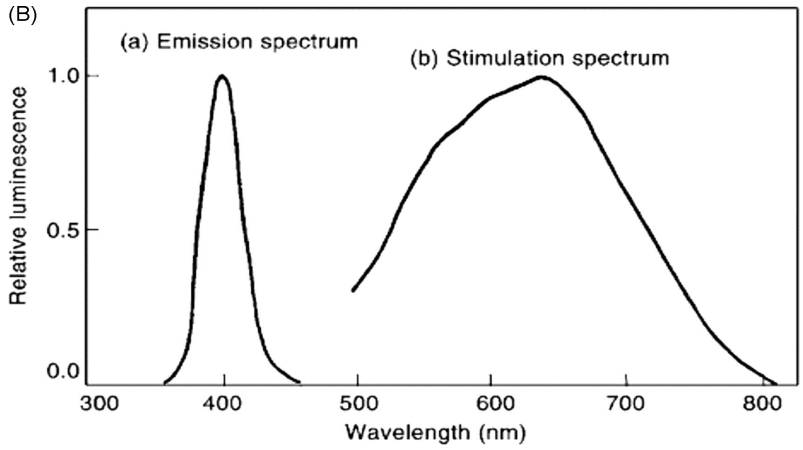

Fig. 3 (*Continued*)

shows the physical principle of the laser-stimulated luminescence phosphor imaging plate. The size of the imaging plate can be 8×10, 10×12, 14×14, or 14×17 square inches. The image produced is $2\,000 \times 2\,500 \times 10$ bits.

Computed Radiography System Block Diagram and its Principle of Operation

The imaging plate is housed inside a cassette just like a screen/film receptor. Exposure of the imaging plate (IP) to X-ray radiation results in the formation of a latent image on the plate (similar to the latent image formed in a screen/film receptor). The exposed plate is processed through a CR Reader to extract the latent image — analogous to the exposed film developed by a film developer. The processed imaging plate can be erased by bright light and be used again. The imaging plate can either be removable or nonremovable. An image processor is used to optimize the display (e.g. lookup tables) based on types of exam and body regions.

The output of this system can be one of two forms — a printed film or a digital image — the latter can be stored in a digital storage device and be displayed on a video monitor. Figure 4 illustrates the

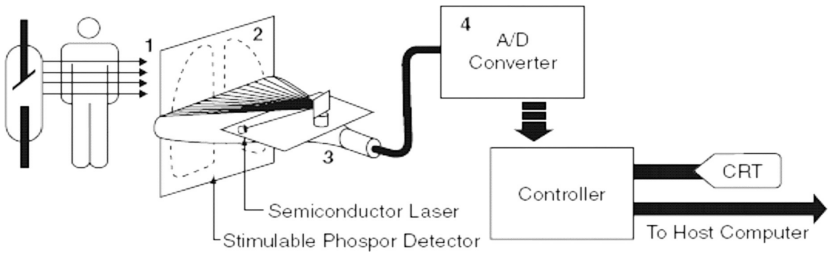

Fig. 4 Dataflow of an upright CR system with nonremovable imaging plates (IP). (1) Formation of the latent image on the IP. (2) The IP is scanned by the laser beam. (3) Light photons are converted to electronic signals. (4) Electronic signals are converted to digital signals which form a CR image (courtesy of Konica Corporation, Japan).

dataflow of an upright CR system with three un-removable imaging plates. Figure 5 shows the latest XG-5000 multiplate reader system with removable imaging plate and its components.

Operating Characteristics of the CR System

A major advantage of the CR system compared to the conventional screen/film system is that the imaging plate is linear and has a large dynamic range between the X-ray exposure and the relative intensity of the stimulated phosphors. Hence, under a similar X-ray exposure condition, the image reader is capable of producing images with density resolution comparable or superior to those from the conventional screen/film system. Since the image reader automatically adjusts the amount of exposure received by the plate, over- or under-exposure within a certain limit would not affect the appearance of the image. This useful feature can best be explained by the two examples given in Fig. 6.

In quadrant A of Fig. 6, example I represents the plate exposed to a higher relative exposure level but with a narrower exposure range (10^3–10^4). The linear response of the plate after laser scanning yields a high level but narrow light intensity (photostimulable luminescence, PSL) range from 10^3–10^4. These light photons are converted into electronic output signals representing the latent image

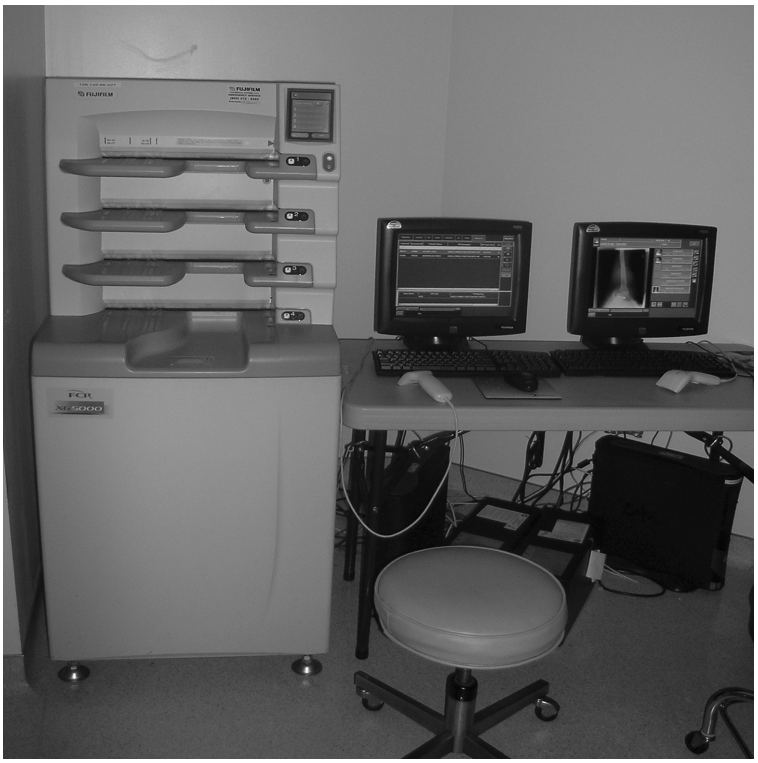

Fig. 5 A Fuji XG-5000 CR System with the multiimaging plate reader and two QA/Image Processing workstations (IIP and IIP Lite). Note that the second workstation shares the same database as the first workstation so that an X-ray technician can perform QA and image processing while another is operating the plate reader and processing the imaging plates.

stored on the image plate. The image processor senses a narrow range of electronic signals and selects a special look-up table [the linear line in Fig. 6(B)], which converts the narrow dynamic range 10^3–10^4 to a large light relative exposure of 1 to 50 [Fig. 6(B)]. If hardcopy is needed, a large latitude film can be used that covers the dynamic range of the light exposure from 1 to 50, as shown in quadrant C, these output signals will register the entire optical density (OD) range from OD 0.2 to OD 2.8 on the film. The total system response including the imaging plate, the look-up table, and the

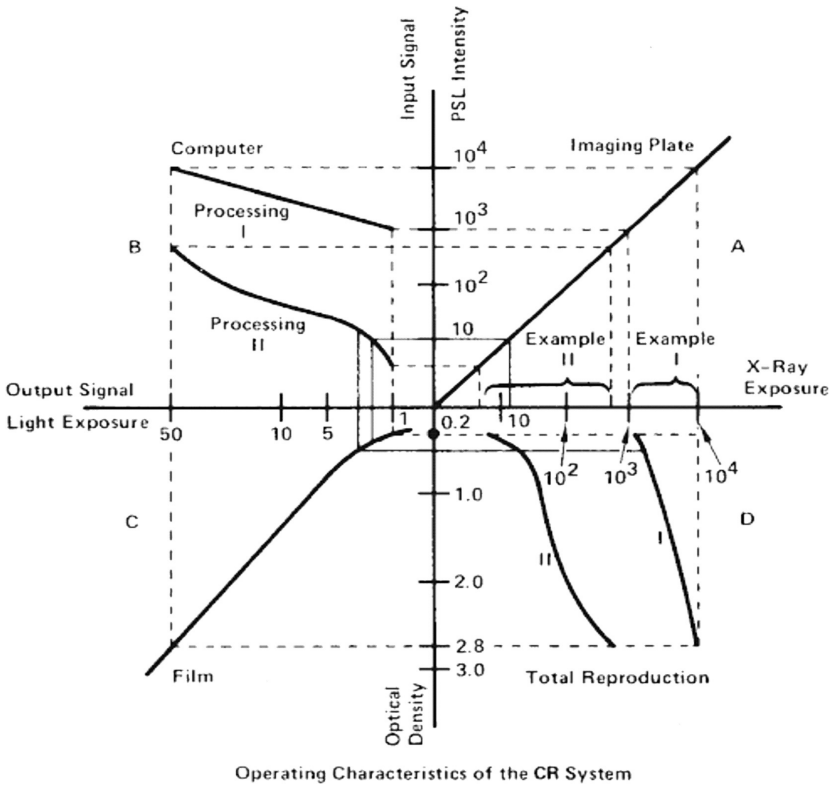

Fig. 6 Two examples, I and II, illustrate the operating characteristics of the CR system and explain how it compensates for over and under exposures.

film subject to this exposure range is depicted as curve I in quadrant D. The system-response curve, relating the relative exposure on the plate and the OD of the output film, shows a high gamma value and is quite linear. This example demonstrates how the system accommodates a high exposure level with a narrow exposure range.

Consider example II, in which the plate receives a lower exposure level but with wider exposure range. The CR system automatically selects a different look-up table in the image processor to accommodate this range of exposure so that the output signals again span the entire light exposure range form 1 to 50. The system-response curve

is shown as curve II in quadrant D. The key in selecting the correct look-up table is that the range of the exposure has to span the total light exposure of the film, namely from 1 to 50. It is noted that in both examples, the entire useful optical density range for diagnostic radiology is utilized.

If a conventional screen/film combination system was used, exposure on example I in Fig. 6 would only utilize the higher optical density region of the film, whereas in example II it would utilize the lower region. Neither case would utilize the full dynamic range of the optical density in the film. From these two examples, it is seen that the CR system allows the utilization of the full optical density dynamic range, regardless whether the plate is overexposed or underexposed. Figure 7 shows an example comparing the results of using screen/film versus CR under identical X-ray exposures. The

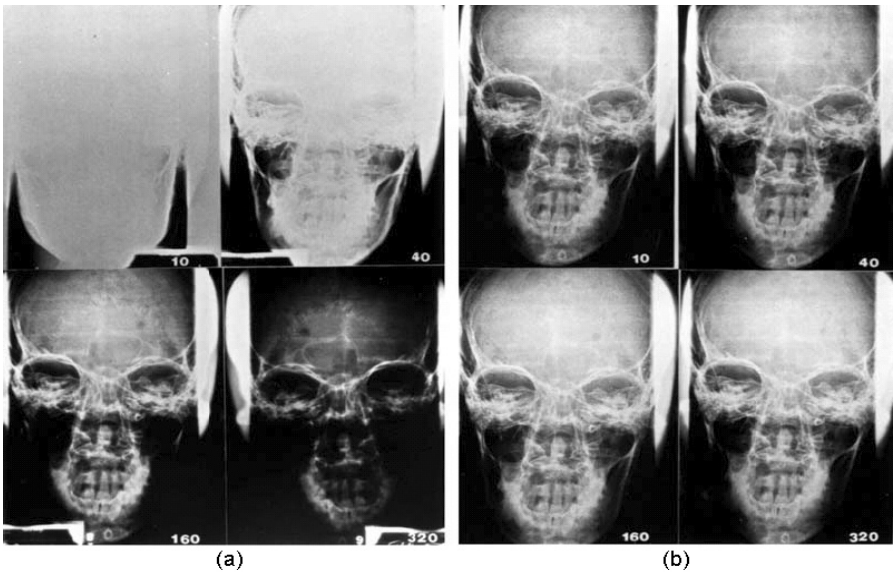

Fig. 7 Comparison of quality of images obtained by using (A) the conventional screen/film method and (B) CR techniques. Exposures were 70 kVp; 10 mAs, 40 mAs, 160 mAs, 320 mAs on a skull phantom. It is seen that in this example that the CR technique is almost dose independent (courtesy of Dr S Balter).

same effect is achieved if the image signals are for digital output, and not for hard copy film. That is, the digital image produced from the image reader and the image processor will also utilize the full dynamic range from quadrant D to produce 10-bit digital numbers.

FULL-FIELD DIRECT DIGITAL MAMMOGRAPHY

Screen/Film and Digital Mammography

Conventional screen/film mammography produces a very high quality mammogram on an 8 sq in $\times$ 10 sq in film. Some abnormalities in the mammogram require 50 μm spatial resolution to be recognized. For this reason, it is difficult to use CR or a laser film scanner to convert a mammogram to a digital image, hindering the integration of the modality images to PACS. Yet, mammography examinations account for about 8% of all diagnostic procedures in a typical radiology department. During the past several years, due to much support from the National Cancer Institute and the United States Army Medical Research and Development Command, some direct digital mammography systems have been developed by joint efforts between academic institutions and private industry. Some of these systems are in clinical use. In the next section, we describe the principle of digital mammography, a very critical component in a totally digital imaging system in a hospital.

Full Field Direct Digital Mammography

There are two methods of obtaining a full field direct digital mammogram, one is the imaging plate technology described in Sec. 3.3 but with higher resolution imaging plate of different materials and higher quantum efficient detector systems. The other is the slot-scanning method. This section summarizes the slot scanning method.

The slot-scanning technology modifies the image receptor of a conventional mammography system by using a slot-scanning

mechanism and detector system. The slot-scanning mechanism scans a breast by an X-ray fan beam and the image is recorded by a charged-couple device (CCD) camera encompassed in the Bucky antiscatter grid of the mammography unit. Figure 8 shows a picture of a FFDDM system. The X-ray photons emitted from the X-ray tube are shaped by a collimator to become a fan beam. The width of the fan beam covers one dimension of the image area (e.g. x-axis) and the fan beam sweeps in the other direction (y-axis). The movement of the detector system is synchronous with the scan of the fan beam. The detector system of the FFDDM shown is composed of a thin phosphor screen coupled with four CCD detector arrays via a tapered fiber optic bundle. Each CCD array is composed of $1\,100 \times 300$ CCD cells. The gap between any two adjacent CCD arrays

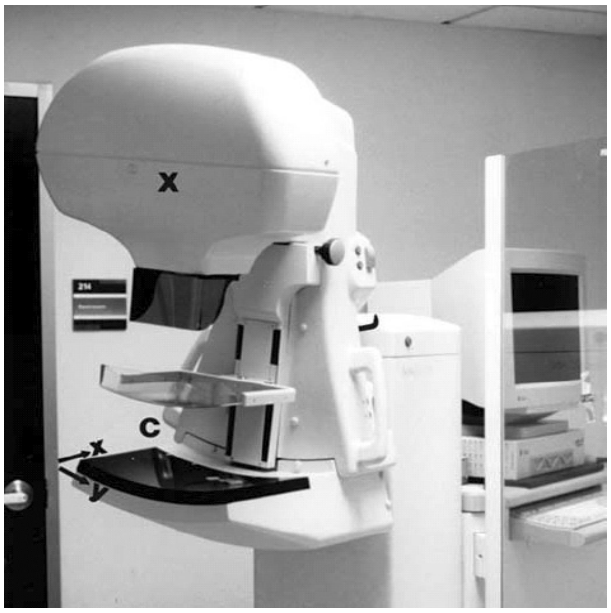

Fig. 8 A slot-scanning digital mammography system. The slot with 300 pixel width covering the x-axis (4 400 pixels). The X-ray beam sweeps (arrow) in the y-direction producing over 5 500 pixels. X: X-ray and collimator housing, C: breast compressor.

requires a procedure called "butting" to minimize the loss of pixels. The phosphor screen converts the penetrated X-ray photons (i.e. the latent image) to light photons. The light photons pass through the fiber optic bundle, reach the CCD cells, and then are transformed to electronic signals. The more light photons received by each CCD cell, the larger the signal is transformed. The electronic signals are quantized by an analog to digital converter to create a digital image. Finally, the image pixels travel through a data channel to the system memory of the FFDDM acquisition computer. Figure 9 shows a $4\,K \times 5\,K \times 12$ bit digital mammogram obtained with the system shown in Fig. 8. A screening mammography examination requires four images, two for each breast, producing a total of 160 Mbytes of image data.

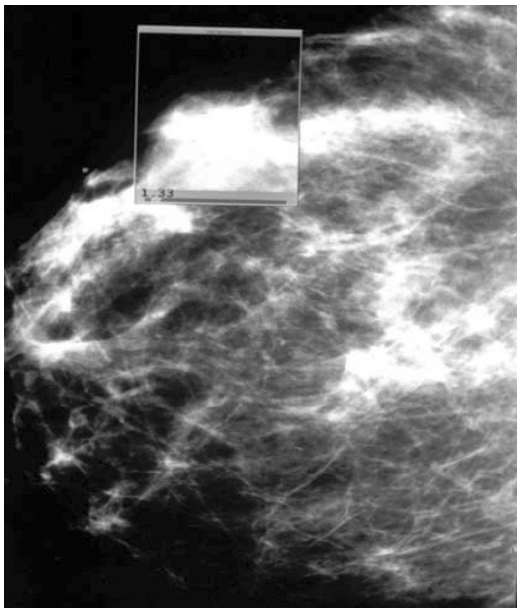

Fig. 9 A $4\,K \times 5\,K \times 12$ bit digital mammogram obtained with the slot-scanning FFDDM shown on a $2\,K \times 2.5\,K$ monitor. The window at the upper part of the image is the magnified glass showing a true $4\,K \times 5\,K$ region (courtesy of Drs E Sickles and SL Lou).

DIGITAL RADIOGRAPHY

During the past five years, research laboratories and manufacturers have devoted tremendous energy and resources investigating new digital radiography systems other than CR. The main emphases are to improve the image quality and operation efficiency, and to reduce the cost of projection radiography examination. Digital radiography (DR) is an ideal candidate. In order to compete with conventional screen/film and CR, a good DR system should:

- Have a high detector quantum efficiency (DQE) detector with 2–3 or higher line pair/mm spatial resolution, and a higher signal to noise ratio;
- Produce digital images of high quality;
- Deliver low dosage to patients;
- Produce the digital image within seconds after X-ray exposure;
- Comply with industrial standards;
- Have an open architecture for connectivity;
- Be easy to operate;
- Be compact in size; and
- Offer competitive cost savings.

Depending on the method used for the X-ray photon conversion, DR can be categorized into direct and indirect image capture methods. In indirect image capture, attenuated X-ray photons are first converted to light photons by the phosphor or the scintillator, from which the light photons are converted to electronic signals to form the DR image. The direct image capture method generates a digital image without going through the light photon conversion process. Figure 10 shows the difference between the direct and the indirect digital capture method. The advantage of the direct image capture method is that it eliminates the intermediate step of light photon conversion. The disadvantages are that the engineering involved in direct digital capture is more elaborate, and that it is inherently difficult to use the detector for dynamic image acquisition due to the necessity of recharging the detector after each read out. The

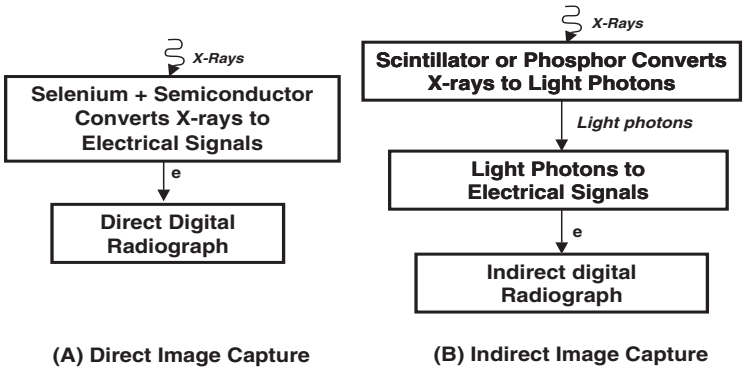

Fig. 10 Direct and indirect image capture methods in digital radiography.

indirect capture method uses either the amorphous silicon phosphor or scintillator panels. The direct capture method uses the amorphous selenium panel. It appears that the direct capture method has the advantage over the indirect capture method since it eliminates the intermediate step of light photon conversion.

Two prevailing scanning modes in digital radiography are slot and areal scanning. The digital mammography system discussed in the last section uses the slot-scanning method. Current technology for areal detection mode uses the flat-panel sensors. The flat-panel can be one large or several smaller panels put together. The areal scan method has the advantage of being fast in image capture, but it also has two disadvantages, one being the high X-ray scattering. The second is the manufacturing of the large flat panels is technically difficult.

Digital radiography (DR) design is flexible which can be used as an add-on unit in a typical radiography room or a dedicated system. In the dedicated system, some design can be used both as a table top unit attached to a C-arm radiographic device or as an upright unit shown in Fig. 11. Figure 12 illustrates the formation of a DR image, comparing it with Fig. 4 on that of a CR image. A typical DR unit produces a $2\,000 \times 2\,500 \times 12$ bit image instantaneously after the exposure.

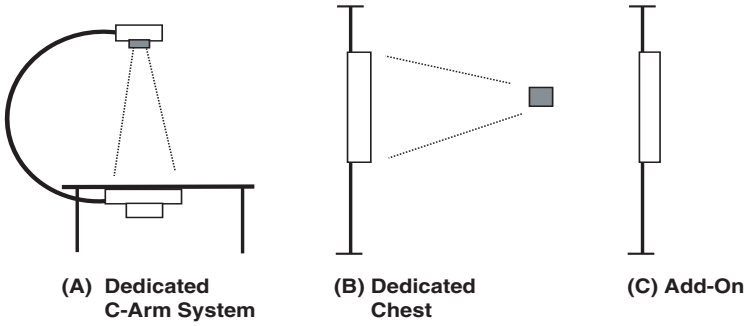

Fig. 11 Three configurations of digital radiography design.

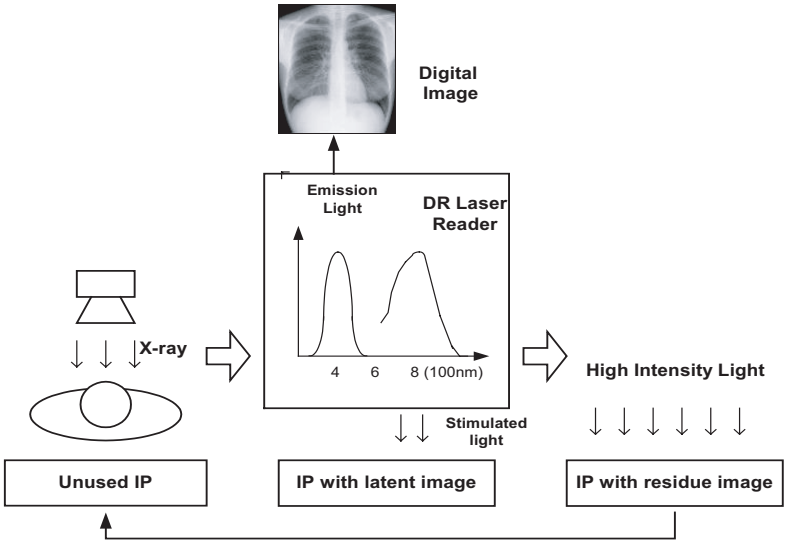

Fig. 12 Steps in the formation of a DR image, comparing it with that of a CR image shown in Fig. 4.

X-RAY CT AND MULTISLICE CT

Image Reconstruction from Projections

Since most sectional images, like CT, are generated based on image reconstruction from projections, we first summarize the Fourier projection theorem, the algebraic reconstruction, and the filtered back-projection method before the discussion of imaging modalities.

The Fourier Projection Theorem

Let $f(x, y)$ be a 2D cross-sectional image of a three-dimensional object. The image reconstruction theorem states that $f(x, y)$ can be reconstructed from the cross-sectional one-dimensional projections. In general, 180 different projections in one degree increments are necessary to produce a satisfactory image, and using more projections always result in a better reconstructed image.

Mathematically, the image reconstruction theorem can be described with the help of the Fourier transform (FT). Let $f(x, y)$ represent the two-dimensional image to be reconstructed and let p(x) be the one-dimensional projection of $f(x, y)$ onto the horizontal axis, which can be measured experimentally (see Fig. 13, the zero degree projection). In the case of X-ray CT, we can consider p(x) as the total linear attenuation of tissues transverses by a collimated X-ray beam at location x.

Then

$$p(x, 0) = \int_{-\infty}^{+\infty} f(x, y)\mathrm{dy} \tag{1}$$

The 1-D Fourier transform of p(x) has the form

$$P(u) = \int_{-\infty}^{+\infty} \left(\int_{-\infty}^{+\infty} f(x, y)\mathrm{dy} \right) \exp\left(-\mathrm{i}2\pi ux \right) \mathrm{dx} \tag{2}$$

Equations (3.1) and (3.2) imply that the 1D Fourier transform of a one-dimensional projection of a two-dimensional image is identical to the corresponding central section of the two-dimensional Fourier transform of the object. For example, the two-dimensional image can be a transverse (cross) sectional X-ray image of the body, and

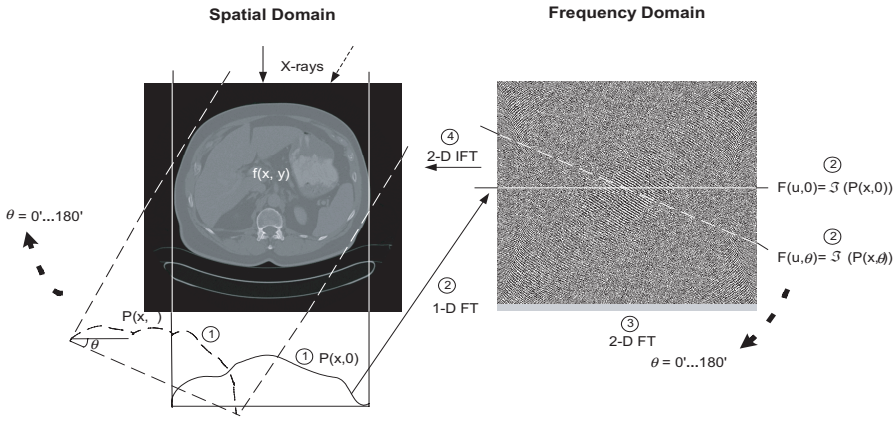

Fig. 13 Principle of the Fourier projection theorem for image reconstruction from projections. F(0,0) is at the center of the 2D FT, low frequency components are represented at the center region. The numerals represent the steps described in the text.
P(x, θ): X-rays projection at angle θ
F(u, θ): 1D Fourier transform of p(x, θ)
IFT: Inverse Fourier transform

the one-dimensional projections can be the X-ray attenuation profiles (projection) of the same section obtained from a linear X-ray scan at certain angles. If 180 projections at one degree increments are accumulated and their 1D FTs performed, each of these 180 1D Fourier transform represents a corresponding central line of the two-dimensional Fourier transform of the X-ray cross-sectional image. The collection of all these 180 1D Fourier transform is the 2D Fourier transform of $f(x, y)$.

The steps of a 2D image reconstruction from its 1D projections shown in Fig. 13 are as follows:

(1) Obtain 180 1D projections of $f(x, y)$, $p(x, \theta)$ where $\theta = 1, \ldots, 180$.
(2) Perform the FT on each 1D projection.
(3) Arrange all these 1D FTs according to their corresponding angles in the frequency domain. The result is the 2D FT of $f(x, y)$.
(4) Perform the inverse 2D FT of (3), which gives $f(x, y)$.

The Fourier projection theorem forms the basis of tomographic image reconstruction. Other methods that can also be used to reconstruct a 2D image from its projections are discussed later in this chapter. We emphasize that the reconstructed image from projections is not always exact; it is only an approximation of the original image. A different reconstruction method will give a slightly different version of the original image. Since all these methods require extensive computation, specially designed image reconstruction hardware is normally used to implement the algorithm. The term "computerized (computed) tomography" (CT) is often used to represent that the image is obtained from its projections using a reconstruction method. If the 1D projections are obtained from X-ray transmission (attenuation) profiles, the procedure is called XCT or X-ray CT. In the following sections, we summarize the algebraic and filtered back-projection methods with simple numerical examples.

The Algebraic Reconstruction Method

The algebraic reconstruction method is often used for the reconstruction of images from an incomplete number of projections (i.e. $<180°$). The result is an exact reconstruction (a pure chance) of the original image f(x,y). For a 512×512 image, it will require over 180 projections, each with sufficient data points in the projection, to render a good quality image.

The Filtered (Convolution) Back-Projection Method

The filtered back-projection method requires two components, the back-projection algorithm, and the selection of a filter to modify the projection data. The selection of a proper filter for a given anatomical region is the key in obtaining a good reconstruction from filtered (convolution) back-projection method. This is the method of choice for almost all XCT scanners. The result of this method, is an exact reconstruction (again, by pure chance) of the original $f(x, y)$. The mathematical formulation of the filtered back-projection method is

given in Eq. (3):

$$f(x, y) = \int_0^{\pi} h(t)^* m(t, \theta) \mathrm{d}\theta, \tag{3}$$

where $m(t, \theta)$ is the "t" sampling point at "θ" angle projection, h(t) is the filtered function, and "*" is the convolution operator.

Transmission X-ray Computed Tomography (XCT)

Conventional XCT

A CT scanner consists of a scanning gantry housing an X-ray tube and a detector unit, and a movable bed which can align a specific cross section of the patient with the gantry. The gantry provides a fixed relative position between the X-ray tube and the detector unit. A scanning mode is the procedure of collecting X-ray attenuation profiles (projections) from a transverse (cross) section of the body. From these projections, the CT scanner's computer program or back-projector hardware reconstructs the corresponding cross-sectional image of the body. Figures 14 and 15 show the schematic of two most popular XCT scanners (third and fourth generations), both using an X-ray fan beam. These types of XCT take about 5 seconds for one sectional scan, and more time for image reconstruction.

Spiral (Helical) XCT

Three other configurations can improve the scanning speed: the helical (spiral) CT, the cine CT (Sec. 3.6.2.3), and the multislice CT (Sec. 3.6.2.4). The helical CT is based on the design of the third-, or the fourth-generation scanner, the cine CT uses a scanning electron beam X-ray tube, and multi-slice CT uses a cone beam instead of a fan beam.

The CT configurations shown in Figs. 14 and 15 have one common characteristic: the patient's bed remains stationary during the scanning; after a complete scan, the patient's bed advances a certain distance and the second scan resumes. The start-and-stop motions of the bed slow down the scanning operation. If the patient's

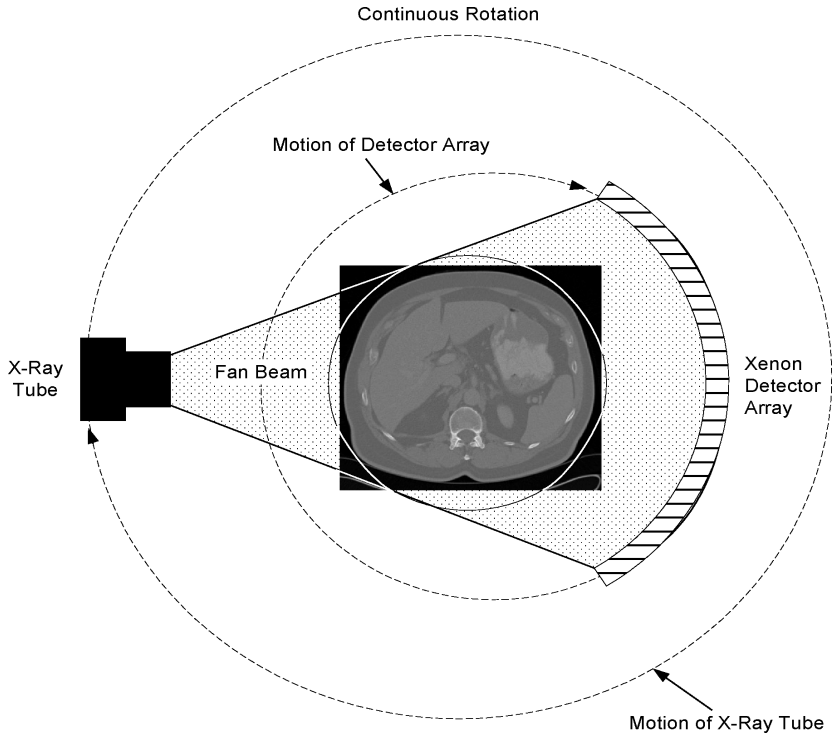

Fig. 14 Schematic of the rotation scanning mode using a fan-beam X-ray. The detector array rotates with the X-ray tube as a unit.

bed can assume a forward motion at a constant speed while the scanning gantry rotated continuously, the total scanning time of a multiple section examination could be reduced. Such a configuration is not possible, however, because the scanning gantry is connected to the external high energy transformer and power supply is through the cables. The spiral or helical CT design does not involve cables.

Figure 16 illustrates the principle of spiral CT. There are two possible scanning modes: single helical and cluster helical. In the single helical mode, the bed advances linearly while the gantry rotates in sync for a period of time, say 30 seconds. In the cluster helical

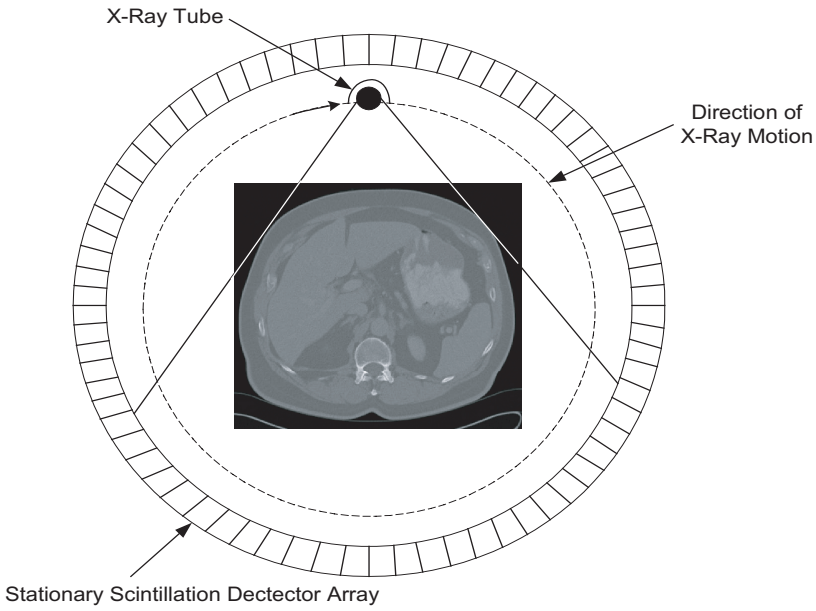

Fig. 15 Schematic of the rotation scanning mode with a stationary scintillation detector array, only X-ray source rotates.

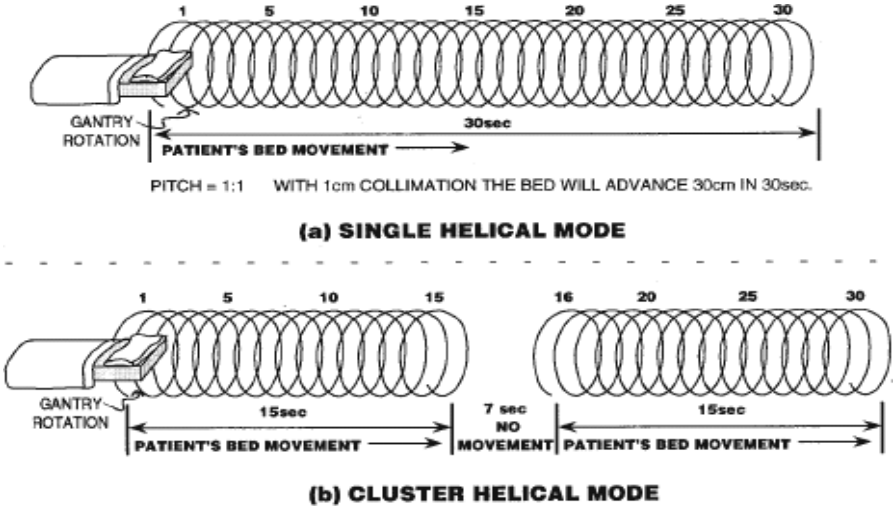

Fig. 16 Helical (spiral) CT scanning modes.

mode, the simultaneous rotation and translation lasts only 15 seconds, whereupon both motions stop for 7 seconds before resuming again. The single helical mode is used for patients who can hold their breath for a longer period of time, while the cluster helical mode is for patients who need to take a breath after 15 seconds.

The design of the helical XCT introduced in the late 1980s. It is based on three technological advances: the slip-ring gantry, improved detector efficiency, and greater X-ray tube cooling capability. The slip-ring gantry contains a set of rings and electrical components that rotate, slide and make contact to generate both high energy (to supply the X-ray tube and generator) and standard energy (to supply powers to other electrical and computer components). For this reason, no electrical cables are necessary to connect the gantry and external components. During the helical scanning, the term "pitch" is used to define the relationship between the X-ray beam collimation and the velocity of the bed movement.

Pitch = Table movement in mm per gantry rotation/slice thickness.

Thus, a pitch equals to "1" means that the gantry rotates a complete 360° as the bed advances 1.5 mm in one second which gives a slice thickness of 1.5 mm. During this time, raw data is collected covering 360 degrees and 1.5 mm. Assuming one rotation takes one second, then for the single helical scan mode, 30 seconds of raw data are continuously collected while the bed moves 45 mm. After the data collection phase, the raw data are interpolated and/or extrapolated to sectional projections. These organized projections are used to reconstruct individual sectional images. In this case, they are 1.5 mm contiguous slices. Reconstruction slice thickness can be from 1.5 mm to 1 cm, depending on the interpolation and extrapolation methods used.

The advantages of the spiral CT scans are speed of scanning, allowing the user to select slices from continuous data to reconstruct slices with peak contrast medium, retrospective creation of overlapping or thin slices, and volumetric data collection. The disadvantages are the helical reconstruction artifacts and potential object boundary unsharpness.

Cine XCT

Cine XCT, introduced in early 1980s, uses a completely different X-ray technology, namely, an electron beam X-ray tube: this scanner is fast enough to capture the motion of the heart. The detector array of the system is based on the fourth-generation stationary detector array (scintillator and photodiode). As shown schematically in Fig. 17, an electron beam (1) is accelerated through the X-ray tube and bent by the deflection coil (2) toward one of the four target rings (3). Collimators at the exit of the tube restrict the X-ray beam to a 30° fan beam, which forms the energy source of scanning. Since there are four tungsten target rings, each of which has a fairly large area (210° tungsten, 90 cm radius) for heat dissipation, the X-ray fan beam can sustain the energy level required for scanning continuously for various scanning modes. In addition, the detector and data collection technologies used in this system allow very rapid data acquisition. Two detector rings (indicated by 4 in Fig. 17) allow data acquisition for two consecutive sections simultaneously. For example, in the slow acquisition mode with a 100 ms scanning time, and a 8 ms interscan delay, cine XCT can provide 9 scans/s, or in the fast acquisition mode with a 20 ms scanning time, 34 scans/s.

The scanning can be done continuously on the same body section (to collect dynamic motion data of the section) or along the axis of the patient (to observe the vascular motion). Because of its fast scanning speed, cine XCT is used for cardiac motion and vascular studies and

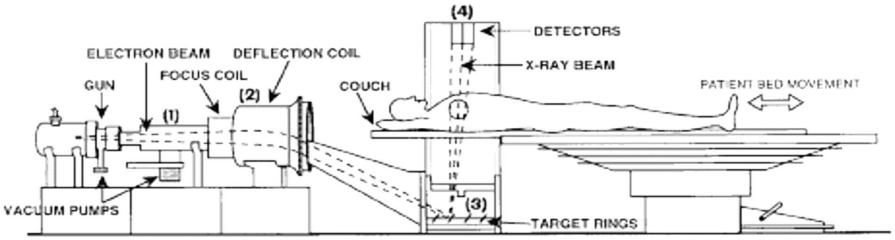

Fig. 17 Schematic of the cine XCT. Source: Diagram adapted from a technical brochure of Imatron Inc.

emergency room scans. Until the availability of the multislice XCT, cine XCT is the fast scanner for dynamic studies.

Multislice XCT

In spiral XCT, the patient's bed moves during scan, but the X-ray beam is a fan beam perpendicular to the patient axis, and the detector system is built to collect data for the reconstruction of one slice. If the X-ray beam is shaped to a three-dimensional cone beam with the z-axis parallel to the patient's axis, and if a multiple detector array (in the z-direction) system is used to collect the data, then we have a multislice XCT scanner (see Fig. 18). Multislice XCT, in essence, is also spiral scan except that the X-ray beam is shaped to a cone beam geometry. Multislice XCT can obtain many images in one examination with a very rapid acquisition time, for example, 160 images in 20 seconds, or 8 images/sec, or 4 MB/sec of raw data. Figure 18 shows the schematic. It is seen from this figure that a full rotation of the cone beam is necessary to collect sufficient projection data to reconstruct the number of slides equal to the z-axis collimation of the detector system (see below for definition). Multislice XCT uses several new technologies:

(1) New detector: Ceramic type detector is used to replace traditional crystal technology. Ceramic detector has the advantages of more light photons in the output, less afterglow time, higher resistance to radiation and mechanical damage, and can be shaped much thinner (1/2) for equivalent amount of X-ray absorption, compared with the crystal scintillators.
(2) Real-time dose modulation: A method to minimize dose delivered to the patient using the cone beam geometry by modulating the mAs (milliampere-seconds) of the X-rays beam during the scan.
(3) Cone beam geometry image reconstruction algorithm: Efficient collection and recombination of cone beam X-ray projections (raw data) for sectional reconstruction.

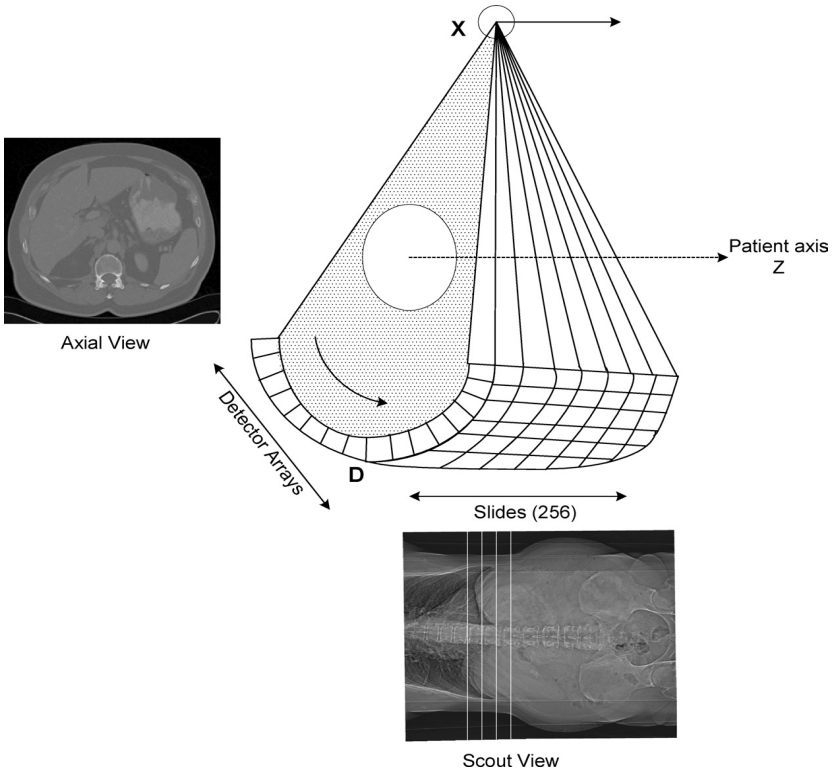

Fig. 18 Geometry of the multislice XCT. The patient axis is in the z-direction. The X-rays (X) shaped as a collimated cone beam rotates around the z-axis 360° in sync continuously with the patient's bed moving linearly in z-direction. The detector system (D) is a combination of detector arrays shaped in a concave surface facing the X-ray beam. The number of slices per 360° rotation are determined by two factors: the number of detector arrays in the z-direction, and the method used to recombine the cone beam projection data into transverse sectional projections (Fig. 13). The reconstructed images are transverse view perpendicular to the z-axis. If the cone beam does not rotate while the patient's bed is moving, the reconstructed image is equivalent to a digital fluorographic image.

(4) High speed data output channel: During one examination, say, for 160 images, much more data have to be collected during the scanning. Fast I/O data channels from the detector system to image reconstruction are necessary.

If the patient bed is moving linearly, but the gantry does not rotate, the result is a digital fluorographic image with better image quality than that discussed in Sec. 3.2. Currently, 16-slice and 32-slice detector CT scanners are in heavy clinical use with the 64, 128, and 256-slice detector CT scanners on the near horizon. Figure 19 shows a 3D rendered volume image of acquisition data from a 64-slice detector CT scan of a human heart. With the advent of the 256-slice detector CT scanner, it will be feasible to acquire image data for an entire organ such as the heart in a single scan cycle as shown in the figure.

Some standard terminology used in multi-slice XCT

Recall the term "pitch" defined in spiral XCT, with cone beam-multidetector scanning, because of the multi-detector arrays in the z-direction (Fig. 18) the table movement can be many times the thickness of an individual slice. For example, take a 16 mm × 1.5 mm detector system (16 arrays with 1.5 mm thickness per array), and

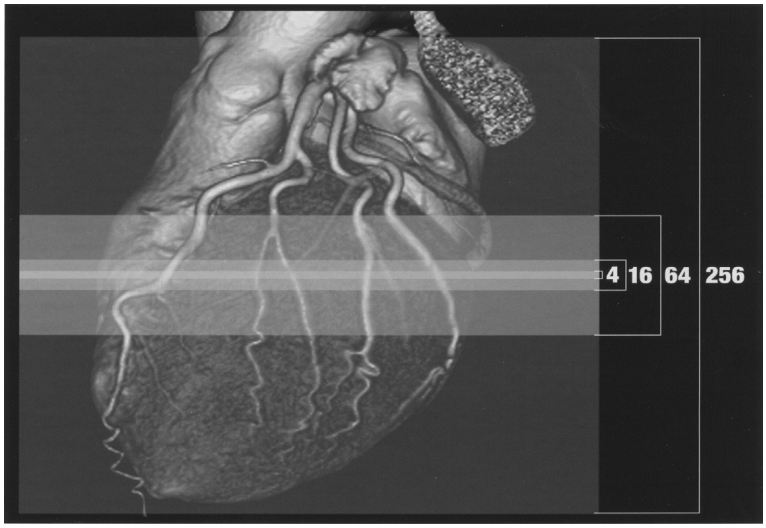

Fig. 19 A 3D volume rendered image of the heart from data acquired by a 64-slice CT scanner. Note that a 256-slice CT scanner would be able to scan the entire heart in one single rotation (courtesy of Toshiba Medical Systems).

with the slice thickness of an individual image being 1.5 mm, then use the definition of "pitch" in spiral scan:

$$\text{Pitch} = \text{Table movement in mm per gantry rotation/Slice thickness} = 16$$
$$= (16 \times 1.5\,\text{mm/rotation})/1.5\,\text{mm} = (24\,\text{mm/rotation})/1.5\,\text{mm}.$$

That means the table moves 24 mm/rotation with a reconstructed slice thickness of 1.5 mm would have a pitch of 16. (Sec. 3.6.2.2) This case also represents contiguous scans. Comparing this example with that shown in Section 3.6.2.2 for single slice scan, the definition of "pitch" shows some discrepancy due to the size of the multidetector arrays. Since different manufacturers produce different sizes of multidetector arrays, the word "pitch" becomes confusing. For this reason, the international electrotechnical commission (IEC) accepts the following definition of pitch (now often referred to as the IEC pitch):

z-axis collimation (T) = the width of the tomographic section along the z-axis imaged by one data channel (array). In multidetector row (multislice) CT scanners, several detector elements may be grouped together to form one data channel (array).

Number of data channels (N) = the number of tomographic sections imaged in a single axial scan.

Table Speed or Increment (I) = the table increment per axial scan or the table increment per rotation of the X-ray tube in a helical (spiral) scan.

Pitch (P) = Table speed (I mm/rotation)/(N · T)

Thus, for a 16 detector scanner in a 16 × 1.5 mm scan mode, N = 16 and T = 1.5 mm, and if the table speed = 24 mm/rotation, then P = 1, a contiguous scan. If the table speed is 36 mm/rotation, then the pitch is 36/(16*1.5) = 1.5.

Four-Dimensional (4D) XCT

Refer to Fig. 17, with the bed stationary, but the gantry continuously rotates, we would have a four-dimensional XCT, with the fourth

dimension as time. In this scanning mode, human body physiological dynamic can be visualized in 3D. Current multislice XCT with a limited size of detector arrays in z-direction, and data collection system of 100 MB/sec can only visualize a limited segment of the body. In order to realize the potential clinical applications of 4D XCT, several challenges are in order:

(1) Extend the cone beam X-ray and the length of the detector array in the z-direction. Currently, detector system with 256 arrays with 912 detectors per array is available in some prototype 4D XCT systems.
(2) Improve the efficiency and performance of the A/D conversion at the detector.
(3) Increase the data transfer rate between the data acquisition system to the display system from the 100 MB/sec to 1 GB/sec.
(4) Revolutionize display method for 4D images.

4D XCT can produce images of gigabyte range per examination. Methods of archive, communication, and display become challenging issues.

PET/XCT Fusion Scanner

XCT is excellent for anatomical delineation with fast scanning time, while positron emission tomography (PET) is slow in obtaining physiological images of poorer resolution, but good for the differentiation between benign and malignant tumors. PET requires attenuation correction in image reconstruction, and the fast CT scan time can provide the anatomical tissue attenuation in seconds which can be used as a base for PET data correction. Thus, the combination of a CT and a PET scanner during a scan would give a very powerful tool for improving the clinical diagnostic accuracy when neither alone would be able to provide such result. Yet, the two scanners have to be combined as one system otherwise the misregistration between CT and PET images would sometimes give misinformation. CT/PET Fusion scanner is such a hybrid scanner which can

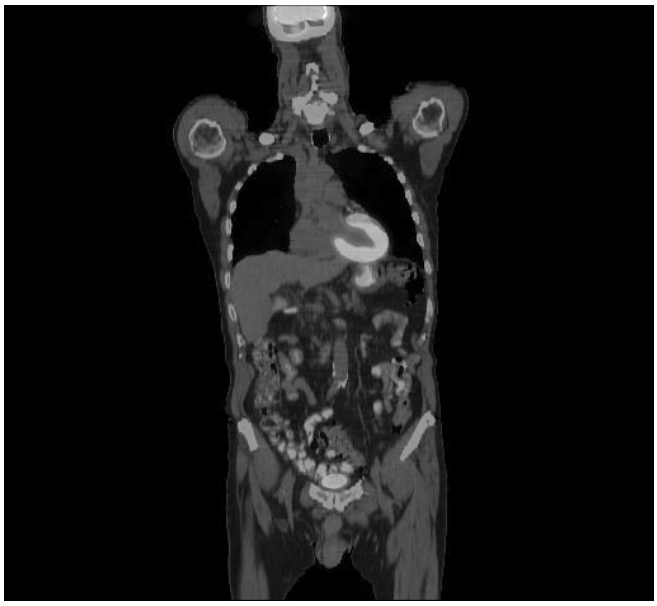

Fig. 20 Reconstructed image showing fusion of both CT image data and positron emission tomography (PET) image data into a single image. Note that PET image data shows physiological function while the CT image data shows the anatomical features. Tools allow the user to dynamically change how much PET or CT data is displayed in the fused image. Note the areas in the body such as the heart with high activity signal from the acquired PET data.

obtain the CT images as well as PET images during an examination. The PET images so obtained actually have better resolution than that without using the CT attenuation correction. The output of a PET/CT fusion scanner is two sets of images, CT and PET with the same coordinate system for easy fusing of the images together. Figure 20 shows an example of CT/PET fused image data set showing both anatomical as well as physiological function.

Components and Data Flow of an XCT Scanner

The major components and data flow of an XCT include a gantry housing the X-ray tube, the detector system, and signal processing/conditioning circuits; a front-end preprocessor unit for

cone/fan beam projection data corrections and recombination to transverse sectional projection data; a high-speed computational processor; a hardware back-projector unit; and a video controller for displaying images. In XCT, its CT number, or pixel/voxel value, or Hounsfield number, represents the relative X-ray attenuation coefficient of the tissue in the pixel/voxel, is defined as follows:

$$\text{CT number} = \text{K}(\mu - \mu_{\text{w}})/\mu_{\text{w}},$$

where μ is the attenuation coefficient of the material under consideration, μ_{w} is the attenuation coefficient of water, and K is a constant set by the manufacturer.

XCT Image Data

Slice Thickness

Current multislice CT scanners can feature up to 32 detectors in an array. In a spiral scan, multiple slices of data can be acquired simultaneously for different detector sizes, and 0.75 mm, 1 mm, 2 mm, 3 mm, 4 mm, 5 mm, 6 mm, 7 mm, 8 mm, and 10 mm slice thickness can be reconstructed.

Image Data Size

A standard Chest CT of coverage size between 300 mm–400 mm can yield image sets from 150–200 images all the way up to 600–800 images depending on the slice thickness, or data sizes from 75 MB up to 400 MB. Performance-wise, that same standard chest CT can be acquired in 0.75 mm slices in 10 seconds. A whole body CT can produce up to 2 500 images or 1 250 MB (1.25 GB) of data. Each image is $512 \times 512 \times 2$ byte size.

Data Flow/Post-Processing

The fan/cone beam raw data are obtained by the acquisition host computer. Slice thickness reconstructions are performed on the raw

data. Once the set of images is acquired in DICOM format, any post-processing is performed on the DICOM data. This includes sagittal, coronal, and off-axis slice reformats as well as 3D post processing. Sometimes the cone beam raw data are saved for future reconstruction of different slice thicknesses.

Some newer scanners feature a secondary computer, which shares the same database as the acquisition host computer. This secondary computer can perform the same post-processing functions while the scanner is acquiring new patient data. This secondary computer also can perform network send jobs to data storage or another DICOM destination (e.g. highly specialized 3D processing workstation) and maintains a send queue, thus alleviating the acquisition host computer from these functions and improving system throughput.

References

1. Cao X, **Huang HK**, Current status and future advances of digital radiography and PACS, *IEEE Eng Med & Bio*, **19**(5), 80–88, 2000.
2. Feldkamp LA, Davis, LC, Kress JW, Practical cone-beam algorithm, *J Optical Society Amer A*, **1**, 612–619, 1984.
3. Huang HK, *PACS and Imaging Informatics: Basic Principles and Applications*, Wiley & Sons, NY, 2004.
4. Stahl JN, Zhang J, Chou TM, Zellner C, Pomerantsev EV, Huang HK, A new approach to tele-conferencing with intravascular ultrasound and cardiac angiography in a low-bandwidth environment, *RadioGraphics*, **20**, 1495–1503, 2000.
5. Taguchi K, Aradate H, Algorithm for image reconstruction in multislice helical CT, *Medical Physics* **25**(4), 550–561, 1998.

Lossless Digital Signature Embedding Methods for Assuring 2-D and 3-D Medical Image Integrity*

Zheng Zhou, H.K. Huang, Brent J. Liu

Image Processing and Informatics Laboratory (IPI), Departments of Radiology and Biomedical Engineering, University of Southern California,
hkhuang@aol.com

* Will appear in "Principles and Recent Advances in Medical Imaging and Image Analysis", AP Dhawan, HK Huang, and DS Kim, Ed., Chapter 22. World Scientific Publications, Singapore**.**

Keywords: image security, image integrity, lossless embedding, digital signature, 2-D medical image, 3-D medical image.

Abstract

Medical image integrity, which assures that the original image is not accidentally or deliberately modified by unauthorized person, has become critical when medical images are stored in an archive or transmitted over public networks. A two-dimensional (2-D) lossless digital signature embedding (LDSE) method has been developed for assuring the image integrity by permanently embedding the digital signature (DS) of an image into image pixels. Experimental results show that the 2-D LDSE method is effective for assuring image integrity. With the advent of multi-detectors and volume acquisition technologies, a CT, MR, or US examination can generate hundreds to thousands of three-dimensional (3-D) volumetric image sets, further aggregating the importance of the individual image as well as the 3-D volume integrity. The 2-D LDSE method or other security technology such as DICOM transport layer security (TLS) is not effective and efficient for assuring the integrity of 3-D image volumes. A novel 3-D LDSE method has been developed for assuring the integrity of large 3-D image volumes. Experimental results with various 3-D medical images demonstrate that the method is effective and efficient for assuring the integrity of 3-D volumetric images both for archive and during transmission. In order to apply the 2-D and 3-D LDSE methods to clinical diagnostic workflow, the integration of the LDSE methods with a PACS has been developed. The 3-D LDSE method has also been integrated with two relevant IHE (Integrating the Healthcare Enterprise) Profiles, Key Image Note Profile and Post-Processing Workflow Profile, accordingly.

1. Introduction

Image security is a critical issue when medical images with pertinent patient information are transmitted over public networks [1]-[3]. With integrated medical imaging systems being extensively used in clinics for healthcare delivery, image security consideration is no longer limited to images in transit but also in storage. Generally, medical image security can be characterized by three major issues: privacy (or confidentiality), authenticity, and integrity [4]. Privacy seeks to protect image data from being accessible or disclosed to unauthorized individuals. Authenticity verifies that the source of an image is what it claims to be. Integrity assures that image data is not altered, destroyed, or deleted by unauthorized person.

With current information technology and knowledge of its use, it is easy to alter a medical image without detection when the image is in transit or in storage. The consequence of such alteration could influence the intended objectives, behavior, and functionalities of healthcare services, and even worse, could cause legal problems [5], [6]. For these reasons, image integrity is one of the most paramount concerns of current clinical imaging systems. Traditional methods, such as encryption, firewall, virtual private network, and access control by user password, have been used to protect the privacy and authenticity of image data. These methods, however, are not effective for assuring the image integrity, because the image can

still be altered or destroyed by an intruder who does not need to have the knowledge of the content of the image.

A lossless digital signature embedding (LDSE) [7] method has been developed for assuring the integrity of two-dimensional (2-D) medical images in transit and in storage. Experimental results show that the method is effective in the assurance of 2-D medical image integrity. With the advent of multi-detectors and volume acquisition technologies, a CT, MR or US examination can generate various three-dimensional (3-D) volumetric image sets consisting of hundreds or even thousands of images. To perform conventional DICOM TLS [8], SSL [9], or the 2-D LDSE methods on each individual image in the volume would be time consuming and inefficient. In order to overcome these, a novel 3-D LDSE method has also been developed for assuring the integrity of 3-D medical images.

2. Procedures and Methods

The goal of LDSE is to provide robust integrity assurance to medical images in various application environments. In pursuing this goal, it is important to permanently embed the digital signature (DS) in the image pixels. A permanently embedded DS would provide image integrity assurance for medical images during their lifetime.

2.1. General LDSE Method

The LDSE method consists of two processes (Figure 1):

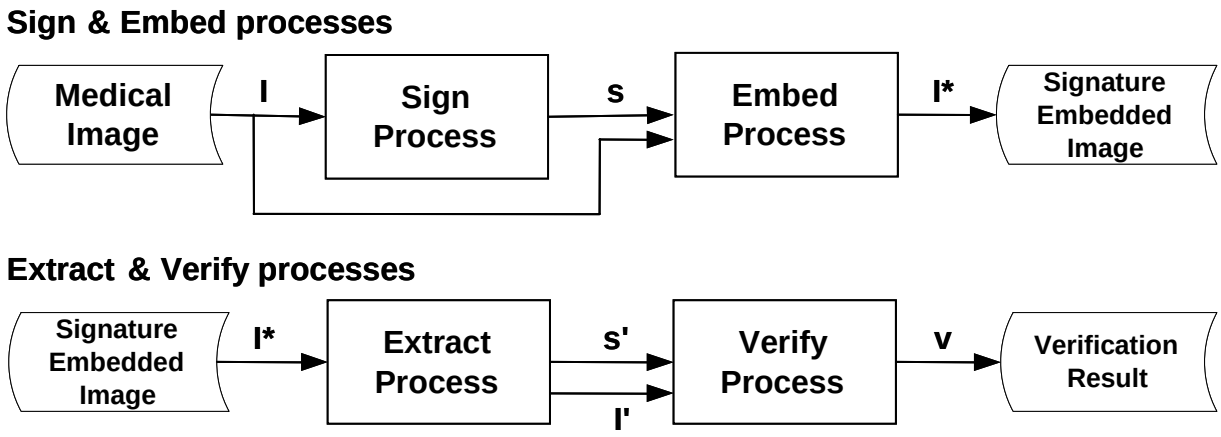

Figure 1 Data flow of Sign & Embed, and Extract & Verify processes in the LDSE method. I: original image, s: signature of the original image I*: signature embedded image, s': recovered signature, I': recovered image, v: verification result.

1) Sign & Embed Processes

a. Generate the DS of the image pixels with the image owner's private key

$$s = S_{k,\,priv}(I) \qquad (1)$$

where *s* is the digital signature (DS) of the image, S denotes the signature signing process[1], k,priv is the owner's private key, and *I* is the image.

b. Embed the bit stream of DS into the image pixels using lossless data embedding approaches

$$I^* = I \oplus s \qquad (2)$$

where *I** is the signature embedded image, $\oplus$ denotes the lossless data embedding process, and *s* is the DS.

2) Extract & Verify processes

a. Extract the DS from the signature embedded image and recover the image from the embedding process

[1] Signature signing process begins by computing a hash value of all pixels of the image using cryptographic hash functions (e.g., SHA1) and follows by encrypting the hash value with public key encryption method.

$$(s, I') = \Theta I^* \quad (3)$$

where *s* is the DS, I' is the recovered image, Θ denotes the data extraction process, *I** is the signature embedded image.

b. Verify the extracted DS with the owner's public key

$$v = \mathrm{V}_{\mathrm{k,\,pub}}(I', s) \quad (4)$$

where *v* is the verification result, V denotes the signature verification process[2], k,pub is the owner's public key, I' is the recovered image, and *s* is the DS of *I*. If the verification result is true, which means the image has not been altered, the image integrity is assured. If the verification is false, the image has been altered.

2.2. 2-D LDSERS Algorithm [10], [11]

1) Algorithm Definition: Consider the original N x M medical image with pixel values in the set P = {0, …, 4095, or higher}. The algorithm starts by dividing the original image into disjoint groups of n adjacent horizontal pixels (p_1, …, p_n) (e.g., (p_1, …, p_4), where p stands for the value of pixel and n is an integer greater than 1. A discrimination function '*f*', defined in (5), computes the correlation coefficients of each pixel group G = (p_1, …, p_n). The function '*f*' converts the vector G into a number *f* (G).

$$f(\mathrm{G}) = \sum_{1}^{n-1} | p_{i+1} - p_i | \quad (5)$$

An invertible operation F on G called "flipping" is also defined. Flipping of a given bit in a pixel is defined as "0" $\rightarrow$ "1" or "1" $\rightarrow$ "0". The flipping would change the value of pixel and the value change would depend on the bit locations in the pixel. Appendix I describes the flipping operation in more detail. F has the property that $\mathrm{F}(\mathrm{F}(p)) = p$ for all *p* in G. Thus, there are three possibilities if *f*(F(G)) is compared to *f*(G). These three possibilities are defined as three groups: R, S and U.

Regular (R) group: if $f(\mathrm{F}(\mathrm{G})) > f(\mathrm{G})$

Singular (S) group: if $f(\mathrm{F}(\mathrm{G})) < f(\mathrm{G})$

Unusable (U) group: if $f(\mathrm{F}(\mathrm{G})) = f(\mathrm{G})$

A new grouped image is formed with these three possible states in the selected bit plane.

2) *Embedding (Figure 2):* the embedding starts with the scanning of image pixels to find R and S groups. The U groups are skipped during scanning. For n = 4, G = (p_1, …, p_4), our experimental results with the current medical images used in clinical practice show that $f(\mathrm{F}(\mathrm{G})) > f(\mathrm{G})$ after the flipping operation F. This is because F makes G less correlated, where the adjacent pixels are usually correlated. The relationship of the four pixels in every found group can be converted to an "R" (R group) or "S" (S group) symbol. As a result, an "R" and "S" sequence of the image is formed. One bit is assigned to every "R" or "S" symbol in this sequence and the value in this bit would be "1" for "R" and "0" for "S". Thus, the "R" and "S" sequence is converted to a bit stream of 1s and 0s, which is called an "RS bit stream". The RS bit stream is then losslessly compressed using adaptive arithmetic coding [12]. The RS bit stream extraction and compression processes are complete until

$$l_{RS} - (l_{RScomp} + l_{DS}) \geq 0 \quad (6)$$

where l_{LSB} denotes the binary length of the RS bit stream, $l_{LSBcomp}$ denotes the binary length of the compressed RS bit stream, and l_{DS} denotes the binary length of the DS.

Afterward, the bit stream of DS is appended to the compressed RS bit stream to form a new bit stream. This new bit stream is then compared with the RS bit stream bit by bit. If there is no difference in the bit value, no change is made. If there is a difference, the corresponding group of pixels (R or S group) is flipped. After all the bits are compared, the embedding process is complete and the result is a signature embedded image.

Since the forming of R and S groups as well as the embedding are all reversible processes, the original image can be completely recovered after the DS is extracted. The extracting process starts with the same scanning to find R and S groups from the signature embedded image. As a result, the embedded bit

[2] Signature verification process begins by decrypting the DS to get the original hash value and then compares this hash value to a second hash value computed from the recovered image using the same hash function used in signing process.

stream is reconstructed from the R and S groups. The bit stream is then broken down into the compressed RS bit stream and the DS. The compressed RS bit stream is decompressed to recover the original R and S groups. The original R and S groups are compared to the extracted groups and the corresponding group of pixels is flipped if there is any difference. Since the flip operation is reversible, the original image pixels can be completely recovered. The recovered DS is verified with the restored image. If verification result is true, there is no alteration of the image and the image integrity is assured.
Figure 2 Embed the DS in an MR image using 2-D LDSERS. The U groups are not used. C1: counter 1 to record the length of the compressed RS bit stream. C2: counter 2 to record the length of the DS.

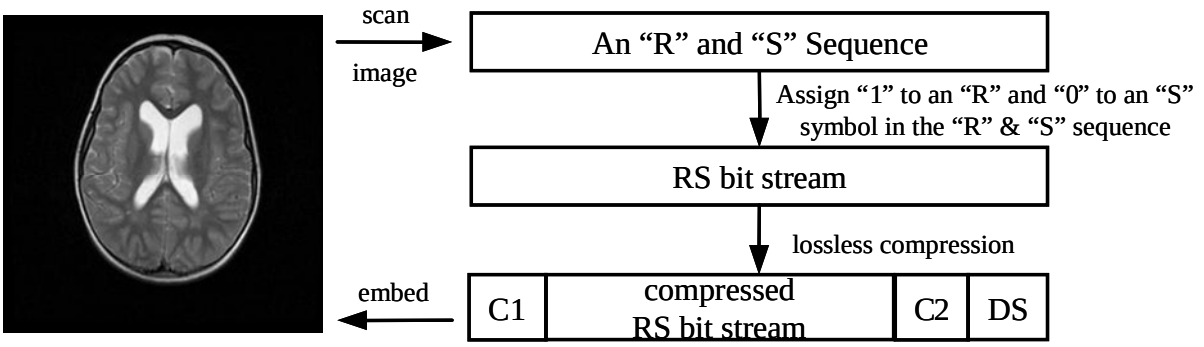

Figure 2 Embed the DS in an MR image using 2-D LDSERS. The U groups are not used. C1: counter 1 to record the length of the compressed RS bit stream. C2: counter 2 to record the length of the DS.

2.3 General 3-D LDSE Method

The general 3-D LDSE method consists of two processes: Signing & Embedding and Extracting & Verifying. A 3-D volume of a single CT series with *n* images is used as an example to illustrate the method in the following sections. If there are multiple series in an exam, the method can be applied to each series separately.

1) Signing & Embedding

In order to make it more difficult to extract the embedded digital signature, randomization is utilized to re-arrange the image order in the CT volume before actual embedding. The random order is generated based on a set of pseudo-random numbers r_k computed by the random number generator [13], [14]. After the re-arrangement, all the pixels are arranged into a pixel stream starting from the first pixel of the first image "1" to the last pixel of the last image "2" as shown in Figure 3. The n is the random order. A hash value is computed for all pixels in the pixel stream using cryptography hash functions such as SHA1 [15]. The hash value is then encrypted to form a digital signature (DS) of the whole volume using public-key encryption method such as RSA [16], [17]. Finally, the DS is embedded in pixels of all images within the volume using a lossless embedding algorithm. Since the images are still in random order, the DS is embedded according to this order. The result of embedding is a signature embedded image volume. After embedding, the images within the volume are re-arranged into the original order; therefore the LDSE method will not affect clinical data flow.
The embedding algorithm used in the 3-D LDSE method is different than the 2-D LDSE method in that it uses all images of the volume as a whole for embedding. In comparison, the 2-D method embeds the 2-D image signature in each individual image within the volume.

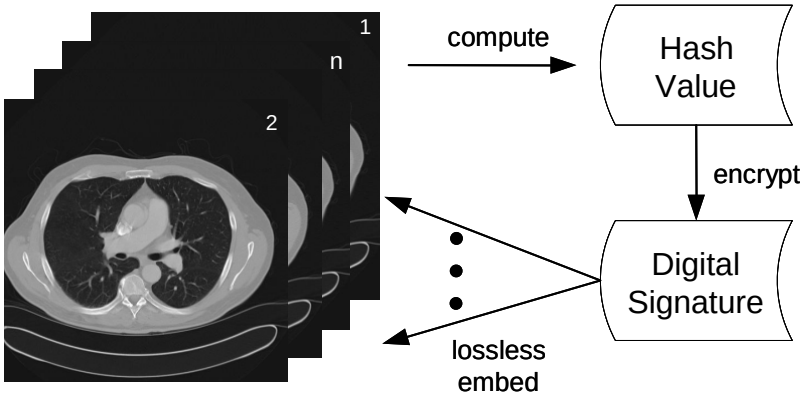

Figure 3 The general 3-D lossless digital signature embedding (LDSE) method. A single digital signature is generated for a CT volume for assuring the integrity of the volume. The original 3-D volume set with 1,…,n images has been randomized (1,n, …,2).

2) Extracting & Verifying

When extracting and verifying, the same random seed is used to reproduce the same random order in the signature embedded volume. Images in the 3-D volume are then re-arranged according to this random order. Since embedding is an invertible process, the DS can be extracted and the original volume can be completely recovered. The extracted DS is then decrypted and verified with the hash value computed from the recovered volume. The verified volume is re-arranged into the original order for clinical use.

7.3. 3-D LDSERS Algorithm

To embed a digital signature in a 3-D image volume is a complex problem. A 3-D LDSERS (Regular/Singular Groups) algorithm has been developed extended from 2-D LDSERS described in Section 7.2.

1) Embedding

The embedding starts by searching R and S groups in the images of the CT volume. A Z-shape walking pattern (Figure 4) is utilized to search the R and S groups, which consist of 4 voxels in each group, in the CT volume. Our experimental results showed that 4 works best for all tested image sets. A voxel is defined as $p_{x,y,z}$, where x represents the horizontal line (or row), y the vertical line (or column), and z the image number in the randomized volume. For example, $p_{1,1,1}$ represents the voxel in the first row and the first column of the first image. After the Z-shape walking, the extracted groups of voxels are ($p_{1,1,1}$, $p_{1,2,1}$, $p_{1,3,1}$, $p_{1,4,1}$), ($p_{1,1,n}$, $p_{1,2,n}$, $p_{1,3,n}$, $p_{1,4,n}$), ..., ($p_{1,1,2}$, $p_{1,2,2}$, $p_{1,3,2}$, $p_{1,4,2}$), ($p_{1,5,1}$, $p_{1,6,1}$, $p_{1,7,1}$, $p_{1,8,1}$), …. A discriminate function 'f' is defined for computing the correlation coefficients of the group of voxels.

$$f(p_{i,j,k},\ldots,p_{i,j+3,k}) = \sum_{j=1}^{3} | p_{i,j+1,k} - p_{i,j,k} | \qquad (7)$$

The R and S groups are found in the volume of randomized images and converted into an RS bit stream by applying (5) and the flipping operation F defined in 2-D LDSERS on the extracted groups obtained from the Z-shape walking. The RS bit steam is then lossless compressed. The walking and compress processes end until there is sufficient space, which can be estimated before hand from characteristics of the image volume, in the RS bit stream to embed the DS. The DS is converted to a DS bit stream, which is appended to the compressed RS bit stream to form a new bit stream. This new bit stream is then compared with the original RS bit stream bit by bit. If there is no difference in the bit value, no change is made. If there is a difference, the corresponding group of voxels (R or S group) is flipped. After all the bits are compared, the embedding process is complete and the result is a signature embedded volume. After embedding, the 3-D volume is re-arranged to the original order.

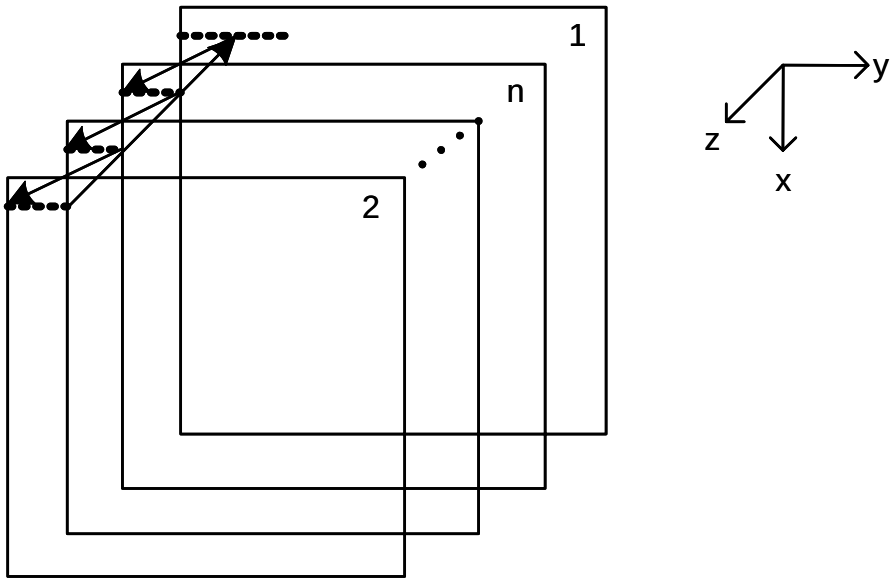

Figure 4 The 3-D LDSERS uses a Z-shape walking pattern to search the R and S groups for data embedding. Four voxels are used to form a group in order to increase the bit compression ratio to accommodate digital signature embedding.

2) Extracting

When extracting, the images in the CT volume is re-arranged in the same order as in the embedding process. The R and S groups are then found based on the same Z-shape walking pattern. The embedded bit stream is reconstructed from the R and S groups. This bit stream is broken down into the compressed RS bit stream and the DS. The compressed RS bit stream is decompressed to recover the original R and S groups. The original R and S groups are compared to the extracted groups and the corresponding group of voxels is flipped if there is any difference. Since the flip operation is reversible, the original CT volume can be completely recovered. The verification of the DS has been described in Section 7.3.

7.5 From A 3-D Volume to 2-D Image(s)

In many clinical scenarios such as a referring physician retrieving images for clinical review, only several 2-D images from a 3-D volume would be needed instead of the entire volume. These several images are usually the significant images that radiologists had selected for referring physician's review. How to protect these several 2-D images in transit and in storage becomes a new data integrity issue.

For example, assuming only the third image in the CT volume is needed, and that 3-D volume already has a signature embedded using the 3-D LDSERS algorithm described in Section 7.4. The procedure how to protect the image integrity of this selected image is as follows:

1) The method starts by recovering the original 3-D CT volume using the Extract & Verify process of the 3-D LDSERS algorithm.

2) Once the verification result assures the integrity of the CT volume, a copy of the third image is extracted.

3) A digital signature of this single CT image is generated and embedded in the image pixels using the 2-D LDSERS algorithm described in Section 7.2. The signature embedded image is sent to the physician for review.

If more than one single image is required, then step 3 is repeated for each image.

By using this method, the integrity of both the 3-D volume and the extracted 2-D images can be assured during the workflow where a physician is retrieving specific images from a 3-D volume. This method can be directly applied to IHE (Integrating the Healthcare Enterprise) Key Image Note Profiles to be discussed in Section 9 [18].

8. RESULTS

8.1. Data Collection

The 2-D LDSERS algorithms was tested with four major modality types of 2-D images used in current clinical practice, including CR, CT, grayscale US, and MR. Although color US images were not evaluated in the experiments, the LDSERS method can be used for color US images by embedding the digital signature in the three chrominance components of the color image. A total of 762 images, including 152 CR images, 204 CT images, 204 grayscale US images and 202 MR images, have been collected. Most of the images collected have standard spatial and density resolution: MR (256x256x12), CT (512x512x12), and US (640x480x8), and CR images varying from 2010x1670x12 to 2510x2000x12.

Thirty image sets from three most common 3-D imaging modalities, CT, US, and MR, were collected for evaluating the performance of the 3-D LDSERS algorithm. The maximum number of images in these image sets was 176, while the minimum number was 10.

8.2. 2-D LDSERS Results

Examples of the tested images and their corresponding results are shown in Figure 5. Figure 5 (a) and (b) depict the signature embedded CT chest image using the 2-D LDSERS algorithm and the subtracted image between the signature embedded image and the original image, Figure 5 (c) and (d) the signature embedded US OBGYN image and the corresponding subtracted image, and Figure 5 (e) and (f) the signature embedded CR hand image and the corresponding subtracted image. The subtracted images were obtained by subtracting the original image from the corresponding signature embedded image. The subtracted image appears black in a regular window/level display. After window/level adjustments, the embedded data becomes visible. A horizontal strip shape pattern is observed in the subtracted images (e.g., Fig. 5(b)). The strip shape shows that every bit embedding changes four adjacent pixels in 2-D LDSERS.

8.3. Time Performance of 2-D LDSERS

The time performance of Sign & Embed processes as well as Extract & Verify processes of the 2-D LDSERS algorithm have been computed and tabulated in Table I. The process time of “Embed” or “Extract” was in hundredth seconds level for all four types of images. This demonstrates that the 2-D LDSERS is efficient for assuring the integrity of a single 2-D image. However, the processing time for an image examination with hundreds of those images could still have a lengthy overall time, which can be shorten using 3-D LDSERS.

Table I. Time performance of the 2-D LDSERS method

Per image	Average Process Time of the LDSE method (seconds)			
	Sign	Embed	Extract	Verify
MRI	0.013	0.018	0.019	0.013
CT	0.019	0.041	0.029	0.016
US	0.014	0.033	0.042	0.013
CR	0.19	0.09	0.08	0.19

[a]STDEV: standard deviation

8.4. 3-D LDSERS Results

The 3-D LDSERS algorithm was evaluated in two steps. First, one digital signature is generated for the entire volume set and the signature is embedded in the volume set using the 3-D LDSERS algorithm. Second, the digital signature was extracted from the signature embedded volume set and verified. Figures 6-8 show three examples of an MR breast, an US OBGYN, and a CT reformatted coronal chest volume set from our results. Each figure depicts four consecutive images from each of these three volumes sets with a partial signature embedded, and the subtracted images between the original and the corresponding signature embedded images. An intuitive view of the pixels changed after the data embedding process can be observed from the subtracted images in Figures 6-8 (b). A horizontal strip can be observed in every subtracted image of the volume set (e.g., Figure 6 (b)). The strip shows that every 1/0 bit embedding process changes four adjacent pixels in the 3-D LDSERS algorithm. As it can be seen, the portion of pixels being changed in every image is small, which means that plenty of space is still available for embedding more data. This is one of the advantages of the 3-D over the 2-D image embedding methods [7], because the embedded data can be distributed in the entire volume instead of just a single image.

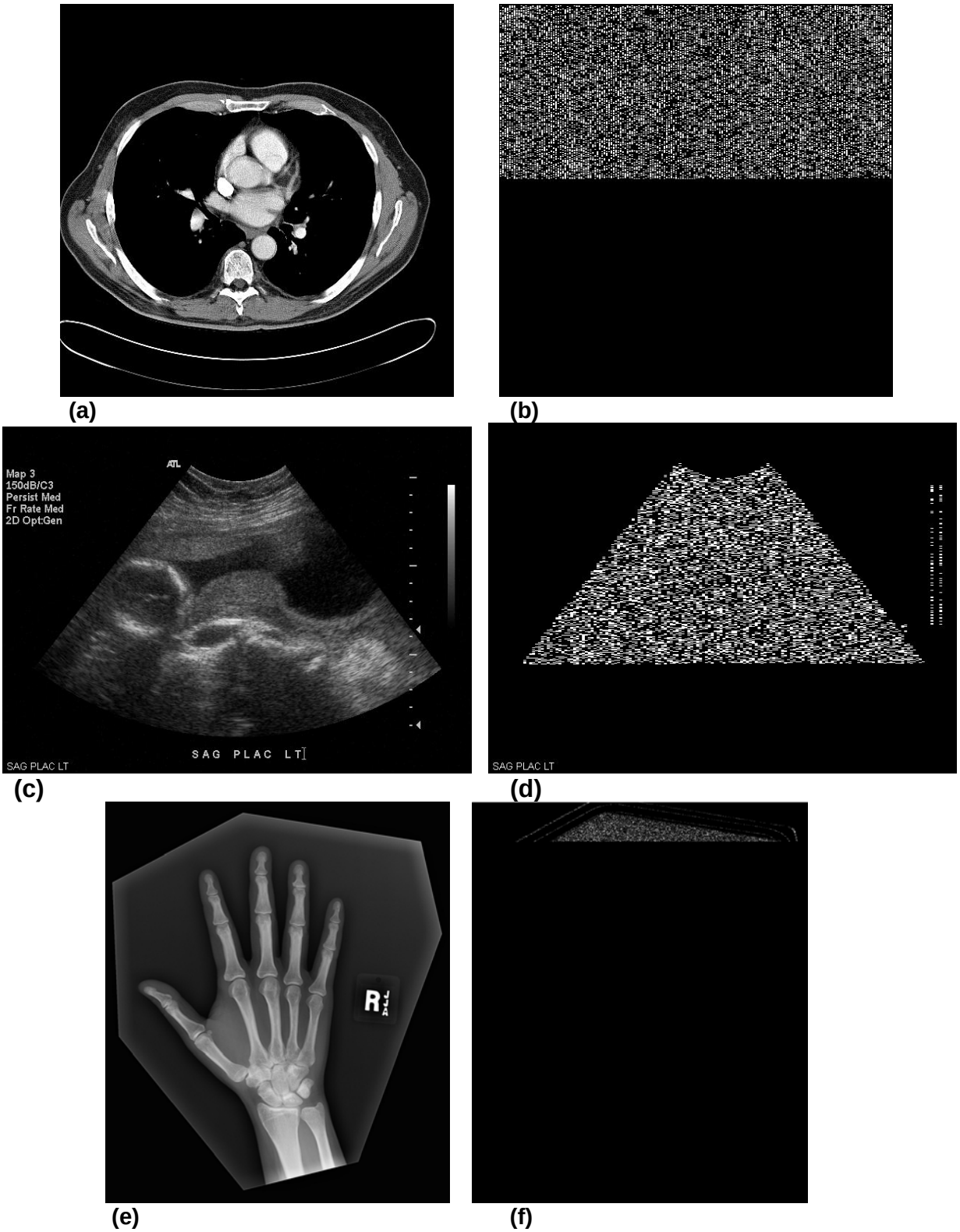

Figure 5 Example of the 2-D LDSERS results. (a) CT chest image with signature embedded; (b) The subtracted image between the original CT chest image and (a) showing where the digital signature is embedded; (c) US OBGYN image with signature embedded; (d) The subtracted image between the original US image and (c); (e) CR hand image with signature embedded; (f) The subtracted image between the original CR image and (e).

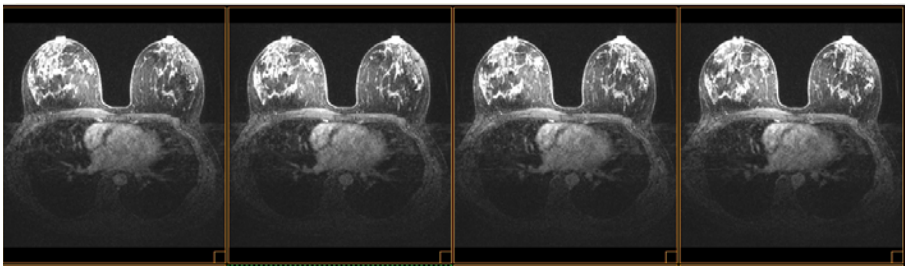

(a)

(b)

Figure 6 Example of the 3-D LDSERS results of MR Breast volume. (a) Four consecutive images of the MR volume with a partial digital signature embedded; (b) The subtracted images between the four original MR images and (a) showing where the digital signature is embedded.

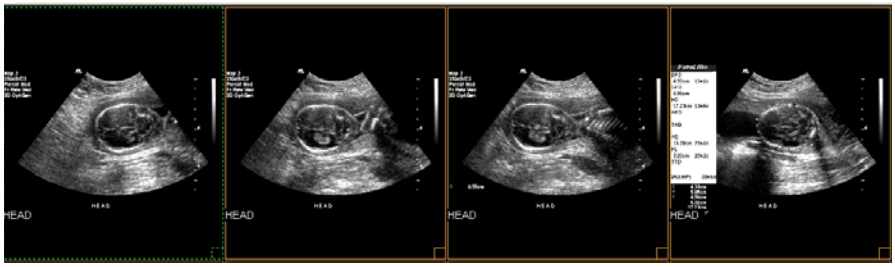

(a)

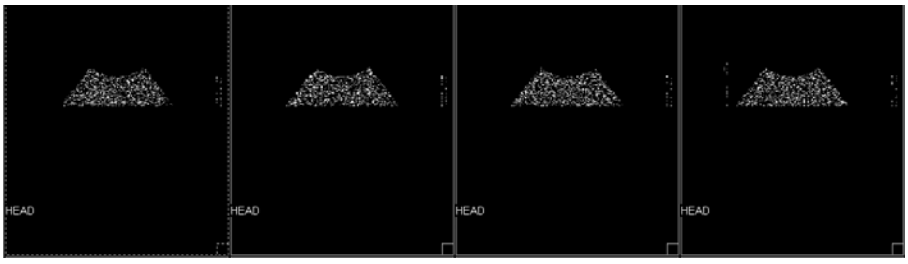

(b)

Figure 7 Example of the 3-D LDSERS results of US OBGYN volume. (a) Four consecutive images of the US volume with a partial digital signature embedded; (b) The subtracted images between the four original US images and (a) showing where the digital signature is embedded.

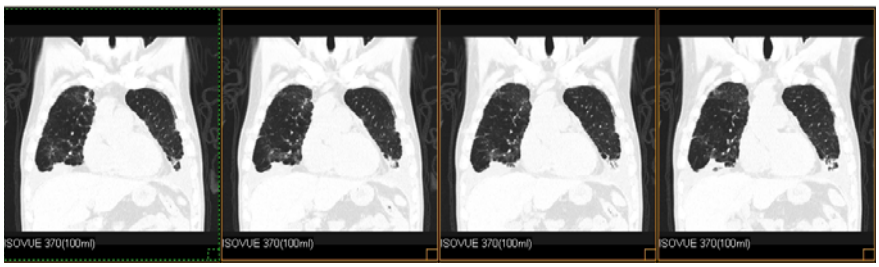

(a)

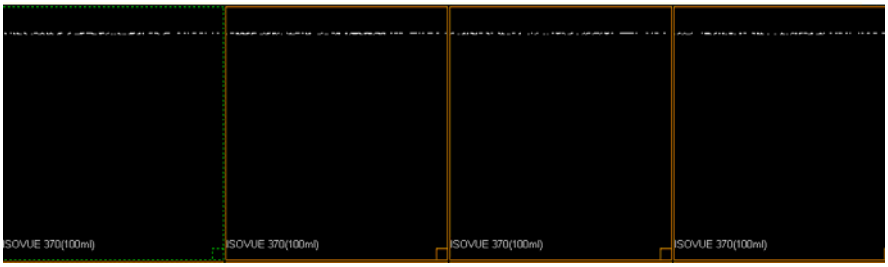

(b)

Figure 8 Example of the 3-D LDSERS results of a reformatted CT Coronal Chest Volume. The images are reformatted and displayed from anterior to posterior. (a) Four consecutive images of the CT volume with a partial digital signature embedded; (b) The subtracted images between the four original CT images and (a) showing where the digital signature is embedded.

8.5. Time Performance of 3-D LDSERS

The time performance of the 3-D LDSERS has been recorded and the results tabulated in Table II. The results demonstrate:

1) Sign or Verify

- The process time to Sign or Verify increased steeply as the total size of the image sets increased. For instance, the time to sign is 0.125 seconds for the MR set 5 (3.16 megabytes), whereas it is 2.516 seconds for the MR set 14 (94.4 megabytes).
- The size of the image but not the number of images contained in an image set was a main factor in determining the process time of the digital signature. For instance, although the MR set 10 contains more images than the MR set 1, the process time to Sign for MR set 10 is much shorter than the MR set 1 that is larger than the MR set 10 in total size of images.
- Different digital signature algorithms will also affect the process time. Our experimental results show that SHA1withRSA [16] has a faster process time for medical images than other digital signature algorithms, including SHA1withDSA [16] and RIPEMD160withRSA [16].

2) Embed or Extract

The process time to Embed or Extract is mainly determined by correlation of adjacent pixels of each image in an image set because of the concept of LDSERS algorithm. For images with a high correlation between adjacent pixels, the process time to Embed or Extract is short. For example, MR sets 11 and 12 contain the same number of images and the same total size of images, whereas the process time to Embed for the MR set 12 is more than three times longer than the MR set 11.

3) 3-D LDSERS vs. 2-D LDSERS

a. Sign or Verify

In order to compare the time performance between the 3-D LDSERS and the 2-D LDSERS applied to all images in the volume, the 2-D LDSERS algorithm was applied to every image in each image set in Table II. The process time of 2-D LDSERS has been measured and the results are tabulated in Table II as well. The process time to “Sign” or “Verify” of every volume set using 3-D LDSERS is faster than 2-D LDSERS. For instance, the process time to sign for MR set 2 using 3-D LDSERS is about 0.3 seconds less than 2-D

LDSERS. This is because only one digital signature was generated for a volume set in 3-D LDSERS resulting in a faster performance time for public key encryption required in digital signature. For example, to generate 10 digital signatures for 10 images in the volume would need ten times public key encryption, whereas it only needs one encryption using 3-D LDSERS. This reduction saves process time, since the public-key encryption was a relatively slow process [16]. The 3-D LDSERS saves even more process time when the number of images in the volume increased. For instance, the process time to sign is about 0.7 seconds less for the MR set 14 using 3-D LDSERS than 2-D LDSERS.

b. Embed or Extract

A more significant improvement in time performance occurs in the "Embed" or "Extract" processes. The processing time using 3-D LDSERS remained in the tenth to hundredth of seconds for most volume sets, whereas most of the process time using 2-D LDSERS was more than 1 second for the same volume set shown in Table II. The maximum difference was more than 60 times less for the CT set 12 by using 3-D LDSERS than by 2-D LDSERS.

c. Embed or Extract versus Sign or Verify

The time to "Embed" or "Extract" process was shorter than the time to "Sign" or "Verify". When the number of images in the volume set became larger, the former could be only about a tenth of the latter. For instance, the time to Embed for the CT set 10 is 0.188 seconds versus the time to Sign 1.422 seconds. These results show that the time to "Embed" or "Extract" process becomes almost negligible when the number of images increases in volume.

All these results indicate that using the 3-D LDSE method for 3-D volumes is far more efficient than using the 2-D LDSE method.

9. Application of 2-D and 3-D LDSE in Clinical Image Data flow

9.1. Application of the LDSE Method in a Large Medical Imaging System like PACS

The goal of the integration of the LDSE method with imaging systems is to assure the integrity of an image right after it is generated from an imaging modality. Thus, the LDSE Sign & Embed process should be positioned near the imaging modality as close as possible. A PACS simulator [19], [20] has been developed as a test bed for evaluating the system integration of the LDSE method with a PACS.

Currently, no network security, such as DICOM Transport Layer Security (TLS), has been applied in current clinical PACS; therefore the communication between any two PACS components is not safe. Each of the PACS components is not safe either. The image integrity in every point after the image modality, therefore, has to be assured using the LDSE method. Figure 9 shows the ideal system integration of the LDSE method with the PACS simulator. The data flow is as following:

1) Modality Simulator passes the DICOM image to the signer "a", which calls the LDSE Sign & Embed process to embed the DS of the image in the pixels. Once the DS is embedded, it becomes a permanent part of the image. This is the only place where the digital signature is signed and embedded.
2) "a" sends the signature embedded image to the verifier "b" using the DICOM communication protocol.
3) "b" calls the LDSE Extract & Verify process to verify digital signature. If the signature is valid, "b" forwards the image to the DICOM gateway.
4) DICOM gateway receives the signature embedded image and stores it in its local disk. It then reads the image file back from the local disk and passes it to the verifier "c".

Steps 5)-11) repeat steps 3 and 4 verifying the digital signature in each imaging component and the communications between every two different components.

By verifying the signature from "b"-"f", the image integrity is completely assured in transit and in storage within each component until the image reaches the viewing workstation.

If DICOM TLS is applied in the PACS simulator, then the protection of the image integrity in transit (e.g., verifiers "b", "d", and "f") can be omitted. Besides these verifiers, other procedures are still necessary for assuring the image integrity in the archive of each component. By combining the LDSE method with DICOM TLS, the image integrity in PACS is completely assured.

If an image is found altered during the transmission, the verifiers (e.g., "b") would reject the image and ask the sending component to re-send the image.

Table II. Time performance of the image volume sets using 3-D LDSERS vs 2-D LDSERS

3-D Volume sets (number of images)	3-D LDSERS		2-D LDSERS	
	Sign + Embed (seconds)	Extract + Verify (seconds)	Sign + Embed (seconds)	Extract + Verify (seconds)
MR set1 (20)	0.25 + 0.14	0.19 + 0.25	0.34 + 0.55	0.34 + 0.34
MR set2 (23)	0.11 + 0.05	0.05 + 0.11	0.42 + 0.51	0.40 + 0.38
MR set3 (23)	0.12 + 0.06	0.06 + 0.11	0.38 + 0.38	0.53 + 0.38
MR set4 (23)	0.30 + 0.06	0.05 + 0.30	0.42 + 0.58	0.66 + 0.39
MR set5 (25)	0.12 + 0.06	0.06 + 0.12	0.38 + 0.53	0.62 + 0.43
MR set6 (36)	0.46 + 0.06	0.05 + 0.48	0.65 + 0.62	1.05 + 0.62
MR set7 (40)	0.59 + 0.05	0.05 + 0.58	0.78 + 0.65	0.67 + 0.66
MR set8 (40)	0.59 + 0.06	0.05 + 0.61	0.74 + 0.66	0.65 + 0.66
MR set9 (49)	0.22 + 0.06	0.06 + 0.20	0.70 + 0.94	0.88 + 0.77
MR set10 (57)	0.09 + 0.06	0.05 + 0.09	0.71 + 0.88	0.89 + 0.88
MR set11 (160)	1.69 + 0.37	0.51 + 1.67	2.51 + 4.30	3.03 + 2.65
MR set12 (160)	1.73 + 1.11	1.26 + 1.67	2.49 + 4.34	3.04 + 2.43
MR set13 (160)	1.69 + 0.52	0.64 + 1.67	2.59 + 4.09	2.51 + 2.55
MR set14 (176)	2.52 + 0.34	0.19 + 2.42	3.21 + 3.27	2.89 + 2.97
US set1 (30)	0.28 + 1.10	0.53 + 0.28	0.42 + 0.99	1.26 + 0.39
US set2 (54)	0.48 + 0.86	0.39 + 0.76	0.82 + 1.48	1.89 + 0.85
US set3 (38)	0.34 + 0.05	0.03 + 0.34	0.53 + 1.25	1.60 + 0.49
US set4 (42)	0.39 + 0.05	0.05 + 0.37	0.59 + 1.38	1.76 + 0.55
CT set1 (10)	0.17 + 0.06	0.06 + 0.17	0.19 + 0.41	0.29 + 0.16
CT set2 (20)	0.33 + 0.06	0.08 + 0.31	0.38 + 0.82	0.58 + 0.32
CT set3 (29)	0.44 + 0.06	0.06 + 0.44	0.55 + 1.19	0.84 + 0.46
CT set4 (42)	0.62 + 0.06	0.06 + 0.61	0.80 + 1.72	1.22 + 0.67
CT set5 (51)	0.73 + 0.19	0.14 + 0.73	0.97 + 2.09	1.48 + 0.81
CT set6 (59)	0.84 + 0.08	0.06 + 0.83	1.12 + 2.42	1.71 + 0.94
CT set7 (72)	1.00 + 0.06	0.08 + 1.00	1.37 + 2.95	2.09 + 1.15
CT set8 (80)	1.12 + 0.06	0.08 + 1.11	1.52 + 3.28	2.32 + 1.28
CT set9 (90)	1.28 + 0.20	0.16 + 1.25	1.71 + 3.69	2.61 + 1.44
CT set10 (100)	1.42 + 0.19	0.11 + 1.39	1.84 + 3.42	2.17 + 1.63
CT set 11 (69)	1.15 + 0.16	0.17 + 1.05	1.31 + 2.83	2.00 + 1.10
CT set 12 (97)	1.37 + **0.06**	0.05 + 1.33	1.84 + **3.98**	2.81 + 1.55

9.2 Integration of the 3-D LDSE method with the Two IHE Profiles

3-D imaging modalities can greatly improve the quality of clinical diagnosis by providing additional features. For example, a series of reformatted CT coronal images generated from 3-D post-processing provides more information for diagnosis when it is reviewed together with original axial CT images. To integrate these features with clinical imaging systems like PACS seamlessly, however, novel clinical image data flow is required. Integrating the Healthcare Enterprise (IHE) has released two important profiles relevant to 3-D volume image data. One is Key Image Note profile and the other is Post-Processing Workflow profile. In order to apply the 3-D LDSE method in PACS, the 3-D LDSE method must be able to integrate with these two profiles. The integration of these two IHE profiles in PACS with the 3-D LDSE method has been developed.

Integration of the 3-D LDSE method with these two IHE profiles is focused on how to protect the integrity of all images involved in the workflow profiles anytime at anywhere without interrupt the clinical data flow.

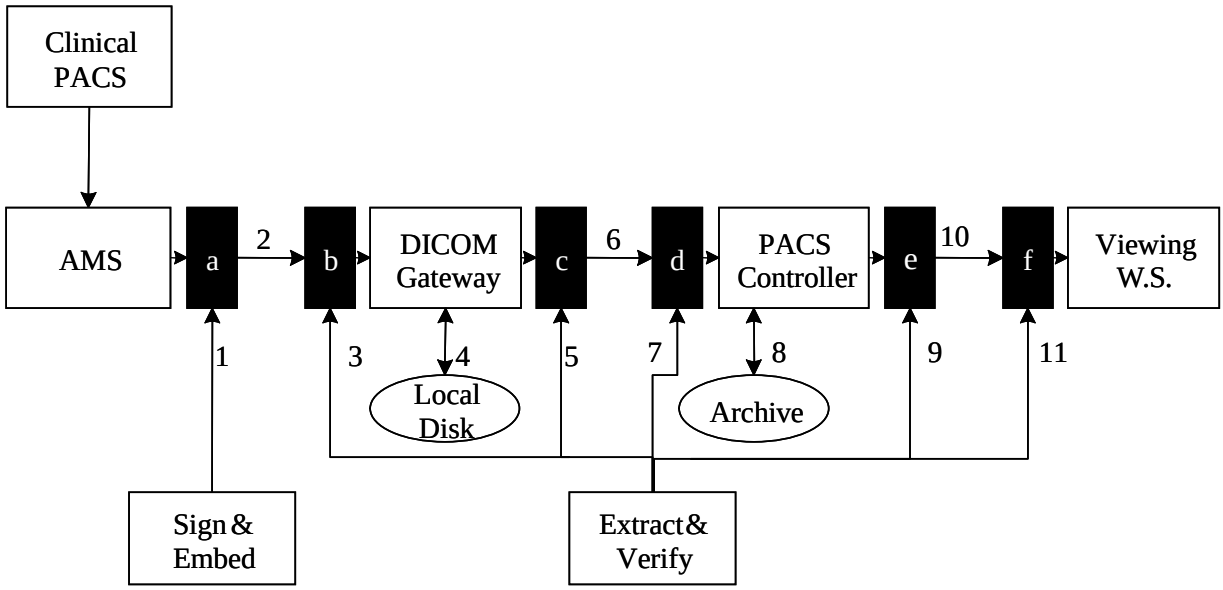

Figure 9 System integration of the LDSE methods with the PACS simulator without Transport Layer Security (TLS). The PACS simulator consists of an acquisition modality simulator (AMS), a DICOM gateway, a PACS Controller, and viewing workstations (W.S.). The connection between these components can be private or public networks. Black boxes represent the LDSE processes. a: signer (Sign & Embed processes), b-f: verifier (Extract & Verify processes).

a) Integration of the 3-D LDSE method with Key Image Note

As shown in Figure 10, the image set of the exam stored in the archive already has a digital signature embedded when the exam is generated in the 3-D image modality. The lack of the protection is when several flagged 2-D images are sent to the viewing workstation for review. The 2-D LDSE method described previously in Section 7.2 can be used in this situation to embed the signature of every 2-D image in the flagged image correspondingly; therefore, the physician at the viewing workstation can verify the integrity of the flagged images whenever they are viewed.

b) Integration of the 3-D LDSE method with 3-D Post-Processing Workflow

As shown in Figure 10, the integration of the 3-D LDSE method with the 3-D Post-Processing Workflow is as follows:

1) The original exam is generated in a 3-D imaging modality. Before the exam is stored in the archive, a signature of each series of the exam is embedded in the image set of the series using the 3-D LDSE method. The signature embedded exam is then sent to the image server for archiving. Thus, the integrity of the original image exam is assured when the exam is in transit and in archive.

2) The signature embedded exam is sent to a 3-D post-processing workstation.

3) When a series of reformatted images (e.g., a CT coronal reformatted series) is generated in the 3-D post-processing workstation, a signature of this image set is also generated and embedded in the image set using the 3-D LDSE method that has been installed in the workstation.

4) The signature embedded series of reformatted images is sent to the image server for archiving. It is important to notice that no changes are made to the signature embedded original exam because the new signature is only embedded in the reformatted image series.

5) & 6) Once the exam is retrieved to the diagnosis workstation or the review workstation, the integrity of the exam can be verified anytime on demand. If there is a key image note, then only several significant images are retrieved to the review workstation. The integration method described previously in Section 7.5 can be used to protect the integrity of these significant images.

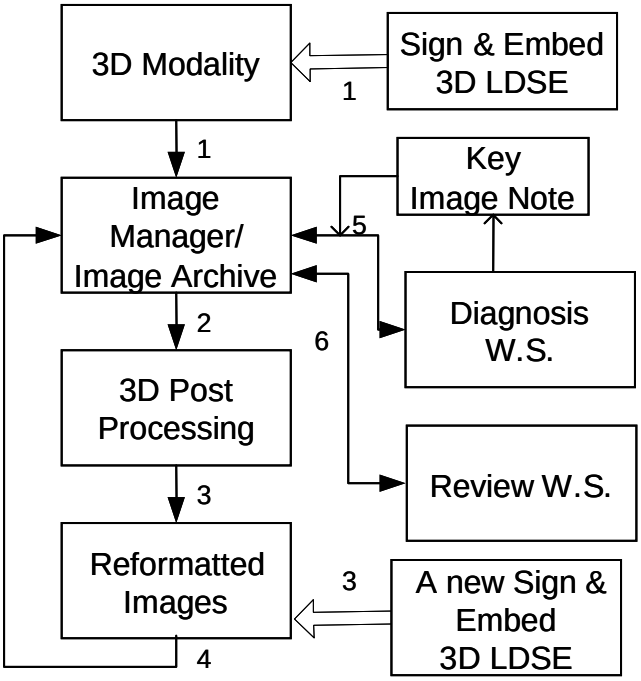

Figure 10 Integrate the 3-D LDSE method with the IHE 3-D Post-Processing Workflow and Key Image Note profiles in a clinical PACS.

10. Concluding Remarks

We have proposed a novel LDSE method for assuring the integrity of 2-D medical images. Experimental results demonstrated that the 2-D LDSERS algorithm is effective for assuring the integrity of an image individually or in a large medical imaging system like PACS. As more and more three dimensional (3-D) imaging modalities are used for clinical diagnosis, an examination created by a 3-D imaging modality could generate hundreds or thousands of images. To apply the 2-D LDSE method for these large amount of images would be time consuming and inefficient. In order to improve the efficiency, the 3-D LDSE method has been developed for assuring the integrity of clinical 3-D image data specifically. Experimental results of the 3-D LDSE method show a significant improvement in the time performance when dealing with a large amount of images in the 3-D CT, MR, or US volume sets compared with the 2-D LDSE method. This shows that the 3-D LDSE method can be used to assure data integrity of 3-D volumes in clinical imaging systems. The integration of the 3-D LDSE method with the IHE profiles related to 3-D image workflow has also been investigated and developed.

Acknowledgements

This research has been partially supported by NIH R01 LM07606 grants, and a contract from MI^2.

References

[1] S.B. Berger and B.B. Cepelewicz, “Medical-legal issues in tele-radiology,” *Am. J. Roentgenoloy*, vol. 166, pp. 505-510, 1996.

[2] L. Berlin, “Malpractice issue in radiology-teleradiology,” *Am. J. Roentgenoloy*, vol. 170, pp. 1417-1422, 1998.

[3] X. Q. Zhou, H. K. Huang, and S. L. Lou, “Authenticity and Integrity of Digital Mammography Images,” *IEEE Trans. Medical Imaging*, vol. 20, no. 8, pp. 784 – 791, 2001.

[4] Information processing systems, Open systems Interconnection, Basic Reference Model-Part 2: Security Architecture, *ISO* 7498-2, 1989.

[5] J.G. Hodge Jr., G.O. Lawrence, and P.D. Jacobson, “Legal issues concerning electronic health information: privacy, quality, and liability,” *J American Medical Association*, vol. 282(15), pp. 1466-1471, 1999.

[6] A.E. James Jr., E. James III, B. Johnson, and J. James, “Legal considerations of medical imaging,” *J Legal Medicine*, pp. 87-113, 1993.

[7] Z. Zhou, “Lossless digital signature embedding for medical image integrity assurance”, *Ph.D. dissertation Chapter 2*, Univ. of Southern California, Los Angeles, CA, Aug. 2005.

[8] Digital Imaging and Communications in Medicine (DICOM) Part 15 Security and System Management Profiles, 2004.

[9] Secure Socket Layer (SSL), http://wp.netscape.com/eng/ssl3/draft302.txt.

[10] J. Fridrich, M. Goljan, and R. Du, “Lossless Data Embedding For All Image Formats,” in *Proc. SPIE Photonics West, Electronic Imaging*, vol. 4675, pp. 572–583, 2002.

[11] J. Fridrich, M. Goljan, and R. Du, “Lossless Data Embedding – New Paradigm in Digital Watermarking,” *EURASIP J. Appl. Sig. Proc*., vol. 2002, no. 2, pp. 185–196, 2002.

[12] M. Nelson. (1991). Arithmetic Coding + Statistical Modeling = Data Compression. Available: http://dogma.net/markn/articles/arith/part1.htm.

[13] D. H. Lehmer, “Mathematical methods in large-scale computing units,” in *Proc. 2nd symposium on Large-Scale Digital Calculating Machinery*, Cambridge, MA, 1949, pp. 141-146.

[14] S. K. Park and K. W. Miller, “Random number generators: good ones are hard to find,” *Comm. ACM*, vol. 31, pp. 1192-201, 1988.

[15] Secure hash standard, *Federal Information Processing Standards* Publication 180-1, 1995.

[16] A.J. Menezes, P.C. Oorschot, and S.A. Vanstone, *Handbook of Applied Cryptography*, CRC Press, 1997.

[17] R.L. Rivest, A. Shamir, and L.M. Adleman, “A method for obtaining digital signatures and public-key cryptosystems,” *Communications of the ACM*, vol. 21, pp. 120-126, 1978.

[18] Integrating the Healthcare Enterprise (IHE) Technical Framework Volume I: Integration Profiles, 2005.

[19] Z. Zhou, H. K. Huang, F. Cao, B. J. Liu, J. Zhang, and G. T. Mogal, “Educational RIS/PACS Simulator,” *SPIE Medical Imaging*, vol. 4, pp. 139-147, 2003.

[20] M. Y. Y. Law and Z. Zhou, “New direction in PACS education and training,” *Computerized Medical Imaging and Graphics J.*, vol. 27, pp. 147-156. 2003.

APPENDIX
FLIPPING OPERATION

An invertible operation "F" is defined as a flipping on individual bit(s) of an image pixel. Flipping of a given bit is always "0" $\rightarrow$ "1" or "1" $\rightarrow$ "0". The absolute value change of the pixel by flipping, however, depends on the bit locations in the pixel. The following show some examples of the absolute value change based on the flipping operation on different bits of the pixel:

	F_{LSB}	F_{1B}	…	F_{7B}
The bit flipped	0^{th} (LSB)	1^{st} bit		7^{th} bit
If the pixel value is the "left", then it is changed to the "right"	$0 \rightarrow 1$, $1 \rightarrow 0$, $2 \rightarrow 3$, $3 \rightarrow 1$, …, $125 \rightarrow 124$, $126 \rightarrow 127$, $127 \rightarrow 126$, $128 \rightarrow 129$, …, $254 \rightarrow 255$, $255 \rightarrow 254$,	$0 \rightarrow 2$, $2 \rightarrow 0$, $1 \rightarrow 3$, $3 \rightarrow 1$, …, $253 \rightarrow 255$, $255 \rightarrow 253$,	• • •	$0 \rightarrow 128$, $128 \rightarrow 0$, $1 \rightarrow 129$, $129 \rightarrow 1$, …, $127 \rightarrow 255$, $255 \rightarrow 127$,

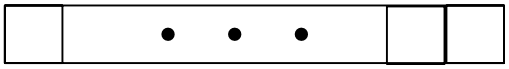

When a flipping operation is performed on the LSB (see Column 2) of a group of four pixels G (see Section II), the value of these four pixels changes accordingly. For example, assuming that $G = (127, 125, 128, 126)$, we would have $F(G) = (126, 124, 129, 127)$ after the flipping operation. Thus, the original second and third pixels (125, 128) become less correlated after flipping (124, 129). In other words, if Equation (8) (see Section II) is applied in G, then $f(F(G)) > f(G)$.

The number of pixels in the group G can be set to other numbers instead of 4, such as 3 or 5. The numbers 3 - 6 have been tested in our experiments. Experimental results show that "4" works best for all tested medical images.

Grid Methods for Large Scale Medical Image Archiving and Analysis

H.K. Huang, Zheng Zhou, Brent Liu,

Image Processing and Informatics Laboratory (IPI), Departments of Radiology and Biomedical Engineering, University of Southern California,
hkhuang@aol.com

* Will appear in “Principles and Recent Advances in Medical Imaging and Image Analysis”, AP Dhawan, HK Huang, and DS Kim, Ed., Chapter 20. World Scientific Publications, Singapore**.**

ABSTRACT

Grid computing is the integrated use of geographically distributed computers, networks, and storage systems to create a virtual computing and communication system environment for solving large-scale, data-intensive problems, for example, in various medical image applications. This chapter uses medical imaging PACS (Picture Arching and Communication System), described in Section 1, as a means to present how Grid Computing can be used to solve several difficult problems facing PACS clinical operations. In Section 2 we introduce Grid Computing fundamentals including topics in the Globus 4.0 five-layered toolkit and the integration of PACS DCIOM technology with the Globus. Section 3 describes the concept of Data Grid and its applications in PACS. We first define the needs of fault-tolerant PACS archive and backup, and three main tasks of Data Grid during disaster recovery. Two important new developments in Data Grid are the dynamic metadata database and the management system which are essential to guarantee the fault-tolerance of an enterprise PACS. Section 4 introduces Grid Computing which extends the Data Grid infrastructure with computational services to cover certain application oriented computing requirements when computer-aided diagnosis (CAD) is integrated with PACS for daily clinical operation. The CAD of multiple sclerosis of the brain on MRI is used as an example to illustrate steps involved.

Keywords

PACS, Grid Computing, Data Grid, Computational Services, Fault-tolerance Archive, Disaster Recovery, Image Analysis, Image Data Mining, CAD of Multiple Sclerosis

1. Introduction

Background

Grid computing is the integrated use of geographically distributed computers, networks, and storage systems to create a virtual computing system environment for solving large-scale, data-intensive problems in science, engineering, commerce, and healthcare. [1-7] A grid is a high-performance hardware and software infrastructure providing scalable, dependable and secure access to the distributed resources. Unlike distributed computing and cluster computing, the individual resources in grid computing maintain administrative autonomy and are allowed system heterogeneity; this aspect of grid computing guarantees scalability and vigor. Therefore, the grid’s resources must adhere to agreed-upon standards to remain open and scalable. A formal taxonomy, composed of five layers has been defined by the Globus Toolkit 4.0 of grid computing to assure this standardization (Figure 1) which will be described in greater detail in Section 2.2. [8]

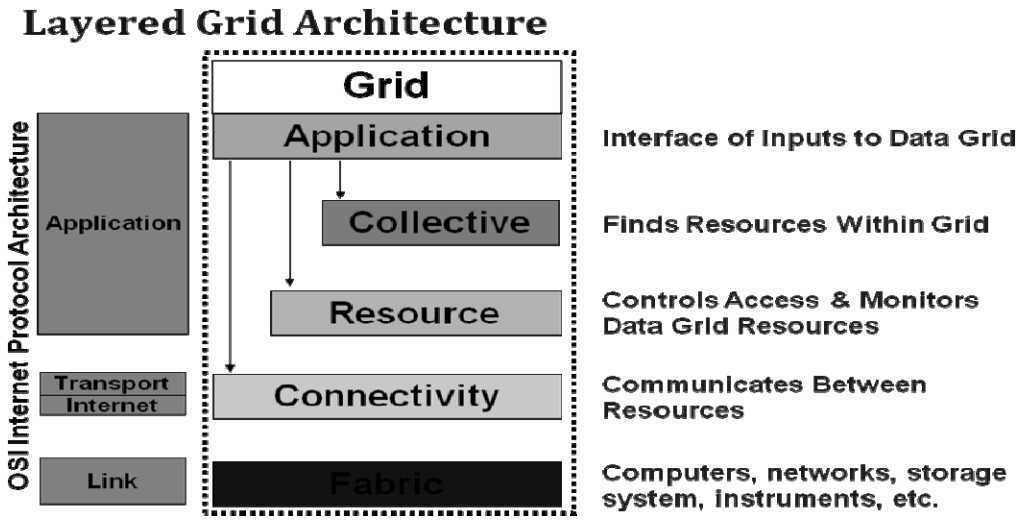

Figure 1. The Five Layer Grid Architecture defined by the Globus Toolkit 4.0: Fabric, Connectivity, Resource, Collective, and Application. The left-hand side depicts its correspondence to the OSI (Open System Interconnection) seven-layer Internet Protocol.

Large-scale Medical Imaging Systems – PACS

PACS (Picture Archiving and Communication system) is a large-scale integral imaging system responsible for 24/7 clinical diagnostic operation in a healthcare delivery system.[9] We use it to illustrate the usefulness of Grid Computing in medical image application. Two current research topics are discussed, the fault-tolerance image archive and recovery after disaster [10], and the integration of computer-aided diagnosis (CAD) with PACS [11]. These two applications explain the concepts of Data Grid and Grid Computing in large-scale medical imaging systems.

A PACS is a system integration of computers, servers, workstations, communication networks, and software to form a system for medical image information archive, distribution, and display. It consists of the following components:

- A data acquisition gateway connected to the Radiology Information System (RIS) and the Hospital Information system (HIS) for acquiring patient and examination related data,
- An array of image acquisitions gateways connected to various medical imaging modalities including light image sensors, film digitizer, CR (computed radiography), DR (digital radiology), DM (digital mammography), US (ultrasonic), CT (computed tomography), MRI (magnetic resonance image), SPECT (Single Photon Emission tomography), and PET (Positron Emission Tomography),
- A PACS Controller and Archive Server including storage devices,
- Image display workstations (WS), and
- An image management system software for image archival, distribution, and manipulation.

These components are interconnected by digital networks, communication protocols and application software using the Digital Imaging and Communications in Medicine (DICOM) [12] standard for data communication protocol and image data format, and Health 7 (HL7) standard [13] for data format shown in Figure 2. The DICOM standard contains many parts each of which was designed for a given type of connection, and as a whole, it is commonly referred to as DICOM technology, resources, or services. When multiple PAC systems are connected together to share some resources and operations such as storages and image distribution, it is referred to as the Enterprise PACS.

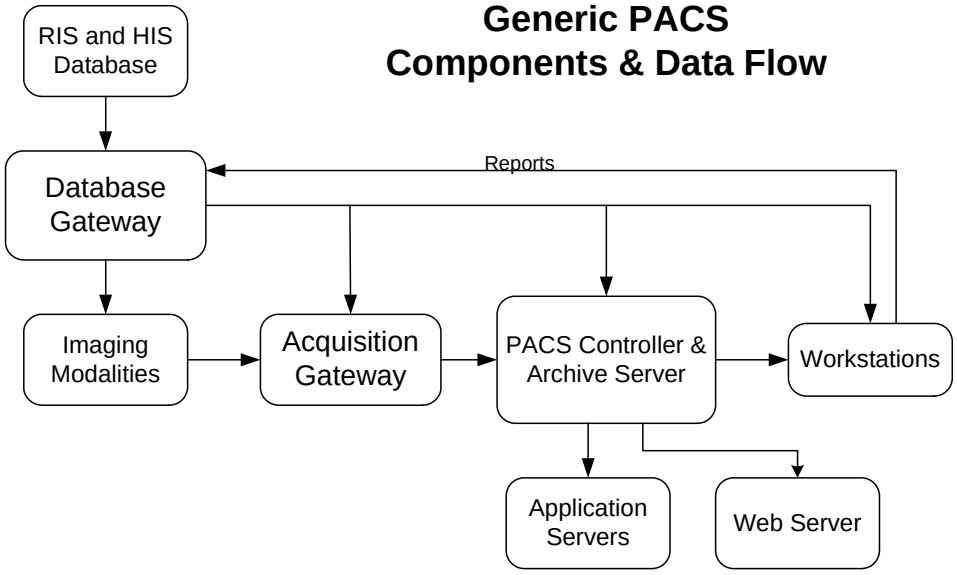

Figure 2. Generic PACS Components and its Data Flow. DICOM and HL7 are two standards used for image and textual information, respectively.

2. Grid Computing Fundamentals

Grid Computing

Grid computing is based on an open set of standards and protocols in its core infrastructure. In this chapter, we use the Open Grid Services Architecture (OGSA) [5,6]] as a guide to discuss the computational services and the data services of the Globus Toolkit 4.0 co-developed by ANL (Argon National Laboratory), University of Chicago and ISI (Information Sciences Institute), University of Southern California [2-4] for medical image applications [8].

a. *Computational Services* support specific applications on distributed computational resources, such as supercomputers or a cluster of computers. A grid for this purpose is called a Computational Grid.

b. *Data Services* allow the sharing and management of distributed datasets. A grid for this purpose is called a Data Grid.

c.

The Globus Five-Layer Toolkit

Figure 1 shows the five layers of the grid computing technology defined by the Globus toolkit 4.0 and the layers correspondence with the OSI (Open System Interconnection) architecture. Figure 3 describes the tools available in each of the five layers.

Integration of DICOM with Globus

Grid Computing technology can be used for specific PACS operations by integrating a selected subset of DICOM resources with the Globus toolkit. We present two examples, the PACS Data Grid and the CAD/PACS (Computer-aided diagnosis) Computing Grid. The former is for PACS backup archive and disaster recovery operation by using the DICOM Image Store, Query and Retrieve (Q/R) services. The CAD/PACS Computing Grid is for integrating CAD with PACS application, which requires additional DICOM resources including the Screen Captured (SC) and Structure Report (SR).[12] In order to assure the fault-tolerance of the integration, a new database and service dedicated for CAD/PACS Computing Grid defined as the DICOM Data Model Metadata database and MetaData Catalog Service are also necessary. Figure 3 depicts

the positions of these DICOM services and the Metadata in the Globus Grid five layer infrastructure. Sections 3 and 4 detail the characteristics, functions, and workflow of the Data Grid and the CAD/PACS Computing Grid of these applications, respectively.

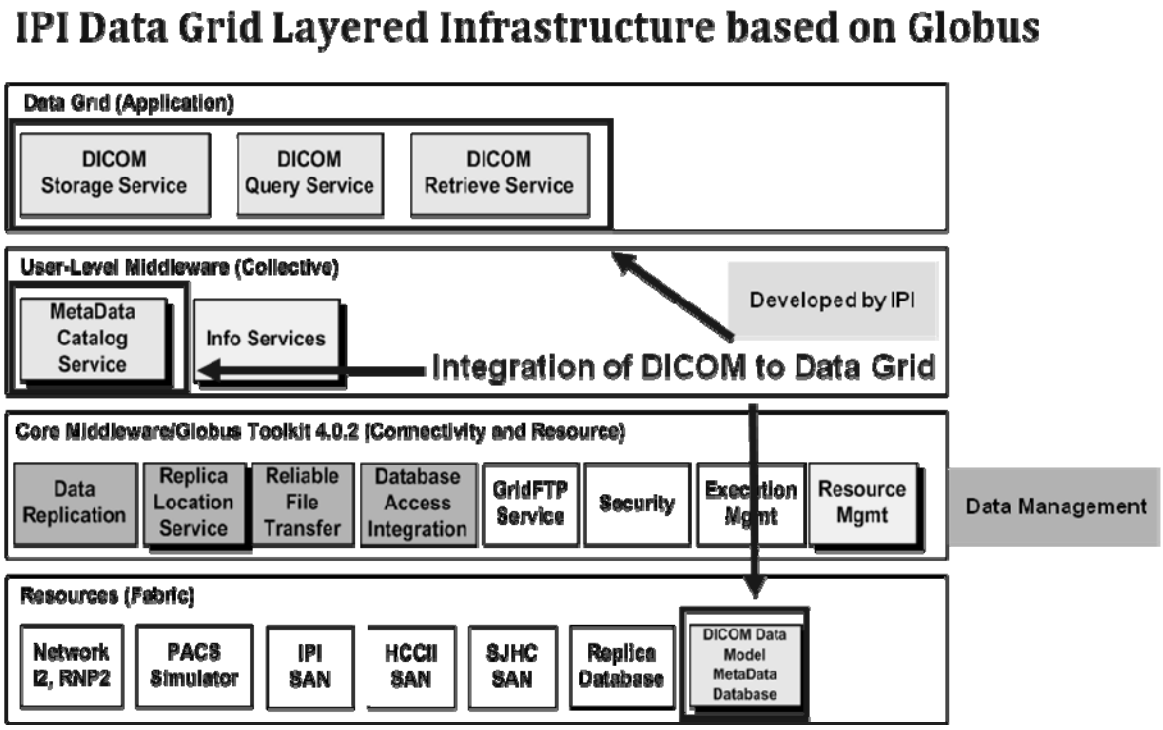

Figure 3. The Five Layer Grid Architecture for medical image PACS Data Grid and CAD/PACS Computing Grid (see Shadow boxes) applications.
Fabric Layer: The leftmost five clear boxes are existing resources from PAC systems, SAN: Storage Area Network [14]; Replica Database is a Globus tool; the rightmost Metadata Database is for fault-tolerant Data Grid and Computing Grid (Shadow) application.
Core Middleware (Connectivity and Resource Layers): The four boxes at the leftmost are Globus tools used for data management in PACS Data Grid, the rest are other Globus tools. Replica (Shadow) and Resource Mgmt (Shadow) are also used for Computing Grid.
User Level Middleware (Collective) Layer includes the Info Service Globus tool and the Metadata Catalog Service for fault-tolerance. Both resources are also used for Computing Grid applications (Shadow boxes)
The Data Grid Application Layer consists of the DICOM Storage, Query, and Retrieve Services. Light shaded boxes with bold external rectangles are DICOM resources, and the Metadata database for fault-tolerance developed at the Image Processing and Informatics (IPI) Laboratory, USC.

3. Data Grid: Large-Scale Medical Image Management Systems for Clinical Services

Three topics will be presented: use Data Grid in large-scale enterprise PACS operation, methods of integrating multiple PAC systems with the Data Grid, and three tasks of the Data Grid during a PACS disaster recovery.

Data Grid for PACS Archive and Q/R

Figure 3 illustrates the integration of DICOM image Store and DICOM image Q/R in the Application Layer of Globus toolkit to form the Data Grid for storage backup of multiple PAC systems. We use three PACS sites shown in Figure 4 to demonstrate the fault tolerance features of the Data Grid.

The operation environment is as follows: Three PACS sites operate total independently as three separate PAC systems, each supports its own clinical site. Each site has a standalone PACS with its own Server, workstations (WS), SAN (Storage Area Network [14]) archive and storage backup. A WS at each site can Q/R images from its own SAN to display image data. A WS of any of these three PAC systems can also Q/R images from other sites using a Web client Common View mechanism.

There are several weaknesses of using this method of integrating multiple PACS operations:

1. The two single-points-of failure (SPOF) in each PACS are the Server and the SAN archive.
2. If the Server of a PACS goes down, its WS would not be able to retrieve images from the SAN of its own PACS or review images of other PAC systems because the workflow (see workflow arrows in Figure 4) relies on the availability of the PACS server.
3. It the SAN of a PACS goes down, two possibilities could happen. First, its WS would not be able to view its own images from SAN. Even though the backup archive may work, it will take time for it to be on-line and supply images for its own WS. It is because most of the backup storage nowadays is low cost and its priority is to preserve a second copy of the archive data instead of immediately failover for continuing operation. The backup is usually without an automatic switch function for primary operation. Second, the PACS would not be able to support Q/R of its images by a WS from other PAC systems.

Therefore, two problems under consideration for the Data Grid are to minimize the impact due to the failure of the Server or the SAN of each PACS.

The PACS Data Grid can be designed as a means of linking these three sites together such that the Data Grid can be used: 1) to support the backup archive and disaster recovery for the three sites, and 2) to allow a WS of any site to retrieve and review image data from any other sites. The former is a Data Grid with functions for PACS backup and disaster recovery, and the latter involves functions of image distribution and review.

In the PACS Data Grid, there are three primary components to the DICOM imbedded Data Grid. Figure 4 illustrates the overall architecture of the Data Grid which is located at the IPI, USC; other SANs are located at three clinical PAC systems as shared storage resources.

1. **Storage Node:** Computer(s) and storage devices, for examples, multiple copies of SAN, provide storage resources for the Data Grid. In this case, each image has three copies, one is in its own PACS SAN, and two are in two SANs within the Data Grid (See Figure 4).

2. **Database:** A Service that keeps track of metadata as well as file locations of different storage nodes within the Data Grid. Dynamic and robust access to data is provided by the Data Access Interface (DAI) in the Globus toolkit integrated with the database. [15]

3. **PACS or DICOM Grid Access Point (GAP):** A Service provides DICOM compliant storage and Query/Retrieve capabilities for WS of any PAC system to access data within the Data Grid. There are multiple GAPs in the Data Grid (See Figure 4)and can be used as the backup for each other.

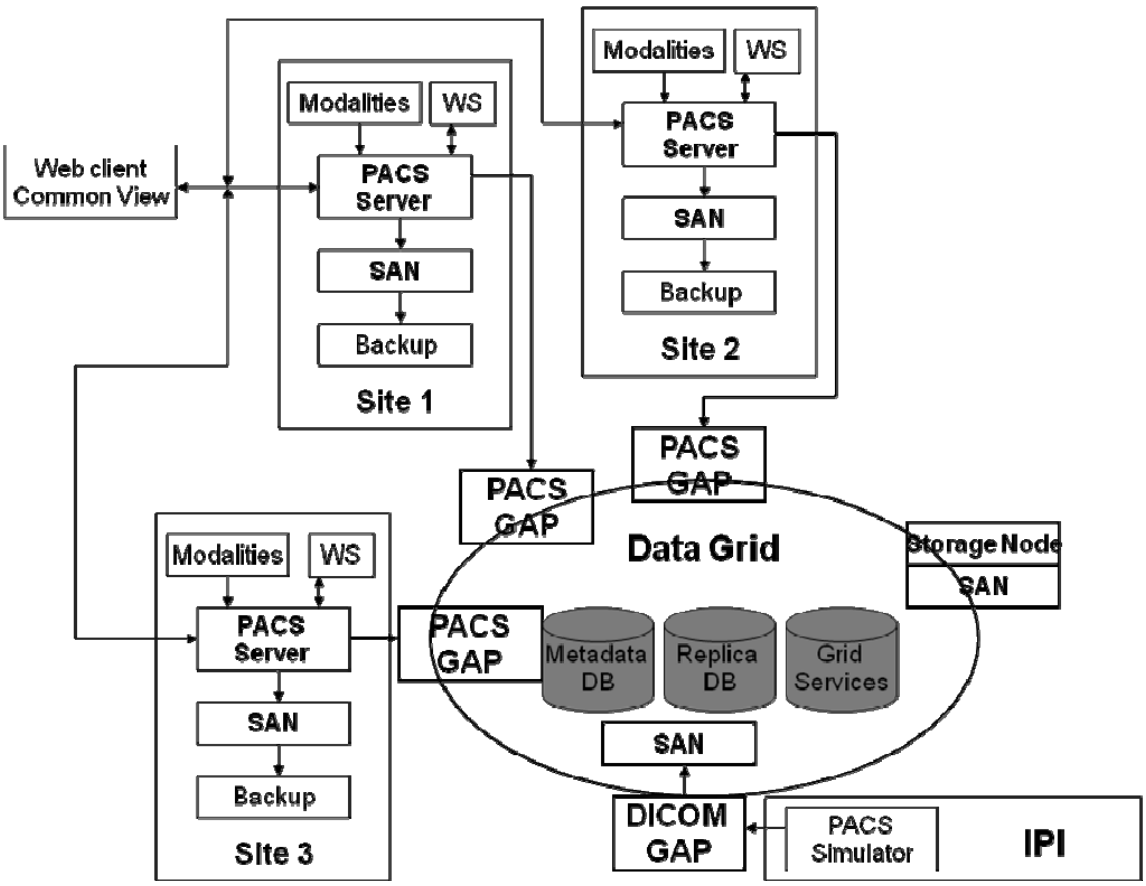

Figure 4. Three PACS sites operate total independently as three separate PAC systems, each supports its own clinical site. Each site has a standalone PACS with its own Server, workstations (WS), SAN (Storage Area Network) archive and storage backup. An enterprise PACS is when these three PAC systems (or more) are connected together. In an enterprise PACS, a WS at each site can Q/R images from its own SAN for image display. A WS of any three PAC systems can also Q/R images from other sites using a Web client Common View mechanism. The weaknesses of this three PACS system interconnection are the two single-points-of-failure. When either each PACS Server or SAN fails, the interconnectivity of three PAC systems breaks down. Data Grid architecture can take away the backup and the connection to the Web client Common View by each PACS. It maintains interconnectivity of these three systems in real-time without human intervention. There are two types of PACS GAP in this architecture, DICOM GAP (bottom) and PACS GAP (middle left). The former is for PACS WS which uses DICOM standard for image Q/R, the latter is for none DICOM file transfer used by some PAC systems.

Data Back Up and Disaster Recover

Let us consider the workflows of data backup and disaster recovery of the Data Grid.

The GAP Under normal operation condition (Figure 5a, solid lines), the image is sent from the DICOM 1 to the Data Grid through its designated GAP1 (Figure 5a). GAP1 is then sent two copies of the image to two Grid Storage Resource SAN1, and SAN2 respectively. Suppose GAP1 fails (cross-lines), GAP2 (dotted lines) would take over and complete the task.

DICOM Q/R Figures 5b solid lines show the normal operation of DICOM Q/R at DICOM 1. Under normal operation condition (solid lines), the WS queries GAP1 for the location of required image data at the metadata database which identifies SAN1 as the location. It returns query results to the GAP, then the WS. The WS retrieves the image data from SAN1. Suppose SAN1 fails during

Q/R (cross-lines), GAP1 would find SAN2 and pass Q/R information to SAN2 which would complete the task (dotted lines).

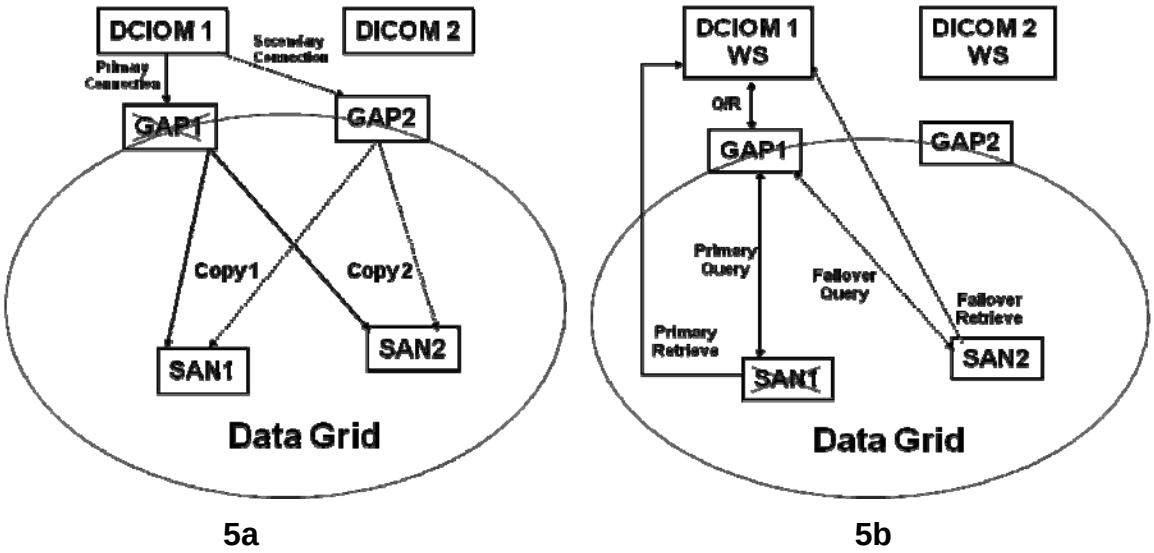

Figure 5. Workflows of Data Grid during image data store and query/retrieve.

5a. Image backup: Solid lines show the normal operation, the image is sent from the DICOM 1 to the Data Grid through its designated GAP1 for backup storage. Dotted lines show GAP1 fails (cross-lines), and GAP 2 takes over automatically.

5b. Query/retrieve: Solid lines show the normal operation, DICOM 1 queries images then retrieves from SAN1 through GAP1. Dotted lines show SAN1 fails (cross-lines), GAP1 finds SAN2 automatically and completes the task.

The Metadata Database Metadata includes all DICOM image header and Data model information extract from each image when it is acquired from the imaging modality. It is organized and stored in the Metadata database (Figure 3) which provides all necessary information of the image including the pointer to where the image is located in the Data Grid SANs. Properly query the database, any image data can be retrieved by the WS through the GAP. The Metadata database without backup databases becomes a single-point-of-failure in the Data Grid. For this reason, a middle layer called the DAI (Data Access Interface [8]) servers is added in-between GAPs and metadata storage nodes. Therefore, there are two layers in the metadata database, the multiple DAI servers and multiple metadata storage nodes (or SANs) shown in Figure 6 which allows multiple GAPs access multiple DAI servers and multiple metadata storage nodes. The three main roles of the DAI server are: centralization of metadata access, replication of metadata into multiple storage nodes, and handling metadata for different PACS archive.[15]

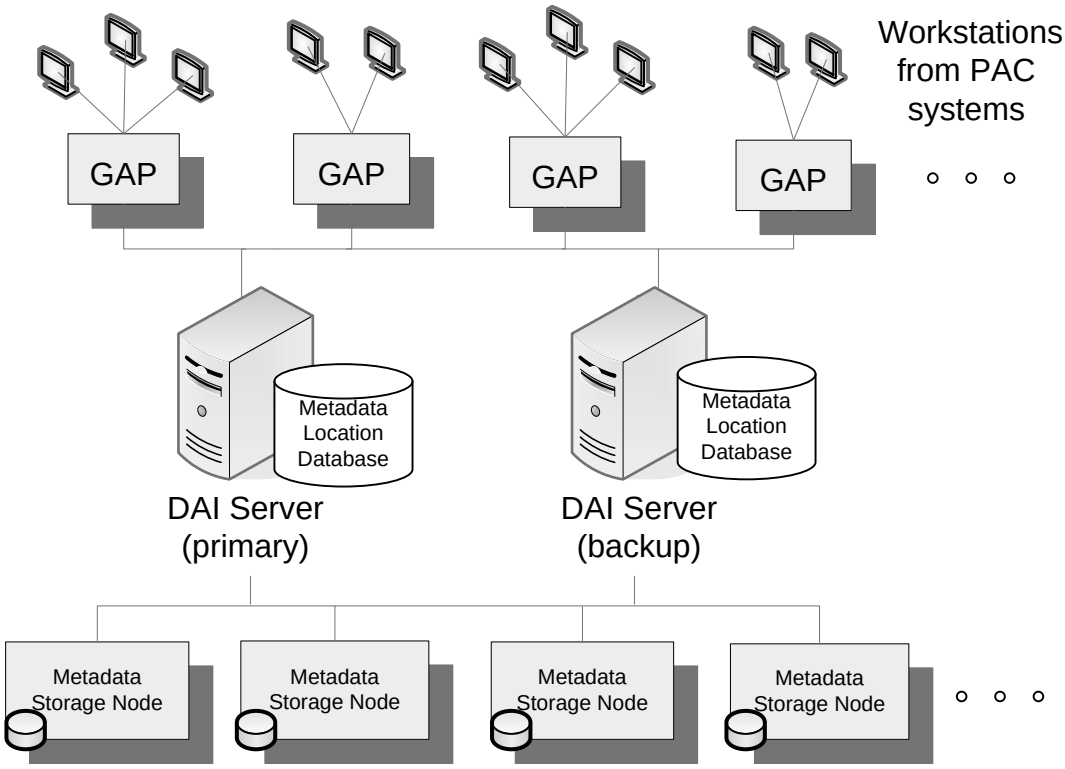

Figure 6.

Figure 6. General Architecture of the fault-tolerance Metadata System for the Data Grid. Fault-tolerance is from Top: Multiple GAPs; Middle: DAI servers; and Lower: Multiple metadata storage nodes (SANs). Contributed by J. Lee..

Three Tasks of the Data Grid during the PACS Server or Archive Failure

Following Figure 4 in which each PACS relies on its own backup archive and the connection of the server through a Web client Common View mechanism for Q/R images of other PAC systems. The failure of the server or the SAN in a PACS would shut down its connectivity with the enterprise PACS. With the Data Grid connected to the multiple PAC systems architecture shown in Figure 7, the enterprise PACS could achieve the fault-tolerance status. Note that in this architecture, which differs from that shown in Figure 4, all backup storages and connections to the Web client Common View for image Q/R from three PACS servers are discarded. Also, the connection of PACS to the Data Grid is at WSs instead of servers.

In this Data Grid architecture, two single-points-of-failure (SPOF) of any PACS are still the PACS server and the SAN storage device. When these two SPOF fail, the Data Grid has to overcome three major tasks in order to be fault-tolerant. First, it has to maintain continuing clinical operation allowing WSs of this PACS Q/R images from the Data Grid. Second and third, after the sever and the SAN have been repaired, it has to rebuild the PACS own archive, and the backup archive for other PAC systems. Figure 7 describes, as an example, these three tasks during the PACS failure (dotted lines) at Site 2 in which either the server or the SAN or both fails (cross-lines). SAN2 is partitioned into P1 and P2. P1 is for its own PACS archive, and P2 is Site 2's storage resource committed to the Data Grid. Task 1 has the highest priority among three tasks shown in dotted lines. All three tasks are performed automatically without human intervention.

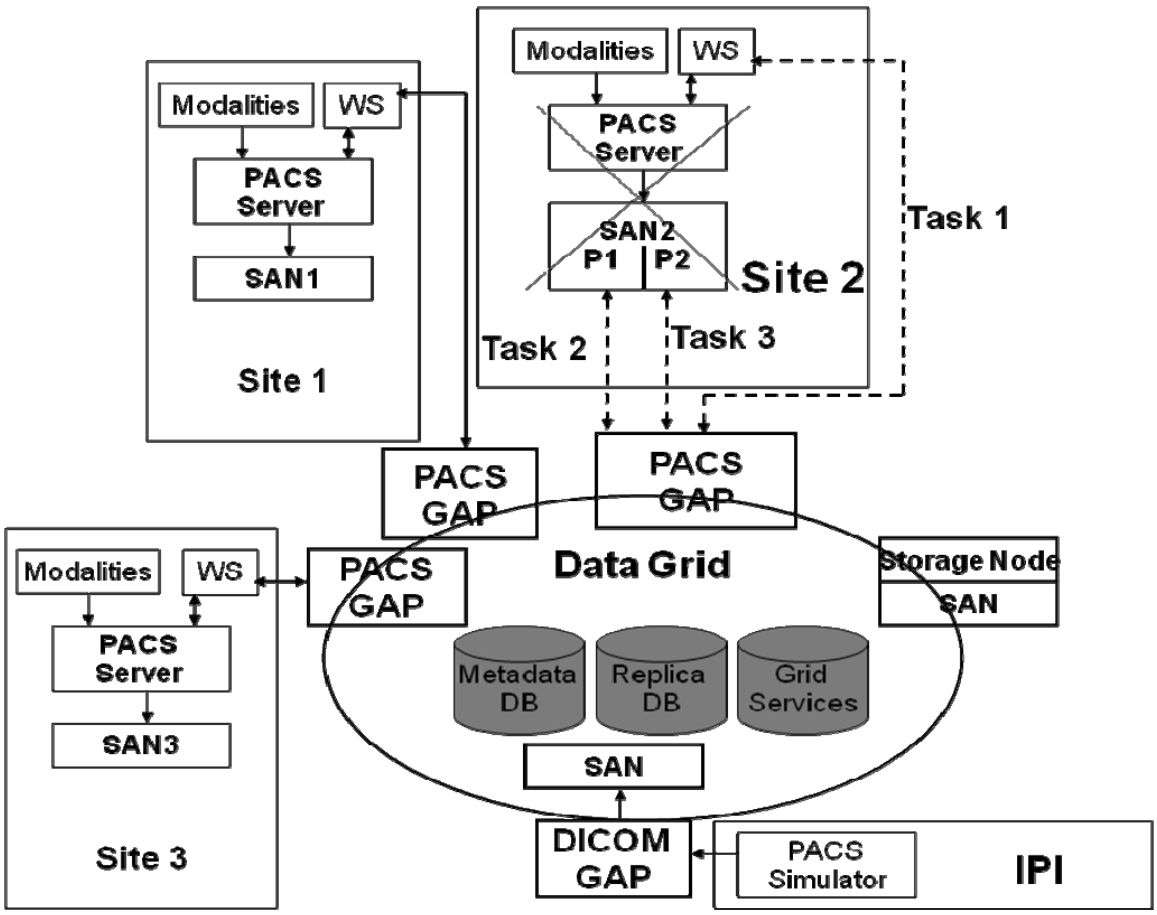

Figure 7. Three Tasks (dotted lines) of the Data Grid during PACS Server or Archive Failure. The PACS at Site 2 is used as an example in which either the server or the SAN or both fails (cross-lines). SAN2 is partitioned into P1 and P2. P1 is its own PACS archive, and P2 is Site 2's storage resource committed to the Data Grid. Task 1. Allowing its WS to Q/R its own images from the Data Grid for continuing clinical operation. Task 2. After its server and SAN have been repaired, the Data Grid rebuilds P1 of SAN2 installing the PACS own images. Task3. After its server and SAN have been repaired, the Data Grid rebuilds P2 of SAN2 which have the backup images of other PAC systems connected to the Data Grid. All three tasks are performed automatically without human intervention. Note that all backup storages and connections to the Web client Common View for image Q/R from the three PACS servers are not necessary and thus discarded (Compare with Figure 4). Courtesy of J Lee.

4. Grid Computing – Combining Image Management and Analysis

A computational service infrastructure in the Data Grid provides dependable, consistent, pervasive, and inexpensive access to computational capabilities. Globus toolkit described in Sections 2 and 3 including Fabric, Core and User-level middleware services (refer to Figure. 3 shadow boxes) enable the expansion of Data Grid to Grid Computing applications. The Grid execution environment includes computing and storage services with diverse capabilities. [16] Five computational services using the Globus toolkit in the Data Grid infrastructure have been developed. We first describe the basic infrastructure and then in Sections 4.2 and 4.3 use this infrastructure to present CAD of multiple sclerosis (MS) on MRI, and CAD/PACS integration, respectively. [17]

Computational Services Architecture in the Data Grid

In Grid environment, an application component can be implemented in different source files; each compiled to run in a different type of target architecture. Exact replicas of the executable file can be stored in many locations, which helps reduce execution time. Data files can also be replicated in various locations. Each file has a description of its contents in terms of application-specific metadata. The Metadata Service including Catalog Service (See User-level Shadow box of Figure 3) responds to queries based on application-specific metadata and returns the logical names of files containing the required data. Given a logical file name that uniquely identifies a file without specifying a location, the Replica Location Service (RLS, Shadow in Core Middleware, Figure 3) can be used to find physical location for the file on the Grid.

In Grid Computing, a specific application may require a certain type of resources for execution. Figure 8 shows the operation architecture of the computational services as follows:

1. The client requests resources from GRID MDS (Monitoring and Discovery System) server, which manages the resources and distributes the jobs to computational services.
2. The index service finds resources appropriate to the requirements of application components and notifies the client to send the application to the Grid Resource Allocation and Management (GRAM) service.
3. The GRAM service acknowledges MDS after it receives the application, jobs that completely specified for execution are sent to the scheduler that manage the resources and monitor execution progress. Execute acknowledges MDS server the completion of the job.
4. MDS notifies the client that the job is completed.

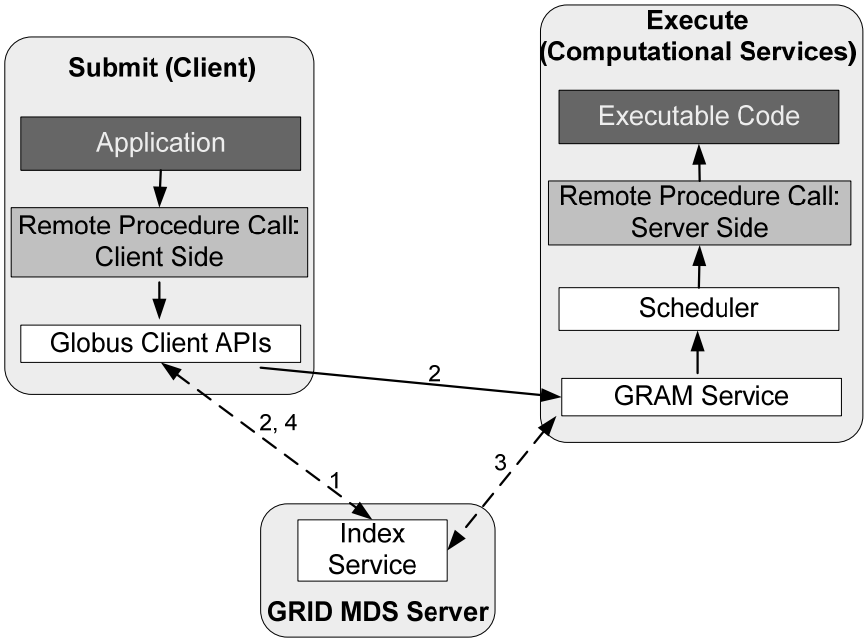

Figure 8. Operation architecture of the Grid Computing. Left: A client, Right: Computational Services. MDS: Monitoring and Discovery System, GRAM (Grid Resource Allocation and Management). Numerals represent the workflow, see text.

An Example of the Computing Grid – CAD of Multiple Sclerosis (MS) on MRI

Multiple Sclerosis

Multiple sclerosis (MS) is a progressive neurological disease affecting myelin pathways. Multiple lesions in the white matter (myelin pathways) can cause paralysis and severe motor disabilities. Symptoms are Changes in sensation, visual problems, muscle weakness, depression. MRI has become the medical imaging study of choice both for the diagnosis and for the follow-up and monitoring of multiple sclerosis. The progression of the disease is variable, and requires routine follow-up to document disease exacerbation, improvement, or stability of the characteristic MS lesions. Current status is that it is easy to make diagnosis from MRI, but time consuming to quantify the number and size of lesions, and its poor reproducibility. Imaging Informatics using CAD is considered an ideal quantitative tool to monitor progression of MS. [18] Two-Dimensional CAD using MRI T1 and FLAIR sequences with 5 mm slice are the most common imaging techniques to make MS diagnosis, with the former for brain anatomy and the latter for MS locations. Several commercially available CAD techniques for MS detection are being used in clinical environment, however, these methods have several weaknesses. First, they are mostly 2-D and often require human intervention to identify the MS lesions. Second, these methods lack the informatics component to organize and accurately measure the many lesions detected for disease progression comparison with time and/or treatment. Third, these methods are mostly stand alone CAD and can not be readily integrated with PACS for routine use in daily clinical operation. Data Grid and CAD/PACS Computing Grid can be used to alleviate these shortcomings of current methods. Based on anatomical and pathological knowledge guided, we have developed a 3-D CAD to quantify MS lesions on MRI with thinner slice for comparative quantitative studies. Here, we will not discuss the details of 3-D CAD methodology except the image processing steps, instead we describe the Data Grid and Computing aspect of the 3-D MS CAD. Section 4.3 will present the CAD-PACS integration with the Data Grid and Computing Grid.

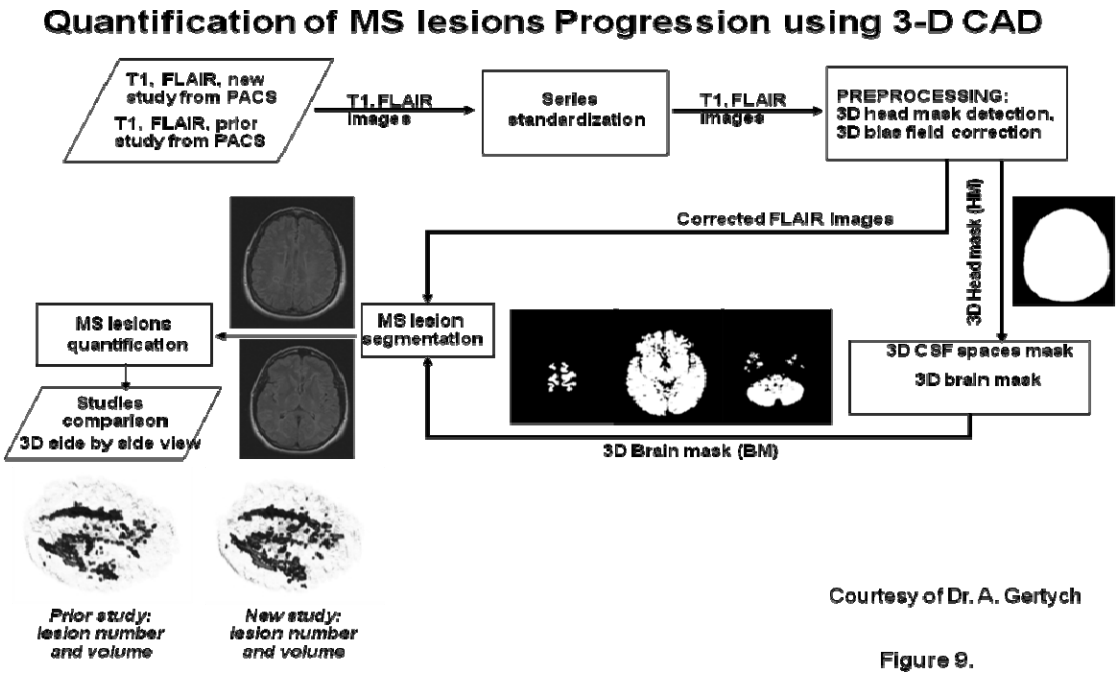

Figure 9. The image analysis work-flow of 3-D MS CAD. T1 and FLAIR sequences are first standardized and preprocessed followed by detection, segmentation, quantification, and visualization of 3-D MS lesions. Quantitative and visualization Comparison between original and follow-up 3-D MRI studies are also available.

Integration of MS CAD with Data Grid and Grid Computing

The steps required in the computational procedure of quantitative diagnosis of MS using CAD are shown in Figure 9. Assuming that such a 3-D CAD software package is available, Figures 10 depicts the workflow steps 1 – 4 of the MS CAD modified for the computational resources based on the Data Grid and the Computing Grid architectures discussed in Figure 8 and CAD workflow in Figure 9. Figure 11A, B, C, D show MS CAD results and the corresponding DICOM Structured Report file of a patient with twenty-six lesions

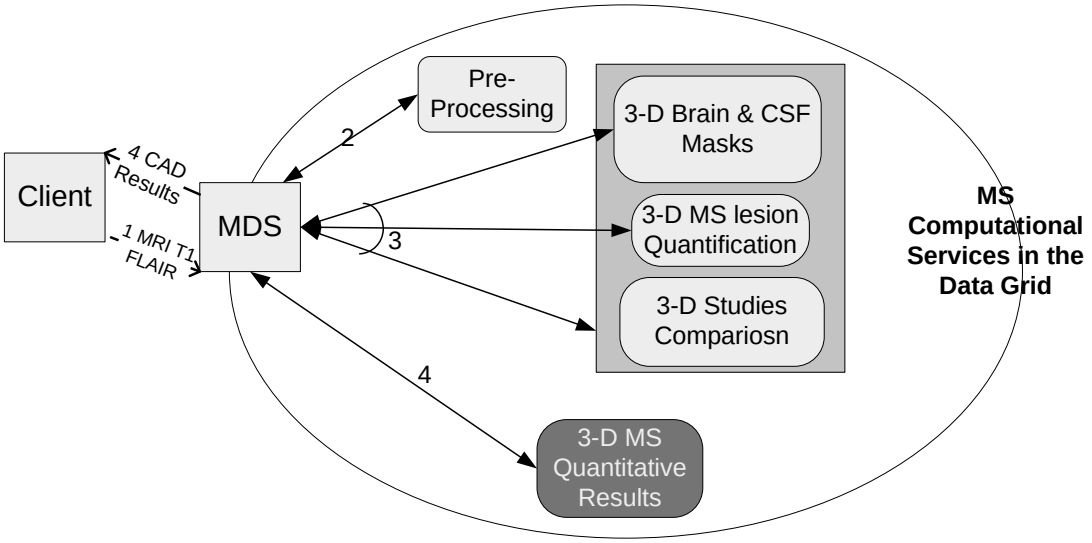

Figure 10. Operation workflow of MS CAD in computational services of the Data Grid and Computing Grid. The MDS allocates the computation requirements according to available services in the Data Grid. Numerals, see text, represent the workflow within the MS computational services. MDS: Monitoring and Discovering System server.

1. MRI T1 and FLAIR image sequences are sent by the Data Grid client to the Data Grid MDS (Monitoring and Discovering System) server.
2. MDS distributes sequence images to the preprocessing resource which performs series standardization, 3-D head mask detection, and 3-D bias field correction.
3. MDS distributes preprocessed sequence images to 3-D brain and CSF (cranial spinal fluid) masks, MS lesion detection and quantification, and studies comparison computational services for processing; and receives processed results.
4. MDS sends processed results to 3-D quantification results resource for organization and receives the compiled single or comparison study results. MDS returns compiled study results to the client with visualization and display.

The advantages of developing the computational services in the Data Grid for MS CAD versus using the conventional standalone CAD method are:

1. It utilizes the existing Data Grid technology which saves the job distribution and computation time.
2. It does not require to significant rewrite the image processing codes for the computational services in the Data Grid, this approach of distributing computations to available resources would result in substantial acceleration of data analysis speed.
3. With the progressively increasing use of MS CAD in clinical centers, utilizing Data Grid architecture can assure easier distribution of computational services throughout the Data Grid

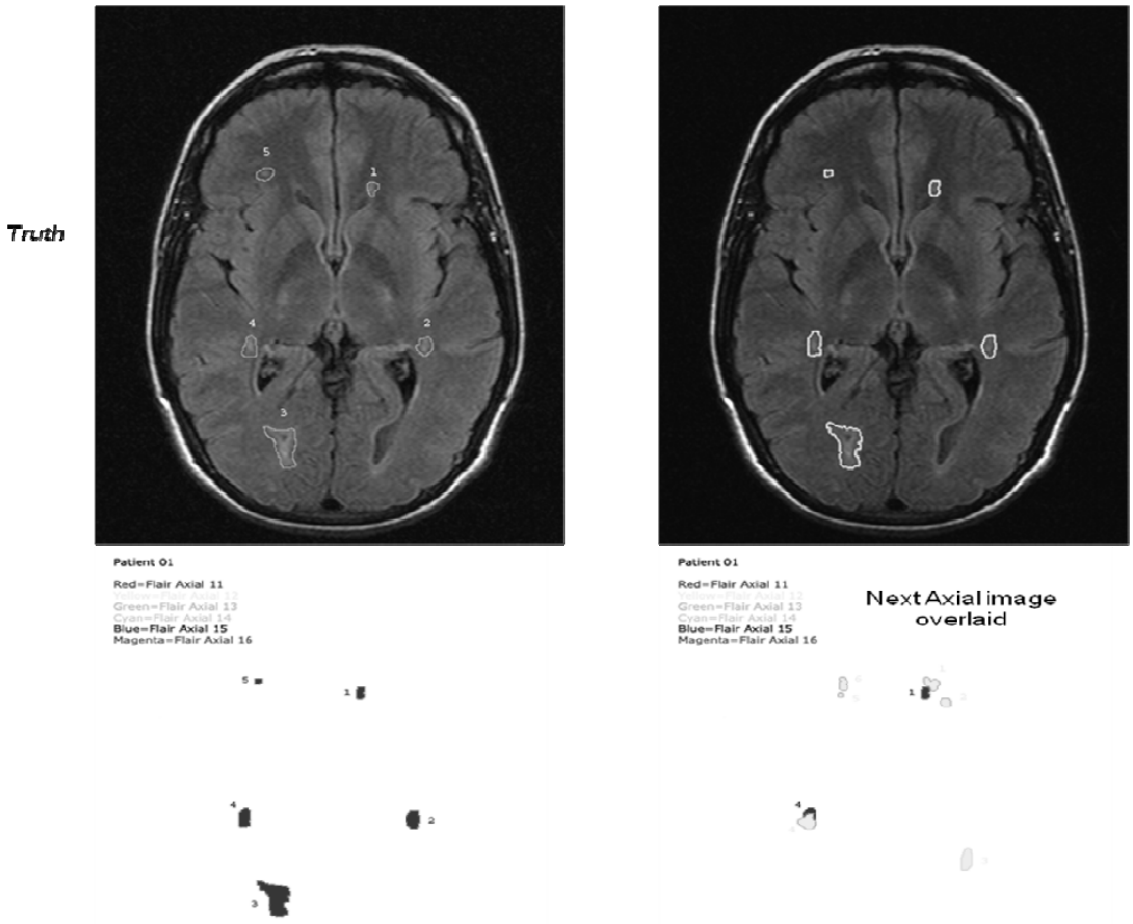

Fig 11 B.

DICOM Structured Report of MS in a PACS WS

Lesion Name	Slice areas included in lesion	Total Count	Red	Yellow	Green	Cyan	Blue	Magenta
A	red 1, yellow 1	**213**	82	131				
B	red 2	172	172					
C	red 3	617	617					
D	red 4, yellow 4, Green 3	**501**	188	212	101			
E	red 5	24	24					
F	yellow 2	65		65				
G	yellow 3	194		194				
H	yellow 5	16		16				
I	yellow 6	79		79				
J	Green 1, Cyan 5, 8, 9-10, 6*, Blue 5*	**1058**			143	634	281	
K	Green 2	250			250			
L	Cyan 1	50				50		
M	Cyan 2	50				50		
N	Cyan 3	120				120		
O	Cyan 4	82				82		
P	Cyan 6	58				58		
Q	Cyan 7	55				55		
R	Cyan11, Blue 6-7 Magenta 2	**393**				151	170	72
S	Blue 1	37					37	
T	Blue 2	111					111	
U	Blue 3	0					0	
V	Blue 4	102					102	
W	Blue 8	125					125	
X	Blue 9	52					52	
Y	Blue 10	88					88	
Z	Magenta 1	89						89
* Cyan 5 and 6 are not connected in slice 14 but join lesion J through Blue 5.								

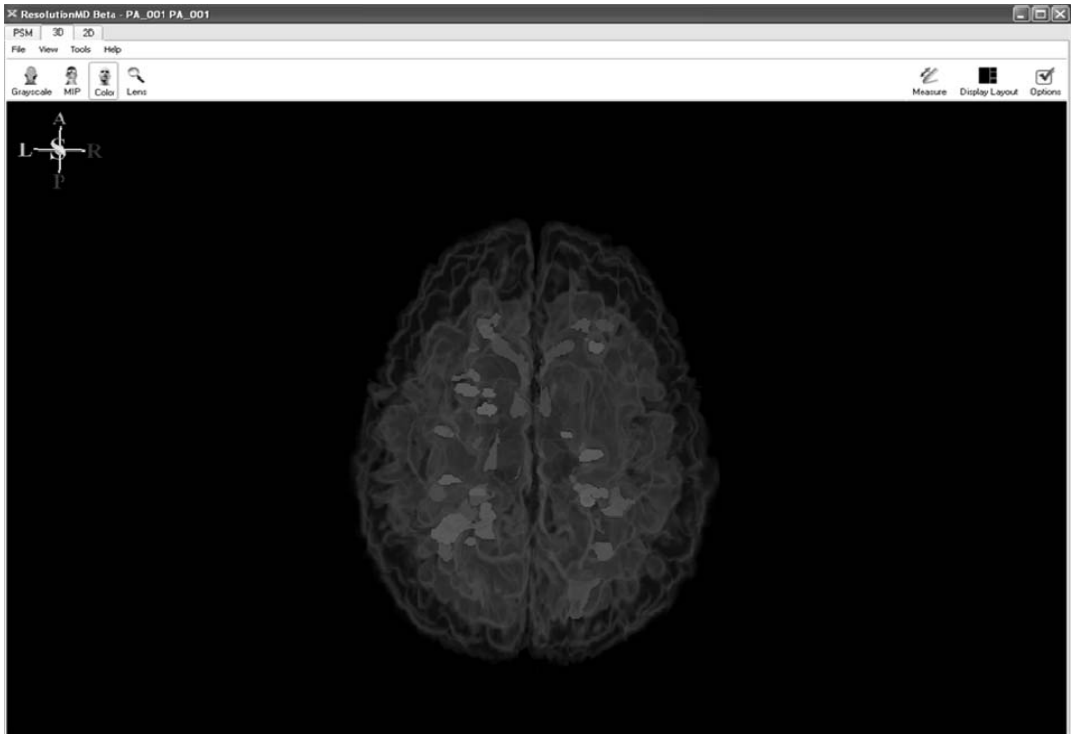

Figure 11. CAD identified, organized with provided quantitative measurements of twenty-six Multiple Sclerosis (MS) lesions of a patient shown in the DICOM Structured Report. Structured Report information could be extracted by the Metadata database in the Data Grid for storage, distribution and future analysis. See legends A, B, C, D, and E in next page.

1. Fig. 11, Top Left: Identifying and Quantification of MS in an MRI FLAIR image, comparing radiologist reading (True from diagnosis, Left) with CAD results (Right).
2. Middle Left: Two consecutive images in which MS lesions were identified and aligned with colors. Courtesy of Guardian Technology.
3. Bottom Left: Twenty-six MS lesions were identified in the case and organized in color code. Courtesy of Guardian Technology.
4. Top Right: Twenty-six (A-Z) MS lesions were detected and organized, the quantitative results of each in number of pixels shown in the DICOM Structured Report in color code. Courtesy of Guardian Technology.
5. Bottom Right: A screen capture of the top view of 3-D rendering of the brain with MS lesions. The brain ventricular system was used as a reference of positions of the lesions.

Integration of CAD/PACS with the Computational Services in the Data Grid

Most CAD method is a developed for standalone operation as a second reader, it does not integrate with PACS clinical workflow. Recently, a CAD-PACS toolkit was introduced which allows CAD to be integrated with PACS workflow enhancing the usefulness of CAD. [17] Integration of the CAD-PACS toolkit with Data Grid and Grid Computing would allow streamlining of CAD results and PACS operation in Grid environment. The PACS-CAD toolkit consists of two components, a DICOM Secondary Capture (DICOM-SC™) and a DICOM-IHE™ component to accommodate various PACS operations (Figure 12).

The DICOM-SC™ component installed on a CAD workstation converts the screen shot of video display of CAD results to a DICOM image file for storing in a PACS server and displaying on PACS workstations. The workflow is as follows (Figure 13):

1. The PACS WS sends DICOM image files to CAD WS for process. The CAD WS receives DICOM files and performs the CAD.
2. The DICOM-SC with i-CAD-SC package installed in CAD WS converts the screen shot of CAD results to DICOM files and sends it to PACS Server. If the CAD does not have the capability to provide screenshot, the i-CAD Screen Capture is used to capture the CAD windows creating the screen shot. This output image is created as a DICOM secondary capture image having the same patient information of the original DICOM image with a new generated series information called Screen Capture in DICOM header. Therefore, it will be stored as additional series under the same study of patient data model in PACS server.
3. When the PACS WS queries the PACS Server, the new series containing the CAD results will appear as a series under the study of patient. Radiologists can retrieve the CAD results with the study to their PACS WS. The CAD results are shown as a DICOM image.

The DICOM-IHE™ component follows DICOM standard and IHE (Integrating the Healthcare Enterprise) [19] workflow profiles using DICOM Structured Report and Post-Processing Workflow Profiles. Thus, results from various CAD software can be integrated into diagnosis workflow of a PACS having DICOM and IHE-compliance and, most importantly, these quantified CAD results in Structured Report format can be archived in the metadata services of the Data Grid (See Figure 3). Computational services can be developed in the Grid Computing to directly query and retrieve CAD results within PACS for future data analysis and mining applications. Figure 14 shows the workflow.

1. PACS server pushes a DICOM worklist to i-PPM (Post-Processing Manager) to requesting a CAD process for the studies. If PACS server cannot push the worklist, the i-PPM can query the PACS server for DICOM worklist automatically.
2. The CAD WS queries the CAD worklist from i-PPM. The CAD claims work items to be performed.
3. The CAD WS queries/retrieves DICOM images from the PACS server for CAD process.
4. The CAD WS sends "work item in progress" message to the i-PPM.
5. The CAD WS performs CAD process and stores the CAD results in the Receive-SR installed in the PACS server. The CAD WS uses computational services described in Figure 10 for CAD process.
6. The CAD WS reports Work Item PPS & Work Item Completed Message to the i-PPM.
7. The PACS WS retrieves the DICOM SR CAD results for physicians' review. The web-based Display-SR can be used in the PACS WS to view the CAD results and perform future analysis.

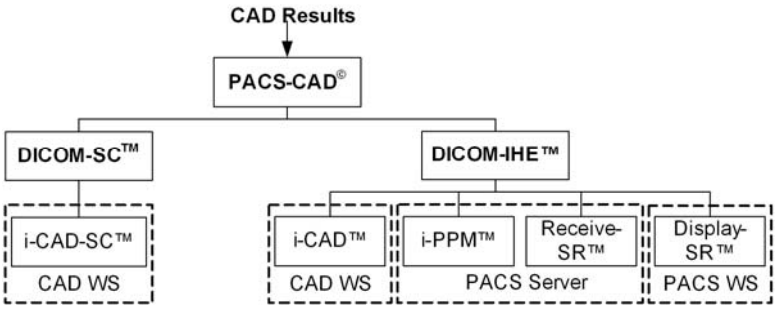

Figure 12. PACS-CAD Model Toolkit. The PACS-CAD toolkit consists of two components, a DICOM Secondary Capture (DICOM-SC™) and a DICOM-IHE™ component to accommodate various PACS operations. DICOM-SC is easy to implement but the data is in screen capture format which does not allow for data manipulation and analysis. DICOM-IHE involves system integration which requires cooperation of PACS manufacturers to implement. Once implemented CAD results are in the PACS workflow which allows for data analysis and mining.

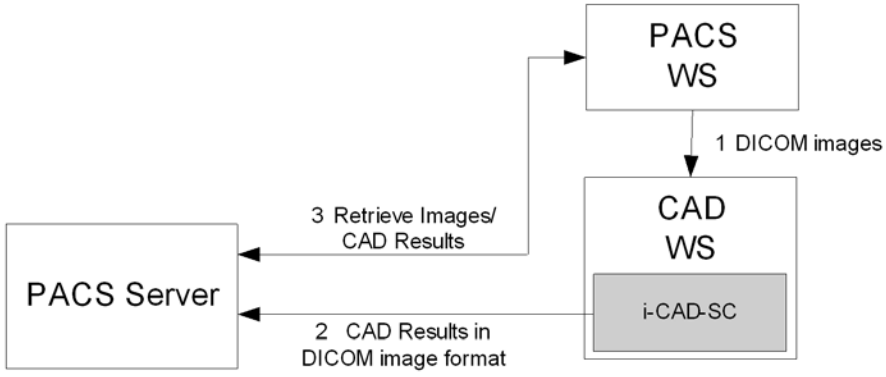

Figure 13. DICOM-SC (Secondary Captured). The DICOM-SC toolkit installed on a CAD workstation converts the screen shot of CAD results to a DICOM image file for storing in a PACS server and displaying on PACS workstations. See text for its workflow.

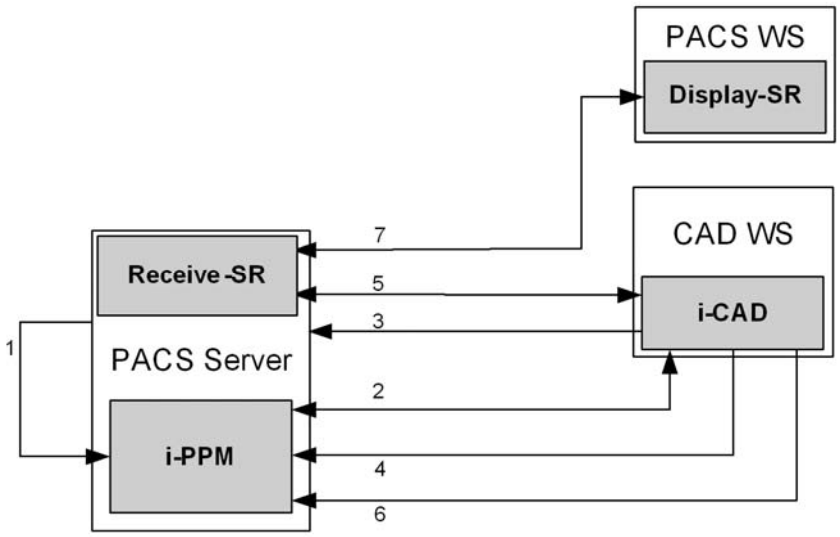

Figure 14. DICOM-IHE Workflow. The DICOM-IHE toolkit follows DICOM standard and IHE workflow profiles using DICOM Structured Report and Post-Processing Workflow Profiles. Results from CAD can be integrated into diagnosis workflow of a PACS having DICOM and IHE-compliance. Quantified CAD results in Structured Report format can be archived in the metadata services of the Data Grid (See Figure 3).

5. SUMMARY

Grid computing is a powerful tool for large-scale computation and storage requirements. In this chapter we present a novel concept of Data Grid for medical image application, in particular, for daily clinical PACS on-site archive, off-site backup, and disaster recovery. PACS Data Grid is based on the Globus 4.0 toolkit, with SAN storage technology and some DICOM resources to form an integrated fault-tolerant archive system.

Grid Computing utilizes the Data Grid infrastructure for specific medical imaging applications by adding necessary computational services. We use computer-aided diagnosis (CAD) of multiple sclerosis (MS) of brain on MRI as an example. The computational services required in CAD MS include image preprocessing followed by detection, segmentation, quantification, and visualization of 3-D MS lesions. Grid computing for large-scale medical image archiving and analysis is still in its infancy, we anticipate many fruitful results will materialize in the near future.

ACKNOWLEDGEMENTS

This research has been partially supported by NIH R01 EB 00298 and NIH R01 LM07606 grants, and a contract from MI^2.

REFERENCES

[1] What is grid computing, http://www-1.ibm.com/grid/about_grid/what_is.shtml

[2] Baker M, et al, Grids and Grid technologies for wide-area distributed computing, *Proceedings of SPIE Medical Imaging*, *February,* 2002.

[3] The Grid: A New Infrastructure for 21st Century Science, http://www.aip.org/pt/vol-55/iss-2/p42.html,

[4] Morgan K, Computational Grids, *The Grid: Blueprint for a New Computing Infrastructure*, Chap 2, 1999.

[5] Foster I, Kesselman C, Nick J, Tuecke S, The Physiology of the Grid: An Open Grid Services Architecture for Distributed Systems Integration. In Open Grid Service Infrastructure WG, *Global Grid Forum*, June 22, 2002.

[6] Foster I, Kesselman A, Tuecke S. The Anatomy of the Grid: Enabling Scalable Virtual Organizations. *International J. Supercomp Applications*, 15(3), 2001.

[7] Foster I, Kesselman C, Nick J, Tuecke S. Grid Services for Distributed System Integration. *Computer*, 35(6), 2002.

[8] Globus Toolkit 4, http://www.globus.org/toolkit/docs/4.0/

[9] Huang HK, PACS and imaging informatics. Hoboken, NJ: John Wiley & Sons, 2004.

[10] Liu BJ, Zhou MZ, and Documet J, Utilizing data grid architecture for the backup and recovery of clinical image data, *J Comput Med Imag Graph* 29, 95-102, 2005.

[11] Doi K, Huang, HK. Special Issue Editorial: Computer-aided diagnosis and image-guided decision support, J *Comput Med Imag Graph* 31, No 3-4, 195-197, 2007.

[12] DICOM, http://medical.nema.org/, accessed on November 18 2006.

[13] HL7, http://www.hl7.org/, accessed on April 20, 2007.

[14] SAN Technology: http://www.storage.ibm.com/ibmsan/whitepaper.html

[15] Lee J, Zhou Z, Talini E, Documet, j, Liu B. Design and Implementation of a fault-tolerant and dynamic metadata database for clinical trials. *Proceedings of SPIE Medical Imaging*, Vol. 6516 0O-1-7, February 2007.

[16] Blythe J, Deelman E, Transparent Grid Computing: a Knowledge-Based Approach. *Fifteenth Innovative Applications of Artificial Intelligence Conference* (IAAI-03), Acapulco, August 12-14 2003.

[17] Zhou Z, Liu BJ, Le AH, CAD-PACS integration toolkit based on DICOM secondary capture, structured report and IHE workflow profiles. J *Comput Med Imag Graph* 31, No 3-4, 346-352, 2007.

[18] Wong A, Gertych A, Zee CS, Guo B, Liu BJ, A CAD system for assessment of MRI findings to track the progression of multiple sclerosis. *Proceedings of SPIE Medical Imaging*, Vol. 65142U-1-7, February 2007.

[19] IHE, http://www.ihe.net/, accessed on November 18 2006.

Chapter 28

Image-Assisted Knowledge Discovery and Decision Support in Radiation Therapy Planning

Brent J. Liu, Ph.D.

Assistant Professor and Deputy Director of Informatics,
Department of Radiology,
Keck School of Medicine
Department of Biomedical Engineering,
Viterbi School of Engineering
University of Southern California

Mailing Address:
Image Processing and Informatics Laboratory,
Department of Radiology
4676 Admiralty Way, Suite 601
Marina del Rey, California 90292
310-448-9440 (Direct)
310-448-9441 (Fax)
brentliu@usc.edu

ABSTRACT

This chapter introduces an application of a medical imaging informatics approach to develop a unified patient-oriented information system to handle complex Radiation Therapy (RT) imaging and informatics data during the course of the patient treatment. Currently, this data is scattered throughout each of the different treatment and information systems in the Oncology department. Additionally in this chapter, as an example, the methodology will be used to develop quantified knowledge and decision support tools for a brain tumor patient case treated by Intensity Modulated Radiation Therapy (IMRT). The use of the "inverse treatment planning" nature of IMRT allows for the extraction of quantified knowledge and the development of decision-support tools to assist in the decision-making process. This *a priori* knowledge, whether the dose distribution to the target tumor is acceptable while limiting dose to critical structures, resides within the expertise of oncologists and physicists. It is currently used in evaluating the acceptance of a treatment plan and this research will quantify this knowledge to derive decision support tools. As a result, the development of quantified knowledge can augment the conventional "inverse treatment planning" approach into an improved "knowledge-based treatment planning" process with better workflow efficiency and more precise dose predictions. The imaging and informatics methodology and approach can be extended to various clinical decision-making scenarios during the course of the patient's treatment for not only a specific RT treatment type but also a specific lesion type in any body region.

Chapter 28

Image-Assisted Knowledge Discovery and Decision Support in Radiation Therapy Planning

28.1 Introduction

28.1.1 Need for Imaging Informatics in Radiation Therapy Planning

The essence of medical imaging informatics is to use informatics methods to extract and synthesize the information-rich Picture Archiving and Communication Systems (PACS) and other patient-related databases to further advance medical research, education, and clinical services. Along the way, we need to develop methodology, tools, infrastructure, and applications. In this chapter, we first present the basic fundamental concepts of building a patient-oriented information system to integrate standardized imaging and informatics data based on DICOM and then introduce methodologies for developing quantified knowledge and decision-support tools during the Radiation Therapy (RT) Planning process. This application not only relies on PACS as a decision support tool but also must combine PACS image data with other medical specialty's data like in radiation therapy to form a new medical informatics server with decision support.

The need for comprehensive clinical imaging informatics in image-intensive Radiation Therapy (RT) is steadily recognizable because of ever increasing demands for better diagnostic and treatment equipment and more accurate information. Traditionally, multiple information systems acquire the necessary data during the RT treatment course of a patient, however, most of the data is scattered throughout each of the varying treatment and information systems. In addition, RT utilizes some of the most technological advancements in diagnostic imaging, therapeutic radiation, and computerized treatment planning systems, which adds to the complexity of the collection and navigation of pertinent RT data. Therefore, imaging informatics tools are needed for knowledge discovery to extract treatment planning data in support of oncologists and physicists' decision making process during daily practice. DICOM (Digital Imaging and Communication in Medicine) is the de facto imaging standard for imaging departments like Radiology, along with clinical workflow profiles (Integrating the Healthcare Enterprise, or IHE). This in turn led to their successful development and utilization of PACS which has become an indispensable integrated imaging system in diagnostic radiology. Furthermore, recently accepted concepts of Computer-Aided Diagnosis (CAD) integrated with PACS advances radiology to the next level of excellence in clinical care.
1,3,14-17] The readily available HL7 (Health Level 7), DICOM, and IHE are basic tools in the realm of medical imaging informatics which can be applied to RT. In addition, other more advanced and powerful imaging informatics methods such as data mining for knowledge discovery, CAD, and outcomes analysis can also be adopted and invented for the benefit of more accurate and efficient patient treatment planning.

28.1.2 Current State of Imaging Informatics in RT

Currently in RT, the practical use of imaging informatics tools is limited. DICOM is mostly used for transmitting PACS images to an RT system; and imaging-guided treatment planning systems are limited to dose computations and graphical data displays. Pertinent RT data results do not have a standardized protocol.

To address these shortcomings, the DICOM Standard Committee extended DICOM for the RT application by ratifying seven DICOM-RT objects [7]. Although some of these objects are utilized within the daily clinical operation in piece-meal fashion, they are not integrated. There are still data crucial to the decision-making process that has not utilized these standards. The need for a system integration infrastructure based on standards is crucial for the establishment of patient outcomes related medical informatics research. The methodology of developing quantified knowledge with decision-support that would augment the current robust and complex therapeutic clinical processes to ultimately improve the quality of patient care is needed. One such system integration infrastructure is the imaging-based electronic patient record (ePR), which is a patient-based digital virtual folder of clinical information obtained from various information sources. [2] The inclusion of imaging data and built-in decision support makes the ePR stand out amongst general clinical information systems, thus opening new doors to the possibility of improvement in clinical decision outcomes of the future in RT.

This chapter will discuss a methodology for research and development of a DICOM-Based ePR system with quantified knowledge-base decision-support tools to facilitate RT in therapeutic treatment planning. As an example, this chapter will discuss the development of necessary imaging informatics research tools on a specific clinical scenario for RT of brain tumor patients treated with Intensity-Modulated Radiation Therapy (IMRT), and specifically, the "inverse treatment planning" nature of IMRT using a Treatment Planning System (TPS). Quantified knowledge and decision-support tools based on the expertise of Oncologists and Physicists to assist in their decision-making process are designed and developed, thus augmenting the conventional treatment planning approach into a "***knowledge-based*** treatment planning." This methodology can be extended for future clinical decision-making scenarios during the course of the patient's treatment for not only a specific RT treatment type but also a specific lesion type in any body region. Let us review briefly the concept of ePR in the next section.

28.1.3 Review of Electronic Patient Record (EPR)

Electronic patient record is an emerging concept to replace or supplement the hospital- or clinic-based healthcare information systems. The concept of the ePR is a patient-based digital virtual folder of clinical information obtained from various information sources. The components of an ePR include an information model, a clinical data repository, a web-based application for the users, along with a security model and built-in decision support. The inclusion of imaging data

and built-in decision support makes the ePR stand out amongst general clinical information systems such as HIS and RIS (Hospital and Radiology Information Systems). The imaging data within the ePR data model has opened new doors to the possibility of improvement in clinical decision outcomes of the future. However, the difficulties involved in system integration across the healthcare enterprise have slowed the developmental progress. Currently, the United States Department of Veterans Affairs Healthcare Enterprise (VAHE) information system, VistA [2], is probably the most advanced enterprise-level ePR integrated with images compared with others in the field.

The major functions of an ePR system are:

- Accept direct digital input of patient data.
- Analyze across patients and providers
- Provide clinical decision support and suggest courses of treatment
- Perform outcome analysis, and patient and physician profiling
- Distribute information across different platforms and health information systems

The concept of the DICOM-RT based ePR System uses the ePR architecture with an individual patient as the focus.

28.2 Procedures and Methods

28.2.1 Introduction to the Medical Imaging Informatics Approach for Developing Quantified Knowledge and Decision-Support Tools

Figure 28.1 shows the overview of the methodology for designing and developing a DICOM-RT based ePR system and standardizing RT data into DICOM-RT objects. Once the standardized data objects are integrated, the next steps in the imaging informatics methodology is to develop the knowledge base, the data mining, and quantification and visualization tools which ultimately become add-on features to a DICOM-RT based ePR system. This methodology can be utilized for developing a knowledge base and clinical decision-making tools for a DICOM-RT ePR based system. Secondly, the integration of DICOM data from both RT and Radiology in a DICOM RT ePR server will be the foundation for the integration of future treatment planning systems for an efficient one-stop-shop source where clinicians can track and review their patient cases with decision-support tools and a knowledge base. The methodology steps will be discussed further in the following paragraphs.

28.2.2 Workflow Model Development

One of the most important first steps for system integration of clinical image and information systems is to research the workflow model of the clinical operations. The example that will be described in this chapter is patients with brain lesions who will be undergoing Intensity-Modulated Radiation Therapy (IMRT). The workflow related to these particular treatment cases should be studied to develop the workflow model. A general clinical workflow model for IMRT of brain tumor cases was developed for the Departments of Radiology and Radiation Oncology, Saint John's Health Center (SJHC), Santa Monica as shown in Figure 28.2. Although this workflow may be specific to SJHC, the workflow steps can be

extended to other institutions with further refinement. The treatment begins with the patient diagnosed with brain lesion or multiple brain lesions. The patient meets with the physician(s) and determines whether to treat the tumor(s) but also what type of radiotherapy will be performed. The patient is entered in an oncology information system and is scheduled for treatment. If conventional RT is prescribed, then a simulator image may be acquired. Otherwise, depending on the treatment type, such as IMRT, a diagnostic CT will be acquired to plan the treatment. The Radiologist and Radiation Oncologist review the patient's case and then the Radiation Oncologist defines the initial plan parameters such as dose limits and constraints, critical structures, and tumor volume to be treated. The physics team then computes the plan based on these dose constraints on the corresponding TPS. Once the initial plan is computed, the Oncologist reviews the results and makes any necessary changes. This process can be iterative and the feedback loop is defined in Figure 28.2 by a dashed line region. Once the treatment plan has been approved, the treatment session is executed by the Radiation Therapist, the corresponding RT plan data are stored in the treatment planning systems of the RT modalities and some results are also inputted into the oncology information system or a Record and Verify system. Since there are a variety of brain tumor types, and the treatment paths can differ, it is important to develop a robust workflow model that can accommodate the various treatment paths and identify points within the workflow that can be improved. Not only would this enhance the design of the DICOM-based ePR System, but also serve as the foundation for a methodology to build quantification and visualization tools for decision-support. In our example for this chapter, the iterative feedback loop is identified as a potential area of improvement. The feedback loop represents the inverse treatment planning process and can be quite tedious if much iteration is necessary. This becomes the area of focus where decision-support tools may benefit during the decision-making. If more *a priori* knowledge and robust quantification and visualization tools can be included during the decision-making process of the initial plan parameters, then it is possible to reduce the iterative process.

28.2.3 DICOM-RT Data Model Development and Data Collection

The DICOM (Digital Communication in Medicine) standard has been well established and widely successful for clinical imaging systems in Radiology, in particular PACS (Picture Archiving and Communication System). Image data acquired from equipment from different vendors can readily communicate with each other and integrate into a system through the DICOM standard. In 1997, the DICOM standard was extended to include radiotherapy information and further updated in the latest version released in 2003. [4,5] Seven DICOM radiotherapy (DICOM-RT) objects have been included by the DICOM standards committee for transmission and storage of radiotherapy images and related information [6]:

RT Image (1997)

- includes all images taken using radiotherapy equipment such as conventional simulators, digitizers or electronic portal imagers

RT dose (1997)

- contains dose data such as dose distribution generated by treatment planning system, DVH (Dose Volume Histogram), dose points etc.

RT Structure Set (1997)

- contains information related to patient structures, markers, isocenter, target volume, contours and related data.

RT Plan (1997)

- refers to information contained in a treatment plan such as beam angles, collimator openings and beam modifiers, etc.

RT Beams Treatment Record (1999)

- records for external beam treatment

RT Brachy Treatment Record (1999)

- records for brachytherapy

RT Treatment Summary Record (1999)

- summary of a patient's radiation treatment

Most RT vendors are at the various stages of implementing these objects, in particular the 1997 ratified objects, RT Structure Set, Plan, Image, and Dose. The three Record objects are still in their preliminary stage of implementation by vendors. Figure 28.3 categorizes these objects and their contents against those of diagnostic radiology. The advantages of having these DICOM objects in RT are obvious. First, information and images within an object can be transferred across the boundary of different RT vendors with minimum efforts from the users. Second, it allows the total integration of RT components from various vendors. Third, the workflow of RT treatment can be closely monitored and analyzed resulting in a better healthcare delivery to the patient. Fourth, an individual patient's RT treatment can be integrated under the scheme of Electronic Patient Record (ePR), a current trend of patient-oriented healthcare delivery system. The individual RT treatment ePR can be combined with other related information including demographic, diagnostic, pharmacy, clinical laboratory, and others under the same format and standard. This will result in a portable ePR of the patient, a giant leap from the current hospital or healthcare information system which is organization-oriented. The DICOM-RT object information models can be utilized to develop the data structure for the electronic patient record. To develop a conceptual data model, the RT workflow must be reviewed to define the data required. Additionally, clinical user input is needed as well. Along with the input sources mentioned above, a conceptual model can be developed for an RT electronic patient record.

A data survey should be performed to track and collect patient cases utilizing any related clinical oncology information systems as well as diagnostic images from PACS. In our example, cases that exhibit brain tumors were tracked to determine the treatment path and outcome. The preliminary data collection survey was performed to determine the feasibility of data collection for the treatment of brain tumors. A sample data set from an IMRT TPS at Saint John's Health Center (SJHC, Santa Monica, CA will be presented and discussed in the further sections.

28.2.4 DICOM-RT Data Conversion and System Integration

Based on the clinical workflow model as well as the guidance of expert users such as oncologists and physicists, a data model can be developed to determine which data will be needed to convert into DICOM-RT objects and which are already in the DICOM-RT format. The data model includes:

1) Patient demographic data
2) CT images
3) Reference and portal images (eg, Simulator Images, Digitally Reconstructed Radiographs - DRR)
4) Critical structure curves
5) Isodose curves
6) Dose limits and weighting factors
7) Dose Volume Histogram (DVH) curves
8) Radiation beams records.

The data not in DICOM-RT format are converted into the seven DICOM-RT objects described in Section 28.2.3. Integration of these data objects into the DICOM-RT ePR system is the next step. For the DICOM RT ePR system, a three-tier architecture was developed [8]: 1) The RT archive server manages, archives and distributes DICOM images and DICOM-RT objects, 2) The RT web-based application server processes patient planning and treatment data, and 3) the RT web-based client application presents the RT data. The database schema reflects this three-tiered system by physically representing the data as well as providing data structures, file organizations and mechanisms for system operation as well as data storage. In the design of the RT workflow, there are two database schemas developed; one for the RT archive server and the second for the RT web-based ePR application server. Because there is more RT data presentation at the web-based application server level, the latter database schema is much more complex as compared to the RT archive server. Based on the Data Model and the Clinical Workflow Model, the data workflow was designed as shown in Figure 28.4 for system integration [9-11].

Data from the Oncology Information System and the IMRT TPS are converted into DICOM-RT objects and sent to the DICOM RT Gateway. The diagnostic images are sent from the PACS Server into the DICOM RT Gateway as well. Once the DICOM-RT objects have been received by the DICOM RT gateway, they are sent to the Archive server. A database schema is developed for the archive server so that the DICOM RT objects can be archived and distributed to the web-based application server. The archive server should be a Continuous Available (CA) server design with 99.999% uptime that has been previously utilized for a variety of clinical applications. [12, 13] Integration of the DICOM-RT ePR System within the clinical environment includes, in our example, evaluating the target feedback loop shown in Figure 28.2. The iterative process of inverse treatment planning is an example where additional knowledge and decision-support tools can improve the overall decision-making process. Based on input from both Radiation Oncologists and Radiation Therapists at SJHC, married with existing data and workflow models, a database schema and user

interface design was developed to meet the clinical needs. This is implemented in the Web-based application server as well as the web client. [8]

28.2.5 Knowledge Base Development

Knowledge is defined and quantified based on the expert's ability, either the oncologist or physicist, to utilize data and other criteria in evaluating, grouping, and defining certain clinical characteristics that are extracted from the standardized DICOM-RT objects stored within the ePR system. The knowledge base is designed in an object-oriented and modular fashion so that additional knowledge and new object classes defined in the future can be easily integrated without affecting the overall design. An example of quantified knowledge modeling is the dose constraint relationship between the weighting factor and the DVH curve of each critical structure and target tumor which can be loosely defined mathematically as:

$$w_i = f\left[DVH_1 \ldots DVH_N\right],$$

where the weighting factor *i* of a particular tumor or critical structure has a value function relationship with all DVH curves from 1 to *N* in the treatment plan. This relationship can be defined by analyzing the DVH curves and the changes to each of them when a particular weighting factor is modified between iterations. The functional form "f" can be defined further when more clinical experience is gained during the course of research and development. Likewise, the relationship between the DVH curves and the isodose curve lines on each of the image slices can be loosely defined as:

$$DVH_i = \sum_{j=1}^{M} isodose_j ,$$

where a particular tumor or critical structure's DVH curve *i* is a summation of all the 1 to *M* isodose curves within the diagnostic image slices of the treatment plan. The two models above will depend on rudimentary quantified knowledge data elements. These data elements can be derived from the knowledge base schema which can be defined into class objects. A few of these are shown in Figure 28.5 along with their attributes:

- Class Object 1) DVH
- Class Object 2) Isodose curve
- Class Object 3) Critical Structure
- Class Object 4) CT image.

Then, for each of these classes, attributes can be defined as shown. For example, for the CT Image class object, there are the primary key (PK) identifier and five attributes: Critical Structure Curve; Isodose Curve; Spatial Coordinates of the image including x, y, and z-directions; Pointer to the image data; and DICOM header data. The relationships between each of the class objects are through the Foreign Keys (FK). For example, in Figure 28.5, Isodose Curve FK1, and Critical Structure FK2 are related to CT Image object. This is because a CT image would contain multiple isodose curves and multiple critical structures. Another example is that the DVH class uses the critical structure volume attribute to relate to the FK1 Volume of the Critical Structure object. Once the knowledge

has been defined and knowledge base schema developed, the knowledge can be extracted and stored within the knowledge base. A search engine can be built to perform queries on the quantified knowledge for automatic extraction of particular knowledge described and further illustrated in the next section.

28.2.6 Data Mining for Knowledge and Development of a Quantification and Visualization Tool

Referring again to the clinical scenario described in section 28.2.2, a quantification and visualization tool can be developed to automatically mine the knowledge base for the information needed to assess a treatment. The tool design used as an example in this chapter and user interface was developed through the guidance of the oncologist and physicist at SJHC. Figure 28.6 shows an illustration of a mockup for data mining utilizing quantification and visualization tools to be developed for decision-support of treatment plan assessment. This proof-of-concept method shows how quantified knowledge can be mined for and then visually presented as an example for further development of powerful and effective decision-support tools. This specific tool example eliminates the tedious manual procedure of first analyzing the DVH curves, which is a 2-D plot graph, and then having to toggle through a 3-D volume of CT image slices overlaid with multiple isodose curves to identify locations and characteristics of regions within critical structures that are receiving radiation overdose. These areas are sometimes called “hot spots”. The exact diagnostic CT image slice together with the exact critical structure and tumor contours and isodose curves representing hot spots can be automatically displayed as a warning and red flag to the oncologist during the review of the treatment plan. In addition to the illustration presented in Figure 28.6, important quantified knowledge measurements can also be displayed. The results of the research and development based on this mockup design and the quantified knowledge measurements will be further discussed in section 28.3. Any design of what quantified knowledge to present and how it will be presented should be closely guided by the oncologist and physicist. Some of this knowledge can include:

- Percent region of critical structure covered by an isodose curve
- Shape models of overdose and prescription dose regions
- Ratio of overdose to critical structure regions
- Shape models of DVH curves
- Location models of dose of target tumor and critical structure regions.

The decision-support tools can be used real-time by the expert users anywhere since the ePR is web-based and portable. In the long term, as more knowledge data is collected from additional brain tumor patients treated with IMRT, as in this example, the knowledge base will be enriched accordingly.

28.3 Results of Developed Quantified Knowledge and Decision-Support Tools for an Example of a Brain Tumor Patient Treated with IMRT

28.3.1 DICOM-RT ePR Timeline Overview Display

This section describes some of the results of an example of a brain tumor case treated by IMRT utilizing the TPS for treatment planning and integrated within the DICOM-RT based ePR system. The end result is a comparison between what clinical information is displayed by a conventional RT information system provided by a manufacturer versus that of the richer database of the preliminary DICOM-RT based ePR system which can provide more information in the display. In addition, some preliminary development of the knowledge base, quantification, and visualization tools is presented based on the particular clinical scenario of assessing treatment plans of brain tumor patients. Figure 28.7 is a timeline overview display showing that a CT and MR diagnostic exam was acquired for a sample patient. Referring to Figure 28.7 (bottom), a conventional RT management information system or record & verify system only has the DICOM RT records but no DICOM RT plan, RT images, and DICOM images. On the other hand, the DICOM-RT based ePR system is able to display information extracted from all of the DICOM-RT objects and can be expanded for more detailed views from the icons on the timeline in the User Interface (both bottom & upper sections). The data reconstructed in the DICOM-RT based ePR system were converted to DICOM-RT objects that can be further distributed to other clinical areas and DICOM-compliant clinical systems while the data from the TPS are proprietary and difficult to distribute throughout the healthcare enterprise. In addition, this standardized data can be used to develop knowledge based on clinical scenarios as well as data mining tools to extract this knowledge for decision-support.

28.3.2 Development of a Visualization Tool with Quantified Knowledge

As an example for this chapter in the medical imaging and informatics approach towards the development of decision-support tools, a clinical scenario where an oncologist needs to assess the isodose plan of critical structures from a treatment plan for a brain tumor patient has been identified and applied to this methodological approach. During treatment planning for brain tumor patients, the treatment plan developed, usually by the physicist, must be approved by the oncologist as shown earlier in the workflow in Figure 28.2. Part of the clinical decision-making process for the physician is to analyze the DVH curves of critical structure areas to evaluate whether the critical structures are receiving an overdose of radiation that is clinically unacceptable. These curves only show dose values in relation to the critical structure volume. The physician must then evaluate the various isodose plans to first locate areas of overdose within the critical structures called “hot spots”, and then to determine whether the plan is acceptable or whether it must be modified and recalculated. In order to make this clinical assessment, the oncologist must navigate through multiple image slices showing multiple isodose curve lines as well as overlapping critical structures to make the assessment. Navigation of all this knowledge, while crucial, is also extremely tedious and complex since there is no tool to quantify and visualize the direct relationship between the DVH curves to the diagnostic images and the corresponding dose and critical structure curves. Based on the methodology described previously, a tool has been designed to automatically

display the DVH curve of a critical structure linked with the diagnostic image slice(s) that contain corresponding isodose curves and critical structure regions.

28.3.3 Development of a Web-Based GUI for Visualization of Quantified Knowledge

Figure 28.8 shows a screenshot of an overview of a particular IMRT Treatment Plan (TP). The Letter A indicates tabs that display different page views. The first view is the TP Overview which shows the general overview showing the DVH curves and the DICOM CT Images with isodose curves overlaid. The TP Evaluation page allows the User to quickly assess a treatment plan for hot spots. The TP Knowledge Base Search page allows users to query for specific knowledge and will be developed in the future. The TP Comparison page shows quantified knowledge for two different TP Iterations in a comparison mode. The Letter B indicates a timeline display showing all TP's, both current and historical, of a particular patient. The letter C indicates a drop-down window which allows the user to view different Iterations within a current plan. The Letter D indicates the DVH Curve of a particular plan with the overdose area shaded for the Optic Chiasm. The letter E indicates DICOM Images with isodose curves overlaid from the TPS. All data is in DICOM-RT Format and standardized. The User can further view each of the DICOM images with isodose curves by selecting one of the images. A pop-up window is generated with a larger image view window. Tools Such as Zoom, Pan, and Window/Level are included as well as the ability to toggle on and/or off particular isodose curves or critical structure curves to allow the User to properly review the plan.

Figure 28.9 shows the TP Evaluation Page with the DVH curve of a specific critical structure, the Optic Chiasm, and the Tumor with the overdose area shaded under the Optic Chiasm curve. In the leftmost column, only the image slices with overdose regions are extracted from the entire CT study and displayed with the regions highlighted. In addition, quantified knowledge such as percent area overdosed is displayed as well. The rightmost column shows only the image slices where the tumor is not receiving the full clinically prescribed radiation dose. In this manner, the User can quickly assess the treatment plan to determine whether the critical structures are being overdosed while at the same time the tumor is being prescribed as much dose as possible without having to review the entire CT Image Study.

Finally, Figure 28.10 presents the TP Comparison page view which shows two Iterations of a current treatment plan side by side evaluation. Only the image slices with overdosed areas to the optic chiasm are extracted and displayed with quantified knowledge. In this case, there is an improvement between Iteration 1 and Iteration 2 in the difference in the shaded area of the DVH Curves with less being shown in Iteration 2. In addition, there is less number of image slices extracted with "hot spots" in Iteration 2 as compared to Iteration 1 and the quantified knowledge also confirms this with the percent areas of overdose. This comparison mode, allows the user to quickly compare between the results of one iteration and a subsequent iteration to assess any improvements in the treatment planning process. In addition, this comparison mode can be used to review

previous approved treatments within the knowledge database to help guide the oncologist and physicist in developing a new treatment plan for a new patient.

The developed tools help in part to assist the user during the tedious manual procedure of first analyzing the DVH curves and then having to toggle through a volume of CT image slices with multiple isodose curves to review and assess the plan. Since data is already mined, the exact diagnostic CT image slice together with the exact structure and isodose curves can be automatically displayed the moment the oncologist opens the case within the ePR system. The oncologist would then have the ability to continue to navigate the presented data or view a different DVH curve if desired to make a quicker assessment of the treatment plan for approval. If the oncologist decides that changes are needed in the treatment plan, the decision-support tools can be used to perform a real-time consult with the physicist either at different locations or at the same location or even directly on the treatment planning system, since the ePR is web-based and portable. If there are historical patients stored within the ePR system, the tools can display all the similar critical structures (eg, in the above example, the Optic Chiasm) of similar treatment plans with the corresponding dose configurations that have been approved. This extracted a priori knowledge would help the clinician to decide on an initial plan for a new brain tumor patient planning to be treated with IMRT and perhaps shorten the iterative process of the inverse treatment planning workflow.

28.4 Discussion

In the previous sections, an imaging informatics methodology was applied to Radiation Therapy planning to develop quantified knowledge and decision support tools. As an example, a DICOM-RT based ePR system for managing patients with brain tumor cases was introduced with an example of patients from the Radiation Oncology Department, Saint John's Health Center, Santa Monica, CA. Data obtained for the example was a brain tumor case where the treatment was planned on the IMRT TPS. The richness of the clinical data available was shown in comparison to standard RT information management systems. The results show that with the availability of standardized DICOM-RT data, further knowledge base and decision-support tools development can be realized to aid the clinicians in critical decision-making processes.

Figure 28.11 shows the new ***knowledge-enhanced*** inverse treatment planning workflow with the ePR system with quantified knowledge integrated in dashed lines within the clinical feedback loop described in the original clinical workflow in Figure 28.2. This knowledge-enhanced inverse treatment planning approach may eliminate the feedback loop and subsequent iterative steps of re-computing of a treatment plan since the first attempt was acceptable based on the prior knowledge. Because each plan is computationally complex and time-consuming, a best practice first computed plan aided by previous knowledge would greatly enhance the decision-making process and ultimately shorten the length of time before the patient undergoes treatment as well as better preserve normal tissue and quality of care. Future progress includes the complete development and collection of a suite of knowledge base and tools as well as a

clinical evaluation of the decision-support tool development and its impact on the overall clinical workflow within the Radiation Oncology Department.

28.5 Concluding Remarks

The imaging and informatics methodology introduced for the development of decision-support tools based on standardized DICOM-RT data within the ePR system represents a new frontier for image-assisted knowledge discovery within the realm of Radiation Therapy planning. As an example in this chapter of how crucial standardized RT data can be, a clinical scenario was developed where knowledge base was defined and quantification and visualization tools were designed to extract the knowledge and display it for a decision-making process for a brain tumor case undergoing IMRT. By implementing this DICOM-RT based ePR system, both clinical image and related informatics data are integrated into a one-stop source of pertinent clinical information necessary for making treatment decisions within the RT department and throughout the healthcare enterprise. With the medical imaging informatics methodology introduced in this chapter, the decision-support and knowledge base development can be easily extended to various lesion types as well as other inverse treatment planning methods.

FIGURE CAPTIONS

Figure 28.1 A Medical Imaging Informatics approach towards development of decision-support tools for the DICOM-RT based ePR system. The final results are add-on features for the ePR system to provide decision-support for new patient cases. This methodology can be applied to different lesion types as well as treatment types to quickly develop new decision-support tools.

Figure 28.2 A General Clinical Workflow for the treatment of Brain Tumors with Intensity-Modulated Radiation Therapy (IMRT).

Figure 28.3 Data Structure of Diagnostic Radiology and the Seven Radiation Therapy (RT) Objects. DRR (Digital Reconstructed Radiography), DVH (Dose Volume Histogram).

Figure 28.4 The RT Data Workflow. 1) RT data input from various different RT sources; 2) Diagnostic images from Radiology PACS; 3) Conversion into DICOM-RT objects by the DICOM-RT Gateway; 4) RT archive server stores, manages, and distributes RT data; 5) RT web-based ePR application server further manages and prepares patient planning and treatment information; 6) Web-based client review workstation displays RT-related data for clinician review. (Courtesy YY Law)

Figure 28.5 Entity-Relationship Example of a Sample Knowledge Base for a Clinical Scenario to perform treatment plan assessment for IMRT. The classes defined have attributes that are extracted from the standardized DICOM-RT data integrated in the ePR system. Each class carries a Primary Key (PK) Identifier, and can contain Foreign Keys (FK) which link it to another class object. For example, the 3) critical structure class object contains FK1 and FK2 that link it to a 1) DVH Curve as well as the 4) CT Image class objects. Each DVH curve is derived from a critical structure and CT images contain critical structure contours. The knowledge base is object-oriented in design and modular to allow for additional or new knowledge to be easily integrated. This knowledge is included in the database schema of the web-based ePR application server**.**

Figure 28.6 Illustration of an Interactive Decision-Support Tool for clinicians. The 2-D nature of the DVH curve (Left) is automatically linked to specific image slices (Right), isodose curves, critical structure and tumor contours which all are extracted from 3-D volumes instead of the manual 2-D to 3-D data registration currently performed by the oncologist and physicist. In this example, the DVH curve for a critical structure volume, the Optic Chiasm, has been automatically

displayed showing where overdose is occurring which is the region past 6,000cGY (See Left: DVH marker). In addition, the DVH curves for the Prescribed Tumor Volume (PTV) as well as the Clinical Tumor Volume (CTV) are displayed. Note that the two DVH curves for the Tumor are nearly overlapping which is a common occurrence. A CT image slice is automatically extracted and displayed superimposed with the optic chiasm region and isodose curves showing overdose. In this special case CT slice, the Optic Chiasm region (light-colored shaded region) overlaps the tumor to be treated (dashed black line contour) which can make the treatment planning complex and where the development of quantified knowledge and tools can be especially beneficial. The user can move the arrows (left, bottom) left and right adjusting the DVH Marker across the DVH curve which links and displays pertinent diagnostic images with both critical structure and superimposed isodose curves automatically. This is one example of the tools that can be developed based on quantified knowledge.

Figure 28.7 Timeline overview display of a patient in the DICOM-RT based ePR system. The RT ePR system has a richer database than the conventional RT information/management system. A given RT information management system has only the DICOM RT records (Bottom of figure), while the RT ePR is able to display the information extracted from all the DICOM objects including the DICOM RT plan, RT images, and DICOM images. (Courtesy YY Law)

Figure 28.8 Screenshot Showing an Overview of a Treatment Plan. A: Tabs that Display Different Page Views. TP Overview - Shows the General Overview showing the DVH curves and the DICOM CT Images with Isodose Curves Overlaid. TP Evaluation Page - Shows Quantified Knowledge. TP Knowledge Base Search Page - Allows Users to Query for Specific Knowledge. TP Comparison Page - Shows Quantified Knowledge for Two Different Treatment Plan iterations in Comparison Mode. B: Timeline Display Showing all Treatment Plans, both Current and Historical of a Particular Patient. C: Drop-Down Window Allowing the User to View Different iterations Within a Current Plan. D: DVH Curve of a Particular Plan with Overdose Region Shaded for the Particular Critical Structure, in this case, the Optic Chiasm. E: DICOM Images with Isodose Curves Overlaid from the TPS. All Data is in DICOM-RT Format**.**

Figure 28.9 TP Evaluation Page Showing the DVH Curves of a Specific Critical Structure and the Tumor (leftmost column). The middle column shows only the image slices with overdose regions extracted from the entire CT Study and displayed with the regions highlighted. In

addition Quantified Knowledge such as Percent Area Overdosed is displayed as well. The rightmost column shows only the image slices where the tumor is not receiving the full clinically prescribed Radiation Dose. In this manner, the User can quickly assess the Treatment Plan to determine whether the critical structures are being Overdosed while at the same time the Tumor is being prescribed as much Dose as possible without having to review the entire CT Image Study.

Figure 28.10 TP Comparison Page View Showing Two Iterations of a Current Treatment Plan. Only the Image Slices with Overdosed Areas to the Optic Chiasm are Extracted and Displayed with Quantified Knowledge. In this Case, There is an Improvement Between Iteration 1 and Iteration 2 Both in the Difference in the Shaded Area (Less Area in Iteration 2 DVH) of the DVH Curves as well as the Number of Image Slices (Two vs. Three) Extracted with Overdose Regions and the Quantified Knowledge Showing Percent Area of Overdose. Note that the Third Image (lower left) Extracted in Iteration 1 is Cut Off Due to the Limitations of the Screen Shot Size and Can be Viewed in the Active GUI by Scrolling the Window.

Figure 28.11 Knowledge-Enhanced Inverse Treatment Planning: Dashed lines show where workflow steps would be performed in the ePR System as compared to the current feedback loop workflow in dash-lined rectangle shown in Figure 28.2.

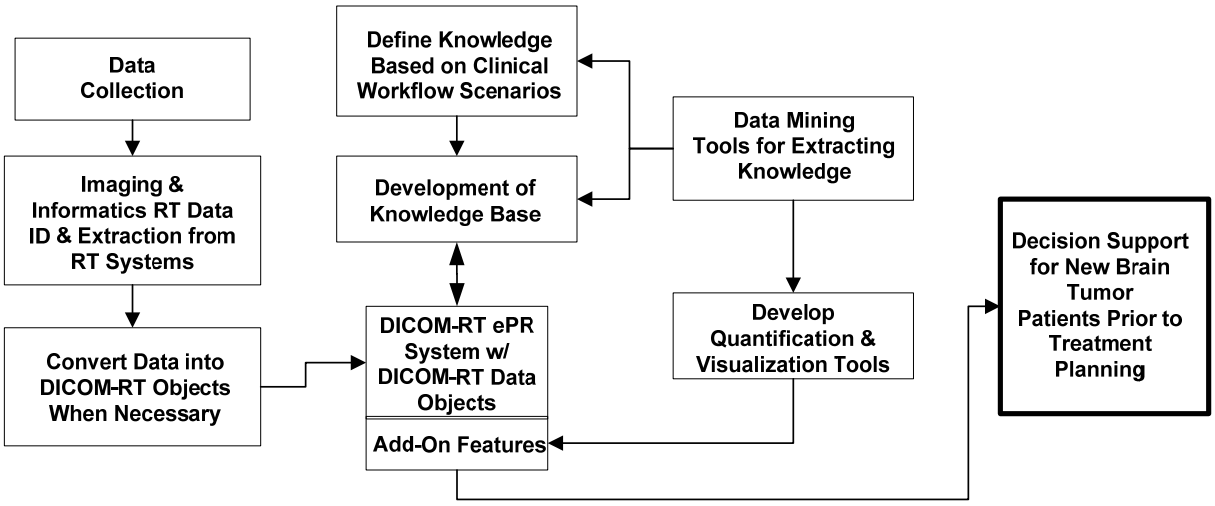
Data Collection
Imaging & Informatics RT Data ID & Extraction from RT Systems
Convert Data into DICOM-RT Objects When Necessary
Define Knowledge Based on Clinical Workflow Scenarios
Development of Knowledge Base
DICOM-RT ePR System w/ DICOM-RT Data Objects
Add-On Features
Data Mining Tools for Extracting Knowledge
Develop Quantification & Visualization Tools
Decision Support for New Brain Tumor Patients Prior to Treatment Planning

Figure 28.1

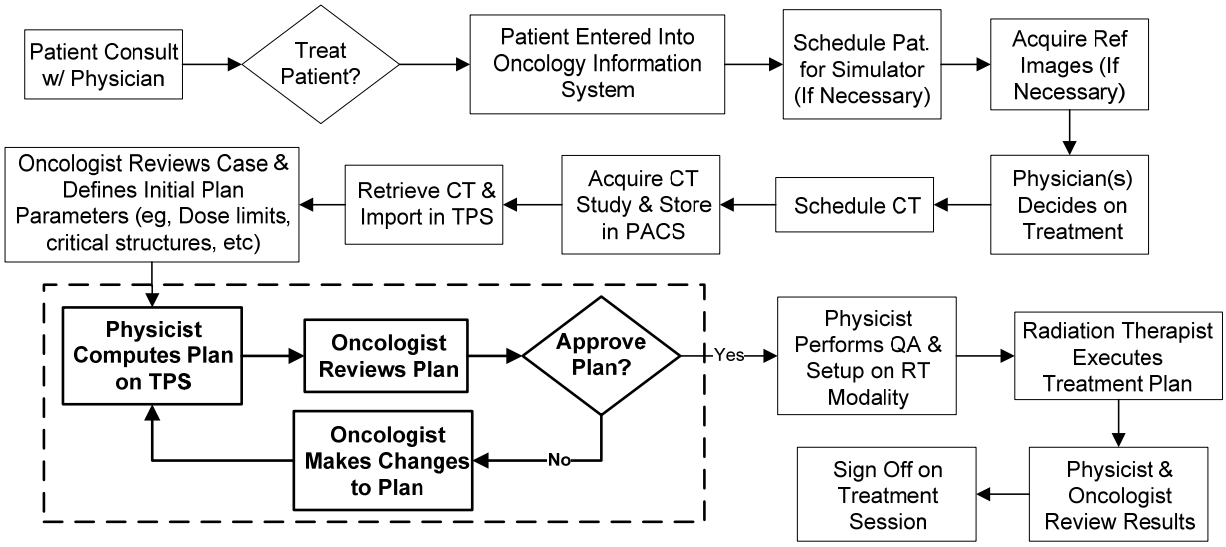
Patient Consult w/ Physician
Treat Patient?
Patient Entered Into Oncology Information System
Schedule Pat. for Simulator (If Necessary)
Acquire Ref Images (If Necessary)
Physician(s) Decides on Treatment
Schedule CT
Acquire CT Study & Store in PACS
Retrieve CT & Import in TPS
Oncologist Reviews Case & Defines Initial Plan Parameters (eg, Dose limits, critical structures, etc)
Physicist Computes Plan on TPS
Oncologist Reviews Plan
Approve Plan?
Yes
No
Oncologist Makes Changes to Plan
Physicist Performs QA & Setup on RT Modality
Radiation Therapist Executes Treatment Plan
Physicist & Oncologist Review Results
Sign Off on Treatment Session

Figure 28.2

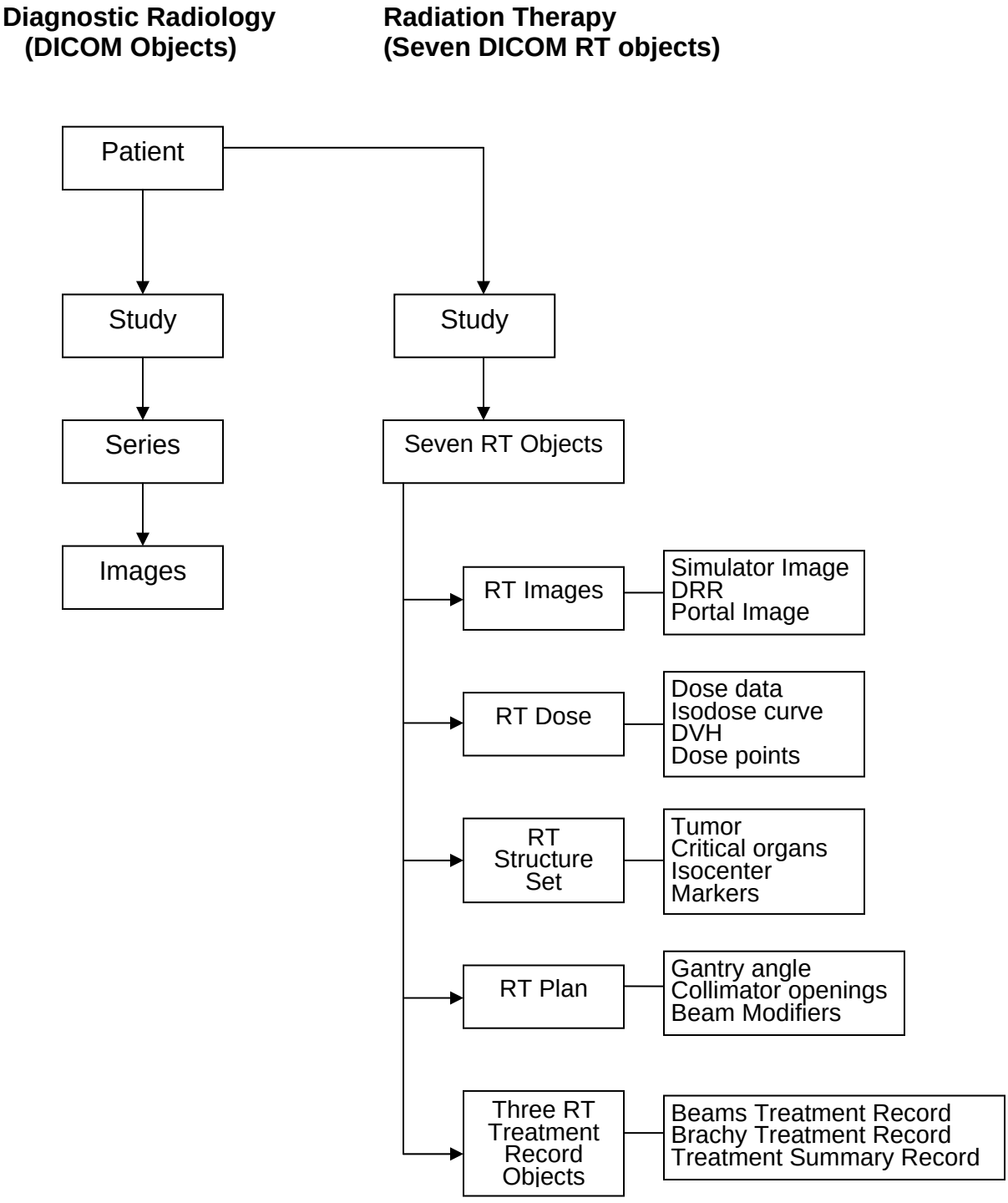
Diagnostic Radiology
(DICOM Objects)
Radiation Therapy
(Seven DICOM RT objects)
Patient
Study
Series
Images
Study
Seven RT Objects
RT Images
Simulator Image
DRR
Portal Image
RT Dose
Dose data
Isodose curve
DVH
Dose points
RT
Structure
Set
Tumor
Critical organs
Isocenter
Markers
RT Plan
Gantry angle
Collimator openings
Beam Modifiers
Three RT
Treatment
Record
Objects
Beams Treatment Record
Brachy Treatment Record
Treatment Summary Record

Figure 28.3

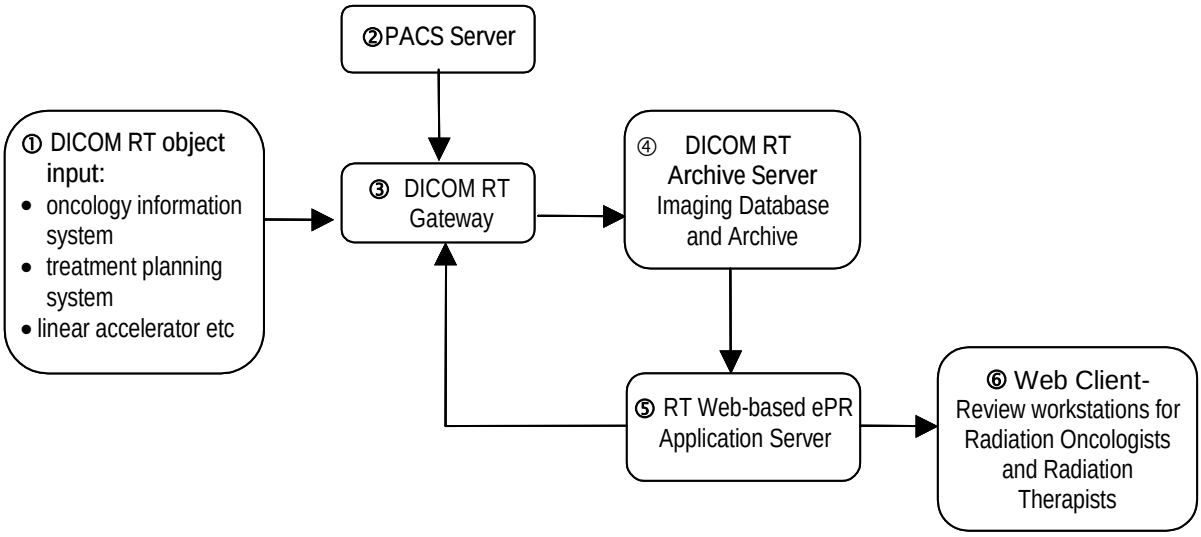
②PACS Server
① DICOM RT object input:
• oncology information system
• treatment planning system
• linear accelerator etc
③ DICOM RT Gateway
④ DICOM RT Archive Server Imaging Database and Archive
⑤ RT Web-based ePR Application Server
⑥ Web Client- Review workstations for Radiation Oncologists and Radiation Therapists

Figure 28.4

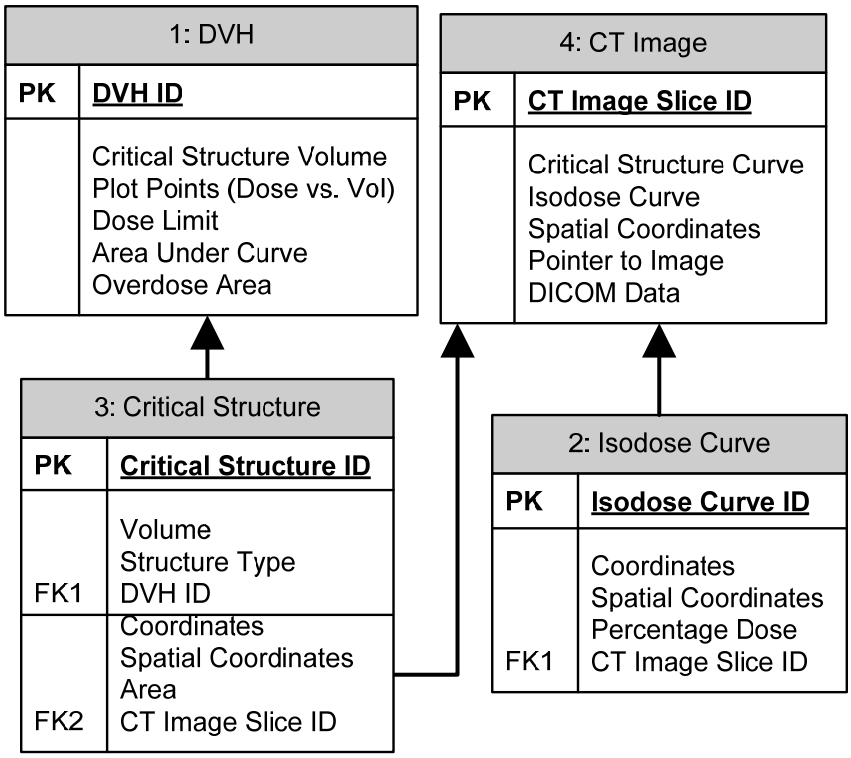
1: DVH
PK
DVH ID
Critical Structure Volume
Plot Points (Dose vs. Vol)
Dose Limit
Area Under Curve
Overdose Area
4: CT Image
PK
CT Image Slice ID
Critical Structure Curve
Isodose Curve
Spatial Coordinates
Pointer to Image
DICOM Data
3: Critical Structure
PK
Critical Structure ID
Volume
Structure Type
FK1
DVH ID
Coordinates
Spatial Coordinates
Area
FK2
CT Image Slice ID
2: Isodose Curve
PK
Isodose Curve ID
Coordinates
Spatial Coordinates
Percentage Dose
FK1
CT Image Slice ID

Figure 28.5

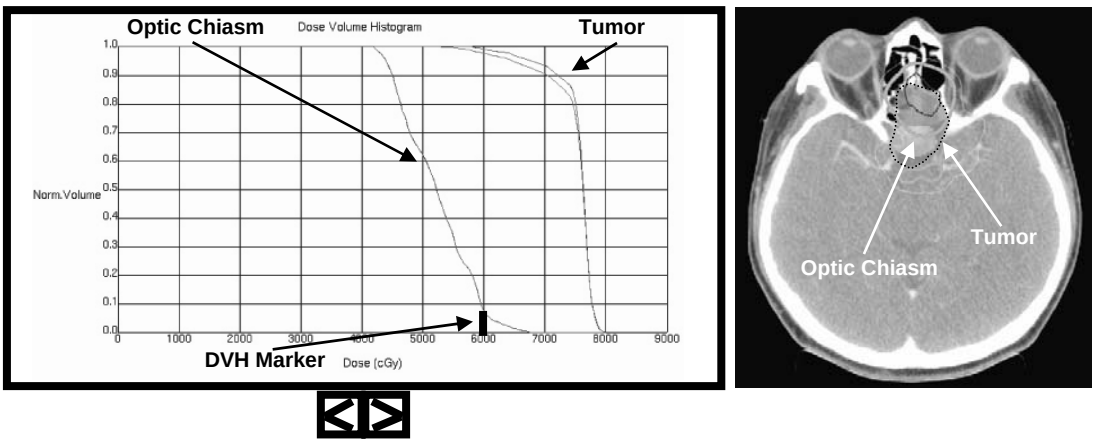
Optic Chiasm
Dose Volume Histogram
Tumor
Norm.Volume
1.0
0.9
0.8
0.7
0.6
0.5
0.4
0.3
0.2
0.1
0.0
0
1000
2000
3000
4000
5000
6000
7000
8000
9000
DVH Marker
Dose (cGy)
Tumor
Optic Chiasm

Figure 28.6

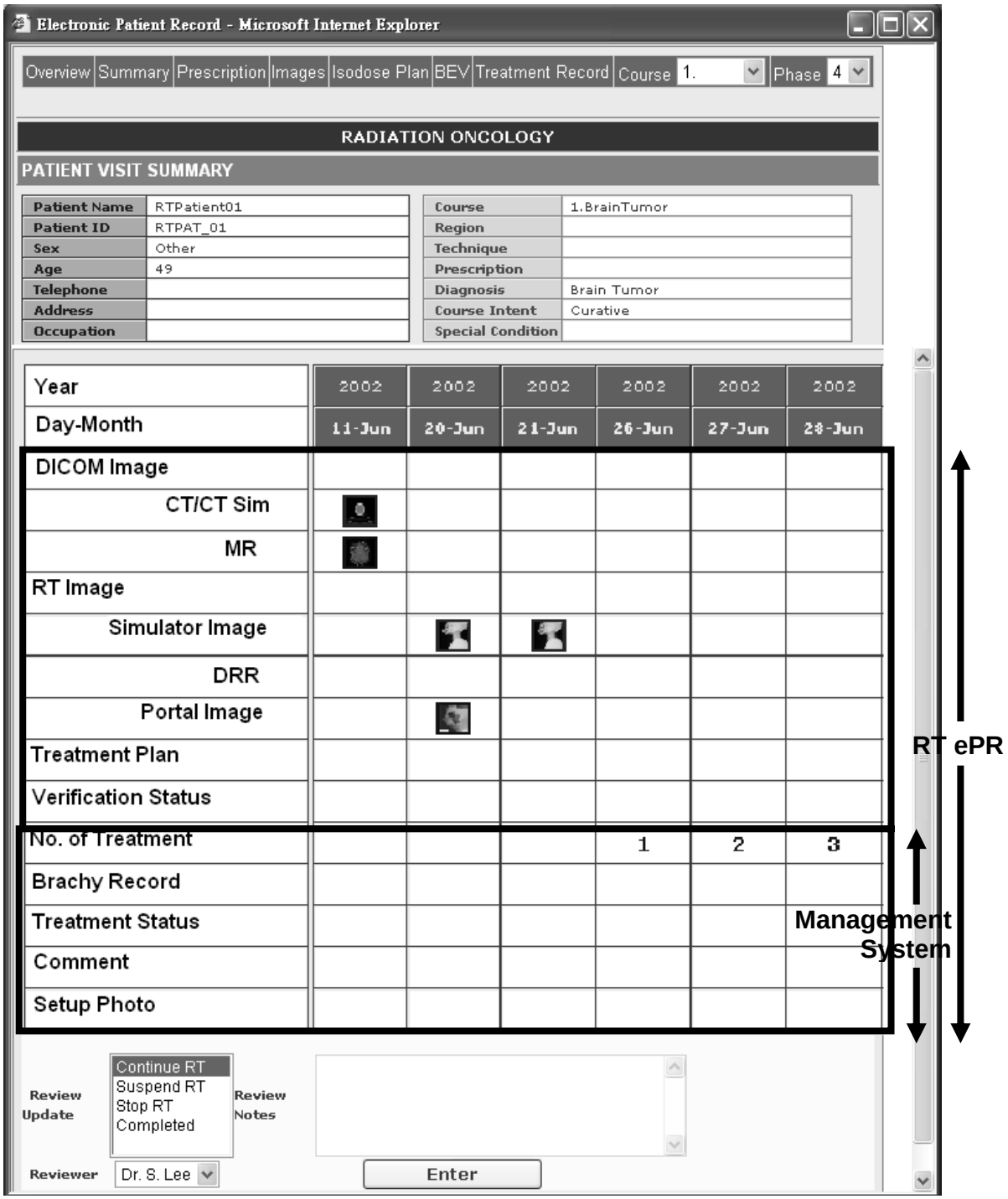
Electronic Patient Record - Microsoft Internet Explorer
Overview
Summary
Prescription
Images
Isodose Plan
BEV
Treatment Record
Course 1.
Phase 4
RADIATION ONCOLOGY
PATIENT VISIT SUMMARY
Patient Name RTPatient01
Patient ID RTPAT_01
Sex Other
Age 49
Telephone
Address
Occupation
Course 1.BrainTumor
Region
Technique
Prescription
Diagnosis Brain Tumor
Course Intent Curative
Special Condition
Year 2002 2002 2002 2002 2002 2002
Day-Month 11-Jun 20-Jun 21-Jun 26-Jun 27-Jun 28-Jun
DICOM Image
CT/CT Sim
MR
RT Image
Simulator Image
DRR
Portal Image
Treatment Plan
Verification Status
No. of Treatment 1 2 3
Brachy Record
Treatment Status
Comment
Setup Photo
Review Update
Continue RT
Suspend RT
Stop RT
Completed
Review Notes
Reviewer Dr. S. Lee
Enter
RT ePR
Management System

Figure 28.7

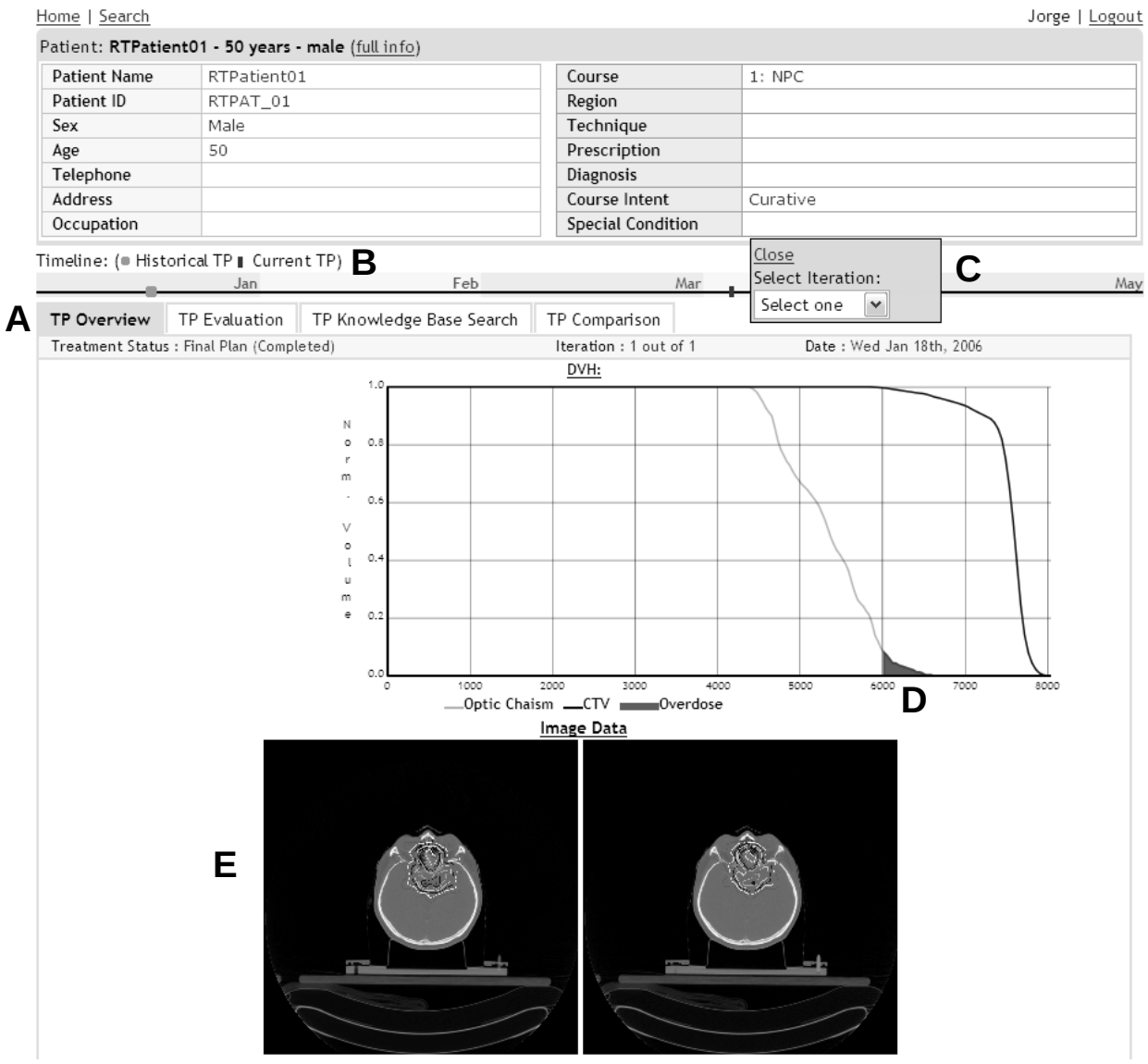
Home | Search
Jorge | Logout
Patient: RTPatient01 - 50 years - male (full info)
Patient Name RTPatient01
Patient ID RTPAT_01
Sex Male
Age 50
Telephone
Address
Occupation
Course 1: NPC
Region
Technique
Prescription
Diagnosis
Course Intent Curative
Special Condition
Timeline: (Historical TP Current TP) B
Jan
Feb
Mar
May
Close
Select Iteration:
Select one
C
A
TP Overview
TP Evaluation
TP Knowledge Base Search
TP Comparison
Treatment Status : Final Plan (Completed)
Iteration : 1 out of 1
Date : Wed Jan 18th, 2006
DVH:
Norm - Volume
1.0
0.8
0.6
0.4
0.2
0.0
0
1000
2000
3000
4000
5000
6000
7000
8000
Optic Chaism
CTV
Overdose
D
Image Data
E

Figure 28.8

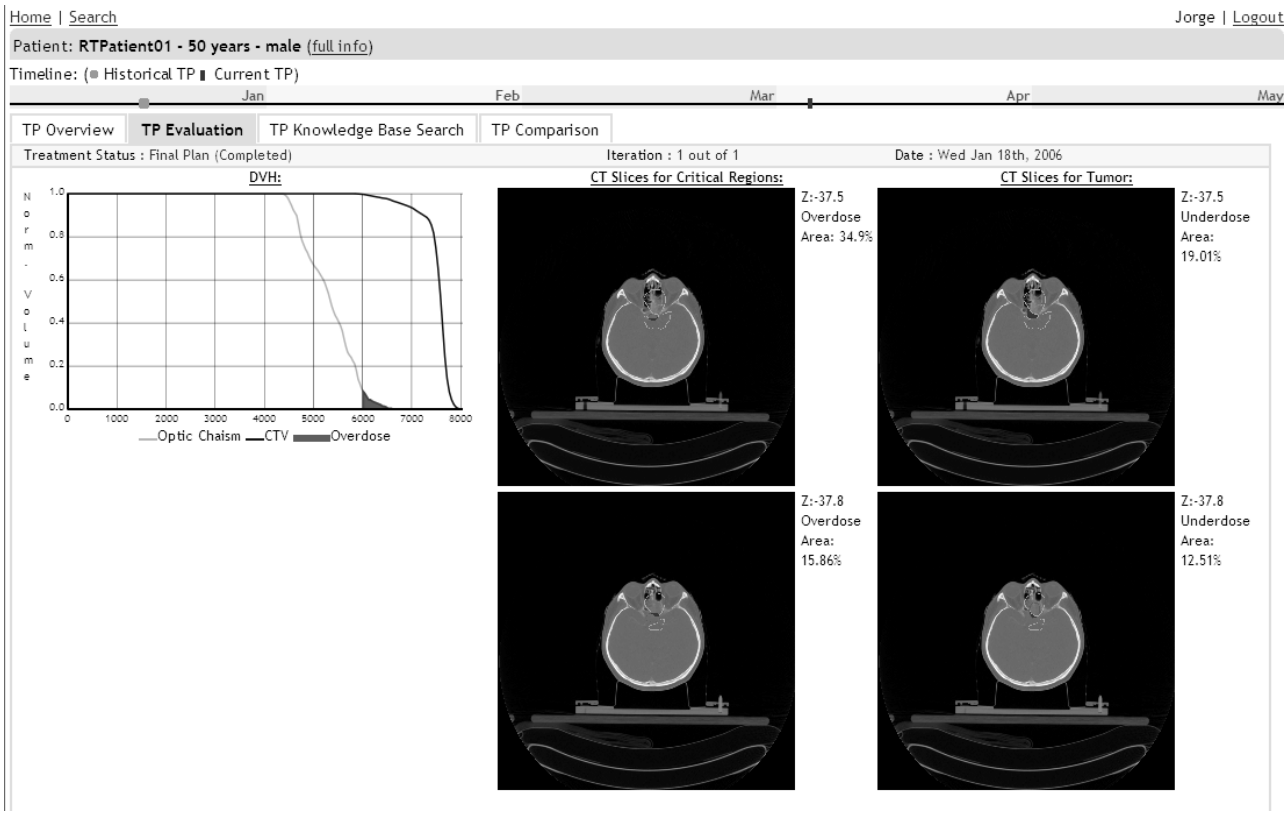
Home | Search
Jorge | Logout
Patient: RTPatient01 - 50 years - male (full info)
Timeline: (Historical TP Current TP)
Jan
Feb
Mar
Apr
May
TP Overview
TP Evaluation
TP Knowledge Base Search
TP Comparison
Treatment Status : Final Plan (Completed)
Iteration : 1 out of 1
Date : Wed Jan 18th, 2006
DVH:
Norm. Volume
1.0
0.8
0.6
0.4
0.2
0.0
0
1000
2000
3000
4000
5000
6000
7000
8000
Optic Chaism
CTV
Overdose
CT Slices for Critical Regions:
Z:-37.5
Overdose
Area: 34.9%
Z:-37.8
Overdose
Area:
15.86%
CT Slices for Tumor:
Z:-37.5
Underdose
Area:
19.01%
Z:-37.8
Underdose
Area:
12.51%

Figure 28.9

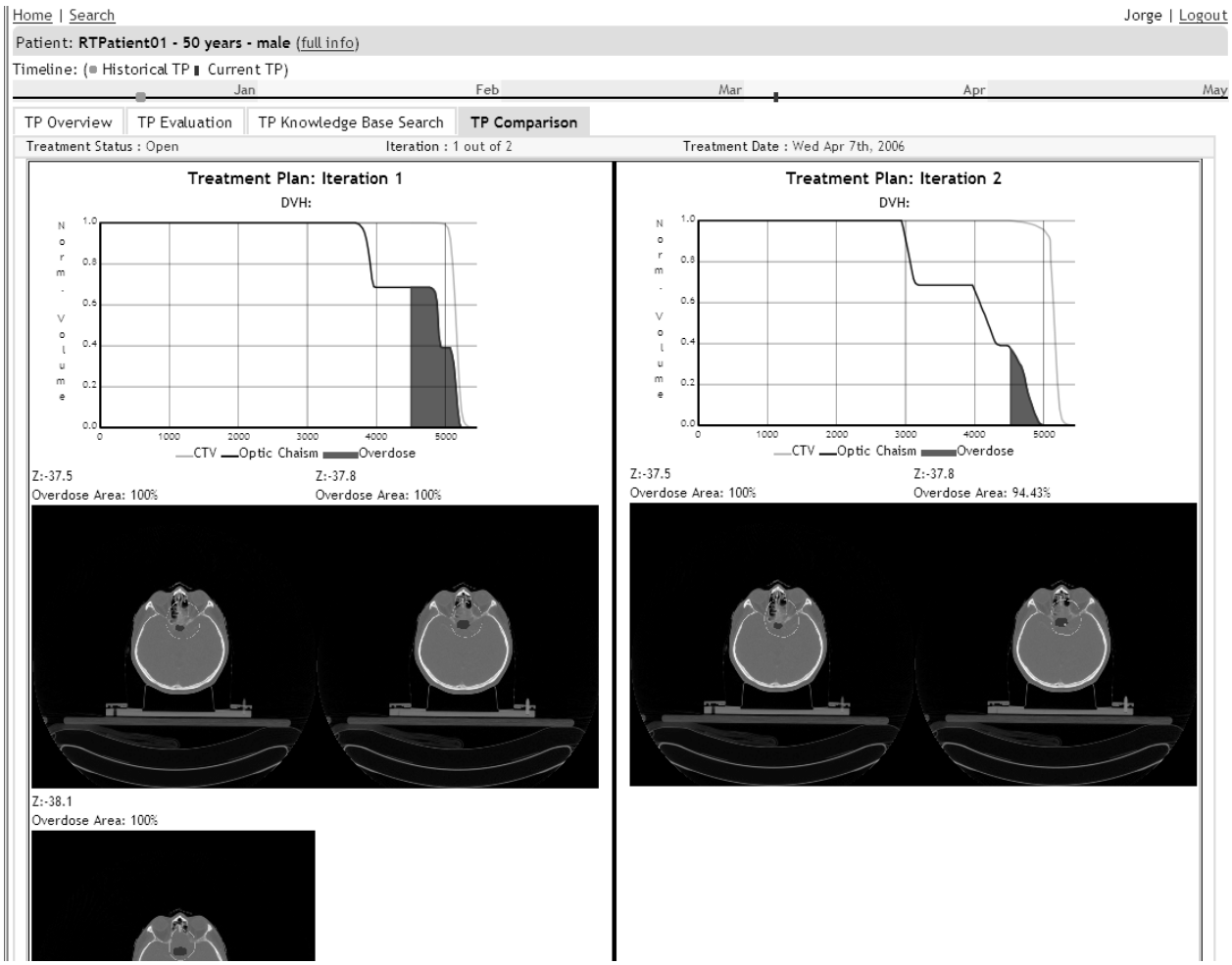
Home | Search
Jorge | Logout
Patient: RTPatient01 - 50 years - male (full info)
Timeline: (Historical TP Current TP)
Jan
Feb
Mar
Apr
May
TP Overview
TP Evaluation
TP Knowledge Base Search
TP Comparison
Treatment Status : Open
Iteration : 1 out of 2
Treatment Date : Wed Apr 7th, 2006
Treatment Plan: Iteration 1
DVH:
Norm. Volume
CTV Optic Chaism Overdose
Z:-37.5
Overdose Area: 100%
Z:-37.8
Overdose Area: 100%
Z:-38.1
Overdose Area: 100%
Treatment Plan: Iteration 2
DVH:
Norm. Volume
CTV Optic Chaism Overdose
Z:-37.5
Overdose Area: 100%
Z:-37.8
Overdose Area: 94.43%

Figure 28.10

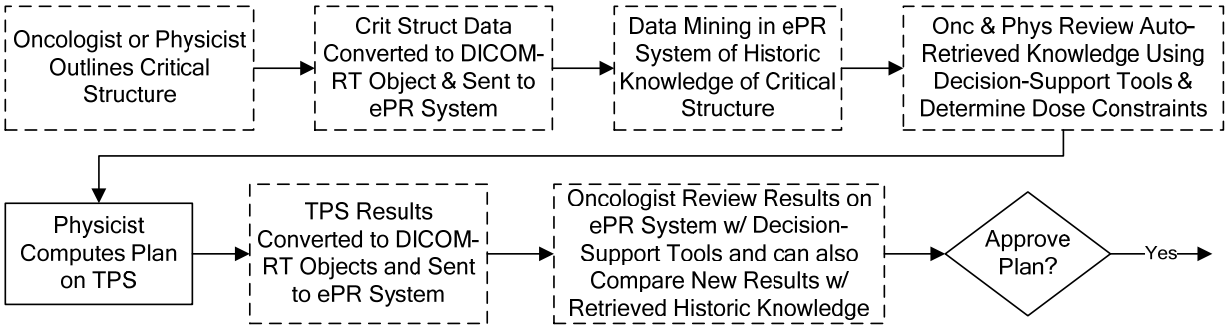
Oncologist or Physicist Outlines Critical Structure
Crit Struct Data Converted to DICOM-RT Object & Sent to ePR System
Data Mining in ePR System of Historic Knowledge of Critical Structure
Onc & Phys Review Auto-Retrieved Knowledge Using Decision-Support Tools & Determine Dose Constraints
Physicist Computes Plan on TPS
TPS Results Converted to DICOM-RT Objects and Sent to ePR System
Oncologist Review Results on ePR System w/ Decision-Support Tools and can also Compare New Results w/ Retrieved Historic Knowledge
Approve Plan?
Yes

Figure 28.11

REFERENCES

Brem R.F., Hoffmeister J.W., Rapelyea J.A., Zisman G., Mohtashemi K., Jindal G., DiSimio M.P., Rogers S.K., Impact of Breast Density on Computer-Aided Detection for Breast Cancer, *Am. J. Roentgenol*., Feb 2005; 184: 439 - 444.

Connolly T., Begg C. *Database Systems – A Practical Approach to Design, Implementation, and Management*, 2nd Ed. England: Addison Wesley, 1998.

Dayhoff R., and Siegel E., Digital Imaging Within and Among Medical Facilities, in R Kolodner (ed): *Computerized Large Integrated Health Networks – The VA Success*. New York: Springer Publishing, 1997: 473-490.

Digital Imaging and Communications in Medicine (DICOM), Supplement 11: Radiotherapy Objects, 1997.

Digital Imaging and Communications in Medicine (DICOM), Supplement 29: Radiotherapy Treatment Records and Radiotherapy Media Extensions, 1999.

DICOM Standard 2003, http://medical.nema.org/dicom/2003.html.

Doi K., MacMahon H., Giger M.L., and Hoffman K.R. (ed), *Computer-Aided Diagnosis in Medical Imaging*. Chicago: Elsevier Science Ltd, 1998.

Huang HK. 1999. *PACS: Basic Principles and Applications*. Wiley & Sons, NY, p. 521.

Law M.Y.Y., Huang H.K. Concept of a PACS and Imaging Informatics-Based Server for Radiation Therapy. *Comput Med Imaging Graph* 27 (1): 1-9, 2003.

Law M.Y.Y., Huang H.K., Chan C.W., Zhang X., Zhang J. A DICOM-Based Radiotherapy Information System. *Proceedings of the SPIE on CD-ROM, Medical Imaging 2004*, 309-317, San Diego, U.S.A.

Law M.Y.Y., Huang H.K., Zhang X., Zhang J. DICOM and Imaging Informatics-Based Radiation Therapy Server. *Proceedings of the SPIE on CD-ROM, Medical Imaging 2002*, 160-167, San Diego, CA, U.S.A.

Law M.Y.Y., Huang H.K., Zhang X., Zhang J. The Data Model of a PACS-Based DICOM Radiation Therapy Server. *Proceedings of the SPIE on CD-ROM, Medical Imaging 2003*, 128-129, San Diego, CA, U.S.A.

Law M.Y.Y. A Model of DICOM-Based Electronic Patient Record in Radiation Therapy. *Comput Med Imaging Graph*, 2004.

Liu B.J., Huang H.K., Cao F., Zhou M.Z., Zhang J.Z., Mogel G., A Complete

Continuous-Availability PACS Archive Server, *Radiographics* 2004; 24:1203-1209.

Liu B.J., Cao F., Zhou M.Z., Mogel G., Documet L. Trends in PACS Image Storage and Archive, *Comput Med Imaging Graph* 2003, 27:165-174.

Palta J.R., Frouhar V.A., Dempsey J.F. Web-based Submission, Archive, and Review of Radiotherapy Data for Clinical Quality Assurance: A New Paradigm. In *J Radiat Oncol Biol Phys*, 2003; 57(5): 1427-1436.

Zhou M.Z., Huang H.K., Cao F., Zhang J., Mogel G., Law M.Y.Y. A RIS/PACS Simulator with Web-Based Image Distribution and Display System for Education. *Proceedings of the SPIE on CD-ROM*, Medical Imaging 2004, 372-381, San Diego, CA, U.S.A.

13

PACS and Medical Imaging Informatics for Filmless Hospitals

Prof. Brent J. Liu[1] and
Prof. H. K. Huang[1,2,3]
[1]*University of Southern California,*
[2]*Hong Kong Polytechnic University*
[3]*The Chinese Academy of Sciences*

13.1 Introduction

Picture archiving and communication systems (PACS) based on digital, communication, display, and information technologies (IT) have revolutionized the practice of radiology, and in a sense, of the entire clinical continuum in medicine during the past 10 years. This chapter introduces the basic concept, terminology, technology development, implementation, integration, and experiences within the clinical practice. There are many advantages to introducing digital, communications, display, and IT to conventional paper- and film-based operations in radiology and medicine.

13.1.1 The Role of PACS in the Clinical Environment

PACS and IT technologies can be used to improve health care delivery workflow efficiency, resulting in speeding up of health care delivery and reducing operating costs. With all these benefits, the digital, communication, and IT technologies are gradually changing the method of acquiring, storing, viewing, and communicating medical images and related information in the health care industry. One natural development along this line is the emergence of digital radiology departments and the digital health care delivery environment. A digital

radiology department has two components: a radiology information management system (RIS) and a digital imaging system. The RIS is a subset of the hospital information system (HIS) or clinical management system (CMS). When these systems are combined with the electronic patient (or medical) record (ePR or eMR) system, which manages selected patient data, the arrival of the total filmless and paperless health care delivery system can become a reality. The digital imaging system, sometimes referred to as a PACS or image management and communication system (IMAC), involves image acquisition, archiving, communication, retrieval, processing, distribution, and display. A digital health care environment consists of the integration of HIS/CMS, ePR, PACS, and other digital clinical systems. The combination of HIS and PACS is sometime referred to as hospital integrated PACS (HI-PACS). The health care delivery system related to PACS and IT is reaching one billion dollars per year (excluding imaging modalities) and continues to grow.

13.1.2 The Role of PACS in Medical Imaging Informatics

PACS originated as an image management system for improving the efficiency of radiology practice. However, it has evolved into a health care enterprise-wide system that integrates information media in multiple forms, including voice, text, medical records, waveform images, and video recordings. To integrate these various data types requires the technology of multimedia: hardware platforms, information systems and databases, communication protocols, display technology, and system interfacing and integration. As the PACS grows in its role within the clinical continuum, it also becomes integrated with these various enterprise-wide media formats and can grow in its richness of content within its database. This wealth of information data becomes the fundamental basis for new approaches in medical research and practice through the discipline of medical imaging informatics, thus ultimately improving the overall health care delivery, research, and education.

13.1.3 General PACS Design

A PACS consists of image and data acquisition, storage, and display subsystems integrated by digital networks and application software. PACS design should emphasize system connectivity. A general multimedia data management system that is easily expandable, flexible, and versatile in its operation calls for both top-down management to integrate various HIS and a bottom-up engineering approach to build a foundation (i.e., PACS infrastructure). From the management point of view, a hospital-wide or enterprise PACS is attractive to administrators because it provides economic justification through a return on investment cost analysis for implementing the system. In addition, proponents of PACS are convinced that its ultimately favorable cost–benefit ratio should not be evaluated as the balance of the resources of the radiology department alone but should extend to the entire hospital or enterprise operation. This concept has gained momentum. Many hospitals and some enterprise-level health care entities around the world have implemented large-scale PACS and have provided solid evidence that PACS improves the efficiency of health care delivery and at the same time saves hospital operational costs. From the engineering point of view, the PACS infrastructure is the basic design concept to ensure that PACS includes features such as standardization, open architecture, expandability for future growth, connectivity, reliability, fault tolerance, and cost-effectiveness. This design philosophy can be constructed in a modular fashion with the infrastructure design described in Section 13.2.

13.1.4 Chapter Overview

This chapter will first describe the PACS infrastructure and its various components in detail. The latter half of the chapter will conclude with implementation and integration strategies for installing a PACS within a health care environment as well as clinical experiences derived from various health care institutions' PACS process.

13.2 PACS Infrastructure

13.2.1 Introduction to PACS Infrastructure Design

The PACS infrastructure design provides the necessary framework for the integration of distributed and heterogeneous imaging devices while supporting intelligent database management of all patient-related information. With this infrastructure, it offers an efficient means of viewing, analyzing, and documenting study results and provides a distribution method for effectively communicating study results to referring physicians. The PACS infrastructure consists of a basic skeleton of hardware components (imaging device interfaces, storage devices, host computers, communication networks, and display systems) integrated with a standardized and robust software system with flexibility for communication, database management, storage management, job scheduling, interprocessor communication, error handling, and network monitoring. The infrastructure as a whole is versatile and can incorporate rules to reliably perform not only basic PACS management operations but also more complex research, clinical service, and educational requests. The software modules of the infrastructure use the ability to handshake and communicate at a system level to permit the components to work together as a system rather than as individual networked computers.

The corresponding hardware components of the general PACS infrastructure include patient data servers, imaging

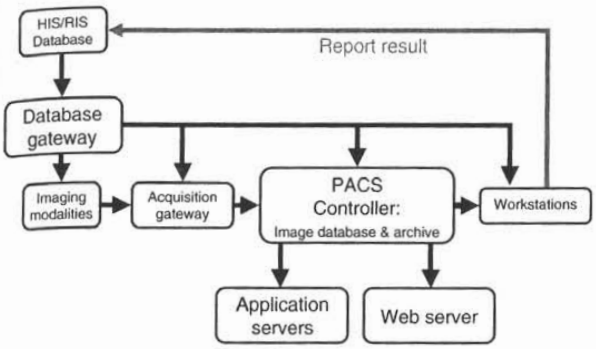

FIGURE 13.1 Generic picture archiving and communication systems components and data flow.

modalities, data/modality interfaces, PACS controllers with database and archive, and display workstations connected by communication networks for handling the data/image flow in the PACS and tuned for a more efficient clinical workflow. Image and data stored in the PACS can be extracted from the archive and transmitted to application servers for various uses. Figure 13.1 shows the basic components and data flow of the PACS. This diagram will be expanded to present additional details in later chapters. The PACS application server concept shown in the bottom of Figure 13.1 broadens the role of PACS in the health care delivery system as a contributor to the advancement of medical imaging informatics field during the past several years. The Web server is optional and is used to distribute PACS studies through wide area networks (WAN) to clinics and physician's offices. Sometimes the Web server is used within the health care enterprise local area network (LAN) to distribute PACS studies throughout the hospital or health care institution.

13.2.2 Industry Standards

Transmission of images and textual information between health care information systems has always been challenging for two major reasons. First, information systems use different computer platforms, and second, images and data are generated from various imaging modalities by made different manufacturers. With the emergent health care industry standards, Health Level 7 (HL7) and Digital Imaging and Communications in Medicine (DICOM), it has become feasible to integrate these heterogeneous, disparate medical images and textual data into an organized system. Interfacing two health care components requires two ingredients, a common data format and a communication protocol. HL7 is a standard textual data format, whereas DICOM includes image and textual data format and communication protocols. In conforming to the HL7 standard, it is possible to share health care information between the HIS, the RIS, and the PACS. By adapting the DICOM standard, medical images generated from a variety of modalities and manufacturers can be interfaced as an integrated health care system. These two standards will be discussed in more detail in the following paragraphs. Integrating health care enterprise (IHE), which is a model for driving the adoption of standards, will also be addressed. IHE combines these available standards with clinical workflow profiles to persuade users and manufacturers to adopt and use this system in daily clinical practice.

13.2.2.1 Health Level 7

HL7, established in March 1987, was organized by a user-vendor committee to develop a standard for electronic data exchange in health care environments, particularly for hospital applications. With the HL7 standard, the level 7 refers to the highest level, which is the application level, in the open systems interconnection (OSI) seven communication levels model. The common goal is to simplify the interface implementation among computer applications from multiple vendors. This standard emphasizes data format and protocol for exchanging certain key textual data among health care information systems, such as HIS, RIS, and PACS. HL7 addresses the highest level (level 7) of the OSI model of the International Standards Organization (ISO), but it does not conform specifically to the defined elements of the OSI's seventh level. It conforms to the conceptual definitions of an application-to-application interface placed in the seventh layer of the OSI model. These definitions were developed to facilitate data communication in a health care setting by providing rules to convert abstract messages associated with real-world events into strings of characters comprising an actual message.

The most commonly used HL7 today is version 2.X, which has many options and is thus flexible. During the past years, version 2.X has been developed continuously, and it is widely and successfully implemented in the health care environment. Version 2.X and other older versions use a bottom-up approach, beginning with very general concepts and adding new features as needed. These new features become options to the implementers so that the standard is very flexible and is easy to adapt to different sites. However, these options and flexibility also make it impossible to have reliable conformance tests of any vendor's implementation. This forces vendors to spend more time in analyzing and planning their interfaces to ensure that the same optional features are used in both interfacing parties. There is also no consistent view of the data when HL7 moves to a new version or when assessing that data's relationship to other data. Therefore, a consistently defined and object-oriented version of HL7 is needed, which is version 3. The initial release of HL7 version 3 was in December 2001. The primary goal of HL7 version 3 is to offer a standard that is definite and testable. Version 3 uses an object-oriented methodology and a reference information model (RIM) to create HL7 messages. The object-oriented method is a top-down

method. RIM is the backbone of HL7 version 3, since it provides an explicit representation of the semantic and lexical connections between the information in the fields of HL7 messages. Because each aspect of the RIM is well-defined, very few options exist in version 3. Through object-oriented method and RIM, HL7 version 3 improves many of the shortcomings of previous 2.X versions. Version 3 uses extensible markup language for message encoding to increase interoperability between systems and will include new data interchange formats beyond the American Standard Code for Information Interchange (ASCII) and support of component-based technology such as ActiveX and CORBA. HL7 version 3 will offer tremendous benefits to providers and vendors as well as analysts and programmers, but complete adoption of the new standard will take time and effort.

13.2.2.2 Digital Imaging and Communications in Medicine Standard

ACR-NEMA, formally known as the American College of Radiology and the National Electrical Manufacturers Association, created a committee to develop a set of standards to serve as the common ground for various medical imaging equipment vendors. The goal was for newly developed instruments to be able to communicate and participate in sharing medical image information, in particular within the PACS environment. The committee, which focused chiefly on issues concerning information exchange, interconnectivity, and communications between medical systems, began work in 1982.The first version, which emerged in 1985, specified standards in point-to-point message transmission, data formatting, and presentation and included a preliminary set of communication commands and a data format dictionary. The second version, ACR-NEMA 2.0, published in 1988, was an enhancement to the first release. It included hardware definitions and software protocols as well as a standard data dictionary. However, networking issues were not addressed adequately in either version. For this reason, a new version aiming to include network protocols was released in 1992. Because of the number of changes and additions, it was given a new name: DICOM 3.0. In 1996, a new version was released consisting of 13 published parts that form the basis of future DICOM new versions and parts. Manufacturers readily adopted this version to their imaging products. Currently, the latest version of DICOM has been expanded to 18 parts. Two fundamental components of DICOM are the information object class and the service class. Information objects define the contents of a set of images and their relationships, and the service classes describe what to do with these objects. The service classes and information object classes are combined to form the fundamental units of DICOM, called service-object pairs (SOPs). The next few paragraphs will describe the DICOM data model, which represents the information object, and the DICOM service classes.

13.2.2.3 DICOM Data Model

There are two components relating to the DICOM data model: the DICOM model of the real world and the DICOM file format. The former is used to define the hierarchical data structure from patient to studies, to series, and to images and waveforms. The latter describes how to encapsulate a DICOM file ready for a DICOM SOP service.

The DICOM model of the real world defines several real-world objects in the clinical imaging arena (e.g., patient, study, series, image) and their interrelationships within the scope of the DICOM standard. It provides a framework for various DICOM information object definitions (IOD). The DICOM Model defines four level objects: (1) patient; (2) study; (3) series and equipment; and (4) image, waveform, and structured report document. Each of the above levels can contain several (1–n or 0–n) sublevels. Figure 13.2 shows the DICOM real-world data model. Note the levels with which the above-mentioned four objects reside.

The DICOM file format defines how to encapsulate the DICOM data set of a SOP instance in a DICOM file. Each file usually contains one SOP instance. The DICOM file starts with the DICOM file meta information (optional), followed by the bit stream of the data set and ends with the image pixel data if it is a DICOM image file. The DICOM file meta information includes file identification information. The meta information uses explicit value representations (VR) transfer syntax for encoding. Therefore, the meta information does not exist in the implicit VR-encoded DICOM file. Explicit VR and implicit VR are two coding methods in DICOM. Vendors or implementers have the option of choosing either one for encoding. DICOM files encoded by both coding methods can be processed by most of the DICOM-compliant software. One data set represents a single SOP instance. A data set is constructed of data elements. Data elements contain the encoded values of the attributes of the DICOM object. If the SOP instance is an image, the last part of the DICOM file is the image pixel data.

13.2.2.4 DICOM Service Classes

DICOM services are used for communication of imaging information objects within a device and for the device to perform a service for the object, for example, to store the object or to display the object. A service is built on top of a set of DICOM message service elements (DIMSEs). These DIMSEs are computer software programs written to perform specific functions. There are two types of DIMSEs: one for the normalized objects and the other for the composite objects. DIMSEs are paired in the sense that a device issues a command request and the receiver responds to the command accordingly. The composite commands are generalized, whereas the normalized commands are more specific. DICOM services are referred to as service classes because of the object-oriented nature of its information structure model. If a device provides a service, it is called a

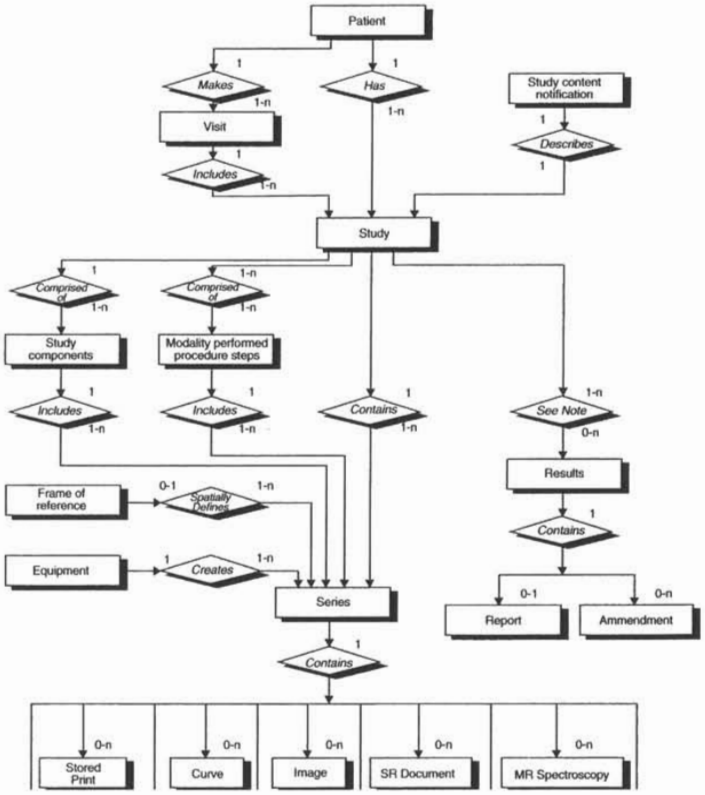

FIGURE 13.2 DICOM model of the real world showing the four main level objects: (1) patient, (2) study, (3) series, and (4) image. Note that there can be multiple instances of each object belonging to the patient.

service class provider; if it uses a service, it is a service class user. Note that a device can be either a service class provider or a service class user or both, depending on how it is used.

DICOM uses existing network communication standards based on the ISO-OSI for imaging information transmission. The ISO-OSI consists of seven layers from the lowest physical (cables) layer to the highest application layer. When imaging information objects are sent between layers in the same device, the process is called a service. When objects are sent between two devices, it is called a protocol. When a protocol is involved, several steps are invoked in two devices; the two devices are referred to as in association using DICOM. If an imaging device transmits an image object with a DICOM command, the receiver must use a DICOM command to receive the information. On the other hand, if a device transmits a DICOM object with a Transmission Control Protocol/Internet Protocol (TCP/IP) communication protocol through a network without invoking the DICOM communication, any device connected to the network can receive the data with the TCP/IP protocol. However, a decoder is still needed to convert the DICOM object for proper use. The most commonly used communication protocol in DICOM is TCP/IP for transmitting DICOM image objects within PACS. To an end user, the two most important DICOM services are (1) send and receive images and (2) query and retrieve images. The query and retrieve services are built on top of the send and receive services.

13.2.2.5 Integrating the Health Care Enterprise

Even with the DICOM and HL7 standards available, there is a need for common consensus on how to use these standards for integrating heterogeneous health care information systems smoothly. IHE is neither a standard nor a certifying authority; instead, it is a high-level information model for driving the adoption of HL7 and DICOM standards. IHE is a joint initiative of RSNA and HIMSS (Health Care Information and Management Systems Society) started in 1998. The mission was to define and guide manufacturers to use DICOM- and HL7-compliant equipment and information systems to facilitate daily clinical workflow operations. The IHE technical framework defines a common information model and vocabulary for using DICOM and HL7 to complete a set of well-defined

radiological and clinical transactions for a certain task. These common vocabularies and models would then facilitate health care providers and technical personnel in understanding each other better, which then would lead to smooth systems integration. The first large-scale demonstration was held at the RSNA annual meeting in 1999. Additional presentations were made at RSNA in 2000 and 2001 and at HIMSS 2001 and 2002. In these demonstrations, manufacturers came together to show how actual products could be integrated based on certain IHE protocols. It is the belief of RSNA and HIMSS that with successful adoption of IHE, life would become more pleasant in health care systems integration for both the users and the providers. The IHE integration profiles provide a common language, vocabulary, and platform for health care providers and manufacturers to discuss integration needs and the integration capabilities of products. As of the 2003 implementation, there are 10 integration profiles; this number will grow over time. The 10 implemented IHE profiles are as follows:

1. Scheduled workflow
2. Patient information reconciliation
3. Consistent presentation of images
4. Presentation-grouped procedures
5. Access to radiology information
6. Key image note
7. Simple image and numeric report
8. Basic security
9. Charge posting
10. Postprocessing workflow

13.2.3 Connectivity and Open Architecture

If PACS modules in the same hospital cannot communicate with each other, they become isolated systems, each with its own images and patient information. It would be difficult to combine these modules to form a total hospital-integrated PACS. Open network design is essential, allowing a standardized method for data and message exchange between heterogeneous systems. Because computer and communications technology changes rapidly, a closed architecture would hinder system upgradeability. For example, suppose an independent imaging workstation from a given manufacturer would, at first glance, make a good additional component to a magnetic resonance imaging scanner for viewing images. If the workstation has a closed proprietary architecture design, however, no components except those specified by the same manufacturer can be augmented to the system. Potential overall system upgrading and improvement would be limited. Considerations of connectivity are important even when a small-scale PACS is planned.

13.2.4 Reliability

Reliability is a major concern in a PACS for two reasons. First, a PACS has many components; the probability of a component failing is high. Second, because PACS manages and displays critical patient information, extended periods of downtime cannot be tolerated. The PACS can be considered a mission-critical system within the health care enterprise that should strive for continuous operation 24 hours a day, 7 days a week. In designing a PACS, it is therefore important to use fault-tolerant measures, including error detection and logging software, external auditing programs (i.e., network management processes that check network circuits, magnetic disk space, database status, processer status, and queue status), hardware redundancy, and intelligent software recovery blocks. Some fail-recovery mechanisms that can be used include automatic retry of failed jobs with alternative resources and algorithms and intelligent bootstrap routines (a software block executed by a computer when it is restarted) that allow a PACS computer to automatically continue operations after a power outage or system failure. Improving reliability is costly; however, it is essential to maintain high reliability of a complex system.

13.2.5 Security

Security, particularly the need for patient confidentiality, is an important consideration because of medical-legal issues and Health Insurance Portability and Accountability Act (HIPAA) mandated in April 2003. The violation of data security can be of three different types: physical intrusion, misuse, and behavioral violations. Physical intrusion relates to facility security, which can be handled by building management. Misuse and behavioral violations can be minimized by account control and privilege control. Most sophisticated database management systems have identification and authorization mechanisms that use accounts and passwords. Application programs may supply additional layers of protection. Privilege control refers to granting and revoking user access to specific tables, columns, or views from the database. These security measures provide the PACS infrastructure with a mechanism for controlling access to clinical and research data. With these mechanisms, the system designer can enforce policy as to which persons have access to clinical studies. In some hospitals, for example, referring clinicians are granted image study access only after a preliminary radiology reading has been performed and attached to the image data. An additional security measure is the use of the image digital signature during data communication. If implemented, this feature would increase the system software overhead, but data transmission through open communication channels would be more secure.

13.2.6 Current PACS Architectures

There are three basic PACS architectures: (1) stand-alone, (2) client/server, and (3) Web-based. From these three basic PACS architectures, there are variations and hybrid design types.

13.2.6.1 Stand-Alone PACS Architecture

The three major features of the stand-alone model are as follows:

1. Images are automatically sent to designated reading and review workstations from the archive server.
2. Workstations can also query/retrieve images from the archive server. Workstations have short-term cache storage.
3. Data workflow of the stand-alone PACS model is shown in Figure 13.3.

Following the numerals in Figure 13.3:

1. Images from an examination acquired by the imaging modality are sent to the PACS archive server.
2. The PACS archive server stores the examination images.
3. A copy of the images is distributed to selected end-user workstations for diagnostic reading and review. The server performs this automatically.
4. Historic examinations are prefetched from the server, and a copy of the images is sent to selected end-user workstations.
5. Ad hoc requests to review PACS examinations are made via query/retrieve from the end-user workstations. In addition, if automatic prefetching fails, end-user workstations can query and retrieve the examination images from the archive server.
6. End-user workstations contain a local storage cache of a finite number of PACS examinations.

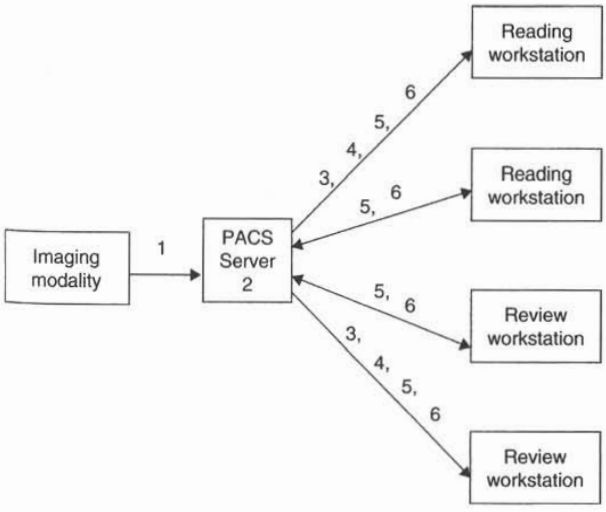

FIGURE 13.3 Stand-alone picture archiving and communication systems architecture and the six workflow steps as described in the text.

The advantages of the stand-alone model are as follows:

- If the PACS server goes down, imaging modalities or acquisition gateways have the flexibility to send directly to the end-user workstation so that the radiologist can continue reading new cases.
- Because multiple copies of the PACS examination are distributed throughout the system, there is less risk of losing PACS data. Some historic PACS examinations will be available in workstations because they have a local storage cache.
- The system is less susceptible to daily changes in network performance because PACS examinations are preloaded onto the local storage cache of end-user workstations and are available for viewing immediately.
- Examination modification to the DICOM header for quality control can be made before archiving.

The disadvantages of the stand-alone system are as follows:

- End-users must rely on correct distribution and prefetching of PACS examinations, which is not possible all the time.
- Because images are sent to designated workstations, each workstation may have a different wordlist, which makes it inconvenient to read/review all examinations at any workstation in one setting.
- End-users depend on the query/retrieve function to retrieve ad hoc PACS examinations from the archive, which can be a complex function compared with the client/server model.
- Radiologists can be reading the same PACS examination at the same time from different workstations because the examination images may be sent to several workstations.

13.2.6.2 Client/Server PACS Architecture

The three major features of the client/server model are:

1. Images are centrally archived at the PACS server.
2. From a single wordlist at the client workstation, an end-user selects images via the archive server.
3. Because workstations have no cache storage, images are flushed after reading.

Data workflow of the client/server PACS model is shown in Figure 13.4.

Following the numerals in Figure 13.4:

1. Images from an examination acquired by the imaging modality are sent to the PACS archive server.
2. The PACS archive server stores the examination.
3. End-user workstations or client workstations have access to the entire patient/study database of the archive server.

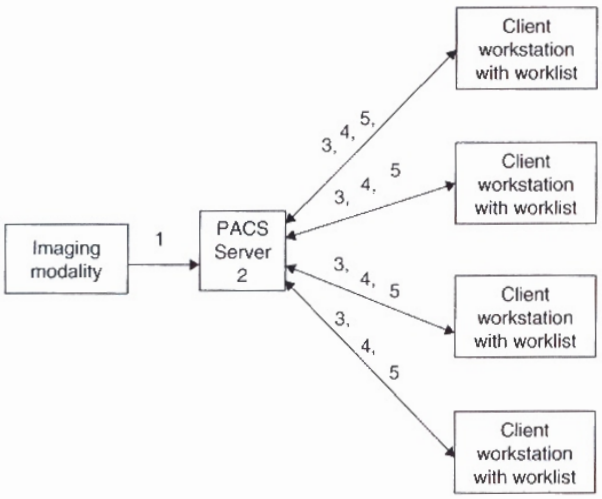

FIGURE 13.4 Client/server picture archiving and communication systems architecture and the five workflow steps as described in the text.

The end-user may select preset filters on the main wordlist to shorten the number of wordlist entries for easier navigation.

4. Once the examination is located on the wordlist and selected, images from the PACS examination are loaded from the server directly into the memory of the client workstation for viewing. Historic PACS examinations are loaded in the same manner.

Once the end-user has completed reading/reviewing the examination, the image data are flushed from memory, leaving no image data in local storage on the client workstation

The advantages of the client/server model are as follows:

- Any PACS examination is available on any end-user workstation at any time, making it convenient to read/review.
- No prefetching or study distribution is needed.
- No query/retrieve function is needed. The end-user just selects the examination from the wordlist on the client workstation, and images are loaded automatically.
- Because the main copy of a PACS examination is located on the PACS server and is shared by the client workstations, radiologists will be aware of when they are reading the same examination at the same time and thus avoid duplicate readings.

The disadvantages of the client/server model are as follows:

- The PACS server is a single point of failure; if it goes down, the entire PACS is down. In this case, end-users will not be able to view any examinations on the client workstations. Newly acquired examinations must be held back from archival at the modalities until the server is back up.
- Because there are more database transactions in the client/server architecture, the system is exposed to more transaction errors, making it less robust compared with the stand-alone architecture.
- The architecture is very dependent on network performance.
- Examination modification to the DICOM header for quality control is not available before archiving.

13.2.6.3 Web-Based Model

The Web-based model PACS is similar to the client/server architecture with regard to data flow. However, the main difference is that the client software is a Web-based application.

Additional advantages as compared with client/server are the following:

- The client workstation hardware can be platform-independent as long as the Web browser is supported.
- The system is a completely portable application that can be used both on-site and at home with an Internet connection.

Additional disadvantages as compared with client/server are as follows:

- The system may be limited in the amount of functionality and performance by the Web browser.

With consistent technology, hardware, and software improvements to database management and performance, clustered and parallel servers, and network communications performance, the client/server and Web-based models have become the architecture of choice for most PACS vendors.

13.3 PACS Components and Workflow

13.3.1 Introduction of Components

This section provides an overview of PACS for two topics. The first topic is the basic concept of PACS and its components, which gives a general architecture and requirements of the system. The second topic is an example of a generic PACS workflow in radiology that highlights the functionalities of these components. As discussed in the previous section, a PACS should be DICOM-compliant. It consists of an image and data acquisition gateway, a PACS controller and archive, and display workstations integrated together by digital

networks as shown in Figure 13.1. The following sections introduce these components in more detail.

13.3.2 Image Acquisition Gateway

PACS requires that images from imaging modalities (devices) and related patient data from the HIS and RIS be sent to the PACS controller and archive server. A major task in PACS is to acquire images reliably and in a timely manner from each radiological imaging modality and relevant patient data including study support text information about the patient, a description of the study, and parameters pertinent to image acquisition and processing.

Image acquisition is a major task for three reasons. First, the imaging modality is not under the auspices of the PACS. Many manufacturers supply various imaging modalities, each of which has its own DICOM-compliant statement. Worse, some older imaging modalities may not even be DICOM-compliant. To connect many imaging modalities to the PACS requires tedious and labor-intensive work and the cooperation of modality manufacturers. Second, image acquisition is a slower operation than other PACS functions because patients are involved, and it takes the imaging modality some time to acquire the necessary data for image reconstruction. Third, images and patient data generated by the modality sometimes may contain format information unacceptable to the PACS operation. To circumvent these difficulties, an image acquisition gateway computer is usually placed between the imaging modality(s) and the rest of the PACS network to isolate the host computer in the radiological imaging modality from the PACS. Isolation is necessary because traditional imaging device computers lack the necessary communication and coordination software that is standardized within the PACS infrastructure. Furthermore, these host computers do not contain enough intelligence to work with the PACS controller to recover various errors. The image acquisition gateway computer has three primary tasks: It acquires image data from the radiological imaging device; it converts the data from manufacturer specifications to a PACS standard format (header format, byte ordering, matrix sizes) that is compliant with the DICOM data formats; and it forwards the image study to the PACS controller or display workstations.

Two types of interfaces are used to connect a general-purpose PACS acquisition gateway computer with a radiological imaging modality. With peer-to-peer network interfaces, which use the TCP/IP ethernet protocol, image transfers can be initiated either by the radiological imaging modality (a push operation) or by the destination PACS acquisition gateway computer (a pull operation). The pull mode is advantageous because if an acquisition gateway computer goes down, images can be queued in the radiological imaging modality computer until the gateway computer becomes operational again, at which time the queued images can be pulled and normal image flow resumed. Assuming that sufficient data buffering is available in the imaging modality computer, the pull mode is the preferred mode of operation because an acquisition computer can be programmed to reschedule study transfers if failure occurs (because of failure of the acquisition computer or failure in the radiological imaging modality). If the designated acquisition gateway computer is down and a delay in acquisition is not acceptable, images from the examination can be rerouted to another networked designated backup acquisition gateway computer or workstation.

Although traditionally the image acquisition gateway is a separate computer device within PACS, improvements in server hardware processing speed and memory have provided some manufacturers with the ability to integrate the image acquisition gateway component within the PACS controller or PACS server. Although the image acquisition gateway shares the same hardware as the PACS controller, the main functionalities remain the same as a standalone image acquisition gateway.

13.3.3 PACS Controller and Image Archive

Imaging examinations along with pertinent patient information from the acquisition gateway computer, the HIS, and the RIS are sent to the PACS controller. The PACS controller is the engine of the PACS and consists of high-end computers or servers; its two major components are a database server and an archive system. The archive system consists of short-term, long-term, and permanent storage. These components are explained in more detail in the next section.

The following lists some major functions of a PACS controller:

1. Receives images from examinations via acquisition gateway computers
2. Extracts text information describing the received examination
3. Updates a network-accessible database management system
4. Determines the destination workstations to which newly generated examinations are to be forwarded
5. Automatically retrieves necessary comparison images from a distributed cache storage or long-term library archive system
6. Automatically corrects the orientation of computed radiography images
7. Determines optimal contrast and brightness parameters for image display
8. Performs image data compression if necessary
9. Performs data integrity check if necessary
10. Archives new examinations onto long-term archive library
11. Deletes images that have been archived from acquisition gateway computers

12. Services query/retrieve requests from workstations and other PACS controllers in the enterprise PACS
13. Interfaces with PACS application servers

13.3.4 Display Workstations

A workstation includes communication network connection, local database, display, resource management, and processing software. The fundamental workstation operations are listed in Table 13.1. There are four types of display workstations categorized by their resolutions: (1) high-resolution (2.5K × 2K) liquid crystal display (LCD) for primary diagnosis at the radiology department, (2) medium-resolution (2000 × 1600 or 1600 × 1K) LCD for primary diagnosis of sectional images and at the hospital wards, (3) physician desktop workstation (1K × 768) LCD, and (4) hard-copy workstations for printing images on film or paper. In a stand-alone primary diagnostic workstation, current and historic images are stored in local high-speed magnetic disks for fast retrieval. It also has access to the PACS controller database for retrieving longer-term historic images if needed. Figures 13.5–13.7 show examples of a typical PACS diagnostic workstation displaying various PACS studies. Note the tool set at the bottom of each figure used for manipulating the digital PACS study for case presentation, interpretation, and documentation.

13.3.5 Communications and Networking

A basic function of any computer network is to provide an access path by which end users (e.g., radiologists and clinicians) at one geographic location can access information (e.g., images and reports) at another location. The important networking data needed for system design include location and function of each network node, frequency of information passed between any two nodes, cost for transmission between nodes with various-speed lines, desired reliability of the communication, and required throughput. The variables in the design include the network topology, communication line capacities, and data flow assignments.

TABLE 13.1 Major functions of a picture archiving and communication systems display workstation

Function	Description
Case preparation	Accumulation of all relevant images and information belonging to a patient examination
Case selection	Selection of cases for a given subpopulation
Image arrangement or hanging protocols	Tools for arranging and grouping images for easy review
Interpretation	Measurement tools for facilitating the diagnosis
Documentation	Tools for image annotation, text, and voice reports
Case presentation	Tools for a comprehensive case presentation
Image reconstruction	Tools for various types of image reconstruction for proper display

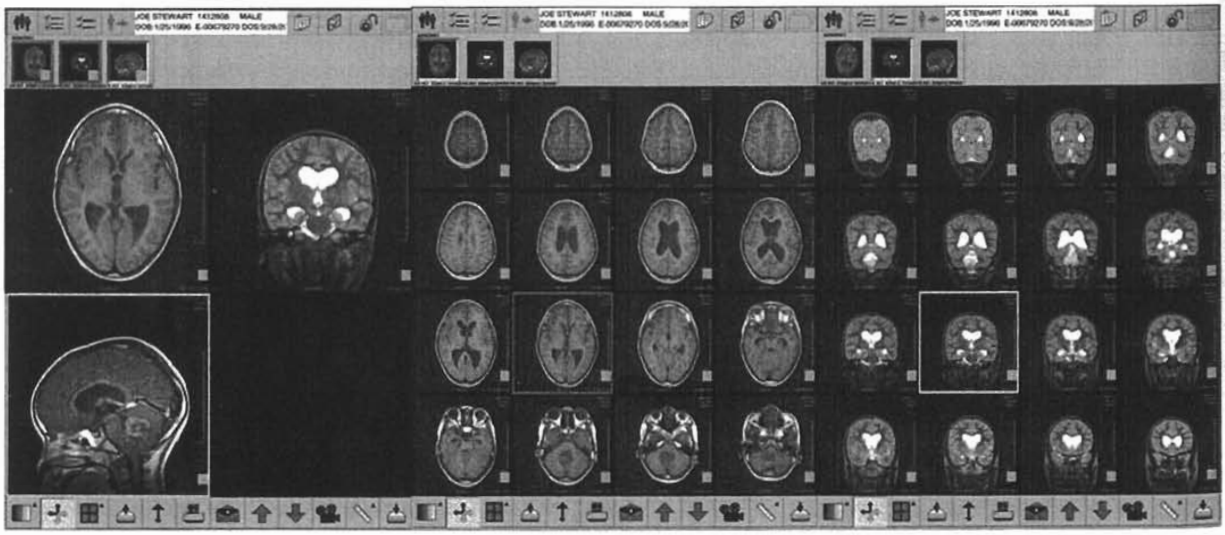

FIGURE 13.5 Example of a picture archiving and communication systems diagnostic workstation displaying a magnetic resonance brain examination.

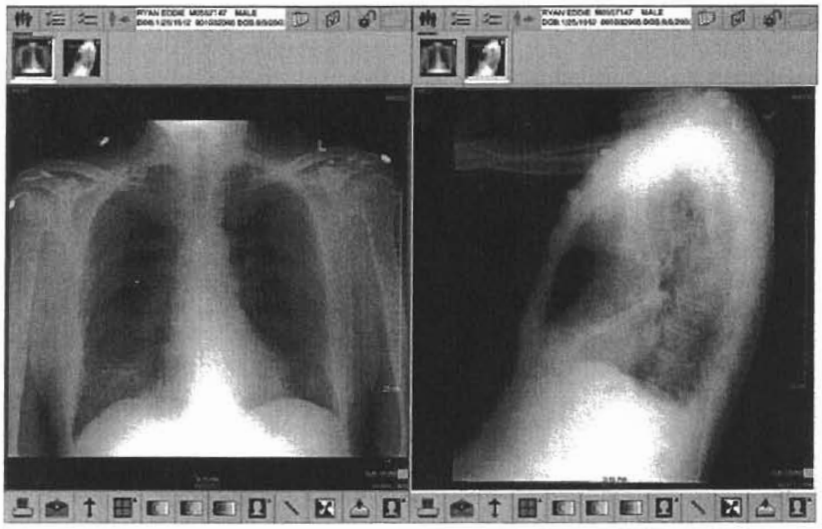

FIGURE 13.6 Example of a picture archiving and communication systems diagnostic workstation displaying a computed radiography chest examination.

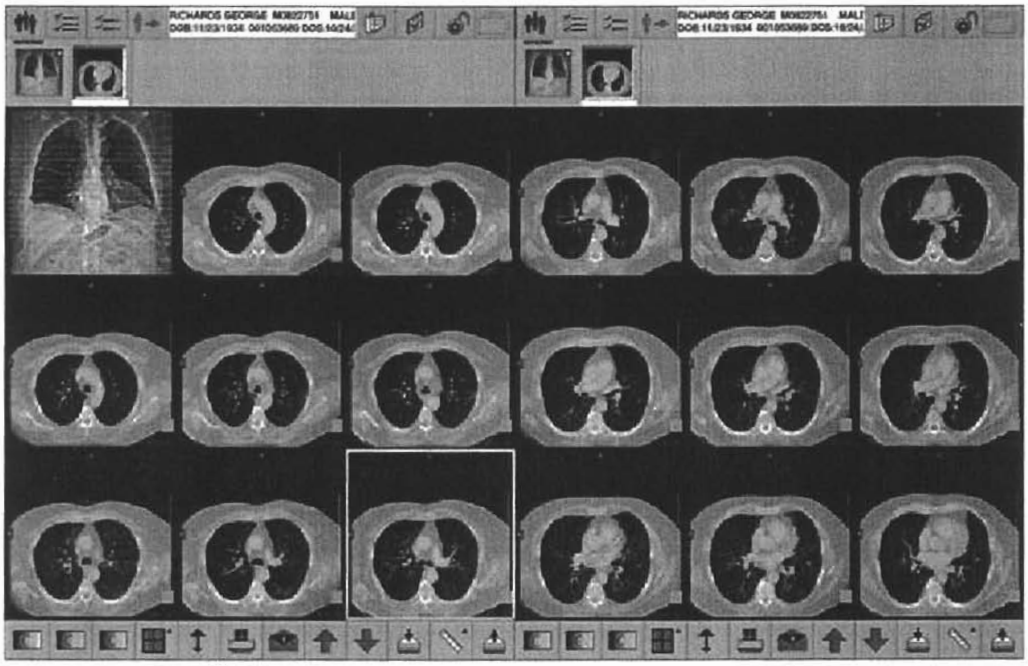

FIGURE 13.7 Example of a picture archiving and communication systems diagnostic workstation displaying a computed radiography chest examination.

At the LAN level, digital communication in the PACS infrastructure design can consist of low-speed Ethernet (10 megabits/s signaling rate), medium-speed (100 megabits/s), or fast-speed (1 gigabit/s) Ethernet, and high-speed asynchronous transfer mode (ATM) technology (155–622 megabits/s and up). In a WAN, various digital service (DS) speeds can be used, which range from DS-0 (56 kilobits/s) and DS-1 (T1, 1.544 megabits/s) to DS-3 (45 megabits/s) and ATM (155–622 megabits/s). There is a trade-off between transmission speed and cost.

The network protocol used should be standard, for example, the TCP/IP and DICOM communication protocol (a higher level of TCP/IP). A low- or medium-speed network is used to connect the imaging modalities (devices) to the acquisition gateway computers because the time-consuming processes during imaging acquisition do not require high-speed connection. Sometimes, several segmented local area Ethernet branches may be used in transferring data from imaging devices to acquisition gateway computers. Medium- and high-speed networks are used on the basis of the balance of data throughput requirements and costs. A faster image network is used between acquisition gateway computers and the PACS controller because several acquisition computers may send large image files to the controller at the same time. High-speed networks are always used between the PACS controller and workstations. It is even more crucial to have high-speed networks to support the client/server PACS architecture because the PACS workstation is highly dependent on data transfer of images from the PACS controller to the PACS workstation's local memory, with performance expectations similar to PACS workstations from a stand-alone architecture where the images are located on the local workstation's hard disk storage.

Process coordination between tasks running on different computers connected to the network is an extremely important issue in system networking. This coordination of processes running either on the same computer or on different computers is accomplished by using interprocessor communication methods with socket-level interfaces to TCP/IP. Commands are exchanged as ASCII messages to ensure standard encoding of messages. Various PACS-related job requests are lined up into disk resident priority queues, which are serviced by various computer system DAEMON (agent) processes. The queue software can have a built-in job scheduler that is programmed to retry a job several times by using either a default set of resources or alternative resources if a hardware error is detected. This mechanism ensures that no jobs will be lost during the complex negotiation for job priority among processes.

13.3.6 PACS Workflow

This section discusses a generic PACS workflow starting from the patient registering in the HIS to the RIS ordering examination, the technologist performing the examination, image viewing, reporting, and archiving. Comparing this PACS workflow with the PACS components and workflow in Figure 13.1 and the general radiology workflow, PACS has replaced many manual steps in the film-based workflow. Figure 13.8 shows the PACS workflow.

13.3.6.1 PACS, Hospital Information Systems, Radiology Information System Workflow

Following the numerals in Figure 13.8:

1. Patient registers in HIS, and a radiology examination is ordered in RIS. An examination accession number is automatically assigned.
2. The RIS outputs HL7 messages of HIS and RIS demographic data to PACS broker/interface engine.
3. The PACS broker notifies the archive server of a scheduled examination for the patient.

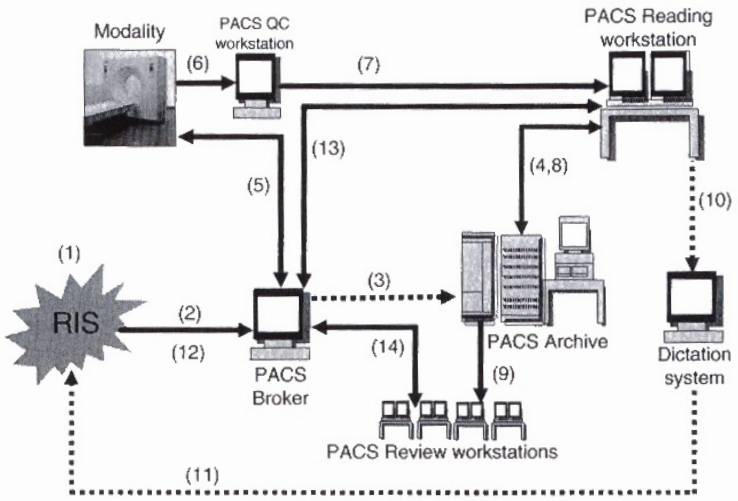

FIGURE 13.8 Generic picture archiving and communication systems workflow showing the numerical steps involved in the clinical workflow as described in the text.

4. Following prefetching rules, historic PACS examinations of the scheduled patient are prefetched from the archive server and sent to the radiologist reading workstation.
5. The patient arrives at examination facility. Modality queries PACS broker/interface engine for DICOM work list.
6. Technologist acquires images and sends PACS examination of images acquired by modality and patient demographic data to QC workstation in DICOM format.
7. Technologist prepares PACS examination and sends to the radiologist reading workstation as prepared status.
8. When the PACS examination arrives at the radiologist reading workstation, it is immediately sent automatically to the archive server. The archive server database is updated, and the PACS examination is marked as prepared status.
9. The archive server automatically distributes the PACS examination to the review workstations in the wards based on patient location received from the HIS/RIS HL7 message.
10. The reading radiologist dictates a report using the examination accession number. The radiologist signs off on PACS examination with any changes. The archive database is updated with changes and marks PACS examination as signed-off status.
11. The transcriptionist retrieves the dictation that corresponds with the examination accession number within RIS and types the report.
12. The RIS outputs HL7 message of results report data along with any previously updated RIS data.
13. The radiologist queries PACS broker/IE for previous reports of PACS examinations on reading workstations.
14. Referring physicians query broker/IE for reports of PACS examinations on review workstations.

13.4 PACS Controller and Image Archive

The PACS central node, considered the engine of the PACS, has two major components: the PACS controller and the archive server. Consisting of both hardware and software architecture, the PACS controller directs the data flow in the entire PACS by using interprocess communication among major processes. The image archive provides a hierarchical image storage management system for short-, medium-, and long-term image archiving.

13.4.1 Image Management and Design Concept

Two major aspects should be considered in the design of the PACS image storage management system: data integrity, which protects against loss of images once they are received by the PACS from the imaging modalities, and system efficiency, which minimizes access time of images at the display workstations. In this section, we only discuss the DICOM-compliant PACS controller and image archive server. To ensure data integrity, the PACS always retains at least two copies of an individual image on separate storage devices until the image has been archived successfully to the long-term storage device (e.g., an optical disk or tape library). This backup scheme is achieved through PACS intercomponent communication among the following PACS components, as shown in Figure 13.1. Figure 13.9 shows the hierarchical image storage management in PACS:

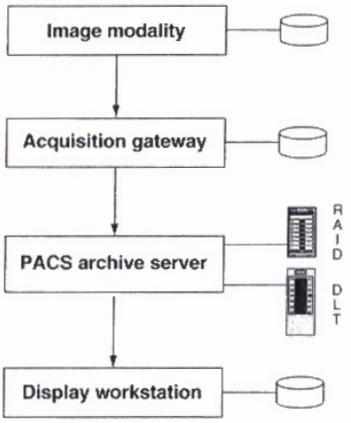

FIGURE 13.9 A diagram showing hierarchic image storage management in picture archiving and communication systems. Note that at least two copies of each picture archiving and communication system image resides on separate storage devices.

1. A copy of the PACS study is stored on the imaging modality until the technologist has verified that the studies have been successfully archived to PACS.
2. A copy of the PACS study is stored on the acquisition gateway computer until the archive subsystem has acknowledged that the study has been received successfully.
3. A copy of the study is retained until the PACS study has been successfully stored to permanent storage (e.g., optical disk or tape library).
4. For stand-alone architecture, a copy of the PACS study is retained on the display workstation until the patient has been discharged or transferred. For client/server architecture, the study is deleted when the review has been completed.

13.4.2 PACS Controller and Archive Server Functions

The PACS controller and the archive server consist of four components: an archive server, a database, a digital linear

tape (DLT) library, and a communication network. Attached to the archive system through the communication network are the acquisition computers and the display workstations. Images acquired by the acquisition computers from various radiological imaging devices are transmitted to the archive server, from which they are archived to the DLT library and routed to the appropriate display workstations. The following is a brief description of each of the four subcomponents as well as some of the major functions.

13.4.2.1 The Archive Server

The archive server consists of multiple powerful central processing units (CPUs), small computer systems interface (SCSI) data buses, and network interfaces (Ethernet and ATM). With its redundant hardware configuration, the archive server can support multiple processes running simultaneously, and image data can be transmitted over different data buses and networks. In addition to its primary function of archiving images, the archive server acts as a PACS controller, directing the flow of images within the entire PACS from the acquisition gateway computers to various destinations such as archive, workstations, or print stations.

The archive server uses its large-capacity redundant array of inexpensive disks (RAID) as a data cache, capable of storing several weeks or months or years worth of images acquired from different radiological imaging devices. As an example, a 20-GB disk storage, without using compression, can hold simultaneously up to 500 computed tomography (CT), 1000 magnetic resonance (MR), and 500 computed radiography (CR) studies. Nowadays, very large RAID and SAN technologies are available in the archive server, especially in the client/server model. The magnetic cache disks configured in the archive server should sustain high data throughput for read operation, which provides fast retrieval of images from the RAID.

13.4.2.2 The Database System

The database system consists of redundant database servers running identical reliable commercial database systems, (e.g., Sybase, Oracle) with structured query language (SQL) utilities. A mirror database with two identical databases can be used to duplicate the data during every PACS transaction (not image) involving the server. The data can be queried from any PACS computer via the communication networks. The mirroring feature of the system provides the entire PACS database with uninterruptible data transactions that guarantee no loss of data in the event of system failure or a disk crash. Besides its primary role of image indexing to support the retrieval of images, the database system is necessary to interface with the RIS and the HIS, allowing the PACS database to collect additional patient information from these two health care databases.

13.4.2.3 The Archive Library

The archive library consists of multiple input/output drives (usually DLT, although some older PAC systems may still use optical erasable, WORM disk, optical tape, or CD-ROM) and disk controllers, which allow concurrent archival and retrieval operations on all of its drives. Newer technologies available as archive library solutions include DVD-ROM, large-scale RAID, and storage area network (SAN). The library must have a large storage capacity of terabytes and support mixed storage media if migrating to newer solutions. In this case, most hospitals opt for migrating PACS studies entirely from one data media solution to another to reduce the complexities of managing mixed storage media. Redundant power supply is essential for uninterrupted operation.

13.4.2.4 Communication Networks

The PACS archive system is connected to both the PACS LAN and the WAN. The PACS LAN can have a two-tiered communication network composed of Ethernet and ATM or high-speed Ethernet networks. The WAN provides connection to remote sites and can consist of T1 lines, ATM, and fast Ethernet. The PACS LAN uses the high-speed ATM or Ethernet switch to transmit high-volume image data from the archive server to 1K and 2K display workstations. An Ethernet using 100 MB/s can be used for interconnecting slower-speed components to the PACS server, including acquisition gateway computers, RIS, and HIS, and as a backup of the ATM or the GB/s Ethernet. Failure of the high-speed network automatically triggers the archive server to reconfigure the communication network so that images can be transmitted to the PACS display workstations over slower Ethernet.

13.4.2.5 PACS Controller and Archive Server Functions

In the controller and archive server, processes of diverse functions run independently and communicate simultaneously with other processes using client/server programming, queuing control mechanisms, and job prioritizing mechanisms. Because the functions of the controller and the archive server are closely related, we sometimes use the term archive server to represent both. Major tasks performed by the archive server include image receiving, image stacking, image routing, image archiving, studies grouping, platter management, RIS interfacing, PACS database updating, image retrieving, and image prefetching. The following subsections describe the functionality carried out by each of these tasks. Whenever appropriate, the DICOM standard is highlighted in these processes.

13.4.2.5.1 Image Receiving. Images acquired from various imaging devices in the gateway computers are converted into DICOM data format if they are not already in DICOM. DICOM images are then transmitted to the archive server via

the Ethernet or ATM by client/server applications over standard TCP/IP protocols. The archive server can accept concurrent connections for receiving images from multiple acquisition computers. DICOM commands can take care of the send and receive processes.

13.4.2.5.2 Image Stacking. Images that come to the archive server from various gateway computers are stored on its local magnetic disks or RAID (temporary archive) based on the DICOM data model and managed by the database. The archive server holds as many images in its several hundred gigabyte disks as possible and manages them on the basis of aging criteria. During a hospital stay, for example, images belonging to a given patient remain in the archive server's temporary archive until the patient is discharged or transferred. Thus all recent images that are not already in a display workstation's local storage can be retrieved from the archive server's high-speed short archive instead of the lower-speed DLT library. This feature is particularly convenient for radiologists or referring physicians who must retrieve images from different display workstations. In the client/server PACS model, the temporary archive is very large, some have terabytes of capacity with the long-term archive library solution a SAN storage device.

13.4.2.5.3 Image Routing. In the stand-alone (or peer-to-peer) PACS model, images that come to the archive server from various acquisition computers are immediately routed to their destination workstations. The routing process is driven by a predefined routing table composed of parameters including examination type, display workstation site, radiologist name, and referring physician name. All images are classified by examination type (1-view chest, CT head, CT body, etc.) as defined in the DICOM standard. The destination display workstations are classified by location (Chest, Pediatrics, CCU, etc.) as well as by resolution (1K or 2K). The routing algorithm performs table lookup based on the aforementioned parameters and determines an image's destination(s). Images are transmitted to the 1K and 2K workstations over Ethernet, LAN, or ATM and to remote sites over dedicated T1 lines, ATM, or high-speed WAN.

13.4.2.5.4 Image Archiving. Images arriving in the archive server from gateway computers are copied from temporary storage to the archive library for long-term storage. When the copy process is complete, the archive server acknowledges the corresponding acquisition gateway, allowing it to delete the images from its local storage and reclaim its disk space. In this way, the PACS always has two copies of an image on separate magnetic disk systems until the image is archived to the permanent storage. Images from multiple examinations that occur during a patient's hospital stay are scattered temporarily across the archive library.

13.4.2.5.5 RIS and HIS Interfacing and PACS Database Updates. The archive server accesses data from HIS/RIS through a PACS gateway computer. The HIS/RIS relays messages regarding patient admission, discharge, and transfer (ADT) to the PACS only when a patient is scheduled for an examination in the radiology department or when a patient in the radiology department is discharged or transferred. Forwarding ADT messages to PACS not only supplies patient demographic data to the PACS but also provides information the archive server needs to initiate the prefetch, image archive, and studies grouping tasks. Exchange of messages among these heterogeneous computer systems can use the HL7 standard data format running TCP/IP communication protocols on a client/server basis. In addition to receiving ADT messages, PACS receives examination data and diagnostic reports from the RIS. This information is used to update the PACS database, which can be queried and reviewed from any display workstation. Data transactions performed in the archive server, such as insertion, deletion, selection, and update, are carried out by using SQL utilities in the database. Data in the PACS database are stored in predefined tables, with each table describing only one kind of entity. The design of these tables should follow the DICOM data model for operation efficiency. Individual PACS processes running in the archive server with information extracted from the DICOM image header update these tables and the RIS interface to reflect any changes of the corresponding tables.

13.4.2.5.6 Image Retrieving. Image retrieval takes place at the display workstations. The display workstations are connected to the archive system through communication networks. The archive library configured with multiple drives can support concurrent image retrievals from multiple tapes. The retrieved data are then transmitted from the archive library to the archive server via the SCSI data buses. The archive server handles retrieve requests from display workstations according to the priority level of these individual requests. Priority is assigned to individual display workstations and users based on different levels of needs. For example, the highest priority is always granted to a display workstation that is used primary for diagnosis or is in a conference session or at an intensive care unit. Thus, a workstation used exclusively for research and teaching purposes is compromised to allow fast service to radiologists and referring physicians in the clinic for immediate patient care.

13.4.2.5.7 Image Prefetching. The prefetching mechanism is initiated as soon as the archive server detects the arrival of a patient by means of the ADT message from HIS/RIS. Selected historic images, patient demographics, and relevant diagnostic reports are retrieved from the archive library and the PACS database. Such data are distributed to the destination workstation(s) before the completion of the patient's current examination or staged at the short-term RAID storage device.

The prefetch algorithm is based on predefined parameters such as examination type, disease category, radiologist name, referring physician name, location of the workstation, and the number and age of the patient's archived images. These parameters determine which historic images should be retrieved, when they should be retrieved, and where they should go.

13.4.3 Digital Imaging and Communications in Medicine-Compliant PACS Archive Server

The purpose of the DICOM standard is to promote a standard communication method for heterogeneous imaging systems, allowing the transfer of images and associated information among them. By using the DICOM standard, a PACS would be able to interconnect its individual components and allow the acquisition gateways to link to imaging devices. However, imaging equipment vendors often select different DICOM-compliant implementations for their own convenience, which may lead to difficulties for these systems in interoperation. Therefore, it is an important step to perform throughput testing of the entire system from PACS study acquisition to archival to ensure that the system is integrated properly. A well-designed DICOM-compliant PACS server can use two mechanisms to ensure system integration. One mechanism is to connect to the acquisition gateway computer with DICOM providing reliable and efficient processes of acquiring images from imaging devices. The other mechanism is to develop specialized server software allowing interoperability of multivendor imaging systems. Both mechanisms can be incorporated in the DICOM-compliant PACS server.

13.4.4 Hardware and Software Components

The PACS archive server generic hardware components consist of the PACS archive server computer, peripheral archive devices, and fast Ethernet interface and SCSI. For large-scale PACS, the server computer used is a mostly UNIX-based machine. The fast Ethernet interfaces the PACS archive server to the fast Ethernet network, where acquisition gateways and display workstations are connected. The SCSI integrates peripheral archive devices with the PACS archive server. The main archive devices for the PACS server include magnetic disk, RAID, DLT, and CD/DVD (digital video disks) jukeboxes, and newer SAN technologies. RAID, because of its fast access speed and reliability, is extensively used as the short-term archive device in PACS. Because of its large data storage capacity, DLT is mostly used for long-term archiving. Many kinds of storage devices are available for PACS application. In the following we describe the two most popular ones, RAID and DLT, along with a third, newer SAN technology.

13.4.4.1 Redundant Array of Inexpensive Disks

RAID is a disk array architecture developed for fast and reliable data access. A RAID groups several magnetic disks (e.g., eight disks) as a disk array and connects the array to one or more RAID controllers. The size of RAID is usually several hundred gigabytes (e.g., 320 GB for eight disks) to terabytes. With the individual disk size increasing, the size of RAID can also be increased. The RAID controller has a SCSI interface to connect to the SCSI interface in the PACS server. Multiple RAID controllers with multiple SCSI interfaces can avoid the single-point failure in the RAID device.

13.4.4.2 Digital Linear Tape

DLT uses a multiple magnetic tape and drive system housed inside a library or jukebox for large-volume and long-term archive. With current tape drive technology, the data storage size can reach 40 to 200 GB/tape. One DLT can hold from 20 to hundreds of tapes. Therefore, the storage size of DLT can be from one to tens of terabytes, which can hold PACS images from one to several years. DLT usually has multiple drives to read and write tapes. The tape drive is connected to the server through SCSI or fiber-optic connection. The data transmission speed is several megabytes per second for each drive. The tape loading time and data locating time are several minutes. Hence, in general, it takes several minutes to retrieve one CR image from DLT. PACS image data in DLT are usually prefetched to RAID for fast access time.

13.4.4.3 Storage Area Network

A current data storage trend in large-scale archiving is SAN technology. With this new configuration, the PACS server will still have a short-term storage solution in local disks containing unread patient studies. However, for long-term storage, the PACS data are stored in a SAN. This SAN is a stand-alone data storage repository with a single IP address. File management and data backup can be achieved with a combination of digital media (e.g., RAID or DLT) smoothly and with total transparency to the user. In addition, the SAN can be partitioned into several different repositories each storing different data file types. The storage manager within the SAN is configured to recognize and distribute the different clients' data files and store them to distinct and separate parts of the SAN.

13.4.4.4 Archive Server Software

PACS archive server software is DICOM-compliant and supports DICOM storage service class and query/retrieve service class. Through DICOM communication, the archive server receives DICOM studies/images from the acquisition gateway, appends study information to the database, and stores the images in the archive device, including the RAID, DLT, or SAN. It receives the DICOM query/retrieve request from

display workstations and sends out the query/retrieve result (patient/study information or images) back to workstations. The DICOM services supported in PACS archive server are C-Store, C-Find, and C-Move. All software implemented in the archive server should be coded in standard programming languages—for example, C and C++ on the UNIX open systems architecture. PACS archive server software is composed of at least six independent components (processes), including receive, insert, routing, send, Q/R-server, and retrieve send. It also includes a PACS database. All of these processes run independently and simultaneously and communicate with other processes through queue control mechanisms.

13.4.5 Disaster Recovery and Backup Archive Solutions

The PACS archive server is the most important component in a PACS, and even though it may have the fault-tolerant feature, chances are it could fail occasionally. A backup archive server is necessary to guarantee its uninterrupted service. Two copies of identical images can be saved through two different paths in the PACS network to two archive libraries. Ideally, the two libraries should be in two different buildings in case of natural disaster. To reduce the cost of redundant archiving, the primary unit can be another DLT library. The backup archive server can be short term (3 months) or long term. The functions of a backup archive server are twofold: maintaining the PACS continuous operation and preventing loss of image data. Data loss is especially troublesome because if a major disaster occurs, it is possible to lose an entire hospital's PACS data. In addition, scheduled downtimes to the main PACS archive have a great impact on a filmless institution. Few current PACS archives feature disaster recovery or a backup archive, and designs are limited at best. Furthermore, current general disaster recovery solutions vary in the approach toward creating redundant copies of PACS data. One novel approach is to provide a short-term fault-tolerant backup archive server using the application service provider (ASP) model at an offsite location. The ASP backup archive provides instantaneous, automatic backup of acquired PACS image data and instantaneous recovery of stored PACS image data, all at a low operational cost because it uses the ASP business model. Figure 13.10 shows the general architecture of an ASP backup archive server. In addition, should the downtime event render the network communication inoperable, a portable solution is available with a data migrator. The data migrator is a portable laptop with a large-capacity hard disk that contains DICOM software for exporting and importing PACS examinations. The data migrator can populate PACS examinations that were stored on the backup archive server directly onto the clinical PACS within hours to allow the radiologists to continue to read previous PACS examinations until new replacement hardware arrives and is installed or until a scheduled downtime event has been completed.

13.5 Large-Scale PACS Implementation

Around the world, because of the need to improve operation efficiency and provide more cost-effective health care, many large-scale health care enterprises have been formed. Each of these enterprises can group hospitals, medical centers, and clinics together as one enterprise health care network. The management of these enterprises recognizes the importance of using PACS and image distribution as a key technology in better-quality and more cost-effective health care delivery at the enterprise level. As a result, many large-scale enterprise-level PACS/image distribution pilot studies, full design, and implementation, are under way. The following are characteristics of these systems:

1. Scale: large enterprise level, from 39 to 399 hospitals and medical centers
2. Complexity: total health care IT integration

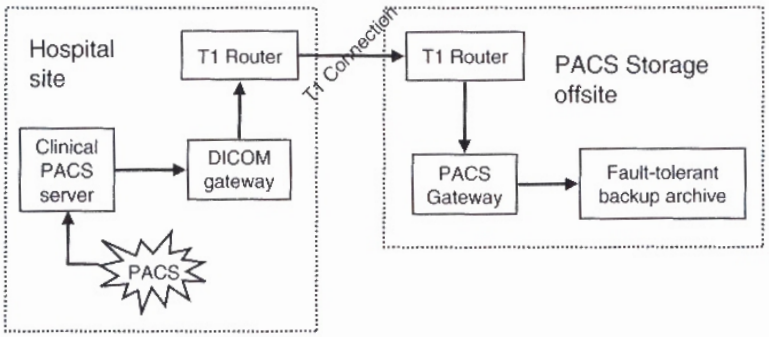

FIGURE 13.10 General architecture of the ASP backup archive server. One DICOM gateway and one picture archiving and communication systems gateway are used as the buffers between the two sites. T1 is used for wide area network (WAN).

3. Goals and Objectives: complete system deployment to the enterprise
4. Costs: extremely expensive
5. Difficulty of Implementation: culture, resources, timeline, and overcoming legacy technologies

13.5.1 Introduction to Hospital Clinical Systems

PACS is a workflow-integrated imaging system designed to streamline operations throughout the entire patient care delivery process. One of its major components, image distribution, delivers relevant electronic images and related patient information to health care providers for timely patient care either within a hospital or in a health care enterprise. Enterprise-level health care delivery emphasizes sharing of enterprise-integrated resources and streamlining operations. In this respect, if an enterprise consists of several hospitals and clinics, it is not necessary for every hospital and clinic to have similar specialist services. A particular clinical service like radiology can be shared among all entities in the enterprise. Under this setup, all patients registered in the same enterprise can be referred to a radiology expert center for examinations. In this scenario, the patient being cared for becomes the focus of the operation. A single index like the patient's name/identification would be sufficient for any health care provider in the enterprise to retrieve the patient's comprehensive record. For this reason, the data management system would not be the conventional HIS, RIS, or other organizational information system. Rather, the ePR or eMR concept will prevail. However, to develop the ePR, the successful integration of the HIS, RIS, and, additionally, voice recognition system, is crucial. The following sections will describe each of the afore-mentioned hospital clinical systems and their interfaces with each other, as well as the ePR concept.

13.5.2 Hospital Information System

The HIS is a computerized management system for handling three categories of tasks in a health care environment:

1. Support clinical and medical patient care activities in the hospital
2. Administer the hospital's daily business transactions (financial, personnel, payroll, bed census, etc.)
3. Evaluate hospital performances and costs and make a long-term forecast

Many clinical departments in a health care center, such as radiology, pathology, pharmacy, clinical laboratories, and other units, have their own specific operational requirements that differ from those of the general hospital operation. For this reason, special information systems may be needed in these departments. Often, these information systems are under the umbrella of the HIS, which maintains their operations. Other departments may have their own separate information systems, and some interface mechanisms are built to integrate data between these systems and the HIS. For example, RIS was originally a component of HIS; later, independent RIS was developed because of the limited support offered by HIS to handle special information required by the radiology departmental operations. However, the integration of these two systems is still extremely important for the health care center to operate as a total functional entity.

Large-scale HIS mostly use mainframe computers. These can be purchased through a manufacturer with certain customization software or homegrown through the integration of many commercial products progressively over years. A homegrown system may contain many reliable legacy components but have out-of-date technology. Therefore, to interface HIS to PACS, caution must be taken to circumvent the legacy problem.

Most HIS are an integration of many information data systems, starting the day the health care data center was established, with older components being replaced by newer ones over many years of operation. In addition to taking care of the clinical operation, the HIS also support hospital and health care center business and administrative functions. They provide automation for such events as patient registration and ADT, as well as patient accounting. They also provide on-line access to patient clinical results (e.g., laboratory, pathology, microbiology, pharmacy, radiology). The system broadcasts in real time the patient demographics and encounters information with HL7 standards to the RIS. Through this path, ADT and other pertinent data can be transmitted to the RIS and the PACS.

13.5.3 Radiology Information System

The RIS is designed to support both the administrative and clinical operation of a radiology department, to reduce administrative overhead, and to improve the quality of radiological examination delivery. Therefore, the RIS manages general radiology patient demographics and billing information, procedure descriptions and scheduling, diagnostic reports, patient arrival scheduling, film location, film movement, and examination room scheduling. The RIS configuration is very similar to the HIS, except that it is on a smaller scale. RIS equipment consists of a computer system with peripheral devices such as RIS workstations (normally no image display), printers, and bar code readers. Most independent RIS are autonomous systems with limited access to HIS. However, some HIS offer embedded RIS as a subsystem with a higher degree of integration.

The RIS maintains many types of patient- and examination-related information, including medical, administrative, patient demographics, examination scheduling, diagnostic

reporting, and billing information. The major tasks of the system include:

1. Process patient and film folder records
2. Monitor the status of patients, examinations, and examination resources
3. Schedule examinations
4. Create, format, and store diagnostic reports with digital signatures
5. Track film folders
6. Maintain timely billing information
7. Perform profile and statistics analysis

The RIS interfaces to PACS based on the HL7 standard through TCP/IP over Ethernet on a client/server model using a trigger mechanism. Events such as examination scheduling, patient arrivals, and actual examination begin and end times trigger the RIS to send previously selected information (patient demographics, examination description, diagnostic report, etc.) associated with the event to the PACS in real time.

13.5.4 Voice Recognition System

Typically, radiological reports are archived and transmitted independently from the image files. They are first dictated by the radiologist and recorded on an audiocassette recorder from which a textual form is transcribed and inserted into the RIS several hours later. The interface between the RIS and the PACS allows for sending and inserting these reports into the PACS database, from which a report corresponding to the images can be displayed on the PACS workstation on request by the user. This process is not efficient because the delay imposed by the transcription prevents the textural report from reaching the referring physician in a timely manner. One method is to append the digital voice recordings of the radiologist to the PACS study. The concept of interfacing this method is to have the digital voice database associated with the PACS image database; thus, before the written report becomes available, the referring physician can look at the images and listen to the report simultaneously. The radiologist views images from the PACS workstation and uses the digital Dictaphone system to dictate the report, which converts it from analog signals to digital format and stores the result in the voice message server. The voice message server in turn sends a message to the PACS data server, which links the voice with the images. The referring physicians at the workstation can, for example, in an intensive care unit, request to review certain images and at the same time listen to the voice report through the voice message server linked to the images. Later, the transcriber transcribes the voice by using the RIS. The transcribed report is inserted into the RIS database server automatically. The RIS server sends a message to the PACS database server. The latter appends the transcribed report to the PACS image file and signals the voice message server to delete the voice message.

The ideal method is to use a voice recognition system that automatically translates voice into text. In this case, the voice recognition system is either called within the PACS application or the RIS application. All the necessary fields are populated (e.g., patient name, medical record number, type of study), and the radiologist can begin to dictate. Once the radiologist has completed the dictation, the report can be edited, reviewed, and electronically signed off. It is then ready for distribution. In addition, report templates can be created for common diagnosis results that allow the radiologist to quickly create a report result via voice recognition commands. The report is then sent to RIS via an interface, and RIS can then forward the report to PACS as needed. When the DICOM-structured report standard becomes available, radiologists can directly enter the report through the structured report format while reviewing the images. Thus, the digital voice dictation system may see less use while the voice recognition system will be enhanced with a full set of automatic templates that can be created on demand once the DICOM-structured report becomes more acceptable to radiologists.

13.5.5 Interfacing PACS, Hospital Information Systems, Radiology Information Systems, and Voice Recognition Systems

There are three methods of transmitting data between information systems: through workstation emulation, through database-to-database transfer, and by means of an interface engine.

13.5.5.1 Workstation Emulation

This method allows a workstation of an information system to emulate a workstation of a second system. As a result, data from the second information system can be accessed by the first system. For example, a PACS workstation can be connected to the RIS with a simple computer program that emulates a RIS workstation. From the PACS workstation, the user can perform any RIS function such as scheduling a new examination, updating patient demographics, recording a film movement, and viewing the diagnostic reports. This method has two disadvantages. First, there is no data exchange between RIS and PACS. Second, the user is required to know how to use both systems. Also, a RIS or HIS workstation cannot be used to emulate a PACS workstation because the latter is too specific for HIS and RIS to emulate.

13.5.5.2 Database-to-Database Transfer

The database-to-database transfer method allows two or more networked information systems to share a subset of data by storing them in a common local area. For example, the ADT data from the HIS can be reformatted to HL7 standard and broadcasted periodically to a certain local database in the HIS.

A TCP/IP communication protocol can be set up between the HIS and the RIS, allowing the HIS to initiate the local database and broadcast the ADT data to the RIS through either a pull or push operation. This method is most often used to share information between the HIS and the RIS. A recent trend is the integration between RIS and PACS databases. In this configuration, common elements are shared between both databases, and any changes or modifications made to the patient, study, or image information are updated once without the need to update both databases manually. In addition, at the diagnostic workstation, the RIS application would call the PACS application to display the particular study. An additional monitor is usually used to display the RIS application. The user will navigate through the RIS application to identify and select the particular radiology study to be diagnosed, and the RIS application makes a function call to the PACS application to display the selected PACS study. This method of workflow is called RIS-driven workflow because the RIS is the driver of the diagnostic workflow and the PACS acts as a client in this instance.

13.5.5.3 Interface Engine

The interface engine provides a single interface and language to access distributed data in networked heterogeneous information systems. In operation, it appears that the user is operating on a single integrated database from his or her workstation. In the interface engine, a query protocol is responsible for analyzing the requested information, identifying the required databases, fetching the data, assembling the results in a standard format, and presenting them at the workstation. Ideally, all these processes are done transparently to the user and without affecting the autonomy of each database system. To build a universal interface engine is not a simple task. Most currently available commercial interface engines are tailored to limited specific information systems.

13.5.5.1 Integrating HIS, RIS, PACS, and VR Systems

Another recent trend to streamline the diagnostic workflow and provide as much clinical information as possible to the radiologist has resulted in the integration of HIS/RIS/PACS/voice recognition (VR) application on one diagnostic workstation. This new integrated workstation is often referred to as the radiology command center and allows the radiologist full access to all available pertinent and historic clinical patient data while making a primary diagnosis. Because this is a fairly recent technology trend, the complexities and challenges of integrating multiple applications on a single workstation have impacted the user with factors such as ease-of-use, reliability, and efficiency. More work in the future is needed to fully realize the potential of such an integrated workstation.

In a hospital environment, interfacing the PACS, RIS, and HIS has become necessary to enhance diagnostic process, PACS image management, RIS administration, and research and training. These are all important aspects to consider when integrating systems.

13.5.6 Electronic Patient Record

The eMR or ePR is the ultimate information system in a health care enterprise. In an even broader sense, if the information system includes the health record of an individual, then it is called the electronic health record (eHR). In this context, we concentrate on ePR. Currently, only small subsets of ePR are actually in clinical operation. One can consider ePR as the big picture of the future health care information system. Although the development of a universal ePR as a commercial product is still years away, its eventual impact on the health care delivery system should not be underestimated. An ePR consists of five major functions:

1. Accepts direct digital input of patient data
2. Analyzes across patients and providers
3. Provides clinical decision support and suggests courses of treatment
4. Performs outcome analysis and patient and physician profiling
5. Distributes information across different platforms and health information systems

HIS and RIS, which deal with patient nonimaging data management and hospital operation, can be considered components of ePR. An integrated HIS-RIS-PACS system, which extends the patient data to include imaging, forms a cornerstone of ePR. Existing ePRs have certain commonalties. They have large data dictionaries with time stamped in their contents and can query and display data flexibly. Examples of successfully implemented EMRs are the Computer-Stored Ambulatory Record developed at Massachusetts General Hospital (in the public domain), the Regenstrief Medical Record System at Indiana University, the Health Evaluation Through Logical Processing system developed at the University of Utah and Latter-Day Saints Hospital, and the Department of Veterans Affairs Health Care Enterprise (VAHE) information system. Among these systems, the VAHE is one of the most advanced systems in the sense that it is being used daily in many of the VA medical centers and it includes images in the ePR. Figure 13.11 shows examples of the ePR from the VAHE system called Veterans Health Information System Technology Architecture (VistA).

As with any other medical information system, the development of the ePR faces several obstacles:

- Finding a common method to input patient examination and related data to the system
- Developing an across-the-board data and communication standard
- Gaining buy-in from manufacturers to adopt the standards
- Gaining acceptance by health care providers

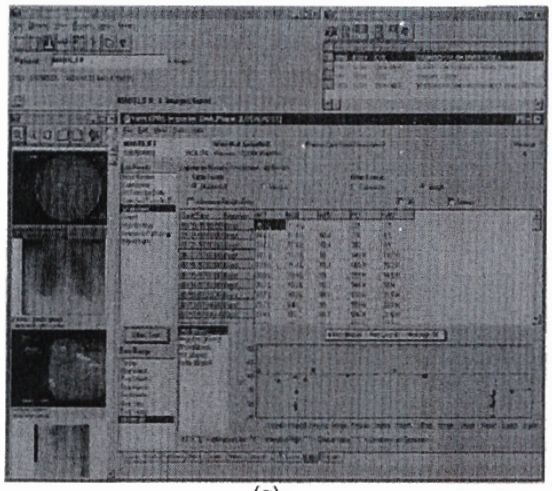

(a)

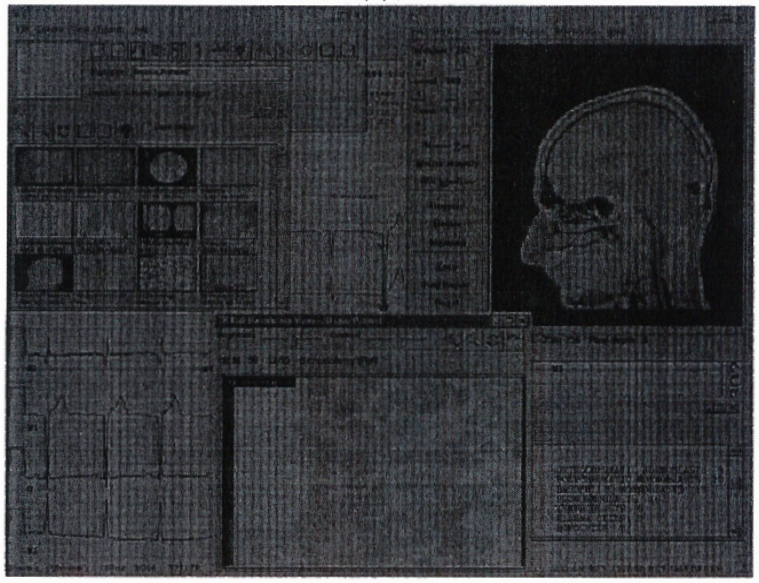

(b)

FIGURE 13.11 (a) VistA imaging displays the patient record with images. (b) VistA imaging displays thumbnail images, microscopic images, magnetic resonance images, and electrocardiogram. Courtesy of Dr. H. Rutherford; Dayhoff, 2000.

An integrated HIS-RIS-PACS system provides solutions for some of these obstacles.

- DICOM and HL7 standards have been adopted for imaging and text, respectively.
- Images and patient-related data are entered into the system almost automatically.
- The majority of imaging manufacturers have adopted DICOM and HL7 as *de facto* industrial standards.

Therefore, in the course of developing an integrated PACS, one should keep in mind the big picture, the ePR. Anticipation of future connections and the integrated PACS as a subsystem of ePR with images should be considered thoroughly.

13.6 PACS Clinical Experiences

13.6.1 Introduction

In this section, methodology and a road map for PACS implementation and system evaluation within a clinical hospital environment will be discussed. In addition, some examples of

clinical experiences and pitfalls will be presented. The philosophy of PACS design and implementation is that, regardless of the scale of the PACS being planned, the strategy should always be to leave room for future expansion, including integration with an enterprise PACS. Thus, if the planning is to have a large-scale PACS now, the PACS architecture should allow its future growth to an enterprise PACS. On the other hand, if only a PACS module is being planned, the connectivity and compatibility of this module with future modules or with a larger-scale PACS are important. The terms we discussed in previous chapters, including open architecture, connectivity, standardization, portability, modularity, and IHE workflow profiles, should all be considered.

13.6.2 PACS Implementation Strategy

When implementing a PACS within a clinical environment, it is very important to recognize some key fundamental concepts that will serve as cornerstones for a successful implementation. First, PACS is an enterprise-wide system or product. It is no longer just for the radiology or imaging department; therefore, careful consideration of all decisions/strategies going forward should include the entire health care continuum, from referring physicians to the radiology department clinical and technical staff to the health care institution's IT department. It is crucial for a successful implementation that some of the key areas within the health care institution have buy-in of the PACS process, including administration, the radiology department, the IT department, and all high-profile customers of radiology (e.g., orthopedics, surgery). Furthermore, a champion or champions should be identified for the PACS process. Usually this is the medical director of radiology, but it can include other physicians as well as IT administrators. Second, PACS is a system with multiple complex components that interact with one another. Each of these components can be an accumulation of multiple hardware components. A general clinical PACS usually includes the archive, the archive server/controller, the DICOM gateway, the Web server, the workstations, and a RIS/PACS interface. Whether considering implementation or acceptance, all components of the system must be assessed. The following sections describe some of the steps involved in implementing a PACS within a health care institution.

13.6.2.1 Risk Assessment Analysis

It is important to perform a risk assessment analysis before implementation so that problem areas and challenges can be mapped out accordingly and timeline schedules can be made to accommodate potential roadblocks. Some areas to focus on are Z the network infrastructure that will be supporting the PACS, the integration of acquisition modality scanners with PACS (e.g., legacy systems, modality work list, quality control workstations), physical space for the PACS equipment, and resource availability. Resource availability is especially crucial because a successful PACS implementation hinges on the support provided by the in-house radiology department. In making risk assessments, it is also helpful to determine areas in which there is a low risk and a high return. These areas are usually departments where there is a high volume of image (film) and a low rate of return of film back to the radiology department (e.g., critical care areas, orthopedics, surgery). These low-risk/high-return areas can help to drive the implementation phase timeline and can also be a good first push in the implementation process.

13.6.2.2 Implementation Phase Development

Implementation of PACS should be performed in distinct phases, which would be tailored based on the risk assessment analysis performed at the health care institution. Usually, the first phase occurs when the main components are implemented such as the archive, archive server/controller, network infrastructure, HIS-RIS-PACS interfaces, workstations, and one or two modality types. The next phases are targeted toward implementing all modality types and a Web server for enterprise-wide and off-site distribution of PACS examinations. The phased approach allows for a gradual introduction of PACS into the clinical environment, with the ultimate goal being the transformation into a filmless department/hospital.

13.6.2.3 Development of Workgroups

Because PACS covers such a broad area within the health care institution, it is important to develop workgroups to handle some of the larger tasks and responsibilities. In addition, a PACS implementation team should be in place to oversee the timely progress of the implementation process. The following are some key workgroups and their responsibilities:

1. RIS-PACS interface and testing: Responsible for integration/testing of RIS/PACS interfaces including the modality work list on the acquisition scanners
2. PACS modalities and system integration: Responsible for the technical integration of modalities with PACS and installation of all PACS devices
3. PACS acquisition workflow and training: Responsible for developing workflow and training for clerical and technical staff and for any construction needed in the clinical areas
4. PACS diagnostic workflow and training: Responsible for developing workflow and training for radiologists and clinicians and for any construction needed in the clinical diagnostic areas (e.g., reading room designs). Figure 13.12 shows an example of the different stages of conversion of a clinical space into a reading room for radiologists.
5. PACS network infrastructure: Responsible for all design and implementation of the network infrastructure to support PACS

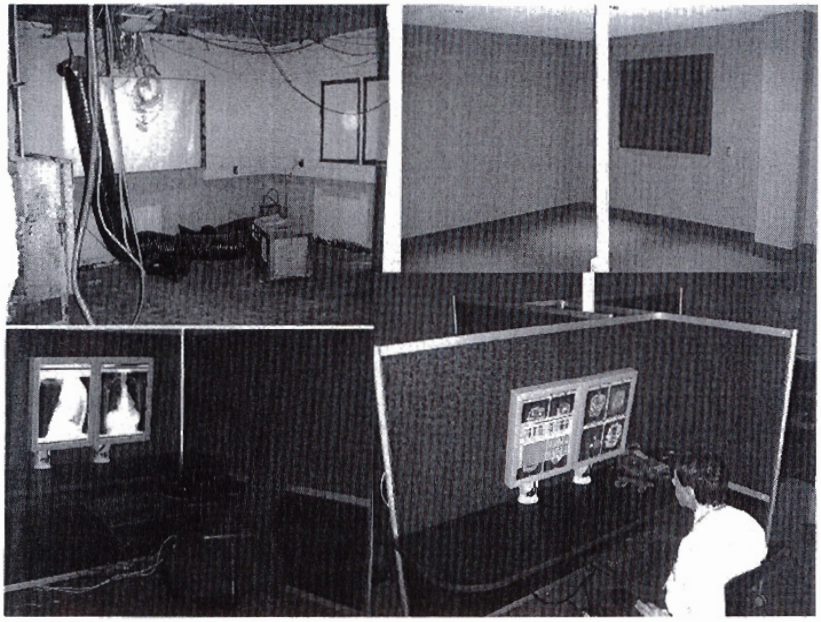

FIGURE 13.12 Different stages of the conversion of a clinical space into a reading room for radiologists. Note the pinwheel-shape design using the center floor of the room. Power and networking are supplied through the column in the center of the floor.

In addition to the above-listed workgroups, a PACS implementation team should be formed to oversee the implementation process. Members should include at least one point person from each workgroup, and additional members should include the PACS implementation manager, the medical director of imaging, the administrative director of imaging, an IT representative, and an engineering/facilities representative. This team should meet at least every 2 weeks and more frequently as the date of live implementation nears. The goals of this team are to update any status items and to highlight any potential stumbling blocks to the implementation process. In addition, this team meeting allows a forum for higher-level administrators to observe the progress of the implementation. It is crucial to identify particular in-house resources for the implementation process. These include a technical supervisor of each modality, a clerical supervisor, a film librarian or film clerk, an RIS support person, and an IT network support person. These resources are an excellent source of information for issues related to PACS such as technologist workflow, clerical workflow, film distribution workflow, design and performance of RIS interface testing with PACS, and overall hospital IT infrastructure.

13.6.2.4 Implementation Management

Developing a schedule and implementation checklist can assist management of the implementation process. This template includes topics such as the task description, the date scheduled for the task, the owner of the task, and a checkmark box to indicate completion of the task. This template allows for finer granularity of the implementation process to protect against overlooked implementation tasks. Input for the checklist can come from the PACS implementation team meetings. Furthermore, the checklist can be broken down into smaller subtask checklists for tracking of issues within each of the workgroups.

13.6.3 System Acceptance

One of the key milestones to system turnover is the completion of the acceptance testing (AT) of PACS. There are a few reasons why AT is important to PACS. First, AT provides vendor accountability for delivering the final product that was initially scoped and promised. It also provides accountability for the in-house administration that there is documentation that the system was tested and accepted. AT also provides a glimpse into determining the characteristics of PACS uptime and whether it will function as promised. Finally, AT provides proof of both PACS performance and functionality as originally promised by the vendor. Most vendors provide their own AT plan; however, usually it is not thorough enough, and the template is not customized to the specific health care institution's needs. The following sections describe some of the steps in designing and developing a robust AT that can be used for final turnover of PACS in the clinical environment.

Acceptance test criteria are divided into two categories. The first category is quality assurance. This includes PACS image quality, functionality, and performance. The second category is technical testing, which focuses on the concept of no single point of failure through the PACS and includes simulation of downtime scenarios. Acceptance criteria should include identifying which PACS components are to be tested. The following are some of the components that should be included are:

1. RIS/PACS interface and/or PACS broker
2. Acquisition gateways
3. Modality scanner(s)
4. Archive server/storage
5. Diagnostic workstation
6. Review workstation
7. Network devices

If the PACS also includes a Web server, then it also should be included within the acceptance testing criteria.

Each of the implementation phases of the PACS process should have an acceptance test performed. Acceptance at each of the phases is also crucial for the vendor because it is only after acceptance that the vendor can collect the remainder of the fee balance, which is negotiated beforehand. The implementation of the AT is a two-phased approach. The first phase should be performed approximately 1 week before the live date. The content of phase one includes the technical component testing focusing on single points of failure, end-to-end testing, contingency solutions for downtime scenarios, and any baseline performance measurements. The second phase should be performed approximately 2 weeks after the live date so that the PACS has stabilized a bit in the clinical environment. The contents of phase two include PACS functional and performance testing as well as any additional network testing, all on a loaded clinical network.

13.6.4 Image/Data Migration

Two scenarios are possible to trigger image/data migration: converting to a new storage technology and increasing data volumes. It is possible for a health care institution to have a dramatic increase in PACS data volumes once it transforms into a filmless institution. This is possible due in part to the continuous image accumulation as well as the integration of new modalities generating mass volumes of PACS data and archiving the large data quantities to PACS. For example, the multislice detector CT scanner is capable of generating up to 1000 images amounting to almost 500 MB of data per examination. It is very likely that a hospital may need to expand the archive storage capacity. Furthermore, most PACS installed in previous years do not have a secondary copy backup of all the archived PACS image data for disaster recovery purposes. It has only been a recent trend for PACS to offer disaster recovery solutions. Therefore, should a hospital decide to upgrade the archive server performance and expand with a higher-capacity data media storage system, there are a few major challenges facing a successful upgrade. One challenge is how to upgrade to a new PACS archive server in a live clinical setting. Another challenge is how to migrate the previous PACS data to a new data media storage system in a live clinical setting.

Some of the issues that surround a migration plan are that the data migration must not hamper the live clinical workflow in any way or reduce system performance. With any migration, it is important that verification be performed to prevent any data loss. Once the data have been successfully migrated to the new data media, the original data media storage system should be removed, which may incur additional downtime of the archive server. Development of a migration plan is key to addressing the surrounding issues and ensuring a data migration that will have the least impact on the live clinical PACS. Because data migration occurs in a live clinical setting, it is important to determine the times at which the data migration will not impact normal clinical workflow. This may include scheduling a heavier data migration rate during off-hours (e.g., nights and weekends) and a lighter rate during operating hours and hours of heavy clinical PACS use. Expert knowledge of the clinical workflow is valuable input toward developing a good schedule data migration. Downtime may be involved both initially and at the end of the data migration process and should be scheduled accordingly with contingency procedures.

It may be necessary to fine-tune the data migration rate because estimates for the migration rate may not be accurate initially. Fine-tuning is very crucial because an aggressive migration rate can adversely affect the performance of the entire clinical PACS. Careful attention to the archive and system performance is especially important during the onset of the data migration. The data migration rate may need to be scaled back. This may be an iterative cycle until an optimal migration rate is achieved that does not adversely affect the clinical PACS.

13.6.5 PACS Clinical Experiences and Pitfalls

The following sections describe an overview of two different PACS clinical experiences from two different sized health care institutions. One is a large-scale health care institution, and the second is a high-profile community-sized hospital. In addition, some PACS pitfalls will be discussed.

13.6.5.1 Clinical Experiences at Baltimore VA Medical Center

The Baltimore VA Medical Center (VAMC) started its PACS implementation in the late 1980s and early 1990s. The VAMC purchased a PACS in late 1991 for approximately $7.8 million, which included $7.0 million for PACS and $800,000 for CR.

The manufacturers involved were Siemens Medical (Erlangen, Germany) and Loral Western Developed Labs (San Jose, CA); the product later changed hands to Loral/Lockheed Martin and then to General Electric Medical Systems. The goals of the project were to integrate with the VA home-grown clinical patient record system (CPRS) and the then to-be-developed VistA imaging system. The project has been under the leadership of Dr. Eliot Siegel, Chairman of the Radiology Department. The system was in operation in the middle of 1993 in the new Baltimore VAMC. This system has since evolved and has been integrated with other VA hospitals in Maryland into a single imaging network, the VA Maryland Health Care System. Four major benefits at the Baltimore VAMC are: changing the operation to filmless, reducing unread cases, reducing retake rates, and drastically improving the clinical workflow.

The two major contributors to the cost of the system are the depreciation and the service contract. The VA depreciates its medical equipment over a period of 8.8 years, whereas computer equipment is typically depreciated over a 5-year time period. The other significant contributor to the cost of the PACS is the service contract, which includes all of the personnel required to operate and maintain the system. It also includes software upgrades and replacement of all hardware components that fail or demonstrate suboptimal performance. This includes replacement of any monitors that do not pass the quality control tests. No additional personnel are required other than those provided by the vendor through the service contract. In the Baltimore VAMC, the radiology administrator, chief technologist, and chief of radiology share the responsibilities of a PACS departmental system administrator. Cost savings attributed to PACS include three areas: (1) film operation costs, (2) space costs, and (3) personnel costs. Films are still used in two circumstances. Mammography examinations are still using films, but they are digitized and integrated to the PACS. Films are also printed for patients who need to have them for hospital or outpatient visits outside the VA health care network. Despite these two uses, film costs have been cut by 95% compared with the figure that would have been required in a conventional film-based department. Additional savings include reductions in film-related supplies such as film folders and film chemistry and processors. The second area in cost savings is space. The ability to recover space in the radiology department because of PACS contributes to a substantial savings in terms of space indirect costs. Finally, the personnel cost savings include radiologists, technicians, and film library clerks. An estimate was made that at least two more radiologists would have been needed to handle the current workload at the VAMC had the PACS not been installed. The efficiency of technologists has improved by about 60% in sectional imaging examinations, which translates to three to four additional technologists had the PACS not been used. Only one clerk is required to maintain the film library and to transport film throughout the medical center.

13.6.5.2 Clinical Experience at Saint John's Health Center

Saint John's Health Center, Santa Monica, CA, has a filmless PACS that acquires approximately 130,000 radiological examinations annually. As the first phase, St. John's implemented the PACS with CR for all critical care areas in April 1999. Phase II, completed in April 2000, included the integration of MR, CT, ultrasound, digital fluorography, and digital angiography within the PACS. Since then, St. John's PACS volumes have increased steadily. The original storage capacity of the PACS archive was a 3.0 TB MOD Jukebox, which would mean that older PACS examinations would have to remain off-line before a year is over. Also, the archive had only a single copy of the PACS data. Therefore, should St. John's encounter a disaster, it might lose all the PACS data because there was no backup. With these considerations, St. John's determined to overhaul its PACS archive system with the following goals:

- Upgrade the archive server to a much larger capacity
- Develop an off-site image/data backup system
- Conduct an image/data migration during the archive system upgrade

These goals were accomplished in late 2001 based on the concepts discussed in this section. With the archive upgrade, all new PACS examinations were archived through a Sun Enterprise 450 platform server with a 270 GB RAID. The examinations were then archived to a network-attached digital tape storage system comprising an additional Sun Enterprise 450 with a 43 GB RAID and a 7.9 TB storage capacity digital tape library. The storage capacity of the tape library technology was forecast to double in the next few years as the tape density doubles, eventually making it a 16 TB library. Figure 13.13 shows the final configuration after the completion of the data migration.

13.6.5.3 PACS Pitfalls

PACS pitfalls are mostly from human error, whereas bottlenecks are due to imperfect design in either the PACS or image acquisition devices. These drawbacks can only be realized through accumulated clinical experience.

Pitfalls resulting from human error are often initiated at imaging acquisition devices and at workstations. Three major errors at the acquisition devices are entering wrong input parameters, stopping an image transmission process improperly, and positioning the patient incorrectly. The errors occur most often at the workstations, where users have to enter many key strokes or click the mouse frequently before the workstation can respond. Other pitfalls at the workstation unrelated to human error are missing location markers in a CT or MR scout view, images displayed with unsuitable lookup tables, and white borders in CR images due to X-ray collimation. Pitfalls created by human intervention can be minimized by implementing a better quality assurance program, providing

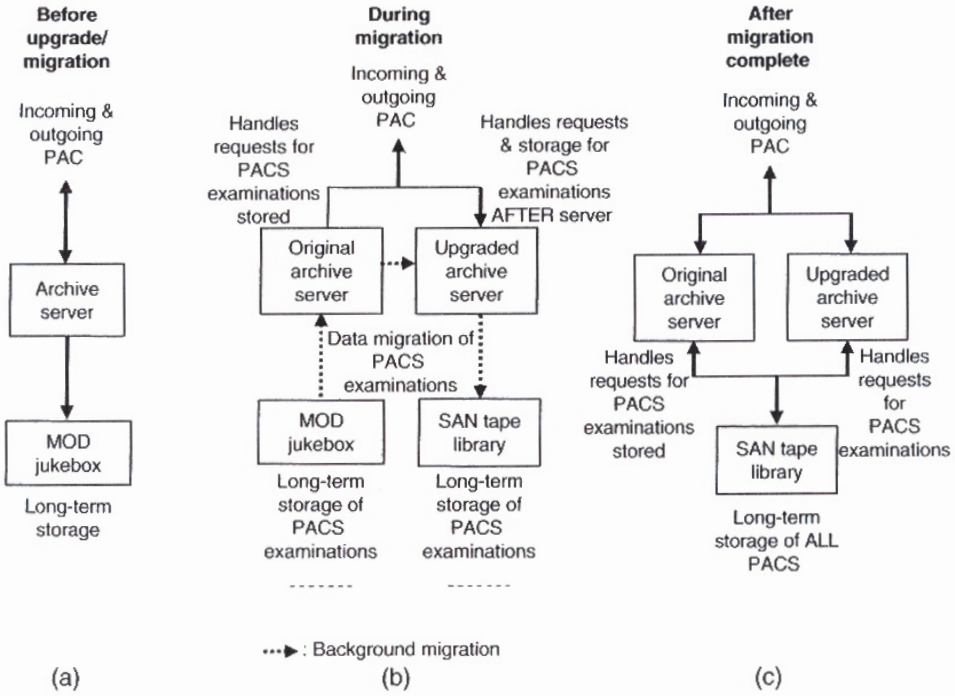

FIGURE 13.13 Before, during, and final archive configuration and process for St. John's Health Center picture archiving and communication system. (a) before, (b) during, (c) after migration with new archive system.

periodic in-service training, and interfacing image acquisition devices directly to the HIS/RIS through a DICOM broker. Bottlenecks affecting the PACS operation include network contention; CR, CT, and MR images stacked up at acquisition devices; slow responses from workstations; and long delays for image retrieval from the long-term archive. Improving the system architecture, reconfiguring the networks, and streamlining operational procedures through a gradual understanding of the PACS clinical environment can alleviate bottlenecks. Utilization of the IHE workflow profiles discussed would also help to circumvent some of the bottleneck problems. During the integration of multivendor PACS components, it should be remembered that, even though each vendor's component may come with a DICOM conformance statement, the components still may not be compatible. These pitfalls can be minimized through the implementation of two DICOM-based mechanisms, one in the image acquisition gateway and the second in the PACS controller, to provide better connectivity solutions for multivendor imaging equipment in a large-scale PACS environment.

13.7 Summary

In this section, various components, terminology, and standards used in PACS were presented and discussed. Integrating the health care enterprise are protocols of image data workflow allowing connectivity of components in PACS from various vendors based on existing standards. The information system used in hospitals is called HIS or CMS, which consists of many clinical databases, like the RIS. These databases are operation-oriented and are designed for special clinical services. The new trend in health care information systems is the ePR, which is patient-oriented (i.e., data goes where the patient goes).

Up-to-date information on these topics can be found in multidisciplinary literature, reports from research laboratories of university hospitals, and medical imaging manufacturers, but not in a coordinated way. Therefore, it is difficult for a radiologist, hospital administrator, medical imaging researcher, radiological technologist, trainee in diagnostic radiology, or student in engineering and computer science to collect and assimilate this information. One major purpose of this section is to provide a brief overview and consolidate PACS-related topics and PACS integration with HIS and ePR. PACS and medical imaging informatics is an ever-growing field that mirrors the ever-changing IT landscape. However, the fundamental concepts remain as important as ever and continue to form the bedrock for this expanding field.

PACS has impacted the health care industry financially and operationally, streamlining clinical workflow and increasing the efficiency of the health care enterprise. Medical

imaging informatics infrastructure is an emerging field focused to take advantage of existing PACS resources and image and related data for large-scale horizontal and longitudinal clinical, research, and education applications that could not be performed previously because of insufficient data.

13.8 Exercises

1. Based on the generic PACS basic components diagram and data flow (Figure 13.1) and the components descriptions, identify the single points of failure for both stand-alone and client/server PACS architectures.
2. Describe how the clinical workflow would be impacted for each of the single points of failure.
3. Provide solutions to address the single points of failure identified.
4. Develop a testing script to perform acceptance testing for each of the single points of failure.

13.9 References and Bibliography

R. A. Bauman, G. Gell, and S. J. Dwyer III. Large picture arching and communication systems of the world—Part 1. *J. Digital Imaging.* 9(3):99–103, 1996.

R. A. Bauman, G. Gell, and S. J. Dwyer III. Large picture arching and communication systems of the world—Part 2. *J. Digital Imaging.* 9(4):172–177, 1996.

R. E. Dayhoff, K. Meldrum, and P. M. Kuzmak. Experience providing a complete online multimedia patient record. Session 38. *Health Care Information and Management Systems Society, 2001 Annual Conference and Exhibition. Feb.4–8,* 2001.

R. Dayhoff and E. L. Siegel. Digital imaging within and among medical facilities. In R. Kolodner (Ed.). *Computerized Large Integrated Health Networks—The VA Success.* Springer Publishing, 473–490, 1997.

D. S. Channin. Integrating the health care enterprise: A primer. II. Seven brides for seven brothers: The IHE integration profiles. *RadioGraphics.* 21:1343–1350, 2001.

D. Channin et al. Integrating the health care enterprise: A primer. III. What does IHE do for me? *Radio Graphics.* 21:1351–1358, 2001a.

D. S. Channin et al. Integrating the health care enterprise: A primer.V. The future of IHE. *RadioGraphics.* 21:1605–1608, 2001b.

DICOM Standard 2003. Available at http://medical.nema.org/.

DICOM: *Digital Imaging and Communication in Medicine.* National Electrical Manufacturers' Association, 1996.

A. J. Duerincks. Picture archiving and communication system (PACS). *Proc. SPIE for Medical Applications.* 318, 1982.

HL7. *Health Level Seven. An application protocol for electronic data exchange in health care environments. Version 2.1.* Health Level Seven, Inc., 1991.

Health Level Seven. Available at http://www.hl7.org/.

HL7 Version 3.0: Preview for CIOs, Managers, and Programmers. Available at http://www.neotool.com/company/press/199912_v3.htm#V3.0_preview.

H. K. Huang. Enterprise PACS and image distribution. *Comp. Med. Imaging Graphics.* 27(2–3):241–253, 2003.

H. K. Huang. *PACS and Imaging Informatics: Basic Principles and Applications.* Wiley & Sons, 2004.

H. K. Huang. *PACS: Principles and Applications.* Wiley & Sons, 1999.

H. K. Huang et al. Design and implementation of a picture archiving and communication system: The second time. *J. Digital Imaging.* 9:47–59, 1996.

H. K. Huang, S. T. C. Wong, and E. Pietka. Medical image informatics infrastructure design and applications. *Med. Informatics.* 22(4):279–289, 1997.

B. J. Liu et al. Trends in PACS image storage and archive. *Comp. Med. Imaging Graphics.* 27(2–3):165–174.

B. J. Liu et al. PACS archive upgrade and data migration: clinical experiences. *Proc. SPIE Medical Imaging.* 4685: 83–88, 2002.

B. J. Liu et al. A fault-tolerant back-up archive using an ASP model for disaster recovery. *Proceeding SPIE Medical Imaging.* 4685:89–95, 2002.

C. J. McDonald. The barrier to electronic medical record systems and how to overcome them. *J. Am. Med. Informatics Assoc.* 4(May/June):213–221, 1997.

R. Osman, M. Swiernik, and J. M. McCoy. From PACS to integrated EMR. *Comp. Med. Imaging Graphics.* 27(2–3): 207–215, 2003.

E. L. Siegel, J. N. Diaconis, S. Pomerantz et al. Making filmless radiology work. *J. Digital Imaging.* 8:151–155, 1995.

E. L. Siegel and B. I. Reiner. Filmless radiology at the Baltimore VA medical center: A nine-year retrospective. *Comp. Med. Imaging Graphics.* 27(2–3):101–109, 2003.

E. L. Siegel and D. S. Channin. Integrating the health care enterprise: A primer—Part 1. Introduction. *RadioGraphics.* 21:1339–1341, 2001. www.rsna.org/IHE

F. Yu et al. Some connectivity and security issues of NGI in medical imaging applications. *J. High Speed Networks.* 9:3–13, 2000.

X. Zhou, H. K. Huang. Authenticity and integrity of digital mammography image. *IEEE Trans. Medical Imaging.* 20(8):784–791, 2001.

imaging informatics infrastructure is an emerging field focused to take advantage of existing PACS resources and image and related data for large-scale horizontal and longitudinal clinical, research, and education applications that could not be performed previously because of insufficient data.

13.8 Exercises

1. Based on the generic PACS basic components diagram and data flow (Figure 13.1) and the components descriptions, identify the single points of failure for both stand-alone and client/server PACS architectures.
2. Describe how the clinical workflow would be impacted for each of the single points of failure.
3. Provide solutions to address the single points of failure identified.
4. Develop a testing script to perform acceptance testing for each of the single points of failure.

13.9 References and Bibliography

R. A. Bauman, G. Gell, and S. J. Dwyer III. Large picture arching and communication systems of the world—Part 1. *J. Digital Imaging.* 9(3):99–103, 1996.

R. A. Bauman, G. Gell, and S. J. Dwyer III. Large picture arching and communication systems of the world—Part 2. *J. Digital Imaging.* 9(4):172–177, 1996.

R. E. Dayhoff, K. Meldrum, and P. M. Kuzmak. Experience providing a complete online multimedia patient record. Session 38. *Health Care Information and Management Systems Society, 2001 Annual Conference and Exhibition. Feb.4–8,* 2001.

R. Dayhoff and E. L. Siegel. Digital imaging within and among medical facilities. In R. Kolodner (Ed.). *Computerized Large Integrated Health Networks—The VA Success.* Springer Publishing, 473–490, 1997.

D. S. Channin. Integrating the health care enterprise: A primer. II. Seven brides for seven brothers: The IHE integration profiles. *RadioGraphics.* 21:1343–1350, 2001.

D. Channin et al. Integrating the health care enterprise: A primer. III. What does IHE do for me? *Radio Graphics.* 21:1351–1358, 2001a.

D. S. Channin et al. Integrating the health care enterprise: A primer.V. The future of IHE. *RadioGraphics.* 21:1605–1608, 2001b.

DICOM Standard 2003. Available at http://medical.nema.org/.

DICOM: *Digital Imaging and Communication in Medicine.* National Electrical Manufacturers' Association, 1996.

A. J. Duerincks. Picture archiving and communication system (PACS). *Proc. SPIE for Medical Applications.* 318, 1982.

HL7. *Health Level Seven. An application protocol for electronic data exchange in health care environments. Version 2.1.* Health Level Seven, Inc., 1991.

Health Level Seven. Available at http://www.hl7.org/.

HL7 Version 3.0: Preview for CIOs, Managers, and Programmers. Available at http://www.neotool.com/company/press/199912_v3.htm#V3.0_preview.

H. K. Huang. Enterprise PACS and image distribution. *Comp. Med. Imaging Graphics.* 27(2–3):241–253, 2003.

H. K. Huang. *PACS and Imaging Informatics: Basic Principles and Applications.* Wiley & Sons, 2004.

H. K. Huang. *PACS: Principles and Applications.* Wiley & Sons, 1999.

H. K. Huang et al. Design and implementation of a picture archiving and communication system: The second time. *J. Digital Imaging.* 9:47–59, 1996.

H. K. Huang, S. T. C. Wong, and E. Pietka. Medical image informatics infrastructure design and applications. *Med. Informatics.* 22(4):279–289, 1997.

B. J. Liu et al. Trends in PACS image storage and archive. *Comp. Med. Imaging Graphics.* 27(2–3):165–174.

B. J. Liu et al. PACS archive upgrade and data migration: clinical experiences. *Proc. SPIE Medical Imaging.* 4685: 83–88, 2002.

B. J. Liu et al. A fault-tolerant back-up archive using an ASP model for disaster recovery. *Proceeding SPIE Medical Imaging.* 4685:89–95, 2002.

C. J. McDonald. The barrier to electronic medical record systems and how to overcome them. *J. Am. Med. Informatics Assoc.* 4(May/June):213–221, 1997.

R. Osman, M. Swiernik, and J. M. McCoy. From PACS to integrated EMR. *Comp. Med. Imaging Graphics.* 27(2–3): 207–215, 2003.

E. L. Siegel, J. N. Diaconis, S. Pomerantz et al. Making filmless radiology work. *J. Digital Imaging.* 8:151–155, 1995.

E. L. Siegel and B. I. Reiner. Filmless radiology at the Baltimore VA medical center: A nine-year retrospective. *Comp. Med. Imaging Graphics.* 27(2–3):101–109, 2003.

E. L. Siegel and D. S. Channin. Integrating the health care enterprise: A primer—Part 1. Introduction. *RadioGraphics.* 21:1339–1341, 2001. www.rsna.org/IHE

F. Yu et al. Some connectivity and security issues of NGI in medical imaging applications. *J. High Speed Networks.* 9:3–13, 2000.

X. Zhou, H. K. Huang. Authenticity and integrity of digital mammography image. *IEEE Trans. Medical Imaging.* 20(8):784–791, 2001.